Technische Universität München
TUM School of Engineering and Design

Monitoring wood moisture content

Methods and specific calibration curves for in-situ measurements in timber structures under temperature and moisture gradients

Nina Flexeder

Vollständiger Abdruck der von der TUM School of Engineering and Design der Technischen Universität München zur Erlangung des akademischen Grades einer Doktorin der Ingenieurwissenschaften (Dr.-Ing.) genehmigten Dissertation.

Vorsitz: Prof. Dr.-Ing. Klaus Sedlbauer

Prüfende der Dissertation:

1. Prof. Dr.-Ing. Stefan Winter
2. Prof. Dr.-Ing. habil. Dr. h.c. Peter Niemz
3. Prof. Dr. Christian Brischke

Die Dissertation wurde am 30.09.2024 bei der Technischen Universität München eingereicht und durch die TUM School of Engineering and Design am 29.11.2024 angenommen.

An erster Stelle möchte ich meinem Doktorvater, Herrn Prof. Dr.-Ing. Stefan Winter, meinen aufrichtigen Dank für seine Unterstützung, seine Expertise und sein wertvolles Feedback aussprechen.

Zudem danke ich ganz herzlich meinem zweiten Betreuer, Herrn Prof. em. Dr.-Ing. habil. Dr. h.c. Peter Niemz, für seine fachliche Beratung und stete persönliche Begleitung meiner Forschungsarbeit.

Ebenso möchte ich meinem dritten Betreuer, Herrn Prof. Dr. Brischke, ein großes Danke für den sehr hilfreichen Austausch und seine konstruktiven Anmerkungen sagen.

Ein wunderbares Dankeschön geht außerdem an meinen Mentor und ehemaligen Kollegen, Herrn Prof. Dr.-Ing. Patrik Aondio, dessen Rat und Inspiration mir den Weg für meine wissenschaftliche Laufbahn geebnet haben.

Nicht zuletzt möchte ich mich bei den ehemaligen Bacheloranden, Masteranden, wissenschaftlichen Hilfskräften, Kolleginnen und Kollegen an der *Technischen Universität München* bedanken, die durch ihre Zusammenarbeit, ihre Hilfsbereitschaft und die gemeinsame Zeit diese Erfahrung bereichert haben.

My special thanks also go to my former colleagues at *The University of Queensland*, who have contributed significantly to the success of this work through their kind support and valuable professional input.

Ganz besonders möchte ich P. danken, für unerschütterliche Geduld, Verständnis, Zuspruch und kulinarische Verpflegung. Ohne diese Unterstützung wäre diese Arbeit nicht möglich gewesen.

THANK YOU!

Parts of the research activities were made possible by the Federal Institute for Research on Building, Urban Affairs and Spatial Development (BBSR), within the framework of the re-search initiative "Zukunft Bau" SWD-10.08.18.7-18.46. Further parts were funded by the Federal Ministry for Economic Affairs and Energy, within the framework of the "Central Innovation Program for SMEs (ZIM)" ZF4777401SA9. International collaboration was supported by the TUM Global Incentive Fund, the TUM-UQ Research Exchange program, and the COST Action CA20139: Holistic design of taller timber buildings. Furthermore, thanks go to the company Binderholz Bausysteme GmbH for the cooperation on the project BBS Thermo, Timberbrain.

MONITORING WOOD MOISTURE CONTENT

Abstract

Analyzing a transient wood moisture gradient at different depths of a timber component over a longer period of time and possibly under the influence of temperature plays an important role in timber engineering. Changes in wood moisture content can have a significant impact in various scenarios and different fields such as in structural design, product development, building physics, maintenance, but also in restoration practice. The underlying issue thus determines the specific requirements for wood moisture monitoring. This dissertation investigates an example from fundamental hygrothermal research, which requires comparatively high precision under fluctuating temperature levels. In a broader context, the results of this thesis are therefore transferable to other applications in timber construction.

The methods include literature research, laboratory experiments on influencing parameters, optimization of measurement methods, collection and improvement of calibration curves, field tests, building monitoring and statistical evaluation of monitoring data.

Two monitoring methods, the electrical resistance method and the sorption method, are being further developed and systematically examined for their precision in laboratory tests. The experiments result in newly parameterized calibration curves for electrical resistance measurement in Norway spruce (*Picea abies Karst.*), European beech (*Fagus sylvatica L.*), laminated spruce veneer lumber and laminated beech veneer lumber; each for different measurement directions and in a temperature range of 5 - 60 °C. As an alternative, the sorption method is optimized using a collection of wood species-specific sorption isotherms. This results in newly parameterized formulas for calculating the equilibrium moisture content for Norway spruce, European beech, Douglas fir (*Pseudotsuga menziesii Franco*) and radiata pine (*Pinus radiata D. Don.).* Systematic laboratory tests on Norway spruce and Douglas fir are complemented by spot checks on radiata pine, spotted gum (*Corymbia maculata*), and shining gum (*Eucalyptus nitens*). The accuracy of both methods is estimated as a function of temperature based on the experiments. Despite successful temperature compensation in the laboratory measurement series, transient experiments show that the electrical resistance method can be error-prone even at slightly lower temperatures. An analysis of possible applications from research and practice determines which method is recommended in each case, with focus on the required measurement accuracy.

The new findings are applied to various projects with exterior walls made from cross-laminated timber. This includes field tests and two monitoring projects, the *Einfach Bauen* dwelling and the *Timberbrain* office building. In the latter, the relationship between thermal conductivity and wood moisture can be confirmed in-situ.

HOLZFEUCHTEMONITORING

Kurzfassung

Die Analyse eines instationären Holzfeuchtegradienten in verschiedenen Tiefen eines Bauteils über einen längeren Zeitraum hinweg und gegebenenfalls unter Temperatureinfluss, spielt im Ingenieurholzbau eine wichtige Rolle. Änderungen des Feuchtegehalts können wesentliche Auswirkungen auf eine Holzkonstruktion haben. In diesem Kontext sind Szenarien aus verschiedenen Fachgebieten wie der Tragwerksplanung, der Bauproduktentwicklung, der Bauphysik, der Instandhaltung, aber auch der Restaurierung möglich. In Abhängigkeit von der zugrundeliegenden Fragestellung ergeben sich spezifische Anforderungen an die Details eines nötigen Holzfeuchtemonitorings. Dies wird in der vorliegenden Dissertation beispielhaft an einem Anwendungsfall der hygrothermischen Grundlagenforschung untersucht, welcher eine vergleichsweise hohe Präzision unter schwankenden Temperaturniveaus erfordert. Die Ergebnisse sind somit auch auf andere Anwendungsfälle übertragbar.

Die Methoden der Arbeit umfassen eine Literaturrecherche, Labormessungen zu Einflussparametern, Optimierung von Messmethoden, Sammlung und Erstellung von Kalibrierkurven, Feldtests, Gebäudemonitoring und statistische Auswertung von Messdaten.

Die elektrische Widerstandsmethode und die Sorptionsmethode werden mittels optimierter Kalibrierkurven weiterentwickelt und systematisch auf ihre Präzision hin in Labortests untersucht. Aus den Experimenten ergeben sich neu parametrisierte Kalibrierkurven für die elektrische Widerstandsmessung in Fichte (*Picea abies Karst.*), Buche (*Fagus sylvatica L.*), Fichtenfurnierschichtholz und Buchenfurnierschichtholz, jeweils für verschiedene Messrichtungen und im Temperaturbereich 5 – 60 °C. Als Alternative wird die Sorptionsmethode anhand einer Sammlung von holzartenspezifischen Sorptionsisothermen optimiert. Daraus resultieren neu parametrisierte Formeln zur Berechnung der Ausgleichsfeuchte für Fichte, Buche, Douglasie (*Pseudotsuga menziesii Franco*) und Radiatakiefer (*Pinus radiata D. Don.*). Systematische Labortests an Fichte und Douglasie werden durch stichprobenhafte Versuche mit Radiatakiefer und zwei Eukalyptusarten (*Corymbia maculata* und *Eucalyptus nitens*) ergänzt. Die Genauigkeit der beiden Methoden wird jeweils in Abhängigkeit von der Temperatur auf Basis der Experimente geschätzt. Obgleich eine erfolgreiche Temperaturkompensation in den Labormessreihen zu verzeichnen ist, zeigt sich in instationären Experimenten, dass die elektrische Widerstandsmethode bereits bei leicht abgesenkten Temperaturen fehleranfällig sein kann. Eine Analyse potenzieller Anwendungsfälle aus der Forschung und Praxis eruiert, welche Methode unter Berücksichtigung der erforderlichen Messgenauigkeit jeweils empfohlen wird.

Die neuen Erkenntnisse werden auf verschiedene Brettsperrholzaußenwände in Feldtests und in zwei Monitoringprojekten, dem *Einfach Bauen*-Wohngebäude und dem *Timberbrain*-Bürogebäude, angewandt. Bei Letzterem kann der aus Referenzen bekannte Zusammenhang von Wärmeleitfähigkeit und Holzfeuchte in-situ bestätigt werden.

CONTENT

Glossar / Symbols and abbreviations

Table 1: Symbols and their physical meaning and unit

Symbol	Quantity	Unit
A	Area	mm^2
AH	Absolute humidity of air	g/m^3
d	Diameter	*mm*
EMC	Equilibrium moisture content	*m.-%*
EWC	Electrode withdrawal peak load capacity	*N*
I	Electric current	*A*
λ	Thermal conductivity	$W/(m \cdot K)$
m	Mass	*g*
MBV	Moisture buffering value	kg/m^2-%RH
MC	Moisture content	*m.-%*
p_S	Saturation vapor pressure	*Pa*
ρ_x	Density at a certain moisture content x	kg/m^3
ρ_{el}	Electrical resistivity	Ωcm
R	Electrical resistance	Ω
RH	Relative humidity of air	%
$\partial RH/\partial t$	Change of relative humidity of air over time	%/h
s_d	Equivalent air layer thickness	*m*
T	Temperature	°C
dT	Temperature difference	*K*
U	Electrical Voltage	*V*
v	Air velocity	*m/s*
$X_{20\,°C}$	Base value of moisture content at 20 °C	*m.-%*

Table 2: Symbols and their mathematical meaning

Symbol	Mathematical meaning
$\bar{X}$	Average of X
Δ	Delta
expx	= e^x, e to the power of x, exponential function of Euler´s number
ln(x)	= $\log_e(x)$, natural logarithm of x
lg(x)	= $\log_{10}(x)$, decadic logarithm of x
NRMSE	Normalized root mean of squared error
SD	Standard deviation
SMA	Simple moving average
Σ	Sum

Table 3: Abbreviations and their meaning

Abbreviation	Meaning
AC	Alternating current
API	Application programming interface
CC	Consequence class
CLT	Cross-laminated timber
$CoCl_2$	Cobalt chloride
CT	X-ray computed tomography
DC	Direct current
ERM	Electrical resistance method
FEM	Finite element method
GPR	Ground penetrating radar
HAM	Heat, air, and moisture transport
HVAC	Heating, Ventilation and Air Conditioning
IL	Inspection level
IRT	Infrared thermography
$KC_2H_3O_2$	Potassium acetate
K_2CO_3	Potassium carbonate
LVL	Laminated veneer lumber
MRI	Magnetic resonance imaging
NaCl	Natrium chloride
NIRS	Near infrared spectroscopy
NMR	Nuclear magnetic resonance
NTC	Negative-temperature-coefficient thermistor
OSB	Oriented strand board
PTC	Positive-temperature-coefficient thermistor
RFID	Radio-frequency identification
RTD	Resistance temperature detector
SI	Système international d'unités (International System of Units)
SHM	Structural health monitoring
SM	Sorption method (also: hygrometric method)
TUM	Technical University of Munich (Germany)
UQ	The University of Queensland (Australia)
UTM	Universal testing machine
WUFI	Wärme und Feuchte instationär (Hygrothermal simulation software)

1 INTRODUCTION

1.1 General structure of this dissertation

This thesis focuses on the improvement and comparison of two existing methods for wood moisture monitoring in the cross-section of a timber element. In addition, a new, third method is presented, which could be used to detect sorption processes at the component surface in long-term studies.

Chapter 1 summarizes the topic of monitoring wood moisture content, establishes the normative basis for wood moisture determination, and explains the objectives of this dissertation.

Chapter 2 examines the relevance of moisture monitoring in various contexts, including historical objects, timber buildings, new developments in timber engineering, and detailed investigations. The Chapter presents a case study from thermal building physics to illustrate the application of moisture monitoring techniques.

Chapter 3 provides a selection of the current state of knowledge in the field of wood physics, elucidating those relationships that extend beyond the fundamental principles of timber construction.

Chapter 4 explains the methods employed in the numerous experiments conducted in this thesis. These include both laboratory tests on a small scale and with different types of wood, as well as several monitoring projects in various exterior walls with cross-laminated timber.

Chapter 5 outlines the results of a series of laboratory experiments designed to enhance the efficacy of wood moisture monitoring techniques. Several novel calibration curves tailored to specific wood types are generated and subsequently tested under a range of conditions to ascertain their reliability.

Chapter 6 employs the newly acquired knowledge in a variety of monitoring projects. Two distinct methods are evaluated and contrasted for their suitability over extended time periods. Two test cubes, two exterior walls of a residential building, and two exterior walls of an office building, all made from cross-laminated timber, serve as the application sites.

Chapter 7 presents a summary of the findings, with a particular focus on the accuracy of the methods under investigation, recommendations regarding the appropriate use of these methods, and suggestions for future research and development. Furthermore, it includes a list of publications and presentations that are not part of this dissertation, but which complement its content.

Appendices A – K address topics that are essential for further use of the results. They include detailed information on the formulations used, measurement data, and calibration curves. Furthermore, they provide the new conversion equations, which are a major outcome of this thesis, compiled in an abridged form and ready for practical use.

1.2 Preface: What is transient wood moisture analysis?

The single measurement of a physical unit to determine the moisture content of a piece of wood has been an established practice for decades and is regulated by various standards. Although some results might also be quite helpful to further advance these known methods (particularly electrical resistance measurements), this is not the primary topic of this work.

This dissertation is about monitoring the wood moisture gradient in a built environment with as little intrusion as possible. This means repeatedly measuring a certain physical unit in-situ over a long period of time and drawing conclusions about the long-term moisture transport in timber, possibly under other influences such as changing temperature.

In order to distinguish this work from the general topic of wood moisture content, this Subsection provides a brief overview of what is already considered as state of the art. There are a variety of physical measurement methods that can be used to estimate the moisture content or moisture distribution in materials. Various resources provide a comparative overview of the methods relevant to building practice, for instance (Riggio et al., 2014), (Dietsch, Franke et al., 2015), (Camuffo, 2018), (Appel, 2020), or (Palma & Steiger, 2020).

In particular, low-destructive measurements using the electrical resistance method are a common practice in timber construction and carpentry. Professionals have been employing this method for indirect estimation of wood moisture content already for several decades. For instance, Figure 1 illustrates a historical apparatus, which was advertised as a new product by the Anglo-Swiss Electrical Co., Ltd. in the year of 1935.

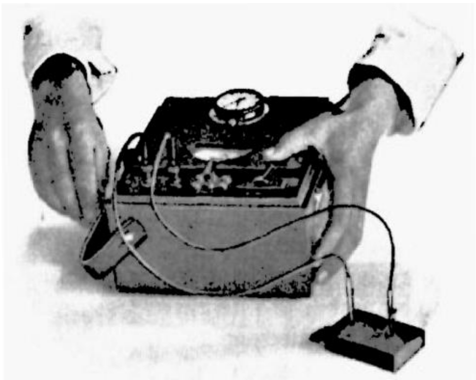

Figure 1: Instrument for the measurement of moisture in wood, sold by the Anglo-Swiss Electrical Co., Ltd., in London and calibrated at the materials testing laboratory of the Polytechnic in Zurich, price of the complete apparatus in 1935: £40 (around 4,175 € today) (Ltd., 1935)

Today, electrical resistance measurements in wood are mainly carried out as a series of random sample measurements using hand-held devices. This method can be found as an adapted solution for continuous monitoring in some cases, cf. also Subchapter 3.3.3. However, there are no standards or similar regulations on how to use and evaluate these adaptations for long-term monitoring yet. Table 4 lists a selection of international standards relevant to the topic of wood moisture analysis.

Table 4: Selection of European, American, and Australian standards regarding wood moisture content analysis

Standard No.	Document title
(EN 13183-1:2002)	Moisture content of a piece of sawn timber - Part 1: Determination by oven dry method
(EN 13183-2:2002)	Moisture content of a piece of sawn timber - Part 2: Estimation by electrical resistance method
(EN 13183-3:2005)	Moisture content of a piece of sawn timber - Part 3: Estimation by capacitance method
(ISO 760:1978-12)	Determination of water; Karl Fischer method (General method)
(EN ISO 12570:2000 + Amd 1:2013 + Amd 2:2018))	Hygrothermal performance of building materials and products – Determination of moisture content by drying at elevated temperature
(EN ISO 12571:2021)	Hygrothermal performance of building materials and products - Determination of hygroscopic sorption properties
(ISO 16979:2003-05)	Wood-based panels — Determination of moisture content
(EN 16682:2017)	Conservation of cultural heritage – Methods of measurement of moisture content, or water content, in materials constituting immovable cultural heritage
(ASTM D4442-20)	Standard Test Methods for Direct Moisture Content Measurement of Wood and Wood-Based Materials
(ASTM D4444-13 [2018])	Standard Test Method for Laboratory Standardization and Calibration of Hand-Held Moisture Meters
(ASTM D4933-16 [2021])	Standard Guide for Moisture Conditioning of Wood and Wood-Based Materials
(ASTM D7438-20)	Practice for Field Calibration and Application of Hand-Held Moisture Meters
(AS/NZS 1080.1:2012)	Timber - Methods of test - Method 1: Moisture content

In order to create uniformity among these different sets of regulations in this thesis, the wood moisture content *MC* is specified in accordance with (EN 13183-1:2002):

$$MC = \frac{m_1 - m_0}{m_0} \cdot 100 \qquad (1)$$

With

MC	Moisture content in mass-percent	[m.-%]
m_1	Mass of the test specimen before drying	[g]
m_0	Mass of the test specimen in oven-dried state	[g]

The moisture content *MC* [m.-%] is therefore defined as the mass of water contained in the wood divided by the mass of dry wood, with the unit being mass percent. It is essential to differentiate between direct/absolute and indirect/relative measurement methods. Direct methods include the oven-drying method, where a specimen is weighed, dried in an oven, and weighed again. The resulting difference is defined as the original moisture content. Oven-drying can alter the specimen´s structure, so it is usually only carried out at the end of an experiment. Furthermore, it is not suited as an in-situ monitoring method. In terms of determining the moisture content of wood, it is the most used absolute reference method, which can actually determine the moisture content with sufficient reliability. Some indirect methods offer the possibility of low or non-destructive repetitive measurements, a prerequisite for monitoring. These methods, some of which are also investigated in this thesis, use physical principles such as Ohm's law, the equilibrium between ambient air and hygroscopic materials, or the sorption enthalpy. As they are indirect, they are subject to certain conversion errors.

1.3 Scientific and practical requirements for monitoring wood moisture content

Moisture monitoring systems could be a key component of future holistic concepts to develop and maintain multi-storey timber buildings (Flexeder, Schenk & Aondio, 2022). General design rules that serve to protect timber structures against moisture have been known to the woodworking trade for centuries. Additional modern moisture monitoring as a part of structural monitoring is considered a preventive concept based on permanent technical installations within structures (Riggio & Dilmaghani, 2020). This type of moisture monitoring is usually carried out to obtain information when progressive damage patterns such as moisture penetration or cracking are suspected. Early intervention during maintenance can prevent, or at least reduce, the cost of major renovations. They are also used to assess the long-term effects of changing environmental conditions (D´Ayala et al., 2014).

The required accuracy of a measurement depends directly on the information needed. If it is only a statement as to whether there is a short-term accumulation of liquid water on the surface or not, a binary answer is sufficient. Statements about the speed of wetting or drying, on the other hand, require the measurement of a gradient. These processes generally take place depending on the ambient conditions, exposure time, and the specific material parameters of the surfaces.

Moisture fluctuations in timber structures can lead to a variety of restrictions within buildings. These include influences on the mechanical properties of materials such as strength and stiffness, and also the occurrence of wood-destroying fungi. In addition, the constant adaptation of the hygroscopic building material to the prevailing ambient climate also changes other material parameters that are relevant in building physics.

In particular, structural changes in existing buildings or changes of use can have an impact on the ambient conditions. If the indoor climate changes, for example because an air conditioning system is retrofitted, this can affect the safety, serviceability, and durability of timber constructions. Very similar problems can also occur outside of traditional timber engineering. For instance, there are similar issues regarding appropriate ambient climate fluctuations in the storage of wooden objects, such as cultural assets or works of art. These challenges include the hygromechanical analysis of panel paintings such as the famous *Mona Lisa* (Riparbelli et al., 2021).

Research into wood moisture analysis and monitoring of transient behavior is therefore not only used for the assessment, strengthening, and monitoring of modern timber structures. In fact, traditional assessment was initially associated with historical structures as a part of restoration practice. Only subsequently, with the use of products in modern construction, did this discipline also become relevant for modern systems. (Kasal, 2013; Riggio et al., 2014)

1.4 Aim and objectives for improving wood moisture monitoring

The time-dependent change in wood moisture content in the hygroscopic range and thus below the fiber saturation point is an important parameter in timber engineering. However, it is a challenge to determine this value accurately in structural elements under temperature gradients. The aim of this dissertation is to improve the measurement techniques for in-situ wood moisture monitoring in different types of wood and under thermal influences as a contribution to advance modern and sustainable building construction.

The work in this dissertation is guided along the following research questions and objectives:

I. Collect and analyze previous approaches for a holistic overview on wood moisture

When, where, why, and to what extent is wood moisture monitoring needed? What factors are influenced by wood moisture content and how can those be utilized?

Several fields of expertise deal with topics related to wood moisture content analysis that stem from different requirements. In order to create synergies in the development of methods, the research approach in Chapters 1, 2, and 3 will also investigate outside of traditional civil engineering.

II. Investigate established methods and develop new ones to quantify moisture gradients

Which methods can be used to investigate the challenges in wood moisture content monitoring? How accurate is the wide-spread electrical resistance method when adapted for repeated measurements under temperature influence? To what extent could the sorption method be a viable option for wood moisture monitoring? Could the idea of using latent heat effects serve for moisture flux detection?

In order to increase the accuracy, various parts of monitoring equipment as well as calibration curves will be designed, created, and tested in Chapters 4 and 5.

III. Apply new findings about methods and their limitations to in-situ monitoring

To what extent can the results obtained in laboratory measurements be transferred to actual exterior walls made of cross-laminated timber? What are influences that cumulate to deviations of each method? Based on the new improved wood moisture monitoring methods, which results can be drawn about the hygrothermal performance of the examined walls? For instance, can the hypotheses about a reduction in thermal conductivity be confirmed?

Monitoring campaigns lasting several months in different buildings with exterior walls made from cross-laminated timber serve as use cases for testing the new methods in Chapter 6. Based on the findings, recommendations for future monitoring projects are provided in Chapter 7.

2 CONTEXT OF RESEARCH ON WOOD MOISTURE ANALYSIS

2.1 Monitoring in the field of conservation and preservation practice

2.1.1 On the need to study the moisture content of wood in historical objects

The basic principles of moisture monitoring in modern timber structures originate from the conservation practice of historical timber structures (Kasal, 2013). Here, in contrast to modern timber engineering, destructive testing methods for extensive material analysis are generally not an option (Camuffo, 2018). Furthermore, if erroneous decisions in climate control lead to irreparable damage to the object, the replacement of the elements made of original material is usually impossible. So ideally, possible damage of historical buildings should be detected before even becoming visible (Lehmann et al., 2018). The examination, observation and, if necessary, the careful correction of moisture gradients in historic wood structures could thus be considered the pinnacle of transient wood moisture analysis. Looking forward, the concept of these methods and models could then be transferred to any timber structure, including modern buildings and bridges. (Konopka et al., 2020; Shabani et al., 2020)

Considering the preservation of historic structures, water has the potential to cause significant damage (Krüger & Lehmann, 2020). Monitoring the moisture content and subsequent drying or humidification therefore plays an important role in the preservation of cultural assets made of any porous material (Krüger & Lehmann, 2019). Hygroscopic materials constantly tend towards dynamic equilibrium between the relative humidity (*RH*) of the ambient air and the moisture content of the sorbent. Consequently, increased relative humidity leads to an increased moisture content of the material, which could promote mold growth. However, the moisture content of historical wooden art objects does not only play a role in mold prevention.

The high hygroscopicity of wood, paper, and other hydrophilic materials are prone to geometric changes (swelling, shrinkage) as humidity changes. Hence, alternating climate conditions can induce mechanical stress and thus damage the structure leading to large deformations and cracks. Temperature and relative humidity of air in particular, are therefore key parameters in preserving cultural heritage (Camuffo & Bertolin, 2012; Konopka et al., 2019). Since fluctuations in indoor humidity are the main cause of mechanical damage to wooden cultural heritage artworks (Backer et al., 2018), it is advisable to maintain these as little as possible. In practice, however, it is often not feasible to continuously air-condition the objects. Changes in the surroundings such as building renovations, relocation of exhibits, outdoor exhibitions with seasonal changes, or storage, can significantly alter the room climate. Oftentimes, conservators are called in when the object has already been visibly damaged by a change in climate that has occurred too quickly. How can such damage be reversed or even prevented?

As the indoor climate of many exhibition spaces and churches has been changed drastically in recent decades, especially due to heating measures to increase comfort levels, there is an increased need for research in restoration. As part of an effort to improve energy efficiency, concepts for exhibition spaces should be designed to allow for a greater hysteresis in their air conditioning systems. An indoor air relative humidity of 50 ±15 %RH is generally considered safe for the storage and display of historical panel paintings; however, it has been argued that these limits require unnecessarily strict control, which in turn fosters high energy consumption (Bratasz, 2013; Holl, 2016; Smith & Ashley-Smith, 2013). In addition, systems that rely solely on mechanical ventilation for the structural health of building components or artwork are vulnerable to potentially catastrophic consequences if such measures fail (Dionisi-Vici et al., 2013).

To assess the risk of mechanical damage, there are approaches to both monitor and model moisture transport in the artwork with respect to a simulated indoor climate. Several projects focus on panel paintings, where low moisture contents cause deformations in the single wooden boards (cupping) and thus damage the paint layer (Backer et al., 2018; Brandt et al., 2023; Gebhardt et al., 2018; Herm et al., 2021; Riparbelli et al., 2023). Figure 2 shows a schematic approach by (Herm et al., 2021), who use climatic measurement data in computer simulations to define a suitable range of ambient climate variations that are just tight enough to prevent any damage on an iconic artwork. By experimenting on a detailed numerical model, they are able to test different scenarios without risking damage to the physical original. In order to create the most accurate digital twin possible, they had to determine and digitally reproduce characteristics such as the wood species, wood density, wood moisture content, the position of the board´s annual rings, the quality of the bond lines, the coating materials, the thickness of the layers, and the application process. Moisture content in particular presented the researchers with a number of challenges, as only a small piece of original wood was available to validate the estimated values by the direct gravimetric method.

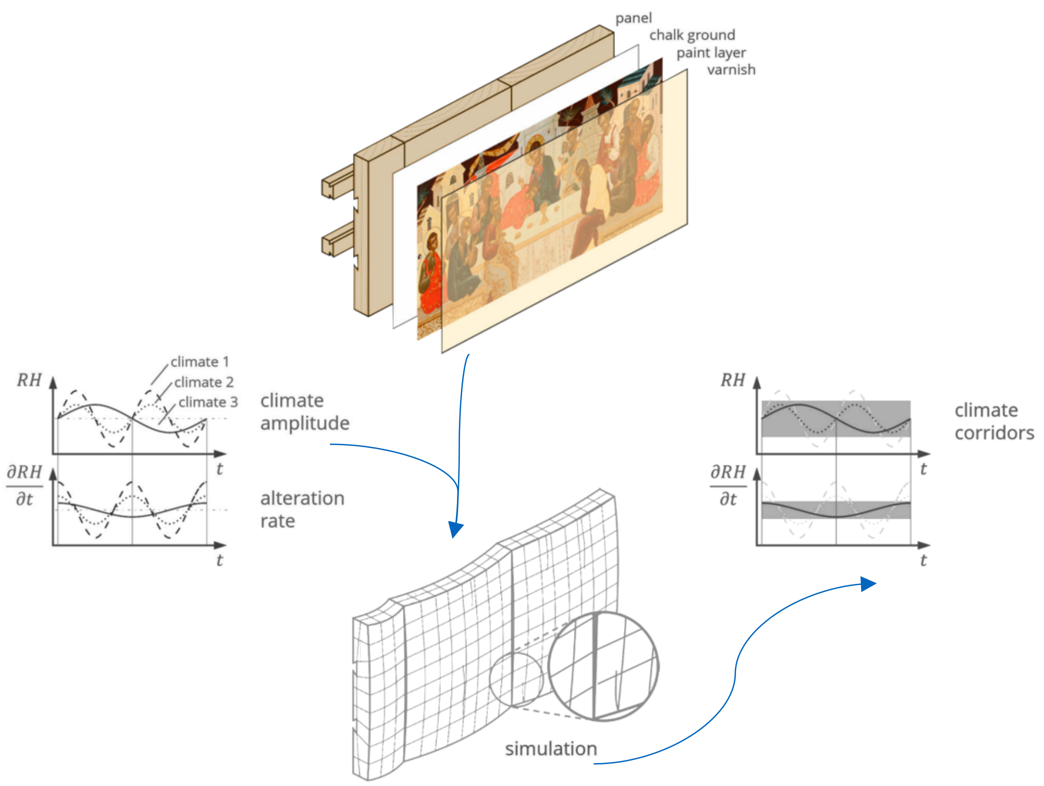

Figure 2: Scheme to predict possible climate corridors for air-conditioning as demonstrated on a historic painting on wooden panels; original illustration by (Herm et al., 2021) with own visual adjustments.

2.1.2 Challenges in validating models on moisture gradients in historical wooden objects

How can modern modeling techniques be used to estimate which climatic loads are still tolerable and which will lead to irreversible damage such as cracking? Several preservation projects on wooden panel paintings, which are a typical work of art in European churches of the 15th and 16th centuries, show the complexity of predicting moisture transport. In this context, a number of cases are documented where hygromechanical phenomena caused by the changing moisture load, in combination with an unsuitable and restrictive structural system, have led to cracking and warping. Simulation studies could be used to predict the general mechanical behavior and help identify the structure´s critical parts and risky climatic situations that could increase the damage. (Backer et al., 2018; Brandt et al., 2023; Gebhardt et al., 2018)

Since the hygrothermal response of wooden artworks is controlled not only by the vapor permeability of the wood but mainly by the barrier effect of the different material layers on top of it, the hygric material properties of all layers are required to reliably simulate the local moisture gradients in the object (Backer et al., 2018; Holl, 2016). The peak response to seasonal moisture changes observed in the material can occur with a significant time delay after the triggering humidity peak (example: delay of about one to two months after the peak summer humidity in (Dionisi-Vici et al., 2013)). How can material parameters, which are required to calculate the long-term behavior and evaluate the preservation strategy, be reproduced using simulations and artificial aging?

In order to investigate the material parameters and validate the simulation models, sufficient monitoring data on the ambient climate, the moisture content in the different material layers, and the resulting geometric changes in the object are required. Monitoring moisture content in aged wood by using electrical resistance measurements might require specific calibration curves. Consequently, it is not clear whether the differences found by (Kozlov & Kisternaya, 2014) in recent and historic Scots pine (*Pinus sylvestris L.*) are really due to different hygroscopicity or only different electrical parameters of the wood. Subchapter 3.2.3 discusses the moisture behavior of this specific wood species further.

When experimentation or destructive measurement methods are not suitable for use on rare original samples, a common method is to experiment on dummies with somewhat similar properties. Dionisi Vici et al. (2006) use this technique to investigate the mechanical response of wooden boards to humidity changes und transfer their findings from fairly new wood panels to the treatment of historical panel paintings. However, their later publication (2013) involving dummies made from both, new and old oak wood, shows distinct differences in the results (Dionisi-Vici et al., 2013; Dionisi-Vici et al., 2006). Whether or not this type of approach could therefore be flawed by a different sorption behavior due to the aging of wood is still under discussion, cf. also Subchapter 3.2.3.

2.1.3 Methods and standards for wood moisture content in historic wooden objects

Various international standards provide guidance on how to measure the moisture content of materials using different methods, cf. Table 4, p. 13. However, these standardized methods only apply to industrially graded materials with homogenous characteristics (Camuffo & Bertolin, 2012). Samples of these materials are usually available in large quantities to ensure a sufficient statistical distribution of the test results. In the case of rare historical objects, taking samples for destructive testing is either not possible at all or if so, rarely provides enough data for statistically representative results. Camuffo (2018) reviews an array of international standards on their suitability to determine the moisture content of historical objects. It is pointed out that if wood was impregnated with oil, wax, resin, or preservatives, it might present erroneous results when tested with the common gravimetric method. These substances are volatile when being heated and will be outgassed during the oven-drying resulting in a greater mass loss than what would be caused just by the difference in water content. In this context, the differences are pointed out between *moisture content* and *water content*, as determined by either by the *gravimetric method* or the *Karl Fischer Titration method*, respectively (Camuffo, 2018; EN 16682:2017).

The standard on the *Conservation of cultural heritage – Methods of measurement of moisture content, or water content, in materials constituting immovable cultural heritage* (EN 16682:2017) specifically focuses on the details of each standardized method in regards to how they can be used on aged and deteriorated materials (Camuffo, 2018). Furthermore, this standard compares three relative methods that are suitable for selective or continuous monitoring (EN 16682:2017, table B.1); yet it does not further discuss the influence that a permanent application might have on the reliability of the results. The experiment by (Melin et al., 2016), comparing two of those methods for monitoring dynamic wood moisture gradients, yields contradictory results. Their study shows that the monitoring methods for the preservation of wood-based materials need to be more accurate and reliable.

The standard on the *Conservation of Cultural Heritage - Test methods - Determination of drying properties* (EN 16322:2013-12) describes a destructive method for comparing the drying time and intensity of various porous inorganic materials such as different types of stone, brick, and plaster in laboratory tests. Appendix B of this standard shows the schematic diagram of an experiment for measuring the dependence of the drying rate on the air velocity. Similar to this topic, see also Subchapter 3.1.3 and the experiments in (Flexeder, Nouman & Hepf, 2022) investigating the influence of different air velocities when humidifying a wooden surface.

In order to combine the preservation of wooden cultural assets with energy efficient measures, it is important to measure reliably and thus understand how changing moisture and temperature relates to moisture gradients and results in dimensional changes. Only when moisture gradients and dimensional changes under dynamic climatic conditions have been monitored and evaluated over an extended period of time, the effects of daily and seasonal changes can be reliably estimated. The challenge in this field of application is to provide non-destructive measuring and monitoring methods that allow conclusions about moisture development, especially in historical and thus very valuable materials.

2.2 Relevance of wood moisture monitoring to assess timber structures

2.2.1 Normative and technical regulations for moisture monitoring in buildings

Human error in structural design and in building construction (mostly disregarding climatic conditions) is proven to be the main cause for failing large span timber structures. Consequently, introducing guidelines and schedules for assessing the structural health might be a vital measure to prevent fatal collapses. (Dietsch & Winter, 2018)

Moisture monitoring is considered an essential part of structural health monitoring (SHM) of all timber structures, both new and existing. The new standard´s draft about the *Assessment and retrofitting of existing structures* (CEN/TS 17440:2020-10) provides general principles on possible testing and monitoring to verify the designer´s assumptions (Flexeder, Schenk & Aondio, 2022). Accordingly, a detailed assessment may include structural calculations and checks, including comparison with monitoring data (CEN/TS 17440:2020-10, 5.6.2(2). In particular, if sufficient structural reliability of cultural heritage buildings cannot be demonstrated using the models, the draft recommends additional material testing or structural monitoring. These results shall then be included in a revised structural analysis (CEN/TS 17440:2020-10, D 6.1). Thus, SHM plays an important role in verifying the safety of older timber structures, as shown for instance in (Arriaga et al., 2021) on an 18th century building in Madrid, Spain.

However, in today´s construction practice, continuous monitoring of all existing timber structures with an electronic monitoring system is not yet common, neither for old nor for new timber structures. This concerns all kinds of relevant parameters, however for timber structures, critical values of wood moisture content are considered to be a major factor for damages (Brandl, 2021; Dietsch & Winter, 2018; Mönck & Erler, 2004).

Eurocode 5 is the standard for the design and construction of buildings and civil engineering structures or timber components for load-bearing purposes. This document is currently under revision and published as a draft European standard (prEN). Part 3 is dedicated to the execution of timber structures, in particular “the minimum requirements for moisture control during transport to building site, storage on site, handling on site and execution.” (prEN 1995-3:2023, 1.1). It states that a so-called *moisture control plan* “should be prepared to ensure that damage to the structure is avoided due to the effects of changing moisture content during execution and on any subsequent drying.” (prEN 1995-3:2023, 5.3).

Although the draft for *Eurocode 5* notes that this moisture control plan is intended to monitor the moisture content of timber components and structures during construction, it does not require actual measurements of moisture content during use. Rather, the moisture content during service should be understood in advance by the planners and operators to ensure the correct climatic conditions during construction. It further states: “The effects of moisture content changes in the timber should be minimized. Before using it in construction, timber should be conditioned to the moisture content appropriate to the intended climatic conditions in the building during its utilization phase, unless the timber is able to desorb or absorb moisture without any detrimental effect on the load-carrying capacity or stiffness of the structure.” (prEN 1995-1-1:2023, 4.3.1.2)

Whilst not specifically required by these standards, moisture monitoring can be a good method for this technical assessment (Flexeder, Schenk & Aondio, 2022).

National standards and regulations provide further guidance on the general topic of moisture protection in construction. In Germany, for instance, several parts of DIN 4108-x are considered essential standards to design for climate-related moisture protection in buildings. They specify corresponding requirements, calculation methods and instructions for planning and execution, which must be provided when applying for a building permit.

The German standard for *Wood preservation* regulates the general requirements to protect installed wood and wood-based materials against degradation and/or destruction by organisms. *Part 1: General* specifies various usage classes in building construction and assigns protective measures to them (DIN 68800-1:2019-06). *Part 2: Preventive constructional measures in buildings* contains numerous rules and detailed drawings for ensuring the durability of components made of wood or wood-based materials (DIN 68800-2:2022-02). Constructive wood protection through structural measures shall always be sought first. If this cannot be implemented, for instance for architectural reasons, planers should refer to *Part 3: Preventive protection of wood with wood preservatives* (DIN 68800-3:2020-03). If timber damage has already occurred in existing structures, guidelines are defined in *Part 4: Curative treatment of wood destroying fungi and insects and refurbishment* (DIN 68800-4:2020-12).

The International Association for Science and Technology of Building Maintenance and Monuments Preservation (WTA) provides various factsheets on the topic of moisture analysis in building construction. The WTA code of practice about the *Assessment of humidity in timber constructions* (WTA 6-8:2016/D) offers simplified verification and simulation methods specifically to appraise moisture in timber constructions. This information can be particularly important for the assessment of flat roofs.

The methods to evaluate moisture content are highly dependent on the prevailing climatic conditions, the implementation of correct measurements, and their evaluation, which requires a great deal of expertise. Accordingly, the *Guidelines on the prevention, detection and remediation of mold in buildings* by the German Federal Environment Agency UBA (Umweltbundesamt) require that only “suitably trained specialists with knowledge of building physics” should carry out moisture measurements, as otherwise misinterpretations could easily occur. (Umweltbundesamt, 2017)

2.2.2 Need for moisture monitoring in a building´s life cycle

The current state of the art usually allows monitoring of timber structures only on a sample basis. Therefore, timing and location of wood moisture monitoring should be carefully selected to ensure representative and meaningful results.

A comprehensive data analysis by (Dietsch & Winter, 2018) with 230 cases of structural failure in large-span timber structures found that the most frequent one was cracking along the grain. This could be caused by tensile stresses perpendicular to the grain and/or low or frequently changing wood moisture contents. This particular finding is later complemented by Brandl (2021), a Master´s thesis supervised by the author, that compiled a total of 90 damage cases in timber structures specifically caused by changes in wood moisture content. These moisture-induced damages include impairment of stability, durability, and/or serviceability and are collected from various sources in Central Europe. Long-term increases in wood moisture were responsible for a large proportion of the documented damage. Statistically, there is an accumulation of damage due to increased wood moisture at the beginning of a component's lifespan. According to Brandl´s analysis, consistently high wood moisture levels led to damage caused by moisture penetration, decay, wood-decay fungi, discoloration, dry rot, maceration, mold growth, and deformation due to swelling. In contrast, elevated wood moisture gradients resulted in shrinkage cracking in 26 documented damage cases. (Brandl, 2021)

If the entire life cycle of a building component is considered, possible moisture gradients could already occur during production in the factory, transportation, storage on the construction site or installation, which then might manifest themselves as moisture damage after the building has been commissioned (Brandl, 2021; Dietsch & Winter, 2018; Gamper et al., 2013; Kordziel et al., 2019; Schmidt & Riggio, 2019).

Most moisture damage cases are discovered either right at the beginning, i.e. within the first five years after construction, or after a longer period of use lasting several decades (Mönck & Erler, 2004). Brandl (2021) therefore differentiated between three time-categories in the data analysis assuming a total service life of fifty years from construction start. Furthermore, a system was developed to account for the severity of the respective damage. This even increased this characteristic distribution, cf. Figure 3 (Brandl, 2021). Accordingly, shrinkage cracking within the first five years is considered the most relevant damage risk, which is consistent with the findings by (Dietsch & Winter, 2018).

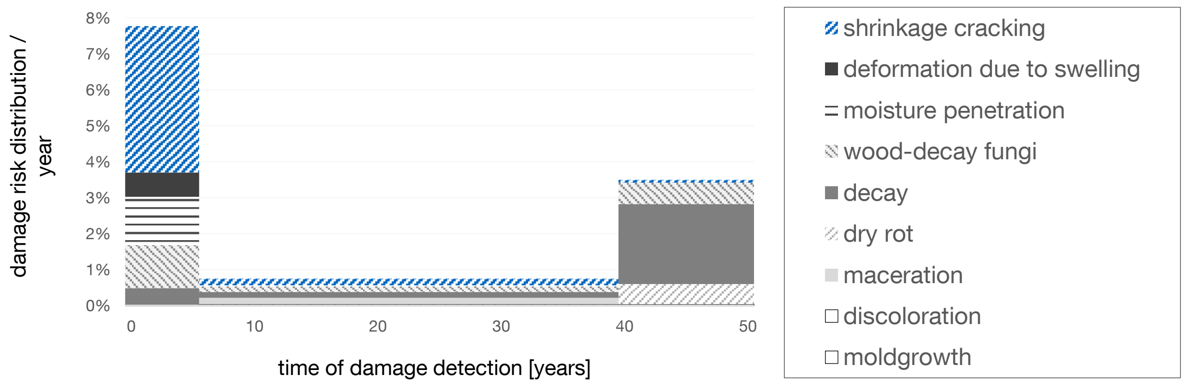

Figure 3: Distribution of documented damage cases per year, analyzed by severity and time of detection, based on the work by (Brandl, 2021)

Assessing how time influences the occurrence of moisture damage according to (Brandl, 2021) is limited in some respects:

1. The analysis shows the risk distribution only within the documented damage cases. It cannot be used to draw conclusions about the general risk of moisture issues in timber construction.

2. The time periods stated are invariably the duration until the user eventually discovered that damage has already occurred. It therefore remains uncertain when a monitoring system could have detected wood moisture at such an early stage that major structural damage could have been avoided.

3. The evaluation includes a total of 63 damage cases that had time specifications available, 20 of which occurred within the first five years, 21 in the 6th to 40th year, and another 22 well after the 40th year. This sample size (n = 63) could simply be too small to allow a general, statistically reliable, statement.

Nevertheless, the analysis provides valuable information on the time periods in which certain wood moisture defects with different severity might typically occur, hence rendering the associated risk. Albeit not specifically investigated by (Brandl, 2021), a single event affecting the overall system, such as changing the use, refurbishing, or remodeling, can cause a substantial change. Installing a heating, ventilation, and air conditioning (HVAC) system, will alter the interior ambient conditions, cf. also discussion in Subchapter 2.1.1. The consequences of such a change, which is often undertaken several decades after the initial construction, might have a very significant impact on a timber structure (Dietsch, Gamper et al., 2015).

Beyond this approach, it is not only the point in time in the life cycle that can determine whether a moisture gradient can cause damage, but also the time interval in which these different moisture levels affect the component. Considering similar amplitudes of moisture variations, Fortino et al. (2013) found that daily changes will provoke greater stresses within a timber element, than a slower variation within the course of a whole year. Accordingly, daily humidity variations are considered a major risk for surface cracking. (Fortino et al., 2013)

However, also slow but very extreme changes in interior climate, such as those that occur in buildings housing an ice rink throughout the year, can also cause critically high levels of wood moisture content in the timber structure (Brandl, 2021; Dietsch, Gamper et al., 2015; Gamper et al., 2013).

2.2.3 Recommended monitoring locations based on probability and severity of damage

In order to position the measuring points for moisture monitoring ideally, the neuralgic points of typical timber structures are analyzed. It is therefore assumed that the weakest points of a structure in terms of probability should be decisive for assessing the overall condition. In order to ascertain the sensitivity of these points, damage reports are used as an indicator of when and where critical moisture loads should have been recognized and averted earlier. It should be noted that such a damage survey usually requires a sufficiently severe case, i.e. there is always a statistical distortion compared to lighter, undocumented cases of damage. On the contrary, when regulations require routine technical inspections for components under high static loads, even minor damage to these components will be detected more frequently.

In current practice, building surveyors often use hand-held tools to detect and appraise damage or suspected cases of microbial infestation. Moisture measurements are thus carried out here on one hand, to determine the extent of damage. On the other hand, the moisture content of the material is determined in order to decide whether microorganisms could possibly grow. In order to estimate the extent of damage, sufficient knowledge of the examined building material is a fundamental prerequisite. A comprehensive analysis investigates both, the extent of the damage in the area and where it occurred in the component´s depth.

The analysis of documented cases of damage due to increased wood moisture by (Brandl, 2021) shows that most of the documented cases of damages occurred in the *roof structure*. Here, the majority of damage was caused by shrinkage cracks. These were primarily due to excessive wood moisture gradients, often caused by high temperatures and low equilibrium moisture content in combination with increased installation moisture. In addition, discoloration, wood-destroying fungi, and decay were commonly found in roof structures. Many other types of damage were found in *exterior structures*, although wood-destroying fungi dominated, followed by shrinkage and decay. Damage to *floor ceilings* was much rarer, and if it did occur, it was usually due to wood decay or dry rot. Damage to *interior walls* was rarely documented, and wood-destroying fungi were much less common. It is therefore advisable to monitor possible weak points with sensors, particularly in roof structures and on exterior main load-bearing components. In general, it has been shown that exposed timber components which are exposed to direct rain and/or sunlight are particularly at risk of developing a very high moisture gradient and thus moisture-induced stresses. (Brandl, 2021)

According to the documented cases, moisture damage in load-bearing timber roof structures are frequent. Here, deficiencies of vapor retarders and too little ventilation are a common cause for moisture accumulation from the inside, while moisture from the exterior is mostly due to precipitation and / or high relative humidity (Gullbrekken et al., 2016). The weather-related moisture risks to the building envelope can be predicted based on the location and its outside macroclimatic conditions (Morishita et al., 2020; Niklewski et al., 2021).

Models for future weather scenarios assume more heavy precipitation events in north-western Europe, meaning that protection against water from outside will have an even higher priority in the future (Bunkholt et al., 2021b). Additionally to general measures to ensure robust assemblies, electronic systems to detect very high moisture contents early on are therefore suggested to limit possible damage (Fouad, 2022). For water ingress through internal pipe leaks as in the examples discussed in (Ott & Aondio, 2020), systems for the detection of liquid water or of pipe pressure loss could possibly also be useful.

On the low end of the hygroscopic spectrum, moisture-induced stresses can have a significant impact on the service life of timber buildings, especially long-span structures in changing climates. Dietsch et al. (2015) conducted a monitoring study on 21 large timber halls (glue-laminated beams from softwood) with various uses and thus varying interior conditions. They suggest to add information about the expected range of interior climatic conditions to the standardized Service Class in order to precondition new timber elements to an equivalent moisture content that is similar to what is to be expected in a later stage after the structure has been built. This should help to reduce large and inhomogeneous moisture gradients and thus reduce the risk of cracking shortly after commission. In their monitoring study they used the electrical resistance method with rammed-in electrodes at different depths, but noticed deviations, especially at lower moisture contents. (Dietsch, Gamper et al., 2015)

In addition to the typology of a wide-span hall with a (partial) thermal envelope, glue-laminated beams are meanwhile also used for bridges (Fortino et al., 2013; Uwizeyimana et al., 2020). Since particularly they are exposed to changing climates, though, timber bridges need to be inspected regularly, possibly including permanent wood moisture monitoring as in (Björngrim et al., 2016; Fortino et al., 2013; B. Franke et al., 2016; B. Franke et al., 2013; Ghazi Wakili et al., 2024; Kasal, 2013; Koch et al., 2016; Mahnert & Hundhausen, 2018; Schiere et al., 2021b; Tannert et al., 2011; Vašková et al., 2016; Wacker et al., 2007). Then combining this monitoring data with numerical results from FEM-modelling allows for early prediction of critical moisture contents. Taking action as early as possible can help to prevent degradation, deformations, and cracking and will therefore reduce the overall costs for maintenance (Fortino et al., 2021).

Once the specific component to be monitored has been selected, the positioning within the object also has a measurable influence on the measurement result. Especially areas that are ventilated well tend to change their conditions more quickly (cf. Subchapter 3.1.3) and are thus also more prone to shrinkage cracking (Niemz, 2022). Ideally, several identical sensors should be distributed in a grid-like pattern over the component (Straube et al., 2002). In order to enable a consistent comparison of the measurement data with results from simulations, the sensors should not be exposed to direct irradiation nor rain (Fortino et al., 2013), even though those might be the locations with the highest risks for cracking and decay.

The challenge in this area of application is to develop a monitoring system that provides reliable information about the entire building at low cost and over the long term, with measurements that should at least be low-destructive and easily accessible, yet barely perceptible to the user. Most relevant damage scenarios are related to longer-term elevated moisture content values, cf. analysis in Subchapter 2.2.2. But since shrinkage cracking within the first years after erection is a major risk, the system will also need to detect decreased *MC* values (<< 12 m.-%) and daily fluctuations.

2.3 Significance for future developments in modern timber engineering

2.3.1 Standardized requirements for moisture control of new technologies and trends

Continuous monitoring of wood moisture can be necessary, especially when new and therefore not yet tested timber construction products are used (Lanata, 2015). The results of this work should aid others with these monitoring measures and thus contribute to the further development of efficient and innovative wood-based materials.

Depending on their respective *inspection level* (IL), the draft for the forthcoming *Eurocode 5* requires the creation and updating of the moisture control plan for a specific structure or part of the structure (prEN 1995-3:2023, 5.3 (1). The inspection level shall in turn be "selected based on the consequence class (CC, where relevant), the complexity of the work and the degree of new technology." (prEN 1995-3:2023, 4.1 (1). The draft for *Eurocode 5* does not explicitly require continuous moisture monitoring, cf. Subchapter 2.2.1. However, such measures could be a very valuable tool, especially when new technologies are being tested for the first time in installed conditions.

If a new timber product´s behavior under moisture fluctuations has not been sufficiently researched and tested in practice yet, moisture monitoring in different depths of an installed building component should give early warnings if critical moisture gradients occur within. Consequently, systematic damage to the structure might be prevented by timely intervention, for example by adjusting the building's climate control or ventilation. Furthermore, the in-situ data can be used to gain a better understanding of the new product´s behavior to further develop numerical models. For instance, current research is focused on refining simulation models to account for glue joints, material inhomogeneities from natural variation, and long-term phenomena such as creep in the simulation of wood structures in the future.

The challenge in this field of application is to offer methods for moisture monitoring for materials or products that have scarcely been investigated to date and for which, accordingly, no characteristic curves are yet available.

Based on current developments, various trends are identified for which solutions are sought in the context of this work. These include:

- Trend of multi-layered glued timber slabs or beams
- Trend of using wood species that have not yet been used in timber engineering
- Trend of using timber engineering in hot and humid climates

To identify typical measurement tasks, a selection of new developments with their respective climate conditions in testing is presented in the following chapters. This selection shall be regarded as exemplary and not exhaustive.

2.3.2 Moisture analysis to support the further improvement of glulam beams

Glulam beams consist of at least three layers of boards glued together, which are traditionally from softwood and with the fibers of each layer aligned in parallel to each other. Some ideas to optimize this construction method use reinforcements at openings, hardwoods, or middle layers with a rotated grain direction, as for instance suggested by (Danzer et al., 2022; Lechner, 2021). Established softwood species such as spruce are combined with other hardwood species such as beech, or with novel cellulose-based composites. These individual materials exhibit different behavior when exposed to moisture fluctuations. Thus, a great concern is about single layers swelling and shrinking in a different pace and hence creating internal stresses when the surrounding climate changes. In case of extensive sorption and thus differently changing geometry of different layers, stress cracks could occur and eventually lead to failure.

In general, drying stresses in a wooden cross-section can cause cracks because differently moist areas in the wood are inhibited from mutual shrinkage. The steep moisture gradients, which form on the board´s surface when drying begins, are very important for the stress development in the further course of time (Welling, 1987). Particularly direct irradiation can cause tensile stress near the surface due to the steep moisture gradient of the wood, resulting in cracking and delamination of the component. If this results in the surface film or even a protective layer of paint getting damaged, water absorption will be unimpeded and fungal attack is all the more likely. (Meierhofer et al., 1982)

Zhou et al. (2010) were modelling the hygrothermal stress in glulam beams and found that usual service conditions can already provide variations of relative humidity *RH* and temperature *T* large enough to lead to cracking and eventually failure of glulam beams. In addition, Angst-Nicollier (2012) showed with experiments that the moisture-induced stresses in glulam were greater during wetting than during drying. However, these results were obtained using the slicing method and there was no non-destructive monitoring of moisture content. (Angst-Nicollier, 2012; Zhou et al., 2010)

For the long-term laboratory testing of more complex glulam products with integrated reinforcing elements, Danzer et al. (2022) also use slicing as a control method for continuous wood moisture monitoring with the electrical resistance method. With the slicing method, the test pieces are completely sawn apart and the moisture content is determined using oven-drying. This method is therefore classified as destructive. For electrical resistance measurements, electrodes are rammed into the element at selected points only. It is therefore considered non-destructive (or low-destructive), as the element can continue to be used after the measurements. Even if both methods, destructive and non-destructive, at least provide results with similar tendencies in the work by Danzer et al., they no longer consider the results from the monitoring to be useful for the evaluation of the tests due to increasing inaccuracies. Consequently, there is a great need for reliable non-destructive methods for moisture determination for such investigations into the effects of stresses due to moisture gradients in complex modern timber engineered products. (Danzer et al., 2022)

For these application examples, a monitoring system would be required that can reliably track hourly local wood moisture changes in different layer depths of the glulam beam in the whole hygroscopic range of around 6 m.-% – 21 m.-% with moderate temperature fluctuations of $\Delta T \approx 10$ K over a period of several months:

- The modelling study by (Zhou et al., 2010) applies daily fluctuations of ambient climate (15 °C – 25 °C) that would cause moisture gradients of 11 m.-% – 13 m.-% within the course of several hours (24 h period).
- The lab experiments by (Danzer et al., 2022) are done in a range of 25 %RH – 60 %RH, 21 °C – 26 °C and 6 m.-% – 13 m.-% within the course of 14 months in glulam made from Norway spruce.
- The lab experiments on smaller scale specimens by (Lechner, 2021) are done in a range of 35 %RH – 70 %RH, 20 °C – 26 °C and 8 m.-% – 21 m.-% with a gradual decrease of humidity in the course of 12 months in glulam made from Norway spruce and beech.

In order to help with similar research tasks, a more reliant monitoring system should be able to track moisture contents in popular soft- and hardwoods as well as glued laminates of such. The measurement range should at least cover a range of moisture contents equivalent to the ambient climate possibly occurring in the life span of such element.

2.3.3 Moisture analysis to investigate internal stresses in cross-laminated timber

In parallel to the investigations on beam-shaped wood-based materials, work is being carried out on the further development of plane wood-based materials, which are usually glued crosswise and thus called *cross-laminated timber* (CLT). Gereke (2009), for instance, carried out extensive investigations on moisture-induced stresses in cross-laminated wood panels by means of sorption tests, cup measurements, and finite element simulations. Yet, non-destructive monitoring of wood moisture contents was completely omitted in this work. Moreover, the method of first splitting the specimens, then weighing, and oven-drying, might have added systemic errors. (Gereke, 2009)

Repeated wetting and drying cycles might not necessarily only have negative effects on the structural system. Bora et al. (2022) even report a slight increase in peak strength after simulating raining-on and re-drying angle bracket connections from CLT panels in a lab environment. However, the observed improved load-carrying capacity of these nailed wall-to-floor brackets could be because the specimens in the lab might have even dried further down than the control samples. Consequently, there might be a need for more research on this topic. (Bora et al., 2022)

Fernando et al. (2015) describe the instrumentation of a new building with an array of sensors to monitor moisture content and its effect on changes in post-tension forces. They investigate columns made of ash wood, timber-concrete hybrid floor systems using beech laminated veneer lumber (LVL) as well as beech cross-laminated timber (CLT) plates. Furthermore, another monitoring study over the course of three years by Larsson et al. (2022) shows a distinct correlation between the natural frequency [Hz] and the moisture content *MC* [m.-%] in a CLT slab. (Fernando et al., 2015; Larsson et al., 2022)

Apart from the homogeneous layered structures, numerous research projects investigate the idea of modifying individual layers in CLT. In addition to the use of pure solid wood structures, CLT is often used in combination with in-situ concrete with various ways of connecting these two materials.

In addition, there are approaches to optimize the individual layers of CLT based on their mechanical properties. Similar to Lechner's approaches for beams, a mixture of softwoods and hardwoods could also optimize the load-bearing capacity of planar components. Bienert & Schumacher are developing approaches for so-called disintegrated hybrid CLT. Here, the individual middle layers are not only constructed from beech, but are also optimized in terms of material consumption and installed with gaps accordingly. (Bienert et al., 2023; Lechner, 2021)

Other approaches redesign individual layers with gaps forming air ducts for additional purposes such as temperature regulation. Mindrup (2020) developed and tested a prototype of a thermally activated CLT element for changes in wood moisture content after repeated heating and subsequent cool-down. This idea of using certain layers of CLT for room temperature control was investigated further in the research project *PHYTAB*. (Flexeder, Schumacher et al., 2022; Mindrup, 2020)

For these application examples, a monitoring system would be required that can reliably track local wood moisture changes in different layer depths of the CLT in the whole hygroscopic range with high temperature fluctuations of $\Delta T > 40$ K over a period of several months:

- The main lab experiments by (Gereke, 2009) are done in a range of 45 %RH – 85 %RH, 20 °C – 20.5 °C, 10 m.-% - 16 m.-% within the course of 1.5 months. In this work, the influence of temperature of the material parameters is neglected because the influence of moisture content would have “a ten times greater effect on wood dimensions than a 1 K change in the temperature” ((Gereke, 2009), p.6, based on (Niemz, 2021)). Considering that CLT may be used as exterior walls, where great temperature variances can occur, similar investigations should be extended to the influences of temperature gradients as well.
- The lab experiments by (Bora et al., 2022) are done in a range of 7 m.-% – 27 m.-% on CLT made from different softwoods (Douglas fir, Southern pine, Norway spruce) in 24 h intervals.
- The weekly taken on-site measurements by (Fernando et al., 2015) show results of 6 m.-% – 20 m.-% in the timber frames and 6 m.-% -11 m.-% in the beech CLT plates.
- The monitoring study by (Larsson et al., 2022) measured values in the range of 45 %RH – 70 %RH, 20 °C – 25 °C, which were calculated to moisture contents of 7 m.-% – 14 m.-% of the CLT slab.
- The lab experiments by (Mindrup, 2020) are done in a range of 16 – 60 °C with resulting values of *EMC* computed at 3 m.-% – 10 m.-%. It should be noted that since the electrical resistance method used might have not been calibrated for temperatures that high, these supposedly very low *EMC* values might be misleading.

2.3.4 Moisture analysis for mold and rot prevention in cross-laminated timber assemblies

In order to use cross-laminated timber (CLT) in the outer shell, it must also be ensured that the drying behavior is sufficient to prevent decay after wetting. Compared to other mineral building materials, wood is highly hygroscopic. It is therefore said to have an advantageously high buffer capacity for fluctuations in relative humidity, which can have a positive effect on mold prevention (Künzel et al., 2004). However, if the moisture content of the building components is too high over a longer period of time, this can be very detrimental to the structural safety of the construction.

McClung et al. (2014) carried out outdoor experiments on various façade structures with CLT made from different types of softwood. *RH/T* measurements and electrical resistance measurements were used to validate their simulation results. They present their results of the wood moisture measurements using the electrical resistance method at various depths only in a very simplified form compared to other measured variables. Furthermore, they note discrepancies between simulation and measurement results. In a similar approach, Kukk et al. (2022) investigated the impact of different initial moisture contents at installation of highly insulated wall assemblies in cold climates with regards to possible mold growth, a risk mainly associated with the thermal gradient in exterior walls. To assess the threat of mold growth, they rely on *RH/T* measurements and use electrical resistance measurements only at the start of their experiments and in the surface layer of the panels. The potential wetting of CLT panels due to rain fall at erection is of special concern, especially water intake at end of grain. (Kalbe et al., 2022; Kukk et al., 2022; McClung et al., 2014)

Hygrothermal simulations, e.g. with products from the WUFI software family, can be used to compare the energy efficiency and serviceability of different wall structures under varying climatic influences. The functionality of such software has already been proven in principle by benchmark tests as described in the standard for *Hygrothermal performance of building components and building elements - Assessment of moisture transfer by numerical simulation* (EN 15026:2023). The numerical method used by WUFI fulfills the general requirements of various currents standards and regulations for the calculation of thermal and moisture protection (Stöckl, 2023). However, these calculations simplify the actual physical behavior to a few mathematical equations and can therefore represent reality only to a limited extent. As calculating of the moisture buffering effect necessitates HAM-models (heat, air, and moisture transport), those models can only be used if they are adequately verified. Verification must be performed at both, the material level as well as at the assembly level, to allow calculation of air and moisture transport under field conditions. Simulation studies utilize theses individual lab results for statements about the hygrothermal behavior of cross-laminated timber walls. However, most in-situ measurement campaigns rather use the resulting values measured somewhere in the ambient indoor air.

There is hardly any measurement-based validation of these statements through real hygrothermal monitoring of the actual timber components. Refined statements about the actual hygrothermal effects of individual assemblies require in-situ monitoring for further validation. Various investigation concepts compare simulation and reality by measurements of relative humidity *RH* and temperature *T* in indoor and outdoor spaces, as for instance in (Kang et al., 2024) or (Künzel et al., 2004). These studies focus on the interior user comfort and compare different structures, such as mass timber with mineral building materials. Consequently, they attribute the differences which they observe between individual indoor air measurement results to the hygrothermal properties of the respective component structures - without, however, even verifying the physical phenomena using measurement technology within the building component itself or on its immediate surface layers. Thus, a comparison of the simulated mechanisms within the respective wall assemblies does not take place due to a lack of measured values. Experimental laboratory measurements have already partially closed this knowledge gap. Measurements with a double climate chamber, which is an environmental test chamber with two adjacent compartments, show the influence of different insulation materials on the values of relative humidity and temperature. These are measured, for instance in (Yoo et al., 2021) at the transition between the CLT surface and the external insulation. Based on that, they recommend certain wall assemblies for avoiding the risk of mold on the CLT surface. They do not investigate the moisture gradient within the CLT element though.

Despite the well-known theories about hygroscopic buffering materials (cf. summary in Subchapter 3.1.3), the in-situ measurement campaign in a used dwelling by (Hameury & Lundström, 2004) could not evidently prove, whether larger areas of exposed massive wood are damping daily fluctuations in relative humidity. Their measurement concept includes relative humidity measurements indoor and outdoor, electrical resistance measurements in the mass timber walls, and numerous temperature measurements. It is possible that the buffer effects were present, but were masked by other effects such as user influence. In this case, methods with more precise measurements on the solid wood surface might possibly have provided further insights. For these application examples, a monitoring system would be required that can reliably track local wood moisture changes in different layer depths of the CLT in the hygroscopic range and even above the fiber saturation point as well with high temperature fluctuations of $\Delta T > 35$ K over a period of several months:

- The in-situ measurement campaign by (Hameury & Lundström, 2004) estimated values in a range of 8 m.-% – 11 m.-% in mass timber.
- The experiments in an outdoor lab setting by (McClung et al., 2014) are done in a range of 20 %RH – 100 %RH, 5 °C – 40 °C and 10 m.-% – 37 m.-% over the course of twelve months in CLT from different softwoods.
- The measurements in an outdoor lab setting by (Kukk et al., 2022) between the CLT and the insulation show values in a range of 15 %RH – 100 %RH, 15 °C – 28 °C over the course of twelve months.
- The on-site measurements by (Kalbe et al., 2022) reveal results estimated in the range of 10 m.-% – 45 m.-% in CLT made from Norway spruce.

The projects presented are mostly related to cold and humid northern European climates. The derivation of typical indoor climates from outdoor climates (weather data) is only possible with sufficient knowledge of the influencing parameters (Kornadt et al., 2010). This means that further research is needed to validate the safe use of CLT in warm and humid or hot climates, with also different challenges such as protection against stormwater (Strang, 2023).

2.4 Importance of wood moisture content in hygrothermal building physics

2.4.1 Estimation of temperature influence on electrical resistance measurements

Another area of application for wood moisture monitoring focuses on the mutually dependent phenomena of moisture and temperature gradients, specifically in building physics in timber construction with a low moisture content (significantly below fiber saturation). Wood moisture measurements are influenced by temperature gradients in several ways. Since the exact correlations will be investigated further in the following chapters, only the general tendencies are briefly described within this subchapter.

The higher the temperature *T*, with otherwise the same absolute amount of water available in the air (*AH* = const.), the lower relative humidity of air *RH* and also the moisture content *MC* in the wood. The higher *T*, with the relative humidity of air kept the same (*RH* = const.), the higher the absolute humidity *AH*, but with a lowered *MC* in the wood. Furthermore, if the common electrical resistance method (ERM) is used for measurements, the following applies: the higher the temperature, the lower the electrical resistance with otherwise identical wood moisture content.

Three examples shall illustrate the relevance of these influencing factors in theory. To simplify this case, the anisotropy is initially neglected and a plane is assumed that is infinite in two directions. A piece of spruce wood is equipped with a pair of electrodes and preconditioned at 10 °C and 50 %RH, resulting in an absolute air humidity of *AH* = 4.7 g/m³ (Figure 4). Assuming the correlations known from the *Keylwerth-diagram* (shown in Figure 13, p. 52), this would result in *EMC* ≈ 9 – 10 m.-%; or possibly slightly higher values of *EMC* ≈ 12 m.-%, when consulting sorption isotherms for Norway spruce.

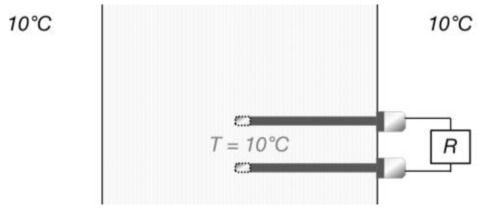

Figure 4: Start at 10 °C, 50 %RH, AH = 4.7 g/m³

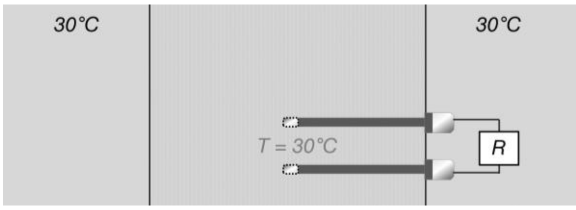

Figure 5: Thoroughly heated test specimen at 30 °C

In the first example, the relative air humidity stays constant at 50 %RH, but the setup is evenly heated by 20 K, from 10 °C to 30 °C (Figure 5) with the absolute humidity in air rising to 15.2 g/m³. In wood, the heat transport happens considerably faster than the moisture transport. Thus, as soon as the wood sample is heated up to 30 °C, the measured electrical resistance value is estimated to drop by approximately 90 %. If the evaluation unit did not take this temperature influence into account, a wood moisture value based on this reduced electrical resistance value would be incorrectly output. Because of this sudden temperature difference of 20 K, the resulting equivalent wood moisture content would then be displayed approximately too high by a difference of *ΔEMC* ≈ 1 - 2 m.-% (cf. Figure 15, p. 58).

As soon as also the moisture transport is completed, the piece of wood will have dried out to a lower moisture content. Depending on the conversion, this new value is approximately

$EMC \approx 8 – 9$ m.-% according to the *Keylwerth-diagram,* and $EMC \approx 9 – 10$ m.-% according to (Weichert, 1963b). This new value does have a higher electrical resistance, however, measured by ERM without temperature compensation, would be erroneously displayed as a too high value of $EMC \approx 11$ m.-%, depending on the used calibration curve. Accordingly, temperature dependence must be considered when measuring electrical resistances, as otherwise wood moisture values will be estimated too high at higher temperatures and too low at lower temperatures. Hence, generic equations for temperature compensation are already widely used and considered state of the art, cf. Subchapter 4.3.3. The application of specific equations for different wood products has not yet been established and will be dealt with in parts of this thesis. Furthermore, changes in moisture content lead to changes in geometry, which will in turn effect the contact pressure between electrode and wood and thus the measured electrical resistance, which will also be investigated.

In the second example, the absolute air humidity stays the same at 4.7 g/m³, the setup is evenly heated by 20 K, from 10 °C to 30 °C, and thus the relative air humidity will drop to 15.5 %RH in Figure 5. In this case, the drying process will be more pronounced. If there is no temperature compensation in the ERM, the sudden rise in temperature will also lead to a value that is erroneously displayed too high as in the first case. Once the drying process in the wood is finished, it will have an actual wood moisture content of $EMC \approx 3 – 5$ m.-% at 30 °C, depending on the reference and the wood species. This corresponds to a very high value of electrical resistance ($R >> 10^{12}$ Ω), which some meters are not even able to detect anymore, therefore already rendering the need to possibly employ another method all together.

In the third example, the same setup is consistently heated by 20 K, but only from one side. The temperature gradient results in a heat flow from the warmer to the colder side. Water vapor will diffuse from the higher level through the element to the lower level of water vapor partial pressure, thus in this case the same direction, cf. Figure 6. If the measuring electrodes are made of metal and therefore greater heat conductors than the surrounding wood, the temperature level in the measurement location might deviate significantly from the rest at this depth. Scilicet, the electrodes acting as thermal bridges might possibly further distort the vital temperature compensation.

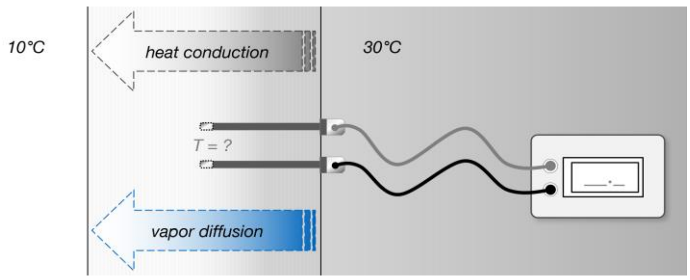

Figure 6: Scheme of temperature gradient and water vapor gradient

Notabene: Unlike in this example, liquid water transport (surface diffusion and capillary conduction) might also take place depending on the relative humidity *RH* of air and even override the main direction of moisture transport as described in (Künzel, 1994). Furthermore, enthalpy effects occur during desorption, which in turn lead to cooling of the material. Accordingly, there are several effects of moisture transport when measuring under real conditions, such as on exterior timber walls.

2.4.2 Concerns about using the electrical resistance method at high temperatures

Since controlling moisture gradients is very important for kiln-drying of sawn timber, Welling (1987) developed a simple simulation program to model the relationships between wood moisture content and resulting drying stresses. In order to validate the predicted moisture distribution within the board profile, smaller spruce specimens in which electrodes had already been driven in before the start of the test are used. The resulting profile measurement by means of electrical resistance measurement always showed a wood moisture content about 3 m.-% lower than the moisture content determined by means of oven-drying. Trübswetter (2009) too, questions the reliability and accuracy of electrical resistance measurement for wood moisture determination in the context of technical drying of sawn timber. Furthermore, it is stated that specifically the wood moisture distribution in the drying kiln would often not be statistically reliable due to insufficient number of measuring points (Trübswetter, 2009, p.59; Welling, 1987).

Welling (1987) already identified the following possible causes for the discrepancies between electrical resistance measurements and the results from the oven-dried specimens:

1. Inaccuracies or drift of the circuit board
2. Deviation of the instrument-internal characteristic curve from the actual resistance characteristic curve of the wood
3. Inaccurate positioning of the electrodes in the cross-section for determining the wood moisture content in the respective profile

According to the findings on the importance of contact pressure in electrical resistance measurements (Christ, 2020), this list could be extended by another possible source of error:

4. Looser fitting electrodes, which could result from the geometry changes of the wood (shrinking) following the rapid reduction in moisture content, leading to an increased electrical resistance R_T at the contact between electrode and wood.

Measuring the electrical resistance with loosened electrodes might lead to higher overall resistance values and thus erroneous results causing the moisture content to appear even lower than it actually is (Dai & Ahmet, 2001; Fredriksson, 2013; Skaar, 1988). Additionally, depending on their material, great temperature variations might also influence the geometry of the electrodes themselves. According to (Welling, 1987), the electrodes were driven in some time before the start of the experiment and then repeatedly used for measurements. However, it is not further specified whether the electrodes could have loosened in the course of the experiment, which might have been a worthwhile investigation step.

2.4.3 Challenges in monitoring wood moisture content under strong temperature gradients

The variety of effects previously discussed in theory makes it challenging to observe the moisture content in mass timber, such as in a real monitoring project with exterior walls made of 234 mm thick cross-laminated timber, cf. Figure 7. The *Timberbrain*, a novel office building, was equipped with numerous sensors for research purposes. Although some measurement tasks were carried out successfully, the electrical resistance measurement still showed ambiguous results. (Flexeder, 2021; Flexeder et al., 2021)

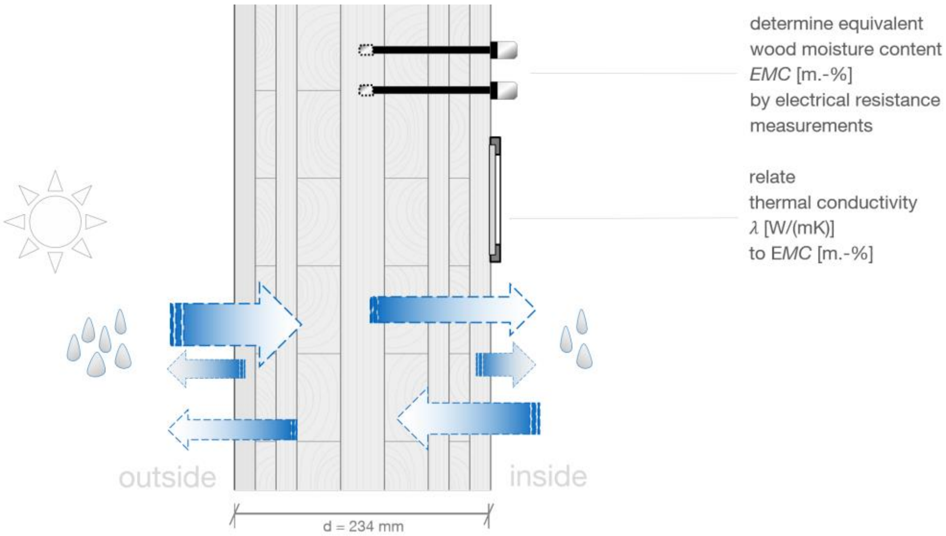

Figure 7: Scheme of various moisture transport phenomena that typically occur in an exterior cross-laminated timber wall, shown with equipment intended for long-term electrical resistance measurements. For the monitoring campaign in the office building Timberbrain, see also Subchapters 2.4.4, 4.7.4, 6.3.1, 6.3.2, and 6.3.3.

When the measured resistance values in the component cross-section are evaluated according to the established electrical resistance method (ERM), the results reveal large scattering with increasing temperature spread. Figure 8 was printed in the original research report and indicated that the values for equilibrium moisture content *EMC* [m.-%], which are derived using the conventional conversion methods on the west-facing wall, would fluctuate by up to 8 m.-% daily. These measurement results appear unrealistic and do not allow a clear statement about the actual moisture behavior of the wall. (Bodemer et al., 2021; Flexeder, 2021)

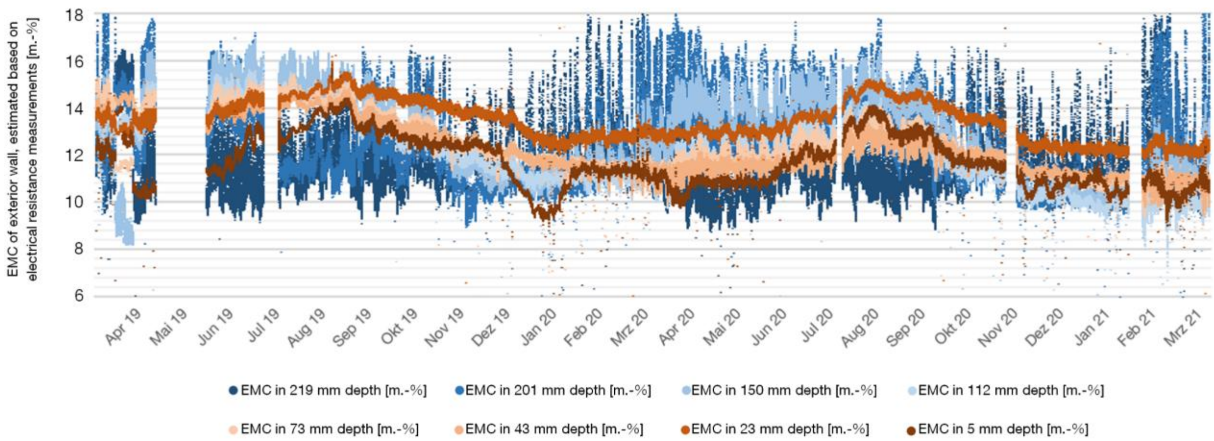

Figure 8: Original results from the Timberbrain, west-facing exterior CLT wall, as printed in (Bodemer et al., 2021).

2.4.4 Transient in-situ thermal conductivity measurements as an application case

Refining the methods for moisture monitoring to such an extent that sufficiently reliable results can be measured in the hygroscopic state even under a great influence of changing temperatures is particularly important when investigating the moisture-dependent heat conduction in exterior walls.

The thermal insulation performance of hygroscopic materials depends not only on material parameters such as the dry bulk density, but also on climatic parameters such as the material´s moisture content, temperature and air flow close to the surface. Accordingly, laboratory results measured on solid wood specimens show that a lower wood moisture content *MC* also means a lower thermal conductivity λ [W/(m·K)] and thus a better insulation capacity, cf. Subchapter 3.1.1.

In-situ, the thermal insulation effect of a solid wood exterior wall made of cross-laminated timber (CLT) is not a steady-state value, but varies with the ambient climate (Thorsell & Bomberg, 2008, 2011). However, current standards suggest to use single physical parameters for the hygrothermal design of exterior wooden envelopes such as CLT walls. These values originate from simplified empirical laboratory experiments and often do not represent the actual transient behavior. For instance, the ISO standard for *Building materials and products - Hygrothermal properties* tabulates design thermal values of λ_{450} = 0.12 W/(m·K) to λ_{500} = 0.13 W/(m·K) for the thermal conductivity of timber and plywood by gross density (EN ISO 10456:2007 + Cor. 1:2009) at an ambient climate of 20 °C/65 %RH.

Although initial indications can be derived from standardized laboratory tests, these values cannot be transferred to the assessment of CLT without restrictions. CLT could significantly underperform these standard values due to increased homogeneity (different orientation of growth rings, compensation of defects) and dynamic hygroscopic behavior, including latent heat effects (Liu et al., 2017; Niemz & Sonderegger, 2011). The increased homogeneity of CLT in contrast to solid wood could mean that using the values specified values for solid wood might be misleading.

Moreover, the individual CLT layers are connected by continuous adhesive bonds, which usually present a water vapor diffusion resistance many times higher than that of pure softwood. Accordingly, this results in a different moisture profile in the cross-section than what would be the case with just solid wood. As a consequence, other values of thermal conductivity adapted to the wood moisture content as well as enthalpy effects are to be expected. Also, due to this increased vapor diffusion resistance of these glue layers, heat transport by water vapor diffusion and onward conduction in the lateral direction through the component is expected to be limited.

For an airtight exterior CLT wall, it is sufficient when only the outer layers consist of boards that are also tightly glued at their narrow sides (Kukk et al., 2021). Thus, CLT walls may have smaller gaps and air pockets in their inner layers due to the production process. In some mass timber products, the principle is also deliberately used for better thermal insulation as shown in the lab experiments by (Joščák, 2013; Niemz & Sonderegger, 2011). Consequently, the built dwelling project *Einfach Bauen* features CLT walls with milled vertical air channels

(2x18 mm) in the middle layer (Flexeder et al., 2021; L. Franke et al., 2024; Jarmer et al., 2021). If these air pockets and the temperature differences are small enough, they can contribute to a further reduced value of thermal conductivity (Niemz & Sonderegger, 2011). However, larger temperature differences (laterally inside-outside, as well as vertically top-bottom) can also result in convection within. Depending on geometry and flow resistance (Rayleigh number), this can lead to a convection roll with greatly increased heat transport (Engelhardt, 2017).

Overall, these differences mean that the insulating capacity of CLT walls might be underestimated if they were simply equated with that of solid wood. Joščák et al. (2011) suggests that stated values for the thermal conductivity of cross laminated timber might be too high by up to 20 - 30 %. It is shown that the material properties required for designing and dimensioning structures reveal certain inconsistencies with those previously given in literature or standards, often from very old sources. Especially in winter, the wood moisture content of a timber wall is claimed to often decrease, which would lead to a lower thermal conductivity of the wood. Thus, the reduced wood moisture content in winter could lead to a reduced thermal conductivity of the wood. The insulating effect of cross laminated timber would therefore be significantly underestimated in the cold season, which is decisive for the dimensioning of thermal performance. In a calculation using steady-state values, the transient moisture distribution within a structure cannot be represented and the potential of wood as a hygroscopic material therefore not exploited. Comparative tests of wall constructions made of new materials and constructions under uniform (comparable) conditions were still lacking. The behavior of the components under practical conditions could therefore only be inadequately estimated. (Joščák et al., 2011)

A brief article by (Griesebner & Egle, 2016) summarizes the findings of the research project *Salzburger Holzbau 2020+*, conducted in Austria, and recommends using a greatly reduced new value of λ = 0.092 W/(m·K) for 3-layered CLT walls. Their laboratory measurements are based on a study that showed buildings with an average moisture content 7.6 m.-% in their exterior walls in winter, unfortunately without further describing their methods or the sampling locations for these measurements. Subsequently, they performed heat flux measurements on CLT specimens that where preconditioned to this *MC* value in the lab. Hence, the actual heat flow density was not determined in-situ.

The aforementioned monitoring project *Timberbrain* also investigated transient thermal conductivity. Even though moisture monitoring using the electrical resistance method (ERM) has not yet generated any reliable results in this respect (Subchapter 2.4.3), the long-term in-situ results from the mere thermal heat flux measurements provide a conclusive statistical evaluation. More details on this topic are given in (Flexeder et al., 2021). The thermal conductivity in this project was determined at around λ = 0.11 W/(m·K) over a period of twelve months shortly after construction and thus also significantly below the normative value. However, the extent to which this result can be attributed to the hygric behavior of the CLT wall remained unanswered, as the measurement method used for this form of application has not yet been sufficiently researched.

3 STATE OF THE ART IN THE DESCRIPTION OF WOOD MOISTURE GRADIENTS

3.1 Hygroscopicity in the context of building physics

3.1.1 Dependence of thermal conductivity on wood moisture content

The thermal conductivity λ [W/(m·K)] of wood is a material parameter that depends on a number of physical factors, and thus can fluctuate under in-situ conditions. It increases with density ρ [kg/m³], moisture content *MC* [m.-%], temperature *T* [°C], and extractive content (Forest Products Laboratory, 2021). In order to facilitate a consistent evaluation of the thermal insulating characteristics of a timber component, it is typically represented as a single fixed value in technical documentation, such as data sheets and guidelines.

Depending on the thermal resistance (expected approximately) and the thickness of the test specimen, different standards are used for the steady-state measurement of thermal conductivity. The European standards for *Thermal performance of building materials and products*, (EN 12667:2001) and (EN 12939:2000), describe the determination of thermal resistance for products of high and medium thermal resistance by means of guarded hot plate and heat flow meter methods. The international code for *Building materials and products – Hygrothermal properties* – (EN ISO 10456:2007 + Cor. 1:2009) specifies the thermal conductivity λ [W/(m·K)] of wood based on its average density ρ [kg/m³]. Consequently, it sets λ_{450} = 0.12 W/(m·K) and λ_{500} = 0.13 W/(m·K) as design values for an average density of ρ = 450 kg/m³ and ρ = 500 kg/m³, respectively. The standard lists these values for an equivalent density at an ambient climate of 20 °C/65 %RH.

The relationship of thermal conductivity and density of wood is a well-known phenomenon with first publications about it dating back to (Rowley, 1933) and (Kollmann, 1934). The empirical linear equation, which Kollmann later derived on the basis of extensive statistical data, can be described by equation (3.1) for a wood moisture content of *MC* = 12 m.-% and perpendicular to the wood fiber (Kollmann, 1951; Niemz, 2021).

$$\lambda_{12}\,(\rho_{12}) = 0.026 + (0.000195\ \cdot \rho_{12}) \tag{3.1}$$

With

λ_{12}	Thermal conductivity at *MC* = 12 m.-%	[W/(m·K)]
ρ_{12}	Density of wood at *MC* = 12 m.-%	[kg/m³]

As indicated in Subchapter 2.4.4, there is possibly a need to re-evaluate the thermal conductivity of cross-laminated timber used in exterior walls. Not only the density ρ, but also the moisture content *MC* shows a significant influence on thermal conductivity. Since the thermal conductivity λ increases with moisture content *MC* of wood, an overestimation of *MC* will lead to an underestimation of the insulation capacity of that wall. According to (Kollmann, 1951, p. 512)the influence of moisture content on thermal conductivity can be approximated with the linear equation (3.2).

$$\lambda_2 = \lambda_1 \cdot (1 - (0.0125 \cdot (MC_1 - MC_2))) \quad (3.2)$$

With

$\lambda_{MC\,1}$	Thermal conductivity at MC_1	[W/(m·K)]
$\lambda_{MC\,2}$	Thermal conductivity at MC_2	[W/(m·K)]
MC	Moisture content	[m.-%]

A literature overview based on equations (3.1) and (3.2) in (Flexeder et al., 2021) summarizes the range of different published values, cf. illustration in Figure 9.

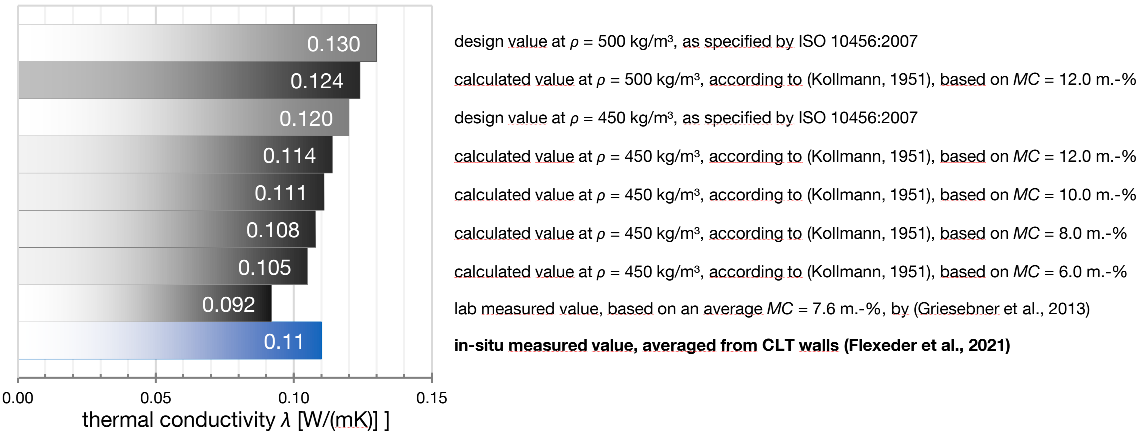

Figure 9: Comparison of values for thermal conductivity λ [W/(m·K)] from different sources

In addition, the measured thermal conductivity also depends on other influencing variables such as the wood species, the extractive content, the annual ring width, the fiber direction (angle), and the measuring temperature (Forest Products Laboratory, 2021; Sonderegger et al., 2011; Vololonirina et al., 2014). The latter in particular can represent a significant difference between in-situ measurements and standardized laboratory measurements.

(Vololonirina et al., 2014) conducted experiments about the influence of moisture content and temperature on the thermal conductivity of spruce and combine their findings into one linear equation. They distinguish between wood with narrow rings and wide rings as well as between the different fiber directions. Equation (3.3) describes the influence of temperature and moisture content on thermal conductivity for narrow-ring spruce (slow growth, oven-dry density of ρ_0 = 383±35 kg/m³) in the radial direction.

$$\lambda_{383}\,(T, MC) = 0.001 \cdot ((((0.034 \cdot T) + 0.95) \cdot MC) + 82) \quad (3.3)$$

With

λ_{383}	Thermal conductivity at a dry bulk density of ρ_0 = 383 kg/m³	[W/(m·K)]
T	Temperature	[°C]
MC	Moisture content	[m.-%]

Assuming an average volumetric swelling of spruce and that Kollmann´s experiments were carried out at an average measurement temperature of $T \approx 27$ °C, equations (3.1) and (3.3) would agree. For more information on this topic, see also (Kollmann, 1951, p. 509).

3.1.2 Transient hygrothermal enthalpy effects on wooden surfaces

Similar to the various phenomena in moisture transport, heat transport in actual exterior walls is usually neither uniform nor exclusively consistent in direction. Rather, there are numerous time-dependent transport and storage effects depending on the ambient conditions.

Particularly heat fluxes can be extremely unsteady. For a proper evaluation, the measurements results must therefore be investigated by statistical tests like in (Flexeder et al., 2021). Furthermore, the heat balance of a component resulting from water vapor diffusion in combination with a phase change can be significantly influenced by enthalpy fluxes (Ineichen, 2020; Künzel, 1994). Consequently, there are also effects that cannot be detected using vapor-tight heat flux measurement plates. These include latent heat effects on the component surface, which occur when the component moisture adapts to a changing ambient air humidity, cf. Subchapter 3.1.2.

Summarized, the hygric behavior of solid wood walls is characterized not only by heat and mass transfer from one surface to the other, but also by thermal and hygric (sorption) storage effects. Depending on its treatment, for instance whether it is unsealed, glazed, or coated, the surface of wood is in constant exchange with the surrounding climate. If the ambient relative humidity changes, the material adapts to it by sorption and enthalpy is released or bound. This hygrothermal effect is known in theory, but the extent to which it contributes to buffering everyday climatic fluctuations in timber construction has not yet been sufficiently investigated.

Since the process of water adsorption is an exothermic reaction (Vidal Bastías & Cloutier, 2005), changes in wood moisture content also show up as a change in temperature. This latent heat effect has been known for decades, specifically in the context of thermal modification and technical drying of wood (Kollmann, 1949).

Based on recent references, the physical principles of latent heat effects have been summarized and calculated as they occur on wooden surfaces and have already been published in (Flexeder, Schumacher et al., 2022, p. 73 - 75). Since the publication is in German, the respective Subchapter is printed in Appendix A, p. 232, as an adapted English translation. The derivation in Appendix A, p. 232 indicates that the binding enthalpy h_B may be disregarded in calculations within the high moisture range. If, for instance, the simplified approach of a constant *adsorption enthalpy* h_{Ad} = *evaporation enthalpy* h_V is assumed, as in a WUFI simulation (Künzel, 1994), this results in a linear equation that solely depends on the adsorbed water quantity x [kg]. Nevertheless, the actual temperature change of the surface is once again dependent on the transient thermal behavior of the component. This simplified linear relationship could therefore be used for a new method in which sorption processes on the surface are detected by high-precision temperature measurements.

The literature review in (Flexeder, Nouman & Hepf, 2022) explains the context and previously existing experimental research on this topic regarding hygroscopic building materials:

“In the context of room cladding materials, latent heat is prospected to have a positive potential. With materials such as wood, the latent heat effect is assumed to have a thermoregulating impact in addition to their purely hygroscopic moisture buffering properties. […]

When moisture is transported into or through a material layer, enthalpy changes occur, which can be experienced or measured by the release of sensible heat. In (Winkler et al., 2014) both the buffering of relative humidity and the heat transport due to sorption are investigated using hygrothermal simulation. In (Dupleix et al., 2018; Kraniotis et al., 2016) laboratory experiments have already been carried out in which the increase in mass and heating of small wooden test specimens after abrupt humidification are documented. In (Nore et al., 2017) hygrothermal simulations of this phenomenon are validated using experiments in two test rooms made of solid wood. Similar room-scale numerical simulations in (Legros et al., 2020) show that a spruce surface has a lower surface temperature and air temperature during the summer period when compared to painted plasterboards. They attribute these findings to the higher hygroscopicity of the spruce.“ (Flexeder, Nouman & Hepf, 2022)

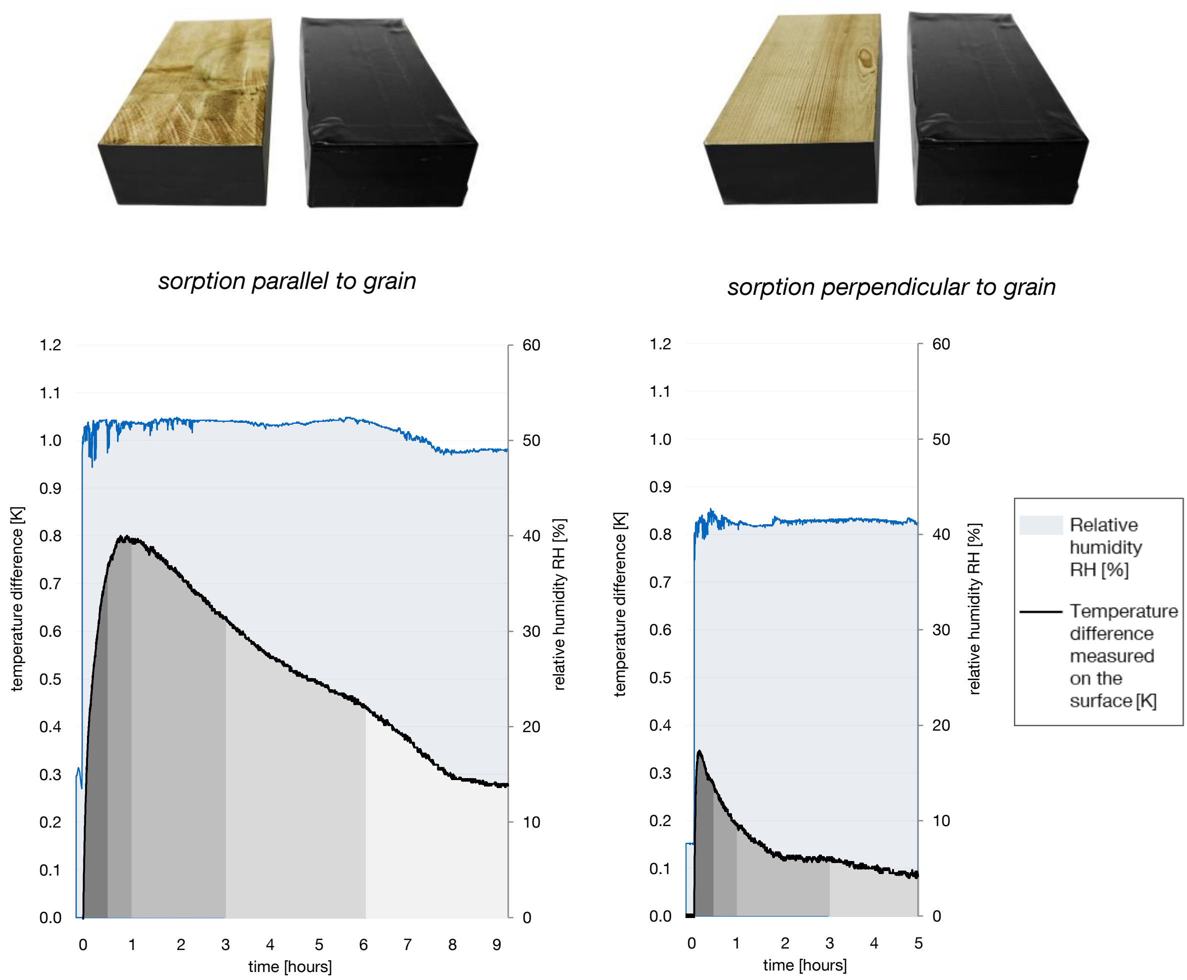

Figure 10: Results for adsorption experiments with surface heating due to enthalpy effects on glulam, parallel vs. perpendicular to the grain. Data previously published in (Flexeder, Kamml & Paulik, 2022)

The measurable heating of a wood surface by adsorption of water vapor due to rapid humidification of the ambient air has also already been demonstrated in (Flexeder, Kamml & Paulik, 2022; Flexeder, Schumacher et al., 2022), cf. Figure 10. Although not exactly obtained at the same *RH* range, these moisture step experiments also indicate the influence of anisotropy on the time-dependent sorption process. The results are thus considered in in-line with the findings by (Dupleix et al., 2018).

Similar to the experiments illustrated in Figure 10,the previous work by (Dupleix et al., 2018; Kraniotis et al., 2016) used measurements of surface temperature changes after artificially generated moisture jumps. It still remained unclear to what extent these findings could be transferred to realistic indoor climates within the course of the day or season. Consequently, the research project *PhyTAB* investigated the extent to which latent heat effects have a significant influence on the indoor climate and whether this phenomenon could be used for active climate control (Flexeder, Schumacher et al., 2022). The experiments concluded that even though the influence is present, latent heat effects only contribute insignificantly to the overall energy balance. Nevertheless, the approaches for monitoring this effect are a novelty. Conversely, the method for thermal measurement of latent heat could be used to detect sorption processes in the layers close to the component surfaces. Accordingly, first tests show the applicability and influencing parameters of this newly adapted method (Flexeder, Nouman & Hepf, 2022).

Notabene: The underlying principal of using temperature measurements to obtain information on changes in wood moisture content has already been considered in technical wood drying, albeit on a very different scale. Although it is not possible to determine the absolute wood moisture content using a heat flow measurement or the so-called temperature difference method, it is already being used for general statements about the major moisture content reduction during the drying process (Trübswetter, 2009, p.38). However, the usually far lower moisture fluctuations of generally dry wood surfaces in the assembled condition have not yet been monitored using this method. Accordingly, there is a need for a monitoring technique to gain knowledge about the everyday moisture sorption activities on wooden surfaces.

3.1.3 Moisture buffering effects and surrounding air movement

Because of their high hygroscopicity, wood and wood-based materials are claimed to be suitable as buffers to compensate for fluctuating levels of indoor humidity (Hameury, 2005; X. Zhang et al., 2016a). Various models have already been developed to assess the buffering effect of hygroscopic building materials. For instance, (Kossatz et al., 1982) compare the sorption rate of different wood-based panels in lab experiments using a method that measures half-life. This is defined as the unit of time it takes for the moisture change in the material to be absorbed by half and is therefore highly dependent on the moisture change that has occurred. Furthermore, recent models such as the *Hygrothermal Mass*, the *Effective Capacitance* (EC), the *Effective Moisture Penetration Depth* (EMPD), the *Moisture Buffering Value* (MBV), and *the Effective Damped Relative Humidity* (EDRH) are presented more detailed in (Flexeder, Schumacher et al., 2022, p. 76 - 78). Particularly the *MBV* value is used in further studies to estimate the moisture buffering effect of surface materials under realistic humidity step changes to simulate everyday fluctuations of indoor humidity. (Ineichen, 2020), a Master´s thesis supervised by the author, found in lab experiments following the *Nordtest protocol* (Rode, Peuhkuri, Hansen et al., 2005; Rode, Peuhkuri, Mortensen et al., 2005) that a glaze alone can significantly reduce the *MBV* of wooden surfaces. The surface of uncoated CLT showed a value of 0.70 kg/m²-%RH. The same material, only with an added thin layer of glaze, proved to already have a significantly reduced buffering effect with an *MBV* of 0.61 kg/m²-%RH. The glazing product was the same as in the project *Timberbrain*, an acrylate dispersion as a water-based and vapor-permeable wood stain for indoor use (Flexeder et al., 2021).

Skulberg et al. (2022) conducted a similar experiment to compare differently treated wood paneling, but at room level. Using electrical resistance measurements, they were able to determine differences between the moisture content of components whose spruce surfaces were sealed with transparent varnish and similar components that were left untreated. Although they attributed the higher hygroscopicity of the untreated surface to a higher hygrothermal mass, they did not measure these effects. They did note, however, that the moisture buffering effect appeared to be lower when the rooms were better ventilated (Skulberg et al., 2022). This is in-line with the experiments by (Li et al., 2012), who found that using an auxiliary fan can lead to significantly faster de- or adsorption and an overall more even distribution of vapor in the indoor air.

The sorption rate, which is how quickly a material can adsorb or desorb water vapor from the air, also depends on the air velocity at the material surface. This could be described as the water vapor resistance at the transition air – material. This value therefore determines how well a certain material can serve as a buffer to mitigate climate fluctuations. Neglecting this correlation can lead to inaccuracies in the simulation of sorption behavior. For example, it should be mentioned that the experimental work of (Winkler et al., 2014) and (Nore et al., 2017), presented in Subchapter 3.1.2, only considered constant air change rates. In contrast, natural ventilation concepts could result in air turbulence in the room and different air velocities near the surface of the room-enclosing surfaces. (Flexeder, Nouman & Hepf, 2022)

In order to quantify the influence of water vapor transfer on component surfaces, Worch (2004) used wind tunnels in their experiments on two different building materials, foam concrete and plaster. As a result, an additional value for transfer resistance might describe the vapor transfer behavior at the surfaces best. In analogy to the thermal resistance, different values are recommended depending on the ambient situation, the surface texture, and the positioning within an internal space regarding convection, Similarly, Steben (2005) also describes the physical principles of the transition of water vapor from ambient air into any component by dividing the water vapor diffusion transition resistance into three components, cf. Figure 11. (Steben, 2005; Worch, 2004)

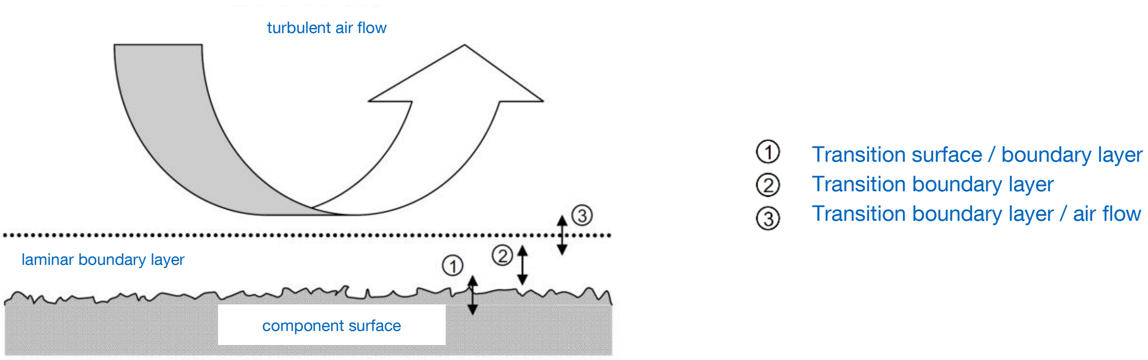

Figure 11: Location of the transfer resistance by (Steben, 2005) with English translations added in blue

Already in 1937, Kamei had demonstrated in tests that a change in air velocity *v* (0.6 m/s versus 6 m/s) leads to a significant increase in the drying rate of pine wood, which is more than twice as high under otherwise identical conditions (40 °C, 40 %RH). (Kamei, 1937)

In 1978, (Rosen H.N., 1978) developed an apparatus to test the hygric behavior of silver maple and black walnut. For these experiments, air was used at relatively high relative humidity of 97 %RH and a temperature of 25 °C (starting conditions unknown), cf. Figure 12.

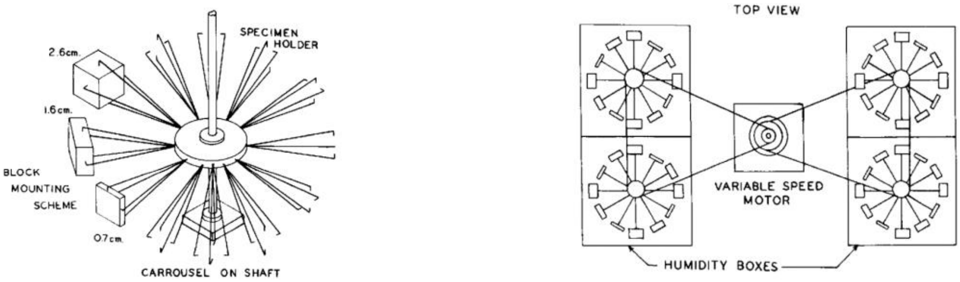

Figure 12: Arrangement of the humidity boxes and specimens on the carrousels for adsorption study (Rosen H.N., 1978)

By hurling the specimens around a common axis at different rotational speeds, air speeds of 0.43 m/s up to 11.70 m/s could be reproduced in the laboratory. It was concluded that “the movement of wood through air at moisture contents below the fiber saturation point influences the external resistance and thus moisture adsorption by the wood. The effect of wood velocity through air becomes more significant for thinner wood and for longitudinal rather than radial flow. The benefits of increasing wood velocity through air to increase adsorption rates are rapidly reduced above 3 m/s […]”. (Rosen H.N., 1978)

Consequently, in terms of a minimal air velocity *v* for effective drying, Trübswetter (2009) recommends at least *v* = 1 m/s, but ideally for softwood *v* = 3 m/s and for heavy hardwood *v* = 1.5 m/s. It is advised to create a jet with turbulent flow, because then the moisture transport away from the wooden surfaces should be much more effective than with a laminar flow. (Trübswetter, 2009)

Furthermore, it is shown that in the drying of wood - unlike some other drying goods such as soap - the ambient temperature and relative humidity have a distinct influence on the drying rate. Accordingly, it is assumed that vapor diffusion through the wooden cross-section has a significant influence on the evaporative drying behavior (Krischer, 1978, p. 326).

Avramidis & Siau (1987) explain the total diffusion resistance of wood by dividing it into two components, the internal diffusion of the material itself and the external diffusion resistance on the surface. Their experiments on small specimens of Western white pine at a constant air velocity of approximately $v = 2.5$ m/s showed that a greater moisture content results in greater emission coefficients, both internal and external. They tested their specimens at 30 °C – 70 °C and found that a rise in temperature usually also means greater emission coefficients as well. As a further development, Rozas et al. (2009) conduct drying experiments with 36 mm thick softwood boards at drying temperatures of 40 °C, 60 °C and 80 °C, relative humidity of 40 %RH and an air velocity of $v = 3.0$ m/s. The starting moisture content of their experiments is far beyond fiber saturation at around MC = 100 m.-% - 160 m.-% and ends in the upper hygroscopic range. They develop a mathematical model that proves to be quite accurate for describing the drying process above fiber saturation. While Chanpet et al. (2020) focus on the drying kinetics of stacked rubberwood lumbers only, they present similar findings as Avramidis & Siau, while varying the parameters of humidity, temperature, and air velocity. By kiln-drying at different values for air velocity (0.5 m/s - 4.0 m/s), relative humidity (6 %RH – 67 %RH), and temperature (60 °C – 100 °C), they state that the drying rate and the overall moisture transfer coefficient could be increased by the following: increasing air velocity, increasing drying temperature, and decreasing relative humidity. (Avramidis & Siau, 1987; Chanpet et al., 2020; Rozas et al., 2009)

3.2 Fundamental correlations regarding the hygroscopicity of wood

3.2.1 Description of sorption phenomena in wood at different temperatures

The next subchapters will only focus on the specifics of wood-water interaction that exceed basic knowledge and are relevant to wood moisture monitoring. General information on wood physics, including the micro- and macroscopic biological structure as well as the correlations with mechanical properties, can be found in established fundamental literature from this comprehensive field (Forest Products Laboratory, 2021; Niemz, 2021; Skaar, 1972, 1988).

The prediction of hygrothermal component behavior, for instance to estimate the transient insulation effect, scenarios of possible mold growth or wood decay, can be supported by hygrothermal simulation. However, the results always depend on the underlying model and the input parameters used. Thus, the water vapor diffusion resistance and the vapor sorption isotherm are the two most important material parameters for describing the transient moisture behavior of wood (Avramidis, 2018; K. Zhang & Richman, 2020; X. Zhang et al., 2016a).

Due to the anisotropy of wood, the diffusion resistance is a parameter depending on direction, temperature, and moisture. The sorption isotherm, also temperature- and moisture-dependent, refers to the entire material thus direction-independent. With increasing temperature, the ability of hygroscopic materials to absorb liquid decreases overall (Krischer, 1978, p. 55). Meanwhile, the rate at which the vapor pressure in the wood and the surrounding air reaches equilibrium, increases with increasing temperature (Kollmann, 1949). Even though sorption isotherms are usually differentiated according to wood species, it should be noted that even solid wood per se does not initially exhibit uniform sorption behavior. Especially in higher ranges of relative humidity, early wood and late wood show different sorption isotherms and hence, differences in hygromechanical behavior, leading to cracks, like shown on Douglas fir by (Bonnet et al., 2017). Although important for material-specific issues on a small scale, the following will focus less on differences in the wood structure itself. In addition, the sorption behavior also depends on the history of the investigated material, both short-term (hysteresis, cf. Subchapter 3.2.2) and long-term (aging, cf. Subchapter 3.2.3).

For decades, knowledge about the wood moisture content in a board´s different depths has been a crucial factor in targeted climate changes, such as technical wood drying. For instance, already in an issue of the journal *Holz-Zentralblatt* from 1949, Rudolph Keylwerth published a nomogram, i.e. a graph for the practical estimation of drying times as a function of initial moisture content, board thickness, wood properties and kiln temperature. Later that year, a graph was published as a guide for estimating wood moisture as a function of relative humidity and temperature. This graph already corresponds to the diagram that later became known as the *Keylwerth-diagram*, cf. Figure 13, p. 52. Since continuous and reliable measurements of relative humidity were still technically difficult for many kiln operators at the time, a trick for calculating the prevailing relative humidity is described using smaller wood sections and a letter scale to gain an indication of the moisture content in the lumber´s surface layers. (Keylwerth, 1949a, 1949b)

It is also well known from the field of wood drying techniques that not only an ambient humidity gradient, but also a temperature gradient by itself can also generate a mass flow. Already in 1940, Voigt et al. carried out experiments on beech wood (radial). A vapor-tight specimen was subjected to a constant temperature gradient so that, due to the diffusion taking place in the pores, moisture accumulated on the cold side and was simultaneously released on the warm side. Avramidis (2018) discussed general considerations about the non-isothermal water diffusion in wood and the fact that diffusion under temperature gradients might contradict Fick´s law. Cases are described where moisture diffusion takes place in the opposite direction of the vapor pressure gradient and attribute this phenomenon to the Soret effect, thermal diffusion in nonequilibrium thermodynamics. Ma et al. (2022) confirmed in experiments with Japanese Cypress that the mass flow is dependent on the drying temperature. Moderate drying temperatures of 30 °C showed a moisture gradient from the outside to the inside (drier). With much more aggressive drying at 90 °C, deformation and cracking appeared quickly, with the surface areas of the specimens showing signs of strongly bonded water. (Avramidis, 2018; Ma et al., 2022; Voigt et al., 1940)

Sorption isotherms describe the water content of a material as a function of the relative humidity for a specific temperature level. For their rough description, established models already exist, which are considered to be sufficiently accurate depending on the field of application. However, the initial hypothesis that individual parameters of the models can actually represent physical parameters is meanwhile being criticized (Thybring et al., 2021; Zelinka et al., 2020). The models and theories widely used on hygroscopic materials include:

- BET (Brunauer & Emmet & Teller), with first ideas from 1938
- HH (Hailwood & Horrobin), published in 1946
- GAB (Guggenheim & Anderson & de Boer), from 1946/1953/1966

Numerous models have since been developed in natural science for estimating the moisture content of hygroscopic materials from at least the variable *RH*. Since the hygroscopicity of materials plays an important role not only in timber engineering, but also, for instance, in conservation practice, HVAC engineering, textiles, and food chemistry, there is plenty of data for the calculation of water activity. A comprehensive compilation of more than 31 approaches to the characterization of sorption isotherms is presented by (Lewicki, 2012) in (Rahman, 2008, p. 67-151). The BET theory, which is often mentioned in the context of wood physics, has thus been further developed in many different approaches. Another approach is the GAB model, which is used both, as a temperature-independent equation in the field of wood research (Bratasz et al., 2012), and can represent temperature dependence in a modified form (Glass et al., 2014; Lewicki, 2012). Simpson (1973) compared ten different approaches specifically to calculate wood moisture contents from the value of relative humidity of ambient air by assessing their fit with the sorption data by Loughborough (1931) from the Wood Handbook of 1955. Only some of these fitted models include temperature as a variable (Simpson, 1973). For the temperature variations that can be expected in the context of wood moisture monitoring, however, a term for fitting the sorption isotherm to temperature, such as the HH-model, is essential.

Hailwood & Horrobin (1946) published an equation for the calculation of *EMC* from *RH* and *T*. Equation (3.4) has been since distributed through various versions of the wood handbook.

Based on the sorption data from Loughborough (1931), it has been used widely to estimate wood moisture contents (Forest Products Laboratory, 2021; Hailwood & Horrobin, 1946):

$$EMC = \frac{1800}{W}\left[\frac{Kh}{1-Kh} + \frac{K_1Kh + 2K_1K_2K^2h^2}{1+ K_1Kh + K_1K_2K^2h^2}\right] \quad (3.4)$$

With

EMC	Equilibrium Moisture Content	[m.-%]
h	Relative Humidity of Air (decimal; $0 \le h \le 1$)	[-]
T	Temperature	[°C]
W	$349 + 1.29\,T + 0.0135\,T^2$	
K	$0.805 + 0.000736\,T - 0.00000273\,T^2$	
K_1	$6.27 - 0.00938\,T - 0.000303\,T^2$	
K_2	$1.91 + 0.0407\,T - 0.000293\,T^2$	

Glass et al. (2014) review historic data and models to calculate *EMC* and suggest to use a simplified version for the same data. Their method originates from an analysis by Avramidis (1989), who examined four approaches for their suitability to reproduce the sorption data from Loughborough as a function of the two variables *RH* and *T*. Accordingly, the best fit is shown by Zuritz's approach, which is similar in structure to the simplified form of the Henderson equation (Avramidis, 1989; Glass et al., 2014; Henderson, 1952; Zuritz et al., 1979):

$$EMC = 100 \cdot \left[A \cdot T \cdot \left(1 - \frac{T}{T_C}\right)^B \cdot \ln(1-h)\right]^{C \cdot T^D} \quad (3.5)$$

$$h = 1 - exp\left[\frac{1}{A \cdot T} \cdot \left(1 - \frac{T}{T_C}\right)^{-B} \cdot \left(\frac{EMC}{100}\right)^{\left(\frac{1}{C}\right) \cdot T^{-D}}\right] \quad (3.6)$$

With

EMC	Equilibrium Moisture Content	[m.-%]
h	Relative Humidity of Air (decimal; $0 \le h \le 1$)	[-]
T	Temperature	[K]
T_c	Critical temperature of water, const. = 647.1 K	[K]
A	-0.000612	
B	2.43	
C	0.0577	
D	0.430	

Accordingly, this approach by equations (3.5) and (3.6) is recommended as an alternative by the recent version of the wood handbook as well (Forest Products Laboratory, 2021). The two equations could be described as today´s state of the art, similar to the diagram by Rudolph Keylwerth (Keylwerth & Noack, 1964, p. 31), which has been mostly used in German-speaking countries for several decades (Böhner, 1996; Fortuin, 2003).

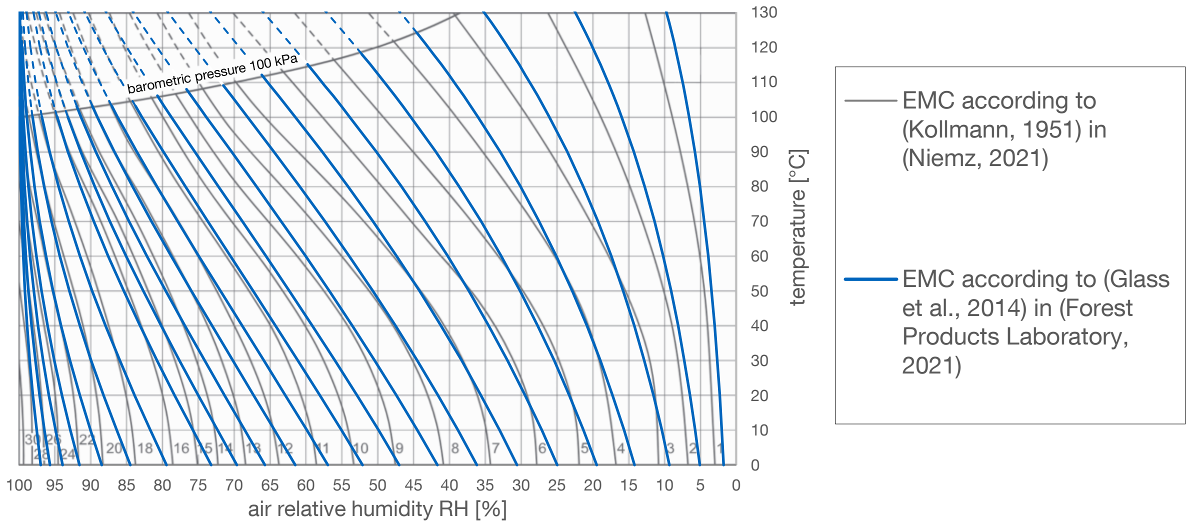

Figure 13: Juxtaposition of the Keylwerth-diagram, shown in black, as published in (Niemz, 2021) to the model by (Glass et al., 2014) in (Forest Products Laboratory, 2021), shown in blue. Both sets of curves for the equilibrium moisture content (EMC) are based on the historic sorption data by Loughborough.

Figure 13 compares the curves for *EMC* by Rudolph Keylwerth with the ones by equation (3.5). There are minor divergences, although both are based on the same historic sorption data. This underlaying data was originally taken from older versions of the wood handbook and originates from Sitka spruce (*Picae sitchensis Carr*.) by W.K. Loughborough in 1931. Even though this data has been used for fitting numerous models, its origin and methodology is not documented well, which is why Glass et al. (2014) consider it unreliable for scientific purposes. Furthermore, it is not clearly specified whether the graph is based on adsorption, desorption or an averaged curve (probably oscillating vapor pressure desorption). (Böhner, 1996; Forest Products Laboratory, 2021; Fortuin, 2003; Glass et al., 2014; Simpson, 1973; Weichert, 1963b; Zelinka et al., 2020).

(Böhner, 1996) had already taken Weichert's sorption data (Weichert, 1963a) as a basis and compared it with Loughborough's data sets. Larger deviations were discovered, especially at low temperatures and at low wood moisture contents. Since Loughborough´s sorption isotherms were initially collected, numerous other data sets for sorption isotherms have been generated. The use of the original Keylwerth diagram thus represents an outdated method and accordingly requires revision. Consequently, material-specific sorption data are collected in Subsection 3.2.2 of this thesis, also with regards to the phenomena of sorption hysteresis. The influence of the latter is larger with greater amplitudes of moisture change, rendering the need to account for the sorption history (Hozjan et al., 2012).

This data is then used in Subchapters 4.4.1 and 5.3 to refine the model approaches for practical use in wood moisture monitoring.

In addition to the currently prevailing temperature, the decisive factors for the course of the sorption isotherm are: whether adsorption or desorption is occurring, how often adsorption and desorption cycles have already been run through, possible wood modifications, the age of the material, and how strong the temperature load on the material was in the past.

3.2.2 Characterization of sorption isotherms as a function for different wood species

Sorption isotherms always refer to a constant temperature. For hygroscopic materials such as wood, the following applies in general: The higher the temperature, the lower the isotherm, since the potential for liquid absorption decreases as the temperature. Furthermore, also water itself changes behavior with increasing temperature. In the temperature range relevant for building physics, the surface tension of water against air decreases by around 20 % (Krischer, 1978, p. 55, p. 211)

Not only wood species, but numerous hygroscopic goods exhibit a similar sorption behavior of the so-called type II isotherm: they show sorption hysteresis, whereby a higher liquid content is present when drying an initially wet material under a certain vapor pressure than when moistening the initially dry material under the same vapor pressure. The desorption isotherm thus always runs above the adsorption isotherm, forming a gap which gets smaller at increased temperatures (Krupińska et al., 2007), cf. Figure 14, p. 54. This phenomenon is more pronounced the broader the sorption cycle (Frandsen et al., 2007; Varnier et al., 2022), and shows the highest amplitude when a sorption cycle is run completely from 0 to 100 %RH.

Since this does not reflect real climate fluctuations though, scanning curves are used to describe the attenuated form of this phenomenon. Using lab experiments on three different wood species accompanied by mathematical modeling, Shi & Avramidis conclude that sorption hysteresis in wood might be related to the cell wall porosity and thus capillary condensation (Shi & Avramidis, 2017a, 2017c). This thesis introduces also an own approach to mitigate the hysteresis effect in a monitoring context, cf. method described in Subchapter 4.4.1.

The studies in the subsequent chapters will investigate the sorption behavior of the following wood species:

> Norway spruce (*Picea abies Karst.*), European beech (*Fagus sylvatica L.*), Douglas fir (*Pseudotsuga menziesii Franco*), radiata pine (*Pinus radiata D. Don*.).

Table 5, p. 55, shows a selection of previously published sorption isotherms of these wood species. In addition, a large number of published sorption data can be found in many more publications. However, some do not meet minimum quality criteria, in terms of accuracy and data sufficiency (Glass et al., 2014; Zelinka et al., 2020). Furthermore, it is pointed out that much of the literature published on this subject is concerned rather with the mathematical description of sorption, but still based on the same measurement data by W. K. Loughborough (1931) as the underlying measurement data, cf. Subchapter 3.2.1. For the sake of completeness, Table 5 also lists the mathematical models with which the respective authors attempted to describe their individual measurement data in a second step in their publications. This column is purely informative, since only the original measurements were used as a basis for this thesis, in order to minimize the falsification by double model fitting. The sorption measurement data employed for further use in this work were thus taken as originals directly from the tables in the publications. In the case of (Weichert, 1963b), it was obtained by precisely measuring in analog graphics in the hard copy of the original dissertation.

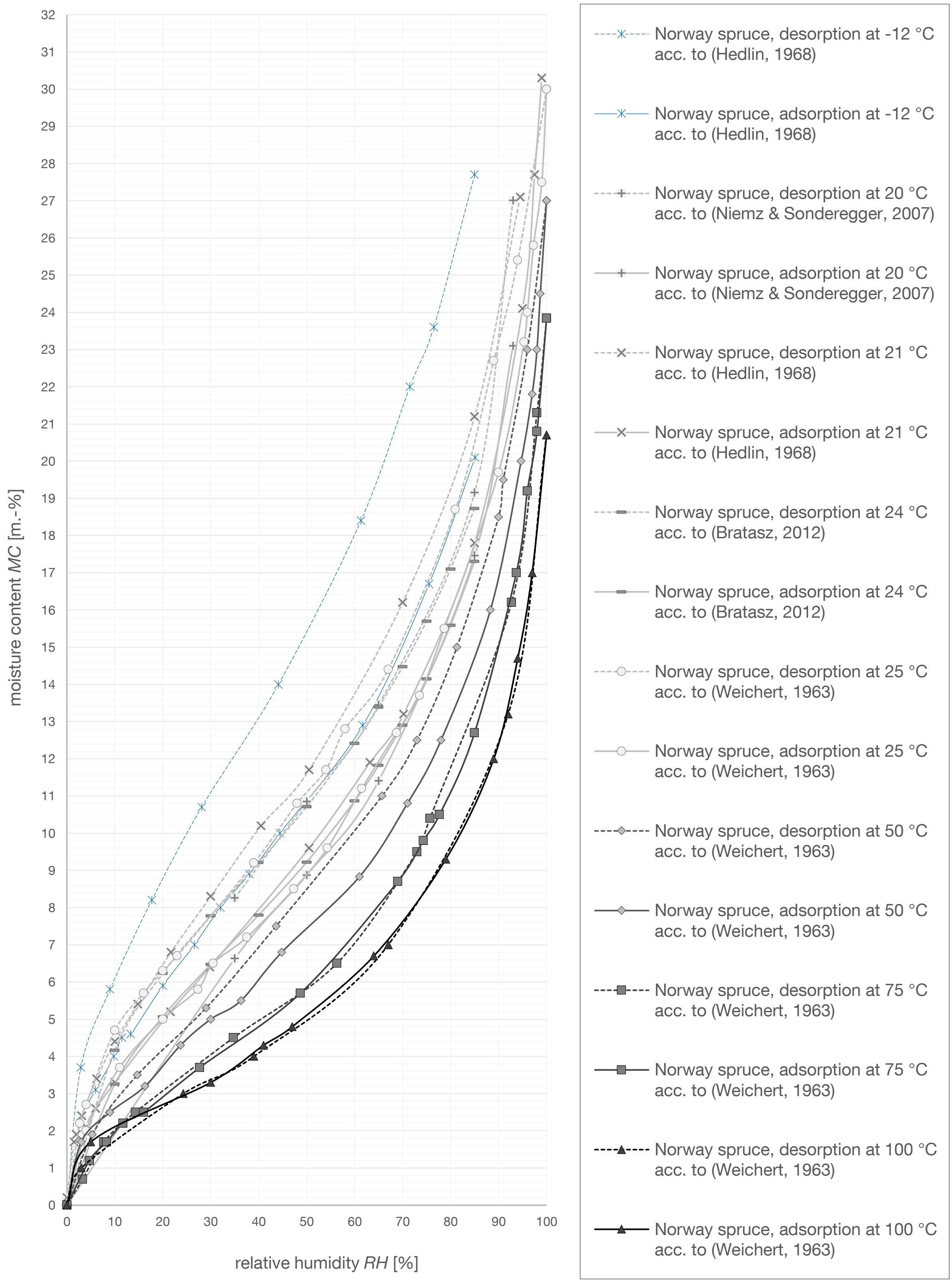

Figure 14: Example for a collection of sorption isotherms for desorption and adsorption in Norway spruce at temperatures between -12 °C and 100 °C. The data is taken from measurement results by (Bratasz et al., 2012; Hedlin, 1968; Niemz & Sonderegger, 2007; Popper & Niemz, 2009; Weichert, 1963b). The lower the temperature, the higher the overall moisture content and also the more pronounced the phenomenon of sorption hysteresis.

Table 5: Selection of published sorption isotherms for different wood species

Authors	Wood Species	Models	Range of measurements	
(Weichert, 1963a, 1963b)	Norway spruce (*Picea abies Karst.*) European beech (*Fagus sylvatica L.*) *Both untreated and modified by irradiation*	BET (Brunauer-Emmet-Teller)	*RH:* *T:* *MC:*	0 % – 99 % 25 °C, 50 °C, 75 °C, 100 °C 0 m.-% – 30 m.-%
(Hedlin, 1968)	Norway spruce (*Picea abies Karst.*) Douglas fir (*Pseudotsuga menziesii Franco*)	-	*RH:* *T:* *MC:*	2 % – 95 % -16 °C, -12 °C, 21 °C 1 m.-% – 30 m.-%
(Fan et al., 1999)	Douglas fir (*Pseudotsuga menziesii Franco*) *Differentiation between heartwood and sapwood*	BET (Brunauer-Emmet-Teller) Adamson FHH (Frenkel-Holsi-Hill)	*RH:* *T:* *MC:*	23 % – 94 % 30 °C, 45 °C, 60 °C 3 m.-% – 24 m.-%
(Ball et al., 2001)	Radiata pine (*Pinus radiata D. Don.*) *Differentiation between heartwood and sapwood*	Day and Nelson HH (Hailwood & Horrobin)	*RH:* *T:* *MC:*	20 % – 80 % 10 °C, 15 °C, 20 °C, 25 °C, 30 °C, 35 °C 5 m.-% – 17 m.-%
(Popper et al., 2005)	Douglas fir (*Pseudotsuga menziesii Franco*) Radiata pine (*Pinus radiata D. Don.*) *untreated and thermally modified at 100 °C / 150 °C / 200 °C for 24 h*	HH (Hailwood & Horrobin)	*RH:* *T:* *MC:*	11 % – 93 % 22 °C 3 m.-% – 23 m.-%
(Niemz & Sonderegger, 2007)	Norway spruce (*Picea abies Karst.*) European beech (*Fagus sylvatica L.*)	-	*RH:* *T:* *MC:*	35 % – 93 % 20 °C 7 m.-% – 27 m.-%
(Popper & Niemz, 2009)	Norway spruce (*Picea abies Karst.*) European beech (*Fagus sylvatica L.*) Douglas fir (*Pseudotsuga menziesii Franco*) Radiata pine (*Pinus radiata D. Don.*) *all: only adsorption curves*	HH (Hailwood & Horrobin)	*RH:* *T:* *MC:*	35 % – 95 % 20 °C 7 m.-% – 27 m.-%
(Bratasz et al., 2012)	Norway spruce (*Picea abies Karst.*) European beech (*Fagus sylvatica L.*)	GAB (Guggen-heim-Anderson-de Boer)	*RH:* *T:* *MC:*	8 % – 85 % 24 °C 3 m.-% – 19 m.-%
(Simón et al., 2016)	Radiata pine (*Pinus radiata D. Don.*)	GAB (Guggen-heim-Anderson-de Boer)	*RH:* *T:* *MC:*	11 % – 98 % 15 °C, 35 °C, 50 °C 3 m.-% – 33 m.-%

3.2.3 Effects of aging and high temperatures on the hygroscopicity of wood

In order to investigate the wood moisture content in older existing timber buildings or historical art objects, the effects of aging on the physiology of the wood might also need to be considered. How does the hygroscopicity of wood change as a result of years of climatic stresses such as changing temperatures and relative humidity fluctuations?

There seems to be no clear answer to this question, as various investigations on wood samples of different ages have produced partly contradictory results (Dremelj & Straže, 2022). Sonderegger et al. (2015) experiment on Norway spruce (*Picea abies Karst*.), silver fir (*Abies alba Mill*.), and European oak (*Quercus robur L./Quercus petraea Liebl.*). They state that the parameters for sorption, swelling, bending, and fracture toughness do not show a distinct correlation to the age of wood (Sonderegger et al., 2015). Erhardt & Mecklenburg (1995) investigate the behavior of cellulose under different climatic conditions to simulate an aging process, distinguished by the differing distribution of reaction products. For their experiments with paper they used different conditions of 60 °C - 90 °C within a relative humidity range of 30 %RH – 80 %RH (Erhardt & Mecklenburg, 1995). In construction practice similar conditions can often be found on surfaces exposed to solar irradiation. Thus, the findings by Erhardt & Mecklenburg (1995) about the strong correlation between relative humidity and the aging process of cellulose might be transferable to wood. A comprehensive literature review on the chemical, mechanical, and physical effects of aging on wood can be found in (Kránitz et al., 2016).

Several examples from the museum context show that aged wood behaves differently than freshly cut wood. In the case of an archaeological wooden ship from the Viking Age (around 1200 years old), it was shown that the young wood specimens (oak) react much faster to climatic changes than the examined parts from the original object (Dionisi-Vici et al., 2013). Regarding the sorption isotherm, various investigations, for instance on historic Hinoki wood, found that their age of several hundred up to 1600 years led to a lower equilibrium moisture content *EMC* then that of recent wood (Inagaki et al., 2008; Kawai et al., 2008; Kohara & Okamoto, 1955; Kránitz et al., 2016; Yokoyama et al., 2009). Similarly, studies on aged Norway spruce (*Picea abies*) and fir (*Abies alba*) show their decreased hygroscopicity compared to recently harvested samples (Lang, 2004).

On the contrary, measuring the sorption isotherms of recent versus 205-year-old Scots pine (*Pinus sylvestris L.*) produced opposite results with the old wood showing clearly higher *EMC*-values and thus a higher hygroscopicity throughout (García Esteban et al., 2006). Explanations for these phenomena could be based on the different cellulose crystallinity, tensions in the material, the cell matrix, rearrangement of amorphous wood polymers, or the temporary closure of micropores (Dremelj & Straže, 2022; Obataya, 2017).

For experimental investigations, artificially aging specimens from recently cut wood by cyclic wetting and heating might be a good option to gain information about how naturally aged wood might behave. In terms of their effect on the wood cell structure, those artificial aging processes could be compared to mild thermal treatment at around 100 °C – 150 °C (Kránitz et al., 2016). Thermal wood modification is the active treatment of wood products, typically at temperatures of around 160 °C - 240 °C, to reduce their hygroscopicity as well as their wettability by water and thus their susceptibility to wood rot and decay fungi. The higher the temperature at treatment, the greater the effect. Even if exact values vary due to the large number of different techniques and types of wood, thermal treatment is typically associated with a decreased equilibrium moisture content *EMC*. (Zelinka et al., 2022)

Interestingly, this rule applies to many common wood species but with the exception of sap-wood Scots pine (*Pinus sylvestris L.*), a wood species with increased liquid water absorption coefficients after mild thermal treatment (Metsä-Kortelainen et al., 2006; Scheiding et al., 2016). Comparing these unusual results with the findings by (García Esteban et al., 2006) on aged Scots pine suggests that this particular wood species might have material properties that distinguish it from others.

Thermal wood modification does not only change the wood´s hygroscopicity, it also changes its overall electrical resistance significantly, cf. Figure 16, p. 60. The latter is important when using the electrical resistance method (ERM) to determine the equivalent moisture content of thermally modified timber. Further investigations of the change in electrical resistance caused by wood treatment can be found in (Boardman, 2011), (Brischke & Lampen, 2014), (Emmerich & Brischke, 2021).

Apart from technical wood modification techniques, situations can also arise, especially on facades, where wood components are systematically exposed to elevated temperatures. These unintentional thermal modifications of components might also have an impact on the physical parameters of the material. Furthermore, the wooden element under investigation might have also been subject to degradation by wood-destroying fungi, which causes mass loss. (Brischke et al., 2019) found that infestation by wood rot leads not only to a decrease in equivalent moisture content *EMC* [m.-%], yet also to a lowered electrical resistance *R* [Ω]. Both phenomena would lead to an overestimation of the actual moisture content *MC,* if in-vestigated by monitoring methods without any adjustments. However, the described effects are not consistent across all scenarios, but considered highly dependent on the wood spe-cies, the type of fungi, and the circumstances of the infestation.

This brief summary shows that both the sorption capacity and the electrical properties of wood can depend not only on the type of wood, but also on its history. Previous stresses on the monitored timber element can mean that conventionally determined calibration curves are only valid to a limited extent. However, there are no generally valid correction factors. The change in material parameters depends on the specific circumstances, as the contrasting example of Scots pine sapwood shows.

Furthermore, it should be noted that even though the effects of long-term natural ageing as well as thermal treatment of wood lead to changes in hygroscopicity, these can be partly reversed when the wood is exposed to high humidity again (Obataya, 2017; Zelinka et al., 2022).

3.2.4 Correlation between wood moisture content, electrical parameters, and temperature

Electrical resistance measurements for wood moisture estimation such as those according to standard (EN 13183-2:2002) use of the pronounced correlation of moisture content and electrical resistance of wood. Figure 15 shows the relationship between electrical resistance *R* [Ω], wood moisture content *MC* [m.-%], and temperature *T* [°C], using *Pinus Sylvestris* as an example (Forsén & Tarvainen, 2000). In general, the lower the wood moisture content *MC,* the higher is the electrical resistance *R*. At the same time, the electrical resistance in the wood decreases with increasing temperature, a phenomenon that might be explained by a percolation model (Boardman et al., 2017; James, 1963; Skaar, 1988; Zelinka et al., 2008).

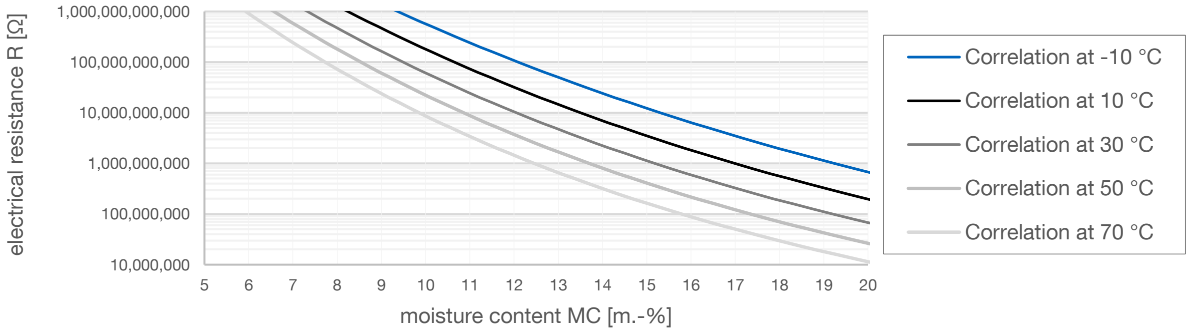

Figure 15: Correlation of wood moisture content MC [m.-%] with measured electrical resistance R [Ω] at different temperature levels in Pinus Sylvestris according to (Forsén & Tarvainen, 2000), shown in a logarithmic scale.

Various authors have already investigated the correlation between the electrical resistance and the moisture content of wood. Relationships derived therefrom can be used as calibration curves for electrical resistance measurements. The main focus of this work is on Norway spruce, since this wood species is currently used a lot in timber engineering. In addition, this thesis will consider current trends in experimental investigations in order to proactively support future developments. These include efforts for the use of other softwood species and the increased use of hardwood, developments for laminated veneer lumber, and a worldwide expansion of cross-laminated timber construction using local species. The studies in the subsequent chapters will investigate the following wood species:

> Norway spruce (*Picea abies Karst.*), European beech (*Fagus sylvatica L.*), Douglas fir (*Pseudotsuga menziesii Franco*), radiata pine (*Pinus radiata D. Don*.), spotted gum (*Corymbia maculata*), shining gum (*Eucalyptus nitens*).

Based on these wood species, there is an array of wood products investigated in this thesis and in related work:

> Cross-laminated timber (CLT) made from spruce (*Picea abies Karst.*), CLT made from radiata pine (*Pinus radiata D. Don*.), laminated veneer lumber (LVL) made from spruce (*Picea abies Karst.*), LVL made from beech (*Fagus sylvatica L.*).

According to this selection, Table 6 presents an overview of published measurement data of these species as well as mathematical models, including their limitations for use in the hygroscopic range.

Table 6: Selection of some published calibration curves for electrical resistance measurements

Authors	Wood Species	Models	Range of measurements	
(Schiere et al., 2021a)	Beech laminated veneer lumber (LVL made of *Fagus sylvatica L.*) *transverse to grain, parallel to grain*	*MC* (R,T)	*RH:* *T:* *MC:*	30 % – 93 % 10 °C, 20 °C 5 m.-% – 20 m.-%
(Grönquist et al., 2021)	Beech laminated veneer lumber (LVL made of *Fagus sylvatica L.*) *in three different variations*	$MC_{22.68\,°C}$ (R) MC ($MC_{22.68\,°C}$,T)	*RH:* *T:* *MC:*	35 % - 85 % ≈ 23 °C (constant) 6 m.-% – 16 m.-%
(Emmerich & Brischke, 2021)	Radiata pine (*Pinus radiata D. Don.*) *Untreated and furfurylated, acetylated*	*MC* (R,T)	*RH:* *T:* *MC:*	> 75 % 4 °C, 20 °C, 36 °C 15 m.-% - 60 m.-%
(Otten et al., 2017)	European beech *(Fagus sylvatica L.)* Douglas fir heartwood *(Pseudotsuga menziesii Franco)* Norway spruce *(Picea abies Karst.)* Norway spruce *(Picea abies Karst.)* TMT *(Thermally modified at 230 °C for 3 hours)*	*MC* (R,T)	*RH:* *T:* *MC:*	> 43 % 4 °C, 20 °C, 36 °C 8 m.-% – 60 m.-%
(Brischke et al., 2014)	Norway spruce *(Picea abies Karst.)* Norway spruce *(Picea abies Karst.)* TMT *(Thermally modified)* European beech *(Fagus sylvatica L.)* European beech *(Fagus sylvatica L.)* TMT *(Thermally modified)*	*MC* (R, T, ML) ML = mass loss caused by the thermal treatment	*T:* *MC:*	4 °C, 20 °C, 36 °C 8 m.-% - 50 m.-%
(Brischke et al., 2008)	Norway spruce *(Picea abies Karst.)* Douglas fir *(Pseudotsuga menziesii Franco)* *Each from three different locations*	$MC_{20\,°C}$ (R) MC ($MC_{20\,°C}$,T)	*T:* *MC:*	20 °C, *(4 °C, 36 °C)* 15 m.-%, 25 m.-%, 50 m.-%
(Forsén & Tarvainen, 2000)	Norway spruce *(Picea abies Karst.)* European beech *(Fagus sylvatica L.)* Scots pine (*Pinus sylvestris L.*) *Various batches from different locations in Europe* *Temperature investigation only on pine*	$MC_{20\,°C}$ (R) MC ($MC_{20\,°C}$,T)	*RH:* *T:* *MC:*	40±5 %, 65±5 %, 85±5 % 20 °C; *only pine:* -10 °C, 5 °C, 20 °C, 40 °C, 60 °C, 70 °C 9 m.-%, 12 m.-%, 16 m.-%
(Du et al., 1991)	Norway spruce *(Picea abies Karst.)* European beech *(Fagus sylvatica L.)* Scots pine (*Pinus sylvestris L.*)	$R_{20\,°C}$ (*MC*)	*RH:* *T:* *MC:*	35 %, 65 %, 85 %, 95 % 20 °C 6 m.-% - 30 m.-%
(James, 1988)	Sitka spruce (*Picea sitchensis.*) Douglas fir, coast region (*Pseudotsuga menziesii* var. menziesii), *measurements along the grain*	no mathematical model, just data $R_{room\ temperature}$ (*MC*)	*T:* *MC:*	"room temperature" 7 m.-% – 25 m.-%

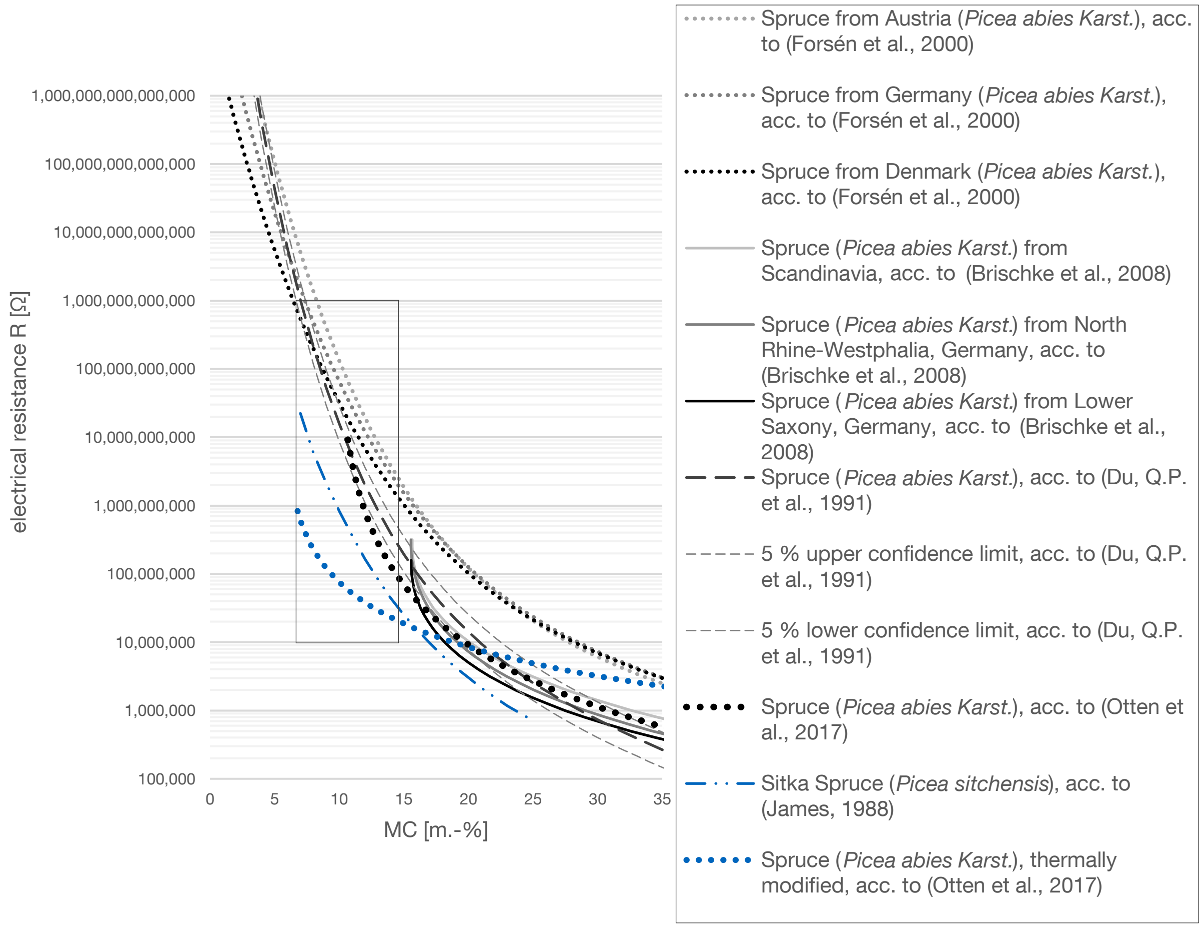

Figure 16: Overview of various published models on the relation of electrical resistance R and moisture content MC [m.-%] of Norway spruce from various locations, both untreated and thermally modified, and Sitka Spruce at 20 °C, shown in a logarithmic scale. The box indicates the range of 7 m.-% – 15 m.-% and 10^7 Ω – 10^{12} Ω, shown for untreated Norway spruce more detailed in Figure 17.

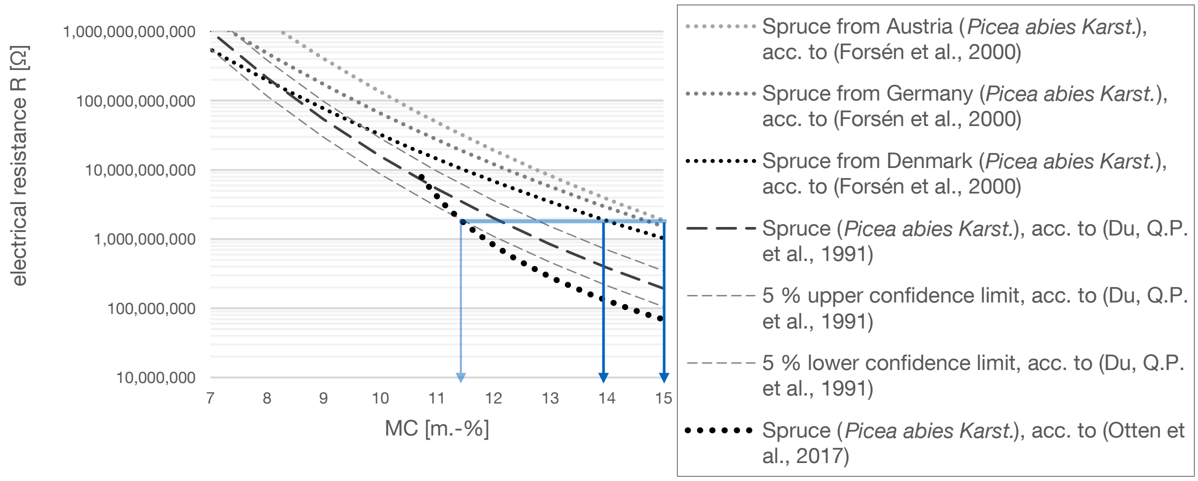

Figure 17: Section showing calibration curves at 20 °C for the moisture range of particular relevance to this work. The arrows illustrate a possible scattering of the calibration curves resulting a) from different locations of the same author by itself and b) within this only limited selection of literature.

Figure 16 compares different calibration curves from the literature for the wood species ´spruce´. Although all these curves were determined empirically at 20 °C, a large scatter is evident for the different batches of Norway spruce (*Picea abies Karst.*). Investigations on the influence of the origin of the same wood species from different growing regions were able to establish a significant difference in the correlation between wood moisture content and electrical resistance (Brischke et al., 2008; Forsén & Tarvainen, 2000).

According to measurements by (Otten et al., 2017), deviations due to thermal modification lead to a reduction in electrical resistance for the same wood moisture content in the range of MC < 20 m.-%. Likewise, a tendency towards lower electrical resistance can be observed in the related species Sitka spruce (*Picea sitchensis)* (James, 1988). Focusing on the hygroscopic range, which is particularly important in the context of this work, it is shown that a back-calculation of electrical resistance values can be sensitively influenced by the model used and the measurement data on which it is based. Figure 17, for instance, shows how a measured value of R = 1.1 10^9 Ω would result in an equivalent wood moisture content of about $EMC \approx$ 11.5 m.-% according to the model by (Otten et al., 2017), but in an equivalent wood moisture content of $EMC \approx$ 15 m.-% according to the model by (Forsén & Tarvainen, 2000). Deviations of this magnitude could be quite sufficient for questions of pure rot prevention. However, they are too large for the investigations of this work, which are primarily concerned with hygrothermal building physics under *normal everyday use*, i.e. dry conditions.

In order to sufficiently specify wood moisture monitoring techniques by means of the electrical resistance method, at least random checks of the calibration curves of known wood species are necessary. In addition, the influencing factors that can lead to further relevant deviations in the overall system must be investigated. The methods of these investigations are explained in the following Subsections 4.1, 4.2, and 4.3. The comparison of own measurement results with these models can then be found in Subsections 5.1 and 5.2.

Complementing the detailed studies on Norway spruce (*Picea abies Karst.*), electrical resistance measurements are also used on European beech (*Fagus sylvatica L.*), Douglas fir (*Pseudotsuga menziesii Franco*) and radiata pine (*Pinus radiata D. Don.),* spotted gum (*Corymbia maculata*), and shining gum (*Eucalyptus nitens*) in the broader context of this thesis. For Douglas fir and radiata pine, only a smaller selection of calibration curves is available in literature. In case of spotted gum and shining gum, unfortunately, no species-specific calibration curves are available at the time of writing. Accordingly, higher inaccuracies are to be expected.

Figure 18 shows a collection of available calibration curves for electrical resistance measurements on Douglas fir (*Pseudotsuga menziesii Franco*) at 20 °C. In addition, data at 4 °C and 36 °C are also available from (Otten et al., 2017) and (Brischke et al., 2008), although their work tends to focus on wood moisture contents above 15 m.-%. Unfortunately, the calibration curves published by them are therefore of limited use for the questions posed in this thesis. In Subsection 5.4, the data are supplemented by the measurement data published by (James, 1988) and used for own curve fitting. It should be noted that the species Douglas fir, despite its common name, is not considered a true fir (*Abies*) (Meier, 2023).

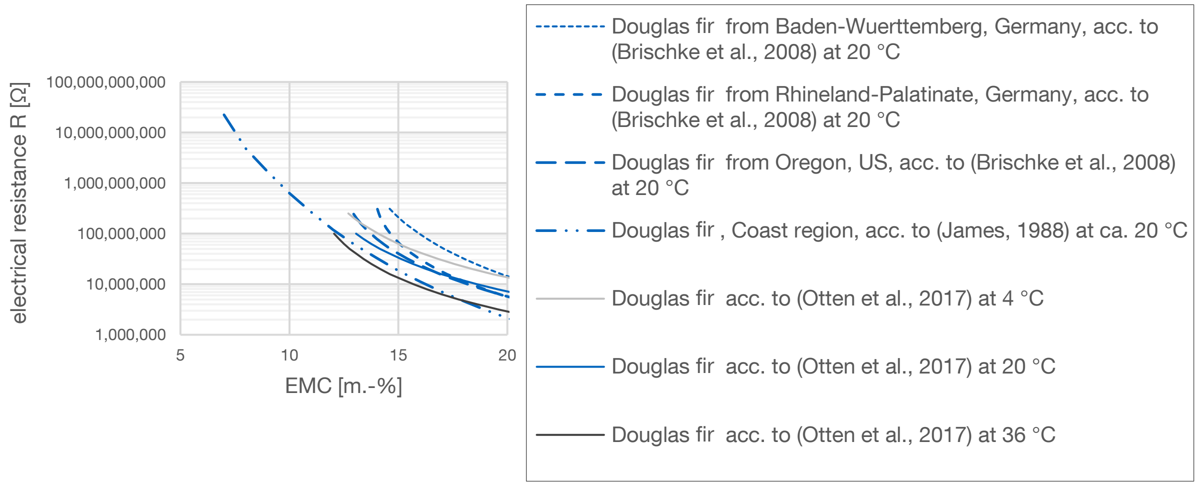

Figure 18: Calibration curves from various publications for different temperature levels of Douglas fir (Pseudotsuga menziesii Franco)

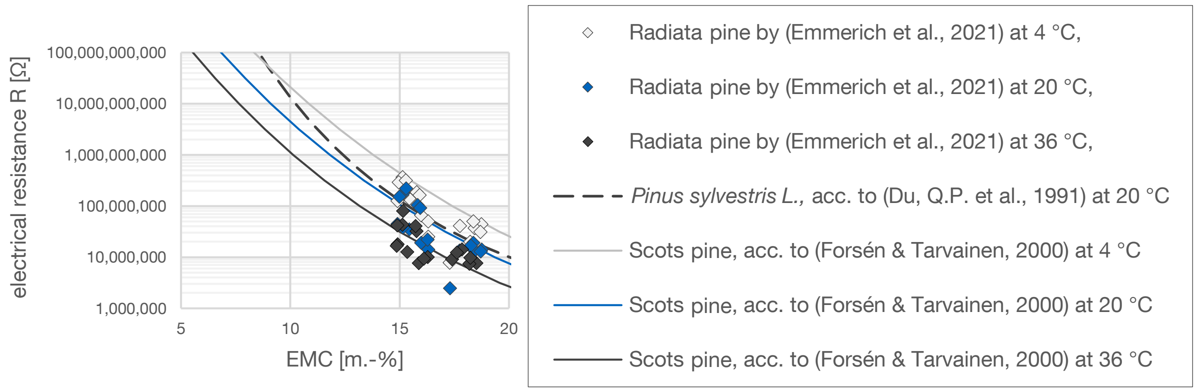

Figure 19: Calibration curves from various publications as well as single measurements for different temperature levels of radiata pine (Pinus radiata D. Don.) and Scots pine (Pinus sylvestris L.)

In order to broaden the data base for investigations on radiata pine (*Pinus radiata D. Don*), the existing data for Scots pine (*Pinus sylvestris L.*) are also used, cf. Figure 19. Despite the fact that both belong to the pines-group, it is important to distinguish between these two wood-species. The former is a subgroup of the yellow pines that grows fast, especially in the sub-tropics such as Australia and Chile. The latter belongs to the red pines, which can be found in the European and North American colder zones. (Meier, 2023)

(Emmerich & Brischke, 2021) conducted measurements on radiata pine at the three different temperature levels 4 °C, 20 °C, and 36 °C, but only in the *MC* range of 15 m.-% and above. Therefore, the data for Scots pine are additionally used for the drier wood moisture ranges. The data collection is used for a separate curve fitting for radiata pine for further application in Subsection 5.4 / Appendix D.

3.3 Approaches for moisture monitoring in timber construction

3.3.1 Overview of various ideas for smart moisture monitoring

In the context of building construction, there are various methods for moisture monitoring, which can be categorized into two major groups: single point measurements at certain locations and laminar measurements covering the whole element (Grönquist et al., 2022). In order to analyze the varying wood moisture contents in single points at different depths of a timber element, the sorption method (Subchapter 3.3.2) and the electrical resistance method (Subchapter 3.3.3) are commonly suitable. For a brief overview, examples for other methods, some of which are still being developed, are collected and summarized in Table 7.

Table 7: Developments for moisture analysis in or on timber and below fiber saturation by handheld devices, in-line production, in-situ monitoring, or leakage detection

Underlying principle	Measurement method	References / examples
anisotropy of wood when shrinking and swelling	Bilayers of two wood sections with different grain direction show different geometric responses to changes in relative humidity.	(Hielscher, 2022) (Informationsdienst Holz, 2022)
increased electrical conductivity on surface of moist/wet material	A special tape printed with two meandering conductive lines will decrease in electrical resistance when wet.	(holzbauaustria, 2021)
	Two closely meandering lines containing conductive graphite are printed next to each other directly on wood.	(Holzforschung Austria, 2023)
increased electrical conductivity in moist wood	Common electrical resistance measurements are in glulam but with the electrodes within two different glue lines.	(Uwizeyimana et al., 2020)
dielectric constant of a polymer changing with humidity	The frequency shift and the intensity variation of the resonance peak of RFID (radio-frequency identification) tags are used to detect variations in relative humidity.	(Mulloni et al., 2024)
dielectric constant of wood changing with moisture content	*Moisture content of a piece of sawn timber – Part 3: Estimation by capacitance method*	(EN 13183-3:2005)
	GPR (ground penetrating radar) is used as a more precise method to measure the transmitted or reflected frequency between sender and receiver of microwaves, which correlates with the material´s dielectric properties (permittivity) and thus with its moisture content.	(Rodríguez-Abad et al., 2010) (Mai et al., 2015) (Razafindratsima et al., 2017)
absorption/reflection and scattering of constant radiation in the visible/infrared range changing with wood properties	NIRS (near infrared spectroscopy) is used to detect changes in wood properties in production processes such as drying.	(Leblon et al., 2013) (Kobori et al., 2013) (Kobori et al., 2015)
	IRT (Infrared thermography) is used to illustrate these changes on a broad surface by comparing shots.	(Barreira & Almeida, 2015) (Dafico et al., 2022)
cobalt chloride ($CoCl_2$) changes color when hexahydrate (with more humidity)	The colorimetric technique could be used on wooden surfaces. Moist wood treated with $CoCl_2$ shows a red hue which turns into blue-green when dryer.	(Yeo et al., 2002)
under a constant magnetic field, the atomic nuclei absorb and emit alternating electric fields depending on the volume fraction of water	NMR (nuclear magnetic resonance) and MRI (magnetic resonance imaging) are used to determine the nuclear magnetization, which can be related to the volume fraction of water.	(Prado, 2001) (Rosenkilde & Glover, 2002) (Senni et al., 2009) (MacMillan et al., 2011)
attenuation of X-ray radiation when interacting with the material correlates with the material´s density	CT scanning (X-ray computed tomography) is used to measure the overall material density, from which the water content could be deducted once the wood´s oven-dry density of the respective section is known.	(Couceiro et al., 2019) *negative*

3.3.2 Use of the sorption method for moisture monitoring

The *sorption method (SM)* is also known as the *sorption isotherm method*, the *sorptive method*, the *bore hole method* (Li et al., 2018) or the *hygrometric method* (Flexeder, 2022). It utilizes laboratory measurements describing correlations between relative humidity of air *RH* [%], temperature *T* [°C], and wood moisture content *MC* [m.-%]. This relationship is usually based on sorption isotherms and used for various purposes such as technical wood drying, cf. Subchapters 3.2.1 and 3.2.2. The results are often referred to as *equivalent moisture content EMC*, a term that will be used in this thesis accordingly. Consequently, the computed values for *EMC* [m.-%] by this indirect method might differ from the actual moisture content *MC* [m.-%] that is obtained by the oven-drying method (EN 13183-1:2002).

The smaller the systematic deviations, the better the accuracy of the monitoring method. The standard for *Conservation of cultural heritage – Methods of measurement of moisture content, or water content, in materials constituting immovable cultural heritage* (EN 16682:2017) specifies the sorption method with a bore-hole as a "relative" method, whereas the gravimetric method is considered "absolute". It notes that the relative humidity in the cavity can be influenced not only by the *MC* of the material but also by any salts contained in the material, for example when used in masonry. The possible presence of soluble salts is only irrelevant until the *RH*-threshold-value for the deliquescence of salt is reached. Above this point, the deliquescent salt begins to form a solution and would therefore keep the equilibrium *RH* constant (EN 16682:2017, B.4.1). The standard does not explicitly explain to what extent the method is suitable for wooden components treated with protective salts. There might be a need for further clarification on this issue. Another limitation is the susceptibility of capacitive RH-sensors to permanently high humidity levels (> 80 %RH), as the moisture absorption by the polymer carrier material can falsify the measured values (EN 16682:2017, B.4.5). The high humidity can alter the dielectric properties of this material and especially excess water condensing on the sensor can cause a drift to higher values as well as longer reaction times, ultimately leading to a systematic error (Ingleby et al., 2013). A brief overview on methods and equipment for measuring relative humidity of air is included in the standard for *Conservation of cultural heritage - Procedures and instruments for measuring humidity in the air and moisture exchanges between air and cultural property* (EN 16242:2012). It describes various techniques and specifies how *RH* [%] can be measured directly or calculated from air temperature, wet bulb temperature and dew point temperature. It also contains recommendations for accurate measurements of ambient conditions and moisture exchange between the air and hygroscopic materials, with a special focus on valuable cultural assets.

In a broader context, the sorption method is also already used in technical timber drying using a so-called stab hygrometers or lay-on hygrometers. Either a perforated probe is inserted or an open flat container is placed on the wood. If the relative humidity is still measured analogously via the change in length of a hair, this is then called a "hair hygrometer" (Trübswetter, 2009, p.38). In the context of this thesis, the sorption method is used to obtain information about the moisture gradient in various depths of the timber component. Figure 20 illustrates how a combination sensor measures the relative humidity *RH* and temperature *T* of a small amount of air enclosed in a little space within the hygroscopic material. In order to ensure that the measurement in this climate cavity is only determined by the surrounding material, it needs to be sealed tightly, cf. methods in Subchapter 4.4.2.

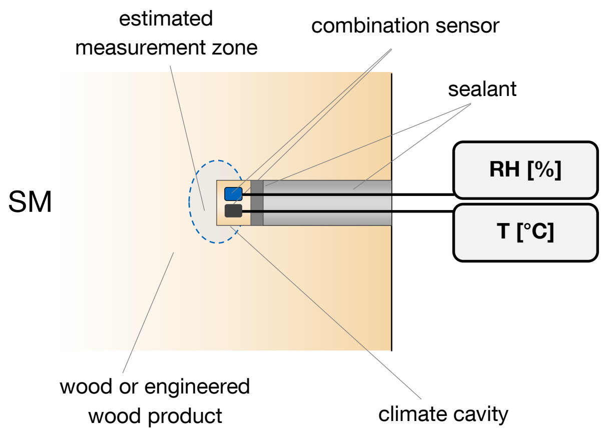

Figure 20: Scheme for wood moisture monitoring using the sorption method (SM), adapted from (Grönquist et al., 2022; Palma & Steiger, 2020)

Several monitoring projects use this concept to measure *RH* and *T* in wood and then calculate to an equilibrium moisture content *EMC* [m.-%] by still using historical sorption data. For example, (Wacker et al., 2007), (Koch et al., 2016), (Ganster et al., 2019), (Schiere et al., 2021a, 2021a, 2021b), (Dorn et al., 2022), (Flexeder, Schenk & Aondio, 2022), (Larsson et al., 2022), (Sieder et al., 2022), (Ghazi Wakili et al., 2024), all utilize variations of equation (3.4), cf. Subchapter 3.2.1, but without accounting for a possibly different wood species than Sitka spruce (*Picae sitchensis Carr*.).

Since equation (3.4) is mainly known through its publication in the wood handbook by the Forest products Laboratory (Madison, WI, USA), Dyken & Kepp (2010) refer to this approach as the "Madison tests". They briefly discuss the fact that employing this equation does not fit their results from laboratory testing, specifically under changing temperature. They suspect that the differences stem from the fact that equation (3.4) is intended for small wooden specimens influenced by a large surrounding volume of ambient air. On the contrary, the sorption method investigates a very small volume of air that depends on a relatively large surrounding volume of wood. They therefore develop new equations based on their laboratory measurements with humidity sensors mounted into specimens of ´Nordic´ pine (*Pinus sylvestris L.*). Their experiments at different temperature levels confirm that their new equations show a better fit than using equation (3.4). However, they do not actually prove that this improvement is due to their hypothesis about the impact of volume ratios. (Dyken & Kepp, 2010)

Melin et al. (2016) also used the sorption method for laboratory measurements with Scots pine (*Pinus sylvestris L.*). For the conversion, they used the sorption isotherm data from spruce by Hedlin (1968) and found great deviations when comparing their results with electrical resistance measurements (Hedlin, 1968; Melin et al., 2016). Fortino et al. (2021) choose a different approach by using the Anderson-McCarthy model to account for temperature-dependent sorption isotherms. However, they do not specify whether the employed parameters are fitted to the respective wood species (Fortino et al., 2021).

3.3.3 Use of electrical resistance measurements for moisture monitoring

The electrical resistance method (ERM) utilizes laboratory measurements describing correlations between electrical resistance *R* [Ω], temperature *T* [°C], and wood moisture content *MC* [m.-%].

Consequently, all results that are acquired with this method can only be as accurate as the calibration curves on which they are based. Although the values resulting from the conversion of electrical resistance and temperature are often simply referred to as "*MC* measurements", this thesis departs from this practice. The following chapters distinguish between the terms based on whether a direct or indirect method is used. In analogy to the sorption method, the results obtained from an indirect method are referred to as "equivalent moisture content" (*EMC*) to indicate that these results are actually only calculated on the basis of calibration curves. Hence, depending on the method and technique used, the results for the value *EMC* might differ significantly from the actual moisture content (*MC*), which in this work is determined exclusively by the oven-drying method (EN 13183-1:2002).

Wood moisture monitoring using the electrical resistance method (ERM) is based on the standardized procedure for estimating the moisture content of a piece of sawn timber using an electrical resistance meter (EN 13183-2:2002). In contrast to the standardized single measurement, repetitive measurements, for example in a fixed cycle, are used on electrodes remaining in the wood.

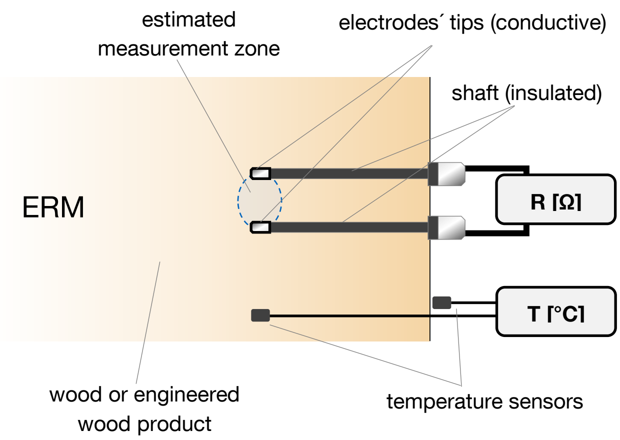

Figure 21: Scheme for wood moisture monitoring using the electrical resistance method (ERM), adapted from (Grönquist et al., 2022; Palma & Steiger, 2020)

Figure 21 shows a typical setup with two insulated pair electrodes, where only the tip at a defined measuring depth is conductive. However, uninsulated electrodes are also used, which then measure over their entire length. Both, rammed-in electrodes with a smooth shaft, similar to a nail with a thickened head, and screwed-in electrodes are common. There are also approaches to simply glue the connection cables directly into place using conductive paste. The investigations in Chapters 4 and 5 will compare these different electrode geometries more in-depth. Since the electrical resistance of wood is dependent on temperature, this value needs to be recorded as well.

In order to investigate a local gradient, several pairs of electrodes can be inserted into the component at the same time for monitoring purposes in different depths. Like this, electrical resistance measurements are already being used for monitoring in various cases, such as in the project *Timberbrain*, cf. Figure 22, Figure 23, and Figure 24.

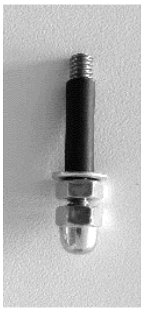

Figure 22: Electrode with galvanized steel thread

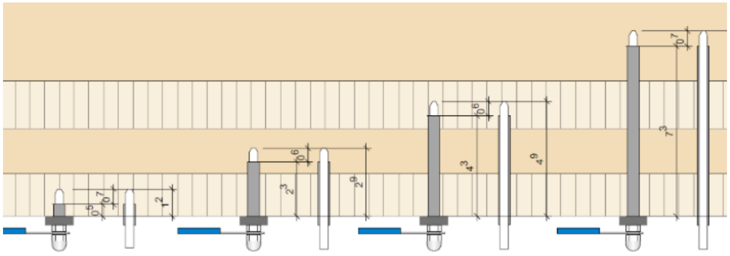

Figure 23: Section of the schematic construction plan (cross-section) of the electrode pairs for the electrical resistance measurements in the monitoring project in the Timberbrain building. The orientation of the electrode pairs is based on the fiber direction of the cross laminated timber lamella at the respective measurement depth.

Figure 24: Interior view of the examined cross-laminated timber wall with the inner heat flux measuring plate and eight pairs of electrodes each

Furthermore, the electrical resistance method (ERM) is quite popular for in-situ monitoring campaigns of large-span timber structures such as beams and columns (Fernando et al., 2015; Kordziel et al., 2019), wide-span roof structures (Bunkholt et al., 2021a; Dietsch, Gamper et al., 2015; Gamper et al., 2013; Jiang et al., 2018), or timber bridges (Björngrim et al., 2016; Fortino et al., 2013; B. Franke et al., 2016; B. Franke et al., 2013; Koch et al., 2016; Schiere et al., 2021a, 2021a, 2021b; Tannert et al., 2011; Wacker et al., 2007).

However, in the majority of these projects, the method is being employed without comprehensive verification of its accuracy over time. Doubts about its applicability primarily arise from the question of whether the technique, which according to the standard is intended for a single measurement after the electrodes have been freshly driven in, is altered by leaving the electrodes in place permanently. Moreover, there might also be more inconsistencies in relation to a temperature gradient.

3.3.4 Systematic wood-independent influences on electrical resistance measurements

In general, the systematic errors due to the measurement setup used, which are independent of the measured wooden component, shall always be taken into account when measuring electrical resistances (Klähn, 2023). Thus, the total resistance measured by a resistance meter is comprised of several individual resistances which could have varying values based on factors such as ambient temperature.

Conventional devices for measuring electrical resistance to determine moisture generally work with direct current (DC). Repeatedly applying the same voltage to one of the two pair electrodes can lead to various electrotechnical phenomena in the material (e.g. displacement polarization, orientation polarization, capacitance formation as a dielectric, ion accumulation). In this thesis, these effects will only be examined in the context of practical applications in monitoring of timber construction. More in-depth investigations of these topics can be found in: (Jakes et al., 2020; Norberg, 1999; Torgovnikov, 1993; Welsh, 1978; Zelinka et al., 2008).

Although initial attempts to use alternating current (AC) for electrical resistance measurements in wood show promising first results (Casans Berga et al., 2019), this technique is not yet established. DC measurements are therefore solely used for the investigations in this thesis.

Figure 25 shows a typical setup for resistance measurements on a wooden component with regards to the partial electrical resistances of the overall measurement set-up. Here, the representation of the evaluation electronics has been greatly simplified; a more detailed approach can be found in (Straube et al., 2002).

The resistance R_W, which correlates with the wood moisture content *MC*, represents the value of interest for the back calculation using the electrical resistance method (ERM). Other resistances to be measured are both internal to the device (R_M and R_V) as well as external. Those resistances, of the electrodes R_E or of the cables R_C, change with varying length of these items. R_T represents the electrical contact resistance at the transition between electrode and wood and can depend on the contact pressure.

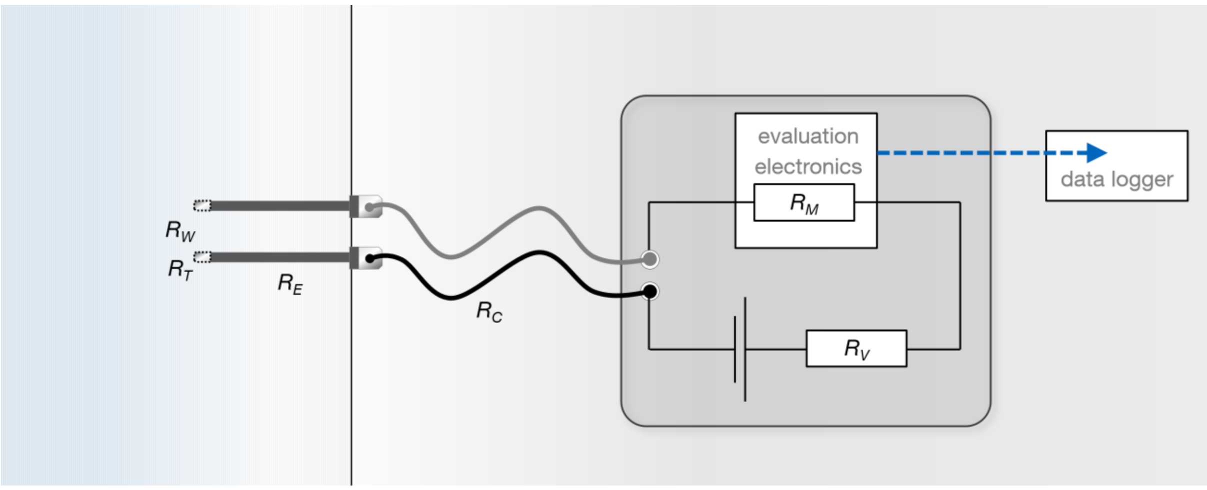

Figure 25: Scheme showing typical set-up for electrical resistance measurements in wood, typical characteristics of thermal gradients. (own illustration, circuit based on (Klähn, 2023).

The specific electrical resistance of any material is generally temperature-dependent, whereby the behavior under the influence of temperature varies from material to material. Consequently, all partial resistances of the overall system would have to be examined for their impact on the overall resistance, including the influence of temperature.

In this subchapter, the individual partial resistances of typical materials for electrodes and cables are calculated with characteristic values and classified according to their relevance for the overall resistance. Electrodes are usually made of stainless steel, yet there are approaches with galvanized steel or composites containing graphite powder, cf. Subchapter 4.2.5. Conductive elements within the device and cables are usually made of copper (oftentimes tin-plated).

The following material properties are taken from the Handbook of Chemistry and Physics, a comprehensive work of reference (*CRC Handbook of Chemistry and Physics*, 2012). The material properties listed in there are given by various authors in different units. Therefore, the values for electrical resistivity ρ_{el} in this subchapter will be provided as both, values converted into Ωcm, as well as the original quotation (in brackets).

The electrical resistivity of copper (Cu) is generally very low. At room temperature (around 20 °C), it is specified at $\rho_{el} = 1.678\ 10^{-6}$ Ωcm ($1.678\ 10^{-8}$ Ωm) and increases with increasing temperature (*CRC Handbook of Chemistry and Physics*, 2012).

The material properties of stainless steel depend on their alloy type as well as other factors such as heat treatment. For instance, the electrical resistivity for stainless steel, type 304, at an ambient temperature of 0 °C - 25 °C, is listed as $\rho_{el} = 72\ 10^{-6}$ Ωcm (72 µ Ωcm) (*CRC Handbook of Chemistry and Physics*, 2012).

The electrical resistivity of graphite dust also depends on the exact material composition. The authors specify values of $\rho_{el} = 1.47\ 10^{-3} - 30\ 10^{-3}$ Ωcm (1.47 – 30 m Ωcm) with a typical temperature correction factor of - 5 10^{-4} °C^{-1}, and thus a lower resistance with higher temperatures (*CRC Handbook of Chemistry and Physics*, 2012).

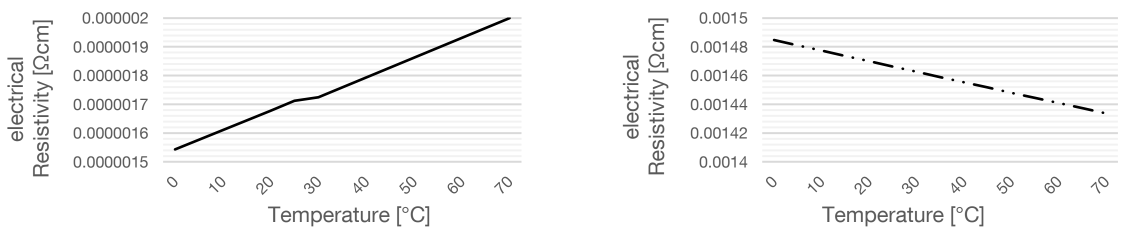

Figure 26: Electrical Resistivity [Ωcm] of copper (left) and graphite (right) in relation to temperature [°C]. Graphs are derived from information compiled in (CRC Handbook of Chemistry and Physics, 2012).

At higher temperatures and therefore stronger atomic vibrations, the electrons in carbon detach from their site and become free charge carriers. However, if the atomic hulls are more densely packed as in metals, the movement of the free electrons is more strongly hindered by the thermal motion of the atoms. Thus, unlike stainless steel or copper, whose electrical resistance increases with temperature (PTC thermistors), the electrical resistance of NTC thermistors such as graphite decreases with temperature (*Fachkunde Elektrotechnik*, 2012, p. 39).

This means that the electrical resistance of the assemblies with stainless steel electrodes increases with increasing temperature as opposed to those with graphite components, where it decreases, cf. Figure 26. Due to this contrast, a separate curve for temperature compensation depending on the electrode material theoretically would be necessary.

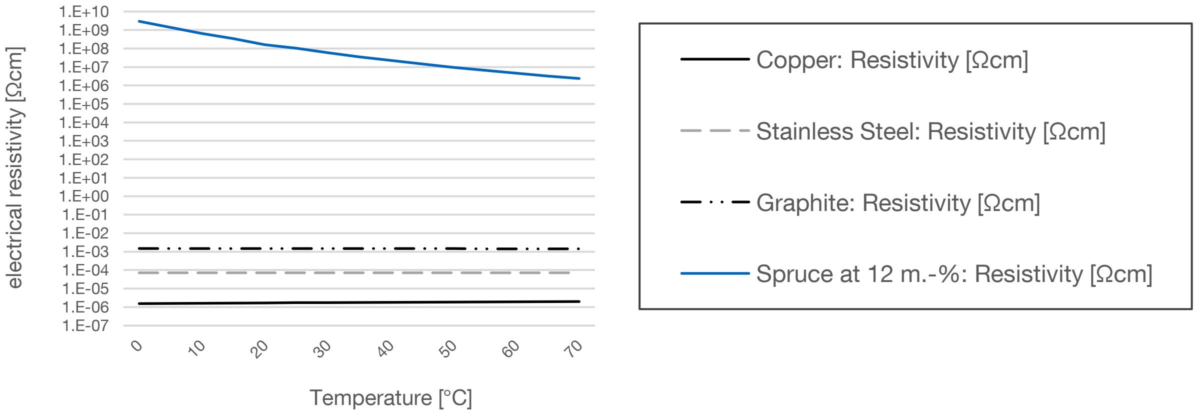

Figure 27: Values for electrical resistivity ρ_{el} of metals and graphite in relation to wood, plotted in a logarithmic scale. The graph for temperature-dependent electrical resisitivity of spruce is calculated based on a typical set-up with pin-type electrodes at a 30 mm distance, the calibration curves for spruce by (Du et al., 1991) and temperature compensation published by (Skaar, 1988).

However, Figure 27 shows that the temperature compensation for the system (electrodes and cables) is considerably lower than that for wood with a typical moisture content of *MC* = 12 m.-%. The influence of the varying behavior of the supporting materials such as copper, stainless steel and graphite dust is therefore estimated to be negligible. Consequently, instrument-specific calibration curves for temperature compensation can be omitted. The temperature influence on the result of the electrical resistance measurement is rather influenced by the characteristics of the measured material such as wood. Therefore, the following Subchapters 4.3.3, 5.2.3, and 5.2.4 only deal with the methods for temperature compensation in different wood species or wood products.

4 METHODS TO IMPROVE THE TECHNIQUES FOR MOISTURE MONITORING

4.1 Theoretical estimation of sensitivities in steady-state and transient models

4.1.1 Method for regression analysis

Subsection 4.1 introduces equations (4.a) – (4.d), which are describing general approaches that are used for the investigations in this thesis.

Regression analysis was used to match the models presented in the following Subchapters with the measured data collected. For this purpose, the optimal numerical values for the respective parameters corresponding to the minimum sum of squared deviations were employed (least squares method). The solution for these nonlinear models was calculated using the generalized reduced gradient method. The normalized root mean square error (*NRMSE*) was calculated as a measure of the quality of the respective regression analyses, similar to the methods used in (Shi & Avramidis, 2017b). The lower the value of *NRMSE*, the better the overall fit of the fitted curve to the measurement data:

$$NRMSE = \frac{\sqrt{\frac{\sum_{n=1}^{i}(m_i - m_{pi})^2}{(n-1)}}}{\frac{1}{n}\sum_{n=1}^{i} m_i} \tag{4.a}$$

With

m_i	measured value at the ith evaluation data point
m_{pi}	predicted value at the ith evaluation data point
n	total number of evaluated data points

Equation (4.a) was used in any approach in Subsections 4.3 and 4.4, where new parameters for a given equation are generated by fitting the model to an array of measurement data.

4.1.2 Measures to account for scattering of natural material parameters

The material parameters of solid wood are naturally variable and depend on factors such as wood species, density, tree origin, and annual ring width. The intended use determines the extent to which detailed investigation and determination of these parameters for monitoring applications is feasible in practice. In addition, there might be other variables in the overall measurement system whose influence exceeds these material parameters, cf. Subchapters 4.2.1 - 4.2.5. Wood species, grain direction, and density distribution are input parameters that can be practically determined from a random sample or the manufacturer's data sheet. The exact origin, e.g. the original forest´s orientation, is usually no longer easily traceable in a large-scale industrial production. The annual ring width of deeper layers can also no longer be determined non-destructively, although these might influence the results of the electrical resistance measurement.

Accordingly, the calibration curves in this thesis were investigated separately by wood products, wood species and measurement directions. Additionally, the oven-dry density ρ_0 is measured after oven-drying to a moisture content of *MC* = 0 m.-% and included in the evaluation. In order to assess the spread of this material parameter within the same batch, the standard deviation *SD* was used. It measures how far the respective values scatter around the mean value (average), with a greater value indicating a broader range and less homogeneity.

$$SD = \sqrt{\frac{\sum(x - \bar{x})^2}{(n-1)}} \tag{4.b}$$

With

x	Value of the individual sample
$\bar{x}$	Sample mean
n	total number of evaluated samples

For comparative studies such as in Subchapters 4.6.1 - 4.6.4, the samples were presorted by weight in advance in order to obtain a density distribution that is as representative as possible.

In some cases, where highly fluctuating data needed to be presented in a cleaner way, the simple moving average SMA was used. However, most of the data in this thesis was not altered in order to not disguise any effects. If curve smoothing by SMA was used as in Subsection 6.2, it was first checked for any effects and also clearly marked.

$$SMA\ (t_k) = \frac{1}{m} \sum_{J=0}^{m-1} x(t_{k-j}) \tag{4.c}$$

With

$x(t_k)$	Value of the individual sample at a certain time t_k
m	Number of time steps that are averaged

4.1.3 Estimation of expected results by means of hygrothermal simulation

Hygrothermal simulation studies using the software WUFI (“Wärme Und Feuchte Instationär”) were used to accompany and prepare the experiments. The simulation tool is based on two governing equations following Fourier´s and Fick´s laws (Künzel, 1994). More details are presented online in the literature collection provided by the Fraunhofer Institute (Fraunhofer IBP).

The attempts to monitor the moisture content in the exterior cross-laminated timber walls of the *Timberbrain* revealed unusual amplitudes in the diurnal rhythm, especially in the strongly irradiated west-facing outer wall, cf. Subchapter 2.4.3. Therefore, a transient hygrothermal component simulation was conducted for individual layer depths based on measured indoor and outdoor air temperature and relative humidity values. Where possible, individually measured material parameters were used. If the necessary material parameters were unknown, they were estimated using literature values. The comparison between transient hygrothermal simulation and *EMC*-values based on the conventional electrical resistance method (cf. Subchapter 2.4.3) resulted in correlating curve shapes with distinct differences, cf. Figure *28*.

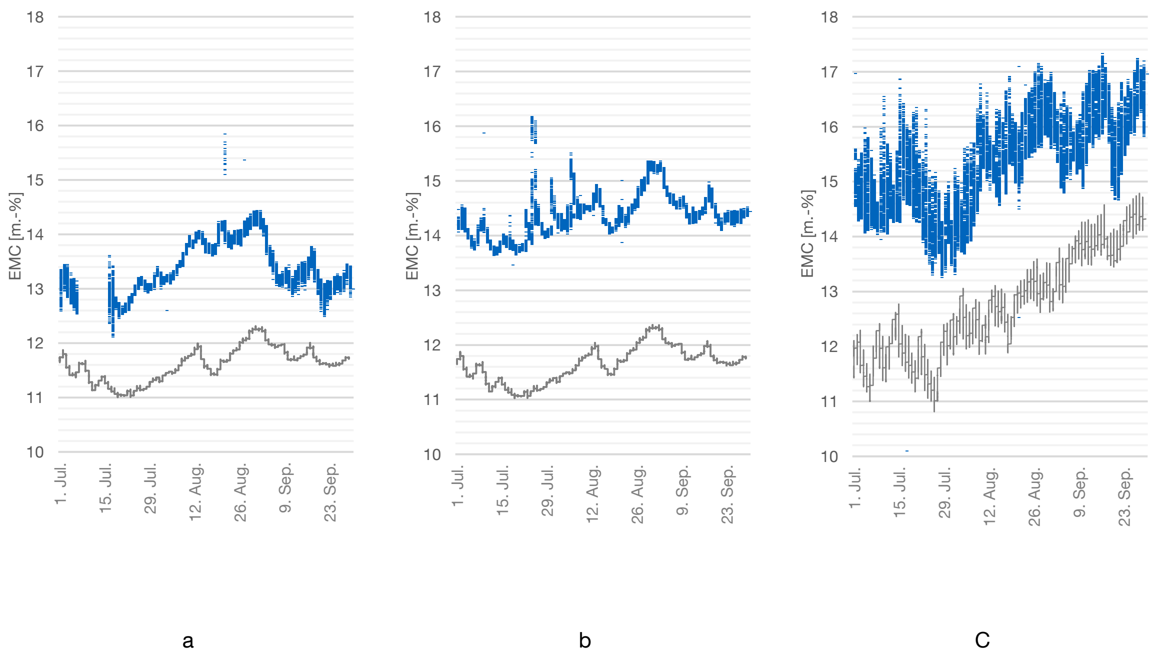

Figure 28: Exemplary comparison of measurements based on the electrical resistance method with a conventional evaluation (blue) and hygrothermal simulation (black) in the exterior walls at different depths, in each case for summer of 2019. Diagram (a) shows the results from the west-facing wall at a depth of 5 mm, diagram (b) from the north-facing wall at a depth of 5 mm, and diagram (c) from the north-facing wall at a depth of 219 mm.

Accordingly, hygrothermal simulations can provide guidance on overall tendencies in realistic scenarios. The methods used for these simulation studies are considered state of the art and will therefore not be explained further.

However, Subsection 5.4 of this thesis covers more in-depth topics, which cannot be simulated with conventional WUFI Pro models as they do not include certain physical phenomena. In order to continue using the simulation tool, the following modifications shall aid to approximate a suitable model on a provisional basis:

1. The model does not provide a term to account for varying air velocities and their influence on the sorption rate. Since the air movement at the surface impacts the moisture flux and hence the overall moisture content, a work-around is described, tested, and discussed in (Flexeder, Nouman & Hepf, 2022). The effects can be modeled by modifying the surface conditions with an additional thermal transfer resistance [(m²K)/W] and adjusting the vapor transfer resistance at the surface by converting it to an equivalent s_d-value. This method uses the experimental findings by (Worch, 2004), which are adapted fixed values in WUFI Pro simulations, cf. Table 8.
   These were used for the simulations presented in Subchapters 5.4.4, 5.4.5, and 5.4.6.

   Table 8: Values for heat and moisture resistance at the surface under different air velocities by (Worch, 2004), adapted to be used in a hygrothermal simulation with WUFI Pro (Flexeder, Nouman & Hepf, 2022)

Air velocity	0 m/s	1 m/s	2 m/s
Heat transfer resistance [(m²K)/W]	0.25	0.125	0.08
s_d-value [m]	0.015	0.00625	0.004

2. The model utilizes a fixed function for moisture storage only and does not account for sorption hysteresis. This issue also occurs when measuring wood moisture using the sorption method. Accordingly, the solution was using a simplified splitting curve, cf. methods in Subchapter 4.4.1.

3. Since the model utilizes only a fixed function for moisture storage, it does not account for the temperature dependency of sorption isotherms either. To address this limitation when investigating wood moisture changes after a sudden temperature rise, the simulation studies presented in Subsection 5.4 each used two input parameter sets. For this purpose, the first part of the simulation was calculated with a different sorption isotherm than the second. To transfer the final results from the first simulation to the next, the wood moisture content was first calculated in thin layers and then used as new input parameters in the second simulation.

Issue 1 could also be solved by using another simulation model such as the Fourier-Fick-analogy (Flexeder, Nouman & Hepf, 2022; Schaffrath, 2015). For instance, (Çolakoğlu, 2009) chose this approach in modelling only mass transport in Ansys finite element analysis to compare the drying time of eight different wood species. However, this approach would have disabled the calculation of any coupled enthalpy effects, which is crucial for the investigations in this thesis.

Regarding issues 2 and 3, studies have already investigated how a hygrothermal model could be extended to include a hysteresis and temperature-dependent sorption function (Rode & Clorius, 2004; X. Zhang et al., 2016a, 2016b). Nevertheless, these ideas have not (yet) been implemented in the regular WUFI software.

4.2 Investigation on the influencing factors in monitoring using the electrical resistance method

4.2.1 Overview of investigations of the influences on electrical resistance measurements

For the investigations on the electrical resistance method (ERM) within this work, physical variables were measured in the SI units Ampere [A] and Kelvin [K]. They are given as electrical resistance *R* [Ω] and temperature *T* [°C], which are converted directly from these. From these raw data, the subsequent derivation of an estimated equivalent wood moisture content *EMC* in mass percent [m.-%] = [g/g] is then a main subject of this work. As a control measure, the wood moisture content *MC* [m.-%] was determined via gravimetric method, which means oven-drying at 103±2 °C until mass constancy is reached according to (EN 13183-1:2002). The experiments in this thesis used a precision balance (KERN KB 360-3N) with a readability and reproducibility of 0.001 g. Before the start of each experiment, the balance was checked and recalibrated using two standard calibration weights with 100 g and 200 g. The electrical resistance *R* [Ω] was either measured with monitoring devices with eight connection ports via BNC-plug each and a measuring range of at least 10^4 Ω - 10^{11} Ω (System I, Gigamodul Scanntronik), which were regularly connected to standard resistors for several hours and checked for accuracy. Or, as in Subchapters 4.3.2 and 4.3.3, the laboratory measurements were undertaken with a high resistance/low current precision electrometer (Keithley 6517B, with a sensitivity of 1 fA, >200 TΩ input impedance for voltage measurements). Unless specified otherwise, insulated electrodes made of stainless steel, with a length of 15 mm, and a thickened cylindrical head were rammed into the wooden specimens.

The results of the electrical resistance measurements can be sensitively distorted by electrical peculiarities of the system. These influences might lead to considerable misinterpretation of the measurement results and include (with respective Subchapter in brackets): increased resistance due to frequent application of a certain voltage (4.2.2), increased resistance due to insufficiently tight contacts or even loss of contact (4.2.3, 4.2.4) and increased resistance due to a different electrode material (4.2.5). Furthermore, the electrical resistance is dependent on commonly known factors that are due to the physical behavior of the actual wood specimen. These material-specific factors include: differences caused by characteristics of individual wood species (4.3.1), deviations of calibration curves within a wood species (4.3.2), and reduced resistance due to an increased measurement temperature (4.3.3, 4.3.4).

The impact of these influences was investigated in various experiments using solid wood specimens and wood-based materials as examples. The focus here was less on the creation of material-specific characteristic curves, but rather on the verification of individual theories and the identification of future research needs. The investigated models were taken from various sources. For better comparability in the context of this work, they had been modified to use the same units. It should be noted that equations (4.1)-(4.14) were not taken directly from the references mentioned, and thus might appear to be new approaches at first glance. However, the mathematical structures are the same as in the source publication. Thus, with the exemption of equation (4.7), there are no novel equations and also no novel models within the context of this work, but only adaptions with mathematical transformations.

4.2.2 Investigation of the influence of the applied voltage for high-ohmic measurements

The measured electrical resistance value R [Ω] is composed of several parts, cf. Subchapter 3.3.4. These include the actual resistance of the wood section between the electrodes R_W and the contact resistances at the electrode - wood contact R_T.

In contrast to the setup shown in (Niemz, 2021; Riedel & Walter, 1989) with a voltage electrode, a protected electrode and a guard-ring-electrode, a simplified setup with two rammed-in electrodes was used for the experiments in this thesis. DC voltage U [V] was applied to one of these two electrodes, the resulting direct current I [A] was measured at the other electrode, and converted to a total resistance R [Ω] based on the measurement voltage. For safety reasons and to ensure energy-saving operation with as few battery changes as possible, it is necessary to use at least a safety extra-low voltage, ideally $U < 10$ V DC for as little time as possible. For example, it would be plausible to apply a voltage of $U = 3.3$ V for 20 seconds and then derive a resistance value from this.

What influence does the level of the measuring voltage have on the result? How does the current flow and thus also the calculated resistance change during the measurement time; are 20 seconds at $U = 3.3$ V already sufficient to produce reasonably accurate results?

In order to investigate the error due to the use of this comparatively low measurement voltage with the relatively high electrical resistances in wood, 30 pre-conditioned specimens (Norway spruce, 50 mm x 50 mm x 50 mm, $\rho = 417$ kg/m³, $SD = 34$ kg/m³) were fitted with rammed-in pair of stainless-steel electrodes (15 mm). They were then examined at the following measurement voltages: 3.3 V; 10 V; 500 V.

For this preliminary testing, a high resistance/low current precision electrometer (Keithley 6517B, with a sensitivity of 1 fA, >200 TΩ input impedance for voltage measurements) was used in combination with a specially made shielded measuring box and specific evaluation software, cf. Figure 29. This laboratory set-up investigates the current intensity I [A] that can be measured over a certain time when a certain measuring voltage U [V] is applied at a wooden specimen. The total electrical resistance $R_{20\,sec}$ [Ω] was then derived from the current $I_{20\,sec}$ [A] finally after 20 seconds:

$$R_{20\,sec} = \frac{U}{I_{20\,sec}} \tag{4.d}$$

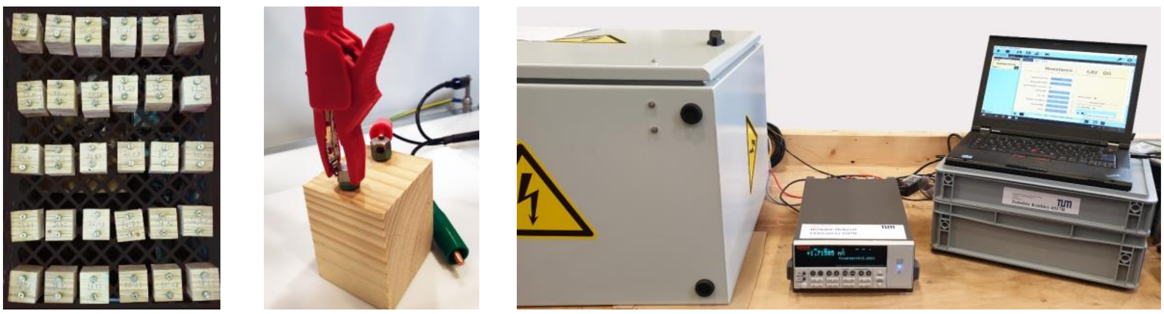

Figure 29: Array of test specimens and experimental set-up for precise electrical measurements

4.2.3 Influence of bore hole width and geometry on contact pressure

In the context of electrical resistance measurements, stainless steel electrodes are often either rammed or screwed into the material in pairs with a fixed spacing, typically by first predrilling two holes with a reduced diameter. In general, the measured electrical resistance increases with decreasing contact pressure. In extreme cases, a disconnected contact will lead to a total loss of electrical conductivity. A significant decrease in contact pressure, for example due to changes in the geometry of the wood, would therefore lead to higher electrical resistance *R* [Ω]. This should be avoided, as it can lead to significant misinterpretation of the measurement result and underestimation of the actual wood moisture content.

What is the effect of the pre-drilled hole diameter on the electrical resistance between the two electrodes? How does R_T, the electrical contact resistance between electrode and wood, change with varying climate and how big is the overall impact on *EMC* [m.-%]?

For the investigation of the influence of this pre-drilling, electrodes with a thickened cylindrical head and insulated shaft (green Teflon lacquer) were rammed into the material, cf. Figure 31. This type of electrode is documented to be employed in several monitoring projects, for instance in (Gamper et al., 2013; Jiang et al., 2018). The tightness or looseness of the electrodes in the wood was checked periodically by carefully moving them by hand. The characteristic curve determined by (Du et al., 1991) for the correlation of electrical resistance and wood moisture content of spruce, including upper and lower confidence limits (95 %), was used to classify the measurement results. For the preliminary test, ten batches of three specimens each were manufactured from Norway spruce with the dimensions 50 mm x 50 mm x 50 mm. The specimens were preconditioned at 20±1 °C / 55±5 %RH over the course of six months. Their oven-dry density was later determined at ρ_0 = 417 kg/m³ with a standard deviation *SD* of 33.8 kg/m³.

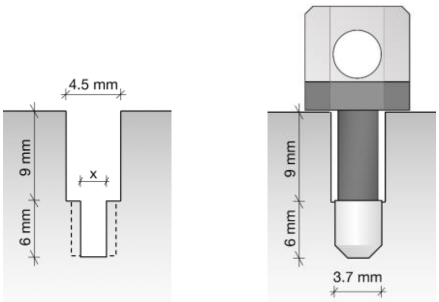

Figure 30: Cross section of predrilled holes and final fit of 15 mm rammed-in electrode

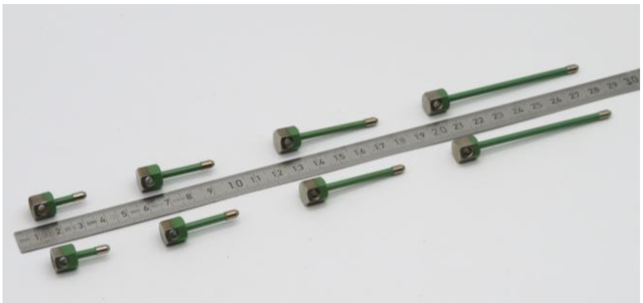

Figure 31: Pair electrodes to be rammed-in, in four different lengths of 15 mm, 25 mm, 40 mm, and 70 mm.

Each specimen was equipped with a pair of electrodes (length: 15 mm) for which two holes were drilled with a center-to-center distance of 30 mm (across the fiber). The upper section had a constant diameter of 4 mm, while the lower section had a variable diameter x to investigate the contact pressure on the conductive head of the impact electrode, cf. Figure 30. The following borehole diameters x (in millimeters) were investigated: 3.8 mm (A), 3.6 mm (B), 3.4 mm (C), 3.2 mm (D), 3.0 mm (E), 2.8 mm (F), 2.6 mm (G), 2.4 mm (H), 2.2 mm (I), and 0.0 mm (no hole, J), cf. Figure 32. The electrical resistance measurements were conducted using the precision electrometer (cf. Subchapter 4.2.2) and supplemented by manual checks of the mechanical resistance to rotation and possible withdrawal of the electrodes, as well as by regular precision weighing. By periodic weighing and checking the strength of the fit, correlations of the accuracy of ERM with the predrilled hole diameter were sought. The influence of the pre-drilled hole diameter on the value of equivalent moisture content *EMC* determined by electrical resistance measurements was thus verified by regular weighing with the precision balance and subsequent oven-drying according to (EN 13183-1:2002). The results were then compared with the calibration curve for Norway spruce described by (Du et al., 1991).

Based on these preliminary tests, series A, B, D, I and J were selected for the subsequent main test. In order to reduce an influence of the flanks on the electric field between the electrodes (Fredriksson et al., 2015), these batches were produced anew from Norway spruce with larger dimensions of 100 mm x 100 mm x 100 mm, cf. Figure 33. As with the specimens used for preliminary testing, those used for the main tests were also preconditioned at 20±1 °C / 55±5 %RH for a minimum of six months. Weighing with the precision balance was carried out between the individual steps to check for changes in the moisture content *MC*.

Figure 32: Specimens for the preliminary tests on bore hole width

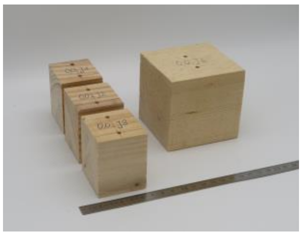

Figure 33: Specimen for the main tests next to three from the preliminary tests

Figure 34: Central piece of the main test series chiseled out by hand, shown as an example

Subsequently, the test specimens were subjected to an isothermal humidity change while connected to monitoring devices (3 x Gigamodul with eight outlets each, 3 x Thermofox). Tightly sealed containers with a solution of potassium acetate ($KC_2H_3O_2$) were used for isothermal drying, following the desiccator method according to the standard for the *Determination of hygroscopic sorption properties* (EN ISO 12571:2021). The specimens were positioned on a grid above the salt solution, with electrodes at the top. These were connected to the monitoring equipment via coaxial cables that pass tightly through the container wall. The test specimens of the main test were thus dried out over 290 days at 20±0.5 °C / 23±1 %RH isothermally until mass constancy, whereby the test specimens were briefly removed at intervals for individual weighing.

This was followed by isothermal humidification at 20±0.5 °C / 75±1 %RH over a sodium chloride (NaCl) solution for 12 days. Due to the moisture gradient, the final weighing and oven-drying could only determine the average total wood moisture content, but not the prevailing wood moisture content in the central piece between the electrodes. Consequently, when concluding the measurement series, a small section of wood was extracted from one specimen of each batch and weighed and oven-dried separately, as illustrated in Figure 34. For removal, machines with high heat generation were being avoided and instead a hand saw and a chisel were used. Furthermore, to prevent the introduction of extraneous variables, the corresponding workpiece was handled exclusively with gloves. In order to keep sorption processes as low as possible, the work was conducted as rapidly as possible (approximately two minutes from opening the desiccator, free chiseling, and sawing, to placing on the fine balance).

4.2.4 Investigating the pull-out resistance of electrodes for the electrical resistance method

Based on the measurement results on Norway spruce (cf. Subchapters 5.1.2 and 5.1.3), the investigation was extended to other, less well-studied wood species, with results in Subchapter 5.1.4. In order to more accurately quantify the contact pressure behavior of the pin-shaped stainless steel electrodes in the wood, the pull-out resistance was additionally being measured similarly to the methods described in (Yermán et al., 2021).

A series of withdrawal tests were conducted on Australian wood species in the laboratories of *The University of Queensland*, using an Instron Universal Testing Machine (UTM) with a 1 kN loadcell, cf. Figure 35.

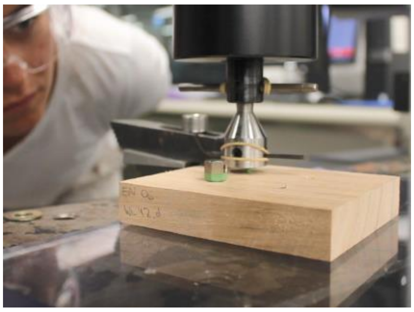

Figure 35: Electrode withdrawal testing with the Instron UTM on a specimen from shining gum.

Figure 36: Selection of four charges of specimens for ERM with pin-type electrodes. From left to right: 8 x radiata pine, 4 x shining gum, 4 x spotted gum.

For this purpose, equal sized test specimens were manufactured and then a total of 36 specimens was selected based on uniformity. The test specimens showed a great variety of oven-dry density ρ_0 with radiata pine (412 kg/m³, *SD* 12.2 kg/m³), shining gum (464 kg/m³, *SD* 17.2 kg/m³), and spotted gum (995 kg/m³, *SD* 57.2 kg/m³). All specimens were uniformly preconditioned at an ambient climate of 23±0.5 °C / 57±2 %RH until uniform moisture content (*MC*) is ensured through mass constancy. Once reached, they were then each prepared for the electrodes with two pairs of pre-drilled holes (diameter at the tip: 3.2 mm). The electrodes were rammed into the first pair of holes per specimen, cf. Figure 36. Subsequently, the specimens were further preconditioned at an ambient climate of 23±0.5 °C / 57±2 %RH.

The first series of measurements investigated low force withdrawal testing on a total of 48 electrodes under isothermal and isohumid conditions. The UTM measured the force required to pull the electrodes vertically out of the holes at a constant rate of 3 mm/minute with no change in the wood moisture content.

The second pull-out tests had the purpose of repeating the same test after a short drying period. For this second series of tests, the electrodes were first driven into the second pair of electrodes of each specimen under the preconditioned climatic conditions. After steady climatization at 23±0.5 °C / 57±2 %RH for over 65 days, the climate was then changed to a warmer and drier ambient climate (35±1 °C / 36±5 %RH) for a duration of 45 hours. The pull-out tests were then immediately carried out again using the same procedure as the first time, with care being taken to ensure that they are carried out as quickly as possible without disturbing the conditioning climate. The experiments were accompanied by periodic weighing with the precision balance and concluded by oven-drying according to (EN 13183-1:2002).

4.2.5 Variations of geometry and materiality to improve contact pressure of the electrodes

Many projects use conventional pair electrodes made of stainless steel that have a thicker head and a thinner shaft insulated with green Teflon lacquer. After predrilling a slightly smaller hole, these are then rammed into the wood, cf. Subchapter 4.2.3. The aim of this subchapter is to investigate the suitability of ideas for alternative geometries or conductive connections that could permanently improve the necessary contact pressure of the electrodes on the material. These initial preliminary tests help to identify further optimization possibilities.

In addition, project-specific dimensions are sometimes simply necessary, which require individual solutions. The associated change in the geometry of the electrodes should also be examined for their metrological deviations from the conventional rammed-in stainless steel electrodes. This comparison will be further elaborated as batch 11 vs. batch 12 in Subchapter 4.6.1. The electrodes installed in the monitoring project *Timberbrain* were made specifically for the project from galvanized threaded rods. Their uninsulated tips are screwed in pairs into a conical hole with a diameter of d = 3.5 mm for the tip and d = 5 mm for the shaft, cf. Subchapters 3.3.3 and 4.7.4. The situation is similar with the longer electrodes (120 mm, 150 mm, 175 mm, and 225 mm) that were installed in the research project *Einfach Bauen*, cf. Subchapter 4.7.3.

Previous investigations involving the application of weights to planar contact surfaces had indicated that the contact pressure of the electrodes on the wood could be enhanced by the use of conductive elastomers (Christ, 2020). Consequently, this thesis´ tests explore an alternative approach, where conventional stainless-steel electrodes were fitted with a prefabricated elastic ring of conductive silicone (specific electrical resistance of 5 Ωcm). Therefore, a slightly larger hole was drilled and the conductive rubber ring inserted first. Then the stainless-steel electrode was rammed in. Although the pressure was sufficient to hold the electrode, it sat relatively loose around the shaft so that it appeared to wobble. The extent to which this would limit possible applications in practice still needs to be investigated. For the first test, four batches, each with three identical specimens (Norway spruce, 50 mm x 50 mm x 50 mm), were preconditioned in a constant laboratory climate (20 °C / 35 %RH) for several weeks cf. Figure 37. After electrodes insertion, they were further conditioned. Then a monitoring device (System I, Scanntronik, Gigamodul) was connected, which measured the electrical resistance R [Ω] every 10 minutes. Additionally, the test involved two different batches of Norway spruce in order to also demonstrate variations that might occur within the same wood species.

Could the measurement setup possibly be simplified by omitting electrodes as an extra component? Instead, the necessary cable could be inserted directly into the wood with a conductive compound.

Figure 37: Schematics from left to right: Charge 1 with rammed-in electrodes, charge 1 with screwed-in electrodes, charge 2 with rammed-in electrodes, and charge 2 with rammed-in electrodes in a larger hole and with conductive silicone rings.

Consequently, as an alternative to rigid metal electrodes, various alternatives were being tested to improve the contact of the measuring system with the wood by using a conductive adhesive or silicone. For this purpose, different mixing ratios of conductive graphite dust and adhesive materials were being investigated (Figure 38).

Preliminary tests had shown: If the graphite content is too low, the electrical resistance turns out to be too high which creates another systematic defect. If the graphite content is too high, there is no sufficient bond after curing. Therefore, the bonding strength of the conductive and the insulating compounds to the wooden material was first tested in small trials, cf. Figure 40. For this purpose, coaxial cables were prepared with the tip stripped of its insulation by 5 mm. The holes in the material were pre-drilled with a diameter of 4 mm and a depth of 15 mm. In addition, conductivity was measured with a multimeter on 10 mm thick disks as retention samples, cf. Figure 39.

Figure 38: Equipment for mixing and injecting of graphite compounds

Figure 39: Commercially available multimeter for approximate measurements of conductivity

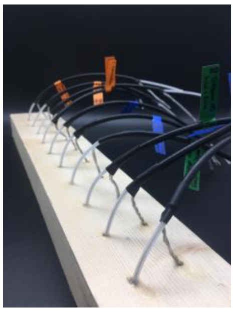

Figure 40: First functional test of various mixtures for gluing in electrodes

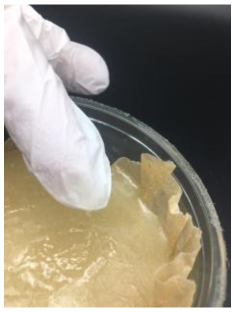

Figure 41: Thumb test on sample with insulation adhesive to check curing time

A conductive adhesive was prepared based on the mixing formula published in (Brischke et al., 2008), a two-component epoxy adhesive, as detailed in Table 21 in Appendix B, p. 235, cf. (1-4). In a separate approach, different formulations for silicone with graphite dust were tested. These are referenced as (5-10) in Table 21 in Appendix B, p. 235. Shortly after thorough stirring, these mixtures were injected with a narrow syringe directly around the conductive cable into the hole in the wood to a fill level of approximately 5 mm. The bond was then made by curing in situ. Finally, the remaining volume was filled with an insulating compound using mixing formulas as listed in Table 22 in Appendix B, p. 236. These compounds were tested also separately on their suitability as an insulating adhesive, cf. Figure 41.

In contrast to (Brischke et al., 2008), who used two polyamide coated stainless steel cables per pair of electrodes, only one coaxial cable per pair was used for the experiments in this work. The coaxial cable (RG 58 C/U 50 Ohm) was split at one end so that the core and shield could each be connected to an electrode. This cable configuration aligns with the setup observed in numerous other experiments and can be connected to the measuring instrument via a BNC connector. The conductive components are made of copper and protected by a thin layer of tin. Fredriksson et al. (2013) also used glued-in copper wires in their experiments, although the rest of the setup differs from the experiments described here (Fredriksson et al., 2013).

4.3 Improving the calibration curves for the electrical resistance method

4.3.1 Verification and adaptation of wood species specific calibration curves

There are already several approaches for the mathematical description of the correlation between measurable electrical resistance *R* [Ω] in wood and the correlating value of wood moisture content *MC* [m.-%], cf. Subchapter 3.2.4. Those approaches are described below that will be used for the subsequent evaluation in Chapter 5. Equation (4.1) was used by (Forsén & Tarvainen, 2000) on different wood species at a temperature of 20 °C and is based on an approach by (Samuelson, 1990). Grönquist et al. (2021) adapted this model for measurements in laminated veneer lumber (LVL) made of beech wood (*Fagus sylvatica L.*). Equation (4.1) can be solved for $X_{20\,°C}$, cf. Equation (4.2). Parameters *a* and *b* are listed as they appear in the original publications by (Forsén & Tarvainen, 2000) and (Grönquist et al., 2021), respectively.

$$\lg\left(\lg\left(10^{-6} \cdot R\right) + 1\right) = \left(-a \cdot X_{20\,°C}\right) + b \qquad (4.1)$$

$$X_{20\,°C} = \frac{b - \lg\left(\lg\left(10^{-6} \cdot R\right) + 1\right)}{a} \qquad (4.2)$$

With

R	Electrical Resistance	[Ω]
$X_{20\,°C}$	Equivalent moisture content at 20 °C, to be used as a base value	[m.-%]

	a	*b*	
Nordic pine (*Pinus sylvestris L.*) by (Forsén & Tarvainen, 2000)	0.039	1.061	-
Nordic spruce *(Picea abies Karst.)* by (Forsén & Tarvainen, 2000)	0.038	1.067	-
European beech *(Fagus sylvatica L.)* by (Forsén & Tarvainen, 2000)	0.046	1.119	-
BauBuche-S, beech LVL, perpendicular to grain, by (Grönquist et al., 2021)	0.07868	1.172	-
BauBuche—Q-Depth 1, beech LVL, perpendicular to grain, by (Grönquist et al., 2021)	0.07441	1.175	-
BauBuche-Q-Depth 2, beech LVL, parallel to grain, by (Grönquist et al., 2021)	0.07924	1.171	-

A more complex mathematical approach than this one, but possibly better suited to mapping the actual correlation between *R* and $X_{20\,°C}$, is the model by (Du et al., 1991).

Similar to the model mentioned above, the correlation in equation (4.3) is described by a double exponential (or logarithmic) function. However, there is an additional component in the model that also depends on $X_{20\,°C}$. This leads to a more complex structure and now four parameters *a* - *d*. Additionally to the parameters fitted for a variety of wood species, (Du et al., 1991) provided parameters for the confidence intervals associated with their measurement results in each wood species. It is therefore considered to be very sound. Equation (4.3) shows the original model and can also be written as (4.4).

$$\ln(R) = a \cdot exp^{(b \cdot X_{20\,°C})} + c \cdot X_{20\,°C} + d \tag{4.3}$$

$$R\ (X_{20\ °C}) = exp^{(a \cdot exp^{(b \cdot X_{20\,°C})} + c \cdot X_{20\,°C} + d)} \tag{4.4}$$

With

R	Electrical Resistance	[Ω]
$X_{20\,°C}$	Equivalent moisture content at 20 °C, to be used as a base value	[m.-%]

	a	*b*	*c*	*d*	
Norway spruce *(Picea abies Karst.),* by (Du et al., 1991)	28.59	-0.1350	-0.153	17.60	-
European beech *(Fagus sylvatica L.),* by (Du et al., 1991)	29.91	-0.1100	-0.037	12.31	-
Scots pine (*Pinus sylvestris L.*), by (Du et al., 1991)	34.06	-0.1350	-0.065	15.14	-

Solving equation (4.3) for the variable $X_{20\,°C}$ is necessary for use in wood moisture determination. However, it is relatively complex and would require several assumptions. A simplification of the model of (Du et al., 1991) could help here. If the parameter *c* is allowed to approach zero, the model could be greatly reduced to the following equations (4.5) and (4.6). This equation can then also be transformed analytically to equation (4.7) without difficulty. Since this is a new, simplified model, new parameters *f*, *g*, and *h* must be determined accordingly, using regression analysis.

$$ln(R) = f \cdot exp^{(g \cdot X_{20\,°C})} + h \tag{4.5}$$

$$R\ (X_{20\ °C}) = exp^{(f \cdot exp^{(g \cdot X_{20\,°C})} + h)} \tag{4.6}$$

$$X_{20\,°C} = \frac{1}{g} \cdot ln(\frac{ln(R) - h}{f}) \tag{4.7}$$

With

R	Electrical Resistance	[Ω]
$X_{20\,°C}$	Equivalent moisture content at 20 °C, to be used as a base value	[m.-%]

Parameters f, g and h are to be determined within the scope of this work.

The structure of the model just derived as model (4.7) would correspond to the same mathematical structure of a double logarithmic expression as in (4.2) after transformations. Therefore, the extent to which this simplified model is sufficient for wood moisture determination will be investigated. Accordingly, an initial data fitting in Subchapter 5.2.1 will examine to what extent this model can be used when fitted to the calibration curves created by (Du et al., 1991). How much accuracy is lost compared to the more complex model (4.3) when using the simplified model (4.7)?

4.3.2 Impact of choice of wood products and sample charges within the same species

The influence of different wood charges has already been indicated by preliminary testing described in Subchapter 4.2.5 with the results presented in Subchapter 5.1.5. The aim of the following experimental series is to elaborate the differences in electrical resistance measurements between two wood species as well as within the same wood species. For this purpose, the following variants are investigated, demonstrated, and compared in Subchapter 5.2.2:

- influence of different wood species
- different batches of the same wood species
- wood glue product versus the raw material of the same wood species
- influence of the measurement directions within the same batch

Figure 42: Four specimens of one batch of solid Norway spruce, electrodes driven in parallel to the grain

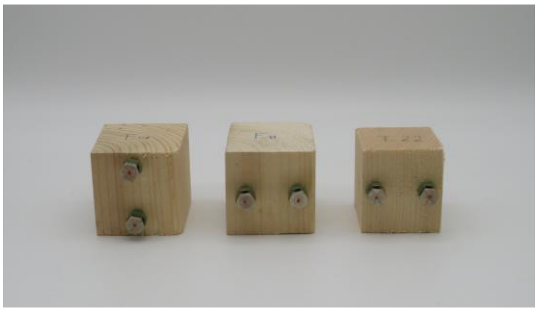

Figure 43: Three specimens of solid Norway spruce, each representing a different batch

Figure 44: Eight specimens of European beech, whole batch shown, with holes drilled in perpendicular to the grain

Figure 45: Spruce LVL, one specimen shown as a single example for each batch

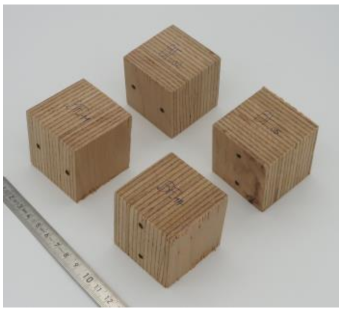

Figure 46: Beech LVL, one specimen shown as a single example for each batch

The study includes batches with differently inserted rammed-in electrodes in specimens of solid Norway spruce and solid European beech, as well as spruce laminated veneer lumber (LVL) and beech LVL. Each batch is represented by at least four specimens, cf. examples in Figure 42 - Figure 46. A total of 56 specimens were preconditioned at a constant climate of 20±1 °C / 55±5 %RH, weighed and fitted with rammed-in electrodes.

These pair electrodes were connected by coaxial cables with the measuring devices for electrical resistance and data loggers (System I, Gigamodul and Thermofox by Scanntronik) just outside the climate chamber. They measured the electrical resistance in a five-minute cycle and had been checked with standard resistors before the start of each experiment.

Table 9 shows the mean values for oven-dry density ρ_0, determined retrospectively at *MC* = 0 m.-%, and its standard deviation *SD*.

Table 9: Sample charges for ERM experiments on different wood species and wood products

	Oven-dry density ρ_0 [kg/m³] at 0 m.-%	*SD* of oven-dry density [kg/m³]	*MC* [m.-%], 1st series	*MC* [m.-%], 2nd series
Norway spruce (*Picea abies Karst.*), Charge 1	**460**	*63.2*	11.2	13.5
Norway spruce (*Picea abies Karst.*), Charge 2	**383**	*31.7*	11.3	14.0
European beech (*Fagus sylvatica L.)*	**615**	*5.5*	9.4	12.3
Spruce laminated veneer lumber (LVL made of *Picea abies Karst*.)	**650**	*10.5*	10.4	12.6
Beech laminated veneer lumber (LVL made of *Fagus sylvatica L.)*	**684**	*18.0*	9.2	11.5

The first series of measurements in the climate chamber took place while maintaining a constant wood moisture content at around 11.2 m.-% (Norway spruce, charge 1) / 11.3 m.-% (Norway spruce, charge 2) / 9.4 m.-% (European beech) / 10.4 m.-% (spruce LVL) / 9.2 m.-% (beech LVL), cf. Table 9.

The adherence to the mass constancy was being checked regularly and sample-wise by weighing with a precision scale (fine balance KERN KB 360-3N with a readability of 0.001 g and a reproducibility of 0.001 g). Once reached, this was followed by isothermal humidification at 20±0.5 °C / 75±1 %RH over a saturated NaCl-solution with conversion to mass consistency after 50 days (defined here as: weight change between at least three weighings 24 hours apart of no more than 0.1 %).

The second series of measurements in the climate chamber then proceeded with the maintenance of a constant wood moisture content of about 13.5 m.-% (Norway spruce, charge 1) / 14.0 m.-% (Norway spruce, charge 2) / 12.3 m.-% (European beech) / 12.6 m.-% (spruce LVL) / 11.5 m.-% (beech LVL), cf. Table 9.

The series of measurements were completed by oven-drying according to standard (EN 13183-1:2002) and a recalculation of the previously determined masses to wood moisture contents *MC* [m.-%].

4.3.3 Investigation of data post-processing for temperature compensation

Subchapter 3.2.4 already indicated the importance of temperature compensation for electrical resistance measurements in wood. In order to take the temperature dependence of the electrical conductivity of wood into account mathematically, there are several approaches, for instance by (Brischke & Lampen, 2014; Forsén & Tarvainen, 2000; Garrahan, 1988; Pfaff et al., 1985; Skaar, 1988; Straube et al., 2002). The methods of the mathematical approaches are presented below. The methods used for the laboratory measurements are discussed more in detail in Subchapter 4.3.4.

Straube et al. (2002) mention several approaches to temperature compensation for moisture contents below fiber saturation. According to their publication, a computational temperature compensation based on the species group should be possible. Their parameters distinguish between spruce, pine, and Douglas fir. Unfortunately, the computational verification of the equations mentioned therein resulted in ambiguities, so that these equations will not be further used in the context of this work. (Straube et al., 2002)

For clarity, only those calculation methods are presented below that are relevant for further processing of the experimental data in the following chapters. Equations (4.8)-(4.10) are based on a two-part approach. First, the measured electrical resistance and a calibration curve are used to determine the equivalent wood moisture content at a standard temperature (usually a value between 20 °C and 25 °C). If the actual temperature deviates from this, the first base value is then corrected by adding a temperature-dependent factor.

In order to simplify this procedure, equations (4.11), (4.12), (4.13), and (4.14) each provide an approach for calculating the equivalent wood moisture content *EMC* [m.-%] directly from the values of the electrical resistance *R* [Ω] and the actual temperature *T* [°C]. Of course, a single equation could also be created from each two-part approach simply by addition. The characteristic of the two-part approaches is that frequently only the first part depends on the wood species used. The second part, the so-called temperature compensation, is then applied across several wood species. This has the advantage that already known approaches can be extended by specific experiments for temperature compensation. In this way, the informative value for the experiments on temperature compensation can be extended when measurements are performed at a large temperature amplitude, but otherwise only to a very limited extent at a small selection of different wood moisture contents.

Equation (4.8) is based on unpublished measurement series by the company Scanntronik Mugrauer GmbH. It was used in the context of several projects conducted at the Technical University of Munich, e.g. (Flexeder et al., 2021; Flexeder, Schenk & Aondio, 2022; Gamper et al., 2013; Jiang et al., 2018). Parameters *a* - *g* in the original equation are confidential and used as a basis for evaluation in the Softfox software. However, modifying and adjusting this model based on the measured data determined within the scope of this work could provide adjusted and possibly more accurate parameters, cf. results in Subchapter 5.2.3. The measurements in the following Subsections use $X_{20\,°C}$ as the base value, which represents the value that would result at a temperature of 20 °C, instead of $X_{25\,°C}$, which corresponds to a temperature of 25 °C.

$$EMC\ (X_{25\,°C}, T) = X_{25\,°C} + \left(\frac{(\mathrm{a} \cdot X_{25\,°C} + \mathrm{b})}{c}\right) \cdot (\mathrm{d} \cdot \mathrm{T}^3 + \mathrm{e} \cdot \mathrm{T}^2 + \mathrm{f} \cdot \mathrm{T} + \mathrm{g})$$

(4.8) *unpublished original*

$$EMC\ (X_{20\,°C}, T) = X_{20\,°C} + \left(\frac{\mathrm{a} \cdot X_{20\,°C}}{b}\right) \cdot (\mathrm{c} \cdot \mathrm{T}^2 - \mathrm{d} \cdot \mathrm{T} + \mathrm{e})$$

(4.8) *modified form in this thesis*

With

T	Temperature	[°C]
$X_{25\,°C}$	Base value for material moisture content at 25 °C	[m.-%]

Equation (4.9) provides a rather simple approach to compensate for wood temperatures that differ from the temperature for which the calibration curves were originally developed. It is published in (Grönquist et al., 2021), who used an approach initially suggested by (Skaar, 1988) and investigated its applicability on beech laminated veneer lumber (LVL). In these two publications, different base values were set (21 °C by Skaar and 22.68 °C by Grönquist et al.). In this thesis, a measurement temperature of 20 °C was chosen and the equation adjusted accordingly.

$$EMC\ (X_{20\,°C}, T) = \frac{X_{20\,°C} - a \cdot (T - 20)}{b \cdot (T - 20) + 1} \qquad (4.9)$$

With

T	Temperature	[°C]
$X_{20\,°C}$	Base value for material moisture content at 20 °C	[m.-%]

	a	*b*	
Beech LVL, by (Grönquist et al., 2021)	0.027	0.0085	-

Accordingly, the equation can be easily transformed so that it could be used to calculate backwards of a hypothetical uniform $X_{20\,°C}$-value from measured values at different temperature levels. Equation 4.9, resolved to $X_{20\,°C}$, gives equation (4.10):

$$X_{20\,°C}\ (EMC, T) = EMC \cdot (b \cdot (T - 20) + 1) + a \cdot (T - 20) \qquad (4.10)$$

With

EMC	Equivalent moisture content of wood at a certain temperature T	[m.-%]
T	Temperature	[°C]

Equation (4.11) originates from (Boardman et al., 2017), who created a correlation to calculate *EMC* directly from resistance and temperature data measured in oriented strand board (OSB). Parameters *a* - *e* thus refer to a wood product that already has a higher electrical conductivity due to the adhesive content. The original equation (4.11) is tested for possible simplification and thus slightly modified and fitted with new parameters in Subchapter 5.2.4.

$$EMC\ (R,T) = \ -a\ +\ b\ \cdot\ (\frac{1000}{T+273.15})^{e} - d\ \cdot\ (\frac{1000}{T+273.15})^{e} \cdot\ \lg\left[\ lg\ (R) -\ c\right] \tag{4.11 original}$$

With

R	Electrical Resistance	[Ω]
T	Temperature	[°C]

	a	*b*	*c*	*d*	*e*	
OSB, by (Boardman et al., 2017)	8.6810	3.7172	3.8974	2.9129	1.9000	-

Equation (4.12) was published by (Schiere et al., 2021a). They used a model by Forsén and Tarvainen (Forsén & Tarvainen, 2000), who had originally trained their model on pine at temperatures from -10 °C to 70 °C, and applied it to their experimental data of beech laminated veneer lumber (LVL). They investigated the electrical resistance measured along as well as transverse to the grain. Hence Equation (4.12) can be used with different parameters, depending on the measurement direction.

$$EMC\ (R,T) = \frac{lg\ (\ lg(R) - 5) - a + (b \cdot T)}{-c - (d\ \cdot T)} \tag{4.12}$$

With

R	Electrical Resistance	[Ω]
T	Temperature	[°C]

	a	*b*	*c*	*d*	
Beech LVL, perpendicular to grain, by (Schiere et al., 2021a)	1.1195	0.0001	0.0512	0.0009	-
Beech LVL, parallel to grain, by (Schiere et al., 2021a)	1.1067	0	0.0512	0.0010	-

The structure of Equation (4.13) was first published by (Brischke & Lampen, 2014) for an array of wood species and treatments with a total of nine parameters (*a*-*i*) in a range of electrical resistances up to 10^9 Ω. The material-specific findings for untreated radiata pine as well as untreated Scots pine are presented in (Emmerich & Brischke, 2021). The values for *EMC (R,T)* can be calculated according to model (4.13), as provided and adapted by Brischke (2023):

$$EMC\ (R,T) = (a \cdot T\ +\ b) \cdot exp^{(c \cdot T\ -\ d) \cdot 10\lg(R)\ +\ e \cdot T\ +\ f}\ -\ g \cdot (10\lg(R))^2\ -\ h \cdot T\ +\ i \qquad (4.13)$$

With

R	Electrical Resistance	[Ω]
T	Temperature	[°C]

	a	*b*	*c*	*d*	*e*	*f*	*g*	*h*	*i*	
Scots pine (Pinus sylvestris L.), by (Emmerich & Brischke, 2021)	0.3408	9.9460	0.0004	0.1033	-0.0555	6.6165	0.0004	0.0708	18.0392	-
Radiata pine (Pinus radiata D. Don), by (Emmerich & Brischke, 2021)	0.1002	15.3986	-0.0018	0.1250	0.0643	6.3328	0.0022	0.0617	30.1706	-

Based on model (4.13), (Otten et al., 2017) used a simplified equation to fit the electrical resistances measured at three different temperature levels in different wood species. Although technically the same model structure, for clarity purposes, it will be referred to as model (4.14).

$$EMC\ (R,T) = (-a \cdot T + b) \cdot exp^{(-c\,\cdot\,10\lg(R)\,+\,d)} + e \qquad (4.14)$$

With

R	Electrical Resistance	[Ω]
T	Temperature	[°C]

	a	*b*	*c*	*d*	*e*	
Norway spruce *(Picea abies Karst.)*, by (Otten et al., 2017)	0.023569824	2.443072848	0.074072840	6.825697870	9.536085058	-
Norway spruce *(Picea abies Karst.),* thermally modified (TMT), by (Otten et al., 2017)	0.062126654	4.185618490	0.123736453	10.166133185	5.540696604	
European beech *(Fagus sylvatica L.)*, by (Otten et al., 2017)	0.037857542	3.354209406	0.081955307	6.722556884	8.672397361	-
Douglas fir *(Pseudotsuga menziesii Franco),* heartwood, by (Otten et al., 2017)	0.075707979	5.039018820	0.106053527	8.301249029	10.122407034	-
Scots pine *(Pinus sylvestris L.),* heartwood, by (Otten et al., 2017)	0.023464707	2.274058840	0.078878169	7.108161627	8.262014601	-
Scots pine *(Pinus sylvestris L.),* sapwood, by (Otten et al., 2017)	0.026547020	2.315552689	0.090230504	7.599716843	8.957435106	-

4.3.4 Methods for lab measurements regarding various temperature levels

The presented models for temperature compensation in the previous Subchapter 4.3.3 are evaluated using the measurement data obtained as part of this work and then refined using parameter fitting. A total of 56 test specimens made of solid Norway spruce, spruce LVL, solid European beech, and beech LVL were selected for the measurement series, cf. Subchapter 4.3.2. For the measurement of electrical resistance, rammed in electrodes and measuring system I (Scanntronik) were used.

Several publications differ in their methodologies for obtaining measurement data at various temperature levels from this thesis´ methods (Boardman et al., 2017; Brischke et al., 2008; Forsén & Tarvainen, 2000; Otten et al., 2017; Schiere et al., 2021a, 2021a). These cited publications describe their experiments as a similar procedure in which test specimens were first preconditioned in a specific climate to a certain target *MC*. Then, plastic bags (e.g. from polyethylene) were used to cover the test specimens tightly before exposing them to different temperature levels. The changes in electrical resistance were measured during the process. According to Forsén & Tarvainen (2000), this procedure allows for adjustments to ambient temperature *T* and relative humidity *RH* without affecting the moisture content *MC* of the specimens. There is no critical discussion of this methodology yet. However, Boardman et al. (2017) report that small amounts of water collected on the inside of the bags during their experiments at higher temperatures (70 °C). Otten et al. (2017) describe that the exposure time to a certain temperature level at their experiments was limited to less than two hours. Schiere et al. (2021a) chose a slightly different method by varying the ambient temperature at a constant relative humidity. None of the publications mentioned above seem to consider that the equilibrium moisture content *EMC* of wood varies with temperature. Sorption isotherms are temperature dependent, cf. Subchapter 3.2.1. Thus, under varying ambient temperatures, it is not possible to achieve mass constancy in wood by maintaining a constant ambient absolute humidity. Accordingly, it is plausible if condensate could be found within the plastic bag like described by Boardman et al. (2017). Moreover, a moisture gradient has most likely already formed in the specimen.

Due to the contradictions between the “plastic-bag-method” and the principles described in Subchapter 3.2.1, a modified method was used for the measurement series in this thesis. Similar to the previously cited work, the test specimens were first pre-conditioned isothermally over several weeks using salt solutions to achieve a constant wood moisture content until mass is constant. After transfer to the same climate in a climate chamber and several days of acclimatization, the individual temperature stages were run through at intervals of five Kelvin. No plastic bags or similar sealing techniques were used. Instead, readjustment of the ambient relative humidity in the climate chamber ensured that the moisture content of the wood remained (somewhat) constant. As the test specimens first had to warm up completely after a temperature step of 5 K, preliminary tests showed asymptotic adjustments in the electrical resistance before a constant value was reached. Each new temperature level was therefore maintained for at least three hours. Only the electrical resistance values recorded within the last hour of each level were then averaged for evaluation. To determine the corresponding value of relative humidity *RH* to be set, Weichert's sorption data was extrapolated into isohumids for the individual temperature levels.

The sorption isotherms in Norway spruce wood were thus used to determine the control regime for the test specimens made of solid Norway spruce wood and spruce LVL. Similarly, the values to be set for solid European beech and beech LVL were derived from the sorption isotherms for beech according to (Weichert, 1963a, 1963b). The respective starting value of the measurement series was derived from the ambient climate in which the preconditioning took place (Round 1: 20 °C / 55 %RH; Round 2: 20 °C / 75 %RH). The resulting values used for climate control are shown in Figure 47 for round 1 and Figure 48 for round 2.

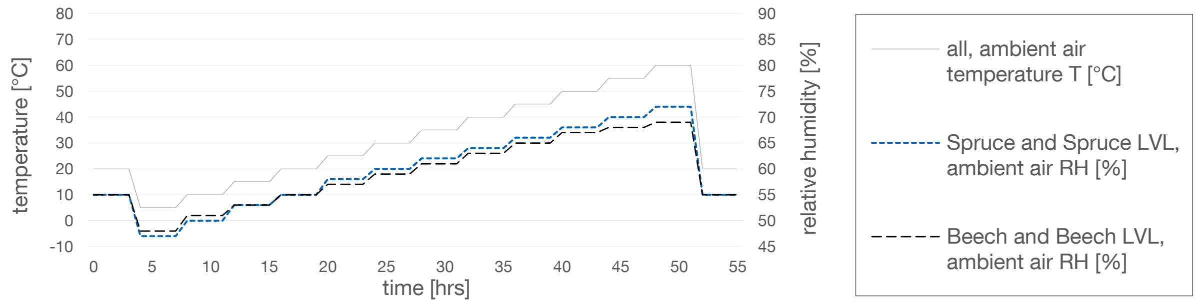

Figure 47: Comparison of the regulation schedules for the climate chamber sustaining a constant sample weight, with adjusted RH values based on the wood species, round 1

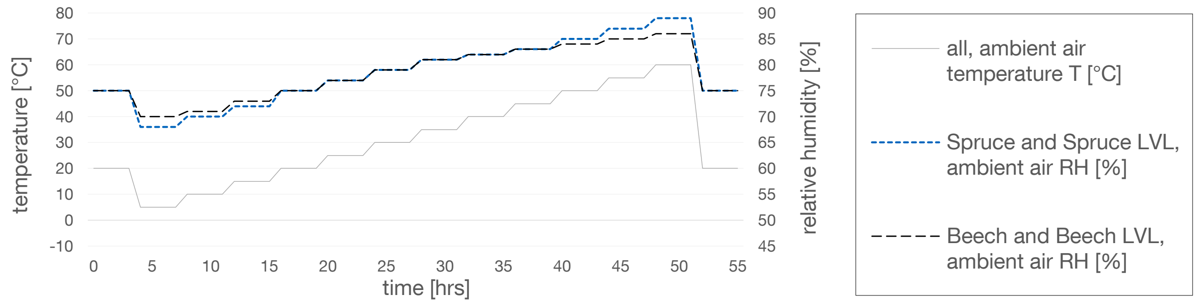

Figure 48: Comparison of the regulation schedules for the climate chamber sustaining a constant sample weight, with adjusted RH values based on the wood species, round 2

Regular precision weighing both during preconditioning and during the temperature steps was used to check if the specimens maintained their constant mass. This ensured that the moisture content of the wood specimens remained constant throughout the procedure. The absolute humidity *AH* [g/m³] of the ambient air in the climate chamber does not remain constant in this control regime, but increases significantly as the temperature rises, cf. Figure 49.

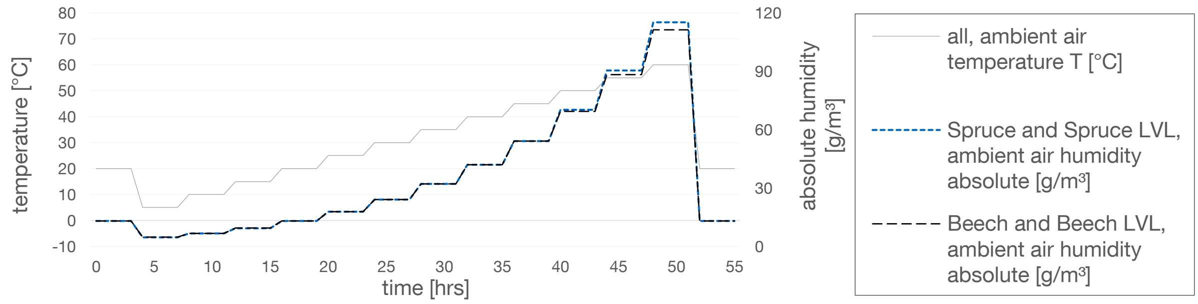

Figure 49: Regulation schedules from Figure 48, round 2, shown as absolute humidity values

Excursus: As part of a further experiment, Subchapter 5.4.4 explores what would actually happen if the absolute humidity *AH* [g/m³] of the ambient air remained the same.

4.4 Further development of the sorption method for monitoring purposes

4.4.1 Extension of the Keylwerth diagram to other wood species

The back-calculation of relative humidity (*RH*) and temperature (*T*) values can be achieved through a variety of methods. For a first approximation and graphical estimation of individual measured values, the Keylwerth diagram could be helpful (cf. also the discussion in Subsection 3.2.1). However, for processing monitoring data using a mathematical algorithm will be inevitable. In order to obtain an unambiguous solution *EMC (RH, T)*, the problem of sorption hysteresis must be solved.

For this purpose, a simplified general splitting curve is generated, similar to the approach used in (Varnier et al., 2022), wherein a step-by-step correction is employed to interpolate an appropriate value between the adsorption and desorption curves. For the interpolation in the course of this thesis, the range of 35 - 85 %RH is selected, cf. Figure 50. This is estimated to be the usual range of fluctuation of the relative humidity indoors. For the curve up to 35 %RH, only the measured desorption values are used. Between 35 %RH and 85 %RH is the range in which ambient humidity values will be fluctuating in a normal operating condition. Hence, a transition to the adsorption curve is introduced here. The values above 85 %RH are taken from the adsorption curve only.

The hysteresis effect is decreasing with higher temperature levels, cf. also Figure 14, p. 54. For instance, in Norway spruce data by (Weichert, 1963b) at 25 °C / 60 %RH, desorption results in *EMC* = 13 m.-% whereas adsorption in *EMC* = 11 m.-%, and thus with a difference of Δ = 2 m.-%. This reduces to Δ = 1 m.-% at 50 °C (11 m.-% at desorption vs. 10 m.-% at adsorption), and to Δ = 0 m.-% at 75 °C (7.3 m.-% at both, desorption and adsorption).

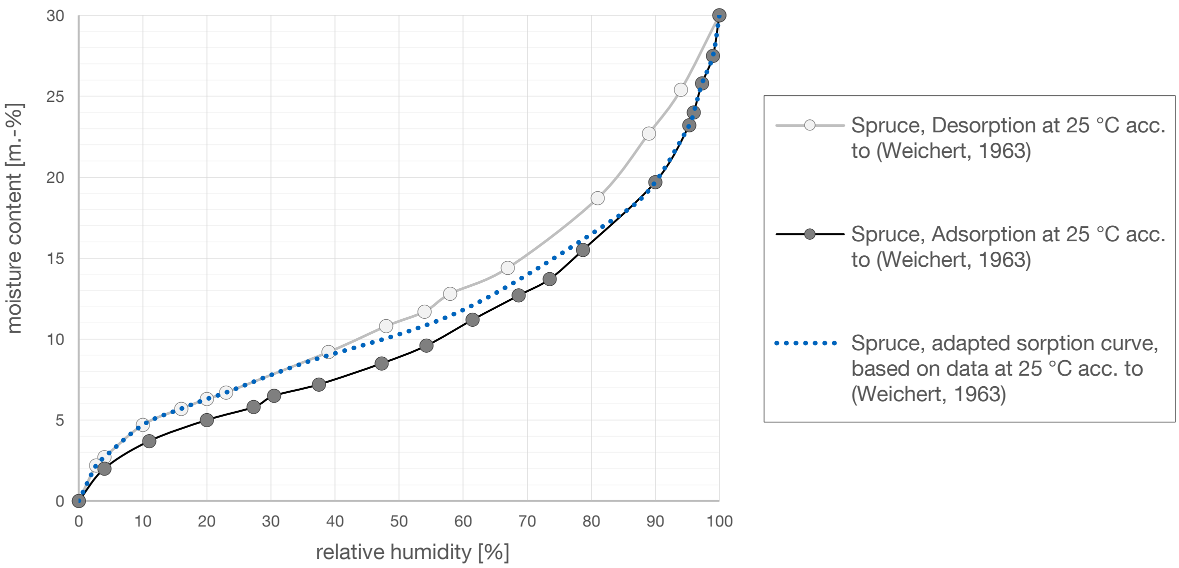

Figure 50: Curves for adsorption and desorption of Norway spruce at 25 °C according to original data by (Weichert, 1963b). The adapted sorption curve is interpolated from this data to generate a scanning curve accounting for sorption hysteresis.

The data from the references listed in Subsection 3.2.2 were compiled and used as the foundation for further evaluation. Table 10 shows the data that is available for training the model.

Table 10: Measurement data of sorption isotherms collected for model training

	Norway spruce *Picea abies Karst.*	**Douglas fir** *Pseudotsuga menziesii Franco*	**Radiata pine** *Pinus radiata D. Don.*	**European beech** *Fagus sylvatica L.*
References	(Weichert, 1963b) (Hedlin, 1968) (Niemz & Sonderegger, 2007) (Popper & Niemz, 2009) (Bratasz et al., 2012)	(Hedlin, 1968) (Fan et al., 1999) (Popper & Niemz, 2009)	(Popper & Niemz, 2009) (Simón et al., 2016)	(Weichert, 1963b) (Niemz & Sonderegger, 2007) (Popper & Niemz, 2009) (Bratasz et al., 2012)
Range of available sorption data	-12 °C – 100 °C 0 %RH – 99 %RH	-12 °C – 60 °C 0 %RH – 99 %RH	15 °C – 50 °C 0 %RH – 98 %RH	20 °C – 100 °C 0 %RH – 95 %RH
Number of data sets	57 data sets	38 data sets	27 data sets	25 data sets

The modified Henderson model was employed to calculate the equilibrium moisture content *EMC*, with an approach developed by (Glass et al., 2014) serving as the underlying equation, cf. equations (3.5) and (3.6) in Subchapter 3.2.1. The original model is published with the parameters fitted to older sorption data by Loughborough for Sitka spruce in (Glass et al., 2014). Equations (4.15) and (4.16) were taken from the publication by (Forest Products Laboratory, 2021) and were only slightly modified within the scope of this work:

$$RH = 100 \cdot \left\{1 - exp\left[\frac{1}{a \cdot (T + 273.15)} \cdot \left(1 - \frac{(T + 273.15)}{647.1}\right)^{-b} \cdot \left(\frac{EMC}{100}\right)^{\frac{1}{c} \cdot (T+273.15)^{-d}}\right]\right\} \tag{4.15}$$

$$EMC = \left[a \cdot (T + 273.15) \cdot \left(1 - \frac{(T + 273.15)}{647.1}\right)^{b} \cdot \ln\left(1 - \frac{1}{100} RH\right)\right]^{c \cdot (T+273.15)^{d}} \tag{4.16}$$

With

EMC	Equilibrium Moisture Content	[m.-%]
RH	Relative Humidity of Air	[%]
T	Temperature	[°C]

Equation (4.15) is based on the same model as equation (4.16), converted to *RH*. In order to refine parameters a-d, the model is trained by parameter fitting based on sorption data taken from the literature from Table 10. Further details on the regression analysis methods are given in Subchapter 4.1.1.

The resulting equations with wood-species-specific parameters for Norway spruce, Douglas fir, radiata pine and European beech are presented in Subchapter 5.3 and Appendix F. These were then tested with the measurement data obtained in the course of this work, with a focus on Norway spruce and Douglas fir, cf. Subsections 4.6 and 5.4.

4.4.2 Conception of the measuring technique for hygrometric moisture measurements

In order to use the sorption method, also called hygrometric method or bore-hole method, RH/T combination sensors need to be inserted and tightly sealed. This means that a small, closed air chamber is drilled into the material at a defined layer depth and instead of the water content of the building material, the water content of the air enclosed in it is measured, and the corresponding equilibrium moisture content *EMC* is inferred, cf. Subchapter 3.3.2.

Depending on the humidity sensors used, the accuracy of the whole method is significantly influenced by the sensor´s quality. Comprehensive details on this topic, which can also be useful for monitoring purposes in general engineering, not only related to cultural heritage, are given in the standard for *Conservation of cultural heritage - Procedures and instruments for measuring humidity in the air and moisture exchanges between air and cultural property* (EN 16242:2012).

The measurement concepts in Subsections 5.4, 6.1, and 6.2 use a system of microcontrollers that are pluggable, connected via application-programming-interface (API) bindings, and compatible to various programming languages (open source). The system offers many advantages in terms of setting up cost-effective individual monitoring concepts via a bus system, but does not offer a prefabricated solution to investigate material moisture content. The system includes a digital humidity sensor with an integrated temperature sensor (3 mm x 3 mm), mounted on a flat sensor plate (a “bricklet”, 25 mm x 15 mm x 5 mm), which needs to be permanently connected to the main system by a 7-pin-cable. The combination sensor itself has an accuracy of ±0.2 °C and ±2 %RH within a range of 10 – 50 °C and 20 – 60 %RH. Outside this range the offset will increase, depending on exposure time. For instance, when exposed to an environment with 85 °C / 85 %RH for 12 hours, the offset will be ±3 %RH; after 24 hours it will increase to ±6 %RH. (Texas Instruments, Incorporated, 2016; Tinker-Forge: Humidity Bricklet 2.0 - Technical Specifications).

In order to use these sensors for the sorption method, a solution was being designed using rapid prototyping. The resulting casing is a cylindrical body weighing 7 g and made of polycarbonate, which the prefabricated bricklet can be snapped into. Considering the thickness of the added sealant, it is recommended to predrill a bore-hole with a diameter of d = 32 mm. The data to reproduce the casings is published open access in (Flexeder, 2022a). These open source files also contain more practical details: “The actual sensor is located at the center of the opening. Aluminum butyl tape is used for vapor-tight masking both on the inside of the borehole and on the surface of the envelope on the room side. Tests with masking on vapor-tight glass surfaces show that the sealing at the 7-pin connector of the sensor cable is the weak point for leaks and thus measurement errors. If the adhesive tape is applied here with high contact pressure and precision, the tests show that the measurement inaccuracy caused by unwanted water vapor diffusion can be kept to a minimum. To remove the glued-in sensor sleeve, it is recommended to remove all aluminum butyl tape first carefully and then pull off the cable. By screwing a longer screw into the opaque semicircle of the sheath, it can then be easily pulled out with pliers and a slight twisting motion. This procedure allows for the sensor to be reused.” (Flexeder, 2022a)

Figure 51 - Figure 62 illustrate the development of the novel sensor envelope, its testing, and installation at various depths of the component cross-section.

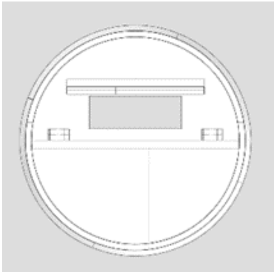

Figure 51: Semi-transparent top view of 3D model

Figure 52: Perspective, showing the optimized geometry for insertion

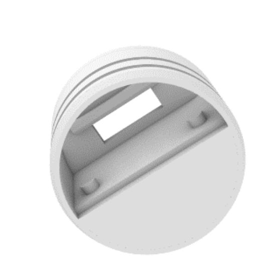

Figure 53: Perspective, showing the inner cavity for the sensor plate

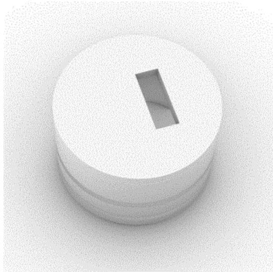

Figure 54: Perspective, showing the casing with cable access

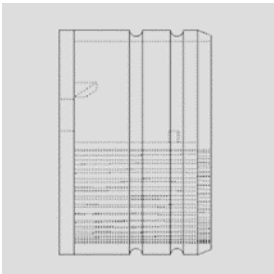

Figure 55: Side view, showing casing division

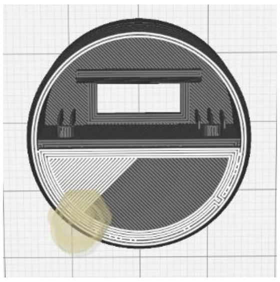

Figure 56: Preparing the geometry for 3D-printing

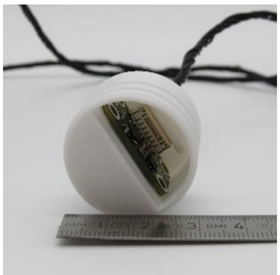

Figure 57: Finished Casing with sensor inserted

Figure 58: Assembling a whole sensor array

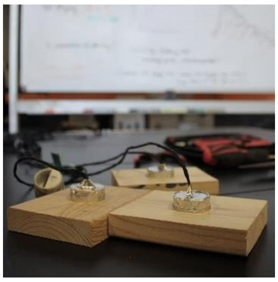

Figure 59: Inserting and sealing sensor casings for SM in Eucalyptus nitens specimens

Figure 60: Specimen of spruce CLT as used in (Flexeder, Schenk & Aondio, 2022)

Figure 61: Sensor inserted in 70 mm depth in spruce CLT in a test cube

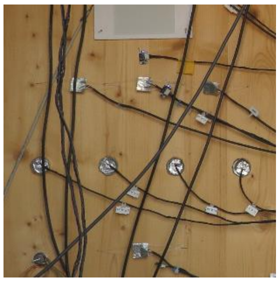

Figure 62: Four sensors in four different depths as part of a monitoring concept in a test cube

The sensor setup has already been installed in the research projects *PhyTAB* and *Einfach Bauen*, cf. Subchapters 4.7.2 and 4.7.3. Even if the investigations in this thesis are limited to measurements in solid wood, the combination of sensor and new sensor envelope can also be used in other dry building materials. Consequently, this constellation had already been tested in various composite wall structures with different insulations and sheet materials (Flexeder, Schumacher et al., 2022; Jarmer et al., 2021).

However, computing *EMC* (*RH, T*) based on wood-species-specific calibration curves as described in Subchapter 4.4.1 is a novel approach within this dissertation.

4.5 Investigation of hygrothermal effects to detect moisture fluxes on the surface

This thesis presents a novel approach to monitoring moisture fluxes on hygroscopic surfaces such as wood. The method employs continuously measured minute temperature differences from a pair of sensors to track the effects of sorption enthalpy. Details of this new method are also published in (Flexeder, 2022b; Flexeder, Kamml & Paulik, 2022; Flexeder, Nouman & Hepf, 2022; Flexeder, Schumacher et al., 2022). As part of the research project *PhyTAB*, the first successful measurements have already been carried out using conventional temperature sensors with a compact cubic shape and a comparatively large contact area (4 mm x 16 mm). Although the experiments were successful in proving the enthalpy effect in principal, systematically less heating was observed in the experiment than in the simulation. The reason for this could be that the surface sensors do not measure the direct heat of sorption. At the point where the surface sensor is located, the material surface is covered by the sensor and therefore cannot absorb or release water vapor. (Flexeder, Schumacher et al., 2022)

The new method is intended to detect moisture fluxes measures the heating or cooling of the room-side surface of a component as a consequence of water vapor sorption in transient behavior. The more pronounced the sorption process, the more distinctive the temperature change at the surface will be under otherwise constant conditions. The enthalpy release or binding as a result of successive changes in the wood moisture content of the near-surface layer can therefore only be observed with very small temperature changes. In addition, there is a logical contradiction in measuring surface temperature changes due to moisture absorption: the surface will not be able to absorb water vapor at the point covered by a sensor. Therefore, any measured surface heating can only originate from the surrounding area.

The following requirements therefore apply to sensors used to monitor surface heating due to water vapor sorption or cooling due to desorption:

- Measurement of the relative temperature change with a high accuracy of at least ±0.1 K
- Minimization of electro-technical measurement errors
- Avoidance of sensor heating due to other effects of heat transfer, such as solar radiation or convection during heating operation
- Smallest possible contact area to minimize error due to logical contradiction of sorption surface coverage
- Implementation within a cost framework that allows a large number of sensors to compensate for the variance of natural building materials

The measurement method used eliminates interferences by measuring with a "twin" in parallel. Here, two identical temperature sensors were mounted on the component, with a vapor barrier previously applied underneath one of them. This allowed a single effect (the change in surface temperature due to water vapor sorption) to be isolated from the temperature variations that are often unavoidable, even in the laboratory. The cover used has a minimum s_d-value of 5 m but ideally much higher, such as aluminium tape with an s_d-value of >1000 m.

Rapid prototyping was used to generate the geometry of the fixture, an inverted pyramid with two internal channels, cf. Figure 63 - Figure 66. This method enabled designing the optimum ratio of curvature and insertion angle to ensure stable solder joints while protecting against condensation and possible short circuits. The final geometry can be produced in a 3d-printer with about 3 g of polycarbonate filament. The data of the final design is published in (Flexeder, 2022b) as open access files.

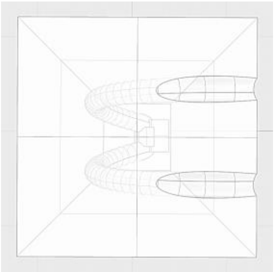

Figure 63: Semi-transparent top view of 3D model with top side and cable outlets

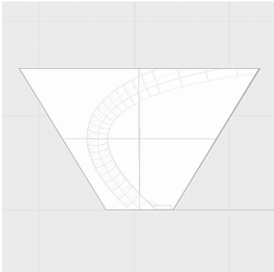

Figure 64: Side view showing the buckle-free cable channel

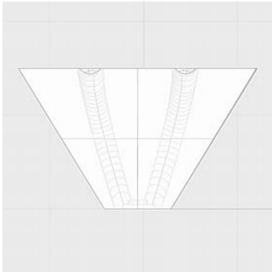

Figure 65: Front view, representation of the axially symmetrical structure

Figure 66: Perspective with bottom recess for platinum thermometer

In order to evaluate the minute temperature deviations on several points of the test elements, four-wire cables were soldered to platinum RTDs (M 222, type: PT1000, accuracy: ±0.1 K, class: 1/3 B). The contact area consists only of the sensor (2.3 mm x 2.1 mm x 0.9 mm). The four wires were passed through the perforations of each pyramid and joined to the pins of the temperature sensors on one end, and on the other end to the RTD-to-digital converter to transfer a compatible signal to the microprocessors (Maxim Integrated Products Inc., 2012). To connect to a 4-wire cable, the two wires were pulled through a channel, then soldered to the platinum thermometer end pieces and pulled back to the stop after cooling. A drop of synthetic resin adhesive (UHU Plast Special) applied with the fine dispensing tip sealed the channels. The area below the PT1000 sensor was covered and sealed with a small piece (about 7 mm x 7 mm) of aluminum butyl tape. The same tape was later used during installation to close off the large area on the room side (approximately 25 mm x 25 mm), which was intended to help to additionally reflect incident radiation. (Flexeder, Nouman & Hepf, 2022)

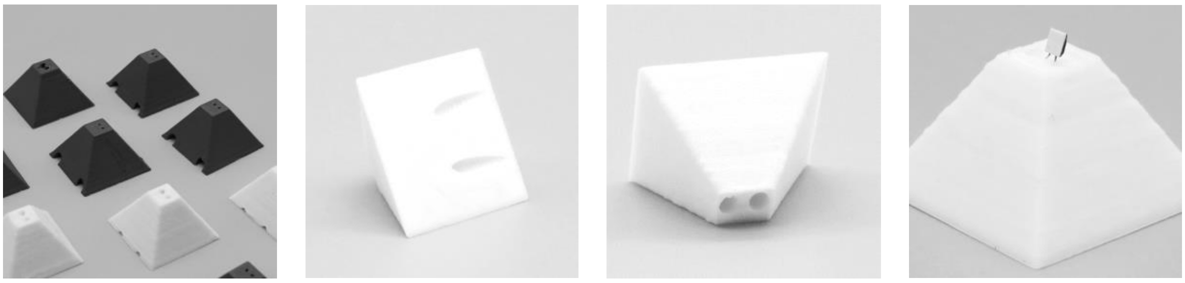

Figure 67: Design of an optimized sensor mount, finding the ideal shape via rapid prototyping for improved attachment of the PT-1000 sensor (tip)

More information and first results on the transient hygrothermal behavior on the inside surface of a cross-laminated timber wall are given in (Flexeder, Nouman & Hepf, 2022; Flexeder, Schumacher et al., 2022) and Appendix I.

4.6 Examination of the new and improved methods in lab trials

4.6.1 Approach to compare measurement instrumentation under lab conditions

Laboratory trials shall prove, which of the improvements from previous subchapters might produce the most accurate results for *EMC*. Different variations of sensor techniques and specimens were used to compare two methods for wood moisture monitoring: the electrical resistance method (*ERM*) versus the sorption method (*SM*). The investigation of variations within each method ensures that the observed phenomena are characteristic for the respective method and not just systematic deviations of the specific sensor product. Some batches refer to known systems, which have been already used in projects, cf. column 5 in Table 11.

In order to minimize the impact of external influences on the results, appropriate precautions were taken in advance to avoid systematic measurement errors. The specimens used in this study were derived from two distinct species: Norway spruce (*Picea abies Karst.*) and Douglas fir (*Pseudotsuga menziesii Franco*). The material was cut into identical external dimensions of 100 mm x 100 mm x 20 mm ±1 mm and preconditioned at 20±1 °C/43±3 %RH over a saturated K_2CO_3 solution, until mass constancy was reached. In order to obtain a statistically uniform density distribution within each batch, the specimens were then sorted by weight, using a precision balance, cf. Subchapter 4.2.1. Although all specimens were obtained from a single log, the Norway spruce specimens conditioned to equilibrium moisture had an average mass of 91.771 g with a standard deviation of 5.129 g (min: 83.991 g – max: 99.583 g) after the first preconditioning phase. The Douglas fir specimens exhibited a significantly higher average mass of 106.306 g with a standard deviation of 7.394 g. (min: 95.826 g – max: 121.844 g), as the overall dry bulk density is higher. This gradient was represented by an allocation with ascending starting weight to the individual batches, cf. Figure 68. Thus, in a batch with four specimens each, there was an even distribution of the average bulk density of the wood used (with xx_a being the lightest and xx_d the heaviest specimen each). The measurements after oven-drying showed a mean oven-dry density ρ_0 for the Norway spruce specimens of 416 kg/m³ (*SD* 23.7 kg/m³) and for the Douglas fir specimens of 490 kg/m³ (*SD* 37.6 kg/m³).

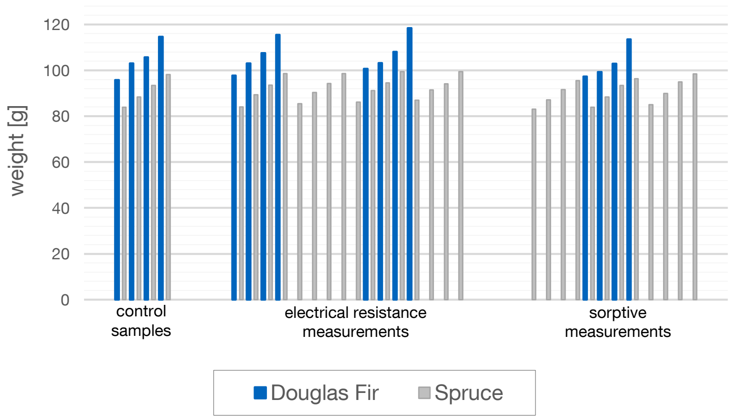

Figure 68: Weight distribution of the specimens a-d of each batch used in the laboratory test, evenly distributed in advance to avoid systematic influences of varying density.

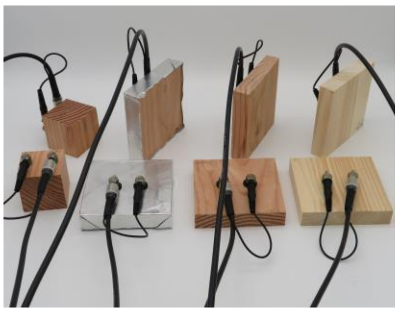

Figure 69: Experimental setup for preliminary testing of systematic influences on electrical resistance.

Table 11: Comparison of methods in lab experiment on European wood species: Norway spruce (Picea abies Karst.) and Douglas fir (Pseudotsuga menziesii Franco).

Technique	No.	Technique / Material	Pre-drilled hole	see also
oven dry method	01_a - d	oven-dry, Norway spruce	-	Moisture content of a piece of sawn timber - Part 1 (EN 13183-1:2002)
	02_a - d	oven-dry, Douglas fir	-	
ERM Electrical resistance method with measure-ments between two electrodes	11_a - d	System I (Scanntronik), rammed-in electrodes, Norway spruce	total length: 15 mm d = 4.4 mm shaft (8.5 mm) d = 3.2 mm tip (6.5 mm)	(Flexeder, Schenk & Aondio, 2022; Gamper et al., 2013) Subchapters 4.7.2 and 4.7.3
	12_a - d	System I (Scanntronik), screwed-in electrodes, Norway spruce	total length: 15 mm d = 5 mm shaft (8.5 mm) d = 3.5 mm tip (6.5 mm)	(Flexeder, 2021; L. Franke et al., 2024) Subchapters 4.7.3 and 4.7.4
	13_a - d	System I (Scanntronik), glued-in electrodes, Norway spruce	d = 4 mm (15 mm)	(Brischke & Lampen, 2014) 01-04 in Subchapter 4.2.5
	14_a - d	System II (Omnisense), screwed-in electrodes, Norway spruce	total length: 15 mm d = 7 mm shaft (8.5 mm) d = 5 mm tip (6.5 mm)	(Kordziel et al., 2019)
	15_a - d	System I (Scanntronik), rammed-in electrodes, Douglas fir	total length: 15 mm d = 4.4 mm shaft (8.5 mm) d = 3.2 mm tip (6.5 mm)	
	16_a - d	System I (Scanntronik), glued-in electrodes, Douglas fir	d = 4 mm (15 mm)	
SM Sorption method with air temper-ature and rela-tive humidity measurements in cavity in the material	21_a - d	System III (Blue Maestro), RH/T-sensor inserted from underneath, Norway spruce	d = 35 mm (15 mm)	Subchapter 4.7.2
	22_a - d	System IV (TinkerForge), RH/T-sen-sor inserted from underneath, Norway spruce	d = 32 mm (11 mm)	(Flexeder, Schenk & Aondio, 2022; Flexe-der, Schumacher et al., 2022; L. Franke et al., 2024) Subchapters 4.7.2 and 4.7.3
	23_a - d	System IV (TinkerForge), RH/T-sen-sor inserted from top, Norway spruce	d = 32 mm (8 mm)	
	24_a - d	System IV (TinkerForge), RH/T-sen-sor inserted from underneath, Douglas fir	d = 32 mm (11 mm)	

To direct the gradient direction in the experiment with constant *AH*, the test specimens were taped tightly on five sides with aluminum foil (s_d-value ≈ 100,000 m). To prevent the aluminum foil from influencing the electrical resistance measurement between two electrodes, the puncture points were cut out generously and sealed with rubber rings (no direct electrical contact). To further investigate the influence of specimen size and geometry, a preliminary experiment was undertaken with variants of specimens 15_a - d (II): Douglas fir specimens but with smaller cube size (I), Douglas fir specimens with a conductive aluminum foil tape (II), Douglas fir specimens without the conductive aluminum foil tape (III), Norway spruce specimens without the conductive aluminum tape (IV), each four times, like shown in Figure 69 with one example representing each batch. These preliminary tests showed no measurable influence of aluminum foil on the electrical resistance measurement. Also, the geometry differences between the cube-shaped and flat Douglas-fir specimens did not appear to produce any significant difference in measurable electrical resistance. However, comparing the Douglas fir specimens with the Norway spruce specimens showed significantly different measurement results, thus proving the relevant influence of the wood species.

In a constant climate of 20±1 °C / 43±3 %RH, the test specimens were weighed, holes for the sensors were drilled, weighed again, taped on five sides with aluminum foil, weighed, fitted with sensors, and weighed again. This procedure ensured that the finally oven-dried specimens referred to the weight of the wood only. The selection of test specimens consisted of nine batches in Norway spruce and five batches in Douglas fir for comparison. Each batch contained four specimens a - d with a representative bulk density distribution. Four batches of Norway spruce specimens and two batches of Douglas fir were equipped with different systems for electrical resistance measurements. The following types of electrodes were investigated: rammed-in (11_a – d; 15_a – d), screwed-in (12_a – d; 14_a – d), glued-in (13_a – d; 16_a – d) as well as two different measuring devices, system I and II. Thus, a total of six batches of four specimens each were examined in parallel for the study of electrical resistance measurements, cf. Figure 70 and Figure 71.

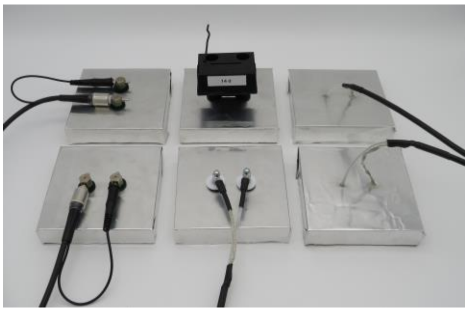

Figure 70: One specimen (d) of each batch for electrical resistance measurements. Top f.l.t.r.: 15_d, 14_d, 16_d Bottom f.l.t.r.: 11_d, 12_d, 13_d

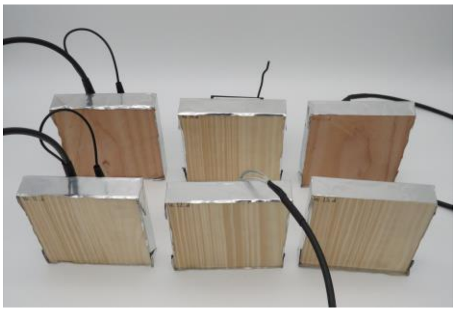

Figure 71: Comparison of two batches made from Douglas fir and four batches made from Norway spruce, each represented by one specimen (d)

Figure 72: Mounting sensor 14-d with insulation rings

Batches 11_a-d and 15_a-d used the rammed-in electrodes with 15 mm length, which were also applied for the investigations in Subsections 4.2 and 4.3. In batch 12_a-d, specially manufactured threaded rods were screwed into a tapered pre-drilled hole, cf. Figure 73 (back). Batches 13_a-d and 16_a-d investigated an alternative approach in which the connecting cables served as electrodes and were glued in directly, cf. Figure 74. They thus corresponded to approach 01-04 from Subchapter 4.2.5. These five test batches (11, 12, 13, 15, 16) used system I as evaluation electronics, cf. Table 11.

Batch 14_a-d was an alternative approach with different evaluation electronics (system II), cf. Figure 72 and Figure 75. Furthermore, two batches, one each in Norway spruce (01_a – d) and Douglas fir (02_a - d) had no sensors and were used for comparison with periodic weighing and a subsequent oven-drying test. Consequently, they were used for the representative estimation of wood moisture content during the experiment, since the actual test specimens with the permanent wiring were not suitable for short random weight checks.

Figure 73: Screw-in electrodes for batch 12 (back) and ram-in electrodes for batch 11 (front)

Figure 74: Cables shown as examples for gluing (orange) in as well as for fastening to ram electrodes (blue) and screw electrodes (purple)

Figure 75: Equipment for wireless resistance measurements on batch 14

To investigate the sorption method, three batches of Norway spruce (21_a – d; 22_a – d; 23_a – d) and one batch of Douglas fir (24_a – d) were fitted with differently inserted systems to measure relative humidity *RH* [%] and temperature *T* [°C], cf. Figure 78. Batches 22, 23, and 24 used system IV as described in Subchapter 4.4.2, cf. Figure 76.

Figure 76: Preparations for the experiment - Example for cable-bound RH/T-sensors in 3d-printed casings

Figure 77: Taping of inner and outer flanks to avoid sorption

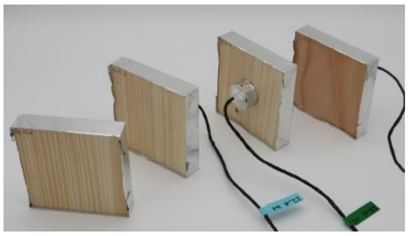

Figure 78: One specimen each representing batches 21, 22, 23 (Norway spruce) and 24 (Douglas fir).

When installing the sensors for determining the wood moisture in the depth of the material, precise attention was paid to a uniform measuring depth of 5 mm below the surface and taping of inner and outer flanks to avoid sorption, cf. Figure 77. The resulting borehole depths and diameters are listed in Table 11, column 4.

Batch 21 employed system III, which are slightly bigger yet wireless RH/T-sensors, cf. Figure 79. They measure relative humidity *RH* [%] and temperature *T* [°C] in a 15 mm deep hole in the specimen and thus 5 mm from the opposite surface, cf. Figure 80 and Figure 81.

Figure 79: Wireless sensors (RH/T), used in Batch 21 as system III. The sensors are placed in the specimen with the air slits first.

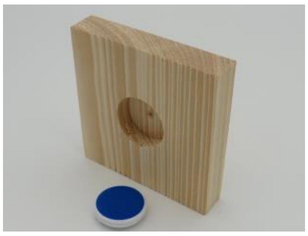

Figure 80: Insertion of RH/T-sensors in 15 mm deep hole

Figure 81: Position of sensor before adding aluminum tape

4.6.2 Additional experiments on latent heat effects in a laboratory environment

Two additional batches, one each from Norway spruce and Douglas fir (31_a – d; 32_a - d) supplemented the main measurements described in Subchapter 4.6.1. They utilized the temperature difference measurement system presented in Subchapter 4.5 to detect sorption mechanisms at the component´s surface, cf. Table 12.

Table 12: Additional method to detect moisture fluxes in lab experiments on European wood species

Technique	No.	Technique / Material	Pre-drilled hole	see also
Temperature differences method	31_a - d	System IV (TinkerForge), 2 precise T-Sensors fitted top and bottom, Norway spruce	-	(Flexeder, Nouman & Hepf, 2022; Flexeder, Schumacher et al., 2022) Appendix I
	32_a - d	System IV (TinkerForge), 2 precise T-Sensors fitted top and bottom, Douglas fir	-	

Four specimens from Norway spruce and four specimens from Douglas fir were fitted with two sensors each (16 total), cf. Figure 82. Each specimen was fitted with one precise temperature sensor on the hygroscopic wooden surface in the front and one on the sealed back, cf. Figure 83 and Figure 84. This new method had already been tentatively proven to work in both, laboratory and field experiments. Since the temperature differences caused by latent heat effects are usually very minute and thus smaller than other temperature fluctuations that might be caused by the surrounding climate, a control measurement on a non-sorbing surface enables cleaning the measurements from these errors. Although this method of temperature differences has been used in several experiments already, none established a direct relationship to the quantity of adsorbed/desorbed water yet. Modelling the sorption process using the hygrothermal simulation tool WUFI with the adjustments explained in Subchapter 4.1.3 investigated the observed sorption phenomena further. The model used the material parameters listed in Appendix G (Norway spruce) and Appendix H (Douglas fir) assuming an effective air velocity of 0 m/s at the specimens´ surfaces.

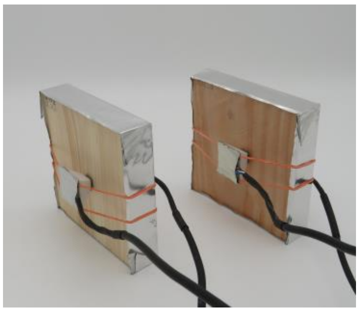

Figure 82: Comparison of two specimens, Norway spruce and Douglas fir respectively, each representative of one batch

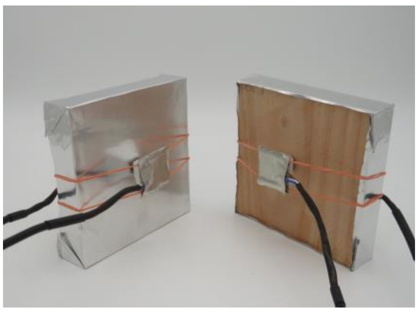

Figure 83: Back and front of two specimens from the same charge of Douglas fir. Each specimen was equipped with two sensors for comparison of changing surface temperatures on the same specimen

Figure 84: Detail showing the mount of the surface temperature sensor, here by stretched rubber strings

4.6.3 Methods to compare various measurement techniques under lab conditions

The trials in Subsection 5.4 assess the moisture monitoring methods, which are improved or even newly developed in this thesis. Therefore, the results in Subchapters 5.4.1, 5.4.2, 5.4.3, 5.4.4, and 5.4.5 are about testing and comparing the electrical resistance method (*ERM*) with the sorption method (*SM*). Furthermore, they are used to prove that the new method of surface temperature differences could be suitable to detect moisture fluxes in Subchapter 5.4.6.

A total of 56 specimens (Norway spruce, Douglas fir) were simultaneously subjected to several series of measurements with humidity and temperature step changes. When positioning the test specimens in the climate chamber, a random distribution was ensured in order to compensate for possible influences of local climatic differences within the chamber. Starting from the preconditioned equilibrium humidity around 21 °C / 50 %RH (*AH* = 9 g/m³), a series of measurements was first run with constant equilibrium humidity (mass constancy). For this purpose, these values of the relative humidity that result in the same equilibrium moisture content at different temperature levels were determined on the basis of the sorption isotherms by (Weichert, 1963a), cf. discussion in Subchapter 4.3.4. By keeping the mass constant in this way, only the temperature changes, but without moisture sorption, cf. theory in Subchapter 3.2.1 as well as adaption for methods in Subchapter 4.4.1. In order to achieve this, the absolute humidity (*AH*) had to raise significantly with the temperature, in this particular case from *AH* = 3 g/m³ (44 %RH at 5 °C) to *AH* = 31 g/m³ (60 %RH at 40 °C), cf. Figure 85.

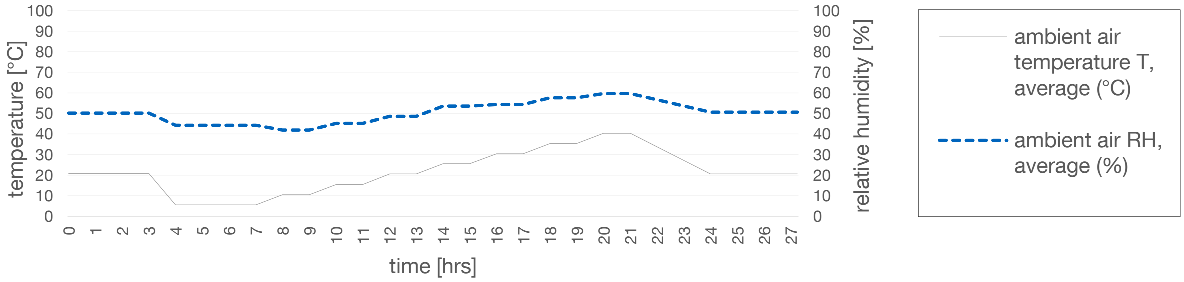

Figure 85: First experiment comparing different moisture monitoring techniques under constant specimen weight

A second measurement series observed the sorption effects that occur when the absolute humidity inside the climate chamber remained constant around 9 g/m³, cf. Figure 86. For this purpose, the temperature in the climate chamber was changed in two major steps, 144 hours apart, with the relative humidity regulated according to the Kelvin relationship in order to keep the absolute humidity constant. These steps were provoking an *MC* gradient.

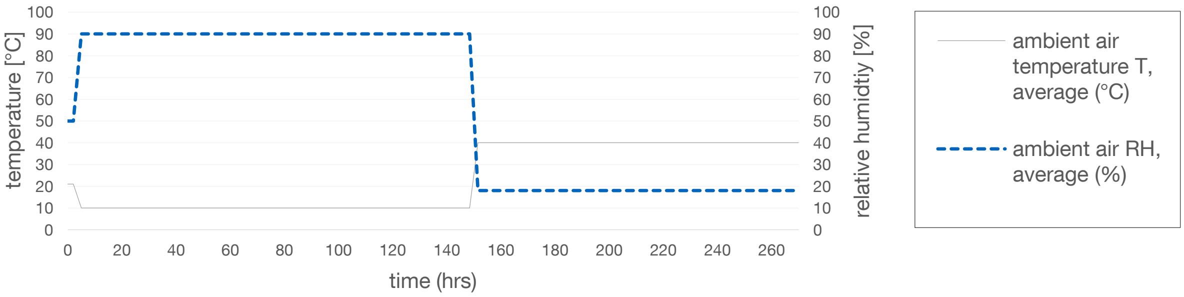

Figure 86: Second experiment comparing different techniques under constant absolute humidity AH

4.6.4 Supplementary lab experiments to compare methods on Australian wood species

The laboratory tests carried out at the *University of Queensland* compared the electrical resistance method (*ERM*) with the sorption method (*SM*), specifically on Australian wood species, cf. Table 13. This method differs from previous subchapters in that the experiments did not take place in a climate chamber with variable relative humidity, but in an air-conditioned laboratory and a kiln. Investigating moisture monitoring methods on these three (sub-)tropical species thus involved a change in wood moisture content with a change in temperature level. This approach differs from the larger main experiment on Norway spruce and Douglas fir, where within a series of tests, *MC* remained constant by readjusting relative humidity (*RH*) as temperature (*T*) changed. However, normalizing the deviations of derived *EMC* to the actual *MC* enables a comparison of the values from the experiments on Australian wood species with the ones on European wood species in Subchapters 5.4.1, 5.4.2, and 5.4.3.

Table 13: Comparison of methods in lab experiment on Australian wood species: spotted gum (Corymbia maculata), shining gum (Eucalyptus nitens), and radiata pine (Pinus radiata D. Don.)

Technique	No.	Technique / Material	Pre-drilled hole	see also
ERM Electrical resistance method with measurements between two electrodes	41_a – d	System I (Scanntronik), rammed-in electrodes, Spotted gum (*Corymbia maculata*)	total length: 15 mm d = 4.4 mm shaft (8.5 mm) d = 3.2 mm tip (6.5 mm)	11_a – d (Norway spruce) 15_a – d (Douglas fir)
	42_a - d	System I (Scanntronik), rammed-in electrodes, Shining gum (*Eucalyptus nitens*)		
	43_a - d	System I (Scanntronik), rammed-in electrodes, Radiata pine (*Pinus radiata D. Don.*)		
	44_a - d	System I (Scanntronik), rammed-in electrodes, Radiata pine (*Pinus radiata D. Don.*)		
	45_a - d	System II (Omnisense), screwed-in electrodes, Radiata pine (*Pinus radiata D. Don.*)	total length: 15 mm d = 7 mm shaft (8.5 mm) d = 5 mm tip (6.5 mm)	14_a – d (Norway spruce) (Strang et al.)
SM Sorption method with air temperature and relative humidity measurements in cavity in the material	51_a - d	System IV (TinkerForge), RH/T-sensor, Spotted gum (*Corymbia maculata*)	d = 32 mm (11 mm)	22_a – d (Norway spruce) 24_a – d (Douglas fir)
	52_a - d	System IV (TinkerForge), RH/T-sensor, Shining gum (*Eucalyptus nitens*)	d = 32 mm (11 mm)	
	53_a - d	System IV (TinkerForge), RH/T-sensor, Radiata pine (*Pinus radiata D. Don.*)	d = 32 mm (11 mm)	
oven dry method	61_a - d	Oven-dry, Spotted gum (*Corymbia maculata*)	-	Moisture content of a piece of sawn timber - Part 1 (EN 13183-1:2002)
	62_a - d	Oven-dry, Shining gum (*Eucalyptus nitens*)	-	
	63_a - d	Oven-dry, Radiata pine (*Pinus radiata D. Don.*)	-	

4.7 Methods using various new moisture monitoring techniques in field tests

4.7.1 Introducing in-situ monitoring concepts to investigate hygrothermal behavior

This thesis summarizes the results from three individual monitoring projects of different sizes and backgrounds. These three have in common that they incorporate various techniques to measure temperature, heat fluxes, and moisture contents in exterior cross-laminated timber walls and thus under temperature gradients. The following Subchapters 4.7.2, 4.7.3, and 4.7.4 describe the respective measurement set-ups.

The temperature in the three projects was measured with an accuracy of at least ±0.2 K in several depths of the respective exterior wall. The monitoring concepts in the two test cubes used RH/T-combination sensors (4.7.2), while the concept in the *Timberbrain* used PT-1000 sensors (4.7.4). The monitoring concept in the *Einfach Bauen* used a mix of both (4.7.3).

The equivalent moisture content *EMC* [m.-%] of the different cross-laminated timber in these three projects is evaluated using the methods improved or developed within this thesis. The test cubes were equipped with both, electrodes for the electrical resistance method and sensors for the sorption method, each in four different depths (4.7.2). The exterior walls of the *Timberbrain* featured electrodes in eight different lengths but no sorption method (4.7.4). The exterior walls in the project *Einfach Bauen* contained electrodes in eight depths, too. For control measures, they also included the sorption method in a single depth (4.7.3). Based on the experiments in this thesis, the temperature-dependent accuracy for both methods, ERM and SM, is estimated and summarized in Subchapters 6.2.2, 6.2.3, and 6.3.2, as a preliminary indication in order to classify monitoring results for *EMC* [m.-%] with regard to their reliability.

What is not depicted on pages 107-109, but will be referred to in the interpretation in Subsections 6.2 and 6.3, are the results from transient heat flux measurements. Heat flux plates (120 mm x 120 mm) were fixed from the inside to the cross-laminated timber walls to measure minute changes in heat flow in mV, which was then transformed into a digital signal by an analog-digital converter. According to the manufacturer, the precision of the converter (Voltage mode) reaches ±0.1 % or better (Phymeas GbR).

In order to investigate the phenomena in greater detail, the illustrations in Subsections 6.2 and 6.3 present the measurement results at a specific time step j. Therefore, the heat flow rates were converted into values of transient thermal conductivity $\lambda'_{in\text{-}situ,\,j}$ [W/(m·K)] at that specific time step *j* with equation (4.17):

$$\lambda'_{in-situ,j} = d \cdot \frac{q_j}{T_{si,j} - T_{se,j}} \tag{4.17}$$

With

$\lambda'_{in-situ,j}$	transient thermal conductivity at time step j	[W/(m·K)]
d	distance between the two measurement points si and se	[m]
q_j	density of heat flow rate at time step j	[W/m²]
$T_{si,j}$	interior surface / material temperature at time step j	[°C]
$T_{se,j}$	exterior surface / material temperature at time step j	[°C]

There is a distinct difference between a fixed value for thermal conductivity λ [W/(m·K)] and the value of transient thermal conductivity $\lambda'_{in\text{-}situ,\,j}$ [W/(m·K)] at that specific time step j.

Monitoring the heat flux q [W/m²] in-situ can result in highly fluctuating results (Flexeder et al., 2021). The *Heat flow meter method* in the standard for *Thermal insulation – Building elements – In-situ measurement of thermal resistance and thermal transmittance* (ISO 9869-1:2014-08) defines several criteria that must be fulfilled by the data, in order to produce statistically sound results and to conclude a single fixed value $\lambda_{in\text{-}situ}$ [W/(m·K)]. The standard describes the procedure of the so-called *Average Method* as in equation (4.18):

$$\lambda_{in-situ} = d \cdot \frac{\sum_{j=1}^{n} q_j}{\sum_{j=1}^{n}(T_{si,j} - T_{se,j})} \tag{4.18}$$

With

$\lambda_{in-situ}$	transient thermal conductivity, averaged from in-situ monitoring	[W/(m·K)]
d	distance between the two measurement points si and se	[m]
q_j	density of heat flow rate at time step j	[W/m²]
$T_{si,j}$	interior surface / material temperature at time step j	[°C]
$T_{se,j}$	exterior surface / material temperature at time step j	[°C]
n	number of time steps required to achieve statistically relevant results	[-]

The data obtained in the project *Timberbrain* did fulfil these criteria under certain circumstances. Consequently, fixed values for $\lambda_{in\text{-}situ}$ [W/(m·K)] could be calculated with equation (4.18). A detailed description of the methods how these resulting values for $\lambda_{in\text{-}situ}$ [W/(m·K)] were obtained and their respective values is given in (Flexeder et al., 2021). The data obtained in the project *Einfach Bauen* in the investigated time frame did not fulfil the statistical criteria explained by (Flexeder et al., 2021; ISO 9869-1:2014-08) for the *Average Method* (L. Franke et al., 2024).

4.7.2 Comparing several techniques and methods in test cubes with insulated CLT walls

As part of the research project *PhyTAB*, various experimental series were carried out in several test cubes in southern Germany. These small buildings were set up solely for research purposes and each have at least one wall with the structure depicted in Figure 87: an inner 5-layer CLT panel (100 mm), insulated by wood fiber insulation (140 mm), and covered by exterior plaster (10 mm). More information on the building of these cubes is given in (Flexeder, Kamml & Paulik, 2022; Flexeder, Schumacher et al., 2022; Kornadt et al., 2019).

Sensors for comparing the sorption method (SM, batch 22/23) with the electrical resistance method (ERM, batch 11), were installed in the cross-laminated timber wall in the north-eastern wall of the cube in Kösching and in the south/south-west facing wall in one of the cubes at the Technical University of Munich (TUM). Only in the latter, additional sensors for wireless measurements (SM, batch 21) were retrofitted in depths of 15 mm and 25 mm.

The raw measurement data were obtained at a 10-minute interval in the larger cube in Kösching and even at a 30-second interval (SM and temperature difference method) / 5-minute interval (ERM) in the smaller cube at the TUM in Munich. The results obtained in Chapter 5 are applied in Subsection 6.1 (6.1.1, 6.1.2) in order to compare the refined methods for transient wood moisture monitoring under test conditions and thus without any user influence.

Additional experiments to detect moisture fluxes on the surface by using the temperature difference method were also carried out in both cubes (not illustrated). Various results of this novel method have already been published in (Flexeder, Nouman & Hepf, 2022) and (Flexeder, Schumacher et al., 2022), cf. also Appendix I.

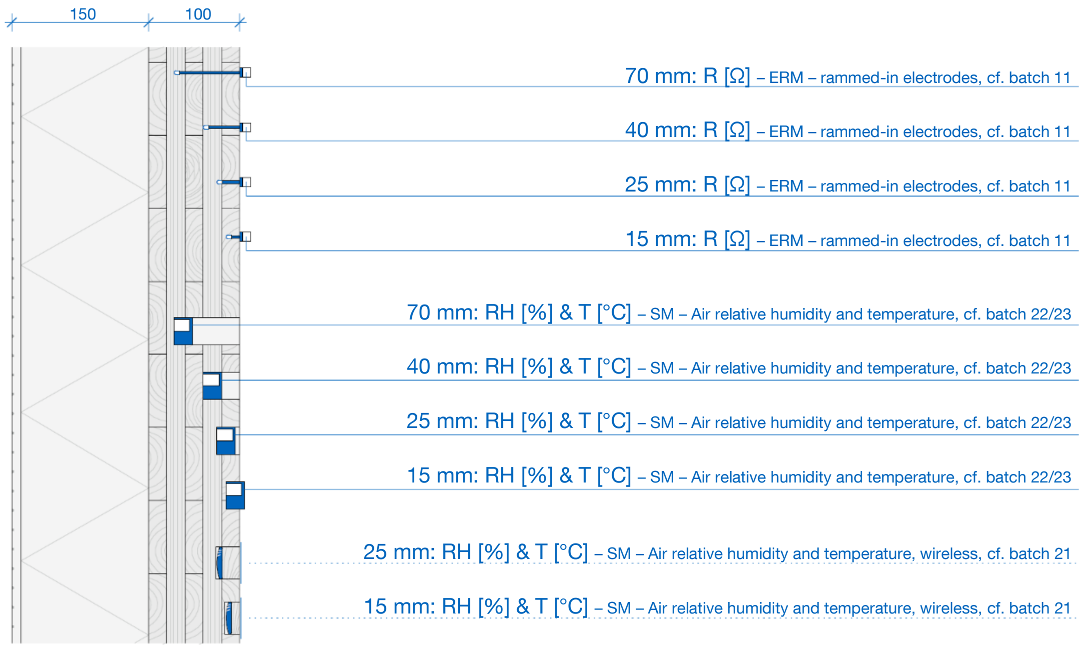

Figure 87: Horizontal section; scheme indicating the position of various sensors in the exterior walls of the test cube located on the Solarstation at the Technical University of Munich. The construction is similar to the exterior walls of the larger test cube in Kösching. The research project PHYTAB used both structures for experiments.

4.7.3 Applying several methods in an experimental dwelling with modified CLT walls

The research project *Einfach Bauen* in Bad Aibling, Germany, investigated the practicality of three newly constructed similar experimental residential buildings with different materials. More detailed information on the project is given in (L. Franke et al., 2024; Jarmer et al., 2021).

The measurement data examined as part of this work originates from two exterior walls of a dwelling in ordinary tenant use. The innovative construction of the north- and west-facing cross-laminated timber exterior walls has no extra insulation layer. Instead, small air slots inserted during production are intended to enhance the insulating effect of the solid timber cross-section. Figure 88 depicts a schematic horizontal section through the exterior wall structure. It should be noted that the positioning of the sensors is only indicated on a diagrammatic scale, they were not indeed all positioned on the same height and distance.

In particular, electrode tips of the measuring depths 70 mm, 150 mm, 175 mm, and 225 mm were possibly located completely or partially within the air slots. The electrode pairs were each mounted with a measuring distance of 30 mm with the measuring direction always perpendicular to the wood fiber. The pairs up to 40 mm in length were therefore placed vertically, the rest horizontally next to each other. In addition to the measuring points shown in Figure 88, the project collected a variety of other data at 10 minute-intervals, including the heat flow measured on the inside of the respective wall. The results of applying two techniques for the electrical resistance method (ERM) and the sorption method (SM), all with improved evaluation models and parameters based on Chapter 5, will be presented and further discussed in Subsection 6.2 (6.2.1, 6.2.2, 6.2.3).

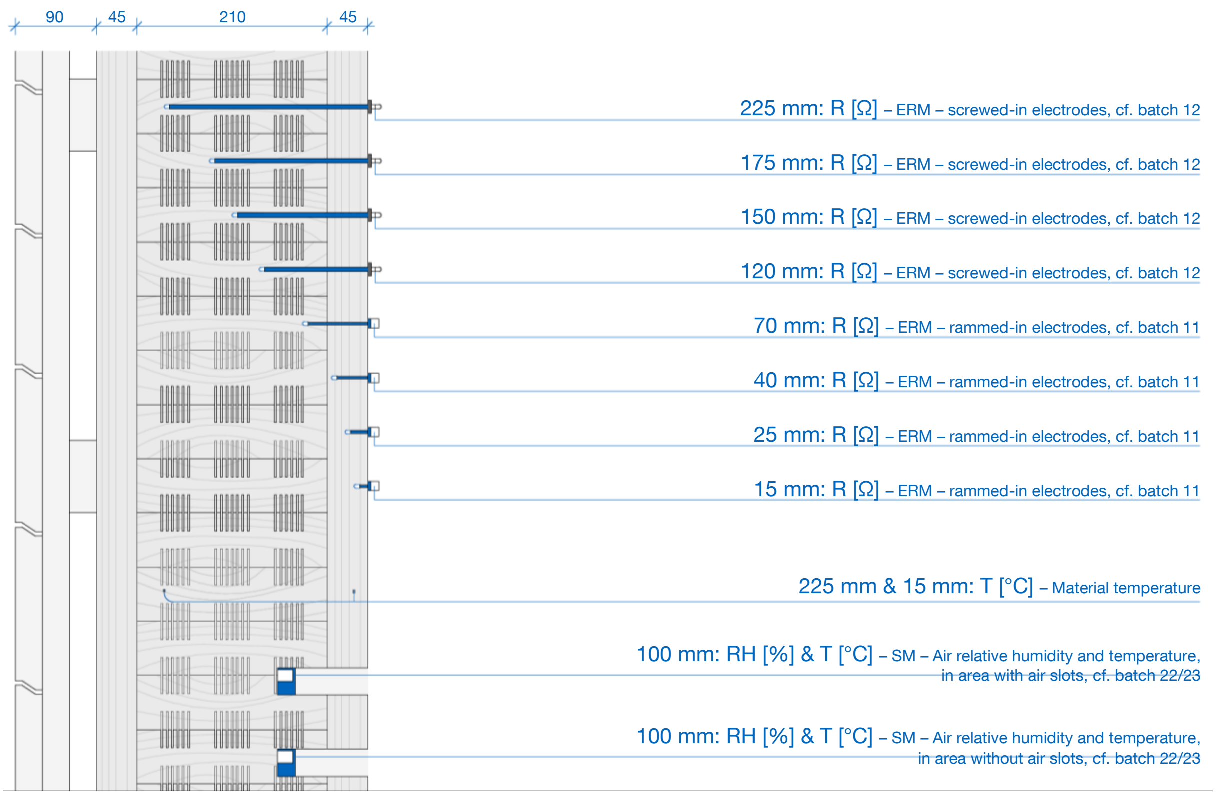

Figure 88: Horizontal section; scheme indicating the position of various sensors in the north- and west-facing exterior walls of the experimental dwelling project EINFACH BAUEN in Bad Aibling, Germany.

4.7.4 Improving the results of monitoring in an office building with uninsulated CLT walls

The first years of operating the new four-story office building *Timberbrain* in Hallein, Austria, were scientifically monitored by the Technical University of Munich. Numerous parameters were recorded in-situ and evaluated using an extensive monitoring concept. Further information about the research project can be found in (Bodemer et al., 2021); more details about the building is presented in (Binderholz Bausysteme GmbH).

The investigations also included recording the transient hygrothermal behavior in the uninsulated, nine-layer cross-laminated timber exterior walls (eight layers spruce and outermost, ninth layer in larch, sealed with biocidal impregnation). The mere thermal behavior of the exterior wall has already been satisfactorily monitored and evaluated in (Flexeder et al., 2021). The results for moisture content, which were obtained using a conventional evaluation method for the electrical resistance measurements, were however not sufficiently accurate (Flexeder, 2021), cf. Subchapter 2.4.3.

The measuring equipment in both the north-facing and west-facing exterior walls was identical and monitoring at a rate of 5 minute-intervals, cf. Figure 89. Eight pairs of electrodes were screwed into the CLT at different depths in each wall, with screws similar to those used in batch 12. The measuring distance between the electrode tips was constant at 30 mm, the alignment varied depending on the grain direction of the respective measuring depth, so that measurements were always taken perpendicular to the grain. In addition, temperature sensors were inserted at various depths via a nearby window reveal. The temperature gradient interpolated from this data was then used to convert the electrical resistance data into equivalent wood moisture values. In addition, a large number of other sensors not shown were installed, including two heat flux measuring plates. The improved methods for converting the values of electrical resistance *R* [Ω] into equivalent moisture content *EMC* [m.-%] from Chapter 5 for Norway spruce are applied in Subsection 6.3 to re-evaluate the raw data from this in-situ project.

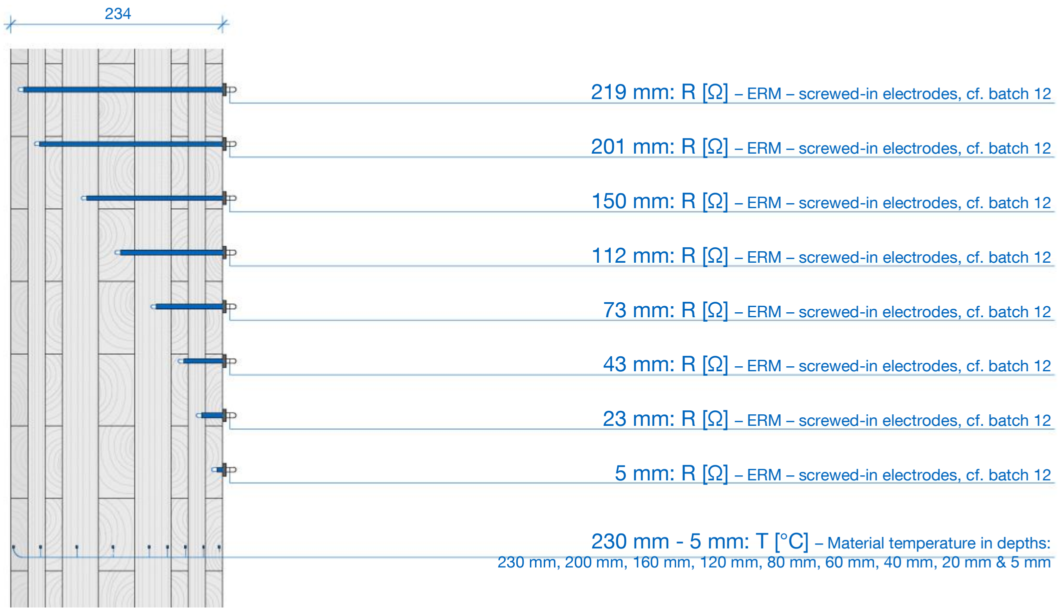

Figure 89: Horizontal section; scheme indicating the position of various sensors in the north- and west-facing exterior cross-laminated timber walls of the office building TIMBERBRAIN in Hallein, Austria.

5 MEASUREMENT RESULTS OF THE INDIVIDUAL APPROACHES TO IMPROVE AND TEST WOOD MOISTURE MONITORING IN LABORATORY STUDIES

5.1 Laboratory studies on the sensitivity of electrical resistance measurements

5.1.1 Investigations on the influence of the applied current voltage

When determining the equilibrium moisture content *EMC* [m.-%] using the electrical resistance method (ERM), the electrical resistance of the material between two electrodes is calculated from the measurement of a current intensity *I* [A] at a certain measurement voltage *U* [V]. What influence does the duration and the level of the measuring voltage have on the resulting electrical resistance when testing a typical wooden specimen?

The greater the applied electrical voltage, the greater the measured current flow (Ohm's law). Accordingly, on the same test specimen, the precision electrometer measures a current of $I_{20\,sec}$ = 0.9 nA (nano Ampere = 10^{-9} A) after 20 seconds when a voltage of 3.3 V is applied, $I_{20\,sec}$ = 3.5 nA at 10 V, and $I_{20\,sec}$ = 115.1 nA at 500 V. After conversion into the respective electrical resistance *R* in Figure 90, it is evident that the measuring voltage also influences the time for reaching a sufficiently constant value of the electrical resistance *R* [Ω].

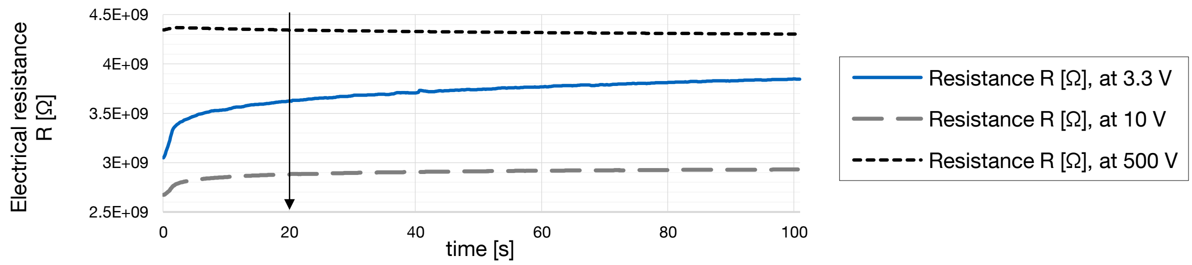

Figure 90: Transient electrical resistance R, obtained by applying three different voltages to rammed-in electrodes, measurement direction perpendicular to the grain, in the same test specimen of Norway spruce with MC = 11.75 m.-%, ρ = 403 kg/m³, and at a temperature of 23±0.5 °C

The evaluation in Figure 91 shows the resistances that were measured with the different voltages after 20 seconds in each case on 15 Norway spruce specimens. The gravimetric method was used to determine the actual wood moisture content *MC* [m.-%]. In order to put these fluctuations in relation, the calibrating curve for Norway spruce by (Du et al., 1991) and its respective confidence limits are added in Figure 91 and Figure 92. They show that most of the values are within or at least close to the confidence interval. The results from 3.3 V, 10 V, and 500 V for the same specimen are so close together that they partly overlap in Figure 91. Although the level of the measurement voltage *U* [V] clearly impacts the resulting electrical resistance $R_{20\,sec}$ [Ω] in the evaluated range, it is considered a tolerable influence on the accuracy on the electrical resistance method (ERM).

Remarkably, the relationship between the measuring voltage and the resulting resistance seems to be not linear. In the example examined, a measuring voltage of *U* = 10 V provides the lowest of the resistance results, which also come closest to the calibration curve for Norway spruce by (Du et al., 1991). It would be beneficial for the future development of wood moisture monitoring devices to investigate the optimal point where the measuring voltage

U [V] is as low as possible and the measuring currents *I* [A] are as high as possible, given the device-specific limitations of the general power supply.

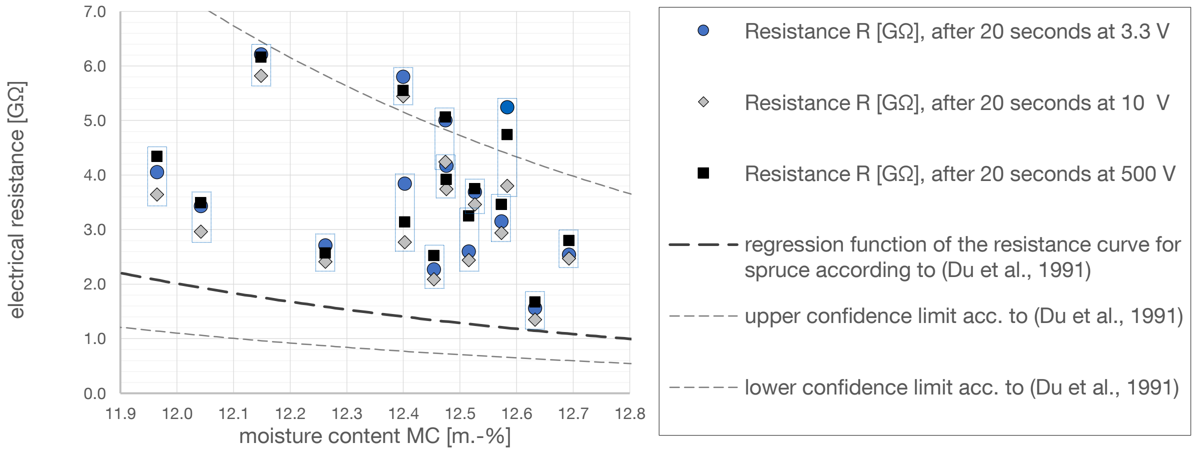

Figure 91: Influence of measurement voltage U [V] on the resulting value of $R_{20\,sec}$ [Ω] at a constant ambient climate. The scale is changed to GΩ (Giga ohm = 10^9 Ω) to provide better readability.

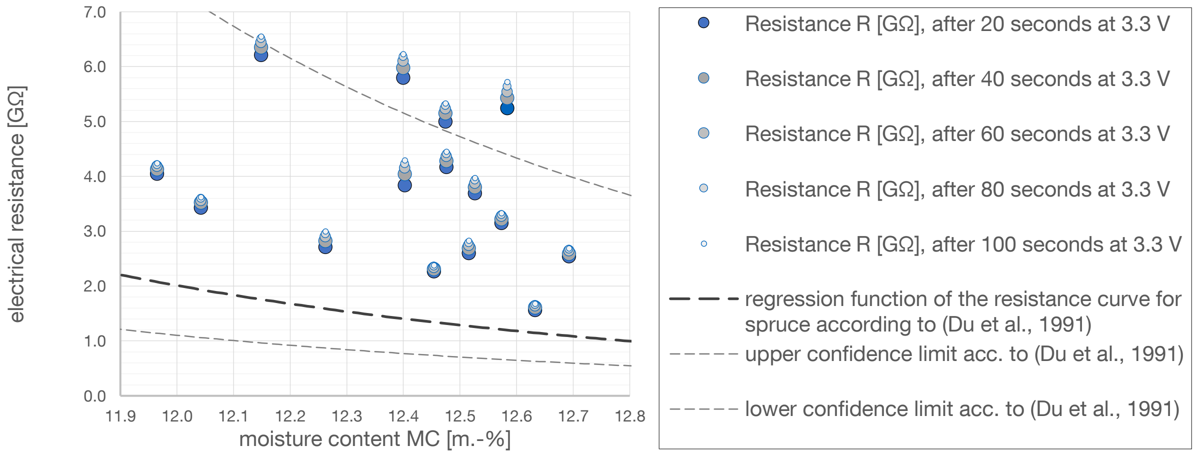

Figure 92: Evolvement of R [Ω] over time at a fixed measurement voltage of U = 3.3 V

The results for current intensity *I* [A] and thus also the calculated resistance *R* [Ω] change due to the chosen measurement time. Figure 92 illustrates as an example how with *U* = 3.3 V, the electrical resistance *R* [Ω] increases slightly over the course of 100 seconds. In relation to the conversion to a wood moisture value, however, this progression is marginal due to the logarithmic relationship. The tests using the high-precision electrometer in the shielded laboratory setup prove that the measurement voltage and duration have an influence on the electrical resistance determined in the wood. However, these influences might be rather minor compared to others.

According to the examples examined, simplifying the measurement strategy to a low voltage such as 3.3 V over 20 seconds seems plausible. In addition, the scattering results indicate that the electrical resistance measurement in wood is in some cases significantly more strongly influenced by other variables, not the electrical resistance measurement by the technical device itself.

5.1.2 Correlation of tight-fitting electrodes with more accurate measurement results

The electrical resistance method (ERM) is influenced by specific factors such as the contact between electrode and wood. Evaluating the mobility of the rammed-in electrodes shows a clear tendency with regard to the expected accuracy. The more firmly the electrodes are anchored in the wood, the closer the correlation determined from electrical resistance *R* [Ω] and moisture content *MC* [m.-%] is to the correlation described for Norway spruce by (Du et al., 1991). The more loosely the electrodes are seated in the material, the higher the measured resistance *R* [Ω] with otherwise very similar actual wood moisture contents *MC* [m.-%], which is determined gravimetrically. Presumably due to the lack of contact pressure, up to three times higher electrical resistance values are measured here, cf. Figure 93.

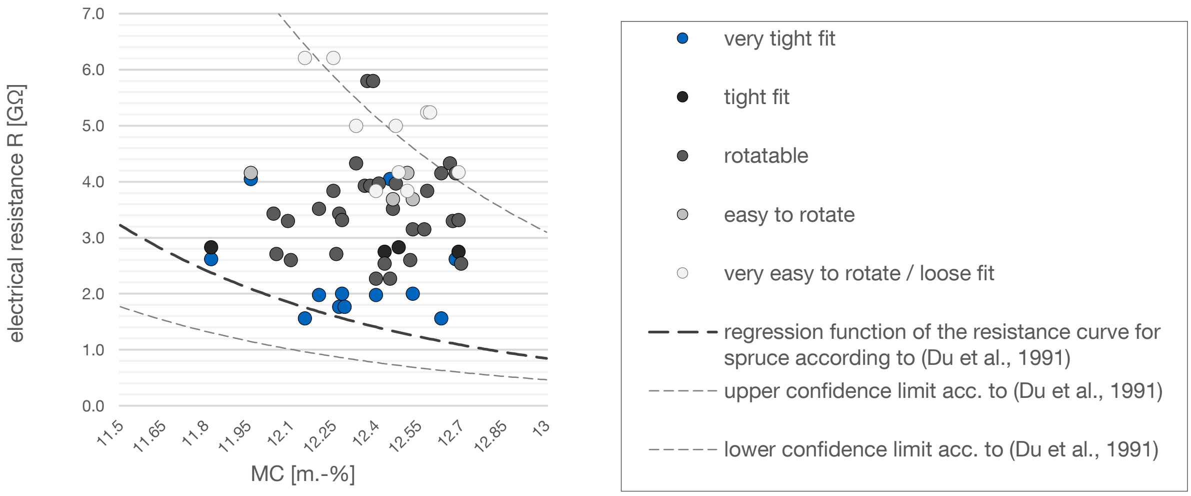

Figure 93: Relationship of measured electrical resistance R [GΩ], MC, and EMC [m.-%], with correlations to the tightness of the electrodes´fit. These results are based on the preliminary experiments with smaller specimen size.

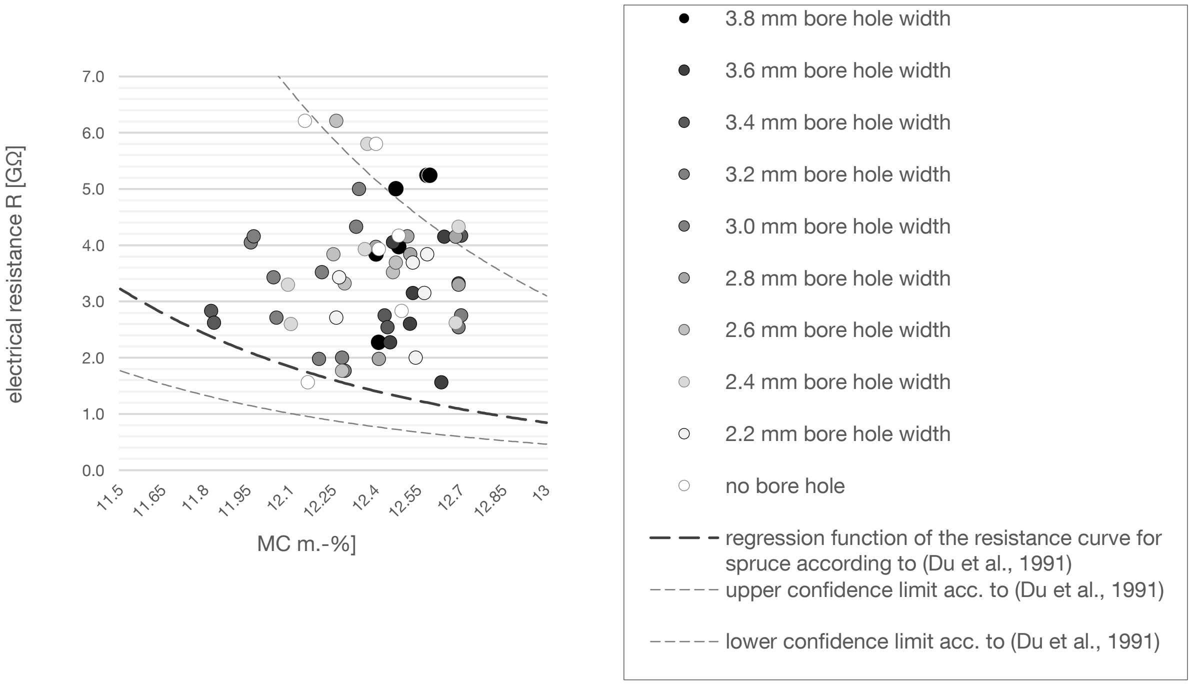

Figure 94: Relationship of measured electrical resistance R [GΩ], MC, and EMC [m.-%], showing no clear correlations to the diameter of the pre-drilled holes. For better readability of single values, refer to Figure 96.

However, in the preliminary experiments, this clear correlation cannot be associated unambiguously with any of the examined hole diameters, cf. Figure 94, Figure 95, and Figure 96. On the basis of these results, it is therefore not possible to provide a clear recommendation for the preparation of the wood prior to insertion of the rammed-in electrodes.

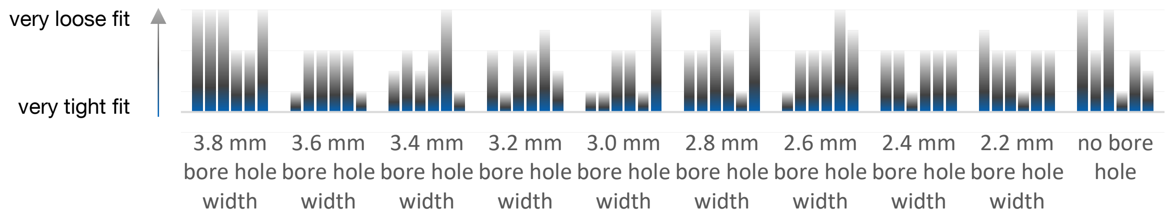

Figure 95: Distribution of rotatability of the electrodes in relation to the diameter of pre-drilled holes for the electrodes´ tips in Norway spruce specimens; results from the preliminary experiments on smaller specimens

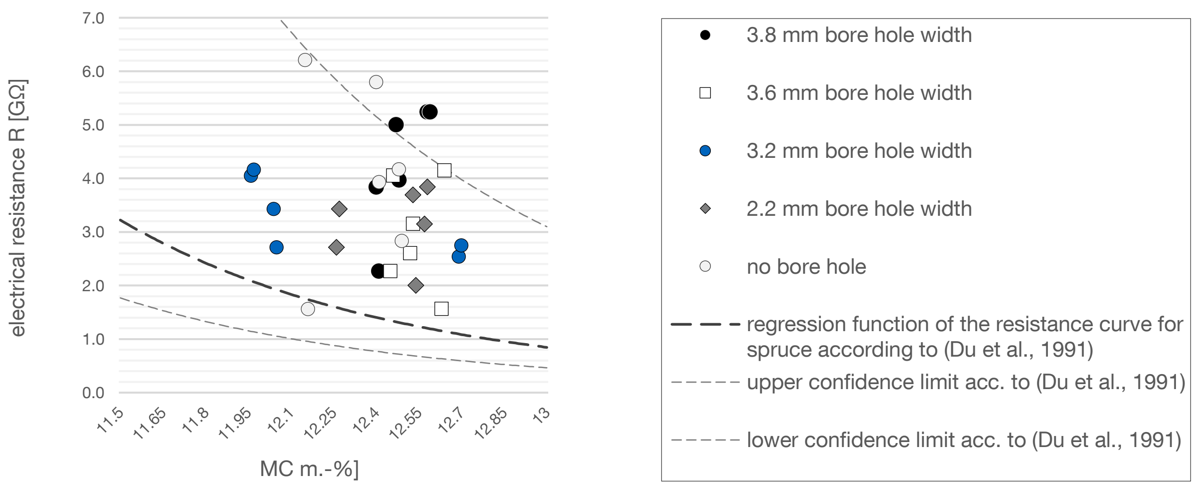

Figure 96: Relationship of measured electrical resistance R [GΩ], MC, and EMC [m.-%], showing no clear correlations to the diameter of the pre-drilled holes in the experiments using the smaller specimen size. For better readability, the illustration only depicts the results from these bore hole widths that are than picked for further evaluation in the main experiment on larger specimens.

Based on the results from the preliminary testing in this subchapter on 10 x 3 specimens with smaller dimensions (50 mm x 50 mm x 50 mm), the results of the following main experiment use larger specimens (100 mm x 100 mm x 100 mm) in order to avoid possible influences at the edges. These larger specimens take considerably longer to achieve a uniform wood moisture content.

Therefore, five diameters (3.8 mm, 3.6 mm, 3.2 mm, 2.2 mm, 0.0 mm) are being selected as representative values, cf. Figure 96. These hole diameters are being further investigated regarding their influence on the measurement results under moisture fluctuations in the next Subchapter 5.1.3.

5.1.3 Results from long-term conditioning series with different bore hole widths

The findings from the previous Subchapter 5.1.2 are investigated further in an experiment with larger but fewer specimens with selected pre-drilled bore hole widths for the rammed-in electrodes (3.8 mm, 3.6 mm, 3.2 mm, 2.2 mm, 0 mm). While the previous experiment only investigated the electrodes´ fit at a steady wood moisture content, the following experiment involves a controlled isothermal shrinking process (290 days), followed by an isothermal swelling process (twelve days), cf. methods in Subchapter 4.2.3 and Figure 97.

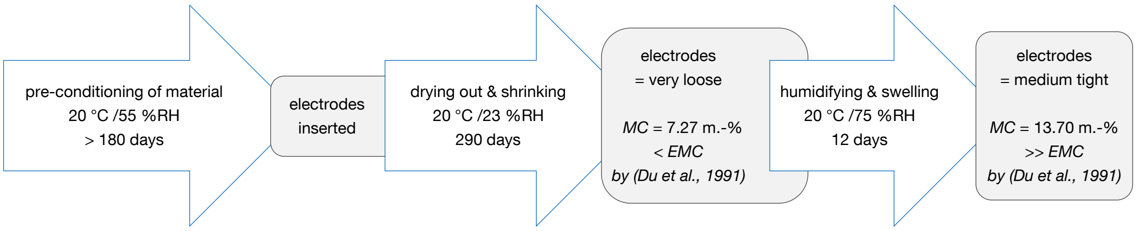

Figure 97: Summary of long-term conditioning and resulting electrodes´fits in Norway spruce

The results show that after drying out at 20±0.5 °C / 23±1 %RH over 290 days, all test specimens had an initial moisture content of *MC* = 7.27 m.-% (mean value with a standard deviation *SD* of 0.07 m.-%). These ambient air conditions would have led to *EMC* ≈ 5.0 m.-% according to Figure 13, p. 52, and to *EMC* ≈ 6.5 m.-% according to Figure 123, p. 138 (SM). After this extended conditioning phase, an initial moisture gradient in the test specimens can be excluded. The isothermal moisture step of ambient relative humidity to 75±1 %RH initially led to a moisture gradient from the outside into the center of the respective specimen.

However, after twelve days, this gradient had already been balanced out to such an extent that the examination of the intermediate piece of wood between the electrodes did not produce any results that deviated significantly from the overall wood moisture content determined. After twelve days, the oven-dry method showed an average moisture content of *MC* = 13.70 m.-% (mean value with a standard deviation *SD* = 0.28 m.-%), for both, the overall the specimens as well as the chiseled out intermediate parts. This observation could be coincidental and does not prove that the moisture transport had already been completed – especially since *EMC* at 20±0.5 °C / 75±1 %RH would be expected to be higher (SM). However, the examination of the exposed intermediate parts assures the findings about the moisture content actually present in the area directly between the electrodes.

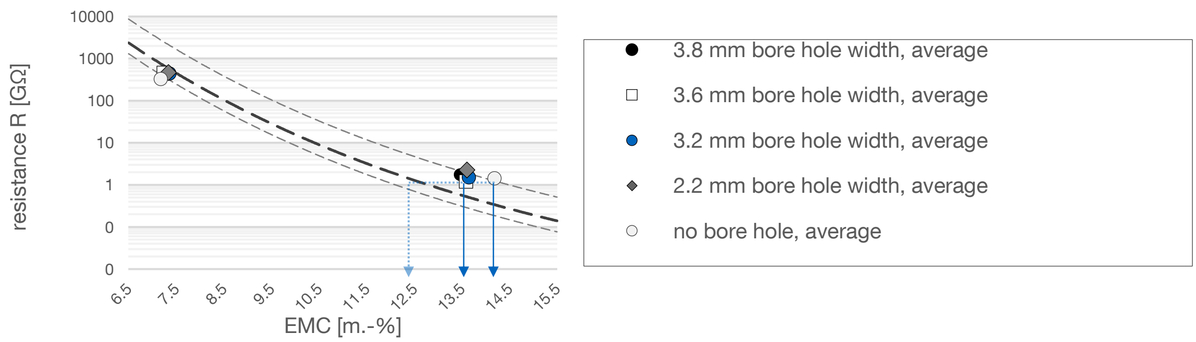

Figure 98: Correlations of measured EMC [m.-%] and electrical resistance [GΩ] before and after the moisture step experiment. Values are averaged and shown in comparison to the correlation given by (Du et al., 1991) with a logarithmic scaling of the ordinate (y-axis). For single results, see Figure 101 and Figure 102, p. 117.

All tested specimens show a significant decrease in electrical resistance *R* after the isothermal moisture step change from 23 %RH to 75 %RH. Within the investigated period of twelve days, the measured electrical resistance *R* between the rammed-in electrodes drops from an average of 400 GΩ (standard deviation *SD* = 63 GΩ) to 1.6 GΩ (*SD* = 0.4 GΩ). According to the correlation given by (Du et al., 1991) for spruce, this would correspond to an increase in equilibrium moisture content *EMC* from around 7.6 m.-% to 12.2 m.-%. However, the actual *MC*s before the moisture step change are first slightly lower and after are even significantly higher than that (around 13.4 m.-% to 14.3 m.-%), cf. Figure 102. This could ultimately mean that after humidification, the actual *MC*s might be systematically underestimated by ERM when evaluated according to (Du et al., 1991), cf. Figure 98. Although the results differ depending on the pre-drilled hole diameter, there is no clear correlation and therefore no clear recommendation for a certain dimension.

Depending on the pre-drilled hole diameter, the decrease in the measured electrical resistance can be observed with different time delays, cf. Figure 99. In particular, the different batches already show significant differences directly after the humidity step. In an interesting development, the electrical resistance measured for the batch with no pre-drilled holes for the electrodes´ tips even increases abruptly at the beginning, cf. Figure 100.

Checking the mobility just before the moisture step experiment results in a very loose fit for all electrodes, no matter which hole diameter was pre-drilled. While the wood moisture content is increasing over the course of the twelve days, this condition changes. At the end of the experiment the electrodes of the batches with a pre-drilled hole diameter of $d \leq 3.6$ mm are all fitting moderately tight in the material and can only be turned slightly. Only the electrodes of the batch with a diameter of $d = 3.8$ mm can still be moved very easily by hand, even with the increased *MC*.

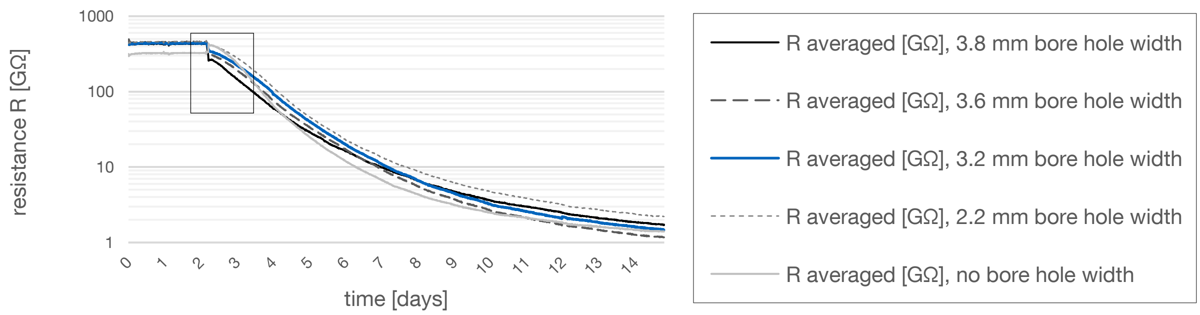

Figure 99: Measured electrical resistance between two electrodes in Norway spruce specimens after an isothermal moisture jump, logarithmic scaling of the ordinate (y-axis). The box indicates the section shown in Figure 100.

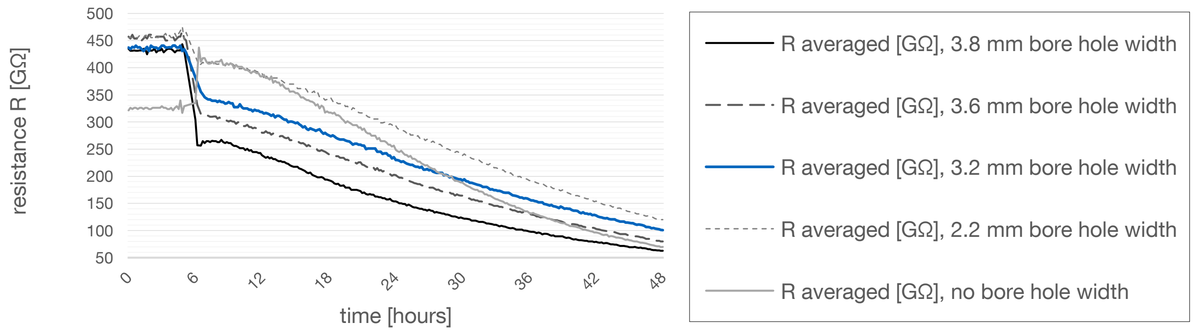

Figure 100: First 48 hours of the experiment with a sudden moisture step change to a more humid environment

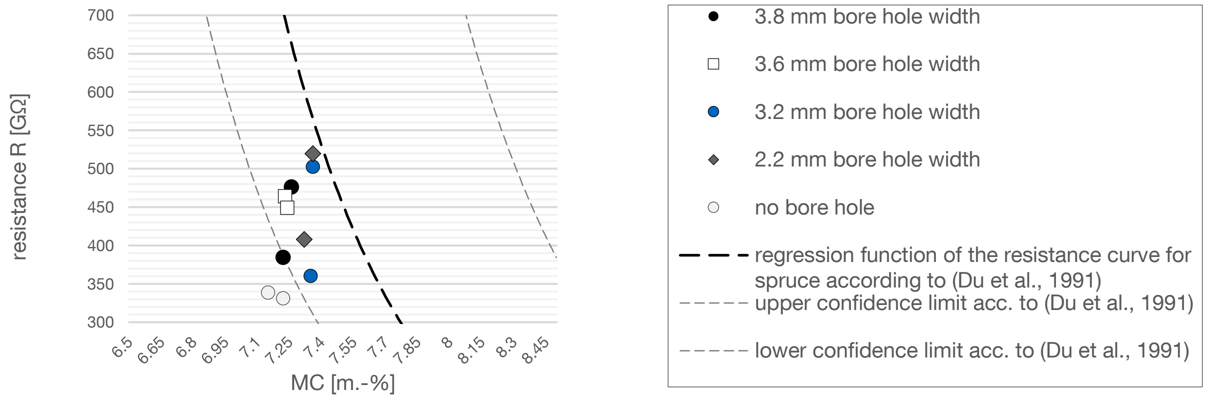

Figure 101: Correlations of measured MC [m.-%] and electrical resistance [GΩ] in Norway spruce specimens after 290 days at 20±0.5 °C / 23±1 %RH, shown in comparison to the correlation given by (Du et al., 1991) for spruce

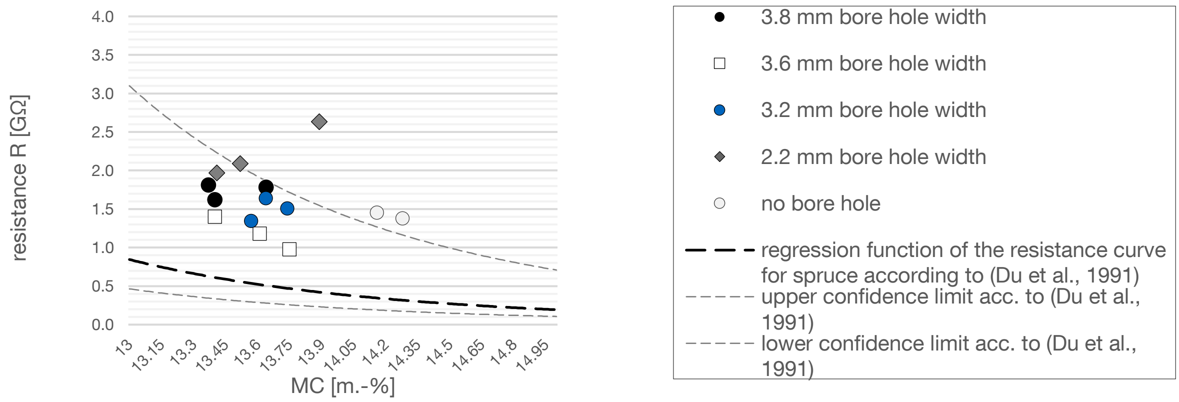

Figure 102: Correlations of measured MC [m.-%] and electrical resistance [GΩ] in Norway spruce specimens after twelve days at 20±0.5 °C / 75±1 %RH, shown in comparison to the correlation given by (Du et al., 1991) for spruce

This correlation, however, is not reflected when analyzing the measurement results in regards to the regression function for Norway spruce by (Du et al., 1991), cf. Figure 102. Accordingly, no general recommendations on the use of a specific hole diameter can be derived from the experimental results. Nevertheless, the experiments show that electrodes with a very loose fit can lead to a falsification by several mass percentage points [m.-%].

In general, the moisture step experiment proves that swelling due to an increase of relative humidity will lead to less rotatability in the electrodes and thus an improved contact pressure. Accordingly, decreases of the contact pressure on the electrodes due to shrinkage processes are also possible by moderate wood moisture changes in the hygroscopic range. The observed deviations are mostly still within the confidence interval (95 %), only those without any pre-drilling (no bore hole) are slightly outside these limits. It is expected that more pronounced changes in wood moisture content will also lead to even more distinct falsifications of presumed wood moisture monitoring results by electrical resistance measurements.

The choice of a certain pre-drilled hole diameter appears to influence these phenomena only to a limited extent. The results with a 3.2 mm diameter pre-drilled hole for a 3.7 mm thick rammed-in electrode tip have so far yielded acceptable results. Consequently, this diameter (d = 3.2 mm) is selected for pre-drilling for these type of rammed-in electrodes in further investigations.

5.1.4 Experiments on electrodes´ fit by withdrawal testing on Australian species

The results from the previous Subchapters 5.1.2 and 5.1.3 do not establish a clear correlation between the pre-drilled hole for the electrodes and the accuracy of the electrical resistance measurement. Therefore, the next experiments only use the same diameter of 3.2 mm. However, there is a correlation between the manually checked position of the electrode and the accuracy of the measurement. Pairs of electrodes, in which both have a very tight fit in the wood, provide results that match a known calibration curve best. In order to additionally quantify this manual inspection and classification later on, mechanical extraction tests are carried out additionally on three Australian wood species.

Figure 103 and Figure 104 show the independently determined "tightness of fit" according to the evaluation matrix that was already introduced as a manual classification in Subchapter 5.1.2, p. 113. In a subsequent investigation using pull-out testing with a universal testing machine (UTM), this shows a correlation to the electrode withdrawal peak load capacity at EWC = 20 N – 150 N. Above that, at EWC > 150 N, electrodes seem to not be moveable by hand anymore and therefore sort as "very tight-fitting" according to the previous manual evaluation. Strikingly, the electrodes in the specimens made of shining gum (*Eucalyptus nitens*) and radiata pine (*Pinus radiata D. Don.*) all show a medium to very tight fit. However, the electrodes rammed into the wood species spotted gum (*Corymbia maculata*), sit either exceptionally loose or exceptionally tight in the material; there are no intermediate stages with this wood species in this experiment. It should be noted that the latter is a hardwood species with more than twice the oven-dry density ρ_0 than the other two, cf. Subchapter 4.2.4.

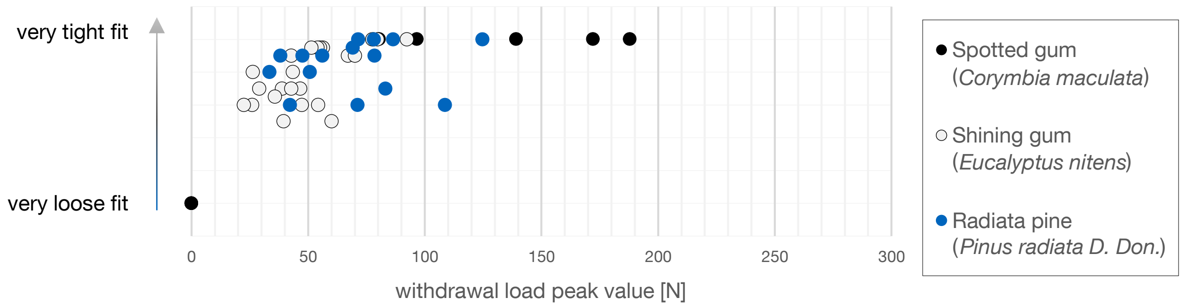

Figure 103: Results of first measurement series showing a correlation between withdrawal peak load capacity [N] and manually estimated movability of electrodes in three different subtropical wood species; measurements at mass constancy, after steady pre-conditioning at 23±0.5 °C / 57±2 %RH for 65 days

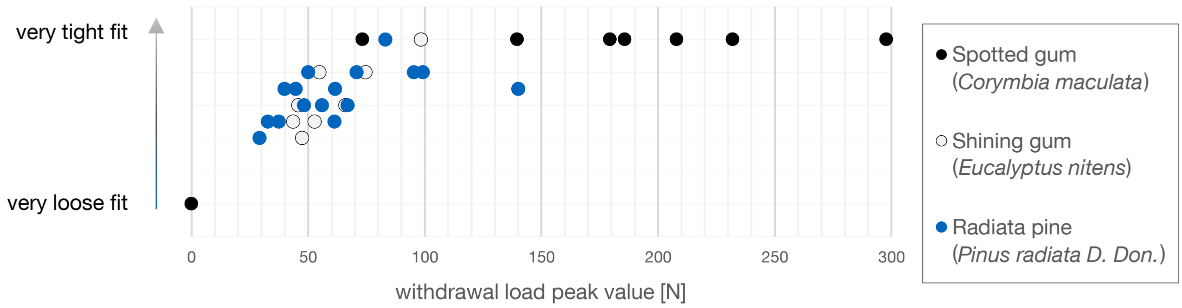

Figure 104: Results of second measurement series showing a correlation between withdrawal peak load capacity [N] and manually estimated movability of electrodes in three different subtropical wood species; measurements after climate step chance to 35±1 °C / 36±5 %RH for 45 hours, possibly with moisture gradients in the specimens

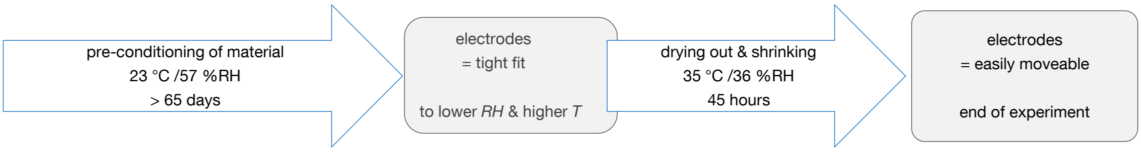

Figure 105: Summary of conditioning and resulting electrodes´ fits in shining gum and radiata pine

Figure 105 summarizes the fact that in both, shining gum and radiata pine, the electrodes show a significantly tighter fit (manually classified) at a constant climate of 23±0.5 °C / 57±2 %RH than later, after the drying phase at 35±1 °C / 36±5 %RH. The observation of the electrodes becoming looser with decreasing wood moisture content is consistent with Subchapter 2.4.2 and the findings from Subchapter 5.1.3 on Norway spruce.

However, the results generated by withdrawal testing are not quite as clear. The first series of withdrawal testing, maintaining the constant climate, result in mean electrode withdrawal peak load capacity of $\overline{EWC}$ = 52 N (*SD* = 19 N) for shining gum and $\overline{EWC}$ = 69 N (*SD* = 29 N) for radiata pine. After the drying-out phase, the force required to pull out the electrodes from the radiata pine specimens is measured at a lower value of $\overline{EWC}$ = 64 N (*SD* = 26 N), as expected. In shining gum, on the other hand, this force even has increased to $\overline{EWC}$ = 60 N (*SD* = 19 N). The reason for this is not yet clear. However, it should also be mentioned that for the second round of measurements, the electrodes were each rammed into new pre-drilled holes; hence there might be significant material differences even within the same test specimen. Furthermore, explicit reference is made to the comparatively high values for standard deviation (*SD*). The number of specimens and tests might simply be too small to allow a statistically reliable statement. Despite this statistical inaccuracy, the measurement results already provide initial indications of trends.

The following figures show results that were determined on the three types of wood after achieving constant mass at 23±0.5 °C / 57±2 %RH. They may therefore also serve as reference points for future calibration curves. Figure 106 shows the electrical resistance values *R* [Ω] measured in the test specimens of the three Australian wood species in relation to the wood moisture content *MC* [m.-%] determined using the gravimetric method. Since the measurement result of the electrical resistance measurement always refers to a pair of electrodes, the looser-fitting electrode of the two is used for evaluation in Figure 107, Figure 108.

Unfortunately, no reliable calibration curve for the electrical resistance measurement in the three types of wood spotted gum (*Corymbia maculata*), shining gum (*Eucalyptus nitens*), and radiata pine (*Pinus radiata D. Don.)* is available at the time of writing. This means that a comparison as in Subchapters 5.1.2 and 5.1.3 of the extent to which the position of the electrodes influences the position of the measuring points within a known confidence interval is not possible. Nevertheless, the results on radiata pine are compared with the characteristic curve determined for Scots pine by (Du et al., 1991). Even though these are two different wood species, the evaluation in Figure 109 indicates results, which are somewhat consistent with the detailed evaluations of Norway spruce in Subchapters 5.1.2 and 5.1.3. Building on the findings from Subchapters 5.1.2 and 5.1.3, in this subchapter, the pre-drilled hole diameter for the rammed-in electrodes was kept uniform at *d* = 3.2 mm.

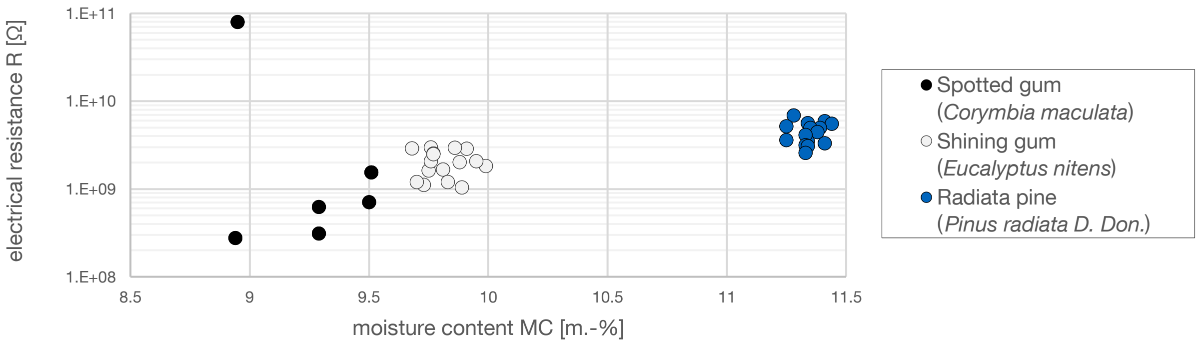

Figure 106: Results of electrical resistance measurements in spotted gum (Corymbia maculata), shining gum (Eucalyptus nitens), and radiata pine (Pinus radiata D. Don.) at 23 °C

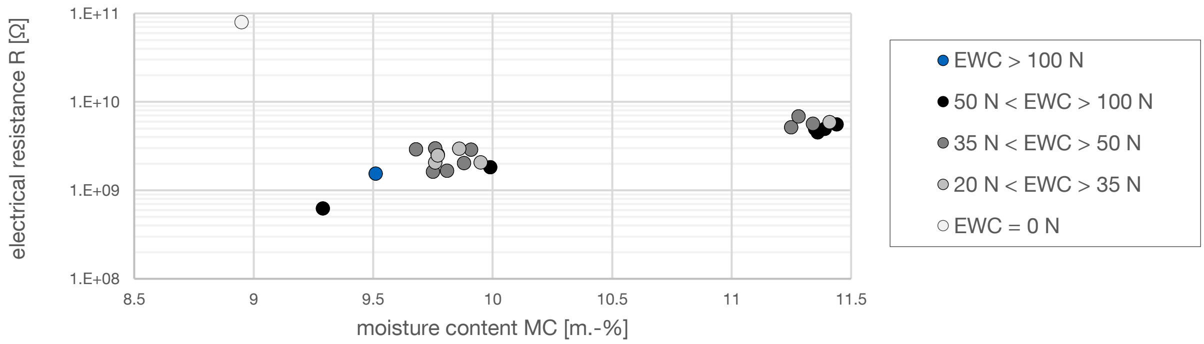

Figure 107: Selection of measurement results shown in Figure 106, sorted by their electrode withdrawal peak load capacity EWC [N] at 23 °C

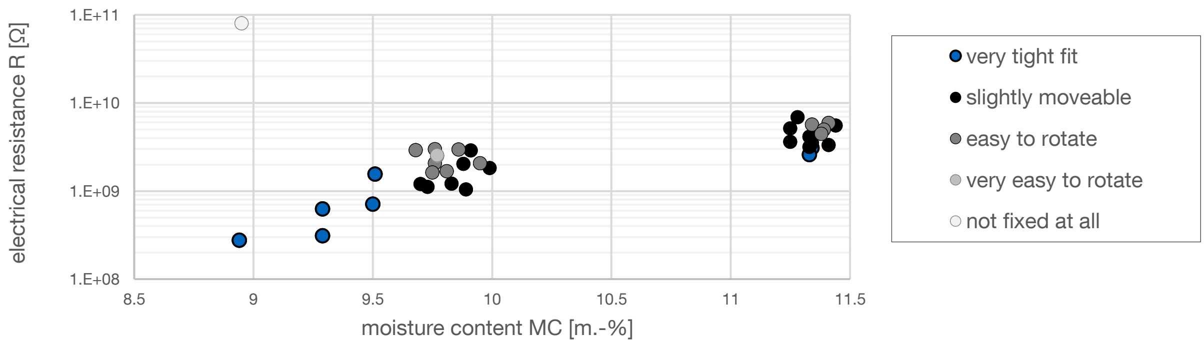

Figure 108: Results, as shown in Figure 106, sorted by the electrodes´manually determined tightness of fit at 23 °C

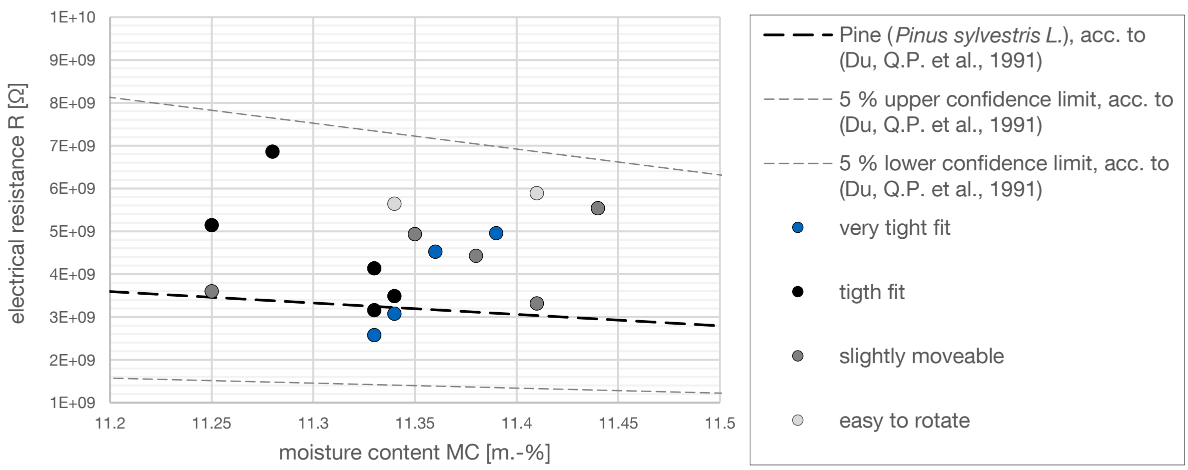

Figure 109: Tightness of fit for electrodes in radiata pine after preconditioning at 23±0.5 °C / 57±2 %RH for >65 days; juxtaposed to the calibration curve for Scots pine by (Du et al., 1991).

5.1.5 Differences of various sensor geometries and conductive materials

Could the issue of a diminished electrical contact between rammed-in electrodes and wood be solved by using a different electrode material? Laboratory tests using electrical resistance measurements at 10-minute intervals in Norway spruce shall tentatively investigate this idea. They show that all three electrode variants introduced in Subchapter 4.2.5 can provide enough conduction to produce plausible resistance values.

With the rammed-in stainless steel electrodes, both with and without an additional silicone ring, as well as the specially manufactured screwed-in threaded rods made of galvanized steel, similar electrical resistances can be measured after a certain delay. Figure 110 shows the average values from twelve test specimens in total over the first six hours of a monitoring test. It is noticeable that all of the constellations fluctuate at the beginning until they output a constant resistance value. In the case of the metal electrodes without any silicone, this point is reached after around 90 minutes. In the case of the rammed-in electrodes with an additional silicone ring, this initial phase takes about twice as long (180 minutes). The resulting initial difference between the two electrode types in batch 2 of $\Delta R \approx 6{\cdot}10^{10}$ Ω corresponds to a difference in equivalent wood moisture content of $\Delta EMC \approx 0.2$ m.-% in Norway spruce at 20 °C.

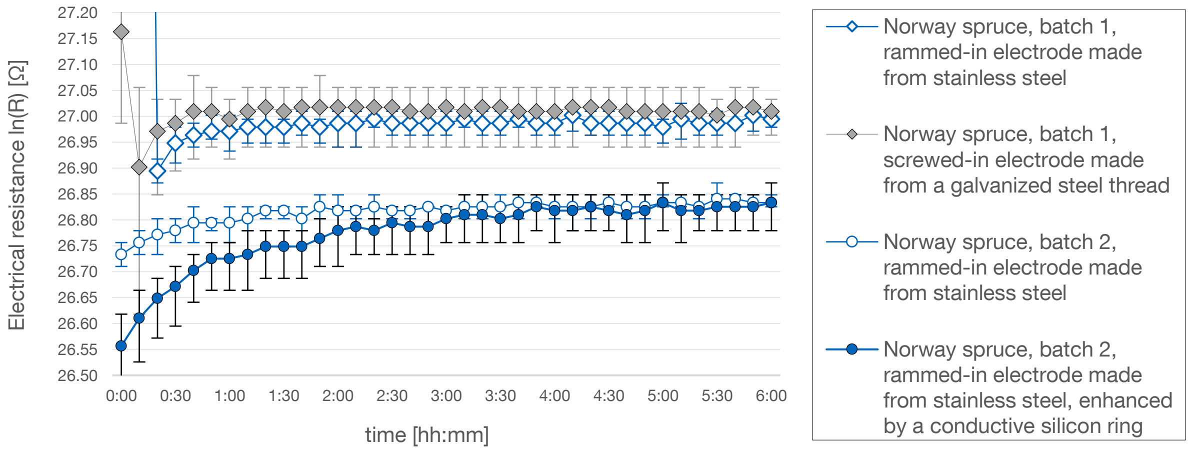

Figure 110: First six hours after start of electrical resistance measurements, shown as a natural logarithm. The graphs show a mean value of three test specimens each with the scattering indicated individually for each measuring point.

After six hours, the measured values in batch 1 are constant at $R \approx e^{27.00}$ Ω, which corresponds to $EMC \approx 7.4$ m.-% in Norway Spruce at 20 °C based on (Du et al., 1991). The measured values in batch 2 result in $R \approx e^{26.84}$ Ω, which would correspond to $EMC \approx 7.5$ m.-% accordingly. From this point onwards, the choice of electrodes appears to have a much smaller influence than the fluctuations caused by different batches from the same type of wood. Consequently, the differences that can arise within the same type of wood are further elaborated in Subchapter 5.2.2.

Furthermore, the hypothesis that the choice between rammed-in electrodes and screwed-in electrodes has no major influence on the measurement result is further tested in Subchapters 5.4.2, 5.4.3, and 5.4.5. Finally, the reevaluation of raw data in Subchapter 6.2.1 uses these findings for in-situ monitoring in an exterior CLT wall. Even though it seems to not produce any major deviations, the variant of the additional silicone ring is not pursued further in this thesis. Instead, the alternative of bonding the cables directly into the wood is being investigated. The various conductive adhesives and silicones produced for this purpose are tested both for their usability as fastenings and for their conductivity. Subchapter 4.2.5 describes the methods and Appendix B the recipes, some of which are based on (Brischke et al., 2008). For all formulations tested in wood, larger quantities of material were also poured into round trays as retention specimens. Figure 111 shows these specimens after several days of curing.

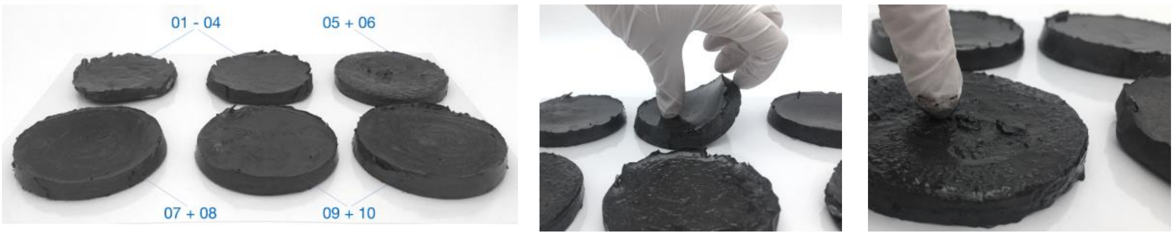

Figure 111: Retention specimens of the mixtures described in Table 21, Appendix B, p. 235

Depending on the mixture used, the retention specimens have a differently smooth surface and elasticity. Testing the conductivity within the disks shows that the electrical conductivity varies greatly. The electrical resistances of all specimens with the mixtures 05 - 10 are so extraordinarily high at a distance of 10 mm that it is already outside the range that can be measured with a conventional multimeter. These formulations (05-10), which use some type of silicone as the base material, are therefore classified as not suitable as a conductive aid.

The measurements on the reference specimens 01 - 04 with the formulation with epoxy resin and hardener show that the conductivity of the material is not homogeneously distributed. Values between 20 kΩ and 60 MΩ are measured over a distance of 10 mm. An electrical conductivity of 10^7 Ω/cm would be already close to the electrical resistance of moist wood, close to the fiber saturation point. These electrical resistance values are thus relatively high for a material considered conductive. However, they appear to be acceptable for measurements in wood well below fiber saturation and thus with much higher resistances. The low electrical conductivity of the composites is due to the carrier material (epoxy or silicone), as the added graphite powder is very conductive in itself, cf. Subchapter 3.3.4. After the curing time, the mixtures produced with extra-fine graphite powder (15-20 µm) hold the inserted cables tightly in the wood. The coarser graphite powder (55 µm) is not sufficient for this, as the cables can still be pulled out. Samples 05 and 06 will be therefore not considered any further.

Figure 112 presents the resulting electrical resistances measured by cables that were fixed in the wood with various mixtures. On the following page, the same results are illustrated using three differently scaled y-axes in order to demonstrate the importance of logarithm. The mean values for *R* [Ω], measured after two hours in the wood, vary significantly between the mixtures containing epoxy and those with silicone. This confirms the previous results measured on the retention specimens. Since lower resistance values indicate a better conduction between measurements system and wood, version 01-04 as in (Brischke et al., 2008) is considered the best option, cf. Table 21 and Table 22 in Appendix B, p. 235. Consequently, this formula is used for further testing in Subchapters 5.4.2, 5.4.3, and 5.4.5.

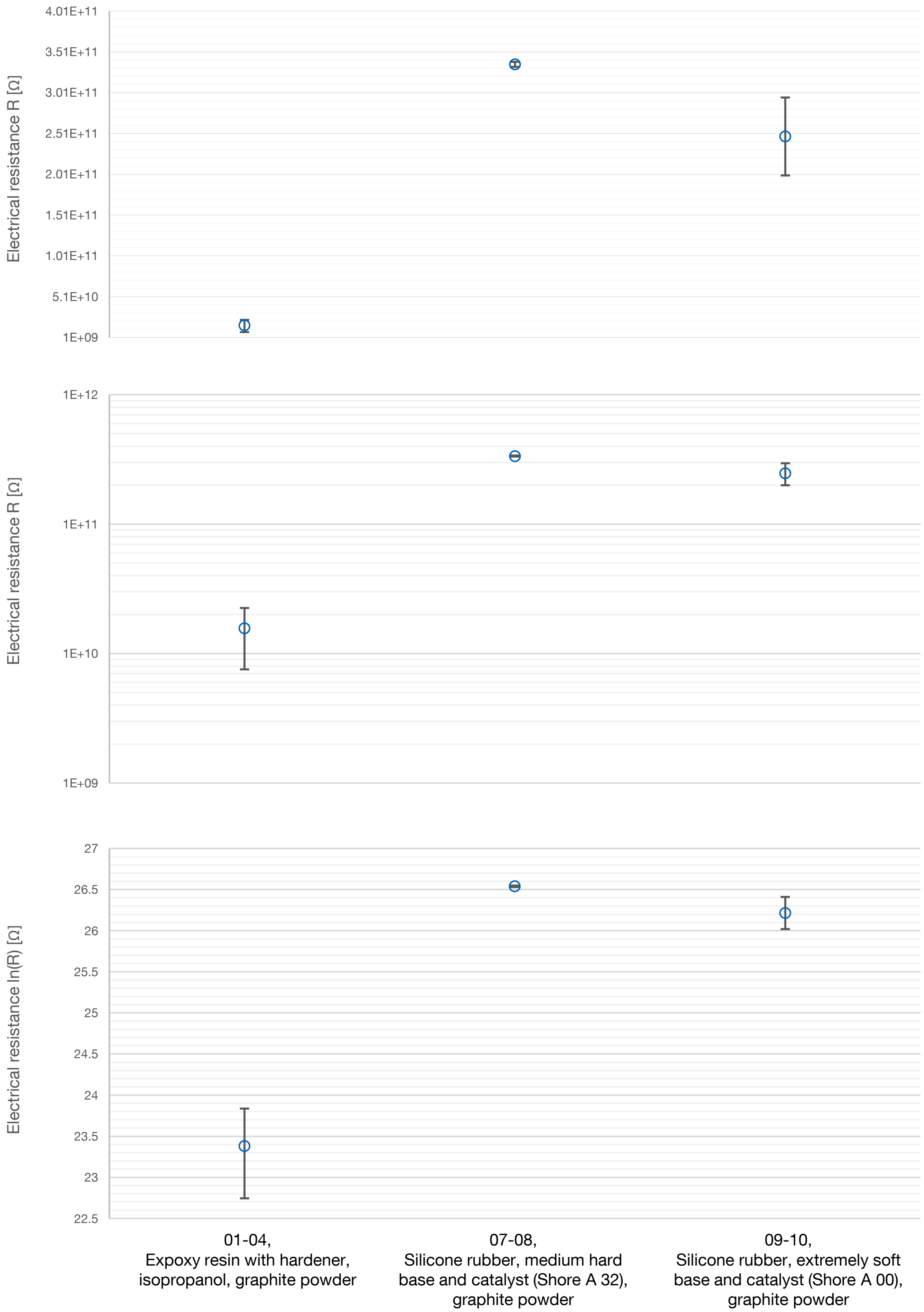

Figure 112: Resistance values, displayed with three different y-axes to demonstrate the variety of results depending on the scaling. The mixtures use epoxy or different silicones according to Table 21 in Appendix B, p. 235.

5.2 Improvement of the electrical resistance method for wood species and products

5.2.1 Checking the calibration curves specific to Norway spruce (*Picea abies Karst*.)

Moisture content monitoring using the electrical resistance method (ERM) is subject to numerous influencing variables, cf. Subchapter 4.2.1 and previous Subsection 5.1. Wood species or timber product, measuring direction, and temperature directly affect the electrical resistance *R* [Ω] of the measured material and are accounted for by calibration curves investigated in this Subsection 5.2. The following evaluation refers to the models presented in Subchapters 3.2.4 and 4.3.1. Using the own, simplified model (4.7) instead of model (4.4) published by (Du et al., 1991) allows to calculate the wood moisture content $X_{20\,°C}(R)$ at a base temperature of 20 °C. In order to be able to utilize the values determined by (Du et al., 1991) in this transformation, model (4.7) is first fitted to the original curves. The following new parameters are thus valid for a wood moisture content range from 0 m.-% to 30 m.-%:

$$X_{20\,°C} = -\frac{1}{g} \cdot ln(\frac{ln(R) - h}{f}) \quad (4.7)$$

With

R Electrical Resistance [Ω]

	f	g	*h*		*NRMSE*
Norway spruce (*Picea abies Karst.*)	31.5	0.109	12.908	-	*0.020*
European beech (*Fagus sylvatica L.*)	30.8	0.105	11.102	-	*0.004*
Scots pine (*Pinus sylvestris L.*)	35.1	0.124	13.213	-	*0.011*

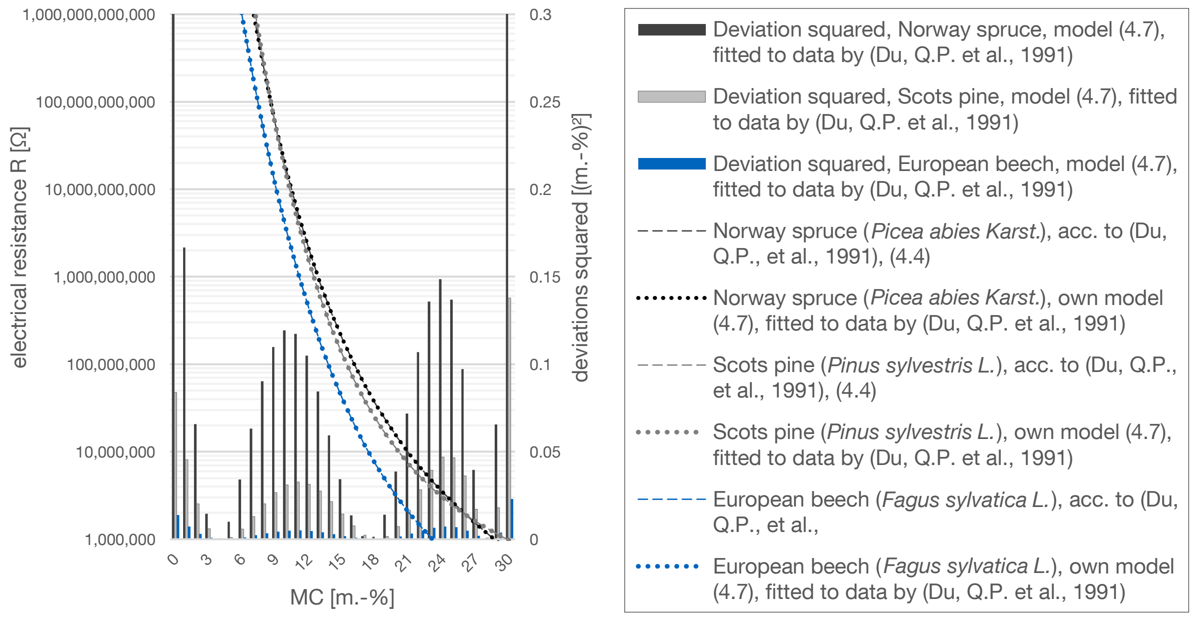

Figure 113: Checking the fit of the new equation (4.7) to the data of the existing model (4.4) by (Du et al., 1991)

Evaluating the fit demonstrates remarkably low levels for the value of the normalized root mean of squared error *(NMRSE)*, thus proving the applicability of the new model (4.7). Accordingly, the curves of the original and the new curves seem superimposed in Figure 113. The squared deviations [(m.-%)²] are additionally plotted on the right axis to illustrate the goodness of fit. They identify increased deviations only in the marginal areas of particularly low and particularly high wood moisture contents.

Next, the electrical resistance measurement data collected in the course of this work are evaluated. The focus hereby is on solid specimens of Norway spruce (*Picea abies Karst*.) with the measurement direction perpendicular to the grain using rammed-in stainless steel electrodes. For a first general check of the existing calibration curves at a constant temperature, all results of own electrical resistance measurements on this wood species are presented as a group.

Figure 114 shows the measurement results on Norway spruce at 20 °C. They are compared with existing calibration curves for Norway spruce originating from different countries by (Forsén & Tarvainen, 2000) and with the calibration curve by (Du et al., 1991), including its confidence interval. The comparison reveals only insufficient agreement, whereby the quality of the measurement data depends on how the respective wood moisture contents were determined. If the moisture content (*MC*), which is determined by the gravimetric method, was only averaged on selected specimens of the entire batch, they are shown in white. If the *MC* was determined individually per each specimen, they are shown in blue.

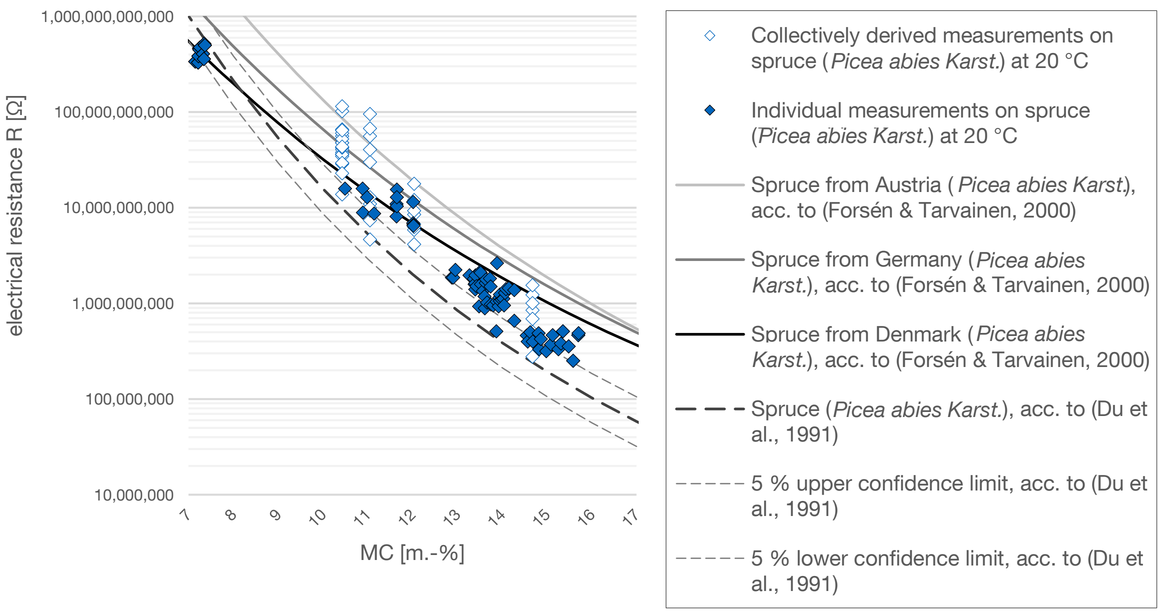

Figure 114: Results obtained from own measurements on different Norway spruce specimens (Picea abies Karst.) at 20 °C, compared with existing calibration curves for Norway spruce at 20 °C

In order to improve the calibration curves in this humidity range, various mathematical models are tested for their fit according to Subchapter 4.3.1. Since the collectively derived measurements (white) are highly scattered, only the individually determined measured data points (blue) are used for curve fitting. The white data points stem from the comparative experiments that will be later used for testing the new equations. In other words: Only the blue data points are used for training the models in this Subsection 5.2, while the white data points are merely shown for preview information here. They will later serve for testing the new models in Subsection 5.4. The specimens used for training the new model to gain new parameters are not the same specimens that are used for testing the model later.

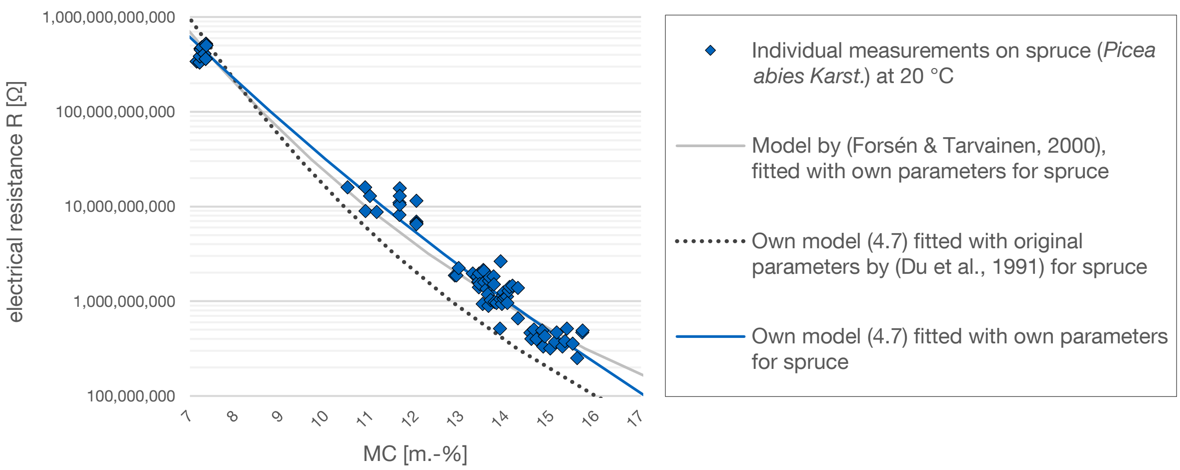

Figure 115: Model (4.2) by (Forsén & Tarvainen, 2000) with parameters fitted to the results obtained from own measurements on different Norway spruce specimens (Picea abies Karst.) at 20 °C, compared with model (4.7), both fitted to data by (Du et al., 1991) as well as fitted to own results

Three models with respective parameters (4.2, 4.4., and 4.7) are compared for their fit to the individually measured data on Norway spruce, cf. Figure 115. The quality of fit can be judged upon by their respective values the normalized root mean of squared error (*NMRSE*) in Table 14, with lower values indicating a better fit. Accordingly, those calibration curves whose parameters were adjusted to the measurement data determined as part of this work, prove a significantly better agreement with the individual measurement points. As a result, model (4.7) fitted with own parameters (printed in bold) is recommended for the further calculation of $X_{20\,°C}$ in solid Norway spruce (*Picea abies Karst.*), measurement direction perpendicular to the grain.

Table 14: Comparison of models for the correlation of electrical resistance R [Ω] and equivalent moisture content $X_{20\,°C}$ [m.-%] for Norway spruce (Picea abies Karst.) at 20 °C, with measurement direction perpendicular to the grain and within the investigated scope of a moisture content MC of 7 m.-% - 16 m.-%.

No.	Model by	Equation	Parameters	*NMRSE*
(4.2) based on own data	Model by (Forsén & Tarvainen, 2000), fitted with own parameters for Norway spruce (*Picea abies Karst.*)	$X_{20\,°C} = \frac{\mathrm{b} - \log(\log(10^{-6} \cdot R) + 1)}{a}$	a 0.042 b 1.06	*0.260*
(4.7) based on (4.4)	Own model, based on (Du et al., 1991), fitted with original parameters for Norway spruce (*Picea abies Karst.*) by (Du et al., 1991)	$X_{20\,°C} = -\frac{1}{g} \cdot ln(\frac{ln(R) - h}{f})$	f 31.5 g 0.109 h 12.908	*4.673*
(4.7) based on own data	Own model, based on (Du et al., 1991), fitted with own parameters for Norway spruce (*Picea abies Karst.*)	$\boldsymbol{X_{20\,°C} = -\frac{1}{g} \cdot ln(\frac{ln(R) - h}{f})}$	f **35.5** g **0.038** h **0.001**	*0.031*

5.2.2 Choice of wood products and sample charges between and within the same species

Comparing individual measurements on solid Norway spruce (*Picea abies Karst.*) in two randomly selected batches demonstrates that slightly different measurement results can indeed be obtained within one wood species. This confirms the findings of the preliminary experiments in the previous Subchapter 5.1.5. The deviations in the present test between batch 1 and batch 2 correspond approximately to a similar order of magnitude resulting from the change in the direction of measurement. Figure 116 shows the results of the individual measurements on two different Norway spruce batches, measured perpendicular to the grain in comparison to parallel to the grain. The newly developed calibration curves (4.7) according to the own measurement data are referenced with (4.7) fitted to the data of (Du et al., 1991).

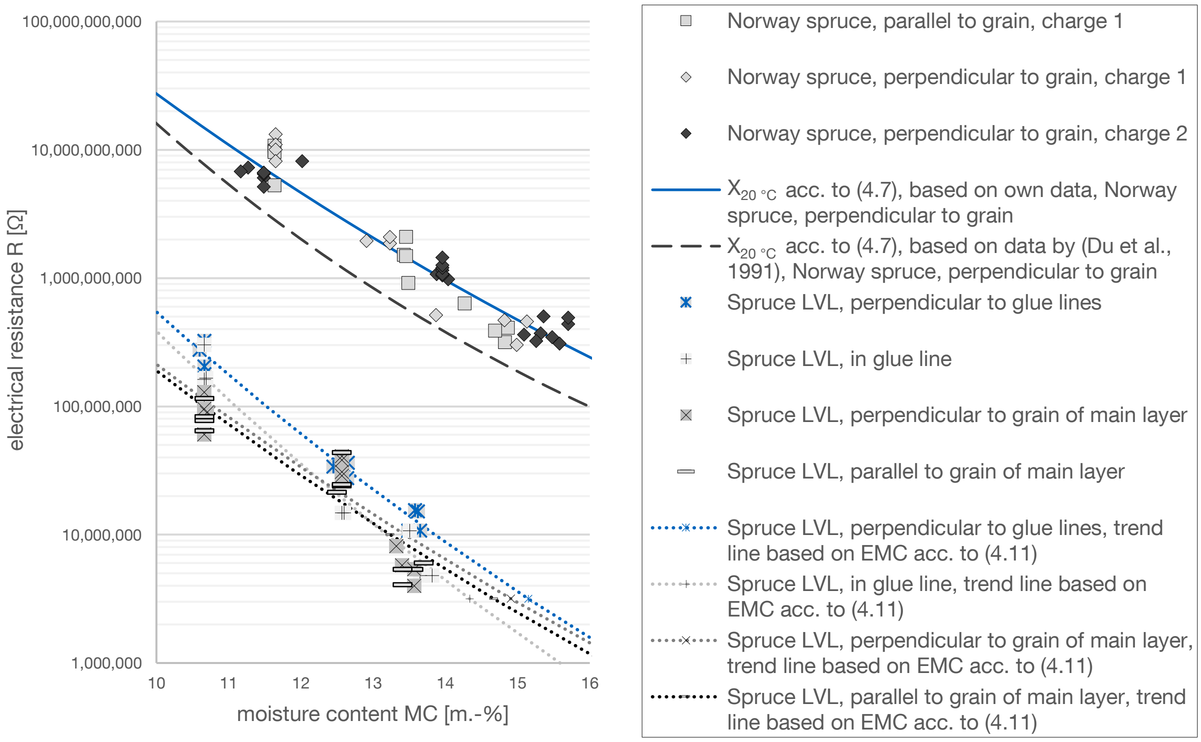

Figure 116: Comparison of own single measurement data in solid Norway spruce and in spruce LVL at 20 °C. The Norway spruce results are supplemented by two calibration curves for $X_{20\ °C}$, (4.7) based on own data, blue line, and (4.7) based on data by (Du et al., 1991), grey dashed line. The results in spruce LVL are supplemented by dotted trend lines, which are based on (4.11) at 20 °C with parameters developed in Subchapter 5.2.4.

Measurements in laminated veneer lumber (LVL) made of spruce reveal significantly lower electrical resistances *R* [Ω]. Furthermore, the direction of glue lines also influences the overall measured electrical resistance *R* [Ω], as indicated by the dotted trend lines in Figure 116. Subchapters 5.2.3 and 5.2.4 will further present and discuss parameter fittings to measurement data on these specimens at a temperature range of 5 °C – 60 °C. The consistently lower resistance values measured in specimens of European beech (*Fagus sylvatica L.*) compared to the Norway spruce specimens confirm and strengthen the need for wood species-specific calibration curves. For comparison, Figure 117 also shows the calibration curve for Norway spruce from the previous Subchapter 5.2.1 with adjusted axis scaling. In addition, however, it also confirms that even calibration curves of the same wood species from the referenced literature can lead to considerable deviations, as the comparison with the calibration curve for beech according to (Du et al., 1991) proves. The measurement results of similarly conducted test series on solid European beech (*Fagus sylvatica L.*) and laminated beech veneer lumber (LVL made of *Fagus sylvatica L.*) reveal similar tendencies to the observations in spruce LVL. Hence, the test results show a clear difference between solid wood and laminated veneer lumber for both types of wood. The resistances measured in laminated veneer lumber are significantly lower than in solid wood at comparable wood moisture contents. Furthermore, it can be observed that in solid wood, the direction of measurement perpendicular to the grain yields slightly higher resistance values. An influence of the measuring direction can also be determined for LVLs. If the electrodes are mounted with the measurement direction perpendicular to the veneer layers, the measured resistances are higher than in measurement setups in which the measurement direction is parallel to the glue lines. These results are consistent with observations by (Schiere et al., 2021a) in beech LVL. If an additional distinction is made between the fiber direction of the veneer layer (parallel or perpendicular to the grain of the layer in which the electrode´s tip is mainly located in), it also becomes apparent that the measurement direction parallel to the fiber yields slightly lower resistance values. This observation about the grain direction of the main layer that the measurement is taking place in, is in line with (Grönquist et al., 2021), who draw similar conclusions in their investigations on beech LVL with transversal layers. However, the differences due to the direction of the fibers in laminated veneer lumber are no longer very great here, and it is questionable to what extent a distinction is even possible and meaningful in practice. Accordingly, these three batches will each be combined into the "measurement parallel to glue lines"-group in the following investigation (Subchapter 5.2.3) to also allow for a broader applicability in-situ.

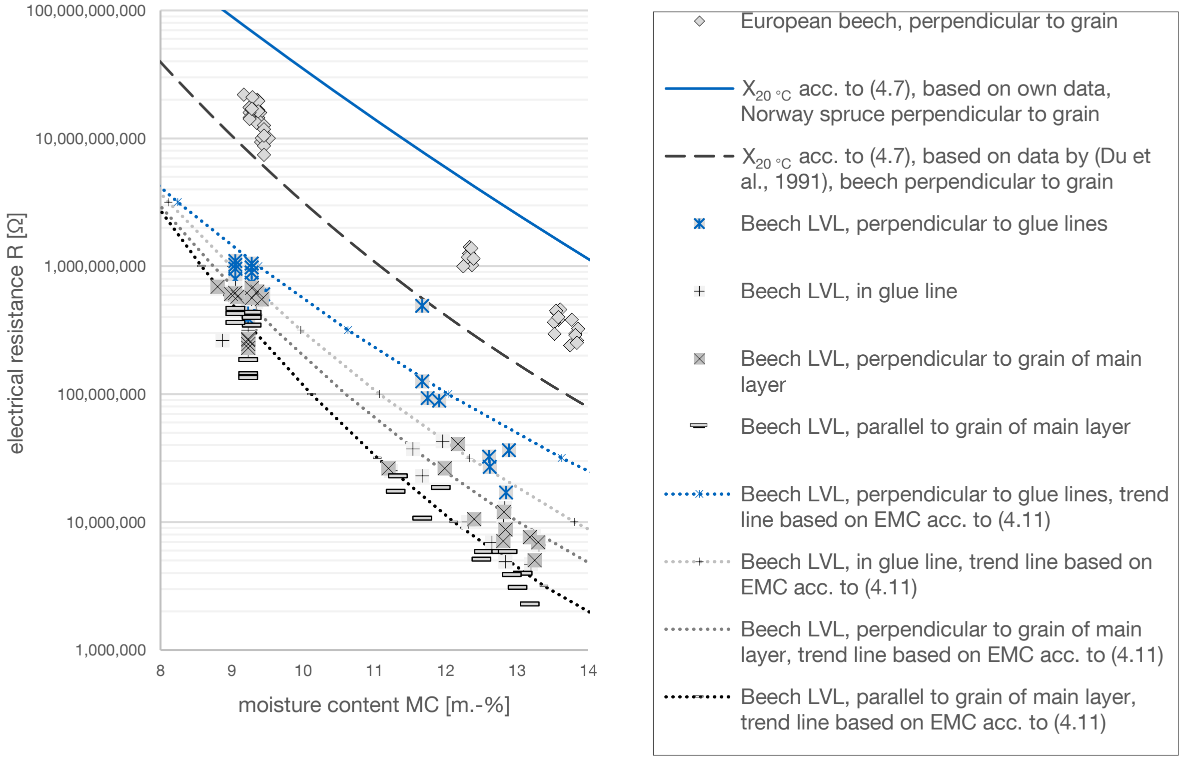

Figure 117: Comparison of own single measurement data in solid European and in beech LVL at 20 °C. These results are juxtaposed to two calibration curves for $X_{20\,°C}$, own (4.7) for Norway spruce, blue line, and (4.7) based on beech data by (Du et al., 1991), grey dashed line. The results in beech LVL are supplemented by dotted trend lines, which are based on (4.11) at 20 °C with parameters developed in Subchapter 5.2.4.

5.2.3 Optimization of temperature compensation to a known base value $X_{20\,°C}(R)$

The measurements on Norway spruce, European beech, spruce LVL as well as beech LVL in the temperature range from 5 °C to 60 °C confirm the general correlations explained in Subchapter 3.2.4. The electrical resistance *R* [Ω] of wood decreases significantly at higher temperatures *T* [°C], while the moisture content *MC* [m.-%] remains constant. The models for taking temperature into account in electrical resistance measurements presented in Subchapter 4.3.3 are investigated using the newly obtained measured values for these four wood products as well as different sensor arrangements. This results in new parameters, which allow for a more precise description of the actual moisture content. Figure 118 depicts a selection of the data measured at different temperatures in solid Norway spruce (*Picea abies Karst*.) and laminated spruce veneer lumber (LVL made of *Picea abies Karst.*) on a logarithmic scale. Similar test series are conducted on solid European beech (*Fagus sylvatica L.*) and laminated beech veneer lumber (LVL made of *Fagus sylvatica L.*), cf. Figure 119. Demonstrated in each case are the mean values determined from numerous individual measurements on four identical specimens from each batch. The trends are consistent with the basics explained in Subchapter 3.2.4 and the results from previous Subchapter 5.2.2.

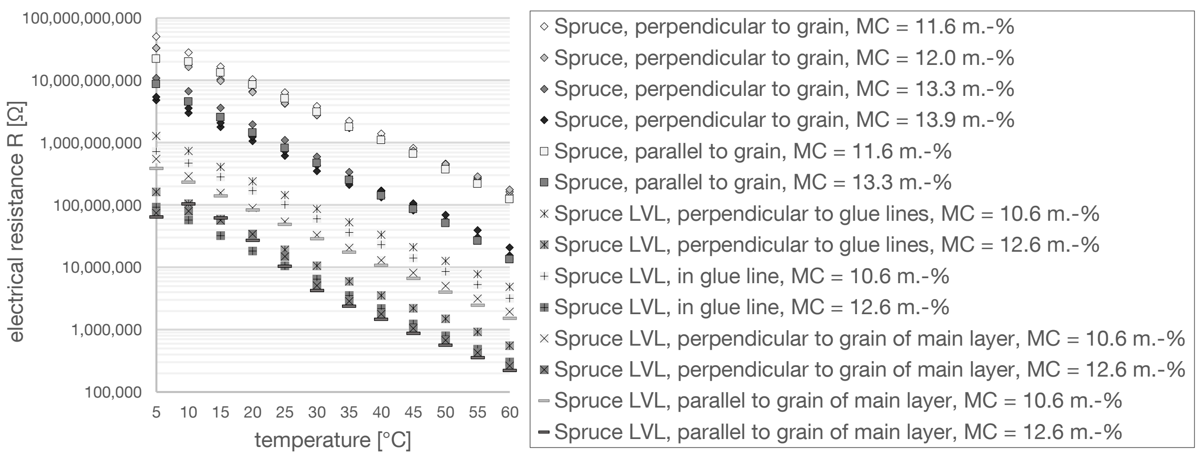

Figure 118: Results of electrical resistance measurements on test specimens made of Norway spruce and spruce LVL under different temperatures at constant wood moisture contents, shown as mean values from four individual test specimens per batch.

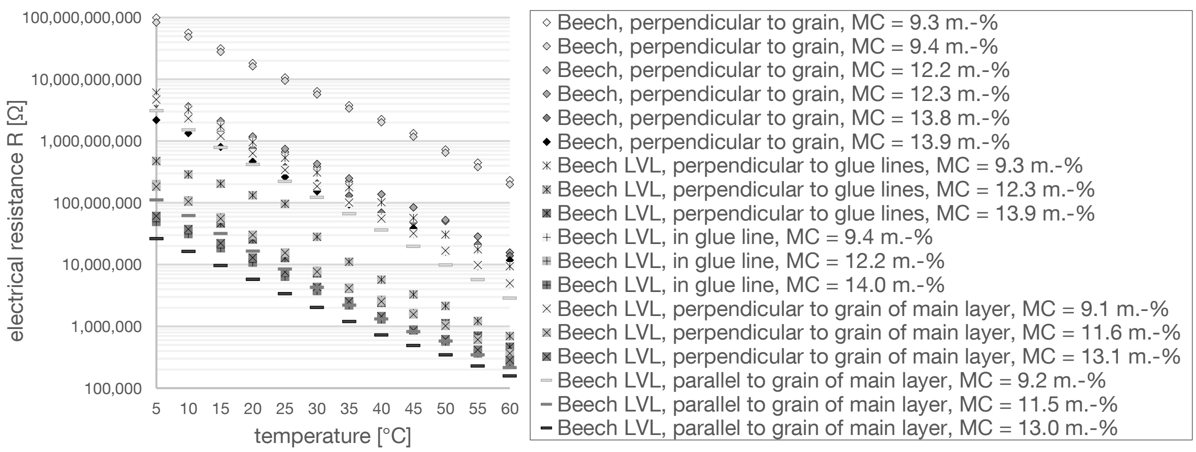

Figure 119: Results of electrical resistance measurements on test specimens made of European beech and beech LVL under different temperatures at constant wood moisture contents (mean values from four specimens).

Figure 120 demonstrates an example of the variations in measured electrical resistance for different wood species and products with coincidentally the same moisture content of $MC \approx 13.9$ m.-%. These differences in the measured electrical resistance with otherwise identical moisture contents should be reflected by wood-species specific parameters.

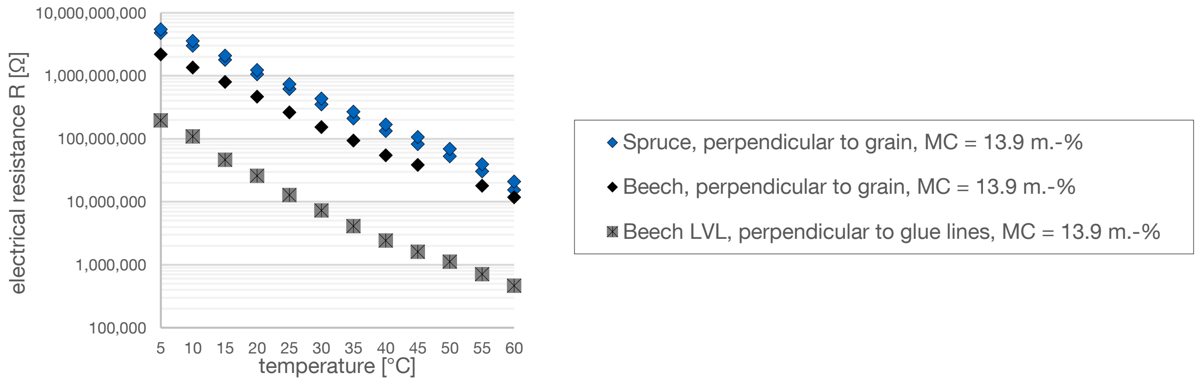

Figure 120: Results of electrical resistance measurements on test specimens made of Norway spruce, European beech, and beech LVL under different temperatures and at a constant wood moisture content of MC ≈ *13.9 m.-%, shown as mean values from four individual test specimens per batch.*

This and the following Subchapter present the refined parameters for the individual models to calculate the equivalent moisture content *EMC* [m.-%] by electrical resistance measurements under the influence of temperature. The equations with newly fitted parameters can be used for future measurement projects on Norway spruce, European beech, spruce LVL, and beech LVL with respect to their individual accuracy and the different areas of application. The *NRMSE* value is used to assess the quality of fit to the experimental data.

Using two-part methods of the form $EMC\ (X_{20\,°C}, T)$, such as models (4.8) or (4.9), the fundamental correlations of R and MC are already captured by the base value $X_{20\,°C}$ [m.-%] at a fixed temperature, cf. Subchapter 5.2.1. Since this procedure requires existing calibration curves for the relationship between electrical resistance and wood moisture content at minimum one constant temperature level, only the batches of Norway spruce, European beech, and beech LVL, all with measurement perpendicular to the grain direction, as well as beech LVL with measurement parallel to the grain direction, will be considered. The subsequent temperature compensation for these groups is investigated to be refined accordingly.

The parameters of equation (4.8) are adapted to the measured data obtained in the course of this work. In contrast to the original model, the theoretical wood moisture value $X_{20\,°C}$ is referenced at 20 °C (not at 25 °C).

The process of parameter fitting confirms that the basic equation structure of the original model, a third-degree polynomial, could be reduced to a second-degree polynomial without relevant loss of accuracy. Similarly, it is proven that another additional parameter can be omitted for a modified shorter equation. This results in the following wood species-specific new parameters for the modified form of equation (4.8) that is similar to the original equation (4.8) with seven parameters presented in Subchapter 4.3.3, but fitted with only five new parameters *a* - *e*.

$$EMC\ (X_{20\,°C}, T) = X_{20\,°C} + \left(\frac{\mathrm{a} \cdot X_{20\,°C}}{b}\right) \cdot (\mathrm{c} \cdot \mathrm{T}^2 - \mathrm{d} \cdot \mathrm{T} + \mathrm{e}) \qquad \text{(4.8) } \textit{modified}$$

With

T	Temperature	[°C]
$X_{20\,°C}$	Base value for material moisture content at 20 °C	[m.-%]

	a	*b*	c	*d*	*e*		*NRMSE*
Norway spruce *(Picea abies Karst.), measurement perpendicular to grain direction*	**0.500**	**8.529**	**0.001**	**0.219**	**3.813**	**-**	***0.031***
European beech *(Fagus sylvatica L.), measurement perpendicular to grain direction*	0.506	13.498	0.0014	0.354	9.742	-	*0.042*
Beech laminated veneer lumber (LVL made of *Fagus sylvatica L.*), *measurement perpendicular to grain of main layer*	0.47	20.186	0.0011	0.602	16.729	-	*0.034*
Beech laminated veneer lumber (LVL made of *Fagus sylvatica L.*), *measurement parallel to grain of main layer*	0.48	19.933	0.0011	0.603	16.729		*0.058*

As an alternative, model (4.9) is tested with the same measurement data. The following fitted parameters are obtained for the temperature compensation:

$$EMC\ (X_{20\,°C}, T) = \frac{X_{20\,°C} - a \cdot (T - 20)}{b \cdot (T - 20) + 1} \qquad (4.9)$$

With

T	Temperature	[°C]
$X_{20\,°C}$	Base value for material moisture content at 20 °C	[m.-%]

	a	*b*		*NRMSE*
Norway spruce *(Picea abies Karst.)*	0.001	0.0071	-	*0.061*
European beech *(Fagus sylvatica L.)*	0.079	0.0001	-	*0.099*
Beech laminated veneer lumber (LVL made of *Fagus sylvatica L.*), *measurement perpendicular to grain of main layer*	**0.001**	**0.0118**	**-**	***0.093***
Beech laminated veneer lumber (LVL made of *Fagus sylvatica L.*), *measurement parallel to grain of main layer*	0.001	0.0142	-	*0.104*

Comparing the values for *NMRSE* (normalized root mean squared errors) of these two models with new parameters proves that the modified equation (4.8) gives much more accurate results and is therefore preferable to equation (4.9).

Printed in **bold** are those specific parameters for Norway spruce and beech LVL, which are shown as resulting curves for later discussion and comparison to references in the following Figure 121, p.135, with beech LVL and Figure 122, p.136, with Norway spruce.

5.2.4 Approaches of the form *EMC (R,T)* for use on several wood species and products

While the two-part approach with *EMC* ($X_{20\,°C}$,*T*) and a known base function $X_{20\,°C}$ *(R)* is being examined in the previous Chapter, the results for the models of the form *MC (R,T)* are presented on Norway spruce, European beech, spruce LVL, and beech LVL below. The best fits are summarized and illustrated ready for practical use in Appendix F. In the following parameterization of the models (4.11) through (4.14), it is important to note the range of validity. They are based on a set of measured data obtained at a wide range of temperatures *T* (5 °C to 60 °C) and electrical resistances *R* (10^5 Ω to 10^{11} Ω), but at a relatively narrow range of actual wood moisture contents *MC* (9 m.-% to 14 m.-% maximum). Hence, the results obtained might have only limited validity for extrapolation outside this measurement range. An exception are measurements on solid Norway spruce that run perpendicular to the grain.

Curve fitting to the measurement data proves that - without significant loss of accuracy - the equation for model (4.11) could be shortened compared to the original of (Boardman et al., 2017) by omitting the first parameter and adjusting the others:

$$EMC\ (R,T) = a \cdot \left(\frac{1000}{T + 273.15}\right)^d - \mathrm{c} \cdot \left(\frac{1000}{T + 273.15}\right)^d \cdot \lg\left[\, lg\ (R) - b\right] \qquad \text{(4.11) } \textit{modified}$$

With

R	Electrical Resistance	[Ω]
T	Temperature	[°C]

	a	*b*	c	*d*	*NRMSE*
Norway spruce *(Picea abies Karst.)*, *measurement perpendicular to grain direction*	**3.4557**	**0**	**2.9052**	**2.4716**	***0.032***
Norway spruce *(Picea abies Karst.)*, *measurement parallel to grain direction*	3.3930	0.0001	2.7875	2.3866	*0.015*
Spruce laminated veneer lumber (LVL made of *Picea abies Karst.*), *measurement perpendicular to glue lines*	0.9765	3.5221	0.8437	2.6860	*0.015*
Spruce laminated veneer lumber (LVL made of *Picea abies Karst.*), *measurement parallel to glue lines*	1.5713	0.2105	1.3592	2.7816	*0.034*
Spruce laminated veneer lumber (LVL made of *Picea abies Karst.*), *measurement perpendicular to grain of main layer*	1.1524	0.0327	1.0218	3.1329	*0.033*
Spruce laminated veneer lumber (LVL made of *Picea abies Karst.*), *measurement parallel to grain of main layer*	1.0887	0.0326	0.9644	3.1651	*0.037*
Spruce laminated veneer lumber (LVL made of *Picea abies Karst.*), *measurement in glue line*	2.3084	0.0571	1.9449	2.4386	*0.015*
European beech *(Fagus sylvatica L.)*, *measurement perpendicular to grain direction*	0.3622	5.4994	0.3438	3.4822	*0.037*
Beech laminated veneer lumber (LVL made of *Fagus sylvatica L.*), *measurement perpendicular to glue lines*	0.2018	4.0549	0.1940	4.0252	*0.025*
Beech laminated veneer lumber (LVL made of *Fagus sylvatica L.*), *measurement parallel to glue lines*	0.6316	3.4845	0.5405	2.9717	*0.056*
Beech laminated veneer lumber (LVL made of *Fagus sylvatica L.*), *measurement perpendicular to grain of main layer*	**0.3911**	**4.1494**	**0.3379**	**3.2634**	***0.027***
Beech laminated veneer lumber (LVL made of *Fagus sylvatica L.*), *measurement parallel to grain of main layer*	0.5083	4.0398	0.4104	2.9746	*0.027*
Beech laminated veneer lumber (LVL made of *Fagus sylvatica L.*), *measurement in glue line*	0.3050	4.2680	0.2722	3.5093	*0.25*

Alternatively, model (4.12), as published by (Forsén & Tarvainen, 2000; Schiere et al., 2021a), is fitted with the same measurement data. The following adjusted parameters are derived for the calculation of the wood moisture content with another equation of the form *MC (R,T)*:

$$EMC\ (R,T) = \frac{a - (b \cdot T) - lg\ (\ lg(R) - 5)}{c + (d\ \cdot T)} \qquad (4.12)$$

With

R	Electrical Resistance	[Ω]
T	Temperature	[°C]

	a	*b*	*c*	*d*	*NRMSE*
Norway spruce *(Picea abies Karst.), measurement perpendicular to grain direction*	**1.0820**	**0**	**0.0268**	**0.0004**	***0.035***
Norway spruce *(Picea abies Karst.), measurement parallel to grain direction*	1.2522	0.0001	0.0408	0.0004	*0.015*
Spruce laminated veneer lumber (LVL made of *Picea abies Karst.*), *measurement perpendicular to glue lines*	1.4129	0	0.0670	0.0007	*0.026*
Spruce laminated veneer lumber (LVL made of *Picea abies Karst.*), *measurement parallel to glue lines*	1.7664	0.0001	0.0978	0.0009	*0.046*
Spruce laminated veneer lumber (LVL made of *(Picea abies Karst.*), *measurement perpendicular to grain of main layer*	1.6535	0	0.0879	0.0009	*0.047*
Spruce laminated veneer lumber (LVL made of *(Picea abies Karst.*), *measurement parallel to grain of main layer*	1.7634	0.0001	0.0971	0.0010	*0.050*
Spruce laminated veneer lumber (LVL made of *(Picea abies Karst.*), *measurement in glue line*	1.7122	0.0001	0.0938	0.0008	*0.033*
European beech *(Fagus sylvatica L.), measurement perpendicular to grain direction*	1.0693	0.0006	0.0283	0.0004	*0.039*
Beech laminated veneer lumber (LVL made of *Fagus sylvatica L.*), *measurement perpendicular to glue lines*	1.1273	0	0.0389	0.0008	*0.045*
Beech laminated veneer lumber (LVL made of *Fagus sylvatica L.*), *measurement parallel to glue lines*	1.5185	0	0.0766	0.0011	*0.074*
Beech laminated veneer lumber (LVL made of *Fagus sylvatica L.*), *measurement perpendicular to grain of main layer*	**1.3420**	**0**	**0.0625**	**0.0010**	***0.044***
Beech laminated veneer lumber (LVL made of *Fagus sylvatica L.*), *measurement parallel to grain of main layer*	1.6414	0	0.0895	0.0012	*0.053*
Beech laminated veneer lumber (LVL made of *Fagus sylvatica L.*), *measurement in glue line*	1.2797	0	0.0541	0.0010	*0.046*

Model (4.13), based on (Brischke & Lampen, 2014), only shows insufficient agreement, especially in the ranges of lower wood moisture content. Thus, in order to maintain the clarity of this thesis, the individual results of the fit with model (4.13) will not be presented in detail. The model will not be recommended for use in the range of moisture contents below 10 m.-%.

Model (4.14) by (Otten et al., 2017) is based on model (4.13). The following adjusted parameters are derived for the calculation of the wood moisture content with another equation of the form *EMC (R,T)*.

$$EMC\ (R,T) = (-a \cdot T + b) \cdot exp^{(-c \cdot 10\lg(R) + d)} + e \qquad (4.14)$$

With

R Electrical Resistance [Ω]

T Temperature [°C]

	a	*b*	*c*	*d*	*e*	*NRMSE*
Norway spruce *(Picea abies Karst.), measurement perpendicular to grain direction*	**0.014**	**2.087**	**0.023**	**4.110**	**0**	***0.042***
Norway spruce *(Picea abies Karst.), measurement parallel to grain direction*	0.012	1.991	0.018	3.670	0	*0.017*
Spruce laminated veneer lumber (LVL made of *Picea abies Karst.*), *measurement perpendicular to glue lines*	0.012	1.935	0.019	3.428	0	*0.026*
Spruce laminated veneer lumber (LVL made of *Picea abies Karst.*), *measurement parallel to glue lines*	0.013	1.970	0.019	3.354	0	*0.039*
Spruce laminated veneer lumber (LVL made of *(Picea abies Karst.*), *measurement perpendicular to grain of main layer*	0.013	1.861	0.020	3.540	0	*0.041*
Spruce laminated veneer lumber (LVL made of *(Picea abies Karst.*), *measurement parallel to grain of main layer*	0.013	1.854	0.020	3.501	0	*0.044*
Spruce laminated veneer lumber (LVL made of *(Picea abies Karst.*), *measurement in glue line*	0.012	1.987	0.018	3.277	0	*0.022*
European beech *(Fagus sylvatica L.), measurement perpendicular to grain direction*	0.015	1.892	0.024	4.214	0	*0.044*
Beech laminated veneer lumber (LVL made of *Fagus sylvatica L.*), *measurement perpendicular to glue lines*	0.015	1.812	0.024	3.993	0	*0.040*
Beech laminated veneer lumber (LVL made of *Fagus sylvatica L.*), *measurement parallel to glue lines*	0.013	1.974	0.018	3.284	0	*0.047*
Beech laminated veneer lumber (LVL made of *Fagus sylvatica L.*), *measurement perpendicular to grain of main layer*	0.014	1.937	0.020	3.492	0	*0.038*
Beech laminated veneer lumber (LVL made of *Fagus sylvatica L.*), *measurement parallel to grain of main layer*	0.013	1.975	0.018	3.261	0	*0.038*
Beech laminated veneer lumber (LVL made of *Fagus sylvatica L.*), *measurement in glue line*	0.014	1.884	0.022	3.703	0	*0.038*

The *NMRSE* values in the right column of each data table can be used to compare the goodness of fit of the newly adjusted models. In this regard, the results of model (4.11) consistently show slightly lower values than the values of model (4.14) and model (4.12). The *NRMSE* values thus point to a higher accuracy of model (4.11), which was originally taken from (Boardman et al., 2017). The modified and fitted version of model (4.11) presented here is therefore encouraged for further use on Norway spruce, European beech, spruce LVL as well as beech LVL within the investigated scope. Only for Norway spruce, measured perpendicular to the grain, could the application of model (4.7) developed in Subsection 5.2.1 in combination with model (4.8) with newly adjusted parameters, lead to even more accurate results.

As beech LVL is increasingly being used in modern wood-based material construction, there has been an urgent need for reliable calibration curves to monitor its moisture content recently. Therefore, the results of the measurements on beech laminated veneer lumber (*LVL made of Fagus sylvatica L.),* measurement perpendicular to the grain of main layer, are discussed in more detail below.

The two-part calculation by model (4.2) in combination with (4.9) using the original parameters published by (Grönquist et al., 2021) can only achieve an approximate agreement with the measurement data from this work (*RMSE: 0.096*). Possibly model (4.2) might not describe the relationship between *R* and base value $X_{20\,°C}$ with sufficient accuracy. Even after adjusting the temperature compensation (4.9) by parameter fitting, only a minimally improved result can be achieved (*NRMSE: 0.093*).

The use of the original parameters for model (4.12), published by (Schiere et al., 2021a), also shows no satisfactory agreement with the measured data (*NRMSE: 0.099*). These discrepancies are possibly due to the experimental methods used by the authors, see critique in Subchapter 4.3.4. However, after parameter optimization, the curve fitting for model (4.12) can be significantly improved (*NRMSE: 0.044*). Surprisingly, model (4.11), which has not yet been published at all in the context of measurements on beech LVL, reveals very good characteristics after curve fitting (*NRMSE: 0.027*). Based on the measurement data collected within this thesis, it might be the most suitable model from this group for modeling laminated veneer lumber and is therefore also recommended for future use in Appendix F.

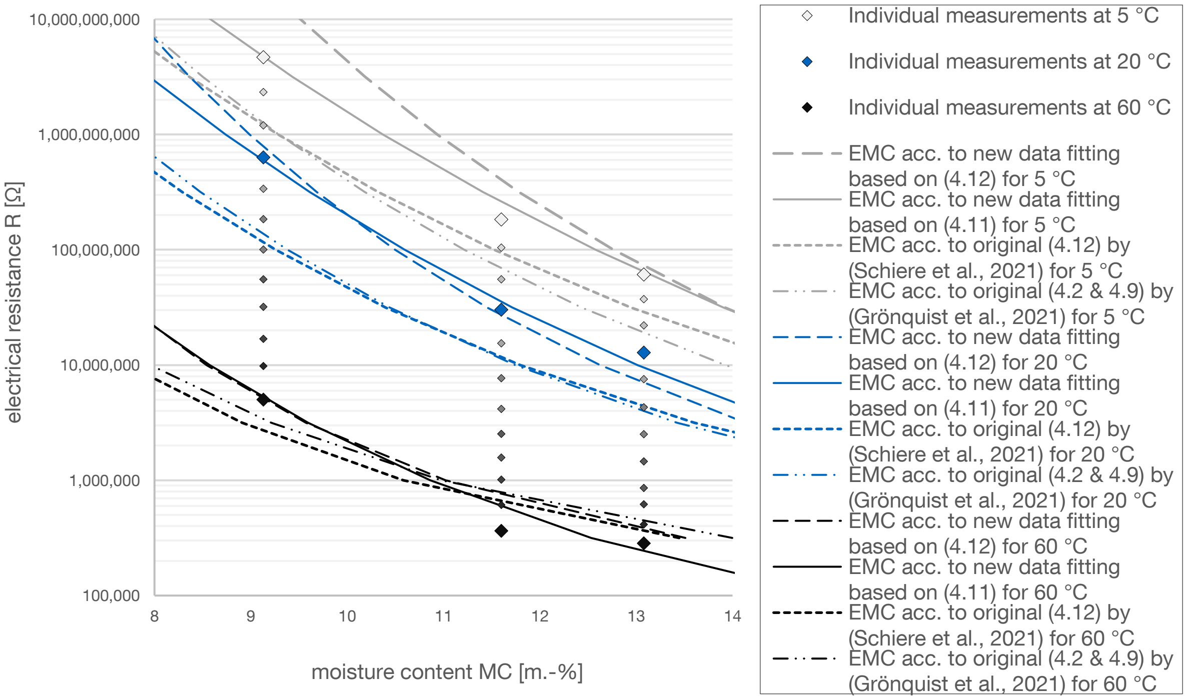

Figure 121: Comparison of models for the correlation of electrical resistance R [Ω], temperature T [°C], and moisture content MC [m.-%] at a range of 5 °C - 60 °C for beech laminated veneer lumber (LVL made of Fagus sylvatica L.*), with measurement direction perpendicular to the grain of the main layer.*

Figure 121 compares the characteristic curves published by (Schiere et al., 2021a), those published by (Grönquist et al., 2021), and those determined within the scope of this work based on models (4.11) and (4.12). For clarity, only the curves for 5 °C, 20 °C, and 60 °C are printed here. However, the curve fitting was performed considering all measured temperature levels, the resulting curves are just not shown in Figure 121. The diagram confirms what the evaluation of the *NMRSE* values revealed: The measured values on beech LVL, measured perpendicular to the fiber of the main layer, are best predicted by a modified version of model (4.11) with adjusted parameters.

Furthermore, there is a need for reliable calibration curves for solid Norway spruce wood under temperature gradients for the main investigations in Chapter 6 of this work. Figure 122 compares the measurement results for solid Norway spruce (measurement direction perpendicular to the grain) with the calculation results derived from models (4.11), (4.12), and (4.7)+(4.8). A more detailed illustration of the results from all twelve temperature levels is given in Appendix C, Figure 209.

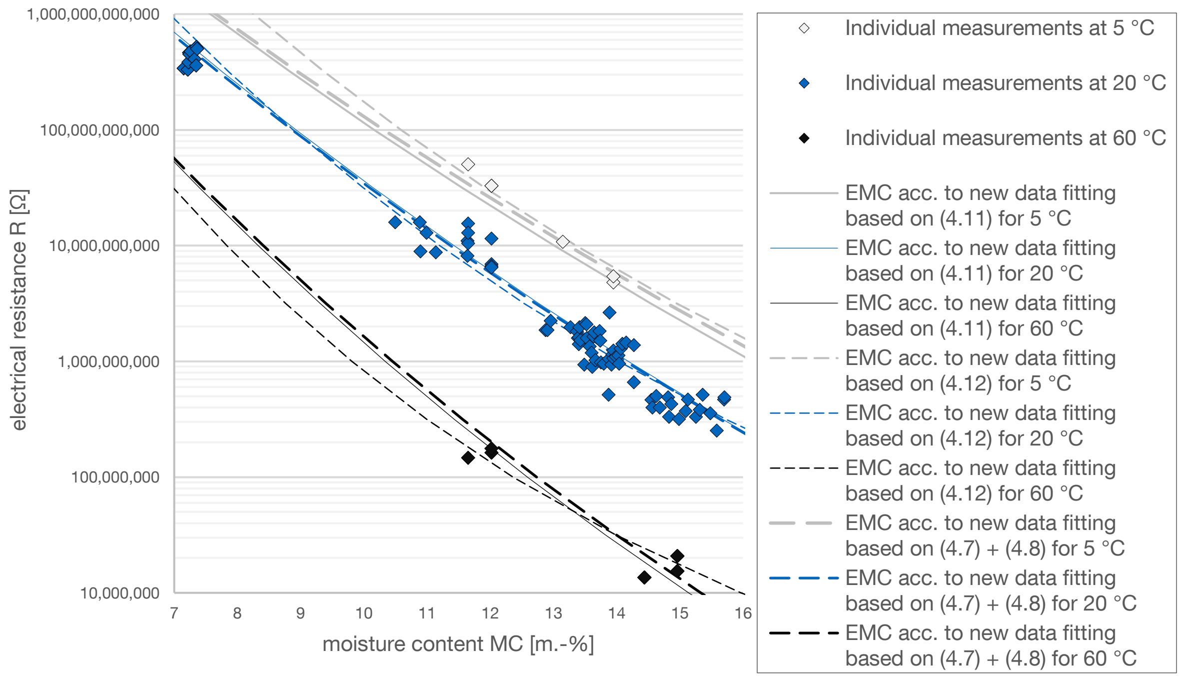

Figure 122: Comparison of models for the correlation of electrical resistance R [Ω], temperature T [°C], and moisture content MC [m.-%] at a range of 5 °C - 60 °C for Norway spruce (Picea abies Karst.), with measurement direction perpendicular to the grain and within the investigated scope of a moisture content MC of 7 m.-% - 16 m.-%.

For the calculation of wood moisture content *MC* [m.-%] from temperature *T* [°C] and electrical resistance *R* [Ω] of massive Norway spruce (*Picea abies Karst.*), measured perpendicular to the fiber, model (4.8) in combination with model (4.7) shows the overall best agreement with the measured data (*NRMSE: 0.031*). Table 14, p. 126, lists the base equation and its parameters. This order of accuracy is followed by the modified model (4.11) (*NMRSE: 0.032*), model (4.12) (*NRMSE: 0.035*), model (4.14) (*NMRSE: 0.042*), and model (4.9) in combination with model (4.7) (*NRMSE: 0.061*).

All values for *NMRSE* (normalized root mean squared errors) are based on evaluations within the investigated scope and after improving the parameters by curve fitting to the obtained measurement data.

Consequently, the two best options for Norway spruce (*Picea abies Karst.*), measured perpendicular to the fiber, two-part-approach (4.7)+(4.8) and one-part-approach (4.11), are illustrated in Appendix F. The detailed analyses from page 141 onwards analyze the results for Norway spruce measured perpendicular to the grain according to option 1, which is utilizing model (4.7) with model (4.8).

5.3 Novel wood species-specific adaptation and optimization of the sorption model

Based on an analysis of previously published sorption data, curve fitting is performed for the wood species Norway spruce (*Picea abies Karst.*), Douglas fir (*Pseudotsuga menziesii Franco*), radiata pine (*Pinus radiata D. Don.*), and European beech (*Fagus sylvatica L.*), cf. Table 5 in Subchapter 3.2.2. The method to generate simple splitting curves between the adsorption and desorption isotherms enables a mathematical solution despite the sorption hysteresis, cf. Subchapter 4.4.1.

Table 15 presents the resulting new parameters, to be used in equations (4.15) and (4.16), which are based on Zuritz's approach, a modified form of Henderson´s model (Avramidis, 1989; Glass et al., 2014):

$$RH = 100 \cdot \left\{1 - exp\left[\frac{1}{a \cdot (T + 273.15)} \cdot \left(1 - \frac{(T + 273.15)}{647.1}\right)^{-b} \cdot \left(\frac{EMC}{100}\right)^{\frac{1}{c} \cdot (T+273.15)^{-d}}\right]\right\} \quad (4.15)$$

$$EMC = \left[a \cdot (T + 273.15) \cdot \left(1 - \frac{(T + 273.15)}{647.1}\right)^{b} \cdot \ln\left(1 - \frac{1}{100} RH\right)\right]^{c \cdot (T+273.15)^{d}} \quad (4.16)$$

With

EMC	Equilibrium Moisture Content	[m.-%]
RH	Relative Humidity of Air	[%]
T	Temperature	[°C]

Table 15: Results for novel wood-species specific parameters to calculate the equivalent moisture content based on equations (4.15) and (4.16)

	Norway spruce *Picea abies Karst.*	**Douglas fir** *Pseudotsuga menziesii Franco*	**Radiata pine** *Pinus radiata D. Don.*	**European beech** *Fagus sylvatica L.*
a	- 0.0001084	- 0.0000982	- 0.0000775	- 0.0004052
b	0.6800	1.1339	0.1389	1.8125
c	0.0005219	0.0010537	0.0008966	0.0072263
d	1.2165	1.0827	1.1173	0.7882
NRMSE	*0.063*	*0.076*	*0.058*	*0.097*
Number of data sets	*57 data sets*	*38 data sets*	*27 data sets*	*25 data sets*
References	(Weichert, 1963b) (Hedlin, 1968) (Niemz & Sonderegger, 2007) (Popper & Niemz, 2009) (Bratasz et al., 2012)	(Hedlin, 1968) (Fan et al., 1999) (Popper & Niemz, 2009)	(Popper & Niemz, 2009) (Simón et al., 2016)	(Weichert, 1963b) (Niemz & Sonderegger, 2007) (Popper & Niemz, 2009) (Bratasz et al., 2012)
Range of available sorption data	-12 °C – 100 °C 0 %RH – 99 %RH	-12 °C – 60 °C 0 %RH – 99 %RH	15 °C – 50 °C 0 %RH – 98 %RH	20 °C – 100 °C 0 %RH – 95 %RH

Equations (4.15) and (4.16) the novel wood-species-specific parameters result in the following adapted diagrams for temperature-dependent wood moisture determination under a regularly changing sorption direction.

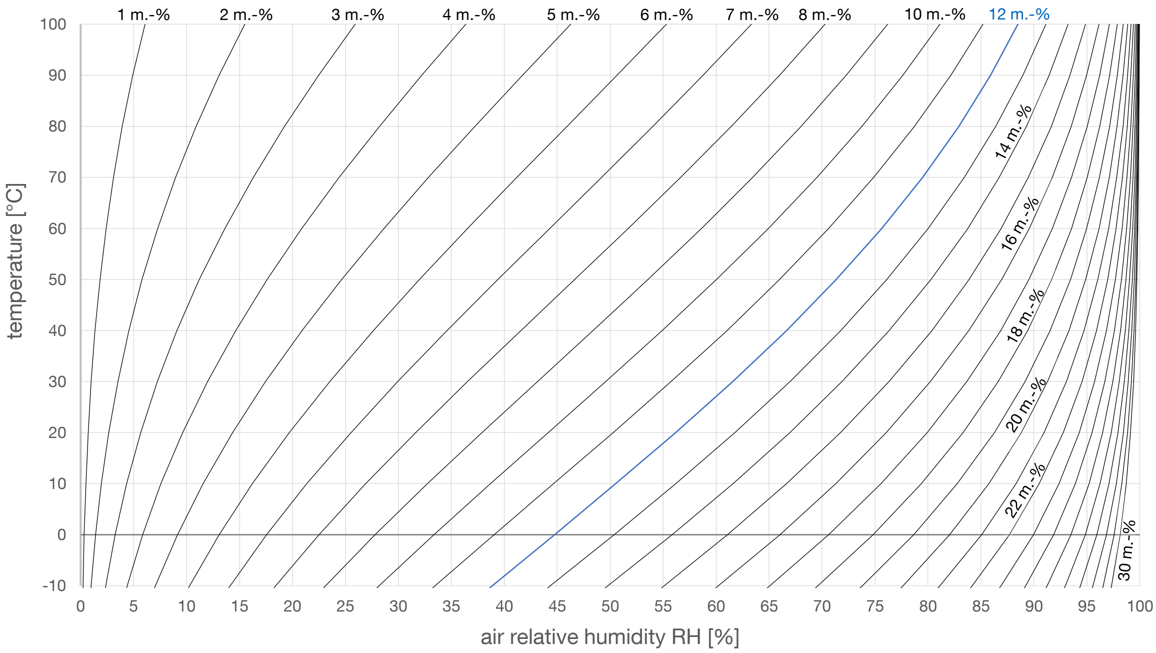

Figure 123: New graph for use in moisture monitoring in Norway spruce, based on own splitting curves derived from data acquisition from (Bratasz et al., 2012; Hedlin, 1968; Niemz & Sonderegger, 2007; Popper & Niemz, 2009; Weichert, 1963b).

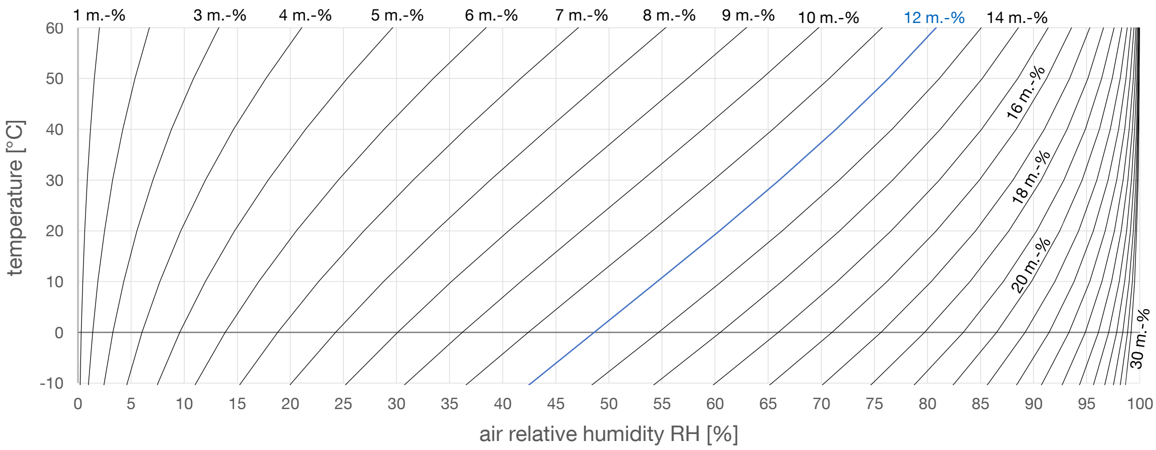

Figure 124: New graph for use in moisture monitoring in Douglas fir, based on own splitting curves derived from data acquisition from (Fan et al., 1999; Hedlin, 1968; Popper & Niemz, 2009).

Figure 123, Figure 124, Figure 125, and Figure 126 show four diagrams that have been newly developed within the scope of this work. They are based on the different sorption capacity of the species Norway spruce, Douglas fir, radiata pine, and European beech.

These diagrams allow a more accurate determination of the wood moisture content under typical wood moisture changes in-situ, considering sorption hysteresis by shifting interpolation. Their applicability to monitoring in different wood species will be tested in comparative laboratory trials and in in-situ experiments in the following Subchapters. In order to facilitate practical application, they are also illustrated in Appendix F as individual data sheets, ready for printing.

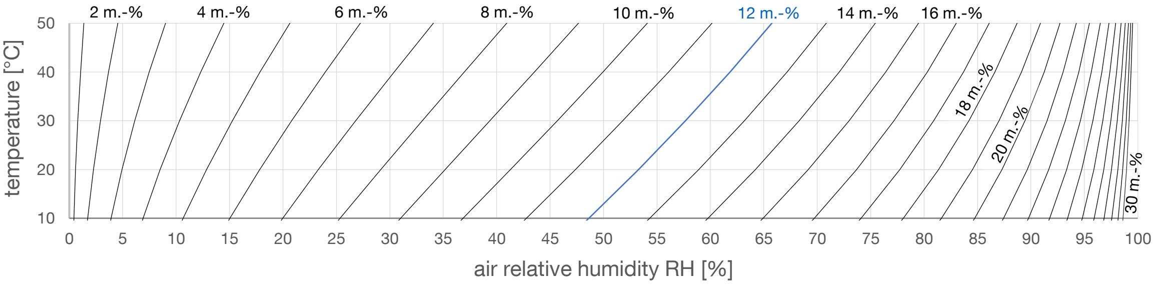

Figure 125: New graph for use in moisture monitoring in radiata pine, based on own splitting curves derived from data acquisition from (Popper & Niemz, 2009; Simón et al., 2016).

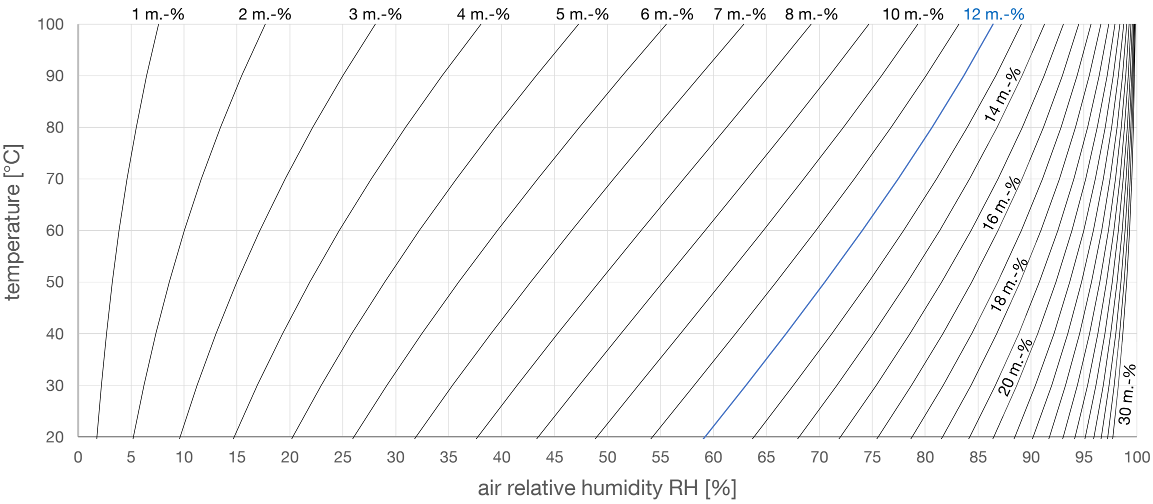

Figure 126: New graph for use in moisture monitoring in European beech, based on own splitting curves derived from data acquisition from (Bratasz et al., 2012; Niemz & Sonderegger, 2007; Popper & Niemz, 2009; Weichert, 1963b).

The graphs shown vary in size due to the different degrees of availability of the underlying sorption data. In each figure, the curve at *EMC* = 12 m.-% is shown in blue to facilitate graphical orientation. The graphs show clear differences for the different wood species.

Figure 127 compares a selection of the four newly generated curve sets with the original values as published by (Glass et al., 2014) and introduced in Subchapter 3.2.1. This shows that the choice of wood species appears to have a significant influence. However, the sorption method is also subject to inaccuracies, which will be further discussed in Subchapter 7.2.1.

The following juxtaposition illustrates the differences between wood-species exemplarily for *EMC*-values of 4 m.-%, 12 m.-%, and 20 m.-%, although without taking deviations into account. For instance, the environmental conditions required to achieve an *EMC* of 4 m.-% are significantly drier for radiata pine than for the original curve for Sitka spruce. According to the conventional graph shown in blue (Glass et al., 2014), an *EMC* of 4 m.-% would be achieved at 17.2 %RH/20 °C. For the same *EMC* in radiata pine, this would already be the case at 8.5 %RH/20 °C. Conversely, radiata pine would already have a significantly higher *EMC* of 5.9 m.-% at the initial conditions of 17.2 %RH/20 °C. At higher equivalent moisture contents, the differences are less pronounced, but still significant. To achieve an *EMC* of 12 m.-%, ambient conditions of 53.3 %RH/20 °C are already sufficient for radiata pine. The original curve for Sitka spruce, however, requires much more humid conditions of 62.9 %RH/20 °C for 12 m.-%. This ambient air humidity would result in an *EMC* of 13.7 m.-% for radiata pine, 13.2 m.-% for Norway spruce, 12.8 m.-% for European beech, and 12.2 m.-% for Douglas fir. As the humidity increases, opposite tendencies are observed. Ambient conditions of about 88.2 %RH/20 °C result in an *EMC* of 20 m.-% for Sitka spruce according to the historical parameter fitting. The same conditions would result in a similar *EMC* of 19.7 m.-% for Norway spruce, 20.4 m.-% for radiata pine, and 20.8 m.-% for European beech according to the new data fitting. Only the curve for Douglas fir is significantly lower at 18.0 m.-%. Figure 127 shows this tendency in terms of a constant *EMC*: For an equivalent moisture content of 20 m.-% to actually occur in Douglas fir according to the new data analysis, the ambient air would have to be closer to 93 %RH/20 °C.

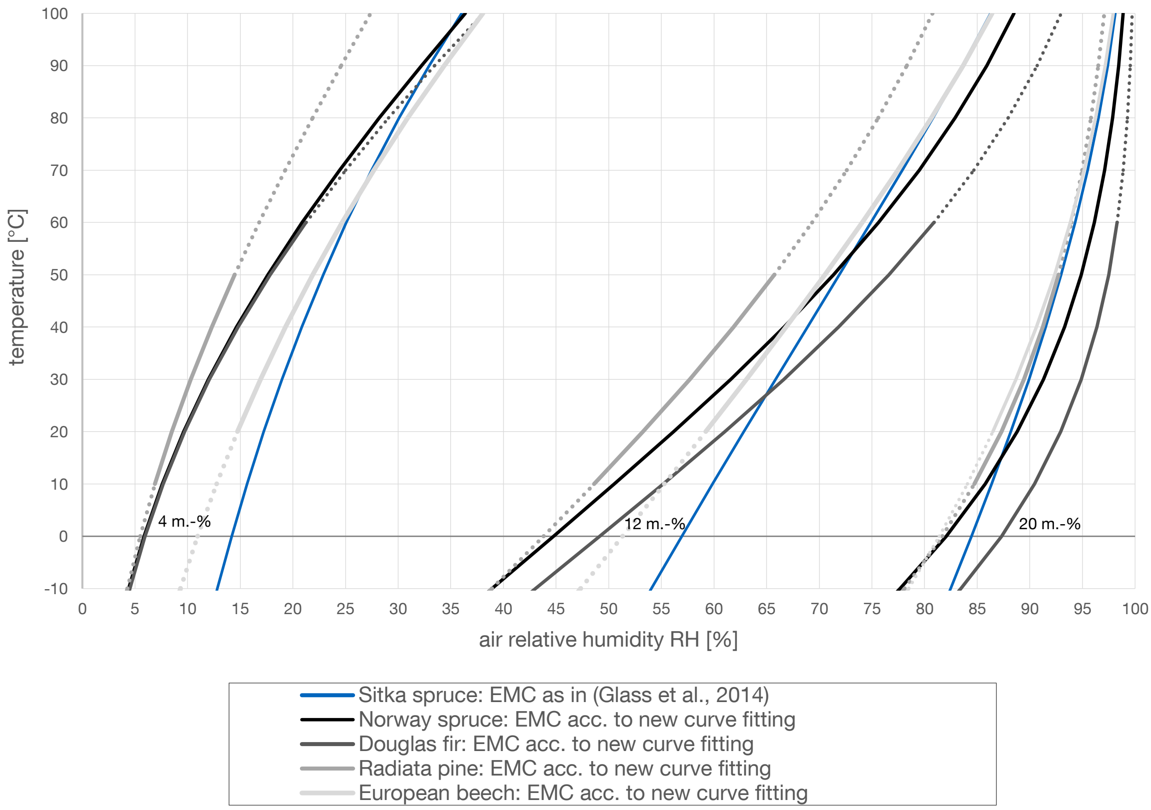

Figure 127: Juxtaposition of newly fitted curves for four different wood species (Norway spruce, Douglas fir, radiata pine, European beech) and the referenced curve based on (Glass et al., 2014), fitted to historic sorption data by Loughborough for Sitka spruce. For a better overview, the graphs only display the equilibrium moisture content at 4 m.-%, 12 m.-%, and 20 m.-%. When extrapolated without underlaying sorption data, the graphs are shown as a dotted line.

Overall, the use of the existing equation by (Glass et al., 2014) seems to lead to an underestimation of the actual wood moisture content at lower, single-digit wood moisture contents. On the other hand, for wood moisture contents above 20 m.-%, it would tend to overestimate the *EMC*s depending on the respective wood species such as in the instance of Douglas fir.

5.4 Laboratory trials on electrical resistance, sorption, and moisture flux methods

5.4.1 Testing the novel sorption method at steady moisture contents in the laboratory

This Subchapter investigates whether the new wood species-specific parameters from the previous Subsection 5.3 would improve moisture monitoring by the sorption method (SM). With this method, the values relative humidity *RH* [%] and temperature *T* [°C] are measured and then transformed into a single value for the equilibrium moisture content *EMC* [m.-%]. In this Subsection, these new parameters, which are based on training data from various references, are now assessed in laboratory experiments using new, independent testing data from other specimens. For the experiment, the ambient climate is changed gradually while keeping the wood moisture constant, as in the first method explained in Subchapter 4.6.3. Figure 128 shows the measurement results of the individual four specimens in batch number 22 (Norway spruce). These use cable-bound combination sensors (*RH*, *T*), which were inserted airtight from below into individual test specimens by means of a specially developed casing, cf. Subchapters 4.4.2 and 4.6.1. The values for *EMC* are calculated from this data using several conversion methods: The conventional equation (3.5) according to (Glass et al., 2014), cf. Subchapter 3.2.1, and the equation with new parameters for Norway spruce, cf. Figure 129.

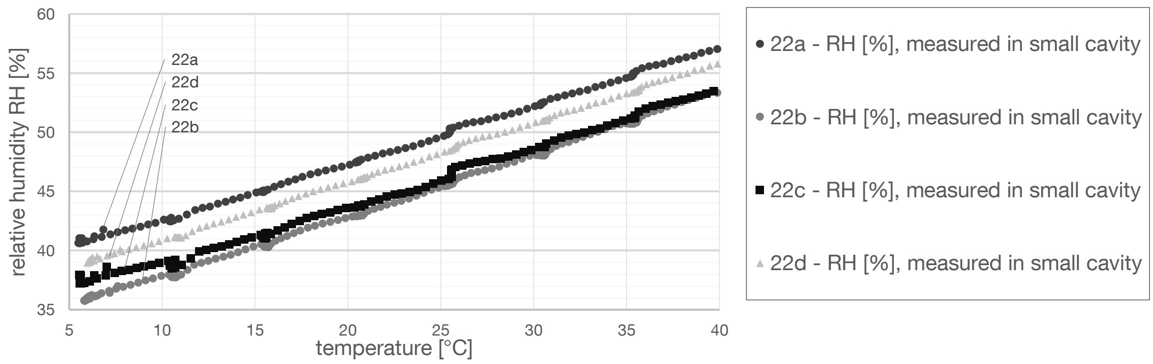

Figure 128: Relative humidity (RH) values measured in the four Norway spruce specimens of batch 22_a-d, graph arranged in dependence of temperature T

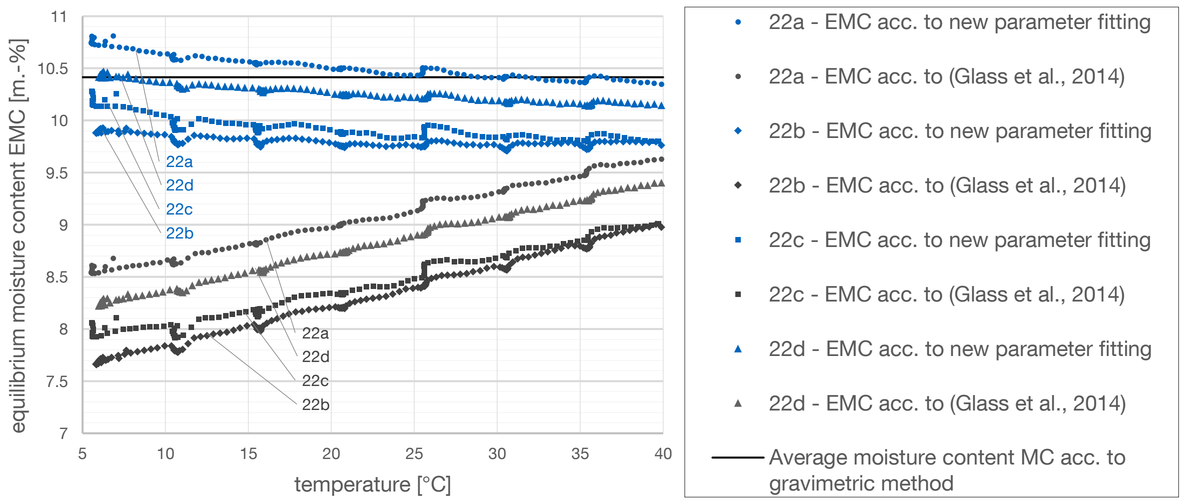

Figure 129: Comparing measurement results of four specimens a-d of the series 22, each analyzed according to (Glass et al., 2014), shown in grey and the new parameter fitting from Subchapter 5.3, shown in blue. The actual moisture content MC this particular experiment was determined at 10.415 ±0.015 m.-% by the gravimetric method.

Comparing the 4 x 260 individual result points shows that there can be deviations of up to Δ*EMC* ≈ 1 m.-% within one batch. These differences can be attributed to the measurement accuracy of the sensors themselves and decrease slightly with increasing temperature, cf. Figure 130.

The two established equations to convert *RH* and *T* to a single *EMC*, (3.4) as tested by (Simpson, 1973), and (3.5) as tested by (Glass et al., 2014), are both fitted to historic sorption data from Sitka spruce by Loughborough (1931), cf. Subchapter 3.2.1. They thus produce very similar results, cf. Figure 130. When using the novel parameters that were fitted specifically for Norway spruce in this thesis, the back-calculation of the values *RH* and *T* leads to results of an equivalent wood moisture *EMC*, which is much closer to the actually measured value of wood moisture content *MC* than with the previously available methods. Especially at low temperatures, the use of the conventional equation (3.5) according to (Glass et al., 2014) would lead to results that are too low by up to Δ*EMC* ≈ 2.8 m.-%. Using equation (3.4) according to (Simpson, 1973) results in even lower values with a difference of up to Δ*EMC* ≈ 3.2 m.-%. This inaccuracy decreases with increasing temperature , but the newly fitted equation still provides more reliable results in the range of 5 °C – 40 °C.

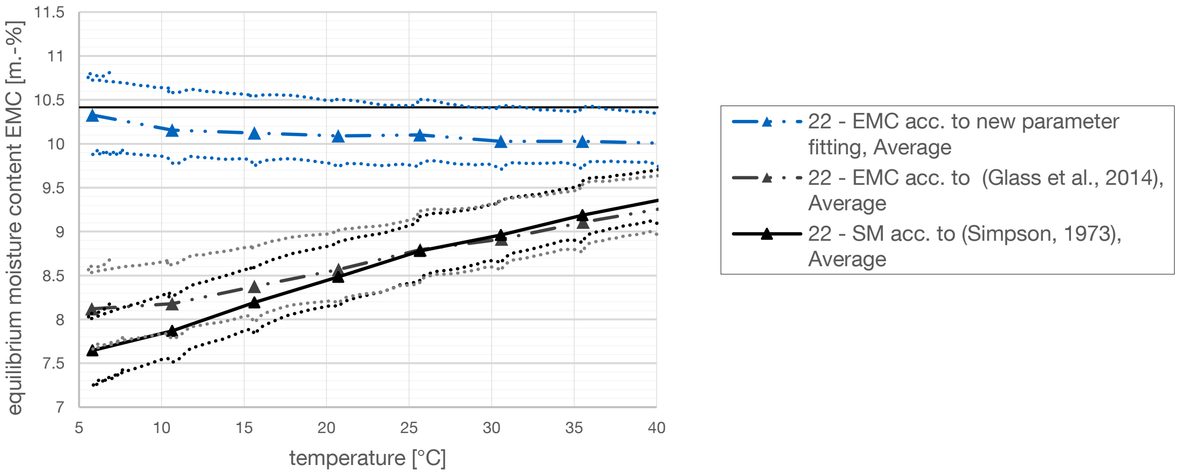

Figure 130: Comparison of three different equations to evaluate the same raw data (22_a-d) using the sorption method. Shown in blue are the averaged results using the new parameter fitting for (4.16) from Subchapter 5.3. Shown in grey and black are the averaged results using the original equations (3.4) as tested by (Simpson, 1973), and (3.5) as tested by (Glass et al., 2014), both as provided by the (Forest Products Laboratory, 2021). The dotted lines each indicate the range of measured data. The actual moisture content MC this particular experiment was determined at 10.415 ±0.015 m.-% by the gravimetric method.

For better readability, the further analysis only employs the averaged values of the individual measurements (x4). Comparing batches 22 and 23 shows that the direction in which the sensor casing was inserted only has a smaller, constant effect on the final result. In contrast, the use of a different combination sensor (*RH*, *T*), here in batch 21, can have a significant and linear impact on the result, cf. Figure 131. Nevertheless, these three different measurement techniques, using the new parameters for Norway spruce (blue), still provide more accurate results for *EMC* compared to those using the conventional parameters for Sitka spruce sorption data (grey).

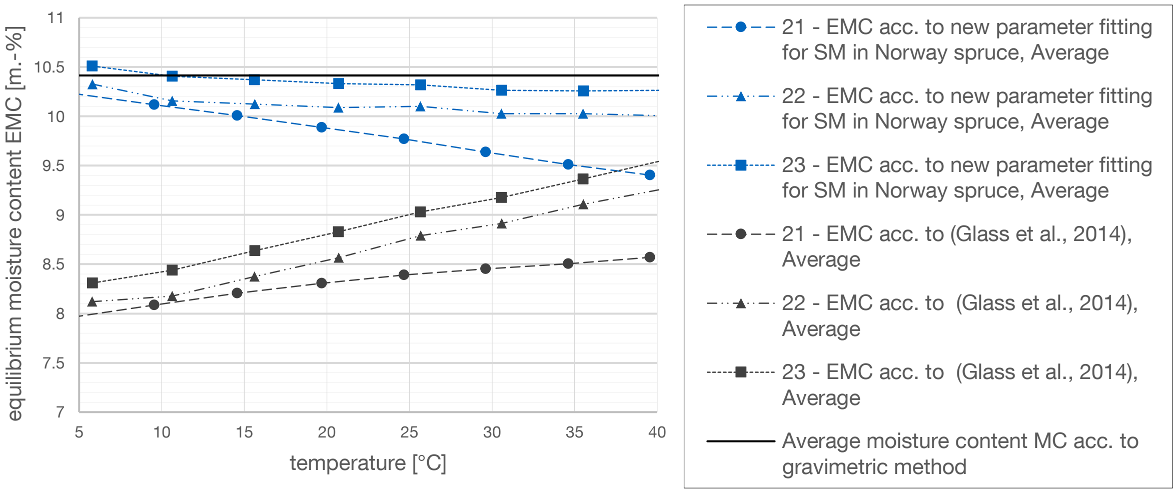

Figure 131: Comparing measurement results of the series 21, 22 and 23 (all in Norway spruce). The averaged values of each series are analyzed according to (3.5) as tested by (Glass et al., 2014), shown in black and the new parameter fitting from Subchapter 5.2.2, shown in blue. The actual moisture content MC in this particular experiment was determined at 10.415 ±0.015 m.-% by the gravimetric method.

Thus, the influence of using the correct, wood-species specific equation for evaluation proves to be more significant in this experiment than the differences caused by using different sensor techniques.

In order to compare the measurement results on different wood species, the deviations are normalized to the actual wood moisture content *MC* determined in each case by gravimetric method (oven-drying). Figure 132, p. 144, shows that the values determined on Douglas fir (batch 24) can be better estimated by using the newly determined parameters than the conventional equation (3.5), especially at cooler temperatures. The new parameters for radiata pine (batch 53), which was randomly tested at 24 °C and 36 °C, also yield a result that is more accurate by about 0.6 m.-%.

Unfortunately, at the time of this study, sorption data sets are not available for the other two Australian wood species investigated, spotted gum (batch 51) and shining gum (batch 52). Therefore, no wood species-specific parameter adjustment for the sorption model could be performed in the previous Subsection 5.3. As an alternative, equation (3.5) as given in (Forest Products Laboratory, 2021) and tested by (Glass et al., 2014) is used, cf. Subchapter 3.2.1. Surprisingly, the results obtained for *EMC* for batches 51 and 52 are relatively close to the respective target *MC*. Since these two hardwood-species differ strongly from the softwood species Sitka spruce, e.g. in terms of grain and density, this might also just be a coincidence.

Overall, it is noticeable that the equivalent wood moisture content using the conventional equation would have led to a significant underestimation of the actual wood moisture content *MC* in most cases, especially at lower temperatures. Within the scope of this investigation (5 °C – 40 °C) on Norway spruce, Douglas fir, and radiata pine, using the new wood species-specific fitting parameters for the sorption method (SM) leads to results which deviate from the actual wood moisture content value *MC* by a maximum of 1 m.-%. These laboratory results serve as evidence that the method developed in Subchapters 4.4.1 and 4.4.2, and the new parameters established accordingly in Subchapter 5.3 work. They allow a much more accurate conversion than the conventional methods used so far. Thus, the new wood species-specific parameters developed in Subchapter 5.3.1 are recommended for further use.

In order to provide a quick overview for practical use, the new findings are designed as convenient data sheets for print in Appendix F, p. 241.

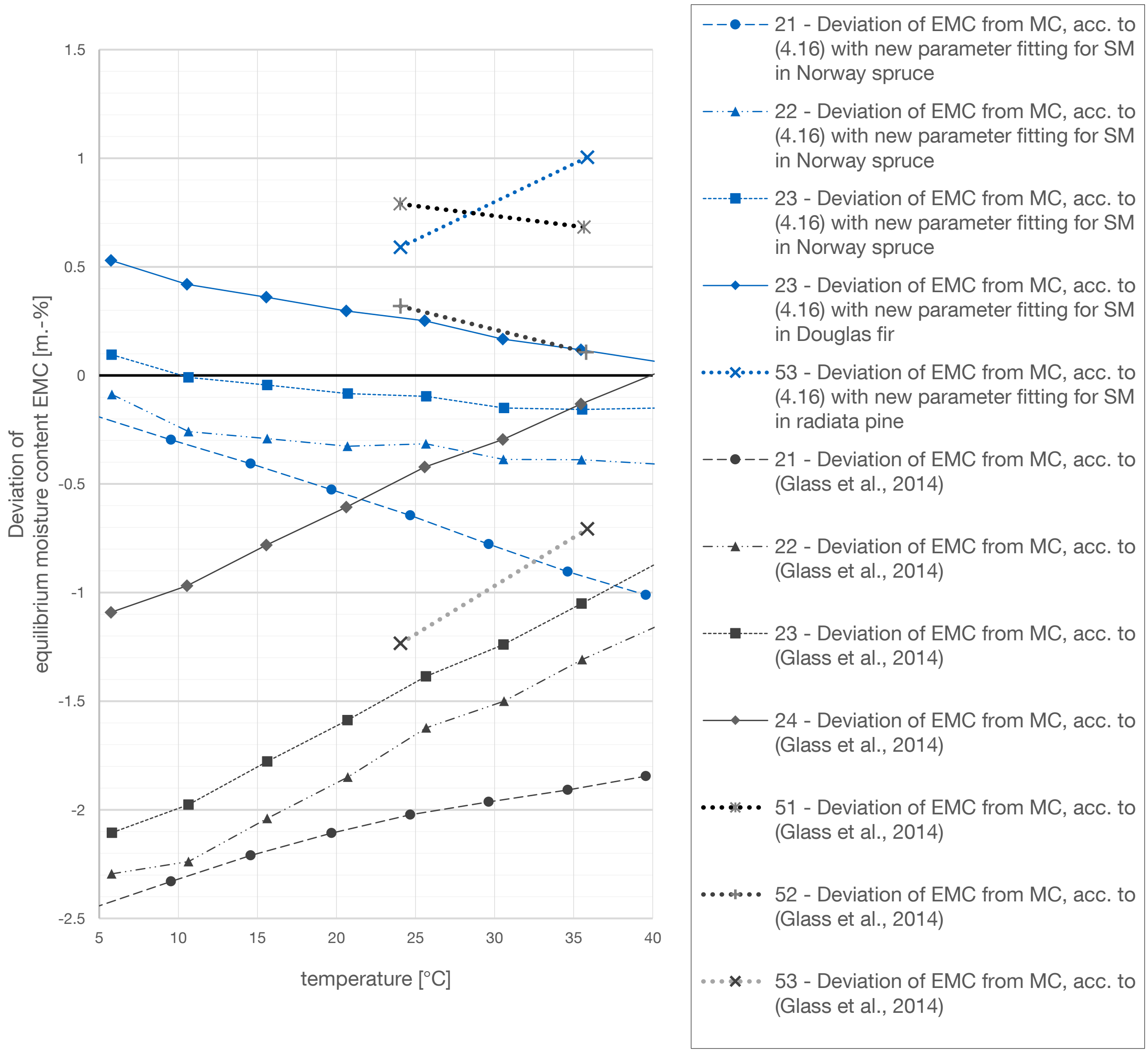

Figure 132: Deviation of differently derived values for equilibrium moisture content EMC by the sorption method (SM) from the actual moisture content MC shown in relation to temperature at measurement. Batches 21, 22 and 23 were experiments in Norway spruce, Batch 24 was in Douglas fir, Batch 51 was in spotted gum, Batch 52 was in shining gum and Batch 53 was in radiata pine (individual MCs are normalized). Shown in blue are the results obtained by using the novel wood-species specific parameters for the sorption method. Shown in grey are the averaged results using the original equation (3.5) as tested by (Glass et al., 2014) and provided by the (Forest Products Laboratory, 2021).

5.4.2 Testing the new electrical resistance method at steady moisture contents

The new parameters for the electrical resistance method (ERM), which are based on training data from previous experiments, are tested on new raw data in comparison to the sorption method (SM). Similar to the previous one, this subchapter discusses the results of the electrical resistance measurements performed in parallel. The detailed methods on investigating the electrical resistance method (ERM) are described in Subchapter 4.6.1.

Three different electrode variations and two different evaluation systems are tested for the measurements in Norway spruce. Figure 133 shows the results of the electrical resistance measurements in batches 11_a-d, 12_a-d, and 13_a-d, averaged from 4 x 260 individual measurements each, all determined with evaluation system I (cf. Table 11, p. 99).

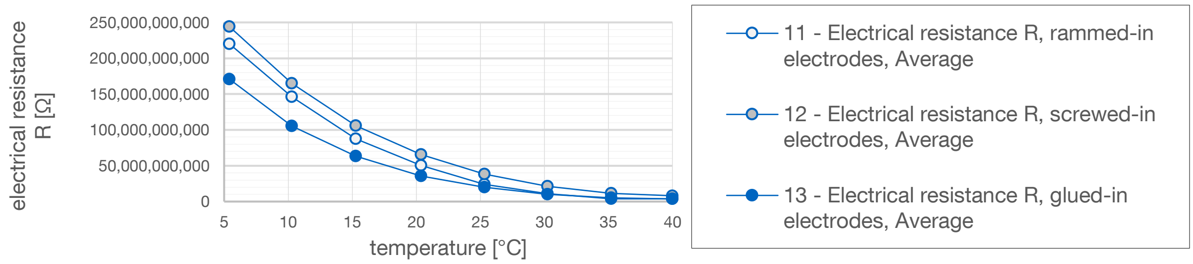

Figure 133: Averaged results from electrical resistance measurements using different electrodes in Norway spruce: batches 11_a-d (rammed-in), 12_a-d (screwed-in), and 13_a-d (glued-in).

The electrical resistances determined with these three different electrode variations are converted using the calibration curve for Norway spruce developed as part of this work in Subsection 5.2. In this experiment all three batches yield results, where the equilibrium moisture contents (*EMCs, shown in blue*) deviate by a maximum of $\Delta EMC \approx 1.2$ m.-% from the actual wood moisture content (*MC*), cf. Figure 134. Along the temperature levels investigated, the resistance values *R* determined with rammed-in electrodes (batch 11) result in the largest variations of *EMC*. The screwed-in electrodes (batch 12) show the smallest fluctuations. The glued-in cable ends (batch 13) also show moderate fluctuation amplitudes, whereby in the present test they provide those results, which are closest to the actual *MC* value.

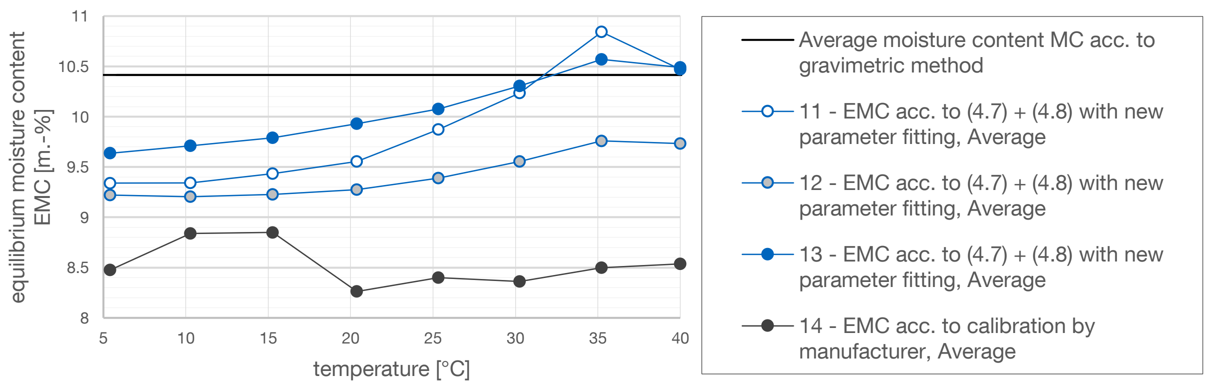

Figure 134: Comparing measurement results of the batches 11_a-d, 12_a-d, and 13_a-d with batch 14_a-d (all in Norway spruce). The averaged values of series 11, 12 and 13 are measured with system I and analyzed according to the new parameter fitting from Subchapter 5.1.3. Results from series 14 were analyzed according to the calibration by the manufacturer of system II. The actual moisture content MC in this particular experiment was determined at MC = 10.415 ±0.015 m.-% by the gravimetric method.

This contrasts with the measurement results with screwed-in electrodes and evaluation system II. This system does not allow any wood species-specific adjustment of the device-internal calibration curve. Accordingly, the results for *EMC* determined in Norway spruce from batch 14 deviate from the actual wood moisture *MC* by up to $\Delta EMC \approx 2.2$ m.-%, cf. gray curve in Figure 134. Furthermore, the individually measured curves show major fluctuations at lower temperatures.

In construction practice, there are cases where it is not possible to separately determine exact calibration curves for the wooden component to be monitored. Accordingly, the following is a random check of how accurate the electrical resistance method could be, if the calibration curves a) have to be compiled from literature values or b) no information is available at all. Notabene: The analysis is limited to a few selected wood species; accordingly, the potential deviations determined do not represent a conclusive, generally valid statement of a maximum amplitude of inaccuracy.

For the investigations on Douglas fir and radiata pine, neither were extra calibration curves created experimentally in advance, nor can calibration curves be found in the literature that would describe *MC* (R,T) sufficiently precisely within the required scope. Therefore, on the basis of collected calibration curves, an own weighted parameter fitting based on a modified model (4.11), cf. Subchapter 5.2.3, is carried out. Figure 135 shows the underlying data from references and the newly generated calibration curve for Douglas fir (*Pseudotsuga menziesii Franco*).

For the species radiata pine, even less data is available at the time of the thesis, which is why the data for the related species Scots pine (*Pinus sylvestris L.*) is used as a supplement, see also the discussion in Subchapter 3.2.4. Figure 136 illustrates the data used and the calibration curve extrapolated from it for radiata pine (*Pinus radiata D. Don*). Because of their imprecision the new parameters obtained by extrapolation are recommended for further use only to a limited extent. They are listed in Appendix D.

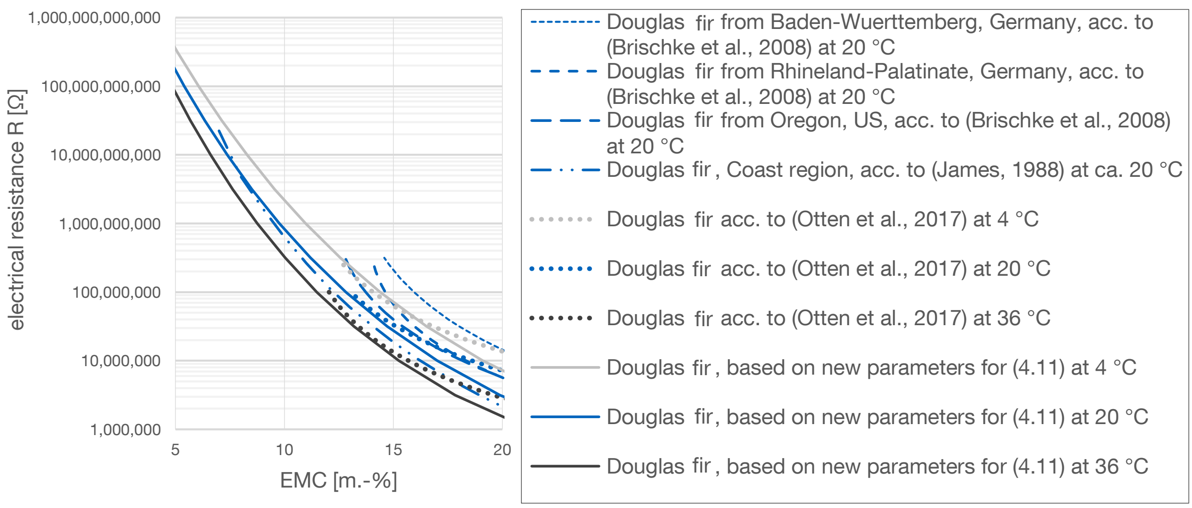

Figure 135: Extrapolation of calibration curves from several publications to generate a new calibration curve to be used on different temperature levels of Douglas fir (Pseudotsuga menziesii Franco)

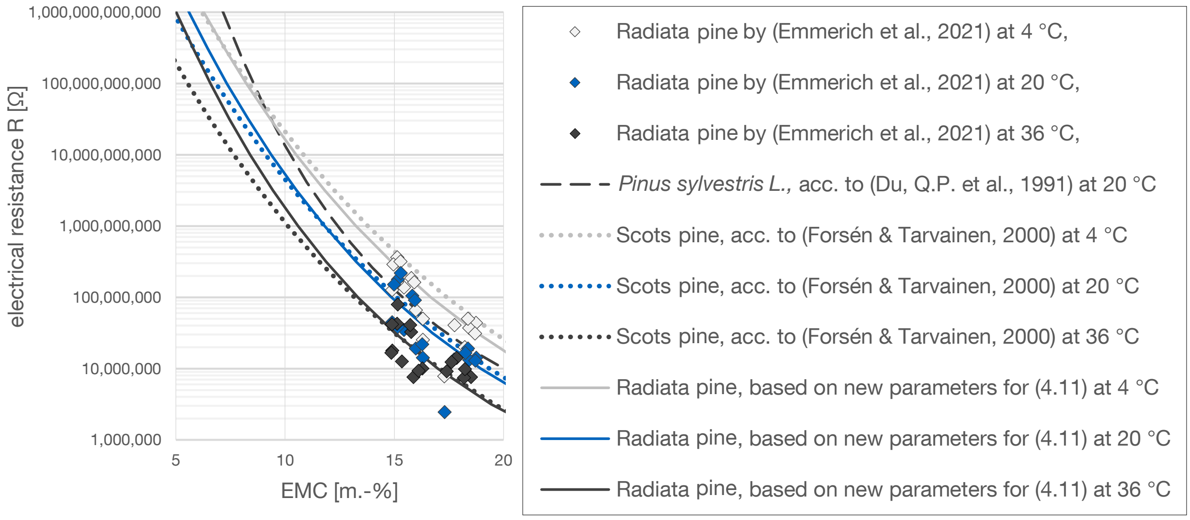

Figure 136: Extrapolation of calibration curves from several publications to generate a new calibration curve to be used on different temperature levels of radiata pine (Pinus radiata D. Don.)

If, as in the case of spotted gum and shining gum, no calibration curves can be found at all, the only option is to fall back on other, well-studied calibration curves. In this case, the parameters used for the wood species Norway spruce with model (4.11) will be applied. Figure 137, Figure 138, and Figure 139 display the deviations between the *EMC* values determined this way and the actual wood moisture *MC*. The curves which are based on measurements within this thesis are shown in solid blue. For comparison, the curves, which have been generated from references in the case of Douglas fir and radiata pine are plotted dashed in blue. The results shaded in grey are those for which the same Norway spruce correlation was applied throughout.

None of the results obtained from extrapolated or substituted calibration curves are consistently as close to the actual wood moisture value as in the case with the previously discussed measurements in Norway spruce using specially measured curves, cf. Figure 137. Rather, the sample tests show that there could be results for *EMC* that are close to the value for *MC*. Under different climatic conditions, however, strongly deviating results could possibly also be obtained. This is evident, for instance, in the case of shining gum (batch 42), where the values for *EMC* are even up to Δ*EMC* ≈ 4.6 m.-% above the actual value, cf. Figure 139.

So far, these deviations do not show a consistent pattern and are therefore generally difficult to correct by mathematical offsetting. Based on the data from measurements on Douglas fir and radiata pine, it is not possible to draw a clear conclusion as to whether it is worth generating species-specific calibration curves synthetically from references. In the case of radiata pine, the experiment indicates that fitting model (4.11) to data by references instead of just using the calibration curve for Norway spruce would improve the accuracy from ±2.7 m.-% to ±1.7 m.-%. However, measurements on Douglas fir provide deviations of up to ±2.8 m.% in both cases and hence seem to render the extra effort pointless, cf. Figure 138.

In all investigated cases, the use of evaluation system I with the calibration curves for Norway spruce on other wood species (Douglas fir, radiata pine, spotted gum, shining gum) leads to an overestimation of the wood moisture content. This means that the *EMC*s calculated from the measured resistance values are mostly significantly higher than the actual wood moisture values *MC*. The tests with evaluation system II show an opposite trend. When testing Norway spruce (batch 14) and radiata pine (batch 45), the *EMC* values output by the system prove to be lower than the actual *MC* measured by gravimetric method.

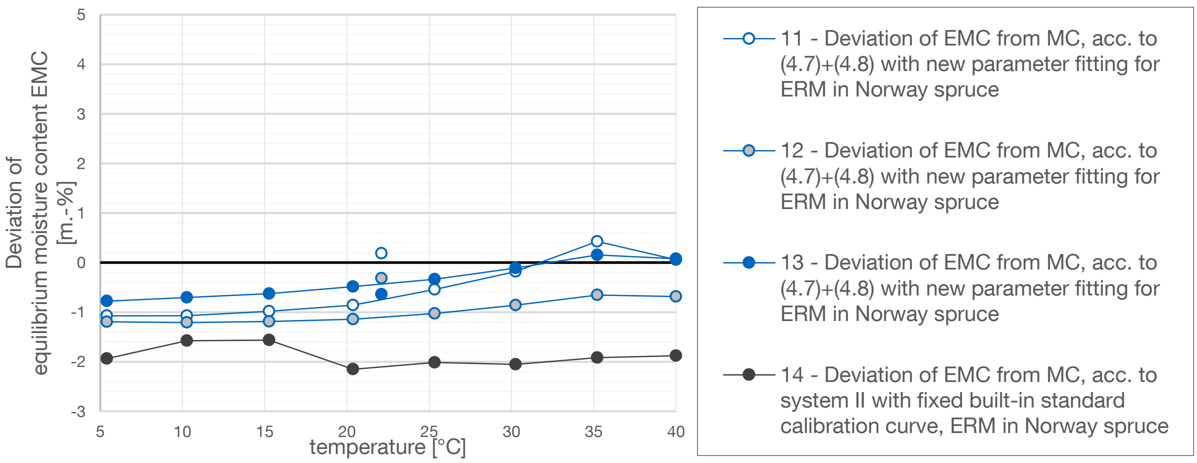

Figure 137: Deviations of results by ERM in Norway spruce in batches 11, 12, 13, and 14.

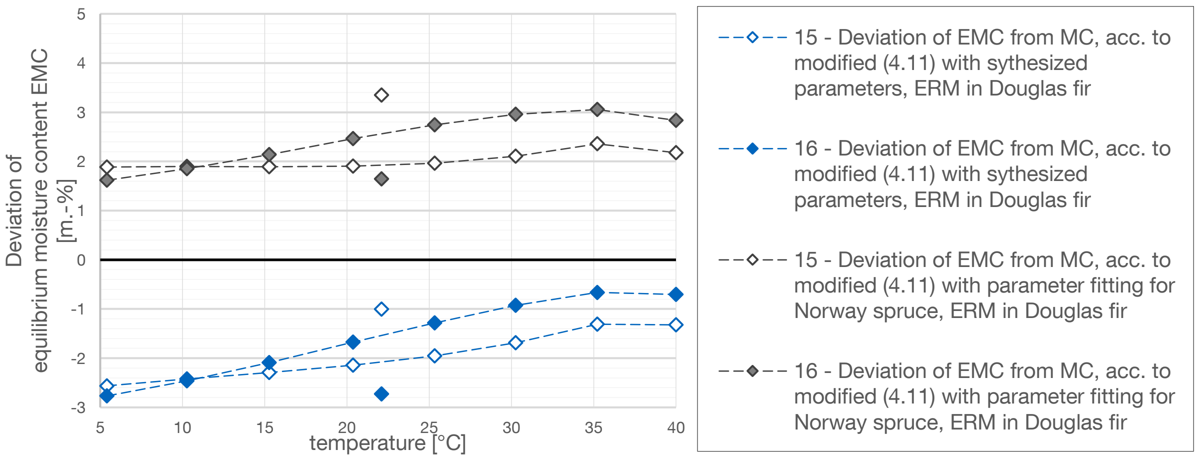

Figure 138: Deviations of results by ERM in Douglas fir in batches 15 and 16

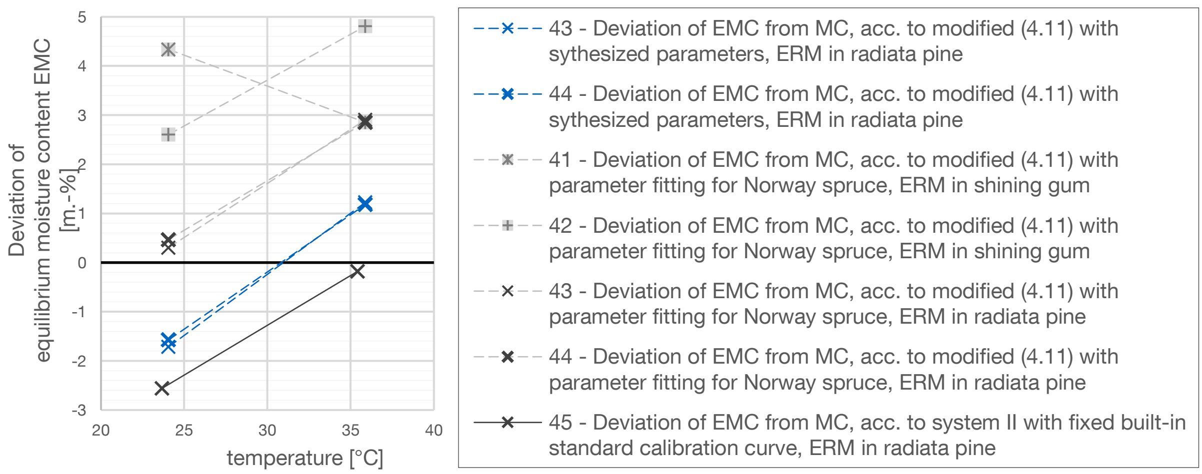

Figure 139: Comparison of experimental results using the electrical resistance method (ERM) for wood moisture monitoring in radiata pine (43, 44, 45), spotted gum (41), and shining gum (42).

5.4.3 Comparing the results at steady wood moisture contents in a laboratory setting

Based on the laboratory trials and the new methods and parameters developed in this thesis: Which method is recommended for wood moisture monitoring in Norway spruce (*Picea abies Karst*.)?

Comparing the individual results from the previous two Subsections for the measurements on Norway spruce, the two methods under investigation – the sorption method (SM) and the electrical resistance method (ERM) - both provide similarly good results for the equilibrium moisture content *EMC*, cf. Figure 140. The results from the sorption method with measuring system IV and the specially developed back-calculation method (batches 22 and 23, shown in blue) tend to consistently give the most accurate results, especially at lower temperatures (5 °C - 20 °C).

At higher temperatures (25 °C - 40 °C), the results of electrical resistance measurements using glued-in electrodes, evaluation system I, and the calibration curve specially determined for Norway spruce (batch 13, shown in blue) can also achieve very accurate results.

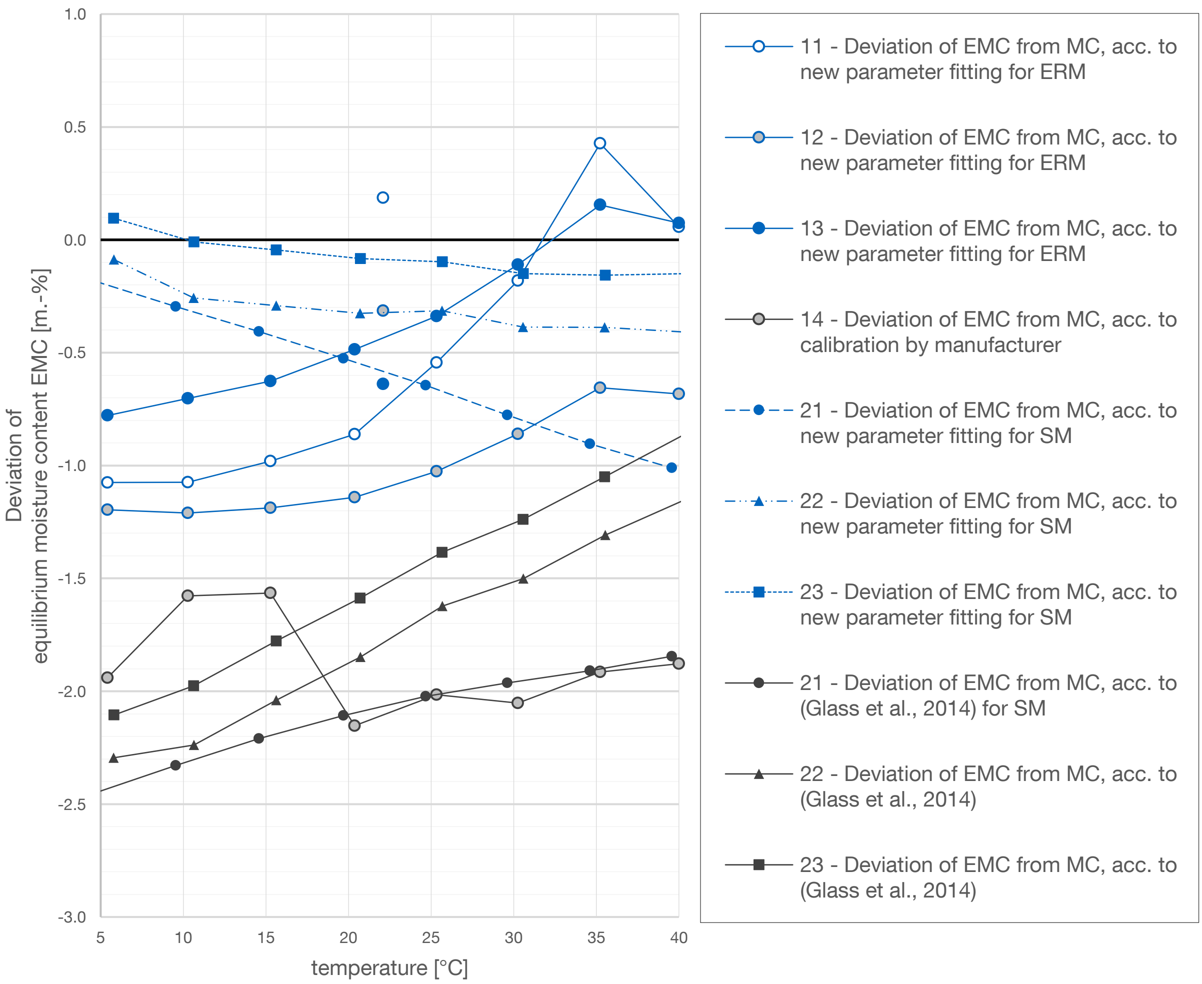

Figure 140: Comparison of deviations based on experimental results using the electrical resistance method (ERM) and the sorption method (SM) for wood moisture monitoring in Norway spruce. The actual moisture content MC in this particular experiment was determined at 10.415 ±0.015 m.-%. The y-axis is differently scaled compared to other figures in this subchapter.

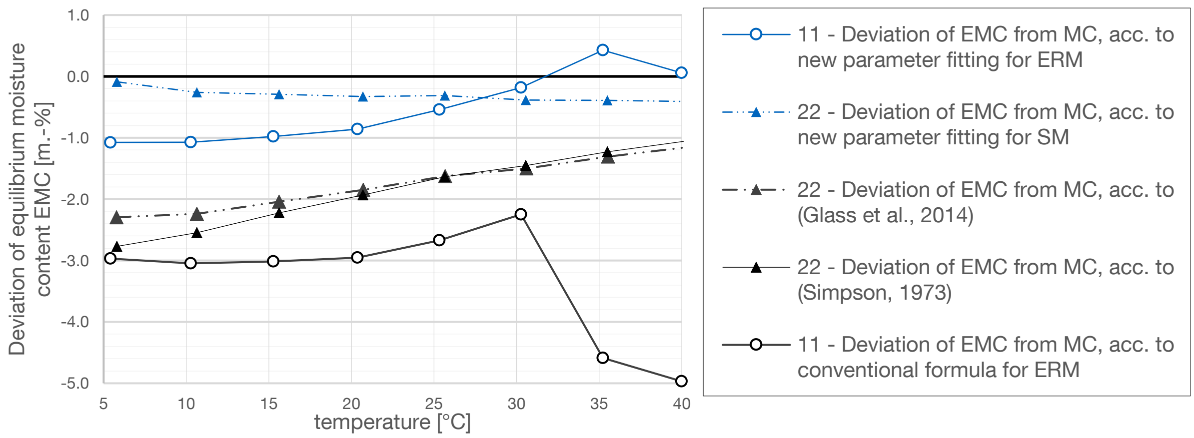

Figure 141: Comparison of deviations obtained with rammed-in electrodes (batch 11) with the new equation for ERM for Norway spruce vs. the conventional one that was used in (Flexeder, Schenk & Aondio, 2022). Additional juxtaposition to the results for SM by the new parameter fitting, the conventional equation by (Glass et al., 2014), and the conventional equation by (Simpson, 1973), which was also used in (Flexeder, Schenk & Aondio, 2022).

Figure 141 demonstrates the deviations resulting from different methods and equations for the same raw data in Norway spruce. The previous publication (Flexeder, Schenk & Aondio, 2022) found very different results when using ERM and SM, both with conventional equations, for monitoring in CLT. Comparing these corresponding lines in Figure 141 proves that all three conventional approaches (grey/black) were actually producing misleading results. Thus, for monitoring in Norway spruce, the newly calibrated methods are significantly more accurate. Which monitoring method provides more accurate results if no exact calibration curves are available for the wood species to be measured? What if no information is available at all?

In the case of the Douglas fir specimens, the sorption method (SM) yields substantially more accurate results than the electrical resistance method (ERM), cf. Figure 142. The application of the back-calculation method developed in Subchapter 5.3 gives the most accurate results (batch 24, shown in blue). In this case, where there are no exact calibration curves for ERM available, preferring SM over ERM is therefore recommended.

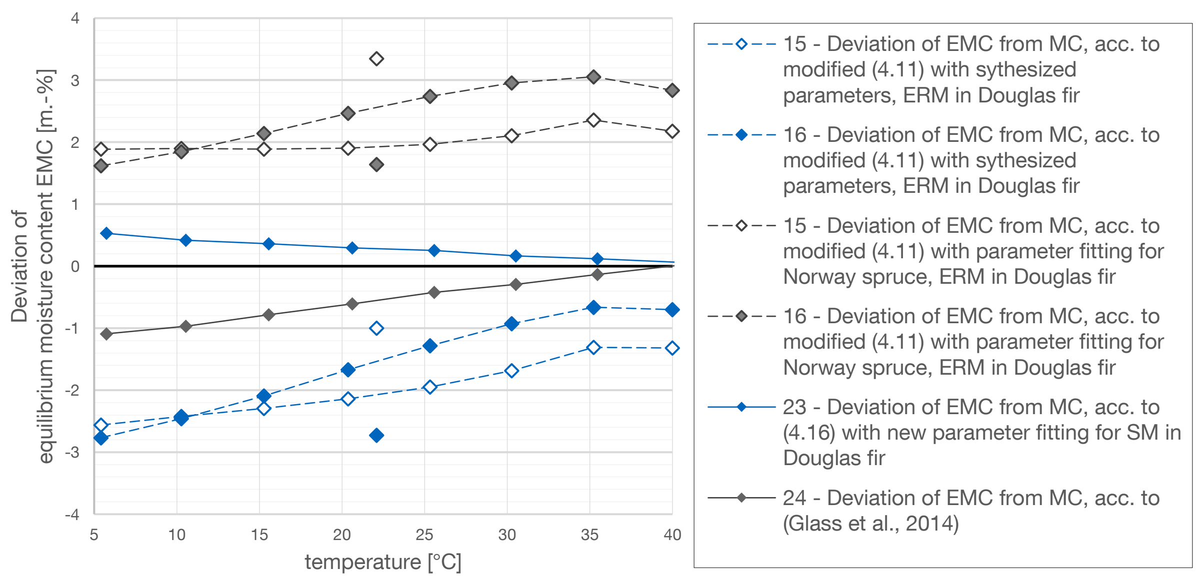

Figure 142: Comparison of experimental results using the electrical resistance method (ERM) in batches 15 and 16, and the sorption method (SM) for wood moisture monitoring in Douglas fir in batch 24.

This applies in particular if, as in the present case, no temperature-dependent calibration curves are available for ERM in the relevant low-moisture range. The results of sampling on the Australian timber species radiata pine support this recommendation, cf. Figure 143. The application of a species-specific back calculation for the use of SM in radiata pine (see dotted blue line, batch 53) provides a more accurate and consistent prediction of wood moisture content than using the calibration curve for ERM synthesized from literature values (blue dashed line, batches 43 and 44).

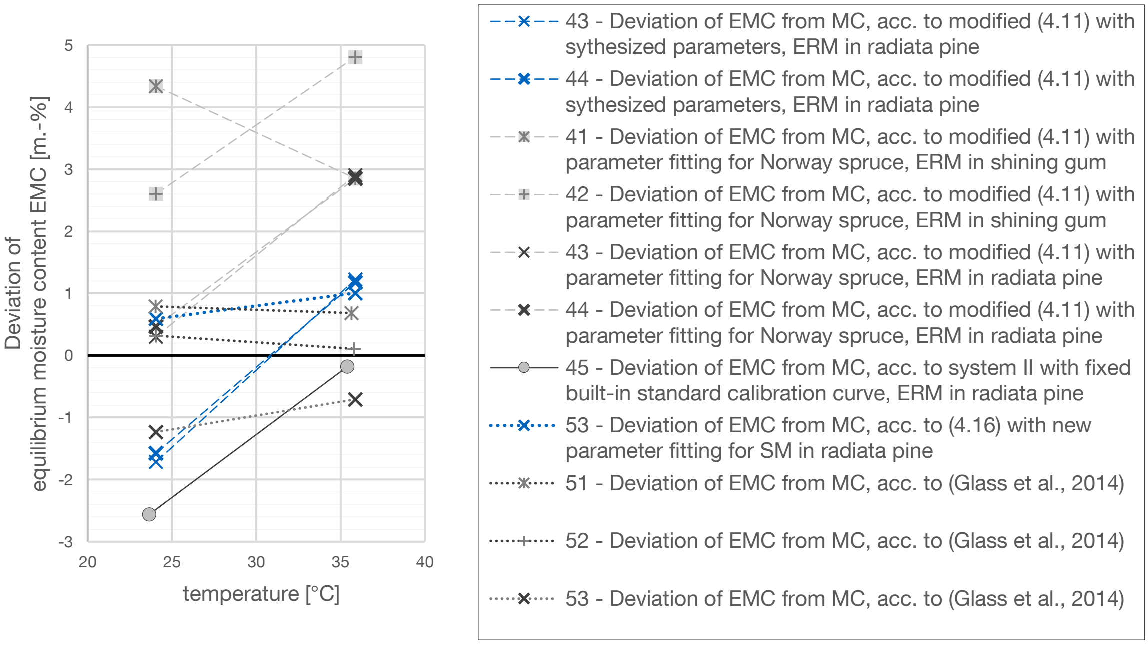

Figure 143: Comparison of experimental results using the electrical resistance method (ERM) in batches 41-45, and the sorption method (SM) for wood moisture monitoring in radiata pine, spotted gum, and shining gum in batches 51-53.

Which monitoring method provides more accurate results if no information is available at all?

Since at the time of writing, no calibration curves were available for the species spotted gum (batches 41 and 51) nor shining gum (batches 42 and 52), only substitutions could be used. When comparing the test results of the wood specimens without any further information, the results using SM (batch 51 and 52, dotted in grey) with a conventional calibration curve based on equation (3.5) by (Glass et al., 2014) show values for *EMC* that are much more constant, as well as closer to *MC*, than the results by ERM (batches 41 and 42, dashed in grey), which were obtained by substituting equation (4.11) with parameters for Norway spruce.

Overall, the results of this Subsection indicate a clear recommendation to use the sorption method (SM). Even if individual series of measurements with ERM produce quite good absolute results, comparisons on different types of wood show a clear picture: deviations obtained by electrical resistance measurement fluctuate on a larger scale than those obtained by the sorption method. This is an important finding for the use of monitoring methods to detect a wood moisture gradient in building components with varying ambient temperatures. Measurement errors, which are not constant but change significantly under the influence of temperature, can lead to incorrect interpretations of wood moisture gradients.

5.4.4 Laboratory results from the sorption method at wood moisture gradients

The second series of experiments using the method described in Subchapter 4.6.2 is intended to show what happens if the absolute humidity *AH* remains constant and the air temperature *T* changes. For this, the specimens are first preconditioned to a constant weight (batches 22/23 from Norway spruce: *MC* = 10.4 m.-%, batch 24 from Douglas fir: *MC* = 9.6 m.-%). Then the temperature is lowered from 21 °C to 10 °C in hour 5, so the relative humidity in the climate chamber rises from 50 %RH to 90 %RH. After keeping this climate constant for six days, the air temperature then rises to 40 °C while the ambient relative humidity drops to 18 %RH. Notabene: According to Subchapter 5.3, an ambient climate of 10 °C / 90 %RH refers to an

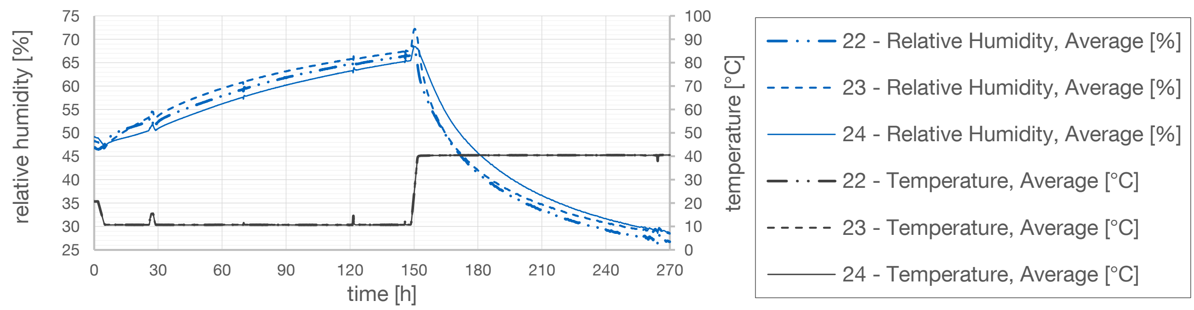

Figure 144: Measured physical variables, averaged from four specimens each, for the calculation of EMC with the sorption method in Norway spruce (batch 22 and 23) and Douglas fir (batch 24). Shown are the measured values for air temperature and relative humidity in the respective measurement cavity within each specimen.

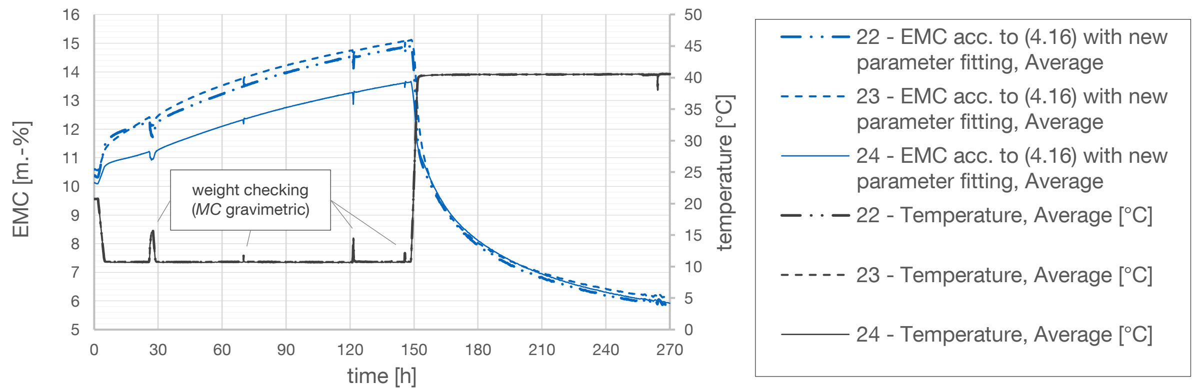

Figure 145: Resulting average EMC values with the sorption method in Norway spruce (22/23) and Douglas fir (24). Opening the climate chamber briefly for weight checks resulted in smaller peaks, cf. Figure 150 and Figure 151.

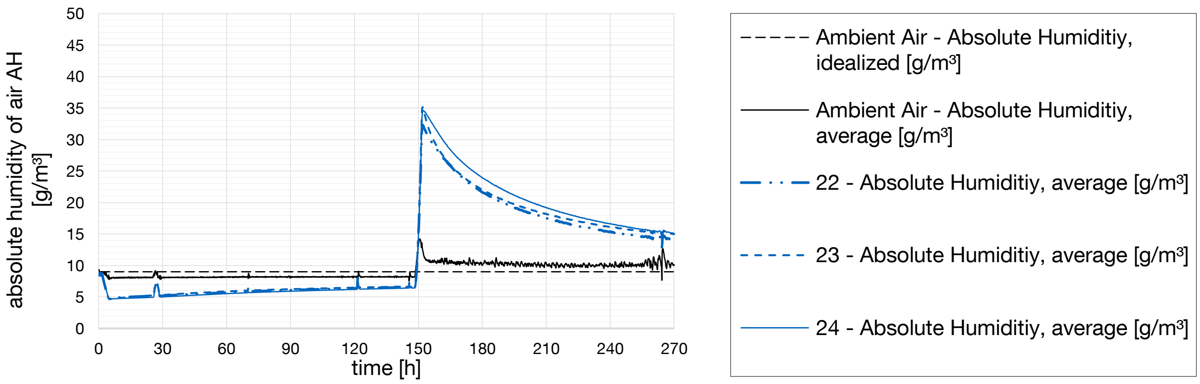

Figure 146: Measured physical variables, averaged and calculated for absolute humidity AH in the ambient air of the climate chamber (black) and the respective measurement cavity within each specimen (blue).

EMC of around 21.8 m.-% for Norway spruce and 19.8 m.-% for Douglas fir. An *EMC* of around 4.5 m.-% is assigned to an ambient climate of 40 °C / 18 %RH for both, Norway spruce and Douglas fir. However, the test period is not sufficient to achieve equilibrium for the 20 mm thick test specimens, hence they exhibit moisture gradients. Figure 144 shows the values detected by the sensors in the small sealed off measurement cavities of the test specimens in series 22_a-d, 23_a-d and 24_a-d in circa 8 mm depth. This means the air chamber is separated from the ambient air by an approximately 8 mm thick layer of wood and tightly sealed on the remaining sides. The change in ambient temperature is detected immediately by the sensors, as heat is transferred very quickly through the thin layer of wood. Diffusion, and therefore the adaptation of the enclosed humidity to the outside conditions, takes considerably longer and is not yet complete even after six days.

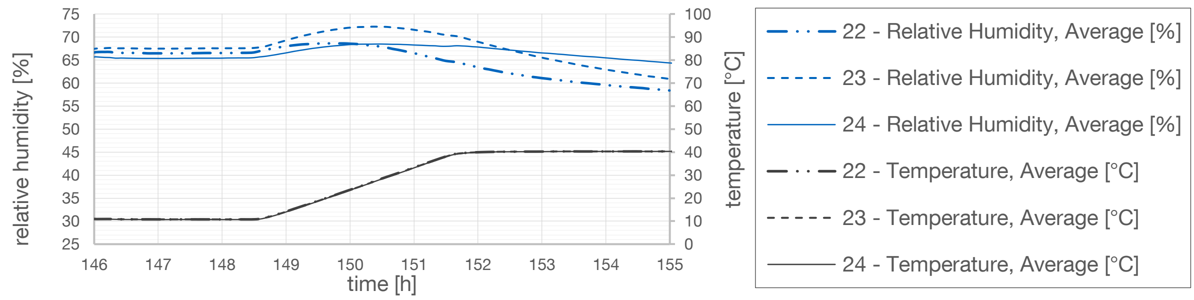

Figure 147: Detail from previous Figure 144. A slight temporary increase of the relative humidity in the measuring cavity can be observed for the material specimens made of Norway spruce (batch 22 and 23) and Douglas fir (24).

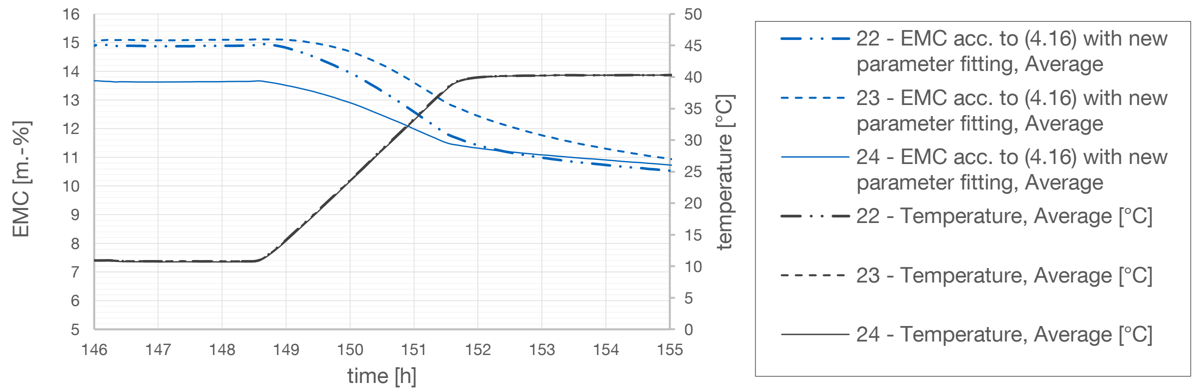

Figure 148: Detail from previous Figure 145. A major decrease of the equilibrium moisture content EMC can be observed for the material specimens made of Norway spruce (batch 22 and 23) and Douglas fir (batch 24) at 8 mm

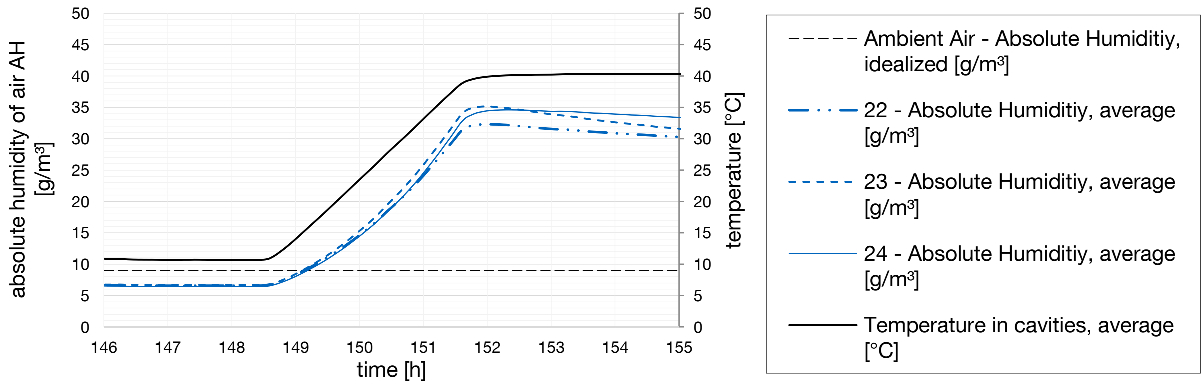

Figure 149: Detail from previous Figure 146. A major increase of absolute humidity in the measuring cavity can be observed for the material specimens made of Norway spruce (batch 22 and 23) and Douglas fir (batch 24).

Figure 145 and Figure 148 show the resulting values for *EMC*, computed by using the findings from Subsection 5.3. If the measurement cavities were completely sealed on all sides, the absolute humidity *AH* [g/m³] within would remain constant. Consequently, the value of the relative humidity *RH* [%] would decrease within a short time as soon as the temperature rises, in a manner similar to the ambient air humidity in the climate chamber. In contrast, the actual measurements in the cavities show only a gradual flattening of the curve for relative humidity between hours 152 and 270 and even a slight increase in the first few hours 148 – 152, cf. Figure 147. This observation is in line with the findings by (Dyken & Kepp, 2010), who, however do not investigate this phenomenon further. Remarkably, when transitioning from 10 °C to 40 °C, the absolute humidity *AH* in the measurement cavities in batches 22, 23, and 24 rises rapidly from around 6 g/m³ to nearly 35 g/m³, cf. Figure 146 and Figure 149. This sudden and major increase of water content in the air within the small, sealed measuring enclosure is a curious phenomenon that merits further investigation.

Why does the absolute humidity *AH* [g/m³] in the measuring cavity increase? A possible explanation could be the thermal inertia of the sensor housing, as explained in (EN 16242:2012, C.3). However, the phenomenon could also be attributed to the temperature-dependent equilibrium moisture content (*EMC*) of the surrounding wood. The wood moisture content in the immediate vicinity of air exhibits a relatively fast adjustment to the rapid rise in temperature. In other words, the temperature change from 10 °C to 40 °C led to a drying process in the wood. Consequently, the material is desorbing the excess water in all available directions, both into the ambient air and into the small air volume in the measurement cavity, which is intended to measure *RH* and *T* for the sorption method. Presumably, there is also a very high humidity at the air boundary layer near the free test specimen´s surface, but this is quickly transported away by convection into the comparatively very large climate chamber volume. The excess water trapped in the measurement cavity can only diffuse through the 8 mm thick wood layer. Consequently, this enclosed air becomes highly humid in a matter of minutes after the temperature rises in the climate chamber, but requires several days to reach equilibrium with the ambient air humidity by water transport through the 8 mm of wood (transverse to grain direction). Regarding the relation of layer thicknesses, the actual quantity of water that evaporates from this layer of wood into the measuring cavity and causes to spike AH up to 35 g/m³ is relatively modest. For a difference in absolute humidity of approximately 29 g/m³, the adjacent wooden layer needs to evaporate around 0.0001044 g of water into the small volume of approximately 3,600 mm³. This equals the difference of water when the *MC* drops from 15.3 m.-% (*EMC* of Norway spruce at 10 °C / 68 %RH) to 12.3 m.-% (40 °C / 68 %RH) in an only 0.0025 mm thick layer of wood covering the area of the measurement cavity (*A* ≈ 200 mm²). The observed increase in absolute humidity *AH* is therefore already caused by a change in wood moisture in a comparatively very thin adjacent layer.

This is considered proof of the functionality of the sorption method under transient conditions. The overall curvature is confirmed by precision weighing of the test specimens throughout the experiment. Since the total weight can only be used to determine the average wood moisture content of the entire specimen, hygrothermal simulations according to Subchapter 4.1.3 shall supplement this analysis with the values to be expected under the moisture gradient at 8 mm depth.

As the simulation tool does not regard temperature-dependent sorption isotherms, the outputs from two simulations need to be combined into one graph, leaving a little gap where the temperature changes. The simulation results show overall similar trends as the measurement results. However, the comparisons in Figure 150 and Figure 151 reveal major deviations in the values obtained for Norway spruce as well as Douglas fir. The total increase in moisture content calculated by the simulation significantly exceeds the wood moisture values determined by the gravimetric method with random samples. In order to facilitate a realistic simulation, the most accurate available values from various references were compiled as material parameters, cf. Appendix G and Appendix H. Nevertheless, the parameters for the moisture transport functions possibly might still not be sufficiently accurate.

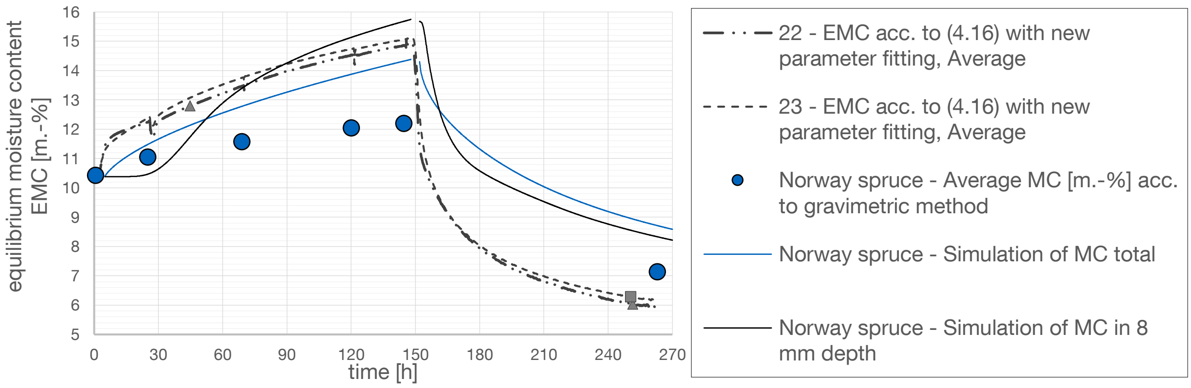

Figure 150: Comparison of values obtained for EMC in 8 mm depth (by sorption method and hygrothermal simulation, shown in black) and overall MC of the specimen (by gravimetric method and hygrothermal simulation, shown in blue) for the average values in Norway spruce, cf. batches 22_a-d and 23_a-d

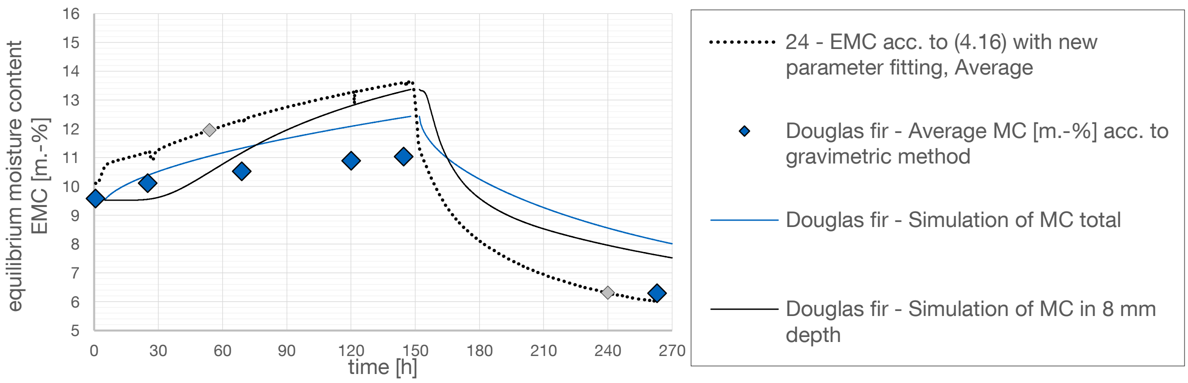

Figure 151: Comparison of values obtained for EMC in 8 mm depth (by sorption method and hygrothermal simulation, shown in black) and overall MC of the specimen (by gravimetric method and hygrothermal simulation, shown in blue) for the average values in Douglas fir, cf. batch 24_a-d

In the first 50 hours of the experiment, the course of the calculated wood moisture at a depth of 8 mm differs fundamentally between the simulation and the sorption method. This deviation has not yet been sufficiently clarified, but it is likely related to the limitations and simplifications of the simulation model described in Subchapter 4.1.3. However, it is also possible that an additional undiscovered systemic disadvantage of the sorption method might be evident here.

In conclusion, the *EMC* curve determined using the sorption method (SM) corresponds, at least in its tendency, to the curve expected by utilizing the hygrothermal simulation tool WUFI with water vapor diffusion according to Fick´s law.

5.4.5 Laboratory results from the electrical resistance method at wood moisture gradients

In addition to the measurements discussed in the previous Subchapter 5.4.4, the quality of the electrical resistance measurements under transient conditions is also evaluated in the same experiment, cf. methods explained in Subchapters 4.6.1 and 4.6.3. The initial temperature change from 20 °C to 10 °C results in erroneous measurements for all batches (11_a-d – 16_a-d) with ERM. The low temperature appears to increase the difficulty of obtaining error-free electrical resistance measurements, cf. Figure 152. Regardless of whether the electrodes are rammed-in, screwed-in, or glued-in, all exhibit highly irregular curves up to hour 150.

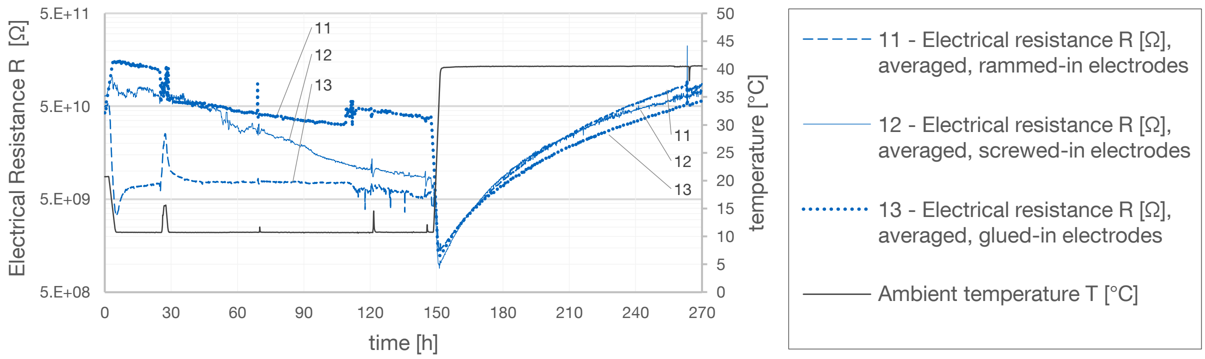

Figure 152: Electrical resistance values measured with system I; temperature change from 20 °C to 10 °C to 40 °C

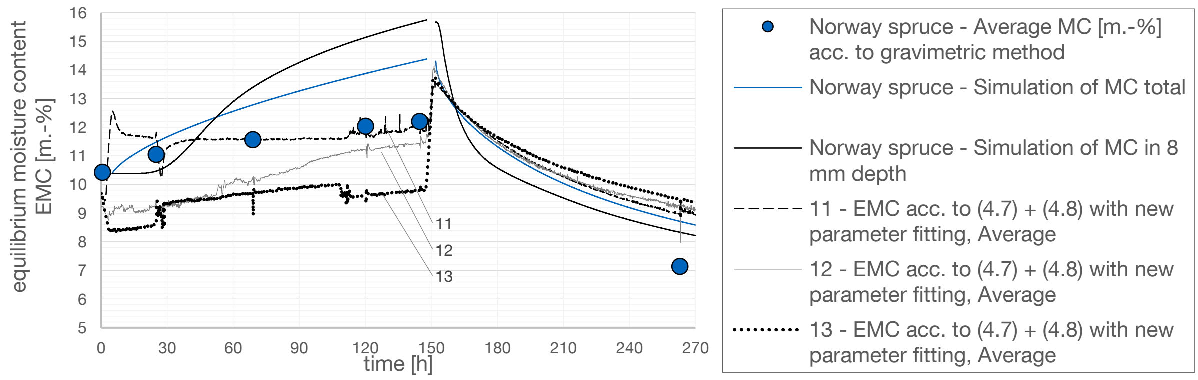

Figure 153: Resulting computed EMC values for Norway spruce (batches 11, 12, and 13)

Figure 153 clearly demonstrates that the wood moisture content determined by electrical resistance measurements at 10 °C in Norway spruce specimens is implausible and the sharp increase of up to 4 m.-% within less than three hours seems unrealistic. The measured values are presumably only reliable after the temperature has risen to 40 °C, hour 151, cf. Figure 154.

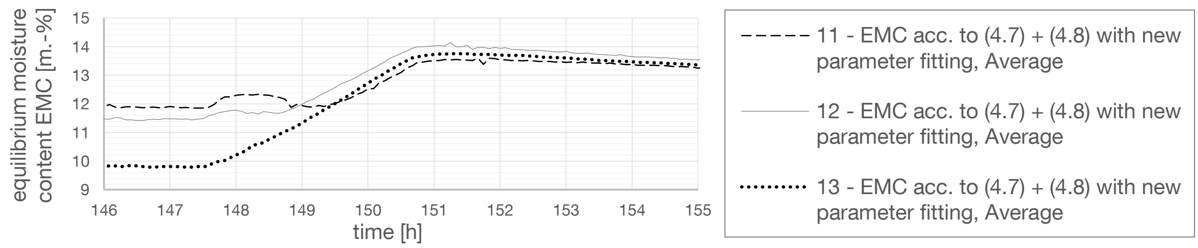

Figure 154: Detail from previous Figure 153. The computed EMC shows a major increase for the specimens made of Norway spruce (batches 11, 12, and 13) with the temperature change from 10 °C to 40 °C.

The measurements in Douglas fir also exhibit a similar contradiction. As shown in Figure 155, the *EMC* curve immediately jumps upwards as soon as the temperature is increased.

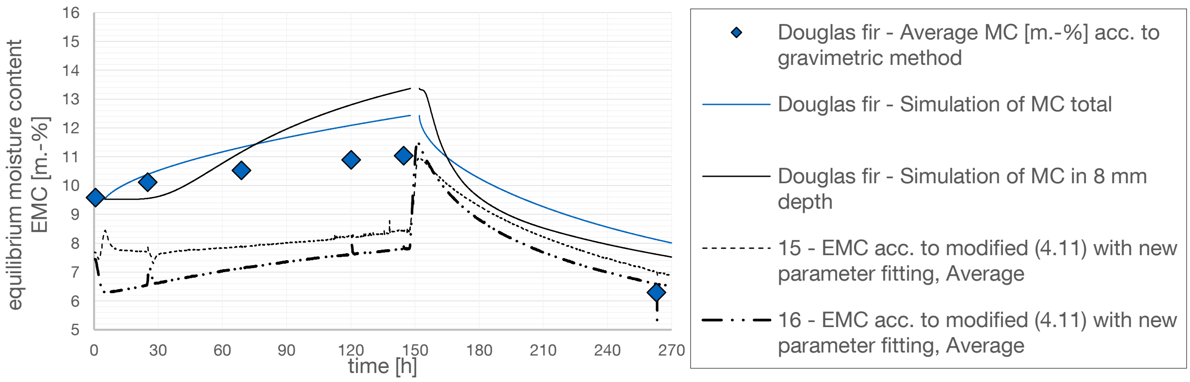

Figure 155: Resulting computed EMC values for Douglas fir (batches 15 and 16)

A similar phenomenon can also be observed in batch 14_a-d, where screwed-in electrodes are used with evaluation system II, cf. Table 11, p. 99. This system incorporates a built-in evaluation with a calibration curve based on (James, 1988) as provided by the manufacturer. The individual curves shown in Figure 156 also demonstrate a significant fluctuation range of up to ΔEMC = 4 m.-%. These results are implausible when compared with the values determined using the gravimetric method and with the transient hygrothermal simulation.

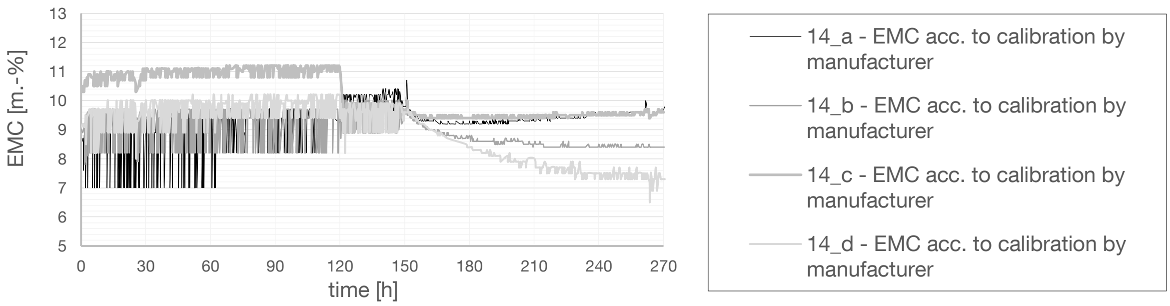

Figure 156: Results for ERM by System II (Omnisense), with screwed in electrodes, in four Norway spruce specimens, batch 14_a-d, The calibration curves are already applied by the manufacturer and based on (James, 1988).

During preparation, the electrodes were inserted into the test specimens at an ambient air temperature of approximately 20 °C. This was followed by months of preconditioning in a constant climate. Following this experiment, it can now be clearly established that a slightly lower temperature of 10 °C is sufficient to trigger incorrect measurements with questionable fluctuations and resulting *EMC*-values that seem too low (dry) overall. Conversely, if the temperature is elevated, the measurement outcomes show less random fluctuations, become more precise, and also exhibit a higher *EMC* [m.-%].

In the context of in-situ wood moisture monitoring, the use of ERM necessitates a degree of caution in the evaluation process, particularly in instances where temperatures decline. This is despite the implementation of optimized temperature compensation, which has been calibrated to account for fluctuations within this temperature range. Furthermore, this caveat applies despite the implementation of measures to improve contact, such as screwed-in or glued-in electrodes.

5.4.6 Validation of the novel temperature differences method for detecting moisture fluxes

The experiment of which some results were already described in Subchapters 5.4.4 and 5.4.5 is further evaluated to develop a new moisture flux detection method. The hygrothermal simulation model used includes latent heat phenomena and thus offers the possibility of calculating the temperature increase on the component surface as a result of water vapor sorption. Furthermore, the results can be transformed to output the computed moisture flux density in the unit [10^{-2} g/(m²s)], as shown for better readability in Figure 157 and Figure 158. These two curves do not exhibit a linear relationship, yet they do share certain similarities.

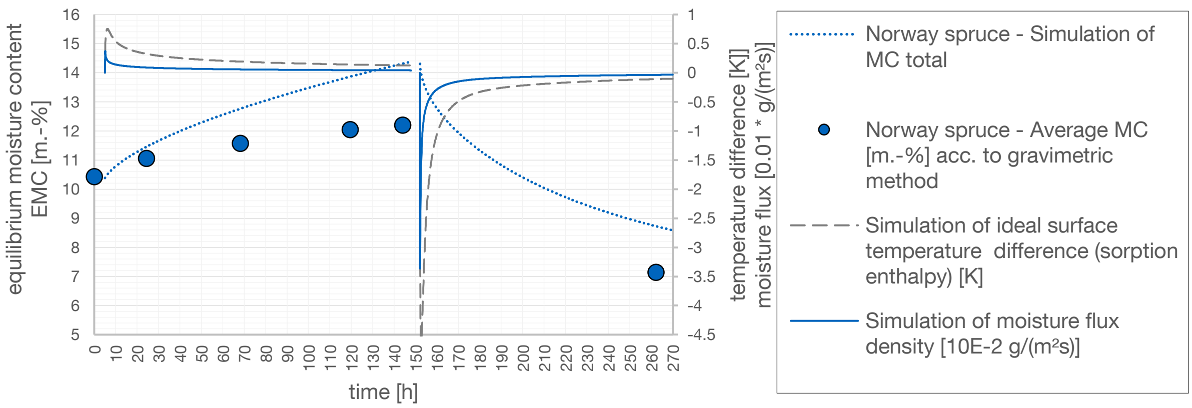

Figure 157: Hygrothermal simulation results for the moisture step experiment in Norway spruce, juxtaposing the change in moisture gradient with the change of temperature and moisture flux density at the sorbing surface

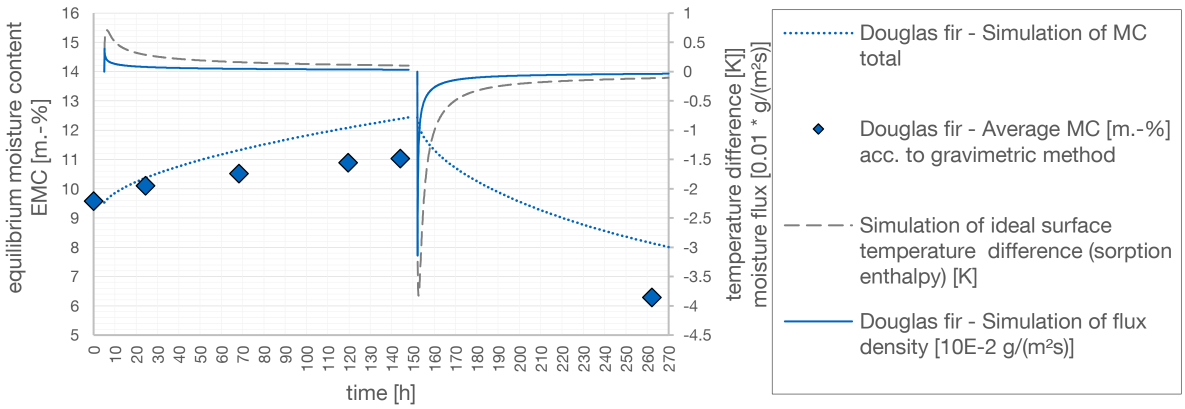

Figure 158: Hygrothermal simulation results for the moisture step experiment in Douglas fir.

As previously noted in in Subchapter 5.4.4, the simulation model exhibits deviations relative to the actual measurements, both for Norway spruce and Douglas fir. This discrepancy is reflected in Figure 157 and Figure 158, where the simulated *MC* total and the gravimetrically determined *MC* average diverge as the experiment progresses.

Figure 159 depicts the details of the simulation results in hours 152 – 154 for Norway spruce, at the start of the desorption phase. As part of the investigation, it is necessary to consider not only the absolute temperature change of the test specimen surface due to latent sorption heat, but also the difference to the second, sealed rear side of the test specimen. Thus, the test setup for this laboratory experiment includes two temperature measurements each on a 20 mm thick test specimen, cf. methods in Subchapter 4.6.2. The front side is free for sorption and heats up accordingly. The rear side does not undergo sorption, but it does heat up with a slight delay due to heat conduction through the wooden specimen. The difference between these two values is referred to here as "simulation of experimental surface temperature differences dt [K]". In a real experiment, this setup is used to correct small temperature changes that occur completely independently of the sorption phenomenon due to external influences.

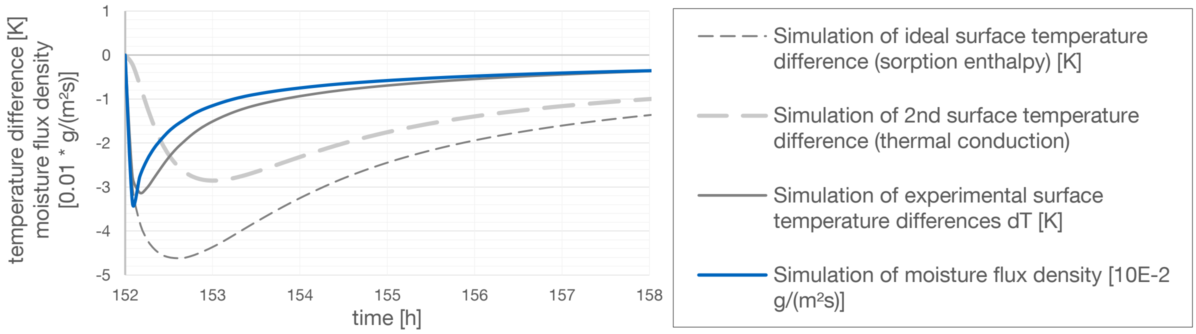

Figure 159: Detail of simulation results for surfaces of Norway spruce specimens; period shown shortly after change of ambient climate from 10 °C / 90 %RH to 40 °C / 18 %RH and thus at the start of a desorption process

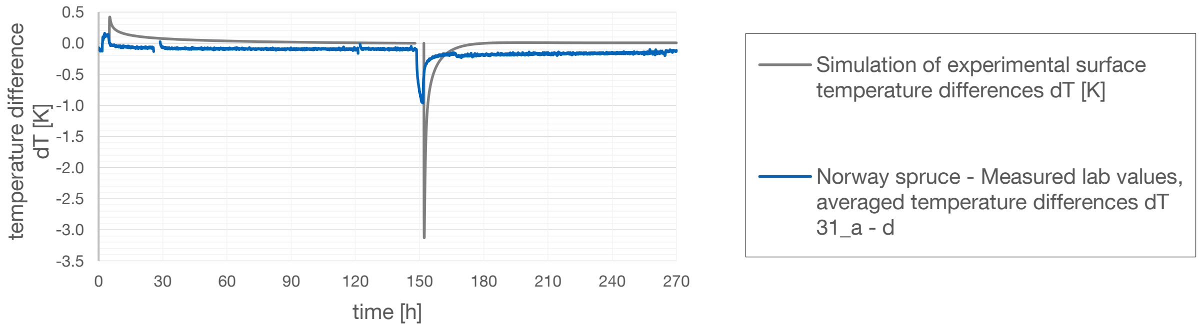

Figure 160: Juxtaposition of measured surface temperature differences vs. simulation results for Norway spruce specimens under transient conditions

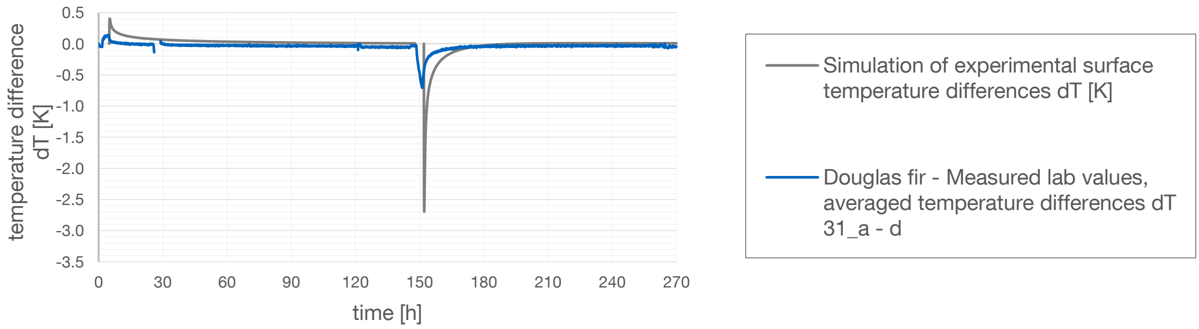

Figure 161: Juxtaposition of measured surface temperature differences vs. simulation results for Douglas fir specimens under transient conditions

Overall, the findings of the surface temperature rising with the test specimen gaining weight (= increasing *MC* = adsorption) and dropping with desorption are in line with (Kraniotis et al., 2016). Furthermore, the compilation in Figure 159 indicates that the surface temperature difference method, described in Subchapter 4.5, could be used to indicate moisture fluxes. There is a clear similarity between the moisture flux density curve, which mathematically corresponds to the derivative of the moisture content, and the surface temperature change due to enthalpy. This surface temperature change, which is based on a comparison of a sorbing with a non-sorbing surface, is achieved in these lab measurements by using vapor-tight aluminum foil, cf. Subchapter 4.6.2. The measurement results show a clear correlation, although the maximum values are significantly lower than in the ideal simulation model, cf. Figure 160 for Norway spruce and Figure 161 for Douglas fir. This proves on a laboratory scale that this new method can be used to detect moisture fluxes on a material´s surface. The relationship between the measured temperature differences and the moisture flux density has not yet shown a clear linear correlation, presumably because the thermal parameters of the material also change with moisture and temperature, cf. Figure 162 and Figure 163. The conversion of measured temperature values into quantitative values of moisture flux density therefore might require further research.

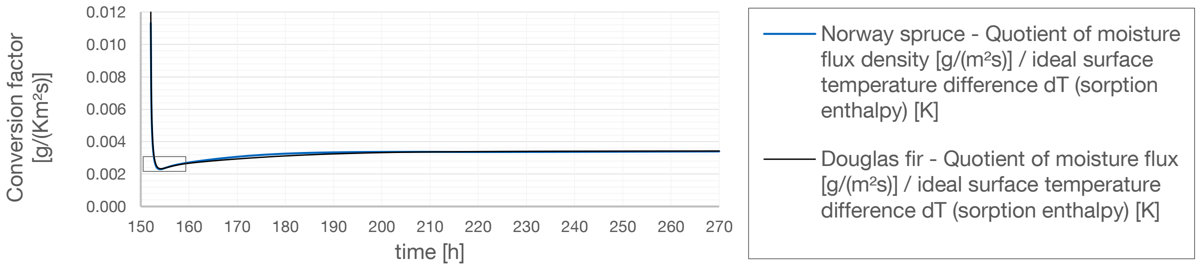

Figure 162: Conversion factor for estimating the moisture flux density from temperature changes at the surface of Norway spruce and Douglas fir. The box on the bottom left is indicating detailed Figure 163.

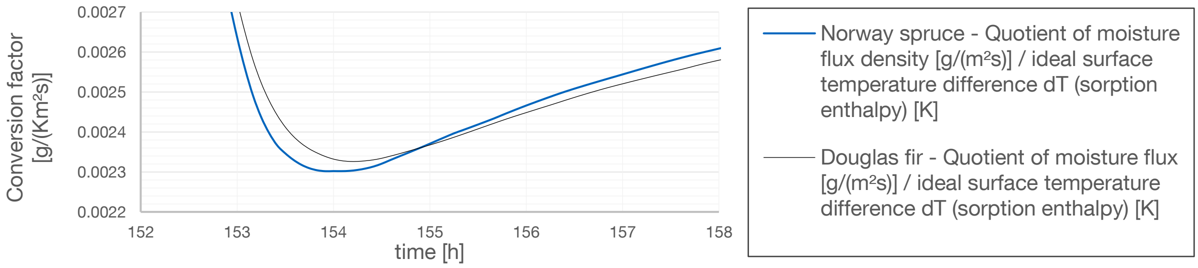

Figure 163: Detail of previous Figure 162 comparing the conversion factor for estimating the moisture flux density from temperature changes at the surface of Norway spruce and Douglas fir.

Regarding just the vague detection of moisture fluxes, this new monitoring method is already being tested in experimental rooms made of CLT. The results of the *PhyTAB* research project show its general applicability in a test cube without any user influence after controlled humidification in (Flexeder, Schumacher et al., 2022). As this publication is written in German, a translated, edited, and adapted version of the respective section can be found in Appendix I, p. 249. Furthermore, the temperature differences method might be employed for qualitative monitoring such as the comparison between materials with different hygroscopic parameters. In this example, Norway spruce has a higher sorption capacity than Douglas fir, which is reflected not only in a greater amplitude of moisture flux density and thus a higher water sorption activity, but also in a greater amplitude of surface temperature difference *dT*. The monitoring results from a test cube prove a measurable difference between the transient sorption capacity of an untreated, glazed and sealed wooden surface (CLT from Norway spruce). The measured differences are further evaluated using an adapted hygrothermal simulation with WUFI Pro. (Flexeder, Nouman & Hepf, 2022)

6 INTERPRETATION OF IN-SITU MONITORING IN CROSS-LAMINATED TIMBER

6.1 Comparing moisture monitoring methods in insulated CLT walls

6.1.1 Effects of rapid humidification under controlled conditions

In order to compare the electrical resistance method (ERM) with new parameters with the new sorption method (SM) under realistic temperature gradients, monitoring equipment corresponding to the sensors and systems used in the laboratory trials was installed in an exterior cross-laminated timber (CLT) wall of a small test room. This way, effects can be evaluated independently, regardless of any user influence. In order to provoke a significant change in wood moisture, the room air was humidified twice at intervals of ten days in September of 2022. This led to a substantial increase in relative humidity each time, cf. Figure 164.

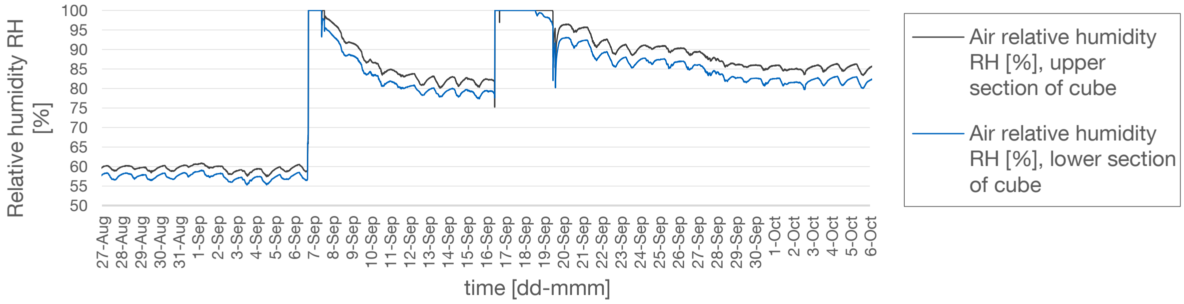

Figure 164: Measured air relative humidity and air temperature in the test cube, close to the CLT surface

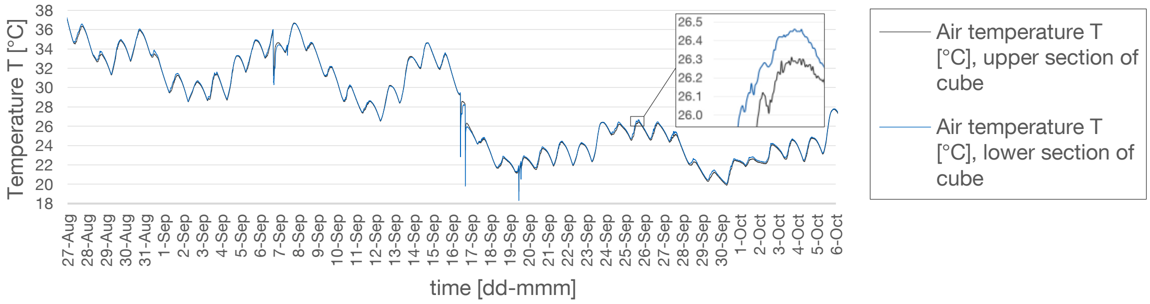

Figure 165: Measured air relative humidity and air temperature in the test cube, close to the CLT surface

Both, air temperature *T* and relative humidity *RH,* show sine-like fluctuations in a daily rhythm, cf. Figure 164 and Figure 165, which is consistent with the observations in previous experiments in the research project *PhyTAB* (Flexeder, Schumacher et al., 2022). Since the sensors for recording the climate in the cube are mounted at different heights, thermal stratification ($T_{upper} > T_{lower}$) would be expected here. However, the temperature readings in Figure 165 show the opposite with a difference of around $\Delta T \approx 0.2$ K/1 m. Although this is only a minor difference, these readings indicating a reversed thermal stratification are surprising - especially since they are not measurement errors but confirmed by four additional sensors (not shown).

Figure 166 schematically depicts a selection of the sensor set-up in the test cube at TUM that is relevant for the further discussion in this subchapter. Relative humidity and temperature of air are being monitored at various locations, for mapping the overall interior climate, but also at several depths in the CLT-part of the façade test element. The results from the RH/T-measurements in the building element are used to derive an equivalent moisture content *EMC* based on the sorption method (SM). Additionally, pairs of electrodes are rammed-in at the same depths to enable a comparison with the electrical resistance method (ERM). The laboratory trials in the previous Subsection 5.4 examined several techniques for both, SM and ERM, cf. also methods in Table 11, p. 99. This subchapter builds on these findings and uses wire-less sensors for SM, equivalent to batch 21_a-d, in two different depths and heights. Furthermore, the RH/T-sensors with special casings for SM, equivalent to batch 22_a-d, are used at a single height but four different depths. For both techniques, the raw data is computed to a value of *EMC* by using equation (4.16) with the new parameters for Norway spruce.

Similarly, the results for *EMC* by the electrical resistance method (ERM) are using the new parameters for equations (4.7)+(4.8). For ERM, stainless-steel electrodes, similar to batch 11_a-d, are rammed-in at a single height and the same four different depths. The electrode pairs are aligned horizontally or vertically, depending on the direction of the CLT-layer (measurement perpendicular to the grain).

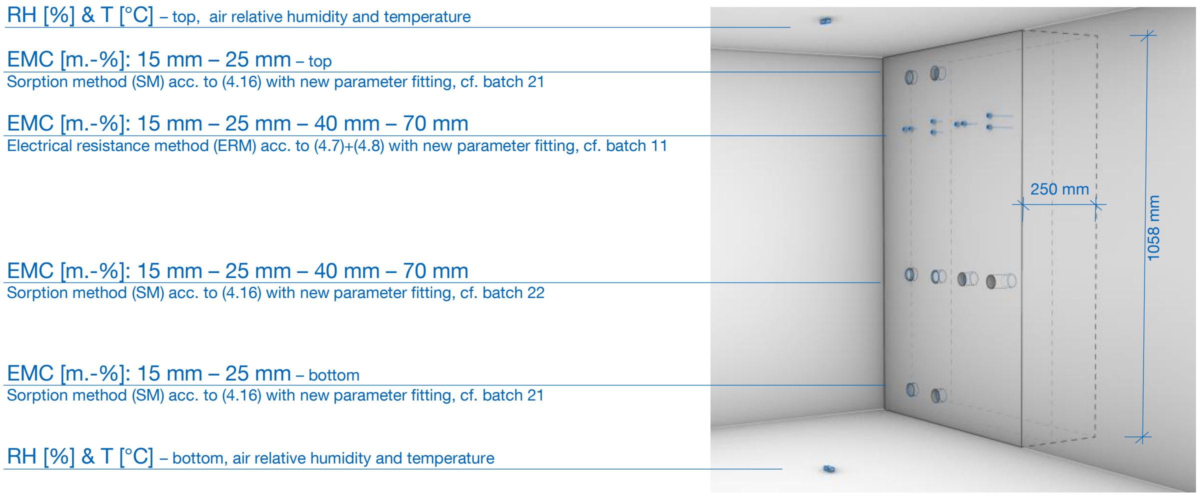

Figure 166: Schematic perspective into the test cube at TUM, showing one of two façade test pieces and a selection of the monitoring equipment.

Figure 167 shows the results from monitoring the wood moisture content using the sorption method (SM) in four different depths (15 mm, 25 mm, 40 mm, 70 mm) in the middle of the CLT wall. The sensor technique and novel method for back-calculation is equivalent to the one used in the trials in Subsection 5.4 on batches 22_a-d in Norway spruce.

The results from this in-situ test under controlled conditions seem plausible with the sensor closest to the inner surface at 15 mm depth detecting a major rise in moisture content while the deeper ones only show a dampened reaction. However, comparing all monitoring results at the 15 mm depth reveals very different results, cf. Figure 168. The values determined using the sorption method show similar trends, albeit with a quantitative difference of over 1 m.-% between the measurements using technique 21 and 22. The two curves using both the technique with the wireless RH/T-sensors, shown in grey and black in Figure 168 and Figure 169, similar to batch 21_a-d, are relatively similar (except for a loss of measurement data) and appear to reflect only minor variances due to the height difference. However, the wood moisture gradient, which is supposedly detected with the electrical resistance method, shows roughly the same tendency, but an unrealistic behavior. Remarkably, the *EMC*-value by ERM rises abruptly as a result of humidification and then appears to fall again within two to three days. The analysis of all *EMC* values determined at a depth of 25 mm yields a similar pattern, cf. Figure 169.

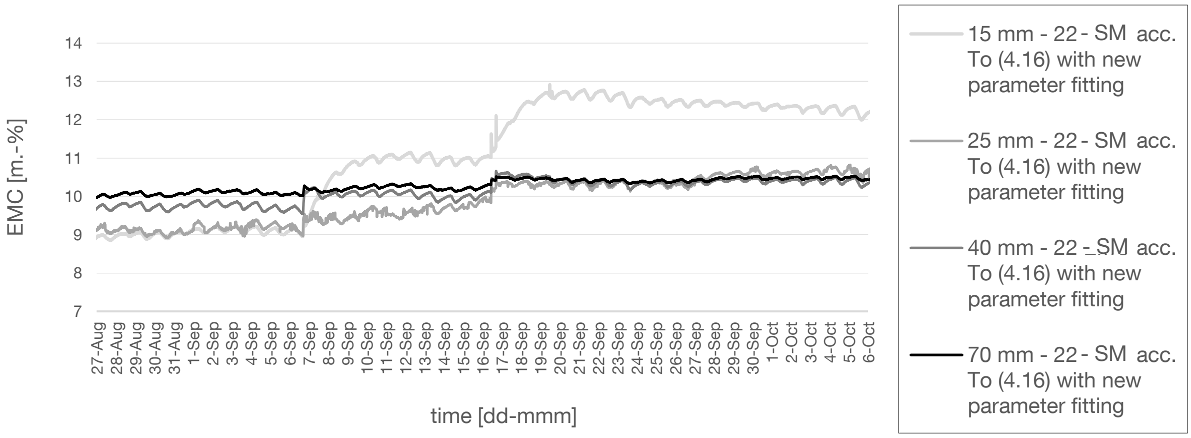

Figure 167: Results from the sorption method (SM) similar to batch series 22_a-d and 23_a-d. The sensors are mounted in four different depths of the exterior CLT wall made from Norway spruce.

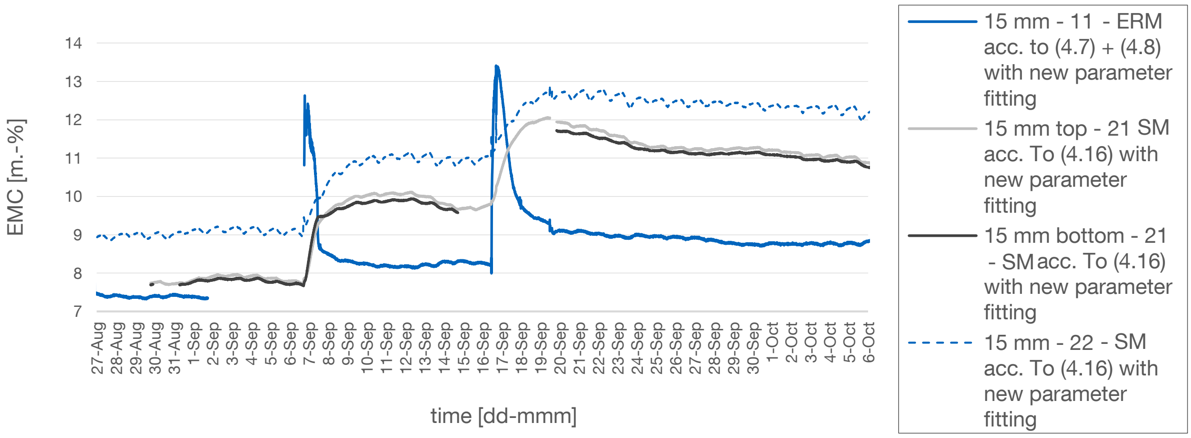

Figure 168: Results from different methods and techniques to monitor the wood moisture content all mounted in the same depth of 15 mm in a CLT wall from Norway spruce.

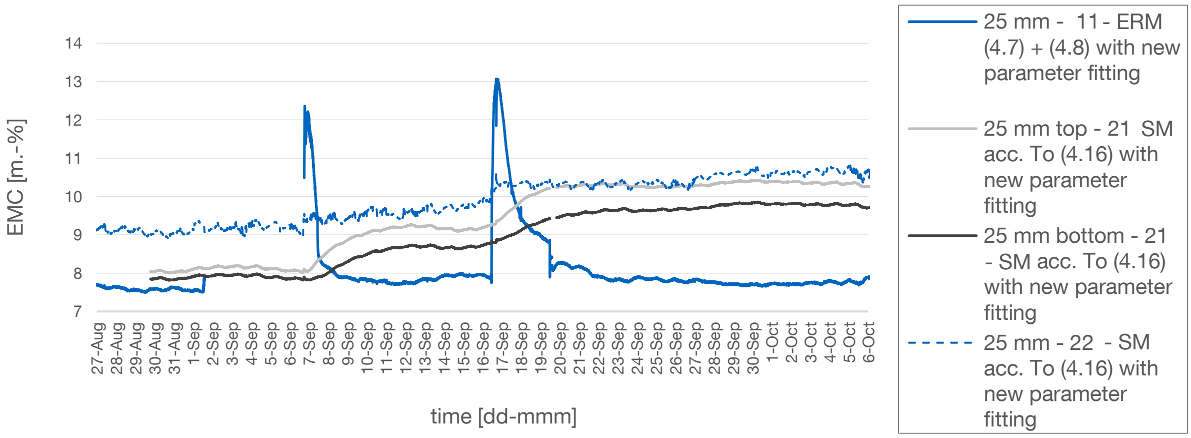

Figure 169: Results from different methods and techniques to monitor the wood moisture content all mounted in the same depth of 25 mm in a CLT wall from Norway spruce.

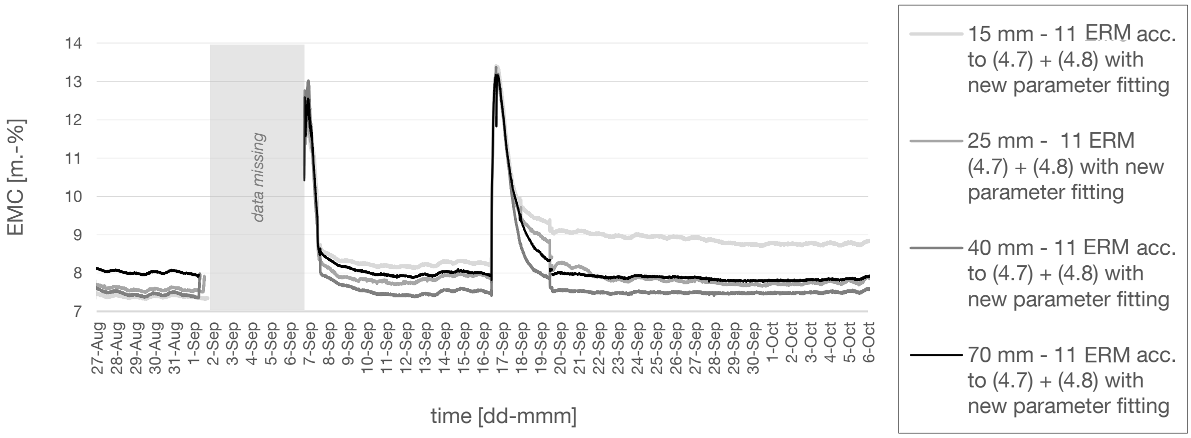

Figure 170: Supposed results from the electrical resistance method (ERM) in a CLT wall from Norway spruce

Figure 170 shows the alleged *EMC* values, which are output according to the electrical resistance method (ERM) similar to that tested in batch 11_a-d. The measurement depths correspond to those of the sorption method (15 mm, 25 mm, 40 mm, 70 mm), cf. Figure 167.

What could be the reason for this sudden spike of the equilibrium moisture content *EMC* determined by the electrical resistance method (ERM)?

Figure 171 depicts the time section around the second peak in indoor air humidity. The values for electrical resistance *R* [Ω] of all four pairs of sensors drop simultaneously and to the same extent to around one hundredth of the original value. It is unlikely that this sudden increase in conductivity is due to an increased water content in the various depths of the cross laminated timber. It is more likely that the very high humidity caused by the mechanical humidification led to a film of moisture and thus to increased conductivity on the surface of the component (short circuit). This also explains the gradual increase in electrical resistance afterwards. Evidently, it took around three days for the increased humidity to subside somewhat and the short circuit to be prevented again.

The experiment proves that monitoring by means of electrical resistance measurements can lead to erroneous results if the humidity in the interior is temporarily very high and thus affecting the measurement set-up. This circumstance must be considered when using ERM under high humidity conditions. A technical solution might need to be further developed.

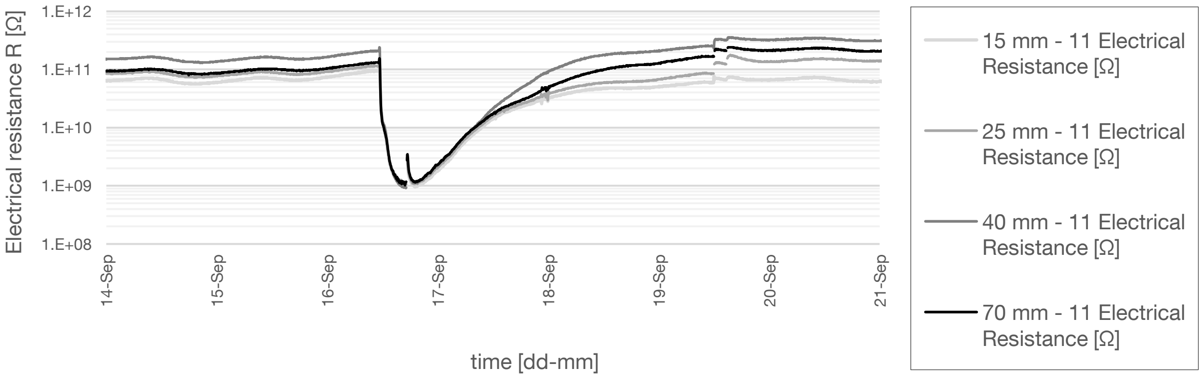

Figure 171: Detail showing the sudden drop in electrical resistance after the second humidification

6.1.2 Juxtaposition of monitoring methods in two independent long-term experiments

As external influences from the user and other technical systems can distort the measurement results, this subchapter discusses long-term measurements in test cubes at two locations in southern Germany. Both experimental buildings are not intended for occupation but used exclusively for scientific investigations. They are accordingly equipped with extensive measurement technology. During the test periods shown, they are neither actively heated nor regularly ventilated; only the window is briefly opened approximately every two to three weeks for access to read out the electronics. Since the test cubes are not actively conditioned, the inner ambient climate conditions are fluctuating with seasonal changes of exterior temperature. Figure 172 is depicting the interior conditions measured in the test cube at TUM.

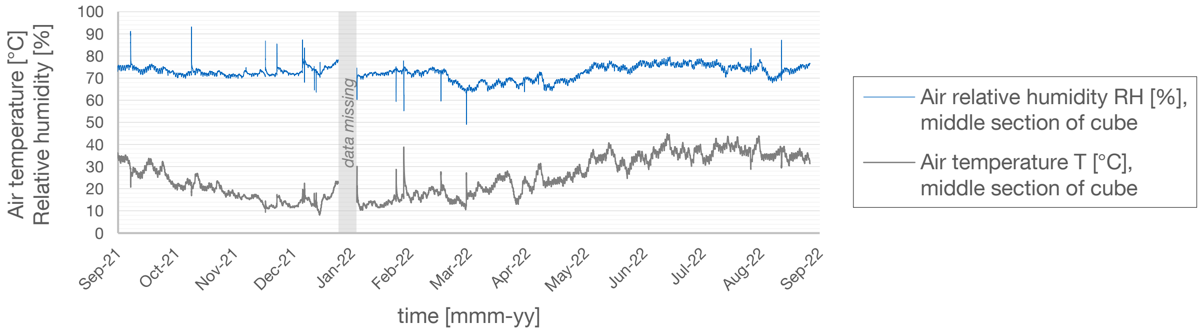

Figure 172: Measured air temperature and relative humidity in the smaller test cube located at TUM with a window facing north/north-east and the investigated CLT wall facing south/south-west

The average air temperature in the test cube during the months of November 2021 – March 2022 was significantly below 20 °C for most of the time rarely even below 10 °C. Individual sudden rises of up to 40 °C were caused by short-term experiments with a radiator. However, this heat dissipated again after a few hours. As the test period progressed, the temperature was rising again due to solar gains and the lack of ventilation losses. It was usually well above 30 °C in the months of June 2022 – September 2022, even reaching peak values of up to 45 °C in some instances.

The investigated wall structure of the two test cubes is identical, cf. Subchapter 4.7.2. They are, however, oriented in different directions: the wall of the smaller test cube at TUM is facing south/south-west; the investigated wall of the larger test cube located in Kösching is facing north-east. Parts of the data obtained in the south/southwest-facing cross-laminated timber wall had already been analyzed in advance using conventional ERM and conventional SM and been published in (Flexeder, Schenk & Aondio, 2022). The values obtained using these conventional methods show larger deviations. For the period September 2021 – May 2022, the curves determined using conventional ERM were in the range of 5 m.-% – 7 m.-%. Using conventional SM with equation (3.4), referenced as the method by (Simpson, 1973), resulted in curves for *EMC*, which were in a range of 8 m.-% – 10 m.-%. More information and additional results from a corresponding laboratory test are presented in the original publication (Flexeder, Schenk & Aondio, 2022).

This Subchapter employs the enhanced methods introduced in this thesis to subject the raw data to further analysis. Applying the improved equation from Subsection 5.3 for the sorption method in Norway spruce results in significantly different *EMC*-values than those previously obtained with the conventional equation (3.4), cf. Figure 173. According to the laboratory tests with batches 22 and 23 in Subsection 5.4, adapting equation (4.16) with new parameters for Norway spruce (see Subchapters 4.4.1 and 5.3) leads to results for *EMC* that are much closer to the actual wood moisture content *MC*. Moreover, the trials in Subchapter 5.4.1 proved that the conventional equation (3.4) with the old parameters according to Loughborough (1931) leads to temperature-dependent deviations, which are especially large at lower temperatures. In Figure 130, p. 142, at a temperature of 5 °C, an estimate using the old equation would lead to an equivalent moisture content that is too low by $\Delta EMC \approx 3$ m.-%. This deviation decreases with increasing temperature and at 40 °C the estimate is only too low by $\Delta EMC \approx 1$ m.-%.

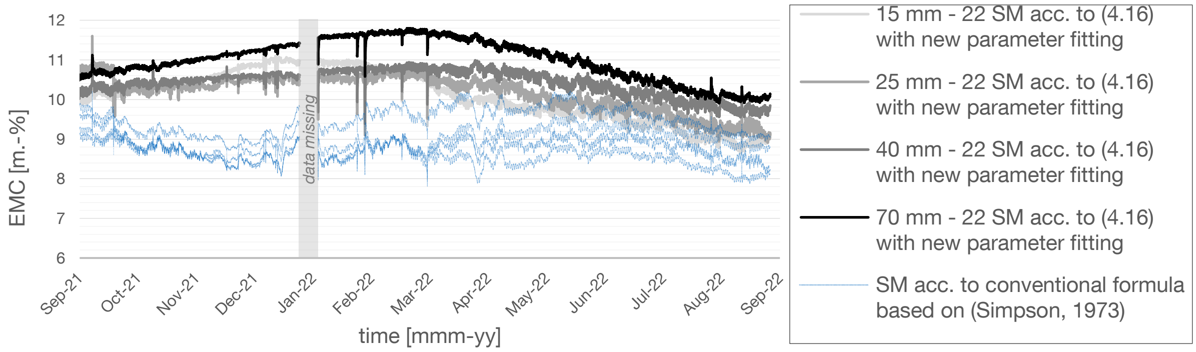

Figure 173: Results for EMC [m.-%] using the sorption method (SM) in four different depths of an insulated cross-laminated timber wall facing south/south-west (test cube at TUM in Munich). The blue graphs indicate the previous results that were obtained using the conventional approach with equation (3.4) discussed by (Simpson, 1973), as already published in (Flexeder, Schenk & Aondio, 2022).

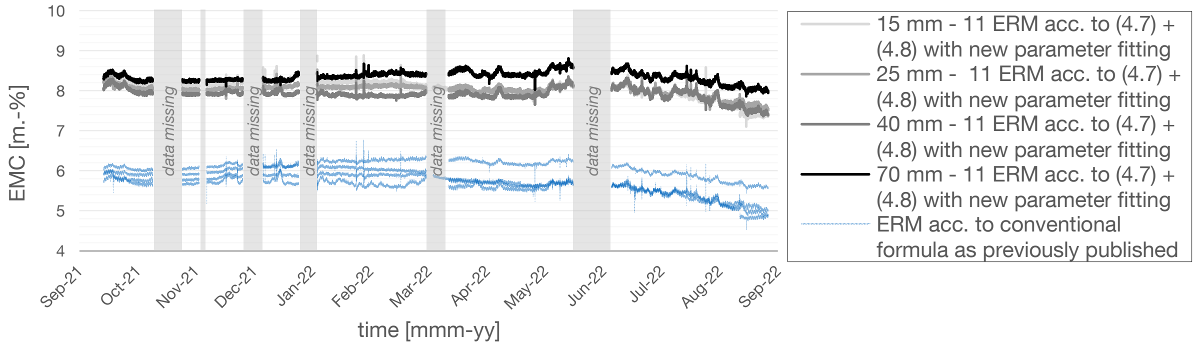

Figure 174: Results for EMC [m.-%] using the electrical resistance method (ERM) in four different depths of an insulated cross-laminated timber wall facing south/south-west (test cube at TUM in Munich). The blue graphs indicate the previous results that were obtained using the conventional approach for ERM, as already published in (Flexeder, Schenk & Aondio, 2022).

Figure 174 shows the values for *EMC* that now result from the temperature and the resistance values measured in the south/southwest-facing exterior wall, according to the new improved ERM. The values fluctuate only slightly in the range of 7 m.-% – 9 m.%, but are significantly higher than those obtained using the conventional method based on the same raw data, shown in blue. Overall, this observation corresponds to the findings presented in Subchapter 5.4.3, Figure 141, p. 150: the refinement of the ERM in Chapter 5 leads to results that are higher than those previously calculated using the conventional ERM. The laboratory tests with batch 11 in the temperature range of 5 °C – 30 °C had shown that the conventional method provides average *EMC*-values that are below the actual *MC*-values by $\Delta \approx 3$ m.-%. At higher temperatures, this deviation increased in Subchapter 5.4.3 significantly, so that at 40 °C a deviation of around Δ ≈ 5 m.-% can be expected. When evaluating the same raw measurement data with the newly calibrated equations (4.7) + (4.8), deviations stayed at a maximum Δ ≈ 1 m.-% in the entire investigated temperature range of 5 °C - 40 °C, cf. Figure 141, p. 150. Strikingly, when comparing Figure 173 with Figure 174, the *EMC*-values obtained using the new methods each still do not match. These deviations between values obtained using the new SM and the new ERM are exceeding the systematic deviations that would be expected based on the steady laboratory tests in Subchapter 5.4.3. These tests showed differences of a maximum Δ ≈ 1 m.-%. However, the in-situ monitoring in this subchapter reveals *EMC*-values that differ by up to a delta of Δ ≈ 3.3 m.-%, depending on the prevailing temperature, cf. Figure 175.

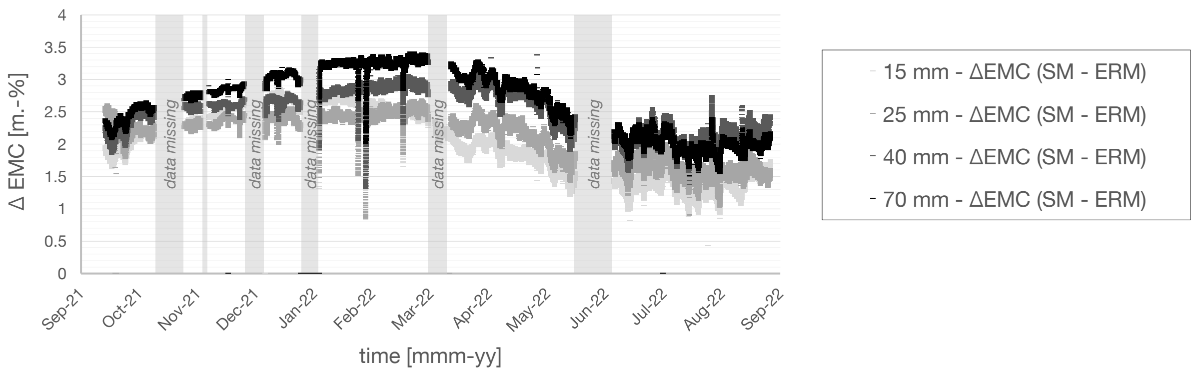

Figure 175: Delta between EMC calculated by the electrical resistance method (ERM) vs. by the sorption method (SM) in close proximity in the same south/southwest-facing exterior CLT-wall. It should be noted that this example might display an indirect proportionality to temperature.

In the months of November 2021 – March 2022, when the average temperature was usually well below 20 °C and sometimes even below 10 °C, the differences between results by SM and ERM are particularly large. Remarkably, the single sudden temperature rises by hourly radiator use in January and February are already sufficient to significantly reduce these differences down to Δ ≈ 1 m.-%. In the months of June 2022 – September 2022, when the average temperature in the cube was mostly well above 30 °C, the *EMC*-values obtained by SM and ERM result in differences of around Δ ≈ 2 m.-%.

The dynamic laboratory experiments in Subchapter 5.4.5 already showed that at low temperatures, the electrical resistance measurement can generate incorrect measurements by up to Δ = 4 m.-%. These laboratory results therefore suggest that the results based on the electrical resistance method are not very accurate, particularly at low ambient temperatures in the test cube. This assessment is all the more important as these systems will still output measurement results, which might appear plausible at first glance.

This subchapter proves that even though both methods, ERM and SM, are calibrated well and also test very similar in steady lab experiments, there could still be larger deviations when utilizing these methods for in-situ monitoring. This phenomenon is suspected to be due to the ERM's susceptibility to systematic faulty measurements at lower temperatures. Figure 175 indicates a relationship between temperature and Δ*EMC* (SM - ERM). If this was a linear correlation, the deviation of ERM in comparison to SM could be mathematically compensated.

Can the monitoring results that were obtained in the test cube at TUM in Munich be reproduced under slightly altered conditions and at a different location?

In a further step, the measurement results from the second experimental CLT-test cube in Kösching are evaluated for verification. These were obtained in an identical exterior wall (cf. Subchapter 4.7.2), but at a different time period, in a different location, and oriented to the north-east. Similarly, the test cube was neither actively heated nor regularly ventilated during the evaluated period. Figure 176 shows the output of the electrical resistance method (ERM) in the north-east wall after evaluation with new calibration curves (4.7) + (4.8). These results from the test cube in Kösching show similarities to those from the first test cube at TUM. The curves, which were determined using the ERM, are relatively horizontal and show hardly any changes over the course of the seasons, cf. Figure 174 and Figure 176. The curves of the alleged wood moisture content at a depth of 25 mm are noticeably offset several times by a difference of around 3 m.-% (marked in blue). This suggests that the electrodes were already relatively loose so that the electrical resistance R_T at the transition between electrode and wood might have increased abruptly in several instances, especially in April and May. Furthermore, the *EMC*-value at a depth of 15 mm shows a noticeably fluctuating behavior.

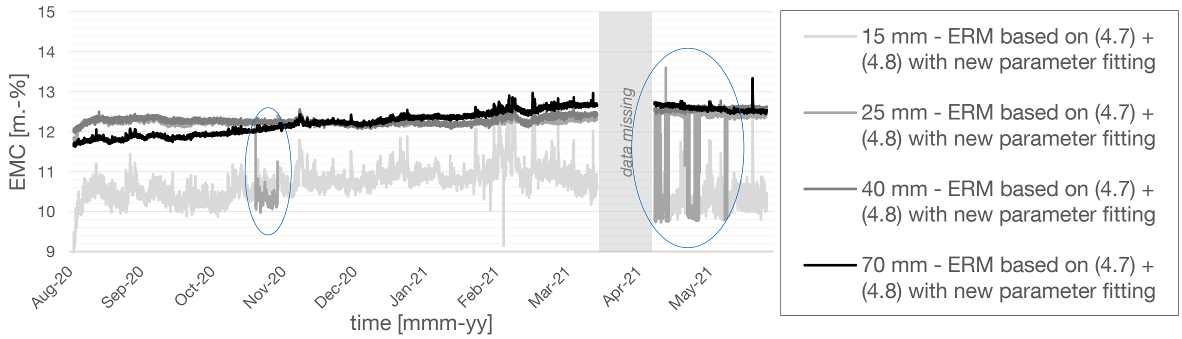

Figure 176: Results for EMC [m.-%] using the electrical resistance method (ERM) in four different depths of an insulated cross-laminated timber wall facing north-east (test cube in Kösching)

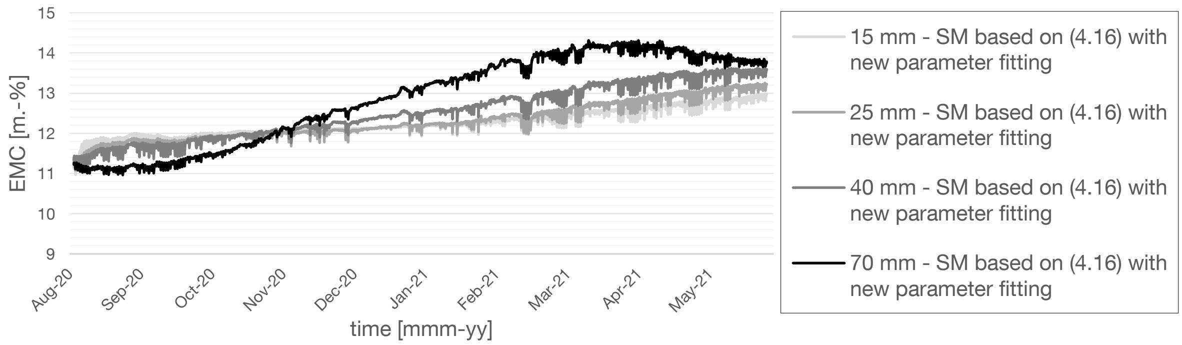

Figure 177: Results for EMC [m.-%] using the sorption method (SM) in four different depths of an insulated cross-laminated timber wall facing north-east (test cube in Kösching)

In contrast, the evaluation of the RH/T-values measured in the immediate vicinity using the sorption method (SM) produces a set of four curves that differs significantly, cf. Figure 177. They show a sine-like progression over the year, whereby the peaks shift with measurement depth. Comparing Figure 173 with Figure 177 reveals various similarities: In the cold months, there is an overall increase in *EMC*. The highest values are estimated at a depth of 70 mm in the months of February/March/April. The *EMC* then gradually decreases at further depths so that the depth closest to the room is usually the one with the lowest *EMC*-value.

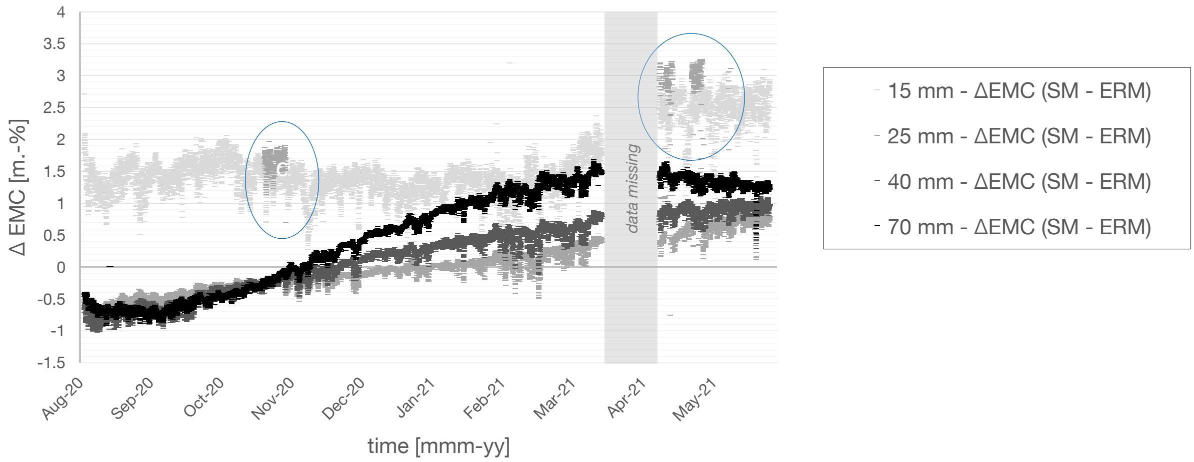

Figure 178: Delta between EMC calculated by the electrical resistance method (ERM) vs. by the sorption method (SM) in close proximity in the same northeast-facing exterior CLT-wall.

Computing the delta between the SM-values and the ERM-values in Figure 178 shows a relationship with larger Δ*EMC* [m.-%] in the springtime, similar to Figure 175. However, the deviations in 15 mm and partly in 25 mm depth observed with ERM also create a greater Δ*EMC* [m.-%], marked in blue. Moreover, the delta values between ERM and SM are significantly lower in Figure 178, than in Figure 175. Figure 179 compilates the results from both test cubes and proves that the observed deviations between SM and ERM do not show a linear correlation to the temperature they were obtained at. This means that the delta between monitoring values obtained using SM or ERM is dependent also on factors other than temperature. Based on temperature only, it cannot be safely predicted.

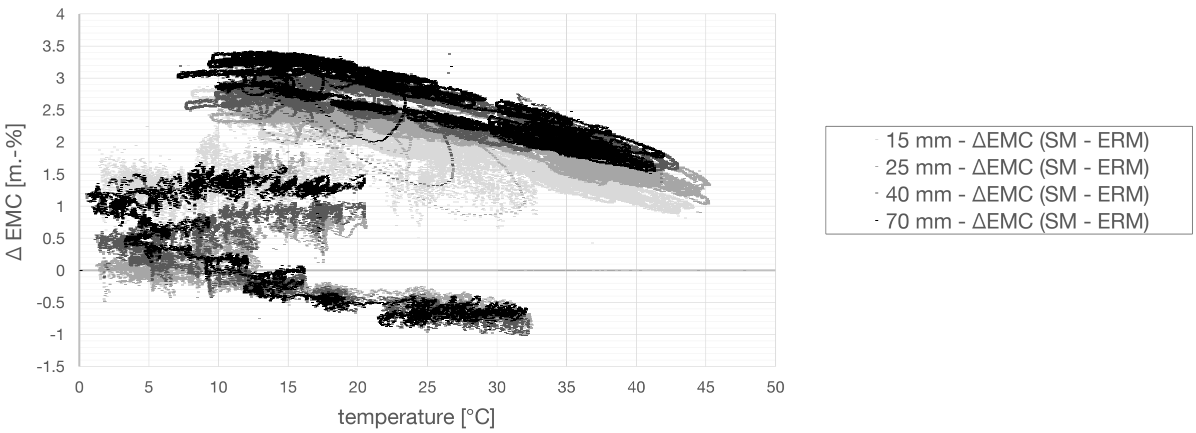

Figure 179: Analysis of Δ EMC [m.-%] between electrical resistance method (ERM) and sorption method (SM), in both test cubes (TUM, Kösching) and in relation to the temperature they were obtained at.

6.2 Monitoring heat flow and moisture content in CLT walls modified with air slots

6.2.1 Different in-situ monitoring techniques in an inhabited experimental building

Analyzing of the measurement data from the exterior mass timber walls in the project *Einfach Bauen* with the novel equations from this thesis reveals new results. These differ significantly from the previously published results in the final project report (L. Franke et al., 2024), which were initially calculated with conventional methods. In the following, the newly calculated results for *EMC* in the north- and west-facing exterior walls of the mass timber building are compared. Both have the same measurement setup, cf. Subchapter 4.7.3 and (L. Franke et al., 2024p. 18 - 20).

The monitoring equipment has been installed in the upper area of two of the exterior CLT walls incorporating air slots inside. The west-facing exterior wall borders the entrance area, a zone with no exceptionally high air humidity production, e.g. no bathroom or kitchen. The north-facing exterior wall is adjacent to the living area. Here, too, there are no sanitary facilities or similar, although the resident occasionally used an iron in the immediate vicinity. Presumably, the electrical resistance measurements are thus not falsified by short circuits on the surface, as observed in the experiment in Subchapter 6.1.1. However, the results produced by the electrical resistance method (ERM) might be significantly distorted by lowered temperatures, cf. findings in Subchapters 5.4.5 and 6.1.2. Consequently, the following Figure 180 - Figure 183 should be analyzed only with great caution. These graphs are merely intended to illustrate what would be output when using the newly improved calibration curves for Norway spruce based on equations (4.7)+(4.8), cf. also Appendix F. They are missing information about possible (but likely) deviations and should not be used for a thorough analysis of the actual hygrothermal behavior of the examined exterior CLT walls. Sections with better readability are given in Appendix J. Additionally, a more reliable analysis including error indicators is discussed in Subchapters 6.2.2 and 6.2.3.

Overall, the measurements in 10-minute-intervalls show wood moisture contents of around 11 m.-% - 16 m.-%. After an initial increase within one month, the values measured by the sorption method (SM, shown in blue) are similar to those determined by the electrical resistance method (ERM, shown in grey). The wood moisture values appear to fluctuate by up to 0.5 m.-% on a daily basis in the inner layers and up to 1 m.-% in the outer layers. However, there are no large unrealistic deviations as for instance shown in Subchapter 2.4.2. This means that the results obtained with the new methods are much more reliable than those previously obtained with conventional methods. The following two pages illustrate these fluctuations with each value computed individually and thus without curve smoothing. Three different measurement techniques are used in the exterior walls of the solid timber house, each of which are being investigated in earlier Chapters. For the measurement points close to the interior (at depths of 15, 25, 40, and 70 mm), ERM was used with rammed-in electrodes, similar to those used in the batch 11 test series. For the measuring points further away from the interior (120, 150, 175, 225 mm), the ERM with screwed-in electrodes was used, cf. batch 12. Alternatively, at the depth of 100 mm, one sensor each for the sorption method (SM) was installed once in solid wood and once in a cross-laminated timber element with small air gaps, following the principle of the test series batch 22/23.

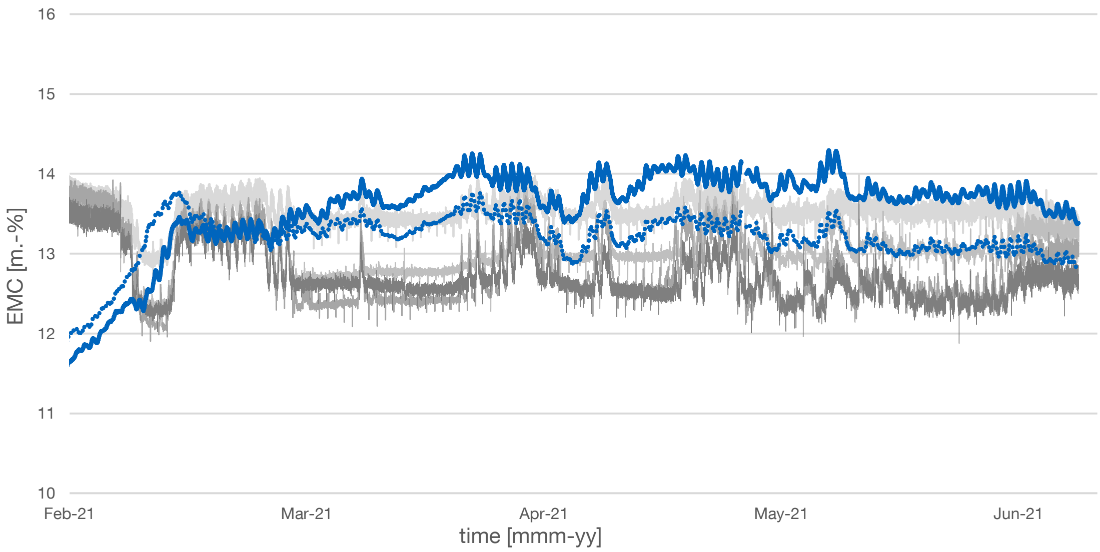

Figure 180: Results with rammed-in electrodes (cf. batch 11) using the electrical resistance method (ERM) with newly improved equations (4.7) and (4.8) and the sorption method (SM, cf. batch 22/23) with equation (4.16), both with new parameter fitting. The graphs show the measurements taken closer to the inside in the west-facing exterior wall of the project Einfach Bauen, February to June of 2021.

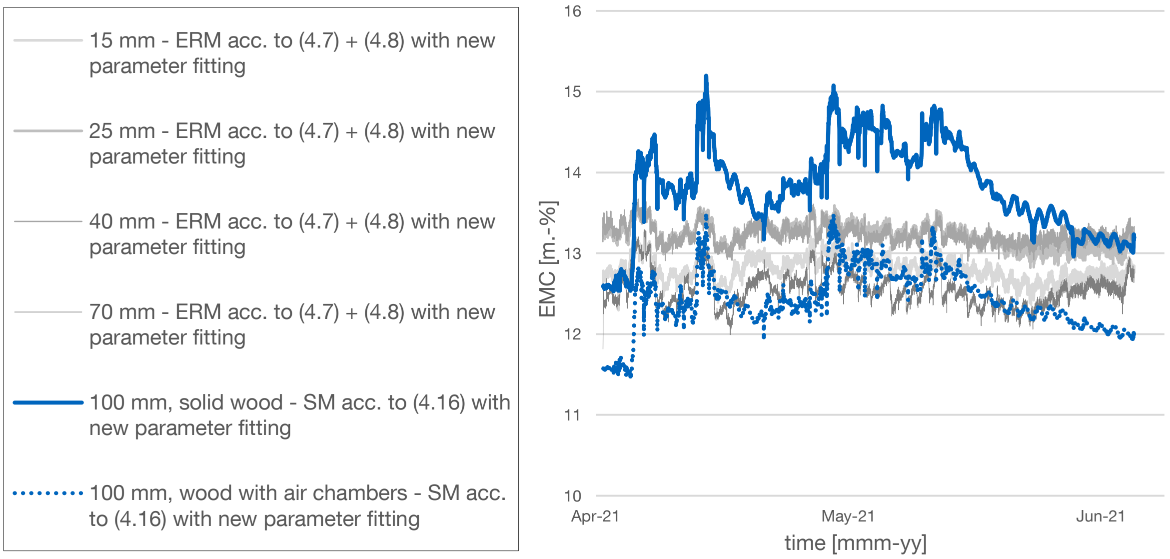

Figure 181: Results with rammed-in electrodes (cf. batch 11) using the electrical resistance method (ERM) with newly improved equations (4.7) and (4.8) and the sorption method (SM, cf. batch 22/23) with equation (4.16), both with new parameter fitting. The graphs show the measurements taken closer to the inside in the north-facing exterior wall of the project Einfach Bauen, April to June of 2021.

For better readability, the newly evaluated results are shown below separately for the inner and outer measuring points. Figure 180 illustrates the results measured in the west-facing exterior wall over a five-month period in 2021. During this time, *EMC* values between approximately 12 m.-% and 14 m.-% are output. Data for the north-facing exterior wall is not available until April 2021, but the results are similar, cf. Figure 181. The *EMC* computed just below the surface on the room side in both walls are a relatively constant at around 12.5 m.-% to 13.5 m.-% over the entire period. The equivalent wood moisture values in the layers behind show a similar pattern with similar fluctuations.

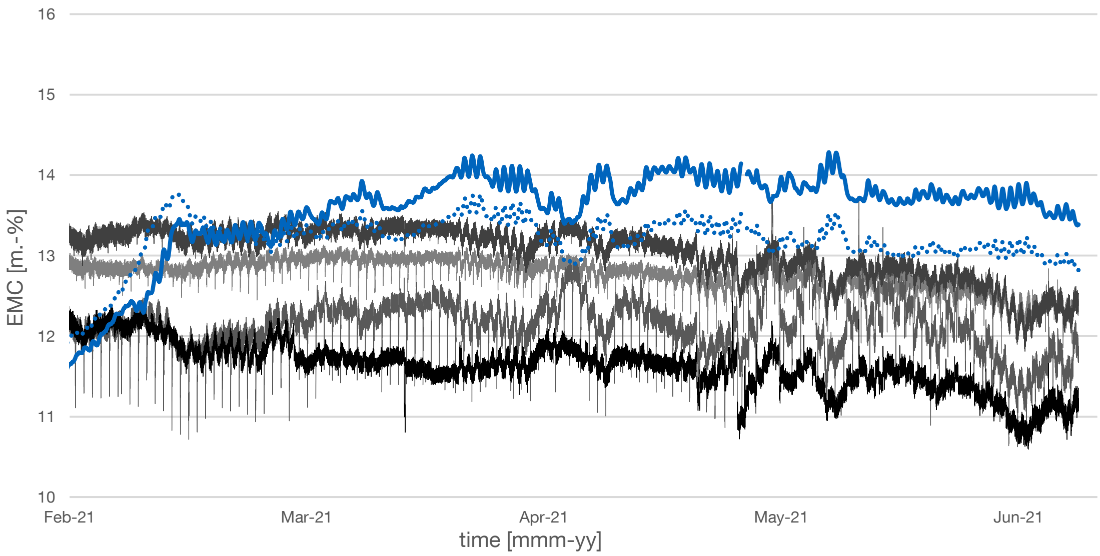

Figure 182: Results with screwed-in electrodes (cf. batch 12) using the electrical resistance method (ERM) with newly improved equations (4.7) and (4.8) and the sorption method (SM, cf. batch 22/23) with equation (4.16), both with new parameter fitting. The graphs show the measurements taken closer to the inside in the west-facing exterior wall of the project Einfach Bauen, February to June of 2021.

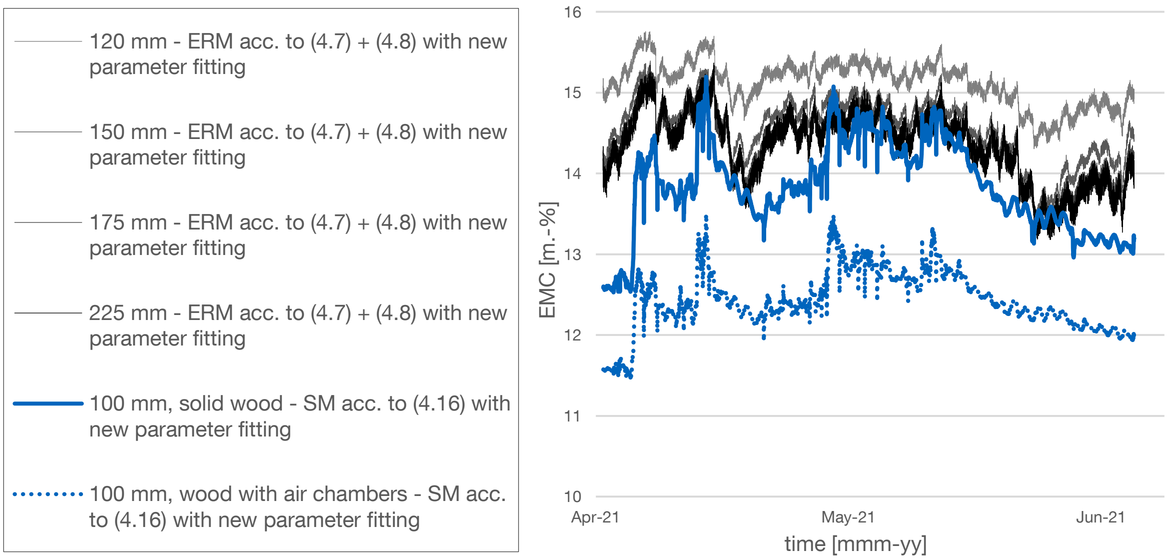

Figure 183: Results with screwed-in electrodes (cf. batch 12) using the electrical resistance method (ERM) with newly improved equations (4.7) and (4.8) and the sorption method (SM, cf. batch 22/23) with equation (4.16), both with new parameter fitting. The graphs show the measurements taken closer to the outside in the north-facing exterior wall of the project Einfach Bauen, April to June of 2021.

The *EMC* determined in the outer layers shows greater amplitudes but also decreases by about one percentage point over the five months observed, cf. Figure 182. The fluctuations in the outer layers of the north-facing exterior wall show the greatest moisture contents overall but also fluctuations during the observation period, cf. Figure 183. The graphs prove that thanks to the improved equations, the daily distortions are not as significant anymore. Hence, the method of simple moving average (SMA) may be used in the further detailed discussion of individual results in Subchapters 6.2.2 and 6.2.3 without altering the results too much.

6.2.2 Comparing the influence of temperature at a similar equivalent moisture distribution

The in-situ monitoring concept in the project *Einfach Bauen* uses a variety of sensors, including several temperature sensors and heat flux plates (L. Franke et al., 2024; Jarmer et al., 2021). The wood moisture monitoring results presented in Subchapter 6.2.1 are related to the transient heat flux density q [W/m²] measured in parallel. Those can be used to compute a transient thermal conductivity $\lambda'_{in\text{-}situ,\,j}$ [W/(m·K)] at any specific time step j (short: λ'), cf. Subchapter 4.7.1. Analyzing the monitoring data from both, the equivalent moisture content and the thermal conductivity measurements was intended to enable conclusions about the transient hygrothermal behavior of the novel CLT wall with air slots. Can the in-situ monitoring data confirm the basic correlations of wood moisture content and thermal conductivity as described in Subchapter 3.1.1?

Figure 184 shows the temperature curves measured in the west-facing exterior wall during February to June 2021. The thermal conductivity calculated from the measured heat flux density and the temperature and position difference generally fluctuates greatly, cf. Figure 185.

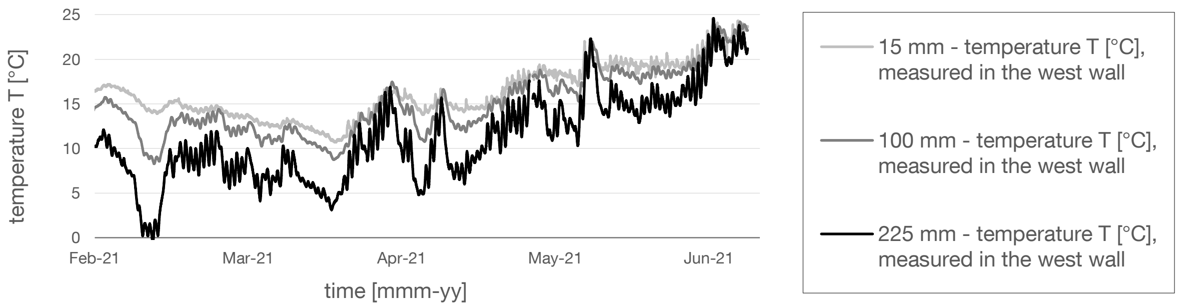

Figure 184: Temperatures measured in February to June 2021 in the west-facing wall of the project Einfach Bauen

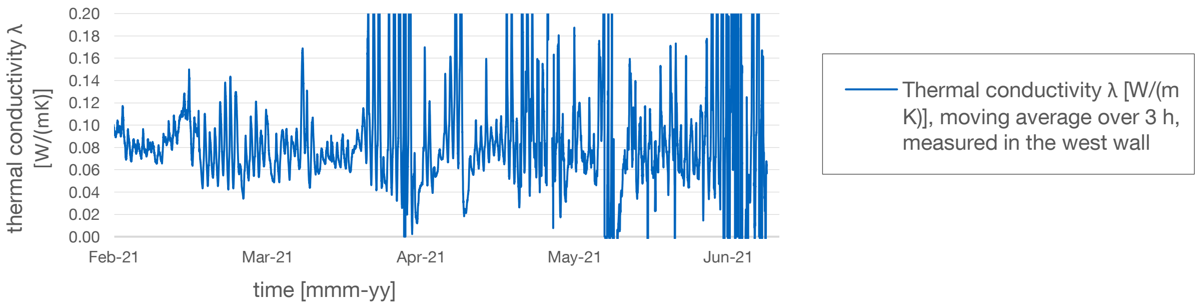

Figure 185: Thermal conductivity computed from the heat flux density measured during February to June 2021 inside the west-facing wall of the project Einfach Bauen

It should be noted that by the method explained in (Flexeder et al., 2021), the measurement data generated in the project *Einfach Bauen* are not sufficient to calculate back to one statistically reliable value for thermal conductivity $\lambda_{in\text{-}situ}$ [W/(m·K)] (L. Franke et al., 2024).

The transient values for thermal conductivity $\lambda'_{in\text{-}situ,\,j}$ [W/(m·K)] shown here are derived from single measured values of heat flux density and therefore rather represent momentary snapshots than uniform values. The greater the temperature gradient, the more reliable the measured heat flow and the more accurate (and uniform!) the determined thermal conductivity.

The following analysis will highlight the influence of the temperature level compared to the influence of the wood moisture distribution on the respective instantaneous thermal conductivity. For this purpose, smaller time sections are specifically selected for discussion. Since the graphs prove in Subchapter 6.2.1 that the distortion of the measurement results is not as significant, the method of simple moving average (SMA) is used. Analyses like in Figure 184 and Figure 185, but that zoom into the respective days of discussion, are given in Appendix J, p. 251.

In order to illustrate the measured curves in the cross section of the outer wall, two points in time in April and May 2021, 31 days apart, are selected and shown in Figure 186. These two data sets indicate a similar moisture content distribution by *EMC* and might illustrate the importance of the prevailing temperature. Even though the monitored wood moisture contents of these two instances show such great similarities, the average temperature level is around 7 K higher in the data from May. Furthermore, the measured thermal conductivity in the example from May at this specific point in time at $\lambda' = 0.11$ W/(m·K) is also significantly higher than in the one from April with $\lambda' = 0.08$ W/(m·K). This example illustrates the dependence of the thermal conductivity on the prevailing temperature level as well as the uncertainties.

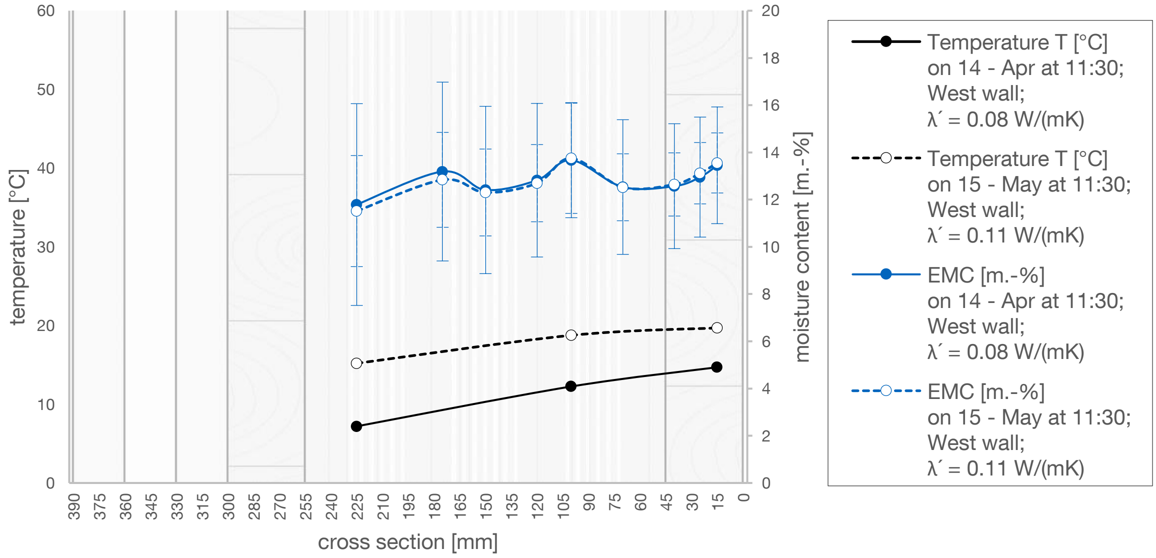

Figure 186: Systematic comparison of two temperature distributions measured 31 days apart in the west wall with very similar equivalent moisture content distribution, but different values for transient thermal conductivity $\lambda'_{\text{in-situ, j}}$ [W/(m·K)] at those two specific points in time

The accuracy of the temperature measurements is listed with ±0.2 K by the manufacturer. The accuracy of the results from moisture monitoring depends on the method used and the prevailing temperature. Based on the findings from this thesis, the potential errors are calculated individually and shown for each point of *EMC*. It should be noted how the value at a depth of 100 mm, determined by the sorption method (SM) in solid wood, demonstrates slightly different error indicators than the other points, which are determined by the electrical resistance method (ERM). Subchapter 4.7.3 presents an overview of the moisture sensors used. The findings about the accuracy of SM and ERM are summarized in Subsection 7.1.

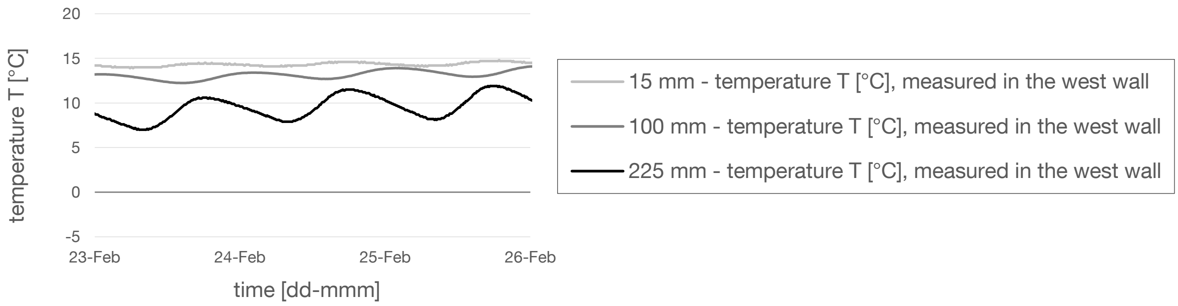

Figure 187: Temperatures measured in February of 2021 in the west-facing wall of the project Einfach Bauen

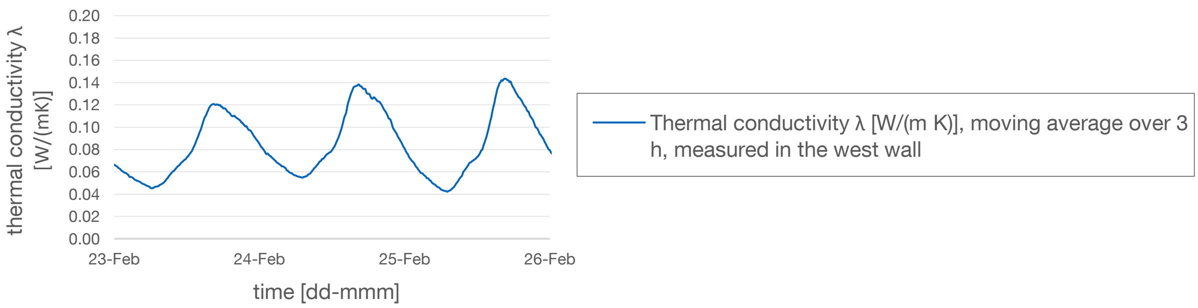

Figure 188: Thermal conductivity computed from the heat flux density measured inside the west-facing wall

The heat flux density measured at a given time can change within a few hours, causing the resulting thermal conductivity to multiply. Accordingly, the computed thermal conductivity is fluctuating a lot with a decreasing temperature gradient, cf. Figure 187 and Figure 188. The illustration in Figure 189 shows two snapshots taken only ten hours apart on February 25th 2021, but where the transient thermal conductivity has increased from $\lambda' = 0.05$ W/(m·K) to $\lambda' = 0.13$ W/(m·K). These changes appear to be regular day/night variations and prove the necessity for a statistically valid evaluation when computing a fixed value for thermal conductivity $\lambda_{in\text{-}situ}$ [W/(m·K)] as in (Flexeder et al., 2021).

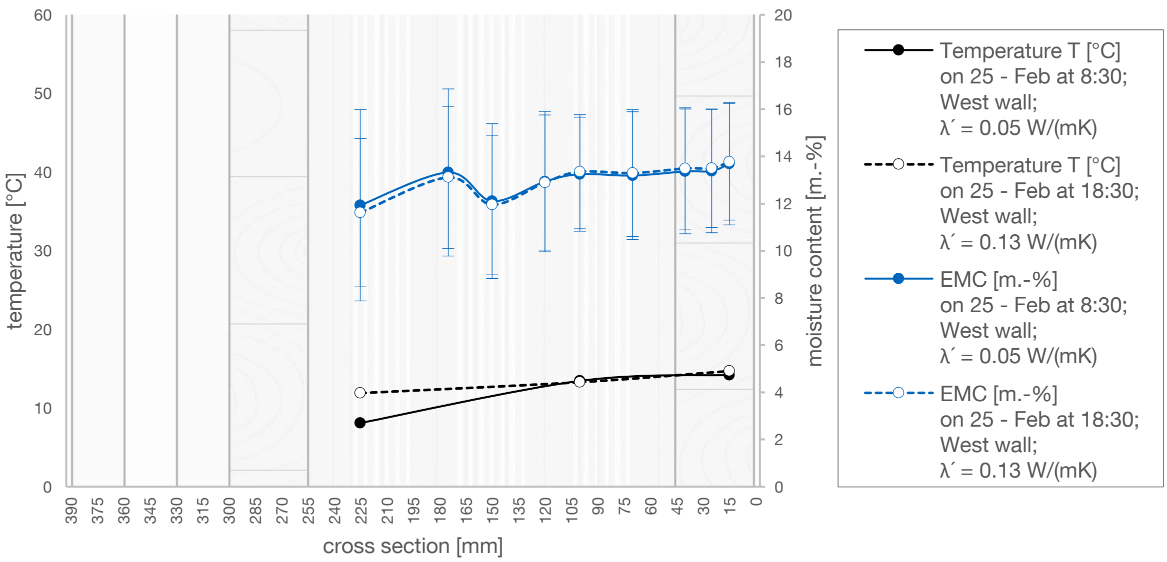

Figure 189: Systematic comparison of two temperature distributions measured only ten hours apart in the west wall with very similar equivalent moisture content distribution, but with different values for transient thermal conductivity $\lambda'_{in\text{-}situ,\,j}$ [W/(m·K)] at those two specific points in time

6.2.3 Comparing the influence of moisture content at a similar temperature distribution

The following examples are specifically picked to illustrate the results when the temperature distribution happened to be approximately the same, but the equivalent moisture content *EMC* [m.-%] seems different. The distributions shown in Figure 190 were measured in the west wall on a day in February and April 2021. Appendix J is presenting the corresponding curves as 36-hour-long sections.

If disregarding the range of accuracy, the moisture distribution between these two data sets would show distinct differences. Although the *EMC* [m.-%] in April would seem to be higher in the deeper layers than in February, it would be read slightly drier in the layer closer to the room. However, the relatively large accuracy ranges indicate that these observed differences might just be measurement errors. Consequently, even though they might seem like a valid finding, they might also just not be relevant at all. This is important to point out, as suspected findings like these might occur quite frequently and would then lead to false conclusions. Furthermore, it should be noted that the selected plot only connects individual measurement points with a line. This creates interpolated values that could be misleading. There might be even greater differences in wood moisture or temperature throughout the component, but they would have just not been detected in this project.

Overall, the transient thermal conductivity computed in the west wall at these two points in time is significantly lower in the April constellation ($\lambda' = 0.08$ W/(m·K)), than in the February constellation ($\lambda' = 0.11$ W/(m·K)). However, based on the present measurement data, it is not possible to prove a reason for this. A similar comparison in the north wall demonstrates the same phenomenon, cf. Figure 191. Here too, measurements conclude to slight differences in the *EMC*, especially at a depth of 100 mm. Yet, these are still within their ranges of accuracy and thus not reliable.

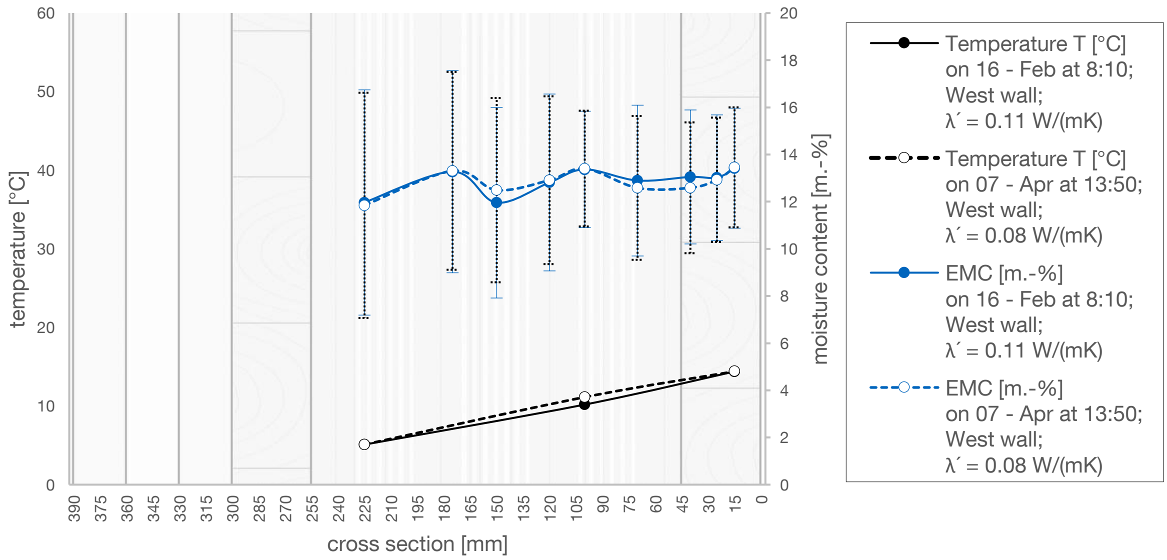

Figure 190: Systematic juxtaposition of two wood moisture distributions measured 50 days apart in the west wall with similar temperature readings, but different values for transient thermal conductivity $\lambda'_{\text{in-situ, j}}$ [W/(m·K)] at those two specific points in time

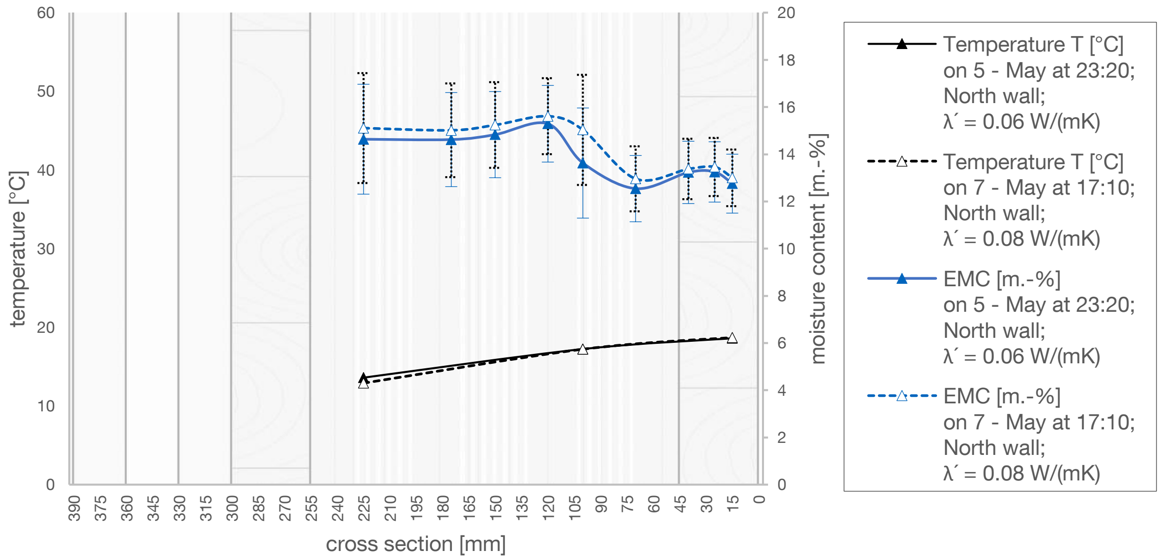

Figure 191: Systematic juxtaposition of two wood moisture distributions measured two days apart in the north wall with similar temperature readings, but different values for transient thermal conductivity $\lambda'_{\text{in-situ, j}}$ [W/(m·K)] at those two specific points in time

Comparing the simultaneous readings from the west and north wall at the same time in Figure 192 reveals a very similar temperature distribution and identical values for transient thermal conductivity of $\lambda' = 0.12$ W/(m·K). This raises the question of whether the actual wood moisture content in the west-facing and north-facing exterior walls differed at all. Based on the errors indicated, the differently appearing curves could also simply be due to systematic measurement deviations. This could mean that apparent differences, such as these in Figure 192, but also those appearing on pages 171 and 172, might not actually exist.

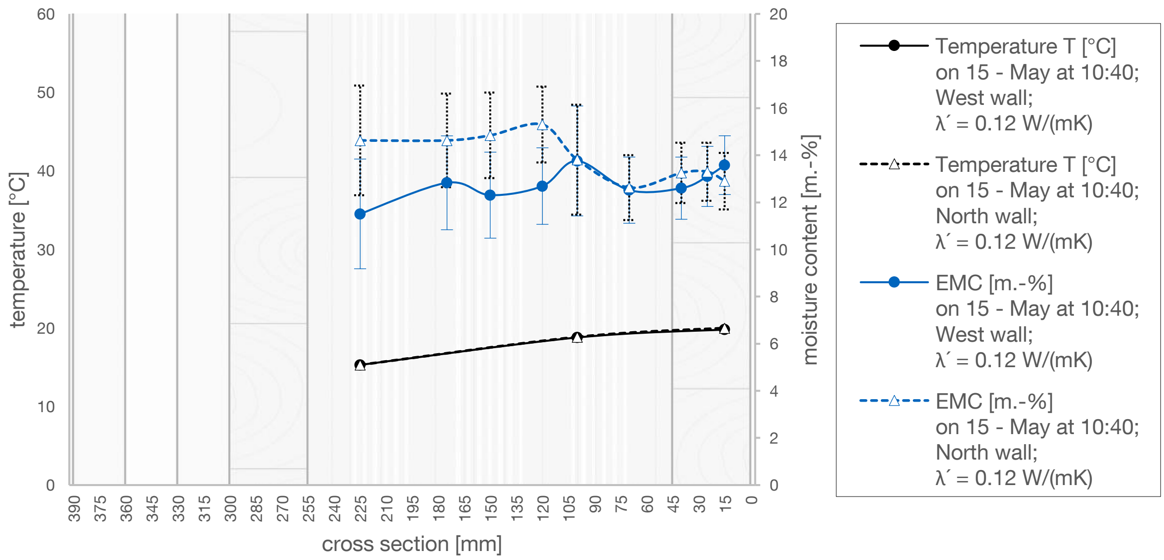

Figure 192: Comparison of the very similar temperature measurements in the west and the north wall at the same time but EMC distributions that seem to be very different, but at the same time the values for transient thermal conductivity $\lambda'_{\text{in-situ, j}}$ [W/(m·K)] at these two sites seem equal.

6.3 Analyzing the hygrothermal behavior of uninsulated CLT walls in-situ

6.3.1 Improving previous monitoring results by the novel electrical resistance method

The new calibration curves for Norway spruce developed as part of this thesis are used below to generate new, more accurate measurement results for the *Timberbrain* project. The exterior walls of this office building consist of a nine-layer cross-laminated timber construction without any additional layers, cf. Subchapter 4.7.4.

As the introduction in Subchapter 2.4.3, p. 37, already indicated, using conventional methods to analyze the moisture distribution did not produce satisfactory results. For instance, the readings for *EMC* in Figure 193 (= Figure 8, p. 37), which are acquired by the conventional resistance method in the west wall, seem to flutter unrealistically. This scattering is presumably due to an initially inadequate scope of the temperature compensation. According to the temperature measurements, temperatures in the range of -5 °C – 65 °C occurred in the investigated west wall, cf. Figure 194.

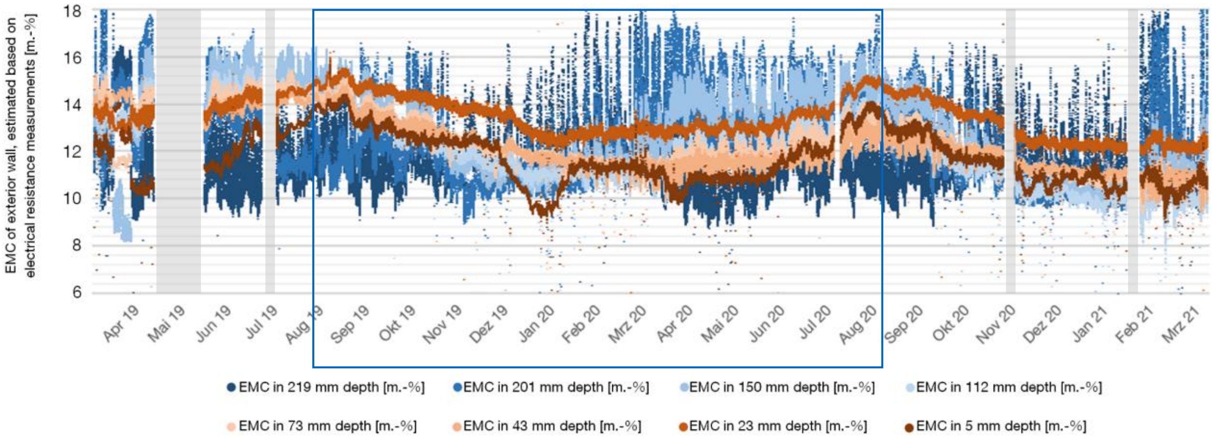

Figure 193: Results from a west-facing exterior CLT wall (Timberbrain project), analyzed with conventional ERM, as in (Bodemer et al., 2021). The blue box indicates the section that is re-evaluated and shown in Figure 195. The grey areas indicate missing data.

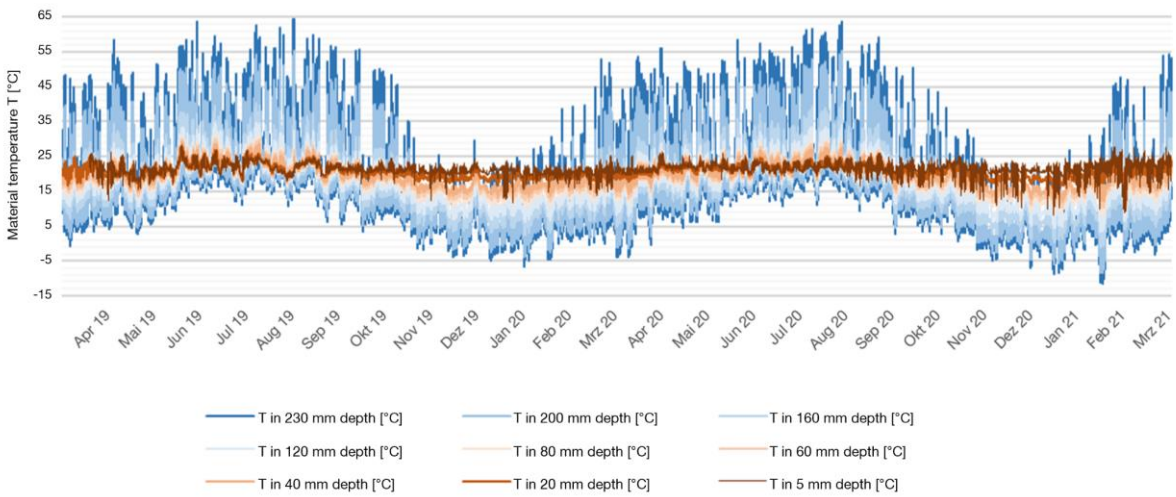

Figure 194: Material temperatures measured in the west-facing exterior CLT wall, as in (Bodemer et al., 2021).

The novel parameters for the equations (4.7) + (4.8) have been newly developed for Norway spruce (*Picea abies Karst.*) in a range of 5 °C – 60 °C | 7 m.-% - 16 m.-% in the context of this thesis. They are illustrated in Appendix F.

Figure 195 shows the results after applying these equations with new parameters to the same original raw data (electrical resistance *R*, temperature *T*). Comparing Figure 193 with Figure 195 demonstrates how these new equations improve the electrical resistance method (ERM). The resulting data are not further adjusted; there is no moving average or similar applied. Thus, Figure 195 depicts the primary results in the 5-minute measurement rhythm without any further post-processing or additional curve-smoothing measures. The curves show a much clearer shape, and by using the newly developed equations, the dubious fluctuations have been largely eliminated. This reaffirms the finding that the newly developed curves for ERM are considerably more suitable and should be preferred over the initially used conventional equation for ERM. Despite the outermost layer being from larch, the data at point 219 mm is also evaluated using the parameters for Norway spruce.

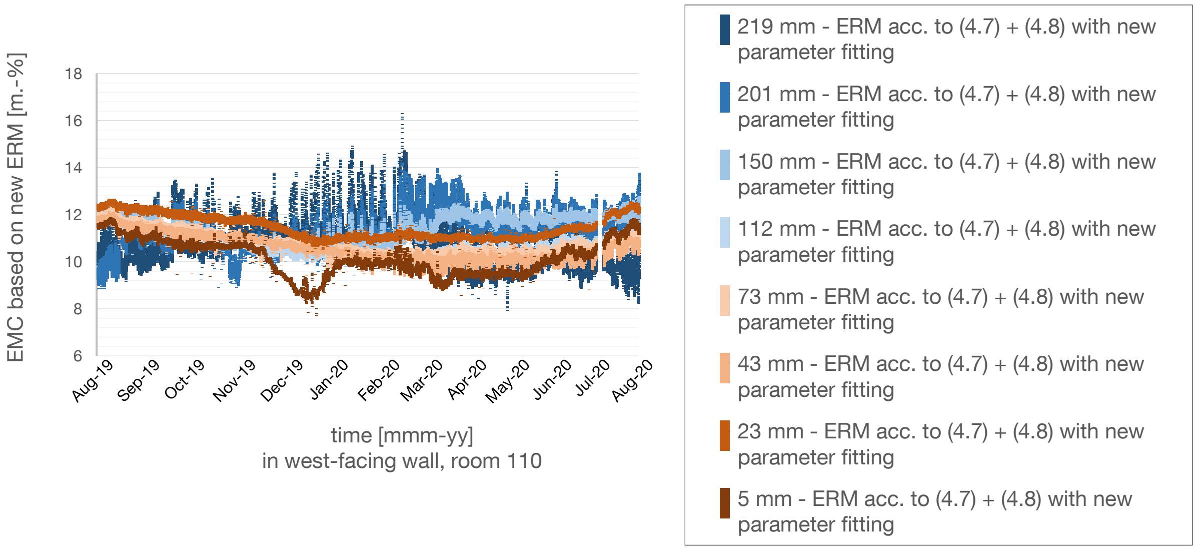

Figure 195: Results from a west-facing exterior CLT wall (Timberbrain project), analyzed with the novel ERM developed in this thesis, equations (4.7)+(4.8) for Norway spruce, measurement direction perpendicular to the gain.

The results presented in Figure 195 and Figure 198 and could therefore be considered a revision of what was originally presented in (Flexeder, 2021). These new results from the west-facing façade are confirmed by the evaluation of the raw data from the north-facing façade. As this side is not heated as extensively by solar radiation as the west, the temperature gradients are less pronounced here, cf. Figure 197. Accordingly, the original results using conventional ERM do not fluctuate quite as much, cf. Figure 196. However, the application of the new calibration curves also brings a significant improvement in the final results here, cf. Figure 198.

Comparing Figure 193 (= Figure 8, p. 37) with Figure 195, and Figure 196 with Figure 198, demonstrates how the overall values using the novel equations (4.7)+(4.8) for *EMC* [m.-%] are differing in the analysis from what would be the average using the conventional ERM.

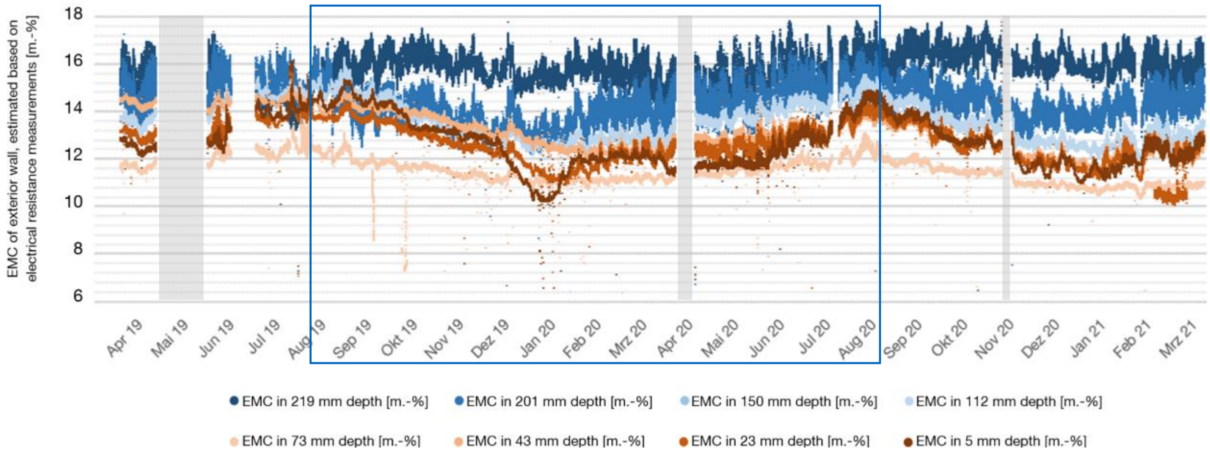

Figure 196: Results from a north-facing exterior CLT wall (Timberbrain project), analyzed with conventional ERM, as in (Bodemer et al., 2021). The blue box indicates the section that is re-evaluated and shown in Figure 198. The grey areas indicate missing data.

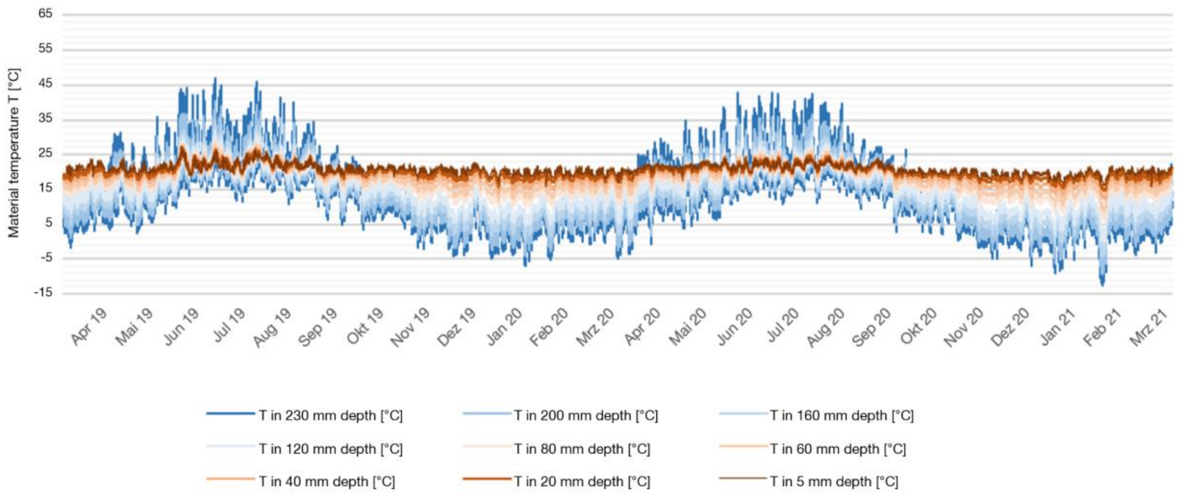

Figure 197: Material temperatures measured in the north-facing exterior CLT wall, as in (Bodemer et al., 2021).

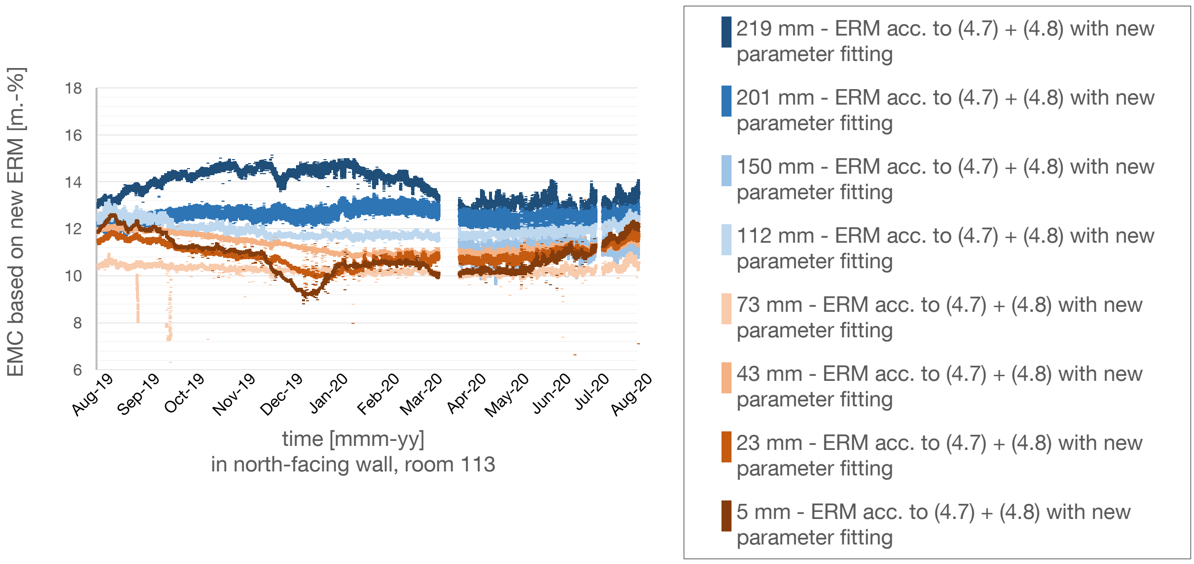

Figure 198: Results from a north-facing exterior CLT wall (Timberbrain project), analyzed with the novel ERM developed in this thesis, equations (4.7)+(4.8) for Norway spruce, measurement direction perpendicular to the gain.

6.3.2 Spot-lighting the influence of temperature gradients on thermal conductivity

The results from the project *Timberbrain* are illustrated in similar way to the previous Subchapters 6.2.2 and 6.2.3. Deviating from the previous investigations on the walls of *Einfach Bauen*, the walls of the *Timberbrain* are exposed directly to both ambient climates, interior and exterior. Consequently, monitoring the temperature gradient shows a large spread.

Figure 201 illustrates how the temperature in the outer layers of the CLT wall is lower in the winter and even higher than inside in the summer. Consequently, the resulting value for the transient thermal conductivity at the time step of August 20th at 18:30, λ' = - 0.04 W/(m·K), is negative. This is caused by a retroverted heat flux when the outside is warmer than the inside.

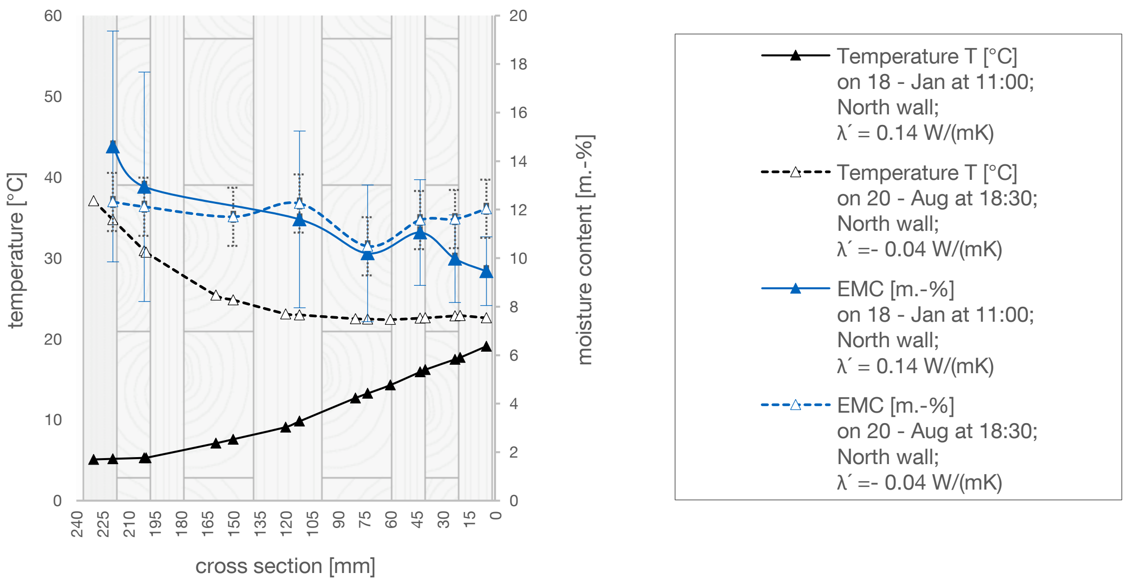

Figure 199: Systematic juxtaposition of two wood moisture distributions determined seven months apart in the north wall with temperature readings and values for transient thermal conductivity $\lambda'_{\text{in-situ, j}}$ [W/(m·K)] that seem very different at those two specific points in time

Remarkably, the values for equivalent moisture content (*EMC*) are significantly lower in the inner layers of the CLT in the winter than in the summer. This is in-line with the hypothesis by (Joščák et al., 2011), who claim that, especially in winter, the wood moisture content of a timber wall would often decrease. They conclude that this phenomenon would then lead to a lower thermal conductivity of the wood in winter, cf. Subchapter 2.4.4. In order to test their hypothesis with applicability for the entire wall section, it would be necessary to obtain monitoring data for *EMC* that are more accurate than the current data. Since the results by the electrical resistance method are less accurate with lower temperatures, it cannot be stated whether there are major differences in *EMC* [m.-%] in the outer layers as well. It is important to note that $\lambda'_{in\text{-}situ,\,j}$ [W/(m·K)] (short: λ'[W/(m·K)]), which illustrates the computed transient thermal conductivity at the time step, is different from $\lambda_{in\text{-}situ}$ [W/(m·K)], which is obtained by the *Average Method* and a statistically valid single value. The values for $\lambda_{in\text{-}situ}$ are listed in the following Subchapter 6.3.3.

Figure 200 illustrates furthermore, how the warm outside temperatures in summer can cause negative values for the transient thermal conductivity λ'[W/(m·K)]. Consequently, the daily fluctuation of the temperature gradient could also be the reason for slightly fluctuating values for *EMC* [m.-%]. However, it should be noted that those recorded differences are still within their respective range of accuracy.

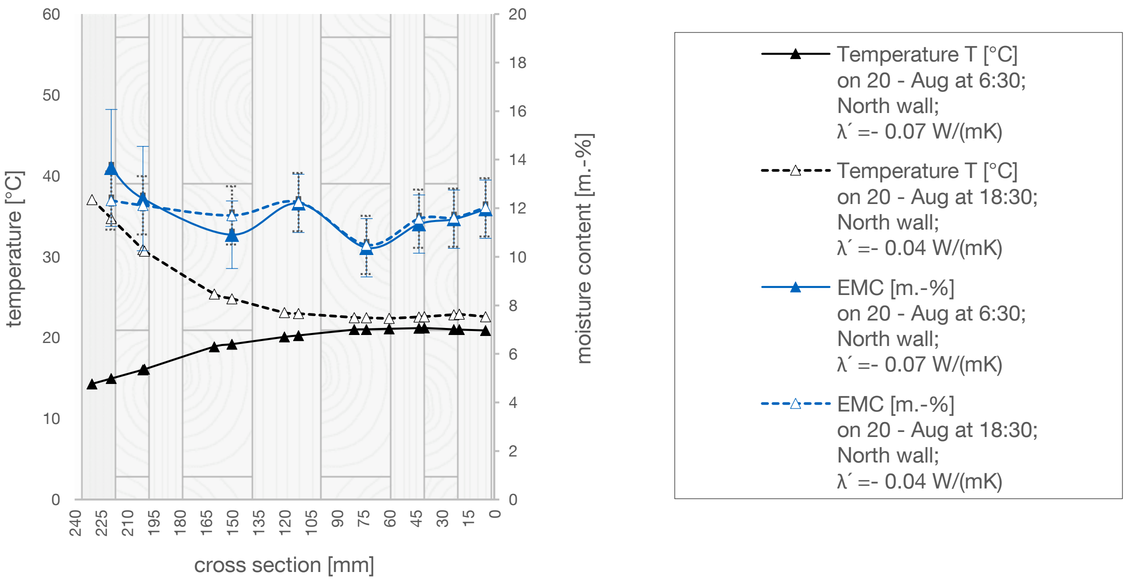

Figure 200: Systematic juxtaposition of two wood moisture distributions determined twelve hours apart in the north wall with very different temperature readings and different values for transient thermal conductivity $\lambda'_{\text{in-situ, j}}$ *[W/(m·K)] at those two specific points in time*

Figure 201 compares the different values for *EMC* [m.-%] that are obtained at the same time in the west-facing and the north-facing wall of the *Timberbrain*. These results are similar to those from the project *Einfach Bauen* in Figure 192, p. 177, which are also obtained in a west-facing and a north-facing exterior wall. In both, *EMCs* in the north seem to be elevated in the outer layers. However, the monitoring data is just not accurate enough to prove this.

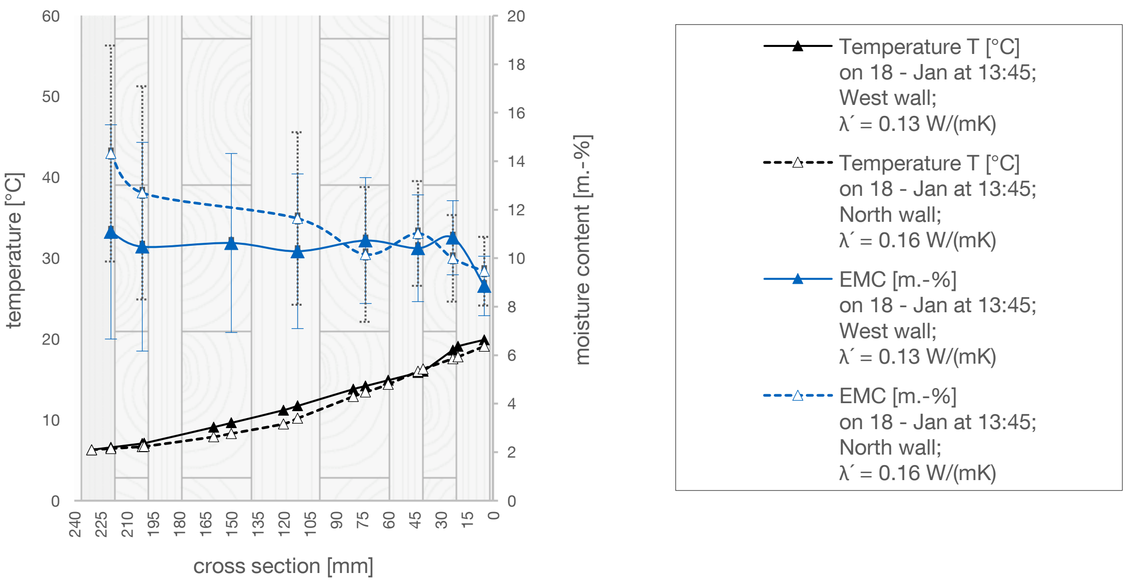

Figure 201: Comparison of the very similar temperature measurements in the west and the north wall at the same time, but EMC distributions and values for transient thermal conductivity $\lambda'_{\text{in-situ, j}}$ *[W/(m·K)] at these two sites seem to be different.*

6.3.3 Linking the results by the electrical resistance method to thermal conductivity

Some of the data within this subchapter have already been presented in context with the industrial research project *Timberbrain* (Flexeder, 2021; Flexeder et al., 2021). The raw data for wood moisture monitoring have been now re-evaluated and discussed according to the new findings and methods developed within this thesis.

Deviating from the other two monitoring projects, the data from the in-situ heat flux measurements in the *Timberbrain* is sufficiently large to conclude on single fixed values for $\lambda_{in\text{-}situ}$ [W/(m·K)] using the *Average Method* according to (ISO 9869-1:2014-08), cf. Subchapter 4.7.1. Consequently, the results discussed in this subchapter are in-line with the mathematical requirements and thus considered statistically sound to represent the conditions that were present in the element at the time. (Flexeder et al., 2021).

The values shown for λ' [W/(m·K)] (short for: $\lambda'_{in\text{-}situ,\,j}$ [W/(m·K)]) in previous Subchapters 6.2.2, 6.2.3, and 6.3.2 on the other hand, should be considered spotlights. They do not represent an averaged value, but shall merely illustrate the volatility of the heat flux, translated into a transient thermal conductivity λ' [W/(m·K)]. Both values, $\lambda_{in\text{-}situ}$ [W/(m·K)] and λ' [W/(m·K)], do not represent the thermal conductivity as it would be in standardized lab testing.

Depending on the circumstances, the investigations on in-situ thermal conductivity of the north-facing and west-facing exterior walls found slightly differing values for $\lambda_{in\text{-}situ}$ [W/(m·K)]. Since these are not laboratory measurements under standardized conditions, but on a real building, ambient conductions such as the prevailing temperature and moisture content can influence thermal conductivity. Table 16 lists the results for thermal conductivity $\lambda_{in\text{-}situ}$ as published in (Flexeder et al., 2021) and compares it to the average temperature *T* and average *EMC* in the respective time span. The standard deviation *SD* is indicating each range of different values that these averages are based on.

Table 16: Results of dynamic heat flow measurements from (Flexeder et al., 2021), juxtaposed to temperature average and the results for EMC by the novel equations (4.7)+(4.8) for electrical resistance measurements

Location	Time range	$\lambda_{in\text{-}situ}$ [W/(m·K)]	$\overline{T}$ [°C]	*SD T [°C]*	$\overline{EMC}$ [m.-%]	*SD EMC [m.-%]*
North	1 year (August 2019 – August 2020)	**0.111**	16.6	*6.0*	11.6	*1.2*
West	1 year (August 2019 – August 2020)	**0.108**	18.0	*6.8*	10.8	*0.8*
North	time span, where Δ surface temperatures (T_{si} - T_{se}) ≥ 10 K	**0.114**	12.7	*6.0*	11.6	*1.4*
West	time span, where Δ surface temperatures (T_{si} - T_{se}) ≥ 10 K	**0.105**	12.7	*6.1*	10.7	*0.6*
North	time span of reduced office use (Lockdown)	**0.113**	17.4	*4.8*	11.3	*1.1*
West	time span of reduced office use (Lockdown)	**0.110**	19.1	*5.7*	10.6	*0.9*

Figure 202 illustrates the analysis from Table 16. Evaluating the in-situ thermal conductivity $\lambda_{in\text{-}situ}$ [W/(m·K)] based on the location of measurement (north vs. west) and the selected time range results in slightly differing values. The corresponding averaged values for *EMC* [m.-%], obtained by the electrical resistance method (ERM), fluctuate as well. However, the established relationship between $\lambda_{in\text{-}situ}$ and *EMC* is not as clearly visible yet.

The measured values are juxtaposed to two sets of curves that both aim to establish a relationship between thermal conductivity, density, and moisture content of wood. The ones shown in black are copied from a graphic in (Kollmann, 1987), edited in (Niemz, 2021, p. 171). The blue dashed ones represent a computed result based on equations (3.1) and (3.2), published by (Niemz, 2021) based on (Kollmann, 1951), cf. also Subchapter 3.1.1, p. 41.

Even though both lines refer to the weight-to-volume ratio, it should be noted that there are several definitions for this parameter in wood science. What is usually referred to as *density* ρ, shown as blue dashed lines, is a moisture-dependent value and refers to the quotient of a wooden specimen´s mass at a certain *MC* and its volume (including potential swelling/shrinking) at the same *MC*. Notabene: The term *oven-dry density* ρ_0 is specifically referring to mass and volume at *MC* = 0 m.-% and considered a moisture-independent material constant.

The lines shown in black, on the other hand, represent the so-called *basic density*, which refers to the quotient of the mass of oven-dry wood (*MC* = 0 m.-%) and the volume of the maximum swollen specimen (*MC* > fiber saturation), cf. (Niemz, 2021, p. 143-145; Niemz et al., 2023, p. 284-285).

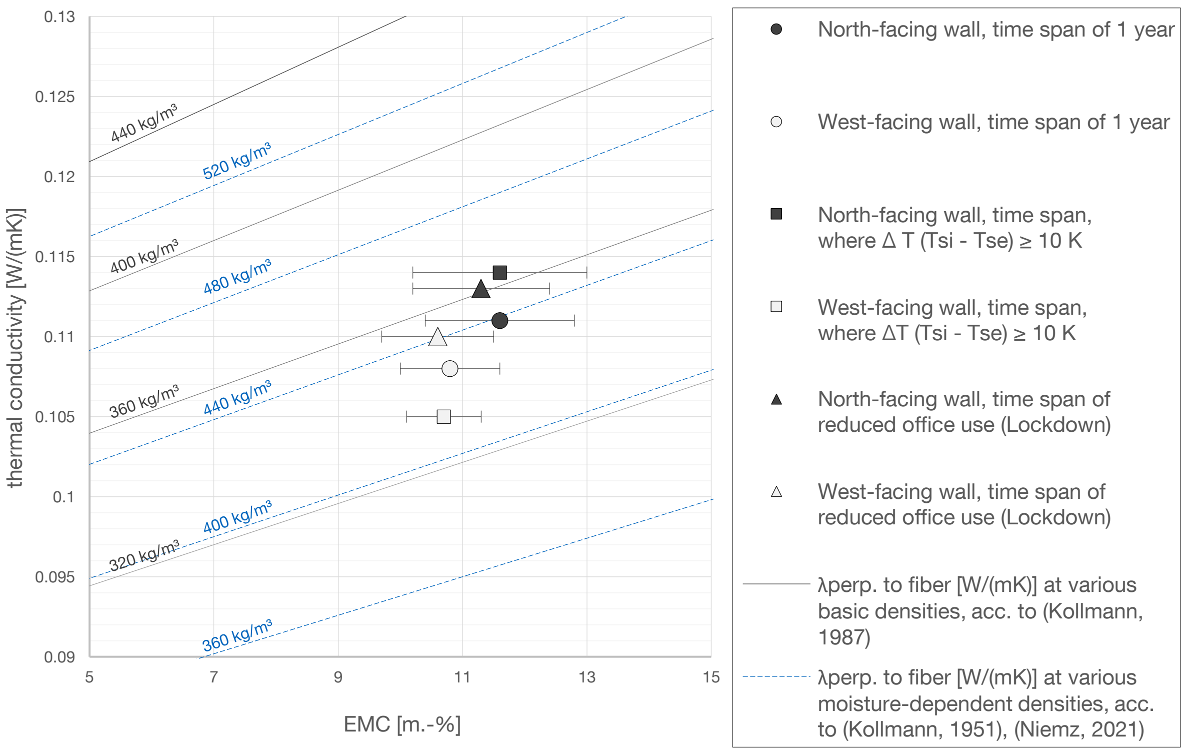

Figure 202: Juxtaposition of the results obtained in this thesis in the Timberbrain with the relationships published according to (Kollmann, 1987), in black, and according to (Kollmann, 1951; Niemz, 2021), dashed in blue.

The investigated exterior walls in the project *Timberbrain* consist of nine-layer cross-laminated timber without any insulation. The manufacturer lists these CLT products with a density of ρ = 450 kg/m³ (Sleik et al., 2018). The blue dashed curves, which are based on equations (3.1) and (3.2) from Subchapter 3.1.1, seem to fit especially the data from the north-facing wall sufficiently well. For reference: The specimens used to generate a calibration curve for the electrical resistance method (ERM) in Norway spruce in this thesis stem from two different spruce batches, cf. Figure 116, p. 127. In the experiments in Subsection 5.2, batch 1 had an average oven-dry density of ρ_0 = 460 kg/m³ (*SD*: 63.2 kg/m³). Batch 2 was significantly lighter with an average oven-dry density of ρ_0 = 383 kg/m³ (*SD*: 32.7 kg/m³), cf. Table 9, p. 85. The resulting differences in R [Ω] between the batches did not seem to be significant for practical use and were therefore neglected when curve fitting equation (4.7) to the experimental data of both batches.

The overall results confirm the general hypothesis from Subchapter 2.4.4, which suggests that the standardized values for thermal conductivity of timber tend to be too high. The results of this work thus agree with the results by (Joščák, 2013), who investigated similar wall structures constructed from solid wood. However, the discrepancies between standardized and in-situ values identified within this thesis are not as pronounced as in (Joščák, 2013) or (Griesebner & Egle, 2016).

Based on the monitoring data analyzed in this thesis, the walls of the *Timberbrain* exhibit only moderately reduced values of $\lambda_{in\text{-}situ} \approx$ 0.11 W/(m·K) at an average equivalent wood moisture content of *EMC* ≈ 11 m.-%. These values are similar to those from laboratory testing on five-layered CLT in (Kordziel et al., 2020), yet with a slightly different layer composition. Furthermore, the hypothesis by (Joščák, 2013) about a lowered thermal conductivity of exterior timber walls especially in winter might be plausible but possibly needs further research. The findings in a heated office building, Subsection 6.3, prove a lowered *EMC* at least in the inner, room-side layer of the northern exterior CLT-wall in January. A decrease in *EMC* [m.-%] would imply a decrease in λ [W/(m·K)]. However, since monitoring by the electrical resistance method showed high inaccuracies at lower temperatures, there are no significant findings about the *EMC* in the outer layers of the wall. Furthermore, if the building was not heated, the *EMC* in the walls might be even higher in winter than in summer, cf. findings in Subchapter 6.1.2. Considering that a decrease in temperature T [°C] would also imply a decrease in thermal conductivity λ [W/(m·K)], incorporating the overall temperature level into further research might add slightly more accuracy. Assuming a moisture content of *MC* = 11 m.-% and based on equation (3.3) in Subchapter 3.1.1, a temperature difference of ΔT = 10 K would result in a difference of thermal conductivity of $\Delta\lambda \approx$ 0.004 W/(m·K). However, the evaluation from the *Timberbrain* within this thesis is not sufficient to consistently prove this correlation based on findings by (Vololonirina et al., 2014).

In conclusion, the density and the moisture content of a timber element have a decisive influence on its thermal conductivity. The constant value of oven-dry density ρ_0 [kg/m³] can be determined in a laboratory by drying, weighing, and measuring material samples. The wood moisture content *MC* [m.-%] is a transient value that changes over time at different depths in the component. In order to track this spatial and temporal gradient, monitoring methods need to be accurate enough to map these differences.

7 CONCLUSION AND OUTLOOK

7.1 General overview on new findings about wood moisture content monitoring

This dissertation is contributing to modern timber construction by improving the measurement techniques for in-situ wood moisture monitoring in different types of wood and under thermal influences. This Subsection 7.1 provides an overview of the findings. The following Subsections 7.2 and 7.3 draw conclusions about the implications of these findings for practical use. The research in this thesis was limited to a small selection of wood species and sample sizes. In order to confirm the findings, further experiments would be beneficial. Furthermore, Subsection 7.4 names more specific suggestions for future research. Personal research that has already been published prior to this dissertation is listed in Subsection 7.5.

The work in the previous chapters were guided along the research questions and objectives posed in Subsection 1.4. The following pages within subchapter summarize the main answers that have been elaborated in this thesis with the respective subsections given in brackets.

I. Collect and analyze previous approaches for a holistic overview on wood moisture

When, where, why, and to what extent is wood moisture monitoring needed? What factors are influenced by wood moisture content and how can those be utilized?

Even though techniques for estimating wood moisture content have been known for several decades and are regulated through corresponding standards (1.2), major knowledge gaps still require research, particularly with regard to long-term monitoring of wood moisture gradients (1.3, 1.4).

For instance, in the field of restoration, valuable works of art such as historic panel paintings show deformations and shrinkage cracks due to recent condition changes. In order to reverse this damage by moderate climatic adjustments, detailed knowledge of the material parameters and non-destructive measuring and monitoring methods are necessary. (2.1)

This topic can be transferred to the monitoring of wooden structures, in which damage patterns increasingly consist of shrinkage cracks in roof structures, occurring within the first five years after construction. Furthermore, according to a statistically evaluated collection of damage cases, the damage pattern of wood-destroying fungi and decay is often found in external structures, yet this type of damage is mostly registered much later in a typical building´s life cycle. (2.2)

For product development in modern timber engineering, low-destructive monitoring systems are needed that can also measure in glue-laminates, previously only little-researched wood types, or hot and humid climate conditions. Depending on the application, wood moisture contents in the very dry hygroscopic range up to and beyond the fiber saturation point, with $MC \approx 5$ m.-% – 45 m.-%, at values for relative humidity of $RH \approx 25$ % – 100 %, and large temperature ranges of $T \approx 5$ °C – 60 °C are of particular interest. (2.3)

Used for monitoring in-situ, electrical resistance measurements show large deviations of $\Delta EMC \approx 8$ m.-% under high temperature gradients of $\Delta T \approx 50$ K, despite applying conventional equations for temperature compensation. More precise measurement results are important, for instance, if the correlation between transient wood moisture content MC and thermal conductivity λ is to be demonstrated in a realistic setting. (2.4)

Depending on the density and the prevailing average moisture content and temperature of the wood, a realistic thermal conductivity in a cross-laminated timber wall is averaged around $\lambda \approx 0.09$ W/(m·K) – 0.13 W/(m·K). Related in-situ phenomena such as the release of latent heat at the surface and dynamic moisture buffering effects depend on the prevailing transient ambient air conditions: The higher the air velocity v (with most significant effects at 0 m/s – 3 m/s), the temperature T, and the greater the moisture difference, the faster occurs the sorption process. (3.1)

In principle, sorption isotherms describing the stationary equilibrium moisture content EMC depend on the type of wood, relative humidity RH, and temperature T. Existing models $EMC\ (RH, T)$ are mostly based on historical data from Sitka spruce, even though various modern data sets with sorption isotherms $EMC_T\ (RH)$ are available and, in this thesis, collected for Norway spruce, Douglas fir, European beech, and radiata pine. For the same wood species, as well as for spruce LVL and beech LVL, the existing calibration curves to calculate the wood moisture content as a function of the electrical resistance R are also collected. Comparing the curves for Norway spruce for $EMC_{20°C}\ (R)$ by different authors demonstrates large deviations of $\Delta EMC \approx 3.5$ m.-%, depending on the place of origin. Furthermore, environmental influences such as age, temperature stress, and fungal degradation, show variable and inconsistent effects on material parameters such as sorption isotherms and electrical resistance in studies on different types of wood. (3.2)

Even though the electrical resistance method (ERM) is standardized for hand-held devices and is also used in an adapted form in some monitoring projects, the permanent installation results in further influencing variables, such as the variable electrical resistance R_T at the transition between electrode and wood. By contrast, material calculations can show that the temperature dependence of the conductive electrode materials is negligible in comparison. The alternative sorption method (SM) is already being tried out in some monitoring projects, although the conversion from RH and T to EMC has not yet been sufficiently accurate yet. In addition, there are numerous other approaches that use physical or chemical effects, which, however, are only briefly mentioned in the context of this work and not pursued further. These include, among others, moisture detection using special conductive tapes placed over the entire surface, RFID technology, or infrared thermography. (3.3)

II. Investigate established methods and develop new ones to quantify moisture gradients

Which methods can be used to investigate the challenges in wood moisture content monitoring? How accurate is the wide-spread electrical resistance method when adapted for repeated measurements under temperature influence? To what extent could the sorption method be a viable option for wood moisture monitoring? Could the idea of using latent heat effects serve for moisture flux detection?

The theoretical methods for estimating sensitivities in the results include regression analysis with calculations for the normalized root mean square error (*NRMSE*), the standard deviation (*SD*), and, where meaningful, the simple moving average (*SMA*). In addition, hygrothermal simulations with WUFI are used to assist in estimating results. However, the models need to be adapted to the phenomena of air velocity influence, temperature dependence of sorption isotherms, and their sorption hysteresis. (4.1)

The variation of the measurement voltage *U* [V] shows that the derived electrical resistance *R* [Ω] fluctuates and also increases with the measuring duration. But this effect is rather small compared to the influence of the contact pressure of the electrodes on the material. The more easily the electrodes can be moved in the Norway spruce specimens, the higher the overall measured electrical resistance *R* [Ω]. Shrinkage, either due to isothermal reduction of ambient *RH* over salt solutions from 55 %RH to 23 %RH, or to a slight temperature increase of 12 K, leads to a significant loosening of the electrodes. Accordingly, monitoring using the ERM leads to an underestimation of the wood moisture content, if the electrodes are not firmly attached. Instead of ramming-in the electrodes, they can also be screwed-in or conductively glued-in, as initial tests at constant wood moisture levels show similar results. A graphite-epoxy mixture is suitable as a conductive adhesive; the tested graphite-silicone mixtures do not show satisfactory results when used for fixing the cables directly into the wood. (4.2, 5.1)

The doubled logarithmic relationship between the moisture content *MC* and electrical resistance *R* measured experimentally in various wood specimens of Norway spruce can be described with satisfactory accuracy for the range of 7 m.-% – 16 m.-% at 20 °C by a rearranged equation with three newly fitted parameters. The laboratory results from investigations into the influence of measurement direction, wood type, product type, and temperature can be used as test data for various equations from the literature. This allows the most suitable calibration curves for Norway spruce, European beech, spruce LVL, and beech LVL to be determined and reparameterized for a temperature range of 5 °C – 60 °C in a series of laboratory measurements. (4.3, 5.2)

The novel idea of adapting sorption curves from published desorption and adsorption isotherms and then fitting these to a model *EMC* (*RH, T*) generates wood-species-specific equations describing the relationship of ambient air and wood moisture content for Norway spruce, European beech, Douglas fir, and radiata pine. In order to use these new equations for the sorption method (SM) in different depths of the material, sensor casings are designed and fabricated using 3D-printing. (4.4, 5.3)

Another novel technique, the temperature difference method, using latent heat effects on the wood surface to detect adsorption or desorption, can be confirmed in dynamic laboratory trials on Norway spruce and Douglas fir. However, according to the accompanying hygrothermal simulation, no linear correlation between detected temperature differences and moisture flux can be determined. Thus, the quantitative evaluation of this measurement method is not (yet) possible. The newly developed sensor casings for these minute temperature measurements have also been developed and produced from polycarbonate using 3D-printing. (4.5, 5.4)

Comparing the novel sorption method (SM) with the newly fitted electrical resistance method (ERM) in various specimens from Norway spruce and Douglas fir proves that both methods can produce sound results in steady laboratory trials at a temperature range of T = 10 °C – 40 °C. Both new methods demonstrate a significantly higher accuracy than the conventional methods. In the dynamic laboratory trials, however, the results by the newly calibrated ERM show great inaccuracies at a lowered temperature of T = 10 °C compared to the novel SM. The newly developed sensor covers for SM and the wood-type-specific conversion matrix from *RH* and *T* to *EMC* are concluded to be a sufficiently accurate and reliable monitoring method in laboratory trials on Norway spruce, Douglas fir, and radiata pine. Consequently, the novel method of consolidating a single diagram and equation *EMC* (*RH, T*) from a set of sorption isotherms emerges to be a viable option. (4.6, 5.4)

III. Apply new findings about methods and their limitations to in-situ monitoring

To what extent can the results obtained in laboratory measurements be transferred to actual exterior walls made of cross-laminated timber? What are influences that cumulate to deviations of each method? Based on the new improved wood moisture monitoring methods, which results can be drawn about the hygrothermal performance of the examined walls? For instance, can the hypotheses about a reduction in thermal conductivity be confirmed?

Applying the sorption method (SM) and the electrical resistance method (ERM) for monitoring in exterior cross-laminated timber (CLT) walls proves that both intensively investigated options can be used in-situ with their respective new calibration curves. However, significant differences are found in field tests in uninhabited test cubes built from cross-laminated timber with an exterior insulation. Temporarily very high values for relative humidity are possibly causing a short circuit in the electrical resistance measurements. Since the test cubes are not heated, the interior temperatures in January are low around 10 °C, which, according to results by SM, is followed by a rise in wood moisture content that has its peak circa two – three months later in a depth of 70 mm. Furthermore, when the temperature is low in winter, the results by SM tend to be significantly above the results by ERM, especially in depths that are further away from the surface, such as in a depth of 70 mm with $\Delta EMC \approx 3.4$ m.-%. Yet, analyzing these deviations for a correlation to temperature does not demonstrate any linear relationship. (4.7, 6.1)

Re-evaluating the raw data from the project *Einfach Bauen* with ERM and SM, both newly calibrated for the use in Norway spruce, yields values for the equivalent moisture content that appear plausible at a range of $EMC \approx 7$ m.-% – 17 m.-%, including assumed deviations. The values derived via SM in the solid part of the cross-laminated timber wall are slightly higher than those derived in the part with the air channels by a difference of $\Delta EMC \approx 1$ m.-%. The results computed for transient thermal conductivity $\lambda'_{in\text{-}situ,\,j}$ [W/(m·K)] are more stable with larger temperature differences. Taking into account the assumed deviations of ERM and SM, the readings in the exterior walls of the experimental dwelling do not allow any definite conclusions about correlations of in-situ *EMC* and the transient thermal conductivity $\lambda'_{in\text{-}situ,\,j}$. (4.7, 6.2)

Using conventional ERM in the project *Timberbrain* was initially resulting in very high and unrealistic fluctuations of the computed values for *EMC*. Since the measurements are taken in nine depths throughout the whole uninsulated CLT-wall, the temperature spread at these points reveals values of $T \approx$ -5 °C – 65°C in the west-facing wall and $T \approx$ -5 °C – 45°C in the north-facing wall. Re-evaluating the raw data from this office building using the newly calibrated calibration curve for ERM in Norway spruce produces results that are much more stable. Considering the fact that ERM is less accurate at lower temperatures, the results for *EMC* in the outer layers in winter might deviate a lot. For the warmer summer months, the moisture content in the west-facing wall can be estimated at $EMC \approx 8$ m.-% – 14 m.-%. Averaging the new values for the equivalent moisture content *EMC* and temperature *T* throughout the entire wall section results in values of $\overline{EMC} \approx 10.6$ m.-% – 11.6 m.-% and $\overline{T} \approx 12.7$ °C – 19.1 °C, depending on the evaluated time interval. Juxtaposing these values with the results from the dynamic heat flow measurements at a range of $\lambda_{in\text{-}situ} \approx 0.105$ W/(m·K) – 0.114 W/(m·K) shows good agreement with the calculations based on fundamentals from Chapter 3. (4.7, 6.3)

The findings obtained based on the objectives I, II, and III of this dissertation can be extended to instructions for practical application. Estimating the accuracy is of particular importance here, which has been already outlined in the context of the evaluations in Chapter 6, but not fully analyzed yet. The following Subsection 7.2 lists the observed partial errors and puts them in relation to each other so that an overall error can be estimated. Subchapter 7.3 evaluates the findings of this dissertation with regard to recommendations for how to proceed with specific measurement tasks.

7.2 Preliminary estimations for the accuracy of wood moisture monitoring methods

7.2.1 Accuracy of the newly developed sorption method and its ambiguities

The newly developed parameters for equations (4.15) and (4.16) result in plausible values for the equivalent moisture content *EMC* [m.-%]. They are listed and illustrated for the wood species Norway spruce (*Picea abies Karst.*), European beech (*Fagus sylvatica L.*), Douglas fir (*Pseudotsuga menziesii Franco*), and radiata pine (*Pinus radiata D. Don*.) in Appendix F. The laboratory experiments in this thesis prove that the sorption method (SM) is generally sound but subject to several influences when used for monitoring purposes. The following summarizes what is evident about the accuracy of SM with novel parameters by findings within this thesis, with the respective subchapters given in brackets.

In general, the method of inverse calculation of an equilibrium moisture content *EMC* from *RH* and *T* requires reliable sorption isotherms. These are usually based on samples without consideration of their history. However, long-term natural ageing and thermal treatment can influence the hygroscopicity of wood and thus, in these cases, lead to incorrect results by reverse calculation (3.2.3). Generating one single curve from the desorption and the adsorption isotherm, creates uncertainty. Since this gap, the hysteresis, is decreasing with higher temperature, the sorption method is more accurate with increasing temperature of the building element (3.2.2, 4.4.1).

If the sorption method uses capacitive RH-sensors, it is limited by the susceptibility to error of the polymer carrier-material for relative humidity > 80 %RH (3.3.2). For measurements at room temperature, this means that - depending on the type of wood - the sorption method is only suitable to a limited extent for wood moisture levels up to *MC* ≈ 16 m.-%.

The accuracy of the sensor itself can also influence the outcome of the sorption method. For instance, a combination RH/T-sensor with a default accuracy of ±0.2 °C and ±2 %RH will add distortions of around *ΔEMC* ≈ 0.35 m.-%. This value increases with elevated relative humidity and with lower temperatures. (4.4.2)

When inserting the RH/T-sensor into a bore-hole to estimate the wood moisture content at a certain depth, the measurement cavity needs to be tightly sealed in order to avoid falsification. In case of leakages, for instance through gaps or vapor permeable taping, the results will be significantly distorted (4.4.2). Even with a taping technique that is verified to be sufficiently tight, the direction how a sensor is inserted into the test specimen still shows slight differences of up to *ΔEMC* ≈ 0.15 m.-% in laboratory measurements (5.4.1, 5.4.4).

Exemplarily comparing two different systems for RH/T-measurements results in temperature-dependent deviations of up to *ΔEMC* ≈ 1 m.-% in laboratory experiments. Consequently, when comparing results measured by the same system, the deviations are smaller, cf. the experiments using only system IV in Subsection 6.2.

Testing the newly developed parameters against conventional ones by (Glass et al., 2014) or (Simpson, 1973), which are based on historic sorption data by Loughborough, proves the significantly improved accuracy, especially at lower temperatures. Using the new equation geared towards the proper wood species leads to experimental results that are more accurate by up to $\Delta EMC \approx 2.8$ m.-%. (5.4.1)

Table 17: Compilation of the identified sources of partial errors in the sorption method (SM) and their respective effects on the measurement results for wood moisture monitoring

Subchapter	Circumstances	Documented range of error (absolute)
3.2.2 4.4.1	Variations that are hysteresis dependent on temperature, exemplified using desorption and adsorption data of Norway spruce	± 1.0 m.-% (at 25 °C / 60 %RH) ± 0.5 m.-% (at 50 °C / 60 %RH) ± 0 m.-% (at 75 °C / 60 %RH)
5.4.1	Variations of RH measurements within the same experiment and system, exemplified using four specimens in one batch of Norway spruce	± 0.5 m.-% (at 5 °C / 40 %RH) ± 0.3 m.-% (at 40 °C / 55 %RH)
5.4.1	Different taping techniques within the same experiment and system, exemplified using two batches of Norway spruce	± 0.1 m.-% (at 5 °C / 40 %RH) ± 0.15 m.-% (at 40 °C / 55 %RH)
4.4.2	Electronic-specific uncertainty, exemplified by a RH/T-combination sensor with a default accuracy of ±0.2 °C and ±2 %RH	± 0.38 m.-% (at 25 °C / 60 %RH) ± 0.34 m.-% (at 50 °C / 60 %RH) ± 0.30 m.-% (at 75 °C / 60 %RH)
5.4.1	Different sensors for RH measurements within the same experiment but different systems, exemplified using two manufacturers	± 0.15 m.-% (at 5 °C / 40 %RH) ± 0.5 m.-% (at 40 °C / 55 %RH)

Table 17 summarizes the errors observed in laboratory measurements with SM that can be transferred to in-situ monitoring. Since these are only approximate values based on the observations from this thesis, they do not provide enough data for a definitive error calculation that could then predict the reliability of other measurements using SM. Various temperature-related influences have opposing effects, resulting in an overall balanced deviation across the temperature range investigated. The random examination of a possible function to describe the influence of humidity on accuracy has not yet yielded any clear results.

Based on the observations from this work, estimating the total error propagation by adding the observed single partial errors results in an overall accuracy of approximately ± 2.5 m.-% (at 10 °C) to ± 2.0 m.-% (at 40 °C) for in-situ monitoring using the sorption method in Norway spruce.

Figure 203 shows the resulting estimated range of potential errors, cumulated as a function of temperature. The schematic analyses in Subsection 6.2 use error indicators for *EMC* (sorption method in 100 mm depth) that are calculated according to this estimation.

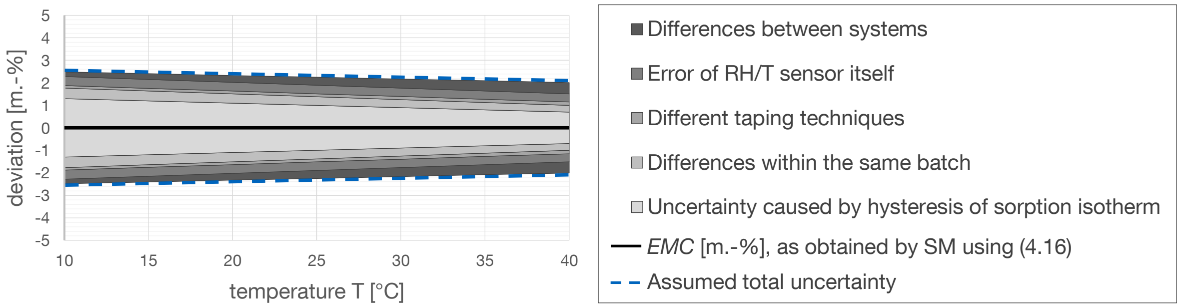

Figure 203: Assumed deviations of computed EMC [m.-%] by the sorption method (SM) at moderate ambient air humidity of RH < 80 % and based on findings in this thesis using the new equation (4.16) for Norway spruce

7.2.2 Accuracy of the improved electrical resistance method and its ambiguities

The newly developed parameters for models (4.7)+(4.8) as well as for model (4.11) result in plausible values for equivalent moisture content *EMC* [m.-%] using the electrical resistance method (ERM). Appendix F provides an illustrated overview for the recommended models and their fitted parameters for Norway spruce (*Picea abies Karst.*), European beech (*Fagus sylvatica L.*), laminated veneer lumber (LVL) made from spruce (*Picea abies Karst.*), and LVL made from beech (*Fagus sylvatica L.*).

The laboratory experiments in this thesis confirm that the electrical resistance method (ERM) is generally sound, but flawed by several influences when used for monitoring purposes under temperature and moisture gradients. The following shall summarize what is evident about the accuracy of ERM by experiments within this thesis (Subchapters given in brackets) and also what can be logically deducted but is not directly shown by experiments yet.

Testing the electrodes´ fit by manually turning each electrode in the wood is a good indicator for the additional electrical contact resistance R_T (5.1.2). This tightness of fit correlates with the peak load [N] when withdrawing the electrode at a fixed speed (5.1.4). Although not experimentally proven within this thesis, logically deducted, this correlation would also apply for the electrical contact resistance R_T. In the experiments on several softwood and hardwood species, drying out leads to shrinkage and loosening of the electrodes (5.1.3, 5.1.4), which would logically result in an increased electrical contact resistance R_T. Similarly, moistening leads to swelling and thus generally to more firmly seated electrodes (5.1.3), which would logically conclude to a reduced electrical contact resistance R_T. It is unclear to what extent other authors have already taken this circumstance of varying electrode´s fits into account. This could explain, why in Subchapter 5.1.3, the loosened electrodes produce lower resistances than the calibration curve by (Du et al., 1991) and why the tighter fit tended to produce higher resistances. This result initially contradicts the expected tendency, but could also simply be due to the fact that the electrodes in the referenced experiment possibly might have been even more extremely tight or loose. In the investigated example this situation by itself already caused an uncertainty of approximately ±1 m.-% (5.1.3).

Furthermore, the influence of an increased electrical contact resistance R_T [Ω] on the overall accuracy of *EMC* [m.-%] is highly dependent on the measurement range. Since the correlation between *R* and *MC* is logarithmic, a deviation of ± 2 GΩ does significantly alter the result for *EMC* in a range of *MC* ≈ 14 m.-%, whereas in a range of *MC* ≈ 7.5 m.-% it does not, cf. examples in Figure 101 and Figure 102 on page 117. Consequently, the range of potential deviation of *EMC* by ERM might be generally increasing with moisture content. This hypothesis could be investigated further in future research.

Choosing the correct calibration curve based on the measurement direction when placing the electrodes shows a minor influence, while distinguishing between solid wood and laminated veneer of the same species is very significant (5.2.2). Targeted curve fitting, in particular the development of temperature compensation for the range of 5 °C – 60 °C (5.2.1, 5.2.3), has been proven to lead to significantly more accurate results in electrical resistance measurements. However, there will always be an uncertainty of at least ±0.1 m.-%, even within the same wood species (5.1.5, 5.2.2).

The trials in Norway spruce at different temperature levels of 5 °C – 40 °C, but with constant wood moisture content, can reproduce measurement results with an accuracy of ±1 m.-% (5.4.2). However, these good testing results can no longer be achieved in a simple laboratory test with larger temperature and moisture step changes. Monitoring at 10 °C and thus approximately 10 K below the starting temperature, shows strong fluctuations of approximately ± 2.5 m.-%. As soon as the temperature rises, the reliability of the measurement results also increases immediately (5.4.5). This means that ERM, although calibrated for a wide temperature range, might be significantly less accurate at lowered temperatures. This observation based on lab experiments could also explain, why in-situ, the major deviations between ERM and SM (detected via monitoring, 6.1.2) improved significantly when the test cube was heated. Unfortunately, these temperature-related deviations do not always show this consistent pattern and are therefore generally difficult to correct by mathematical offsetting.

When using ERM for in-situ monitoring, very high relative humidity in the surrounding air can also lead to erroneous results. Since the system is usually not fully electrically isolated, mist or a thin condensation film might form on the equipment and lead to a short circuit (6.1.1). This will cause the system to output a higher value for EMC than what is actually the case. In the example shown, this circumstance in itself led to an error of up to + 5 m.-% in the deeper measurement spots.

Table 18: Compilation of the identified sources of error in the electrical resistance method (ERM) used in Norway spruce and their respective effects on the measurement result of using ERM for wood moisture monitoring

Subchapter	Circumstances	Documented range of error (absolute)
5.1.5 5.2.2	Variations within the same wood species, exemplified using two batches of Norway spruce	± 0.1 m.-% (at 20 °C / 35 %RH)
5.1.3	Due to swelling or shrinking, the rigid electrodes might fit tighter or looser in the wood than what was the case in the corresponding calibration curve (deviating electrical contact resistance R_T)	± 0.15 m.-% (at 20 °C / 23 %RH) ± 1 m.-% (at 20 °C / 75 %RH)
5.4.5 6.1.2	Disturbed measurements at a temperature level lowered by 10 K, from 20 °C to 10 °C	± 0.1 m.-% (at 20 °C / 50 %RH) + 2.5 m.-% (at 10 °C / 50 %RH) – 2.5 m.-% (at 10 °C / 65 %RH) ± 0.1 m.-% (at 40 °C / 65 %RH)
6.1.1	Slight short-circuit due to very high relative air humidity and possibly mist on the measurement equipment	+ 5 m.-% (at 25 °C / 100 %RH) ± 0 m.-% (at 25 °C / <90 %RH)

Table 18 summarizes the errors observed in the laboratory measurements and in the in-situ monitoring experiments with Norway spruce. It should be noted that these errors are only approximate values based on the observations in this work. They should be rather considered spot-lights. It is therefore not possible to perform a definitive error calculation that could then predict the reliability of other measurements. However, according to the error propagation, the output values of in-situ monitoring using ERM at slightly cooler temperatures might already be deviating significantly.

In conclusion, the resulting accuracy of moisture monitoring by the electrical resistance method (ERM) shows a high temperature- and possibly also humidity-dependency. The findings of this thesis are cumulated to an estimated graph of deviations in relationship to temperature for the example of Norway spruce in Figure 204 under moderate air relative humidity.

This relationship is used for indicating the estimated errors in the schematic analyses in Subsections 6.2 and 6.3 for the results by ERM.

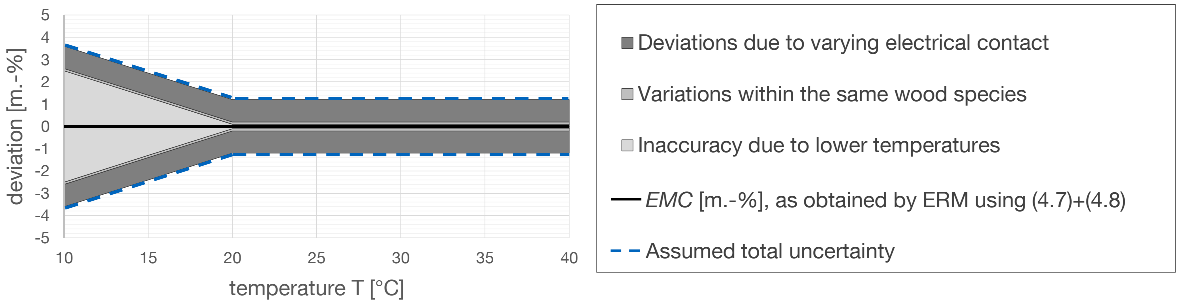

Figure 204: Assumed deviations of computed EMC [m.-%] by the electrical resistance method (ERM) at an elevated ambient air humidity of RH ≈ 75 % and based on findings in this thesis using the improved equations (4.7)+(4.8) with temperature compensation and new parameter fitting for Norway spruce.

The scheme for a temperature-dependent accuracy for moisture monitoring by the electrical resistance method (ERM) is more detailed than what has been published previously.

Forsén & Tarvainen (2000) investigated electrical resistance measurements with hand-held meters and conclude to an accuracy between ±1.5 m.-% and ±2.5 m.-% in laboratory tests. 15 years later, Dietsch et al. describe an accuracy of ±1.0 m.-% as “acceptable” for electrical resistance measurements. They might be referring to datasheets of hand-held meters as well and not long-term monitoring devices, though. (Dietsch, Franke et al., 2015; Forsén & Tarvainen, 2000)

The experiments in this thesis have also proven that some aspects in ERM that do not seem to influence the results as much as previously assumed:

- Although the measurement voltage and duration have an influence on the electrical resistance determined in the wood, these might be rather minor compared to other influences (5.1.1).
- The tightness of the electrodes´ fit does not show a clear correlation to any certain pre-drilled hole diameter for the rammed-in electrodes, as long as it is smaller than the actual electrode´s thickened head (5.1.2, 5.1.3, 5.1.4).
- Furthermore, it is possible to use various geometries for rigid conducting electrodes. The three options that were investigated more in-depth, rammed-in stainless steel nails, screwed-in threaded rods, and cables glued-in with a special epoxy, all showed similar results (5.1.5, 5.4.2, 5.4.5).
- If the actual wood-species specific calibration curve is not available, synthesizing one from a similar species or measurements in a higher humidity range might be a possibility. However, based on the data from Douglas fir and radiata pine, this approach does not necessarily add any more accuracy and thus might not be worth it (5.4.2).

7.3 Recommendations for wood moisture monitoring methods

The literature review in Chapter 2 defines requirements for wood moisture monitoring in various settings. Depending on the matter under investigation and based on the findings in this thesis, different monitoring could be recommended, cf. Table 19.

Table 19: Compilation of the identified requirements for wood moisture monitoring with SM and/or ERM

Subchapter	Circumstances / requirements	Possible solution
2.1	non-destructive conclusions about moisture development historical and valuable materials	SM on the surface (possibly with isotherms adapted to aging)
2.2	information about the entire building early warning about elevated moisture content low cost and over the long term	ERM on the surface, as a leakage warning system no species-specific calibration required
	monitor moisture gradients decreased MC values (<< 12 m.-%) daily fluctuations	SM in different depths of the timber element (ERM only if no cold temperatures)
2.3	multi-layered glued timber slabs or beams monitor moisture gradients in complex modern timber engineered products	ERM for spruce LVL and beech LVL (calibrated for measurement direction)
	utilize wood species that are less explored for construction yet, such as hardwoods or wood from other regions	SM with adapted calibration curves (based on specific sorption isotherms)
	test timber engineering for durability in hot and humid climates	ERM with calibration curves for high temperatures (SM only if with suitable RH/T-combination sensors)
2.4	reliably track local wood moisture changes in different layer depths with high temperature fluctuations over a period of several months	ERM or SM both only with calibration for a wide temperature range

When working with historical wooden objects or art, wood moisture monitoring needs to be non-destructive and suitable for aged materials (Subsection 2.1). A solution could be using lay-on hygrometers combined with the sorption method (SM). If the respective data is available, the calibration curve, which is based on sorption isotherms from recent wood, could possibly be altered to represent aged wood (Subchapters 2.1.2, 3.2.3).

The need for monitoring regular timber structures can be divided into two main causes (Subsection 2.2): On the one hand, there is a risk of moisture damage over the entire life cycle due to leaks or construction defects, which should be detected early on throughout the building. For a comprehensive early warning system, a simple leakage detection based on electrical resistance might be a good solution. These measurements do not necessarily need to be in the timber element, but it might be sufficient to just place them surface-wide onto it. Some ideas are listed in Table 7, p. 63, such as a special conductive tape.

On the other hand, cracks can form in the first few years after construction or any change in building use causing excessive drying-out. In order to observe the drying behavior and, if necessary, counteract it by changing the ambient climate, the wood moisture needs be monitored closely at neuralgic points. This requires a calibrated monitoring system that can reliably track decreased moisture content values (MC << 12 m.-%) and daily fluctuations. Depending on the wood-species, the specific equations with newly fitted parameters from this thesis can be suitable for this task.

In the service life of built wooden structures, dry and moist phases can also alternate in the hygroscopic range due to the influence of common climatic fluctuations, for instance due to seasons, a renovation, or a change in use. If using the electrical resistance method (ERM) for monitoring projects, the installation of electrodes should take place in a rather dry phase. Furthermore, the position of the electrodes should be checked manually after some time in order to avoid an underestimation of critical wood moisture contents.

In order to help develop novel timber products or test them in a new application field, monitoring systems need to be calibrated for the respective material (Subsection 2.3). This thesis offers calibration curves for ERM in laminated veneer lumber (LVL) made from spruce or beech. Furthermore, using three exemplary Australian wood species, it investigates how ERM and SM could be used even when proper calibration curves have not been established yet.

If the monitoring task involves a building element under a strongly fluctuating temperature gradient, the challenge is to reliably account for these various temperature levels (Subsection 2.4). The monitoring method should be chosen based on the expected measurement range. For instance, the intentions for investigating the wood moisture content in an exterior CLT wall could be based on several research questions. Subchapter 2.4.4 introduces an application case from building physics that is mainly discussed in this thesis. However, projects with another focus, such as those described in Subchapters 2.3.3 and 2.3.4, might also pose similar monitoring tasks.

Recommendations for certain calibration curves depend on the wood species and the expected range of measurement. Table 20 summarizes the calibration curves for the electrical resistance method (ERM) and the sorption method (SM) that are recommended for use based on the fitting to experimental data within this thesis. Listed are only those equations that showed the lowest normalized root mean square errors (*NRMSE*) and thus the best fit. They are also illustrated in Appendix F.

Table 20: Compilation of the new calibration curves based on the findings from this thesis

Subchapters	Method	Equations	Wood species / product	Investigated range
5.2.4	ERM	(4.11)	Spruce laminated veneer lumber (LVL made of *Picea abies Karst.*)	5 °C – 60 °C 10 m.-% - 13 m.-%
5.2.4	ERM *Option 1*	(4.11)	Beech laminated veneer lumber (LVL made of *Fagus sylvatica L.*.)	5 °C – 60 °C 9 m.-% - 14 m.-%
5.2.4	ERM *Option 2*	(4.14)		
5.2.1 5.2.3	ERM *Option 1*	(4.7) + (4.8)	Norway spruce *(Picea abies Karst.)*	5 °C – 60 °C 7 m.-% - 16 m.-%
5.2.4	ERM *Option 2*	(4.11)		
5.3	SM	(4.16)		-12 °C – 100 °C 0 %RH – 99 %RH
5.2.4	ERM	(4.11)	European beech *(Fagus sylvatica L.)*	5 °C – 60 °C 9 m.-% - 14 m.-%
5.3	SM	(4.16)		20 °C – 100 °C 0 %RH – 95 %RH
5.3	SM	(4.16)	Douglas fir *(Pseudotsuga menziesii Franco)*	-12 °C – 60 °C 0 %RH – 99 %RH
5.3	SM	(4.16)	Radiata pine *(Pinus radiata D. Don.)*	15 °C – 50 °C 0 %RH – 98 %RH

7.4 Identification of future potentials in research and development

This thesis identifies several aspects that relate to the accuracy of the electrical resistance method (ERM). Consequently, the following ideas could help to improve the accuracy of ERM.

The discussion in Subchapter 2.4.1 mentions that metal electrodes might be conducting more heat into the measurement area than what would be the case without any measurement equipment. The experiments in this thesis can neither prove nor disprove this hypothesis. Future research could investigate the effects of this systematic measurement error and possible solutions using an electrically conductive material that has thermal parameters similar to wood.

Future developments of wood moisture monitoring devices could investigate the optimal point where the measuring voltage U [V] is as low as possible and the measuring currents I [A] are as high as possible. Based on the findings in Subchapter 5.1.1 and general limitations by the power supply, a measuring voltage in the order of U = 10 V might be a good starting point.

The previous lab experiments prove that ordinary geometry changes in the wood can already diminish the electrical contact between electrode and wood, which increases the electrical resistance at the transition R_T [Ω] and thus significantly alters the result. The idea of gluing the connecting cables directly into the wood with a conductive epoxy resin produced good initial results and was therefore pursued further in this thesis. However, the idea of gluing these cables into the wood using a conductive silicone failed due to either too little electrical conductivity or missing adhesive strength. The idea of ramming the stainless-steel electrodes into a prefabricated ring of conductive silicon as in Subchapter 5.1.5 does not produce any adverse results. Although it is not pursued further in this thesis, this approach could be worthwhile for future projects.

The preliminary estimation of accuracy of ERM in Subchapter 7.2.2 is only displayed as a function of temperature. This is used for indicating the estimated errors in the schematic analyses in Subsections 6.2 and 6.3. However, the accuracy of ERM seems to be influenced also by moisture. Accordingly, Figure 205 suggests assumed deviations at a constant temperature but dependent on relative humidity RH, which, according to the experimental results, seems to also influence the accuracy. The blue circle indicates where the scheme would intersect with the temperature-dependent estimation, which is shown in Figure 204, p. 196.

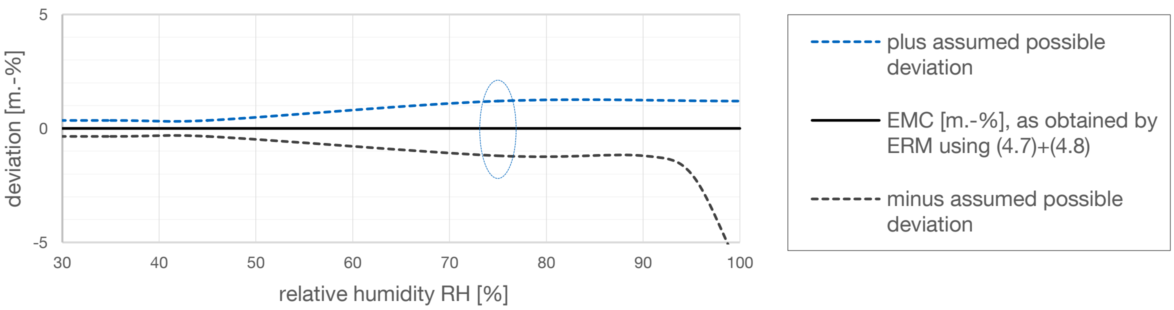

Figure 205: Assumed deviations of computed EMC [m.-%] by the electrical resistance method (ERM) at a moderate temperature of T ≈ 25 °C and based on findings in this thesis using the improved equations (4.7)+(4.8) with temperature compensation and new parameter fitting for Norway spruce.

Using ERM for monitoring in a test cube shows unrealistically high values for *EMC* when the indoor air relative humidity *RH* rises to 100 m.-%, cf. Subchapter 6.1.1. These readings are probably due to a short circuit, either on the CLT surface, despite the electrodes being isolated by Teflon lacquer, or through a thin layer of mist on the monitoring device itself. In order to prevent such errors this phenomenon should be investigated further and possibly remedied by a technical solution. Otherwise, especially in the case of very high ambient humidity, the output values might get significantly falsified as indicated in Figure 205. Furthermore, the logarithmic correlation between *R* and *MC* might cause an inaccuracy that is decreasing with lower humidity values, cf. Subchapter 7.2.2.

The developments in this work regarding the sorption method (SM) could be considered a first approach that needs to be tested further in order to gain a better understanding about its potential future use. The temperature-dependent accuracy estimated in Figure 203, p. 193, is based on the whole range of sorption hysteresis and could possibly be narrowed down by investigating a realistically occurring range. This would be beneficial since this influence accounts for a significant fraction of this method´s estimated overall deviation.

In this thesis, the parametrization of the sorption method is limited to four wood species and a total of 147 data sets. In order to improve the sorption method further, the methods explained in Subchapters 4.1.1 and 4.4.1 could be expanded to a broader collection of sorption isotherms. This could include wider temperature ranges as well as new wood species. Furthermore, the sorption method could be suitable to be also used in other building materials. Especially lower temperature ranges might be a worthwhile investigation as the electrical resistance method (ERM) presents larger inaccuracies here.

The investigations with the sorption method utilize a sensor set-up that requires a bore-hole with a diameter of d = 32 mm, cf. Subchapter 4.4.2. Using smaller RH/T-combination sensors in the future would help to reduce possible interferences. Furthermore, the RH/T-combination sensors tend to drift when exposed to elevated relative humidity RH > 80 % for several hours. Consequently, deploying more resilient sensors might facilitate to expand the potential field of application for monitoring with the sorption method. Even though preliminary tests showed no signs of sorption or diffusion in the 3D-printed polycarbonate covers and their thorough taping, future covers should possibly be manufactured from another material that is not considered hygroscopic.

7.5 Previous personal publications related to this work

A number of publications were produced as part of the scientific activities conducted between 2018 and 2023. While the main contents of this monograph are entirely new and previously unpublished, they are in part based on the results of earlier work, such as figures or raw data. Where content from these publications is used, it is identified by duly cited references.

Moreover, the publications contain a plethora of results that are not discussed in this work, but which might be of interest to the reader in a broader context. They are therefore recommended for more in-depth information.

Flexeder, Nina; Ott, Stephan; Bodemer, Eva; Winter, Stefan (2021): Monitoring of an office building in uninsulated cross laminated timber (CLT) construction regarding hygrothermal component behavior. In: *Proceedings of WCTE 2021 - World Conference on Timber Engineering*.

Bodemer, Eva; Flexeder, Nina; Wagner, Anna (2021): Forschungsprojekt BBS Thermo am Beispiel des neuen Verwaltungsgebäudes der Binderholz Bausysteme GmbH in Hallein. Projektbericht. Confidential industry research report.

Flexeder, Nina (2022): Instationäre Holzfeuchtebestimmung. Verschiedene Anwendungsszenarien mit Bezug zum thermischen Bauteilverhalten. In: *Holzbau Forschung + Praxis. Doktorandenkolloquium der Universität Stuttgart.* III-b.

Flexeder, Nina (2022): Geometry data of a sensor envelope for the hygrometric method to determine material moisture content. Technical University of Munich. doi: 10.14459/2022mp1651104.

Flexeder, Nina (2022): Geometry data of a sensor mount for surface temperature measurements. Technical University of Munich. doi: 10.14459/2022mp1651103.

Grönquist, Philippe; Flexeder, Nina; Franke, Bettina; Franke, Steffen (2022): Monitoring of Wood Moisture Content in Timber Structures by Electrical Resistance and the Sorption Methods: Current Challenges. In: *Sustainability and Durability of Taller Timber Buildings: A State-of-the-Art Report*. COST Action CA20139 Holistic design of taller timber buildings (HELEN). WG4.SG4.02, CA20139 – Working Group 4 Sustainability and Durability. p. 51–54.

Flexeder, Nina; Schenk, Martin; Aondio, Patrik (2022): Moisture Monitoring Techniques for the Protection of Timber Structures. In: *Proceedings of the International Conference on Structural Health Assessment of Timber Structures (SHATIS)*. DOI: 10.14459/2022md1687361.

Flexeder, Nina; Nouman, Ahmad S.; Hepf, Christian (2022): Measurement of Sorption Heat in Laboratory and Field Tests in Comparison with Hygrothermal Simulations. In: *Proceedings of BauSIM 2022*. DOI: 10.14459/2022md1688193.

Flexeder, Nina; Schumacher, Nils; Hepf, Christian; Nouman, Ahmad; Briels, David; Varga, Zsofia et al. (2022): PhyTAB – Potenziale hygrothermisch aktivierter Bauteile. Energieeffiziente Raumkonditionierung mittels luftdurchströmter Massivholzelemente und hygroskopisch optimierter Oberflächen. ISSN 1868-0097. Report. Bonn: BBSR-Online Publikation (BBSR-Online-Publikation, 17/2022).

Flexeder, Nina; Kamml, Michael; Paulik, Johannes (2022): Anlagen zum Forschungsbericht. Potenziale hygrothermisch aktivierter Bauteile (PhyTAB). Anlagen zur BBSR-Online-Publikation 17/2022

Franke, Laura; Niemann, Anne; Jarmer, Tilmann; Varga, Zsofia; Flexeder, Nina; Kränkel, Thomas et al. (2024): Einfach Bauen 3 – Messen, Validieren, Rückkoppeln: Monitoring der Pilothäuser aus Massivholz, Leichtbeton und hochwärmedämmendem Mauerwerk aus Einfach Bauen 2 und Validierung der Ergebnisse. Hg. v. BBSR-Online-Publikation 41/2024. Technische Universität München. Bonn (ISSN 1868-0097).

As part of the scientific activities, there were also a number of presentations in which these topics were discussed. In addition to regular lectures at the Technical University of Munich, this also included several conferences, panel discussions, and international collaborations.

A selection of the most relevant presentations is listed below:

Flexeder, Nina: Potenziale hygrothermisch aktivierter Bauteile. *Forschungsinitiative Zukunft Bau, Bundesinstitut für Bau-, Stadt- und Raumforschung*. *Projektetage der Bauforschung PT12 - Juni 2018*. *Bundesamt für Bauwesen und Raumordnung, Bonn, Germany*. 04.06.2019

Flexeder, Nina: Monitoring of an office building in uninsulated cross laminated timber (CLT) construction regarding hygrothermal component behavior. *WCTE - World Conference on Timber Engineering 2021*. *Online / UC Timber Innovation Center*, *Santiago, Chile*. 09.08.2021

Flexeder, Nina: Instationäre Holzfeuchtebestimmung - Verschiedene Anwendungsszenarien mit Bezug zum thermischen Bauteilverhalten, *Universität Stuttgart, Institut für Konstruktion und Entwurf*. *Doktorandenkolloquium: Holzbau Forschung + Praxis*. *Stuttgart, Germany*. 10.03.2022

Flexeder, Nina: Transient Wood Moisture Analysis: Different Application Scenarios with Reference to Thermal Component Behavior. *ETH Zürich, Institute for Structural Engineering. PhD Colloquium on Timber Engineering Research*. *Zurich, Switzerland*. 29.08.2022

Flexeder, Nina: Measurement of sorption heat in laboratory and field tests in comparison with hygrothermal simulations. *Bauhaus-Universität Weimar und IBPSA Germany / Austria*. *BauSIM 2022 - Tagung zur energetischen Simulation im Gebäudesektor für Fachleute aus Wissenschaft und Praxis*. *Weimar, Germany*. 21.09.2022

Flexeder, Nina: Monitoring of Wood Moisture Content in Timber Structures by Electrical Resistance and Sorption Methods: Current Challenges. *Chalmers University of Technology*. *COSTAction CA20139: Meeting of all working groups. Gothenburg, Sweden*. 04.10.2022

Flexeder, Nina: Research with and on in-situ Moisture Monitoring at the Technical University of Munich. *Department of Agriculture and Fisheries*. *Queensland Government*. *Brisbane, Australia*. 07.02.2023

8 DIRECTORIES

8.1 Referenced standards

AS/NZS 1080.1:2012. *Timber - Methods of test - Method 1: Moisture content*. Joint Standards Australia/Standards New Zealand Committee TM-003, Timber Grading.

ASTM D4442-20. *Test Methods for Direct Moisture Content Measurement of Wood and Wood-Based Materials*. American Society for Testing and Materials (ASTM) International.

ASTM D4444-13 (2018). *Test Method for Laboratory Standardization and Calibration of Hand-Held Moisture Meters*. American Society for Testing and Materials (ASTM) International.

ASTM D4933-16 (2021). *Standard Guide for Moisture Conditioning of Wood and Wood-Based Materials*. American Society for Testing and Materials (ASTM) International.

ASTM D7438-20. *Practice for Field Calibration and Application of Hand-Held Moisture Meters*. American Society for Testing and Materials (ASTM) International.

CEN/TS 17440:2020-10. *Assessment and retrofitting of existing structures; German version DIN CEN/TS 17440:2020*. CEN-CENELEC (ed.).

DIN 68800-1:2019-06. *Wood preservation - Part 1: General*. NA 042-03-01 AA, NHM, NABau, DIN Media GmbH (ed.).

DIN 68800-2:2022-02. *Wood preservation - Part 2: Preventive constructional measures in buildings*. NA 042-03-02 AA, NHM, NABau, DIN Media GmbH (ed.).

DIN 68800-3:2020-03. *Wood preservation - Part 3: Preventive protection of wood with wood preservatives*. NA 042-03-03 AA, NHM, NABau, DIN Media GmbH (ed.).

DIN 68800-4:2020-12. *Wood preservation - Part 4: Curative treatment of wood destroying fungi and insects and refurbishment*. NA 042-03-04 AA, NHM, NABau, DIN Media GmbH (ed.).

EN 12667:2001. *Thermal performance of building materials and products - Determination of thermal resistance by means of guarded hot plate and heat flow meter methods - Products of high and medium thermal resistance; German version DIN EN 12667:2001-05*. CEN/TC 89, CEN-CENELEC (ed.).

EN 12939:2000. *Thermal performance of building materials and products - Determination of thermal resistance by means of guarded hot plate and heat flow meter methods - Thick products of high and medium thermal resistance; German version DIN EN 12939:2001-02*. CEN/TC 89, CEN-CENELEC (ed.).

EN 13183-1:2002. *Moisture content of a piece of sawn timber - Part 1: Determination by oven dry method; German version DIN EN 13183-1:2002-07*. CEN/TC 175, CEN-CENELEC (ed.).

EN 13183-2:2002. *Moisture content of a piece of sawn timber - Part 2: Estimation by electrical resistance method; German version DIN EN 13183-2:2002-07*. CEN/TC 175, CEN-CENELEC (ed.).

EN 13183-3:2005. *Moisture content of a piece of sawn timber - Part 3: Estimation by capacitance method; German version DIN EN 13183-3:2005-06*. CEN/TC 175, CEN-CENELEC (ed.).

EN 15026:2023. *Hygrothermal performance of building components and building elements - Assessment of moisture transfer by numerical simulation; German version DIN EN 15026:2023-12*. CEN/TC 89, CEN-CENELEC (ed.).

EN 16242:2012. *Conservation of cultural heritage - Procedures and instruments for measuring humidity in the air and moisture exchanges between air and cultural property; German version DIN EN 16242:2013-03*. CEN/TC 346, CEN-CENELEC (ed.).

EN 16322:2013-12. *Conservation of Cultural Heritage - Test methods - Determination of drying properties; German version DIN EN 16322:2013-12*. CEN/TC 346, CEN-CENELEC (ed.).

EN 16682:2017. *Conservation of cultural heritage - Methods of measurement of moisture content, or water content, in materials constituting immovable cultural heritage; German version DIN EN 16682:2017-05*. CEN/TC 346, CEN-CENELEC (ed.).

EN ISO 10456:2007 + Cor. 1:2009. *Building materials and products - Hygrothermal properties - Tabulated design values and procedures for determining declared and design thermal values (ISO 10456:2007 + Cor. 1:2009); German version DIN EN ISO 10456:2010-05*. SC 2 ISO/TC 163, CEN/TC 89, CEN-CENELEC (ed.).

EN ISO 12570:2000 + Amd 1:2013 + Amd 2:2018. *Hygrothermal performance of building materials and products - Determination of moisture content by drying at elevated temperature; German version DIN EN ISO 12570:2018-07*. ISO/TC 163, CEN/TC 89, CEN-CENELEC (ed.).

EN ISO 12571:2021. *Hygrothermal performance of building materials and products – Determination of hygroscopic sorption properties; German version DIN EN ISO 12571:2022-04*. ISO/TC 163, CEN/TC 89, CEN-CENELEC (ed.).

ISO 16979:2003-05. *Wood-based panels - Determination of moisture content*. ISO/TC 89, ISO (ed.).

ISO 760:1978-12. *Determination of water; Karl Fischer method (General method)*. ISO/TC 47, ISO (ed.).

ISO 9869-1:2014-08. *Thermal insulation - Building elements - In-situ measurement of thermal resistance and thermal transmittance - Part 1: Heat flow meter method*. SC 1 ISO/TC 163, ISO (ed.).

prEN 1995-1-1:2023. *Eurocode 5 - Design of timber structures - Part 1-1: General rules and rules for buildings; German and English version prEN 1995-1-1:2023 / DIN EN 1995-1-1:2023-10. CEN/TC 250/SC 5,* CEN-CENELEC (ed.).

prEN 1995-3:2023. *Eurocode 5: Design of timber structures - Part 3: Execution; German and English version prEN 1995-3:2023 / DIN EN 1995-3:2023-09. CEN/TC 250/SC 5,* CEN-CENELEC (ed.).

WTA 6-8:2016. *Assessment of humidity in timber constructions - Simplified verifications and simulation; German version 6-8-16/D:2016-08*. WTA-Ref. 6, WTA Publications, DIN Media GmbH (ed.).

8.2 Referenced literature

Angst-Nicollier, V. (2012). *Moisture Induced Stresses in Glulam: Effect of Cross Section Geometry and Screw Reinforcement* [Dissertation]. Norwegian University of Science and Technology, Trondheim.

Appel, A. (2020). *Feuchtemessung: Stand der Technik und Forschung* [Bachelorthesis]. Technische Universität München.

Arriaga, F., Osuna-Sequera, C., Esteban, M., Íñiguez-González, G. & Bobadilla, I. (2021). In situ assessment of the timber structure of an 18th century building in Madrid, Spain. *Construction and Building Materials*, *304*, 124466. https://doi.org/10.1016/j.conbuildmat.2021.124466

Avramidis, S. (1989). Evaluation of three-variable models for the prediction of equilibrium moisture content in wood. *Wood Science and Technology*, *23*(3), 251–257. https://doi.org/10.1007/BF00367738

Avramidis, S. (2018). Bound Water Migration in Wood. In *Advances in the drying of wood: COST E15.*

Avramidis, S. & Siau, J. F. (1987). An investigation of the external and internal resistance to moisture diffusion in wood. *Wood Science and Technology*, *21*(3), 249–256. https://doi.org/10.1007/BF00351396

Backer, L. de, Laverge, J., Janssens, A. & Paepe, M. de (2018). Evaluation of the diffusion coefficient and sorption isotherm of the different layers of early Netherlandish wooden panel paintings. *Wood Science and Technology*, *52*(1), 149–166. https://doi.org/10.1007/s00226-017-0949-y

Ball, R. D., Simpson, I. G. & Pang, S. (2001). Measurement, modelling and prediction of equilibrium moisture content in *Pinus radiata* heartwood and sapwood. *European Journal of Wood and Wood Products*, *59*(6), 457–462. https://doi.org/10.1007/s001070100242

Barreira, E. & Almeida, R. M. (2015). Drying Evaluation Using Infrared Thermography. *Energy Procedia*, *78*, 170–175. https://doi.org/10.1016/j.egypro.2015.11.135

Bienert, L., Schumacher, N., Winter, S. & Richter, K. (2023). Development of Disintegrated Hybrid Cross Laminated Timber: PAPER REF: 19907. *Proceedings of the ICEM20 - 20th International Conference on Experimental Mechanics*, 943–954.

Binderholz Bausysteme GmbH. *REFERENZ binderholz Bürogebäude TimberBrain, Hallein | Österreich*. https://www.binderholz.com/bauloesungen/binderholz-buerogebaeude-timberbrain-hallein-oesterreich/

Björngrim, N., Hagman, O. & Wang, X [Xiaodong] (2016). Moisture Content Monitoring of a Timber Footbridge. *BioResources*, *11*(2). https://doi.org/10.15376/biores.11.2.3904-3913

Boardman, C. R. (2011). Moisture Meter Calibrations for Untreated and ACQ-Treated Southern Yellow Pine Lumber and Plywood.

Boardman, C. R., Glass, S. V. & Lebow, P. K. (2017). Simple and accurate temperature correction for moisture pin calibrations in oriented strand board. *Building and Environment*, *112*, 250–260. https://doi.org/10.1016/j.buildenv.2016.11.039

Bodemer, E., Flexeder, N. & Wagner, A. (2021). *Forschungsprojekt BBS Thermo am Beispiel des neuen Verwaltungsgebäudes der Binderholz Bausys-teme GmbH in Hallein: Projektbericht.* Technical University of Munich.

Böhner, G. (1996). Überlegungen und Ergänzungen zum „Keylwerth-Diagramm". *European Journal of Wood and Wood Products*, *54*(2), 73–79. https://doi.org/10.1007/s001070050139

Bonnet, M., Courtier-Murias, D., Faure, P., Rodts, S. & Care, S. (2017). NMR determination of sorption isotherms in earlywood and latewood of Douglas fir. Identification of bound water components related to their local environment. *Holzforschung*, *71*(6), 481–490. https://doi.org/10.1515/hf-2016-0152

Bora, S., Sinha, A. & Barbosa, A. R. (2022). Effect of Short-Term Simulated Rain Exposure on the Performance of Cross-Laminated Timber Angle Bracket Connections. *Journal of Architectural Engineering*, *28*(4), Artikel 04022025. https://doi.org/10.1061/(ASCE)AE.1943-5568.0000560

Brandl, L. (2021). *Datenauswertung zum Thema Faktoren für Schadensfälle im Holzbau durch Holzfeuchteänderungen* [Master´s Thesis]. Technische Universität München.

Brandt, J., Fröhlich, A., Hilger, T., Holl, K., Hörmann, M. & Pallas, L. (2023). A Heated Situation: In situ Monitoring of a Wooden Altarpiece. *AIC Annual Meeting General Session Postprints. Presentations from the American Institute for Conservations's 51st Annual Meeting in Jacksonville, Florida. General and Concurrent Sessions, Mai 18-20*, *2*, 171–179. https://www.culturalheritage.org/docs/default-source/publications/periodicals/annual-meeting/general-session-postprints/aic-general-session-postprints-volume-2-2023.pdf?Status=Master&sfvrsn=64111120_3

Bratasz, Ł. (2013). Allowable microclimatic variations for painted wood. *Studies in Conservation*, *58*(2), 65–79. https://doi.org/10.1179/2047058412Y.0000000061

Bratasz, Ł., Kozłowska, A. & Kozłowski, R. (2012). Analysis of water adsorption by wood using the Guggenheim-Anderson-de Boer equation. *European Journal of Wood and Wood Products*, *70*(4), 445–451. https://doi.org/10.1007/s00107-011-0571-x

Brischke, C. & Lampen, S. C. (2014). Resistance based moisture content measurements on native, modified and preservative treated wood. *European Journal of Wood and Wood Products*, *72*(2), 289–292. https://doi.org/10.1007/s00107-013-0775-3

Brischke, C., Rapp, A. O. & Bayerbach, R. (2008). Measurement system for long-term recording of wood moisture content with internal conductively glued electrodes. *Building and Environment*, *43*(10), 1566–1574. https://doi.org/10.1016/j.buildenv.2007.10.002

Brischke, C., Sachse, K. A. & Welzbacher, C. R. (2014). Modeling the influence of thermal modification on the electrical conductivity of wood. *Holzforschung*, *68*(2), 185–193. https://doi.org/10.1515/hf-2013-0041

Brischke, C., Stricker, S., Meyer-Veltrup, L. & Emmerich, L. (2019). Changes in sorption and electrical properties of wood caused by fungal decay. *Holzforschung*, *73*(5), 445–455. https://doi.org/10.1515/hf-2018-0171

Bunkholt, N. S., Gullbrekken, L., Time, B. & Kvande, T. (2021a). Pitched unventilated wood frame roof with smart vapour barrier – field measurements. *Journal of Physics: Conference Series*, *2069*(1), 12007. https://doi.org/10.1088/1742-6596/2069/1/012007

Bunkholt, N. S., Gullbrekken, L., Time, B. & Kvande, T. (2021b). Process induced building defects in Norway – development and climate risks. *Journal of Physics: Conference Series*, *2069*(1), 12040. https://doi.org/10.1088/1742-6596/2069/1/012040

Camuffo, D. (2018). Standardization activity in the evaluation of moisture content. *Journal of Cultural Heritage*, *31*, S10-S14. https://doi.org/10.1016/j.culher.2018.03.021

Camuffo, D. & Bertolin, C. (2012). Towards Standardisation of Moisture Content Measurement in Cultural Heritage Materials.

Casans Berga, S., Garcia-Gil, R., Navarro Anton, A. E. & Rosado-Muñoz, A. (2019). Novel Wood Resistance Measurement Method Reducing the Initial Transient Instabilities Arising in DC Methods Due to Polarization Effects. *Electronics*, *8*(11), 1253. https://doi.org/10.3390/electronics8111253

Chanpet, M., Rakmak, N., Matan, N. & Siripatana, C. (2020). Effect of air velocity, temperature, and relative humidity on drying kinetics of rubberwood. *Heliyon*, *6*(10). https://doi.org/10.1016/j.heliyon.2020.e05151

Christ, M. (2020). *Einflussfaktoren der Holzfeuchtemessung: Experimentelle Untersuchung der Einussfaktoren auf die Messgenauigkeit der elektrischen Holzfeuchtemessung nach dem Widerstandsprinzip mit Gleichstrom* [Master´s Thesis]. Technische Universität, München.

Çolakoğlu, M. H. (2009). Determination of change in moisture ratios of some woods during air-drying by finite element analysis. *Journal of Applied Sciences*, *9*(22), 4091–4094. https://doi.org/10.3923/jas.2009.4091.4094

Couceiro, J., Lindgren, O., Hansson, L., Söderström, O. & Sandberg, D. (2019). Real-time wood moisture-content determination using dual-energy X-ray computed tomography scanning. *Wood Material Science & Engineering*, *14*(6), 437–444. https://doi.org/10.1080/17480272.2019.1650828

CRC handbook of chemistry and physics: A ready-reference book of chemical and physical data (93. ed., 2012 - 2013). (2012). CRC Press.

D´Ayala, D., Branco, J. M., Riggio, M., Harte, A., Kurz, J. & Descamps, T. (2014). Assessment, Reinforcement and Monitoring of Timber Structures: FPS COST Action FP1101. *Proceedings of the World Conference on Timber Engineering, WCTE Quebec City*.

Dafico, L. C. M., Barreira, E., Almeida, R. M. S. F. & Carasek, H. (2022). Comparison of Infrared Thermography and Other Traditional Techniques to Assess Moisture Content of Wall Specimens. *Sensors (Basel, Switzerland)*, *22*(9). https://doi.org/10.3390/s22093182

Dai, G. & Ahmet, K. (2001). Long-term monitoring of timber moisture content below the fiber saturation point using wood resistance sensors. *Forest Products Journal*, *51*(5), 52–58.

Danzer, M., Dietsch, P. & Winter, S. (2022). Effect of shrinkage on cracking and structural behaviour of reinforced glulam members. *Construction and Building Materials*, *327*, 125977. https://doi.org/10.1016/j.conbuildmat.2021.125977

Dietsch, P., Franke, S., Franke, B., Gamper, A. & Winter, S. (2015). Methods to determine wood moisture content and their applicability in monitoring concepts. *Journal of Civil Structural Health Monitoring*, *5*(2), 115–127. https://doi.org/10.1007/s13349-014-0082-7

Dietsch, P., Gamper, A., Merk, M. & Winter, S. (2015). Monitoring building climate and timber moisture gradient in large-span timber structures. *Journal of Civil Structural Health Monitoring*, *5*(2), 153–165. https://doi.org/10.1007/s13349-014-0083-6

Dietsch, P. & Winter, S. (2018). Structural failure in large-span timber structures: A comprehensive analysis of 230 cases. *Structural Safety*, *71*, 41–46. https://doi.org/10.1016/j.strusafe.2017.11.004

Dionisi-Vici, P., Allegretti, O., Braovac, S., Hjulstad, G., Jensen, M. & Storbekk, E. (2013). The Oseberg ship. Long-term physical-mechanical monitoring in an uncontrolled RH exhibition environment. Analytical results and hygromechanical modeling. In J. Smith & J. Ashley-Smith (Hrsg.), *Climate for collections: Standards and uncertainties: Postprints of the Munich Climate Conference, 7 to 9 November 2012* (1st. publ, S. 284–298). Archetype Publ. https://doi.org/10.13140/2.1.3385.0567

Dionisi-Vici, P., Mazzanti, P. & Uzielli, L. (2006). Mechanical response of wooden boards subjected to humidity step variations: climatic chamber measurements and fitted mathematical models. *Journal of Cultural Heritage*, *7*(1), 37–48. https://doi.org/10.1016/j.culher.2005.10.005

Dorn, M., Larsson, C. & Abdeljaber, O. (2022). Coupling of Weather Data to Moisture Content in a Timber Building. *Proceedings of the 6th International Conference on Structural Health Assessment of Timber Structures (SHATIS)*, 150–155.

Dremelj, M. & Straže, A. (2022). Vpliv naravnega staranja na izbrane fizikalne in mehanske lastnosti konstrukcijskega lesa. *Les/Wood*, *71*(2), 45–56. https://doi.org/10.26614/les-wood.2022.v71n02a05

Du, Q. P., Geissen, A. & Noack, D. (1991). Widerstandskennlinien einiger Handelshölzer und ihre Meßbarkeit bei der elektrischen Holzfeuchtemessung. *European Journal of Wood and Wood Products*, *49*(7-8), 305–311. https://doi.org/10.1007/BF02663796

Dupleix, A., van Nguyen, T., Vahtikari, K. & Hughes, M. (2018). The anisotropic temperature rise on wood surfaces during adsorption measured by thermal imaging. *Wood Science and Technology*, *52*(1), 167–180. https://doi.org/10.1007/s00226-017-0968-8

Dyken, T. & Kepp, H. (2010). Monitoring the Moisture Content of Timber Bridges. *Proceedings of the International Conference on Timber Bridges (ITCB 2010)*, 223–235.

Emmerich, L. & Brischke, C. (2021). Electrical moisture content measurements of modified wood: Determination of resistance characteristics and outdoor monitoring. *holztechnologie*, *2*(62), 11–22.

Engelhardt, M. (2017, 17. Mai). *Freie Konvektion in Faserdämmstoffen: Hintergrund und praktische Auswirkung.* Forschungsinstitut für Wärmeschutz e.V., München.

Erhardt, W. D. & Mecklenburg, M. F. (1995). Accelerated VS Natural Aging: Effect of Aging Conditions on the Aging Process of Cellulose. *MRS Proceedings*, *352.* https://doi.org/10.1557/PROC-352-247

Fachkunde Elektrotechnik (28., überarb. und erw. Aufl.). (2012). *Europa-Fachbuchreihe für elektrotechnische Berufe*. Verl. Europa-Lehrmittel Nourney Vollmer.

Fan, K., Hatzikiriakos, S. G. & Avramidis, S. (1999). Determination of the surface fractal dimension from sorption isotherms of five softwoods. *Wood Science and Technology*, *33*(2), 139–149. https://doi.org/10.1007/s002260050105

Fernando, D., Teng, J.-G. & Torero, J. L. (2015). Structural Health Monitoring of an Innovative Timber Building. *Proceedings of the Second International Conference on Performance-based and Lifecycle Structural Engineering*, 1383–1392.

Flexeder, N. (2021, 8. September). *WCTE 2021 - MONITORING OF AN OFFICE BUILDING IN UNINSULATED CROSS LAMINATED TIMBER CONSTRUCTION REGARDING HYGROTHERMAL COMPONENT BEHAVIOR: - Video-Presentation by Nina Flexeder.* World Conference on Timber Engineering. WCTE 2021, Round Table on 21/08/09 in Room No. 2. https://www.youtube.com/watch?v=gbck-jrednM

Flexeder, N. (2022a). *Geometry data of a sensor envelope for the hygrometric method to determine material moisture content.* Technische Universität München. doi: 10.14459/2022mp1651104.

Flexeder, N. (2022b). *Geometry data of a sensor mount for surface temperature measurements.* Technische Universität München. doi: 10.14459/2022mp1651103.

Flexeder, N., Kamml, M. & Paulik, J. (2022). *Anlagen zum Forschungsbericht. Potenziale hygrothermisch aktivierter Bauteile (PhyTAB): Anlagen zur BBSR-Online-Publikation 17/2022* (Innovationsprogramm Zukunft Bau, Bundesinstitut für Bau-, Stadt- und Raumforschung im Auftrag des Bundesministeriums für Wohnen, Stadtentwicklung und Bauwesen (BMWSB) Anhang zur ISSN 1868-0097). https://mediatum.ub.tum.de/1713792

Flexeder, N., Nouman, A. S. & Hepf, C. (2022). Measurement of Sorption Heat in Laboratory and Field Tests in Comparison with Hygrothermal Simulations. *Proceedings of BauSIM 2022.* Vorab-Onlinepublikation. https://doi.org/10.14459/2022md1688193

Flexeder, N., Ott, S., Bodemer, E. & Winter, S. (2021). Monitoring of an office building in uninsulated cross laminated timber (CLT) construction regarding hygrothermal component behavior. *Proceedings of WCTE 2021 - World Conference on TImber Engineering*.

Flexeder, N., Schenk, M. & Aondio, P. (2022). Moisture Monitoring Techniques for the Protection of Timber Structures. *Proceedings of the International Conference on Structural Health Assessment of Timber Structures (SHATIS).* Vorab-Onlinepublikation. https://doi.org/10.14459/2022md1687361

Flexeder, N., Schumacher, N., Hepf, C., Nouman, A., Briels, D., Varga, Z., Kamml, M., Paulik, J., Übelhör, V., Winter, S. & Auer, T. (2022). *PhyTAB – Potenziale hygrothermisch aktivierter Bauteile: Energieeffiziente Raumkonditionierung mittels luftdurchströmter Massivholzelemente und hygroskopisch optimierter Oberflächen*. Report. *BBSR-Online-Publikation: 17/2022*. BBSR-Online Publikation.

Forest Products Laboratory. (2021). *Wood handbook—wood as an engineering material: General Technical Report FPL-GTR-282.*

Forsén, H. & Tarvainen, V. (2000). *Accuracy and functionality of hand held wood moisture content meters*. *VTT publications: Bd. 420*. Technical Research Centre of Finland.

Fortino, S [Stefania], Genoese, A [Alessandra], Genoese, A [Andrea], Nunes, L. & Palma, P. (2013). Numerical modelling of the hygro-thermal response of timber bridges during their service life: A monitoring case-study. *Construction and Building Materials*, *47*, 1225–1234. https://doi.org/10.1016/j.conbuildmat.2013.06.009

Fortino, S [Stefania], Hradil, P., Koski, K., Korkealaakso, A., Fülöp, L., Burkart, H. & Tirkkonen, T. (2021). Health Monitoring of Stress-Laminated Timber Bridges Assisted by a Hygro-Thermal Model for Wood Material. *Applied Sciences*, *11*(1), 98. https://doi.org/10.3390/app11010098

Fortuin, G. (2003). *Anwendung mathematischer Modelle zur Beschreibung der technischen Konvektionstrocknung von Schnittholz* [Dissertation]. Universität Hamburg, Hamburg.

Fouad, N. A. (Hrsg.). (2022). *Bauphysik-Kalender Ser*. *Bauphysik-Kalender 2022: Schwerpunkt: Holzbau*. Wilhelm Ernst & Sohn Verlag fur Architektur und Technische.

Frandsen, H. L., Damkilde, L. & Svensson, S. (2007). A revised multi-Fickian moisture transport model to describe non-Fickian effects in wood. *Holzforschung*, *61*(5), 563–572. https://doi.org/10.1515/HF.2007.085

Franke, B., Müller, A., Franke, S. & Magnière, N. (2016). *Langzeituntersuchung zu den Auswirkungen wechselnder Feuchtegradienten in blockverleimten Brettschichtholzträgern: Forschungsbericht*. Berner Fachhochschule Architektur Holz und Bau Institut für Holzbau Tragwerke und Architektur.

Franke, B., Widmann, R., Müller, A. & Tannert, T. (2013). Assessment and monitoring of the moisture content of timber bridges. *Proceedings of the International Conference on Timber Bridges, Las Vegas, Nevada, USA*.

Franke, L., Niemann, A., Jarmer, T., Varga, Z., Flexeder, N., Kränkel, T., Diewald, F., Ficht, R., Nouman, A., Karghuber, J., Auer, T., Nagler, F. & Winter, S. (2024). *Einfach Bauen 3 – Messen, Validieren, Rückkoppeln: Monitoring der Pilothäuser aus Massivholz, Leichtbeton und hochwärmedämmendem Mauerwerk aus Einfach Bauen 2 und Validierung der Ergebnisse.* (ISSN 1868-0097). Technische Universität München.

Fraunhofer IBP. *WUFI Literature*. https://wufi.de/de/literatur/

Fredriksson, M. (2013). *Moisture conditions in rain exposed wood joints - Experimental methods and laboratory measurements*. Division of Building Materials, LTH, Lund University.

Fredriksson, M., Claesson, J. & Wadsö, L. (2015). The Influence of Specimen Size and Distance to a Surface on Resistive Moisture Content Measurements in Wood. *Mathematical Problems in Engineering*, *2015*, 1–7. https://doi.org/10.1155/2015/215758

Fredriksson, M., Wadsö, L. & Johansson, P. (2013). Small resistive wood moisture sensors: a method for moisture content determination in wood structures. *European Journal of Wood and Wood Products*, *71*(4), 515–524. https://doi.org/10.1007/s00107-013-0709-0

Gamper, A., Dietsch, P., Merk, M. & Winter, S. (2013). Gebäudeklima - Langzeitmessung zur Bestimmung der Auswirkungen auf Feuchtegradienten in Holzbauteilen. *Bautechnik*, *90*(8), 508–519. https://doi.org/10.1002/bate.201300010

Ganster, K., Ringhofer, A. & Schickhofer, G. (2019). Experimentelle und numerische Untersuchungen des hygrothermischen Verhaltens von Brettsperrholz am Beispiel einer Außenwand. *Bauphysik*, *41*(5), 252–268. https://doi.org/10.1002/bapi.201900019

García Esteban, L., García Fernández, F., Guindeo Casasús, A., palacios Palacios, P. de & Gril, J. (2006). Comparison of the hygroscopic behaviour of 205-year-old and recently cut juvenile wood from Pinus sylvestris L. *Annals of Forest Science*, *63*(3), 309–317. https://doi.org/10.1051/forest:2006010

Garrahan, P. (1988). Moisture meter correction factors for high temperature dimension lumber. In https://www.semanticscholar.org/paper/Moisture-meter-correction-factors-for-high-lumber-Garrahan/65055f593ca23ac510270f8fe34bd5333666ffbc

Gebhardt, C., Konopka, D., Börner, A., Mäder, M. & Kaliske, M. (2018). Hygro-mechanical numerical investigations of a wooden panel painting from "Katharinenaltar" by Lucas Cranach the Elder. *Journal of Cultural Heritage*, *29*, 1–9. https://doi.org/10.1016/j.culher.2017.08.003

Gereke, T. (2009). *Moisture-induced Stresses in cross-laminated Wood Panels* [Dissertation]. ETH Zurich.

Gertis, K. & Schmidt, T. (2015). Zur Ermittlung der Sorptionsenthalpie von Baustoffen. *Bauphysik*, *37*(2), 71–80. https://doi.org/10.1002/bapi.201510009

Ghazi Wakili, K., Schiere, M., Bonifacio, S., Kauz, U., Maurer, J., Rüegsegger, L. & Müller, A. (2024). Monitoring climatic impacts on the moisture uptake of the first Swiss wildlife bridge made of wood. *European Journal of Wood and Wood Products.* Vorab-Onlinepublikation. https://doi.org/10.1007/s00107-024-02052-8

Glass, S. V., Zelinka, S. L. & Johnson, J. A. (2014). Investigation of Historic Equilibrium Moisture Content Data from the Forest Products Laboratory: General Technical Report FPL–GTR–229. Vorab-Onlinepublikation. https://doi.org/10.2737/FPL-GTR-229

Griesebner, M. & Egle, J. (2016). *Salzburger Holzbau 2020+: „holzAUFbau" Innovationsnetzwerkprojekt zur ökologischen und energetischen Weiterentwicklung marktgängiger Massivholzbaulösungen für zukunftsfähige, ressourcenschonende Bauweisen im Niedrigstenergie- und Plusenergiestandard*. Forschungsprojekt 20102-719/162/2013 RWF-Kooperationsprojekt „Salzburger Holzbau 2020+".

Grönquist, P., Flexeder, N., Franke, B. & Franke, S. (2022). Monitoring of Wood Moisture Content in Timber Structures by Electrical Resistance and the Sorption Methods: Current Challenges: State-of-the-Art Report (STAR) - CA20139 - WG4 Sustainability and Durability. *Sustainability and Durability of Taller Timber Buildings: A State-of-the-Art Report. COST Action CA20139 Holistic design of taller timber buildings (HELEN)*, Artikel WG4.SG4.02, 51–54. https://cahelen.eu/wp-content/uploads/2022/12/CA20139_STAR_WG4.pdf

Grönquist, P., Weibel, G., Leyder, C. & Frangi, A. (2021). Calibration of Electrical Resistance to Moisture Content for Beech Laminated Veneer Lumber "BauBuche S" and "BauBuche Q". *Forests*, *12*(5), 635. https://doi.org/10.3390/f12050635

Gullbrekken, L., Kvande, T., Jelle, B. & Time, B. (2016). Norwegian Pitched Roof Defects. *Buildings*, *6*(2), 24. https://doi.org/10.3390/buildings6020024

Hailwood, A. J. & Horrobin, S. (1946). Absorption of water by polymers: analysis in terms of a simple model. *Trans. Faraday Soc.*, *42*(0), B084-B092. https://doi.org/10.1039/TF946420B084

Hameury, S. (2005). Moisture buffering capacity of heavy timber structures directly exposed to an indoor climate: a numerical study. *Building and Environment*, *40*(10), 1400–1412. https://doi.org/10.1016/j.buildenv.2004.10.017

Hameury, S. & Lundström, T. (2004). Contribution of indoor exposed massive wood to a good indoor climate: in situ measurement campaign. *Energy and Buildings*, *36*(3), 281–292. https://doi.org/10.1016/j.enbuild.2003.12.003

Hedlin, C. P. (1968). Sorption isotherms of twelve woods at subfreezing temperatures. *Forest Products Journal*, *17*(12), 43–48.

Henderson, S. M. (1952). A basic concept of equilibrium moisture. *Agricultural Engineering*(33), 29–32.

Herm, C., Tietze, O., Belik, Z., Konopka, D., Trufanova, O., Fuhrmann, A., Weiß, B., Kaden, J. & Kaliske, M. (2021). The Icon Last Supper of the Iconostasis of the Russian Memorial Church in Leipzig: Technological Investigation as Basis for the Modelling and the Numerical Simulation of Historical Works of Art. *Studies in Conservation*, 1–18. https://doi.org/10.1080/00393630.2021.1940021

Hielscher, M. (2022). Arbeiten erlaubt: Der Rohstoff Holz und seine Eigenschaften. *dds online*. https://www.dds-online.de/technik/eigenschaften-holz_arbeiten-erlaubt/

Holl, K. (2016). *Der Einfluss von Klimaschwankungen auf Kunstwerke im historischen Kontext* [Dissertation]. Technische Universität München.

holzbauaustria. (2021, 4. März). *Den Wert eines Gebäudes nachhaltig sichern* [Pressemitteilung]. https://www.holzbauaustria.at/markt/2021/03/wie-man-den-wert-eines-gebaeudes-nachhaltig-sichert.html

Holzforschung Austria. (2023, 16. Oktober). *ACR-INNO-VA-TI-ONS-PREIS FÜR DIGI-TA-LI-SIERTE HOLZ-BAU-TEILE* [Pressemitteilung]. https://www.holzforschung.at/aktuelles/details/acr-innovationspreis-fuer-digitalisierte-holzbauteile/

Hozjan, T., Turk, G., Srpcic, S. & Svensson, S. (2012). The effect of changing ambient humidity on moisture condition in timber elements. *Proceedings of World Conference on Timber Engineering 2012*, *12*, 316–320.

Inagaki, T., Yonenobu, H. & Tsuchikawa, S. (2008). Near-infrared spectroscopic monitoring of the water adsorption/desorption process in modern and archaeological wood. *Applied spectroscopy*, *62*(8), 860–865. https://doi.org/10.1366/000370208785284312

Ineichen, M. (2020). *Bestimmung und Gegenüberstellung der Materialkennwerte von hygroskopisch aktiven Baustoffen: Messmethoden, Kennlinienerstellung und Validierung zur feuchte- und zeitabhängigen Wasserdampfaufnahme und -abgabe ausgewählter Baustoffe* [Master´s Thesis]. Technische Universität München. https://mediatum.ub.tum.de/1611619

Informationsdienst Holz. (2022, 4. Februar). *Projekt 'Motorholz' im Institut für Holztechnologie Dresden* [Pressemitteilung]. https://informationsdienst-holz.de/details/nutzung-des-schwindens-und-quellens-von-holz

Ingleby, B., Moore, D., Sloan, C. & Dunn, R. (2013). Evolution and Accuracy of Surface Humidity Reports *Journal of Atmospheric and Oceanic Technology*, *30*(9), 2025–2043. https://doi.org/10.1175/JTECH-D-12-00232.1

Jakes, J. E., Zelinka, S. L., Hunt, C. G., Ciesielski, P., Frihart, C. R., Yelle, D., Passarini, L., Gleber, S.-C., Vine, D. & Vogt, S. (2020). Measurement of moisture-dependent ion diffusion constants in wood cell wall layers using time-lapse micro X-ray fluorescence microscopy. *Scientific reports*, *10*(1), 9919. https://doi.org/10.1038/s41598-020-66916-8

James, W. L. (1963). Electric moisture meters for wood: US forest service research note FPL-08. *US Forest Service, Forest Products Laboratory*, 1–24.

James, W. L. (1988). Electric moisture meters for wood. Vorab-Onlinepublikation. https://doi.org/10.2737/FPL-GTR-6

Jarmer, T., Niemann, A., Franke, L., Varga, Z., Diewald, F., Nagler, F. & Auer, T. (2021). *EINFACH BAUEN 2 – Planen, Bauen, Messen.* https://doi.org/10.14459/2021md1617984

Jiang, Y., Dietsch, P., Oberhardt, F. & Simon, J. (2018). *Landwirtschaftliche Nutzgebäude in Holzbauweise ohne vorbeugenden chemischen Holzschutz (Gebrauchsklasse 0 (GK 0): Besondere bauliche Maßnahmen in Anlehnung an DIN 68800* [Forschungsbericht]. Technische Universität München; LfL - Bayerische Landesanstalt für Landwirtschaft, München. https://www.cee.ed.tum.de/fileadmin/w00cbe/hbb/04_Forschung/02_Abgeschlossene_Forschungsprojekte/2018/18_SB_Landwirtschaftliche_Nutzgebaeude.pdf

Joščák, M. (2013). *Experimentelle und rechnerische Charakterisierung des Wärme- und Feuchtetransportes in Holzbauteilen mit variablem Aufbau* [Dissertation]. ETH, Zürich.

Joščák, M., Sonderegger, W., Niemz, P., Holm, A., Krus, M., Großkinsky, T., Lengsfeld, K., Grunewald, J. & Plagge, R. (2011). *Vergleichende Untersuchungen zum Feuchte- und Wärmeverhalten unterschiedlicher Holzbauelemente* (Nr. 5). https://wufi.de/literatur/Joscak,%20Sonderegger%20et%20al%202011%20-%20Vergleichende%20Untersuchungen%20zum%20Feuchte.pdf https://doi.org/10.1002/bapi.201110796

Kalbe, K., Kalamees, T., Kukk, V., Ruus, A. & Annuk, A. (2022). Wetting circumstances, expected moisture content, and drying performance of CLT end-grain edges based on field measurements and laboratory analysis. *Building and Environment*, *221*, 109245. https://doi.org/10.1016/j.buildenv.2022.109245

Kamei, S. (1937). Untersuchung über die Trocknung fester Stoffe: Bd. III. *Memoirs of the College of Engineering, Kyoto Imperial University*(X), 65–115.

Kang, Y., Jo, H. H. & Kim, S. (2024). Enhancing indoor comfort and building energy efficiency with cross-laminated timber (CLT) in hygrothermal environments. *Journal of Building Engineering*, *84*, 108582. https://doi.org/10.1016/j.jobe.2024.108582

Kasal, B [Bo] (2013). Assessment, Reinforcement and Monitoring of Timber Structures – COST FP1101. *Advanced Materials Research*, *778*, 1037–1040. https://doi.org/10.4028/www.scientific.net/AMR.778.1037

Kawai, S [S.], Yokoyama, M [M.], Matsuo, M [M.] & Sugiyama, J [J.] (2008). Research on the aging of wood in RISH. *Wood science for preservation of cultural heritage: mechanical and biological factors*, 52–56.

Keylwerth, R. (1949a). Einfache Kontrollmessung bei der Holztrocknung. *Holz-Zentralblatt*, *75*(26), 307–309.

Keylwerth, R. (1949b). Die Ermittlung der Trockenzeit bei künstlicher Holztrocknung. *Holz-Zentralblatt*, *75*(59), 735.

Keylwerth, R. & Noack, D. (1964). Die Kammertrocknung von Schnittholz: Bundesforschungsanstalt für Forst-und Holzwirtschaft, Reinbek Institut für Holzphysik und mechanische Holztechnologie. *European Journal of Wood and Wood Products*, *22*(1), 29–36. https://doi.org/10.1007/BF02627726

Klähn, G. (2023). *Grundlagen der Elektrotechnik*. https://www.elektrotechnik-fachbuch.de/e_grundlagen_kap_04_5v5.html

Kobori, H., Gorretta, N., Rabatel, G., Bellon-Maurel, V., Chaix, G., Roger, J.-M. & Tsuchikawa, S. (2013). Applicability of Vis-NIR hyperspectral imaging for monitoring wood moisture content (MC). *hfsg*, *67*(3), 307–314. https://doi.org/10.1515/hf-2012-0054

Kobori, H., Inagaki, T., Fujimoto, T., Okura, T. & Tsuchikawa, S. (2015). Fast online NIR technique to predict MOE and moisture content of sawn lumber. *Holzforschung*, *69*(3), 329–335. https://doi.org/10.1515/hf-2014-0021

Koch, J [Johannes], Simon, A. & Arndt, R. W. (2016). Monitoring of Moisture Content of protected Timber Bridges. *Proceedings of World Conference on Timber Engineering 2016*.

Kohara, J. & Okamoto, H. (1955). Studies of Japanese old timbers. *Sci Rep Saikyo University*(7 (1a), 9–20.

Kollmann, F. (1934). Über die wärmetechnischen Eigenschaften der Hölzer. *Gesundheits-Ingenieur*, *57*, 224–238.

Kollmann, F. (1949). Hitzevergütung von Holz und Holzwerkstoffen. *Holz-Zentralblatt*, *75*(6-8), 47–72.

Kollmann, F. (1951). *Technologie des Holzes und der Holzwerkstoffe: Anatomie und Pathologie, Chemie, Physik Elastizität und Festigkeit*. Springer Berlin Heidelberg. https://doi.org/10.1007/978-3-642-49758-2

Kollmann, F. (1987). Poren und Porigkeit in Hölzern. *Holz als Roh- und Werkstoff*(45), 1–9.

Konopka, D., Ehricht, S. & Kaliske, M. (2019). Hygro-mechanical investigations of clavichord replica at cyclic climate load: Experiments and simulations. *Journal of Cultural Heritage*, *36*, 210–221. https://doi.org/10.1016/j.culher.2018.07.006

Konopka, D., Stöcklein, J. & Kaliske, M. (2020). Neue numerische Simulation für alte Holzkonstruktionen. *Bautechnik*, *97*(10), 708–716. https://doi.org/10.1002/bate.202000055

Kordziel, S., Glass, S. V., Boardman, C. R., Munson, R. A., Zelinka, S. L., Pei, S. & Tabares-Velasco, P. C. (2020). Hygrothermal characterization and modeling of cross-laminated timber in the building envelope. *Building and Environment*, *177.* https://doi.org/10.1016/j.buildenv.2020.106866

Kordziel, S., Pei, S., Glass, S. V., Zelinka, S. & Tabares-Velasco, P. C. (2019). Structure Moisture Monitoring of an 8-Story Mass Timber Building in the Pacific Northwest. *Journal of Architectural Engineering*, *25*(4), Artikel 04019019. https://doi.org/10.1061/(ASCE)AE.1943-5568.0000367

Kornadt, O., Carrigan, S., Schöndube, T., Winter, S., Mindrup, K. & Knieriemen, G. (2019). *Dynamisch thermisch-hygrisches Verhalten von Massivbaukonstruktionen: Entwicklung eines Wärmespeicherfähigkeitsindex für Gebäude aus Mauerwerk und thermisch aktivierbare Massivholzelemente*. *Forschungsinitiative Zukunft Bau: F 3129*. Fraunhofer IRB Verlag.

Kornadt, O., Geyer, C. & Hofmann, M. (2010). Abhängigkeiten des Raumklimas im jahreszeitlichen Verlauf. *Bauphysik*, *32*(2), 73–82. https://doi.org/10.1002/bapi.201010009

Kossatz, G., Drewes, H., Kratz, W. & Mehlhorn, L. (1982). Sorptionsverhalten von Holzwerkstoffen in verschiedenen Umgebungsklimaten. In J. Ehlbeck & G. Steck (Hrsg.), *Ingenieurholzbau in Forschung und Praxis: Karl Möhler gewidmet* (S. 75–82). Bruderverl.

Kozlov, V. & Kisternaya, M. (2014). Sorption properties of historic and recent pine wood. *International Biodeterioration & Biodegradation*, *86*, 153–157. https://doi.org/10.1016/j.ibiod.2013.06.020

Kraniotis, D., Nore, K., Brückner, C. & Nyrud, A. Q. (2016). Thermography measurements and latent heat documentation of Norwegian spruce (*Picea abies*) exposed to dynamic indoor climate. *Journal of Wood Science*, *62*(2), 203–209. https://doi.org/10.1007/s10086-015-1528-1

Kránitz, K., Sonderegger, W., Bues, C.-T. & Niemz, P. (2016). Effects of aging on wood: a literature review. *Wood Science and Technology*, *50*(1), 7–22. https://doi.org/10.1007/s00226-015-0766-0

Krischer, O. (1978). *Die wissenschaftlichen Grundlagen der Trocknungstechnik* (3., neubearb. Aufl.). *Trocknungstechnik / von Otto Krischer und Karl Kröll. Begr. von Otto Krischer: Bd. 1*. Springer.

Krüger, M. & Lehmann, F. (2019). Instrumentiertes Feuchtemonitoring von historischen Bauwerken mittels elektrischer Impedanzspektroskopie. *Bautechnik*, *96*(9), 696–701. https://doi.org/10.1002/bate.201900055

Krüger, M. & Lehmann, F. (2020). Instrumentiertes Feuchtemonitoring von historischen Bauwerken mittels elektrischer Impedanzspektroskopie. *Mauerwerk*, *24*(4), 248–253. https://doi.org/10.1002/dama.202010025

Krupińska, B., Strømmen, I., Pakowski, Z. & Eikevik, T. M. (2007). Modeling of Sorption Isotherms of Various Kinds of Wood at Different Temperature Conditions. *Drying Technology*, *25*(9), 1463–1470. https://doi.org/10.1080/07373930701537062

Kukk, V., Adeniyi, B., Kers, J. & Kalamees, T. (2021). Air Permeability Properties of Cross-Laminated Timber Envelopes. *Proceedings of WCTE 2021 - World Conference on TImber Engineering*.

Kukk, V., Kaljula, L., Kers, J. & Kalamees, T. (2022). Designing highly insulated cross-laminated timber external walls in terms of hygrothermal performance: Field measurements and simulations. *Building and Environment*, *212*, 108805. https://doi.org/10.1016/j.buildenv.2022.108805

Künzel, H. M. (1994). *Verfahren zur ein- und zweidimensionalen Berechnung des gekoppelten Wärme- und Feuchtetransports in Bauteilen mit einfachen Kennwerten* [Dissertation]. Universität Stuttgart, Stuttgart.

Künzel, H. M., Holm, A., Sedlbauer, K., Antretter, F. & Ellinger, M. (2004). *Moisture buffering effects of interior linings made from wood or wood based products: Investigations commissioned by Wood Focus Oy and the German Federal Ministry of Economics and Labour* (IBP Report HTB-04/2004/e). Fraunhofer Institut für Bauphysik.

Lanata, F. (2015). Monitoring the long-term behaviour of timber structures. *Journal of Civil Structural Health Monitoring*, *5*(2), 167–182. https://doi.org/10.1007/s13349-014-0095-2

Lang, A. (2004). *Charakterisierung des Altholzaufkommens in Deutschland (Characterisation of the waste wood situation in Germany)* [Dissertation]. Universität Hamburg.

Larsson, C., Abdeljaber, O., Bolmsvik, Å. & Dorn, M. (2022). Long-term analysis of the environmental effects on the global dynamic properties of a hybrid timber-concrete building. *Engineering Structures*, *268*, 114726. https://doi.org/10.1016/j.engstruct.2022.114726

Leblon, B., Adedipe, O., Hans, G., Haddadi, A., Tsuchikawa, S., Burger, J., Stirling, R., Groves, K., Nader, J. & LaRocque, A. (2013). A review of near-infrared spectroscopy for monitoring moisture content and density of solid wood. *The Forestry Chronicle*, *5*(89), 595–606.

Lechner, M. (2021). *Holzbewehrtes Holz - Entwicklung eines furnierverstärkten stabförmigen Holzprodukts für tragende Zwecke: english: Veneer-reinforced timber - Development of a veneer-reinforced timber product for load-bearing purposes* [Dissertation]. Technische Universität München.

Legros, C., Piot, A., Woloszyn, M. & Pailha, M. (2020). Effect of moisture buffering on surface temperature variation: study of different indoor cladding materials. *E3S Web of Conferences*, *172*, 6002. https://doi.org/10.1051/e3sconf/202017206002

Lehmann, F., Schreiner, M. & Reinhardt, H.-W. (2018). Instrumentierte Bauwerksüberwachung im Kontext historischer Bauten. *Bautechnik*, *95*(1), 1–5. https://doi.org/10.1002/bate.201700049

Lewicki, P. P. (2012). Data and Models of Water Activity.: II: Solid Foods. In *CRC handbook of chemistry and physics: A ready-reference book of chemical and physical data* (93. ed., 2012 - 2013, S. 67–151). CRC Press. Chapter 4.

Li, Y., Fazio, P. & Rao, J. (2012). An investigation of moisture buffering performance of wood paneling at room level and its buffering effect on a test room. *Building and Environment*, *47*, 205–216. https://doi.org/10.1016/j.buildenv.2011.07.021

Liu, F., Jia, B., Chen, B. & Geng, W. (2017). Moisture transfer in building envelope and influence on heat transfer. *Procedia Engineering*, *205*, 3654–3661. https://doi.org/10.1016/j.proeng.2017.10.229

Ltd., A.-S. E. C. (1935). *Instrument for the measurement of moisture in wood*.

Ma, T., Morita, G., Inagaki, T. & Tsuchikawa, S. (2022). Moisture transport dynamics in wood during drying studied by long-wave near-infrared hyperspectral imaging. *Cellulose*, *29*(1), 133–145. https://doi.org/10.1007/s10570-021-04290-y

MacMillan, B., Veliyulin, E., Lamason, C. & Balcom, B. J. (2011). Quantitative magnetic resonance measurements of low moisture content wood 1 This article is a contribution to the series The Role of Sensors in the New Forest Products Industry and Bioeconomy. *Canadian Journal of Forest Research*, *41*(11), 2158–2162. https://doi.org/10.1139/x11-081

Mahnert, K.-C. & Hundhausen, U. (2018). A review on the protection of timber bridges. *Wood Material Science & Engineering*, *13*(3), 152–158. https://doi.org/10.1080/17480272.2017.1403955

Mai, T. C., Razafindratsima, S., Sbartaï, Z. M., Demontoux, F. & Bos, F. (2015). Non-destructive evaluation of moisture content of wood material at GPR frequency. *Construction and Building Materials*, *77*, 213–217. https://doi.org/10.1016/j.conbuildmat.2014.12.030

Maxim Integrated Products Inc. (2012). *MAX31865 RTD-to-Digital Converter*. https://datasheets.maximintegrated.com/en/ds/MAX31865.pdf

McClung, R., Ge, H., Straube, J. & Wang, J. (2014). Hygrothermal performance of cross-laminated timber wall assemblies with built-in moisture: field measurements and simulations. *Building and Environment*, *71*, 95–110. https://doi.org/10.1016/j.buildenv.2013.09.008

Meier, E. (August 2023). *The Wood Database: Pine Wood: An Overall Guide*. https://www.wood-database.com/pine-wood-an-overall-guide/

Meierhofer, U., Sell, J. & Strässler, H. (1982). Zur Wetterbeanspruchung tragender Holzbauteile. In J. Ehlbeck & G. Steck (Hrsg.), *Ingenieurholzbau in Forschung und Praxis: Karl Möhler gewidmet* (S. 67–74). Bruderverl.

Melin, C. B., Gebäck, T., Geynts, A. & Bjurman, J. (2016). Monitoring Dynamic Moisture Gradients in Wood using Inserted Relative Humidity and Temperature Sensors. In.

Metsä-Kortelainen, S., Antikainen, T. & Viitaniemi, P. (2006). The water absorption of sapwood and heartwood of Scots pine and Norway spruce heat-treated at 170 °C, 190 °C, 210 °C and 230 °C. *Holz als Roh- und Werkstoff*, *64*(3), 192–197. https://doi.org/10.1007/s00107-005-0063-y

Mindrup, K. (2020). *Raumklimatisierung durch thermisch aktivierte Massivholzelemente* [Dissertation]. Technische Universität München.

Mönck, W. & Erler, K. (2004). *Schäden an Holzkonstruktionen. Analyse und Behebung: das Standardwerk für Sanierung*. 4., stark bearbeitete Auflage. Huss-Medien, Verl. Bauwesen.

Morishita, C., Berger, J. & Mendes, N. (2020). Weather-based indicators for analysis of moisture risks in buildings. *The Science of the total environment*, *709*, 134850. https://doi.org/10.1016/j.scitotenv.2019.134850

Mulloni, V., Marchi, G., Gaiardo, A., Valt, M., Donelli, M. & Lorenzelli, L. (2024). Applications of Chipless RFID Humidity Sensors to Smart Packaging Solutions. *Sensors (Basel, Switzerland)*, *24*(9). https://doi.org/10.3390/s24092879

Niemz, P. (2021). *Holzphysik : Eigenschaften, Prüfung und Kennwerte: Physik des Holzes und der Holzwerkstoffe : mit zahlreichen Bildern und Tabellen*. Hanser. http://www.hanser-fachbuch.de/9783446445260

Niemz, P. (1. Juli 2022). Rissbildung bei BSH und BSP in Innenräumen: Verschiedene Methoden helfen gegen Rissbildung, Delaminierung und Verschmutzung. *Holz-Zentralblatt*, S. 427–429.

Niemz, P. & Sonderegger, W. (2007). Sorptionsisothermen ausgewählter heimischer und fremdländischer Holzarten bei Adsorption und Desorption. *Bauphysik*, *29*(5), 381–382. https://doi.org/10.1002/bapi.200710049

Niemz, P. & Sonderegger, W. (2011). Untersuchungen zur Wärmeleitung von Vollholz und Werkstoffen auf Vollholzbasis, wesentliche Einflussfaktoren. *Bauphysik*, *33*(5), 299–305. https://doi.org/10.1002/bapi.201110793

Niemz, P., Teischinger, A. & Sandberg, D. (Hrsg.). (2023). *Springer Handbook of Wood Science and Technology*. Springer International Publishing. https://doi.org/10.1007/978-3-030-81315-4

Niklewski, J., Brischke, C. & Frühwald Hansson, E. (2021). Numerical study on the effects of macro climate and detailing on the relative decay hazard of Norway spruce. *Wood Material Science & Engineering*, *16*(1), 12–20. https://doi.org/10.1080/17480272.2019.1608296

Norberg, P. (1999). Monitoring wood moisture content using the WETCORR method. *European Journal of Wood and Wood Products*, *57*(6), 448–453. https://doi.org/10.1007/s001070050072

Nore, K [Kristine], Nyrud, A. Q [A. Q.], Kraniotis, D [D.], Skulberg, K. R., Englund, F. & Aurlien, T. (2017). Moisture buffering, energy potential and volatile compound emissions of wood exposed to indoor environments. *Science and Technology for the Built Environment*, *23*, 512–521.

Obataya, E. (2017). Effects of natural and artificial ageing on the physical and acoustic properties of wood in musical instruments. *Journal of Cultural Heritage*, *27*, S63-S69. https://doi.org/10.1016/j.culher.2016.02.011

Ott, S. & Aondio, P. (2020, 20. Oktober). Observations of Moisture Damages in Historic and Modern Wooden Constructions. In *XV International Conference on Durability of Building Materials and Components. eBook of Proceedings.* CIMNE. https://doi.org/10.23967/dbmc.2020.102

Otten, K. A., Brischke, C. & Meyer, C. (2017). Material moisture content of wood and cement mortars – Electrical resistance-based measurements in the high ohmic range. *Construction and Building Materials*, *153*, 640–646. https://doi.org/10.1016/j.conbuildmat.2017.07.090

Palma, P. & Steiger, R. (2020). Structural health monitoring of timber structures – Review of available methods and case studies. *Construction and Building Materials*, *248*, 118528. https://doi.org/10.1016/j.conbuildmat.2020.118528

Pfaff, F., Garrahan, P., Clubs, W. D. K. & Western Dry Kiln Clubs. Meeting (1985). New temperature correction fractors for the portable resistance-type moisture meter. *Forest Products Journal*, *36*, 28–30. https://www.semanticscholar.org/paper/New-temperature-correction-fractors-for-the-meter-Pfaff-Garrahan/28fe4bad71e9be0124e01f6853d8a152c89f9169

Phymeas GbR. *Phymeas Heat Flux Sensors with temperature sensor (PT 100 Kl. A DIN IEC 751)*. https://www.phymeas.de/?page_id=2&lang=en

Popper, R. & Niemz, P. (2009). Wasserdampfsorptionsverhalten ausgewählter heimischer und überseeischer Holzarten. *Bauphysik*, *31*(2), 117–121. https://doi.org/10.1002/bapi.200910017

Popper, R., Niemz, P. & Eberle, G. (2005). Untersuchungen zum Sorptions- und Quellungsverhalten von thermisch behandeltem Holz. *Holz als Roh- und Werkstoff*, *63*(2), 135–148. https://doi.org/10.1007/s00107-004-0554-2

Prado, P. J. (2001). NMR hand-held moisture sensor. *Magnetic resonance imaging*, *19*(3-4), 505–508. https://doi.org/10.1016/S0730-725X(01)00279-X

Rahman, M. S. (Hrsg.). (2008). *Contemporary Food Science: v.v. 3. Food Properties Handbook, Second Edition* (2nd ed.). Taylor and Francis. http://gbv.eblib.com/patron/FullRecord.aspx?p=566061

Razafindratsima, S., Sbartaï, Z. M. & Demontoux, F. (2017). Permittivity measurement of wood material over a wide range of moisture content. *Wood Science and Technology*, *51*(6), 1421–1431. https://doi.org/10.1007/s00226-017-0935-4

Riedel, B. & Walter, T. (1989). Widerstandsmessung von antistatisch beschichteten Holzwerkstoffen. *HK Holz-Möbelindustrie*, *25*(6), 775–777.

Riggio, M., Anthony, R. W., Augelli, F., Kasal, B [Bohumil], Lechner, T., Muller, W. & Tannert, T. (2014). In situ assessment of structural timber using non-destructive techniques. *Materials and Structures*, *47*(5), 749–766. https://doi.org/10.1617/s11527-013-0093-6

Riggio, M. & Dilmaghani, M. (2020). Structural health monitoring of timber buildings: a literature survey. *Building Research & Information*, *48*(8), 817–837. https://doi.org/10.1080/09613218.2019.1681253

Riparbelli, L., Dionisi-Vici, P., Uzielli, L. & Gril, J. (2021). Integration of experimental and numerical methods to study the mechanical risk conditions for the conservation of unique art pieces: the case of the Mona Lisa. In M. Kaliske, D. Konopka, O. Tietze & C. Herm (Hrsg.), *Virt Ex: Virtual experiments for wooden artwork* (S. 58–69). Technische Universität Dresden.

Riparbelli, L., Mazzanti, P., Helfer, T., Manfriani, C., Uzielli, L., Castelli, C., Santacesaria, A., Ricciardi, L., Rossi, S., Gril, J. & Fioravanti, M. (2023). Modelling of hygro-mechanical behaviour of wooden panel paintings: model calibration and artworks characterisation. *Heritage Science*, *11*(1). https://doi.org/10.1186/s40494-023-00958-9

Rode, C. & Clorius, C. O. (2004). Modeling of Moisture Transport in Wood with Hysteresis and Temperature-Dependent Sorption Characteristics. *Buildings*(IX), 1–15.

Rode, C., Peuhkuri, R. H., Hansen, K. K [Kurt Kielsgaard], Time, B. & Svennberg, K. (2005). NORDTEST Project on Moisture Buffer Value of Materials. *AIVC 26th conference: Ventilation in relation to the energy performance of buildings. Air Infiltration and Ventilation*, 47–52.

Rode, C., Peuhkuri, R., Mortensen, L. H., Hansen, K. K [Kurt K.], Time, B., Gustavsen, A., Ojanen, T., Ahonen, J., Svennberg, K., Harderup, L.-E. & Arfvidsson, J. (2005). *Moisture Buffering of Building Materials* (Report BYG·DTU R-126, Proj.Nr.: 04023). Department of Civil Engineering, Technical University of Denmark.

Rodríguez-Abad, I., Martínez-Sala, R., García-García, F. & Capuz-Lladró, R. (2010). Non-destructive methodologies for the evaluation of moisture content in sawn timber structures: ground-penetrating radar and ultrasound techniques. *Near Surface Geophysics*, *8*(6), 475–482. https://doi.org/10.3997/1873-0604.2010048

Rosen H.N. (1978). The influence of external resistance on moisture absorption rates in wood. *J.Wood Fiber*, *10*(3), 218–228.

Rosenkilde, A. & Glover, P. (2002). High Resolution Measurement of the Surface Layer Moisture Content during Drying of Wood Using a Novel Magnetic Resonance Imaging Technique. *Holzforschung*, *56*(3), 312–317. https://doi.org/10.1515/HF.2002.050

Rowley, F. B. (1933). The heat conductivity of wood at climate temperature differences. *Heat. Pip. Air Condit.*, *5*, 313–323.

Rozas, C., Tomaselli, I. & Zanoelo, E. F. (2009). Internal mass transfer coefficient during drying of softwood (Pinus elliottii Engelm.) boards. *Wood Science and Technology*, *43*(5-6), 361–373. https://doi.org/10.1007/s00226-008-0223-4

Schaffrath, J. (2015). *Studies of moisture transport and moisture induced deformations and stresses in various wood species under different climatic conditions* [Dissertation]. Technical University of Munich.

Scheiding, W., Direske, M. & Zauer, M. (2016). Water absorption of untreated and thermally modified sapwood and heartwood of Pinus sylvestris L. *European Journal of Wood and Wood Products*, *74*(4), 585–589. https://doi.org/10.1007/s00107-016-1044-z

Schiere, M., Franke, B., Franke, S. & Müller, A. (2021a). Calibration and comparison of two moisture content measurement methods for in situ monitoring of beech laminated veneer lumber. *Wood Material Science & Engineering*, 1–12. https://doi.org/10.1080/17480272.2021.1958918

Schiere, M., Franke, B., Franke, S. & Müller, A. (2021b). Comparison between Predicted and Measured Moisture Content and Climate in 12 Monitored Timber Structures in Switzerland. *Buildings*, *11*(5), 181. https://doi.org/10.3390/buildings11050181

Schild, K. & Willems, W. M. (2013). *Wärmeschutz*. Springer Fachmedien Wiesbaden. https://doi.org/10.1007/978-3-658-02571-7

Schmidt, E. & Riggio, M. (2019). Monitoring Moisture Performance of Cross-Laminated Timber Building Elements during Construction. *Buildings*, *9*(6), 144. https://doi.org/10.3390/buildings9060144

Senni, L., Casieri, C., Bovino, A., Gaetani, M. C. & Luca, F. de (2009). A portable NMR sensor for moisture monitoring of wooden works of art, particularly of paintings on wood. *Wood Science and Technology*, *43*(1-2), 167–180. https://doi.org/10.1007/s00226-008-0200-y

Shabani, A., Kioumarsi, M., Plevris, V. & Stamatopoulos, H. (2020). Structural Vulnerability Assessment of Heritage Timber Buildings: A Methodological Proposal. *Forests*, *11*(8), 881. https://doi.org/10.3390/f11080881

Shi, J. & Avramidis, S. (2017a). Water sorption hysteresis in wood: I review and experimental patterns – geometric characteristics of scanning curves. *Holzforschung*, *71*(4), 307–316. https://doi.org/10.1515/hf-2016-0120

Shi, J. & Avramidis, S. (2017b). Water sorption hysteresis in wood: II mathematical modeling – functions beyond data fitting. *Holzforschung*, *71*(4), 317–326. https://doi.org/10.1515/hf-2016-0121

Shi, J. & Avramidis, S. (2017c). Water sorption hysteresis in wood: III physical modeling by molecular simulation. *Holzforschung*, *71*(9), 733–741. https://doi.org/10.1515/hf-2016-0231

Sieder, M., Plüss, Y., Biller, P. & tronnier, M. (2022). Erfassen der Feuchtespeicherung in Holz und Potenzial für Messsysteme zur Bauwerksüberwachung. In *Bauphysik-Kalender 2022* (Bd. 31, S. 227–248). https://doi.org/10.1002/9783433611081.ch7 (Erstveröffentlichung 2022)

Simón, C., Esteban, L. G., Palacios, P. de, Fernández, F. G. & García-Iruela, A. (2016). Thermodynamic properties of the water sorption isotherms of wood of limba (*Terminalia superba Engl. & Diels*), obeche (*Triplochiton scleroxylon K. Schum*.), radiata pine (*Pinus radiata D. Don*) and chestnut (*Castanea sativa Mill.). Industrial Crops and Products*, *94*, 122–131. https://doi.org/10.1016/j.indcrop.2016.08.008

Simpson, T. W. (1973). Predicting Equilibrium moisture content of wood by mathematical models. *Wood and Fiber*, *5*(1), 41–49.

Skaar, C. (1972). *Water in wood*. *Syracuse wood science series: Bd. 4*. Syracuse Univ. Pr.

Skaar, C. (1988). *Wood-Water Relations*. Springer Berlin Heidelberg. https://doi.org/10.1007/978-3-642-73683-4

Skulberg, K. R., Nyrud, A. Q [A. Q.] & Nore, K [K.] (2022). Hygroscopic buffering effects in exposed cross-laminated timber surfaces and indoor climate in a Norwegian primary school. *Wood Material Science & Engineering*, 1–10. https://doi.org/10.1080/17480272.2021.2019830

Sleik, T., Kolbitsch, C. & Koch, J [Jens]. (2018). *AUSSENWAND MASSIVHOLZHANDBUCH 2.0: Technical Data Sheet.* Binderholz GmbH & Saint-Gobain Rigips Austria GesmbH.

Smith, J. & Ashley-Smith, J. (Hrsg.). (2013). *Climate for collections: Standards and uncertainties: Postprints of the Munich Climate Conference, 7 to 9 November 2012* (1st. publ). Archetype Publ.

Sonderegger, W., Hering, S. & Niemz, P. (2011). Thermal behaviour of Norway spruce and European beech in and between the principal anatomical directions. *Holzforschung*, *65*(3). https://doi.org/10.1515/hf.2011.036

Sonderegger, W., Kránitz, K., Bues, C.-T. & Niemz, P. (2015). Aging effects on physical and mechanical properties of spruce, fir and oak wood. *Journal of Cultural Heritage*, *16*(6), 883–889. https://doi.org/10.1016/j.culher.2015.02.002

Steben, P. (2005). Vergleichsuntersuchungen zur Wasserdampfdurchlässigkeit von Unterdeck- und Unterspannbahnen und Dampfsperren.

Stöckl, B. (2023). *WUFI® in Normen, Richtlinien und unabhängigen Veröffentlichungen*. https://wufi.de/en/software/validation/

Strang, M. (2023). *Moisture safety for energy-efficient CLT envelopes: pathways to net-zero operational energy for engineered wood multi-storey buildings in Australian tropical and subtropical climates.* https://doi.org/10.14264/80ca907

Strang, M., Leardini, P. & Shirmohammadi, M. VALIDATING MOISTURE-SAFE ENERGY EFFICIENT CLT ASSEMBLIES IN HOT AND HUMID CLIMATES USING EXPERIMENTAL TESTING, 4429–4438. https://doi.org/10.52202/069179-0577

Straube, J., Onysko, D. & Schumacher, C. (2002). Methodology and Design of Field Experiments for Monitoring the Hygrothermal Performance of Wood Frame Enclosures. *Journal of Thermal Envelope and Building Science*, *26*(2), 123–151. https://doi.org/10.1177/0075424202026002098

Tannert, T., Berger, R., Vogel, M. & Müller, A. (2011). Remote moisture monitoring of timber bridges: a case study. *Proceedings of the 5th International Conference on Structural Health Monitoring of Intelligent Infrastructure (SHMII-5), Cancún, México*.

Texas Instruments, Incorporated. (2016). *HDC1080 Low Power, High Accuracy Digital Humidity Sensor with Temperature Sensor (Rev. A): (SNAS672,A)*. https://www.ti.com/product/HDC1080?qgpn=hdc1080&bm-verify=AAQAAAAJ_____wl8-rcZFlbRPJ8bau8GNdyqn55t2ygmRljh9qzHpeHNdSLPqm4had5alqN4FBGxPknuEvb68fEH2DgkyOH4-X40uOEn-wsaTHgfHF-LmOdk_gLw8-90g0xXSxzthCz05v-RCRJ0HgN-3nSs59zhwGNg7ayl_3RDiNqVu0GFNrHvkuYbBCKCnD-bLGJQ4pp6Fs_uPfCnrynXsdPxnbvyo2fNTCGtAi1I1AOsDKTqXmKMqAmTf8TH04ElCRUladC7crCjbrlkP5qKxYisP-bQvqa7x5K79DbPlofza3B33ARAXcUhCf6_abWFvkBLMqbikXj3lWXfnxrKOoCKn1JkQ9nXq5MLqcyNSo7J11U8Q

Thorsell, T. & Bomberg, M. (2008). Integrated Methodology for Evaluation of Energy Performance of Building Enclosures: Part II — Examples of Application to Residential Walls. *Journal of Building Physics*, *32*(1), 49–65. https://doi.org/10.1177/1744259108093317

Thorsell, T. & Bomberg, M. (2011). Integrated methodology for evaluation of energy performance of the building enclosures: Part III — uncertainty in thermal measurements. *Journal of Building Physics*, *35*(1), 83–96. https://doi.org/10.1177/1744259111404381

Thybring, E. E [Emil E.], Boardman, C. R., Zelinka, S. L. & Glass, S. V. (2021). Common sorption isotherm models are not physically valid for water in wood. *Colloids and Surfaces A: Physicochemical and Engineering Aspects*, *627*, 127214. https://doi.org/10.1016/j.colsurfa.2021.127214

TinkerForge: Humidity Bricklet 2.0 - Technical Specifications. *Humidity Bricklet 2.0 - Technical Specifications*. https://www.tinkerforge.com/en/doc/Hardware/Bricklets/Humidity_V2.html

Torgovnikov, G. I. (1993). *Dielectric properties of wood and wood-based materials*. *Springer series in wood science*. Springer.

Trübswetter, T. (2009). *Holztrocknung: Verfahren zur Trocknung von Schnittholz - Planung von Trocknungsanlagen // Verfahren zur Trocknung von Schnittholz - Planung von Trocknungsanlagen ; mit 27 Tabellen* (2., aktualisierte Aufl.). *Holztechnik*. Fachbuchverl. Leipzig im Carl-Hanser-Verl.

Umweltbundesamt. (2017). *Leitfaden zur Vorbeugung, Erfassung und Sanierung von Schimmelbefall in Gebäuden.*

Uwizeyimana, P., Perrin, M. & Eyma, F. (2020). Moisture monitoring in glulam timber structures with embedded resistive sensors: study of influence parameters. *Wood Science and Technology*, *54*(6), 1463–1478. https://doi.org/10.1007/s00226-020-01228-8

Varnier, M., Ulmet, L., Dubois, F. & Sauvat, N. (2022). Characterization and modeling of wood species sorption isotherms for use in civil engineering structures monitoring. Vorab-Onlinepublikation. https://doi.org/10.21203/rs.3.rs-2113454/v1

Vašková, V., Fojtík, R. & Pustka, D. (2016). Monitoring and Failures of Footbridges Made from Glued Laminated Wood. *Procedia Engineering*, *142*, 87–91. https://doi.org/10.1016/j.proeng.2016.02.017

Vidal Bastías, M. & Cloutier, A. (2005). Evaluation of Wood Sorption Models for high Temperatures. *Ciencia y tecnología*, *7*(3), 145–158.

Voigt, H., Krischer, O. & Schauss, H. (1940). Die Feuchtigkeitsbewegung bei der Verdunstungstrocknung von Holz. *European Journal of Wood and Wood Products*, *3*(10), 305–321. https://doi.org/10.1007/BF02718022

Vololonirina, O., Coutand, M. & Perrin, B. (2014). Characterization of hygrothermal properties of wood-based products – Impact of moisture content and temperature. *Construction and Building Materials*, *63*, 223–233. https://doi.org/10.1016/j.conbuildmat.2014.04.014

Wacker, J. P., Joyal, M. R., Murphy, J. F. & Wang, X [Xiping] (2007). Monitoring the performance of timber bridges over the long term. *Proceedings of the 2007 Mid-Continent Transportation Research Symposium, Ames, Iowa, USA*.

Weichert, L. (1963a). Untersuchungen über das Sorption- und Quellungsverhalten von Fichte, Buche und Buchen-Preßvollholz bei Temperaturen zwischen 20° und 100°C. *European Journal of Wood and Wood Products*, *21*(8), 290–300. https://doi.org/10.1007/BF02610962

Weichert, L. (1963b). *Untersuchungen über das Sorptions- und Quellungsverhalten von Fichte, Buche und Buchenpressvollholz bei Temperaturen zwischen 20C °C und 100 °C* [Dissertation]. Technische Hochschule München.

Welling, J. (1987). *Die Erfassung von Trocknungsspannungen während der Kammertrocknung von Schnittholz*. Zugl.: Hamburg, Univ., FB Biologie, Diss., 1987. Ergebnisse-Verl.

Welsh, J. K. (1978). *A model for time-dependent D.C. conduction in moist wood: (Dissertation)*. State University of New York. https://experts.esf.edu/esploro/outputs/doctoral/A-MODEL-FOR-TIME-DEPENDENT-DC-CONDUCTION/99889945304826

Willems, W. (2016). Equilibrium thermodynamics of wood moisture revisited: presentation of a simplified theory. *Holzforschung*, *70*(10), 963–970. https://doi.org/10.1515/hf-2015-0251

Winkler, M., Nore, K [Kristine] & Antretter, F. (2014). Impact of the moisture buffering effect of wooden materials on energy demand and comfort conditions.

Worch, A. (2004). The Behaviour of Vapour Transfer on Building Material Surfaces: The Vapour Transfer Resistance. *Journal of Thermal Envelope and Building Science*, *28*(2), 187–200. https://doi.org/10.1177/1097196304044398

Yeo, H., Smith, W. B. & Hanna, R. B. (2002). Determination of Surface Moisture Content of Wood Utilizing a Colorimetric Technique. *Wood and Fiber Science*, *34*(3), 419–424.

Yermán, L., Ottenhaus, L.-M., Montoya, C. & Morrell, J. J. (2021). Effect of repeated wetting and drying on withdrawal capacity and corrosion of nails in treated and untreated timber. *Construction and Building Materials*, *284*, 122878. https://doi.org/10.1016/j.conbuildmat.2021.122878

Yokoyama, M [Misao], Gril, J., Matsuo, M [Miyuki], Yano, H., Sugiyama, J [Junji], Clair, B., Kubodera, S., Mistutani, T., Sakamoto, M., Ozaki, H., Imamura, M. & Kawai, S [Shuichi] (2009). Mechanical characteristics of aged Hinoki wood from Japanese historical buildings. *Comptes Rendus. Physique*, *10*(7), 601–611. https://doi.org/10.1016/j.crhy.2009.08.009

Yoo, J., Chang, S. J., Yang, S., Wi, S., Kim, Y. U. & Kim, S. (2021). Performance of the hygrothermal behavior of the CLT wall using different types of insulation; XPS, PF board and glass wool. *Case Studies in Thermal Engineering*, *24*, 100846. https://doi.org/10.1016/j.csite.2021.100846

Zelinka, S. L., Altgen, M., Emmerich, L., Guigo, N., Keplinger, T., Kymäläinen, M., Thybring, E. E [Emil Engelund] & Thygesen, L. G. (2022). Review of Wood Modification and Wood Functionalization Technologies. *Forests*, *13*(7), 1004. https://doi.org/10.3390/f13071004

Zelinka, S. L., Glass, S. V. & Stone, D. S. (2008). A percolation model for electrical conduction in wood with implications for woodwater relations. *Wood and Fiber Science*(40), 544–552.

Zelinka, S. L., Glass, S. V. & Thybring, E. E [Emil Engelund] (2020). Evaluation of previous measurements of water vapor sorption in wood at multiple temperatures. *Wood Science and Technology*, *54*(4), 769–786. https://doi.org/10.1007/s00226-020-01195-0

Zhang, K. & Richman, R. (2020). Parametric analysis of moisture sorption isotherms for wood sheathing using hygrothermal modelling. *Journal of Building Engineering*, *28*, 101047. https://doi.org/10.1016/j.jobe.2019.101047

Zhang, X., Zillig, W., Künzel, H. M., Mitterer, C. & Zhang, X [Xu] (2016a). Combined effects of sorption hysteresis and its temperature dependency on wood materials and building enclosures – Part I: Measurements for model validation. *Building and Environment*, *106*, 143–154. https://doi.org/10.1016/j.buildenv.2016.06.025

Zhang, X., Zillig, W., Künzel, H. M., Mitterer, C. & Zhang, X [Xu] (2016b). Combined effects of sorption hysteresis and its temperature dependency on wood materials and building enclosures - Part II: Hygrothermal modeling. *Building and Environment*, *106*, 181–195. https://doi.org/10.1016/j.buildenv.2016.06.033

Zhou, H. Z., Zhu, E. C., Fortino, S [S.] & Toratti, T. (2010). Modelling the hygrothermal stress in curved glulam beams. *The Journal of Strain Analysis for Engineering Design*, *45*(2), 129–140. https://doi.org/10.1243/03093247JSA563

Zuritz, C., Singh, R. P., Moini, S. M. & Henderson, S. M. (1979). Desorption isotherms of rough rice from 10 °C to 40 °C. Transactions of the American Society of Agricultural Engineers(22), 433–440.

8.3 List of figures

Unless cited with a reference in brackets, the figures are created by the author.

8.4 List of tables

All tables are by the author. Unless cited with a reference in brackets, their content is also created by the author.

9 APPENDICES

9.1 Appendix A: Translated and adapted chapter from a previous publication

The physical principles of latent heat effects have been summarized and calculated as they occur on wooden surfaces and have already been published in (Flexeder, Schumacher et al., 2022, p. 73 - 75). Since the publication is in German, the respective Subchapter is quoted below as an adapted English translation:

"Moisture movement in the material can lead to enthalpy currents and thus heat transport in the material. The currents are bound to water as a medium. In particular, enthalpy fluxes due to water vapor diffusion combined with phase changes can have a major influence on the heat balance of the component or material (Künzel, 1994). The enthalpy fluxes due to liquid transport are negligible. When moisture is transported into or through a material layer, enthalpy changes occur that can be experienced or measured by the release of sensible heat. […] This phenomenon can be described as the sum of two components and is referred to as the adsorption enthalpy h_{Ad} (Gertis & Schmidt, 2015).

$$h_{Ad} = h_V + h_B$$

The latent enthalpy of vaporization h_V during the phase change (liquid-gaseous) and the sorptive binding enthalpy h_B of the water molecules in the pores of the material together form the adsorption enthalpy h_{Ad}.

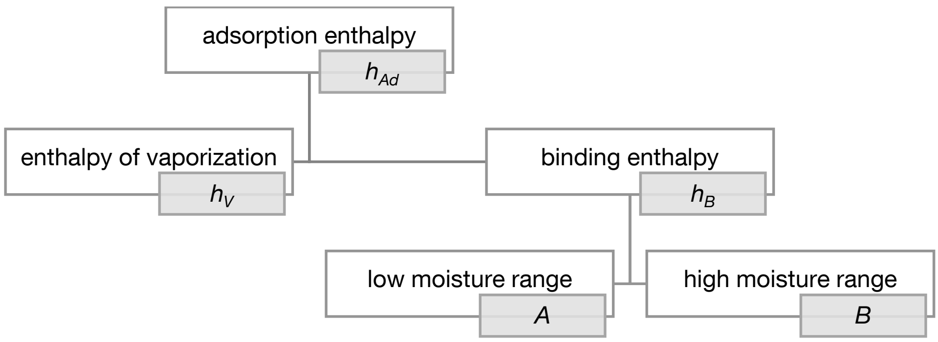

Figure 206: Scheme of the different components constituting adsorption enthalpy

The enthalpy of vaporization h_V of water during the vapor-liquid phase transition is not constant. It decreases linearly from about 2500 kJ/kg at 0 °C to about 2400 kJ/kg at 40 °C in a range of interest for building physics (Gertis & Schmidt, 2015). The entropy change during evaporation is therefore directly proportional to the enthalpy of evaporation as a function of temperature.

$$h_V = T\ \Delta s_V$$

In the simulation with the WUFI programs (transient heat and humidity, Fraunhofer Institute), the enthalpy of vaporization h_V is simplified to a constant value of 2500 kJ/kg (Künzel, 1994). This means that the heat of sorption is slightly overestimated at typical room temperatures of 20 °C. The phenomenon of material heating due to the accumulation of water molecules on the cell wall was observed as early as 1896 by Volbehr as "heat of swelling" and measured experimentally using a calorimeter on spruce samples (Fortuin, 2003; Skaar, 1972). The resulting integral binding enthalpy H_B with the unit [kJ/kg dry wood] can be differentiated step by step according to the respective wood moisture content MC [m.-%]. This results in the differential binding enthalpy h_B [kJ/kg water], which indicates the binding enthalpy in relation to 1 kg of sorbed water as a function of wood moisture content. The sorptive binding enthalpy h_B is also referred to as the *building material-dependent sorption enthalpy* in (Künzel, 1994) and partially in (Gertis & Schmidt, 2015). To avoid confusion, only the term binding enthalpy h_B will be used in the following. According to (Gertis & Schmidt, 2015; Krischer, 1978) it can be understood as the amount of energy needed to compress water vapor isothermally from an arbitrary vapor pressure p (gaseous) to the dew point, i.e. to the saturation vapor pressure p_S. This results in an entropy change Δs_B.

$$h_B = T\,\Delta s_B$$

As the distance between the sorbate and the sorbent increases, the binding enthalpy decreases (Künzel, 1994). The distinction between the sorption enthalpy h_B at low and high humidity is based on the shape of the sorption isotherm curve. The direction of curvature changes in the region around 50% relative humidity; this is where the boundary between moisture regions A and B runs. (Gertis & Schmidt, 2015) derive the following description according to (Krischer, 1978) using the equilibrium vapor pressure in the building material capillary:

$$h_B = -R\,T\,ln\varphi$$

The low moisture region A ends when a monomolecular sorbate layer is reached. Accordingly, van der Waals forces dominate the sorption bond h_B in the low moisture region A [lower, right-curved part of the sorption isotherm]. Capillary condensation results from a multilayer occupation of the inner pore wall. The resulting interfacial forces determine the sorption enthalpy h_B in the high moisture region B [upper part of the sorption isotherm]. In this range, the value of the binding enthalpy h_B becomes almost constant at high humidities due to the logarithmic relationship. This means that the higher the relative humidity φ [%], the lower the influence of the binding enthalpy h_B on the value of the total adsorption enthalpy h_{Ad}. Knowledge of the adsorption enthalpy h_{Ad} of wood species plays a particularly important role in the technical drying of structural timber. A collection of selected approaches for calculating the binding enthalpy h_B (and H_B) by comparing sorption isotherms at different measurement temperatures can be found in (Fortuin, 2003). In addition, values for the binding enthalpy h_B of various materials such as wood or potatoes can be found in (Krischer, 1978). Figure 207 shows an example of the binding enthalpy h_B of the material "spruce" according to the calculations of (Fortuin, 2003) as a function of the wood moisture content in percent by mass [m.-%]. For orientation, the secondary ordinate shows the equivalent relative humidity φ [%], recalculated according to the sorption isotherm for spruce wood at 20 °C (Weichert, 1963a).

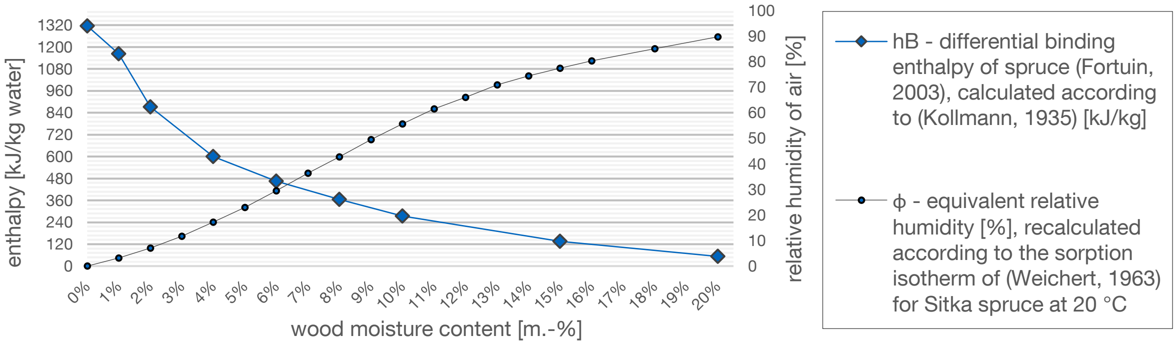

Figure 207: Binding enthalpy of wood according to (Fortuin, 2003) according to (Kollmann, 1935), recalculated based on (Weichert, 1963a)

While the differential enthalpy of binding h_B has relatively high absolute values in the low moisture range, its importance for the total adsorption enthalpy is relativized as soon as the value is related not to the mass of the water, but to the mass of the building material itself, cf. Figure 208. The sum rule of integration applies:

$$h_{Ad} = h_V + h_B$$

$$H_{Ad} = H_V + H_B$$

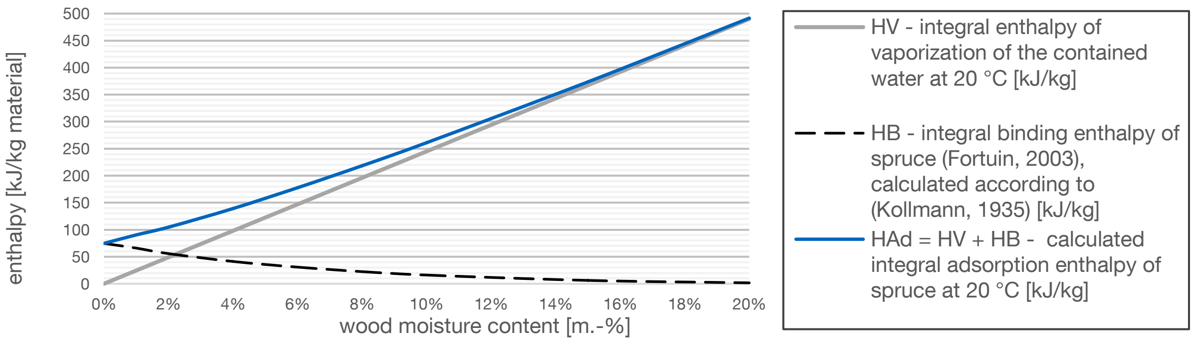

Figure 208: Adsorption enthalpy of wood as a function of water content, calculated based on (Gertis & Schmidt, 2015) after (Fortuin, 2003) according to (Kollmann, 1935)

Accordingly, the binding enthalpy h_B could possibly be neglected for calculations in the high humidity range. Note: The calculation of the binding enthalpy h_B is not integrated in the algorithms of the WUFI simulation (Künzel, 1994). If the simplified approach of a constant adsorption enthalpy h_{Ad} is assumed and equated with the evaporation enthalpy h_V (e.g. with the constant value of 2450 kJ/kg), a linear equation H_V is obtained, which depends only on the adsorbed amount of water x [kg].” (Flexeder, Schumacher et al., 2022)

9.2 Appendix B: Details on experiments with conductive adhesives for ERM

Table 21: Mixing ratios for compounds with conductive silicone or glue; 01-04 in reference to (Brischke et al., 2008)

No.	Ingredients	Properties as specified by manufacturer	Compound ratio
01-04	Epoxy resin	Epoxy L, solvent-free, filler-free Bisphenol A/F resin Density: 1.15 g/cm³ at 20 °C Viscosity: 700 mPas at 25 °C	19.2 m.-%
	Hardener	Modified cycloaliphatic polyamine hardener L Processing time at 23 °C: 40 min Curing time at 23 °C: 24 h	5.8 m.-%
	Isopropanol		40 m.-%
	Graphite powder, extra finely ground d50: 15-20 µm	Content: 99 % Particle size: approx. 15-20 µm Chemical formula: C CAS number: 7782-42-5	35 m.-%
05-06	Silicone rubber, translucent, extremely soft (Shore A 00) Base	Mixture: 1:1 by weight Specific gravity: 1,03 Viscosity: 1500 mPas Processing time at 23 °C: 6 min Curing time at 23 °C: 60 min Breaking load: 1.10 N/mm² Elongation at break 400 ± 20% Tensile strength: 1.5 ± 1 N/mm² Dimensional change after 24 hours: 0.1 %	44.7 m.-%
	Silicone rubber, translucent, extremely soft (Shore A 00) Catalyst		44.7 m.-%
	Graphite powder, ca. 55 µm	Content: 99.7 % Particle size: approx. 55 µm Chemical formula: C CAS number: 7782-42-5	10.6 m.-%
07-08	Silicone rubber, translucent, medium hard (Shore A 32) Base	Mixture: 1:1 by weight Specific gravity: 1,09 Viscosity: 17,500 mPas Processing time at 23 °C: 20 min Curing time at 23 °C: 210 min Breaking load: 6.0 N/mm² Elongation at break 460 ± 20% Tensile strength: 20 ± 2 N/mm² Dimensional change after 24 hours: 0.05 %	45.6 m.-%
	Silicone rubber, translucent, medium hard (Shore A 32) Catalyst		45.6 m.-%
	Graphite powder, extra finely ground d50: 15-20 µm	Content: 99 % Particle size: approx. 15-20 µm Chemical formula: C CAS number: 7782-42-5	8.8 m.-%
09-10	Silicone rubber, translucent, extremely soft (Shore A 00) Base	Mixture: 1:1 by weight Specific gravity: 1,03 Viscosity: 1500 mPas Processing time at 23 °C: 6 min Curing time at 23 °C: 60 min Breaking load: 1.10 N/mm² Elongation at break 400 ± 20% Tensile strength: 1.5 ± 1 N/mm² Dimensional change after 24 hours: 0.1 %	44.7 m.-%
	Silicone rubber, translucent, extremely soft (Shore A 00) Catalyst		44.7 m.-%
	Graphite powder, extra finely ground d50: 15-20 µm	Content: 99 % Particle size: approx. 15-20 µm Chemical formula: C CAS number: 7782-42-5	10.6 m.-%

Table 22: Mixing ratios for compounds with isolating silicone or glue; 01-04 in reference to (Brischke et al., 2008)

<table>
<tr><th>No.</th><th>Ingredients</th><th>Properties as specified by manufacturer</th><th>Compound ratio</th></tr>
<tr><td rowspan="3">01-04</td><td>Epoxy resin</td><td>Epoxy L, solvent-free, filler-free
Bisphenol A/F resin
Density: 1.15 g/cm³ at 20 °C
Viscosity: 700 mPas at 25 °C</td><td>58.8 m.-%</td></tr>
<tr><td>Hardener</td><td>Modified cycloaliphatic polyamine hardener L
Processing time at 23 °C: 40 min
Curing time at 23 °C: 24 h</td><td>17.7 m.-%</td></tr>
<tr><td>Wheat flour type 405</td><td>Light flour with minimal content of shell and germ
Mineral content: 405 mg / 100 g</td><td>23.5 m.-%</td></tr>
<tr><td rowspan="3">05-10</td><td>Silicone rubber, translucent, extremely soft (Shore A 00)
Base</td><td rowspan="2">Mixture: 1:1 by weight
Specific gravity: 1,03
Viscosity: 1500 mPas
Processing time at 23 °C: 6 min
Curing time at 23 °C: 60 min
Breaking load: 1.10 N/mm²
Elongation at break 400 ± 20%
Tensile strength: 1.5 ± 1 N/mm²
Dimensional change after 24 hours: 0.1 %</td><td>44.7 m.-%</td></tr>
<tr><td>Silicone rubber, translucent, extremely soft (Shore A 00)
Catalyst</td><td>44.7 m.-%</td></tr>
<tr><td>Wheat flour type 405</td><td>Light flour with minimal content of shell and germ
Mineral content: 405 mg / 100 g</td><td>10.6 m.-%</td></tr>
</table>

9.3 Appendix C: Illustrated results from ERM in Norway spruce

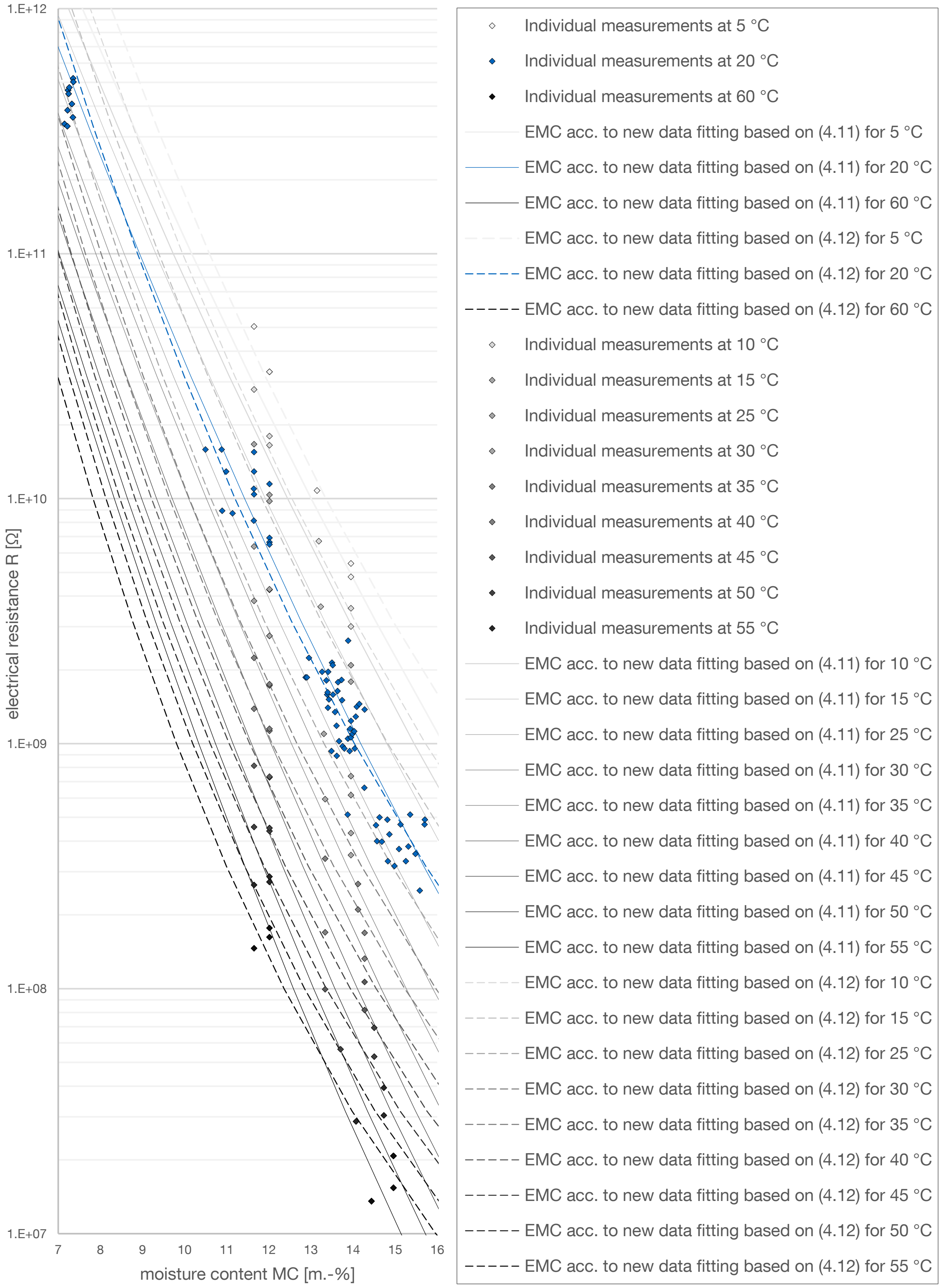

Figure 209: Detailed comparison of modified models (4.11) and (4.12) for the correlation of electrical resistance R [Ω], temperature T [°C] and moisture content MC [m.-%] at a range of 5 - 60 °C for Norway spruce (Picea abies Karst.), with measurement direction perpendicular to the grain and within the investigated scope of a moisture content MC of 7 - 16 m.-%.

9.4 Appendix D: Synthesized calibration curves for ERM in Douglas fir and radiata pine

Because of their imprecision, the new parameters obtained by extrapolation for electrical resistance measurements on Douglas fir and radiata pine are recommended for further use only to a limited extent. The following parameters are obtained by weighted curve fitting to data from references:

$$MC\,(R,T) = a \cdot \left(\frac{1000}{T+273.15}\right)^{d} - c \cdot \left(\frac{1000}{T+273.15}\right)^{d} \cdot log_{10}\,[\,log_{10}\,(R) - b] \qquad \text{(4.11) } \textit{modified}$$

With

R	Electrical Resistance	[Ω]
T	Temperature	[°C]

	a	*b*	*c*	*d*
Douglas fir (*Pseudotsuga menziesii Franco*), *measurement perpendicular to grain direction*	2.0705	5	2.0663	2.0601
Radiata pine (*Pinus radiata D. Don.*), *measurement perpendicular to grain direction*	2.4457	4	2.2750	2.0469

These synthesized calibration curves are used for the comparison in Subsection 5.4 of this dissertation.

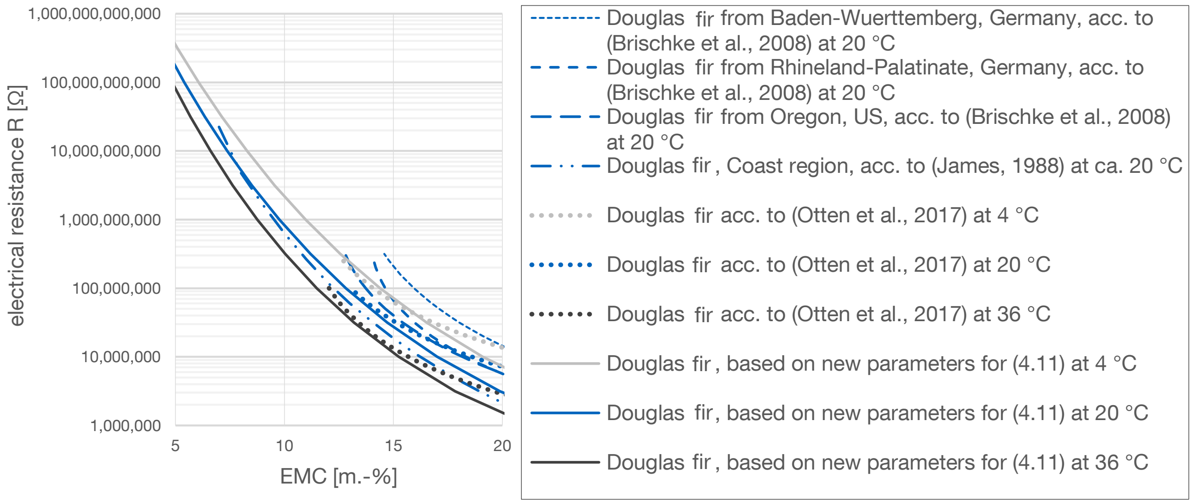

Figure 210: Extrapolation of calibration curves from several publications to generate a new calibration curve to be used on different temperature levels of Douglas fir (Pseudotsuga menziesii Franco)

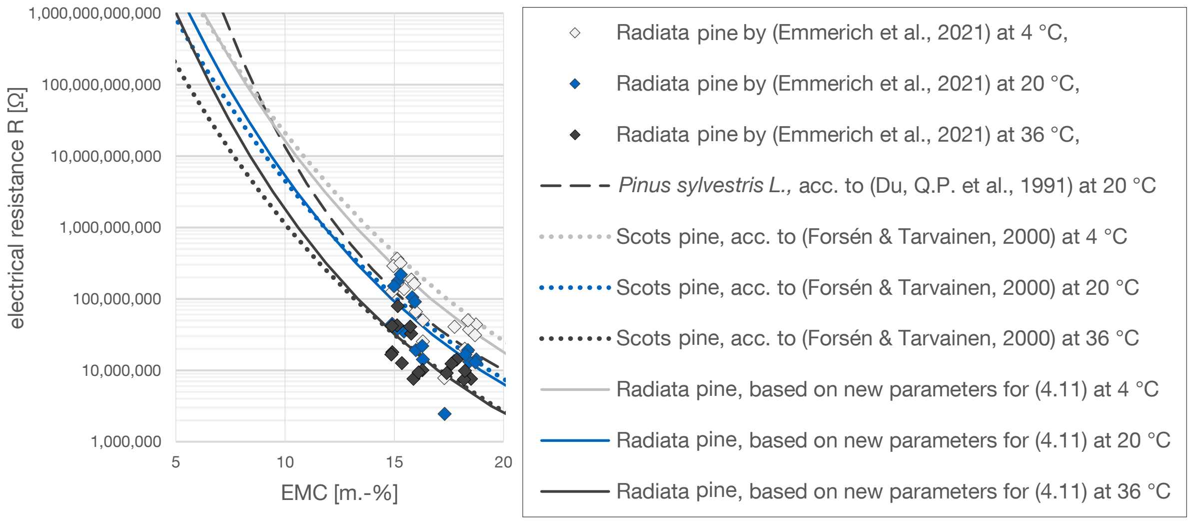

Figure 211: Extrapolation of calibration curves from several publications to generate a new calibration curve to be used on different temperature levels of radiata pine (Pinus radiata D. Don.)

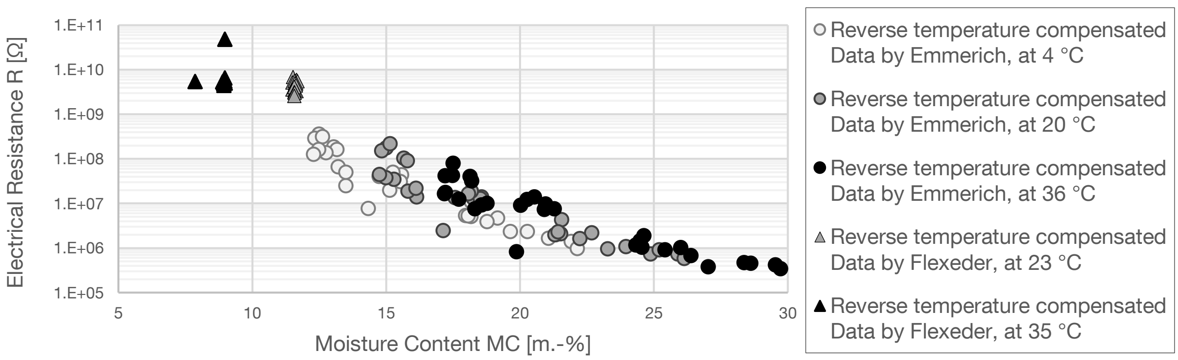

Figure 212: Compilation of resistance measurement data, obtained on radiata pine (Pinus radiata D. Don.) at different temperature levels and reverse-engineered to form a single calibration curve

9.5 Appendix E: Illustrated results from comparing ERM with SM

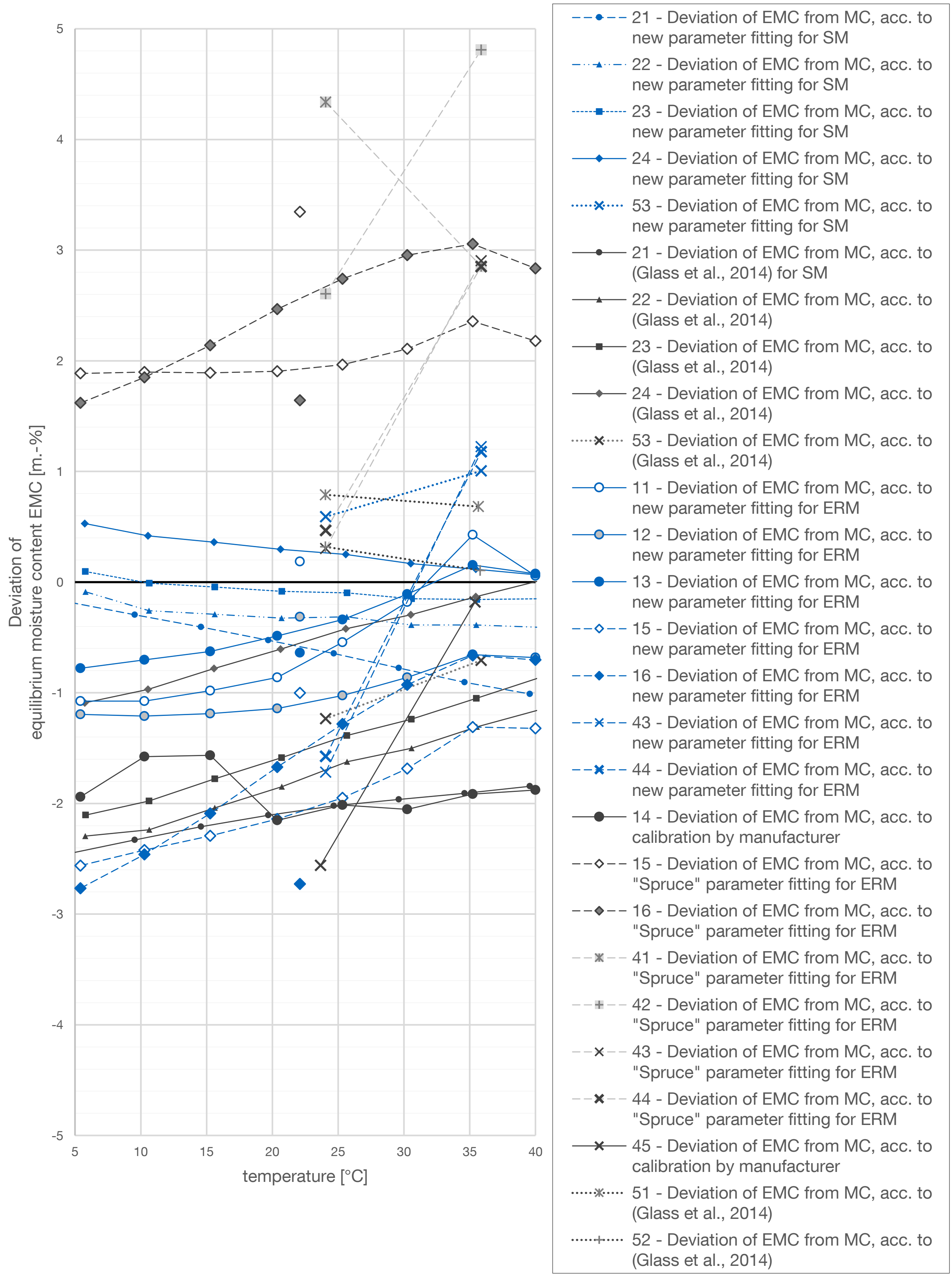

Figure 213: Comparison of experimental results using the electrical resistance method (ERM) and the sorption method (SM) for wood moisture monitoring in Norway spruce (ERM: 11, 12, 13, 14 – SM: 21, 22, 23), Douglas fir (ERM: 15, 16 – SM: 24), spotted gum (ERM: 41 – SM: 51), shining gum (ERM: 42 – SM: 52), and radiata pine (ERM: 43, 44 – SM: 53)

9.6 Appendix F: Recommended new calibration curves for ERM and SM

Spruce laminated veneer lumber (LVL made of *Picea abies Karst*.)

EMC	Equilibrium Moisture Content	[m.-%]
R	Electrical Resistance	[Ω]
T	Temperature	[°C]

Electrical Resistance Method (ERM)

investigated range: 5 °C – 60 °C | 10 m.-% - 13 m.-%

$$\mathrm{EMC\ (R,T)} = \mathrm{a} \cdot \left(\frac{1000}{\mathrm{T}+273.15}\right)^{\mathrm{d}} - \mathrm{c} \cdot \left(\frac{1000}{\mathrm{T}+273.15}\right)^{\mathrm{d}} \cdot \lg\left[\lg(\mathrm{R}) - \mathrm{b}\right]$$

	a	b	c	d
perpendicular to glue lines	0.9765	3.5221	0.8437	2.6860
parallel to glue lines	1.5713	0.2105	1.3592	2.7816
perpendicular to grain of main layer	1.1524	0.0327	1.0218	3.1329
parallel to grain of main layer	1.0887	0.0326	0.9644	3.1651
in glue line	2.3084	0.0571	1.9449	2.4386

Beech laminated veneer lumber (LVL made of *Fagus sylvatica L.*)

EMC	Equilibrium Moisture Content	[m.-%]
R	Electrical Resistance	[Ω]
T	Temperature	[°C]

Electrical Resistance Method (ERM)

investigated range: 5 °C – 60 °C | 9 m.-% - 14 m.-%

Option 1

$$\mathrm{EMC\ (R,T)} = \mathrm{a} \cdot \left(\frac{1000}{\mathrm{T}+273.15}\right)^{\mathrm{d}} - \mathrm{c} \cdot \left(\frac{1000}{\mathrm{T}+273.15}\right)^{\mathrm{d}} \cdot \lg\left[\lg(\mathrm{R}) - \mathrm{b}\right]$$

	a	b	c	d
perpendicular to glue lines	0.2018	4.0549	0.1940	4.0252
parallel to glue lines	0.6316	3.4845	0.5405	2.9717
perpendicular to grain of main layer	0.3911	4.1494	0.3379	3.2634
parallel to grain of main layer	0.5083	4.0398	0.4104	2.9746
in glue line	0.3050	4.2680	0.2722	3.5093

Option 2

$$MC\ (R,T) = (-a \cdot T + b) \cdot exp^{(-c \cdot 10\ \lg(R) + d)}$$

	a	b	c	d
perpendicular to glue lines	0.015	1.812	0.024	3.993
parallel to glue lines	0.013	1.974	0.018	3.284
perpendicular to grain of main layer	0.014	1.937	0.020	3.492
parallel to grain of main layer	0.013	1.975	0.018	3.261
in glue line	0.014	1.884	0.022	3.703

Norway spruce (*Picea abies Karst.*)

EMC	Equilibrium Moisture Content	[m.-%]
$X_{20\,°C}$	Base value for material moisture content at 20 °C	[m.-%]
R	Electrical Resistance	[Ω]
T	Temperature	[°C]
RH	Relative Humidity of Air	[%]

Electrical Resistance Method (ERM)

investigated range: 5 °C – 60 °C | 7 m.-% - 16 m.-%

Option 1

$$\mathrm{EMC}\,(X_{20\,°C}, T) = X_{20\,°C} + \left(\frac{a \cdot X_{20\,°C}}{b}\right) \cdot (c \cdot T^2 - d \cdot T + e)$$

	a	b	c	d	e
perpendicular to grain direction	0.500	8.529	0.001	0.219	3.813

$$X_{20\,°C} = -\frac{1}{g} \cdot ln\left(\frac{ln(R) - h}{f}\right)$$

	f	g	h
perpendicular to grain direction	35.5	0.038	0.001

Option 2

$$\mathrm{EMC}\,(R, T) = a \cdot \left(\frac{1000}{T + 273.15}\right)^d - c \cdot \left(\frac{1000}{T + 273.15}\right)^d \cdot \lg\,[\,\lg\,(R) - b]$$

	a	b	c	d
perpendicular to grain direction	3.4557	0	2.9052	2.4716
parallel to grain direction	3.3930	0.0001	2.7875	2.3866

Sorption Method (SM)

investigated range: -12 °C – 100 °C | 0 %RH – 99 %RH

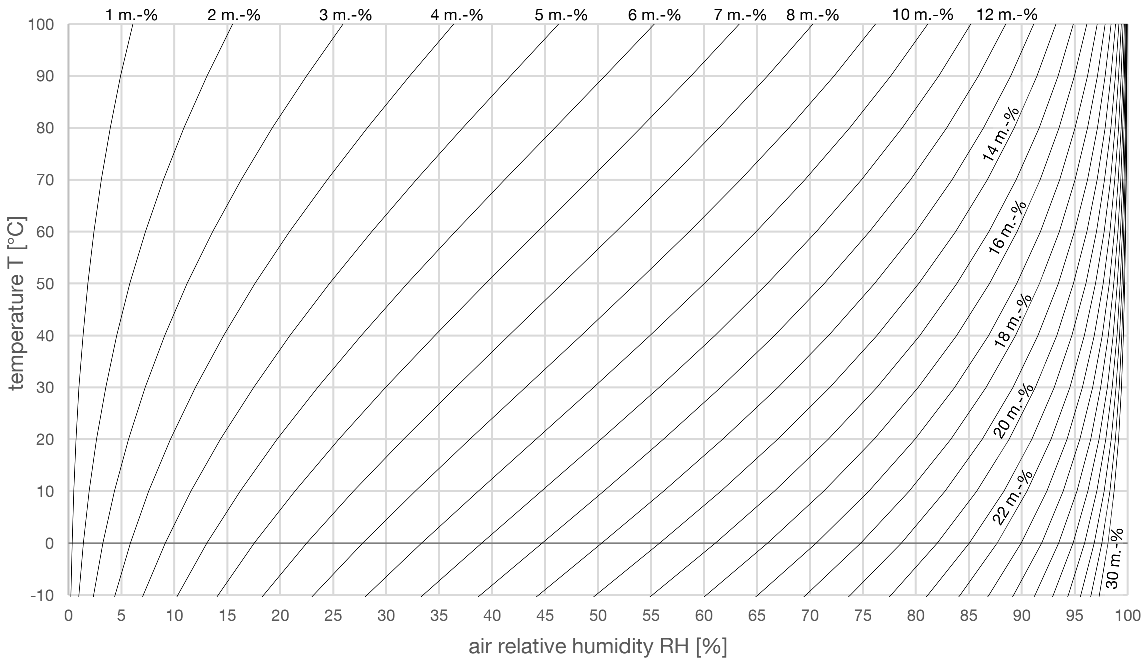

$$\mathrm{EMC} = \left[a \cdot (T + 273.15) \cdot \left(1 - \frac{(T + 273.15)}{647.1}\right)^b \cdot \ln\left(1 - \frac{1}{100}\,RH\right)\right]^{c \cdot (T + 273.15)^d}$$

	a	b	c	d
independent of grain direction	- 0.0001084	0.6800	0.0005219	1.2165

European beech *(Fagus sylvatica L.)*

EMC	Equilibrium Moisture Content	[m.-%]
R	Electrical Resistance	[Ω]
T	Temperature	[°C]
RH	Relative Humidity of Air	[%]

Electrical Resistance Method (ERM)

investigated range: 5 °C – 60 °C | 9 m.-% - 14 m.-%

$$\mathrm{EMC}\,(\mathrm{R},\mathrm{T}) = \mathrm{a} \cdot \left(\frac{1000}{\mathrm{T}+273.15}\right)^{\mathrm{d}} - \mathrm{c} \cdot \left(\frac{1000}{\mathrm{T}+273.15}\right)^{\mathrm{d}} \cdot \lg\left[\lg(\mathrm{R}) - \mathrm{b}\right]$$

	a	b	c	d
perpendicular to grain direction	0.3622	5.4994	0.3438	3.4822

Sorption Method (SM)

investigated range: 20 °C – 100 °C | 0 %RH – 95 %RH

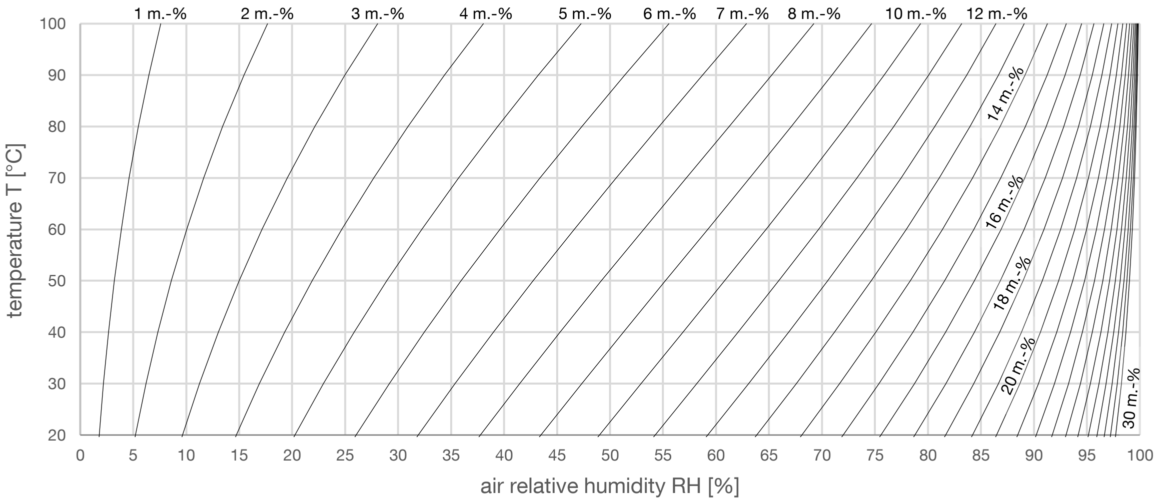

$$\mathrm{EMC} = \left[\mathrm{a} \cdot (\mathrm{T}+273.15) \cdot \left(1 - \frac{(\mathrm{T}+273.15)}{647.1}\right)^{\mathrm{b}} \cdot \ln\left(1 - \frac{1}{100}\,\mathrm{RH}\right)\right]^{\mathrm{c}\cdot(\mathrm{T}+273.15)^{\mathrm{d}}}$$

	a	b	c	d
independent of grain direction	- 0.0004052	1.8125	0.0072263	0.7882

Douglas fir *(Pseudotsuga menziesii Franco)*

EMC	Equilibrium Moisture Content	[m.-%]
T	Temperature	[°C]
RH	Relative Humidity of Air	[%]

Sorption Method (SM)

investigated range: -12 °C – 60 °C | 0 %RH – 99 %RH

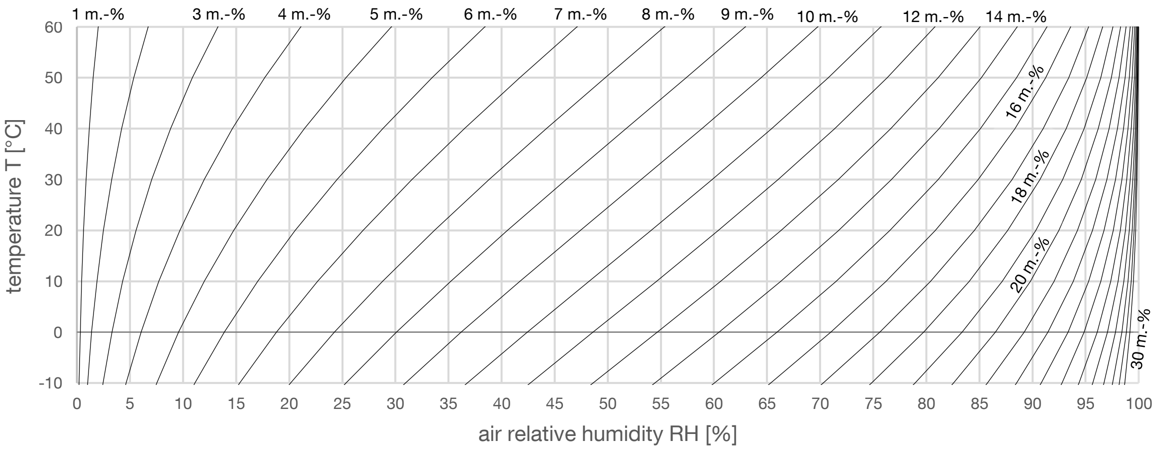

$$\mathrm{EMC} = \left[a \cdot (T + 273.15) \cdot \left(1 - \frac{(T + 273.15)}{647.1}\right)^{b} \cdot \ln\left(1 - \frac{1}{100}\,\mathrm{RH}\right)\right]^{c \cdot (T+273.15)^{d}}$$

	a	b	c	d
independent of grain direction	- 0.0000982	1.1339	0.0010537	1.0827

Radiata pine *(Pinus radiata D. Don.)*

EMC	Equilibrium Moisture Content	[m.-%]
T	Temperature	[°C]
RH	Relative Humidity of Air	[%]

Sorption Method (SM)

investigated range: 15 °C – 50 °C | 0 %RH – 98 %RH

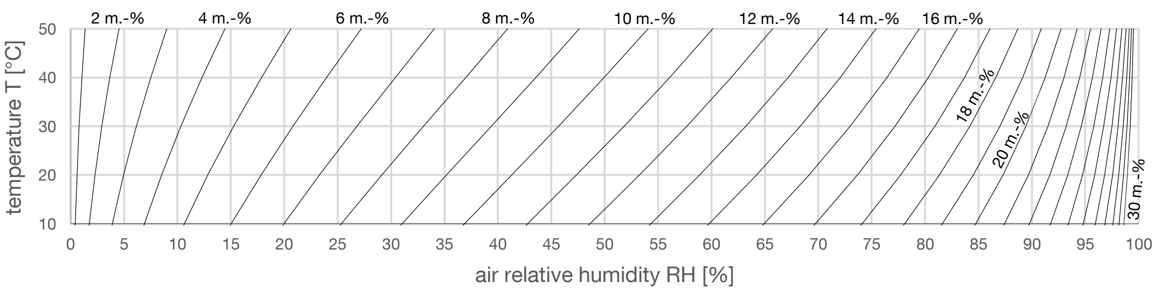

$$\mathrm{EMC} = \left[a \cdot (T + 273.15) \cdot \left(1 - \frac{(T + 273.15)}{647.1}\right)^{b} \cdot \ln\left(1 - \frac{1}{100}\,\mathrm{RH}\right)\right]^{c \cdot (T+273.15)^{d}}$$

	a	b	c	d
independent of grain direction	- 0.0000775	0.1389	0.0008966	1.1173

9.7 Appendix G: Parameters for the hygrothermal simulation of Norway spruce

Table 23: Material parameters for Norway spruce used for hygrothermal simulation with WUFI Pro

Parameter	Value	Unit	Reference
Dry density	416	kg/m³	Own measurements
Porosity	0.73	m³/m³	(Kollmann, 1951)
Heat capacity	1600	J/(kgK)	DIN EN ISO 10456
Thermal conductivity	0.11	W/(m·K)	ASHRAE 1018-RP, cf. function
Diffusion resistance	50	-	ASHRAE 1018-RP, cf. function

Table 24: Moisture storage function at 10 °C and 40 °C for Norway spruce used for hygrothermal simulation with WUFI Pro, based on oven-dry density and findings in Subchapter 5.3

Nr.	Relative humidity [decimal]	Moisture storage of Norway Spruce at 10 °C: water content [kg/m³]	Moisture storage Norway Spruce at 40 °C: water content [kg/m³]
1	0.1	19.2	13.2
2	0.2	28.0	20.2
3	0.3	35.5	26.4
4	0.4	42.5	32.3
5	0.5	49.5	38.4
6	0.6	57.0	45.0
7	0.7	65.3	52.6
8	0.8	75.6	62.0
9	0.9	90.5	76.0
10	0.95	103.2	88.2
11	0.99	128.1	112.5

Table 25: Liquid transport coefficients for Norway spruce used for hygrothermal simulation with WUFI Pro, based on North-American Data for "spruce", ASHRAE 1018-RP

Nr.	Water content [kg/m³]	Liquid transport coefficient, suction DWS [m²/s]	Liquid transport coefficient, redistribution DWW [m²/s]
1	0	0	0
2	55.8	5.19E-14	5.19E-14
3	845	1.14E-10	1.14E-11

Table 26: Water vapor diffusion resistance coefficient, moisture-dependent for Norway spruce used for hygrothermal simulation with WUFI Pro, based on North-American Data for "spruce", ASHRAE 1018-RP

Nr.	Relative humidity [decimal]	Water vapor diffusion resistance coefficient μ [-]
1	0	552
2	0.1	552
3	0.2	326.2
4	0.3	192.7
5	0.4	113.1
6	0.5	66.5
7	0.6	28.8
8	0.7	22.4
9	0.8	12.8
10	0.9	7.1
11	1	3.7

Table 27: Thermal conductivity, moisture-dependent, for Norway spruce used for hygrothermal simulation with WUFI Pro, based on (Kollmann, 1987)

Nr.	Water content [kg/m³]	Thermal conductivity λ [W/(m·K)]
1	0	0.11
2	125	0.16

Table 28: Thermal conductivity, temperature-dependent, for Norway spruce used for hygrothermal simulation with WUFI Pro, based on a thermal conductivity coefficient for temperature of 0.0002 W/(mK²) from (Kollmann, 1951)

Nr.	Temperature [°C]	Thermal conductivity λ [W/(m·K)]
1	- 20	0.104
2	80	0.124

9.8 Appendix H: Parameters for the hygrothermal simulation of Douglas fir

Table 29: Material parameters for Douglas fir used for hygrothermal simulation with WUFI Pro

Parameter	Value	Unit	Reference
Dry density	490	kg/m³	Own measurements
Porosity	0.9	m³/m³	ASHRAE 1018-RP
Heat capacity	1600	J/(kgK)	DIN EN ISO 10456
Thermal conductivity	0.12	W/(m·K)	ASHRAE 1018-RP, cf. function
Diffusion resistance	200	-	ASHRAE 1018-RP, cf. function

Table 30: Moisture storage function at 10 °C and 40 °C for Douglas fir used for hygrothermal simulation with WUFI Pro, based on oven-dry density and findings in Subchapter 5.3

Nr.	Relative humidity [decimal]	Moisture storage of Douglas fir at 10 °C: water content [kg/m³]	Moisture storage Douglas fir at 40 °C: water content [kg/m³]
1	0.1	22.4	15.7
2	0.2	32.0	23.4
3	0.3	40.0	30.0
4	0.4	47.4	36.3
5	0.5	54.8	42.7
6	0.6	62.6	49.5
7	0.7	71.3	57.2
8	0.8	81.9	66.7
9	0.9	97.1	80.7
10	0.95	110.1	92.8
11	0.99	135.0	116.6

Table 31: Liquid transport coefficients for Douglas fir used for hygrothermal simulation with WUFI Pro, based on North-American Data for "Douglas fir", ASHRAE 1018-RP

Nr.	Water content [kg/m³]	Liquid transport coefficient, suction DWS [m²/s]	Liquid transport coefficient, redistribution DWW [m²/s]
1	0	0	0
2	55.8	3.35E-14	3.35E-14
3	845	2.13E-11	2.13E-12

Table 32: Water vapor diffusion resistance coefficient, moisture-dependent for Douglas fir used for hygrothermal simulation with WUFI Pro, based on IEA Annex 14 Catalogue (above a value of 0.7 extrapolation based on the Diplomarbeit by A. Kaufmann from 1995)

Nr.	Relative humidity [decimal]	Water vapor diffusion resistance coefficient μ [-]
1	0	200
2	0.25	180
3	0.5	65
4	0.6	45
5	0.7	30
6	0.9	20
7	1	10

Table 33: Thermal conductivity, moisture-dependent, for Douglas fir used for hygrothermal simulation with WUFI Pro, based on (Kollmann, 1987)

Nr.	Water content [kg/m³]	Thermal conductivity λ [W/(m·K)]
1	0	0.12
2	147	0.18

Table 34: Thermal conductivity, temperature-dependent, for Douglas fir used for hygrothermal simulation with WUFI Pro, based on a thermal conductivity coefficient for temperature of 0.0002 W/(mK²) from (Kollmann, 1951)

Nr.	Temperature [°C]	Thermal conductivity λ [W/(m·K)]
1	- 20	0.114
2	80	0.134

9.9 Appendix I: Translated and adapted chapter from a previous publication

Some of the data for employing the new method for moisture flux detection on CLT in field tests have already been presented in the final report of the research project *PhyTAB* (Flexeder, Schumacher et al., 2022). The following is an adapted and summarized translation of the results detecting moisture gradients in a controlled humidification.

The method to detect moisture fluxes on wooden surfaces validated in Subchapter 5.4.6 is transferred to the scale of an entire room. The first step is to investigate the suitability of the measurement method using two temperature sensors for measurements in field tests. The pairs consist of two PT-1000 sensors with a four-wire circuit and the specially developed pyramidal sheaths, cf. Subchapter 4.5. The first sensor is placed directly on the material. The second, identical sensor is placed on a surface directly adjacent to it, on which a vapor retardant film (s_d-value 5 m) has been previously applied. Three of these pairs of sensors are installed inside the cube: in the center of the northeast wall, in the center of the northwest wall, and on the ceiling. For an isothermal humidity jump, the door to the cube is closed after the installation is complete and the humidification is started remotely for a period of 50 minutes. The humidifier was connected to a relay and placed on a scale to track the amount of water evaporated.

The results of the first experiment with active humidification without air exchange and under otherwise constant conditions in July 2020 show that the methods of laboratory operation can in principle be transferred to field tests. Operating the humidifier for 50 minutes results in the release of about 400 g of water (in vapor form) into the room air, cf. Figure 214.

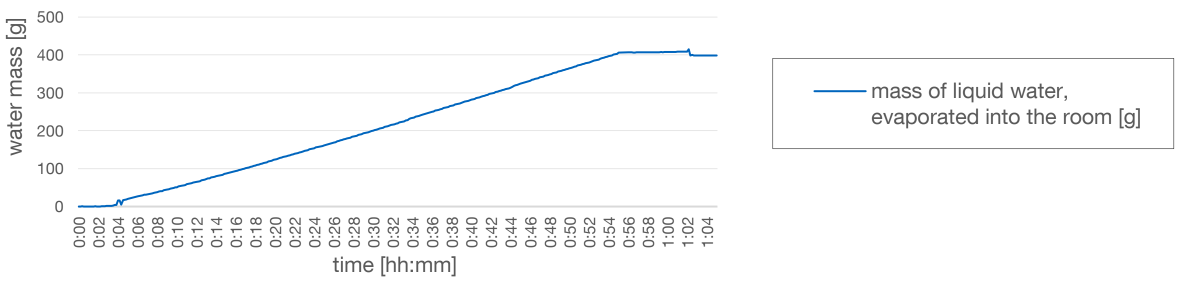

Figure 214: Rapid humidification to generate a moisture jump reaction in the test cube

This leads to a change in the room´s air relative humidity. The resulting values measured in the air layers near the enclosing wooden surfaces, the so-called boundary layers, are shown in Figure 215.

To evaluate the surface heating, the difference between the temperature measured on the wooden surface and the temperature measured on the masked surface in the immediate vicinity is calculated. The delta *dT* [K] of these two measurements is plotted against time and interpreted as the heating of the material surface due to the release of sorption enthalpy. For the period of active humidification (50 minutes), all three measuring points (ceiling, northwest wall and northeast wall) show a warming of about 0.15 Kelvin due to this hygrothermal effect, cf. Figure 216. Once the relative humidity of air drops, the temperature differences drop as well, even into the negative indicating a sudden reverse moisture flux (desorption).

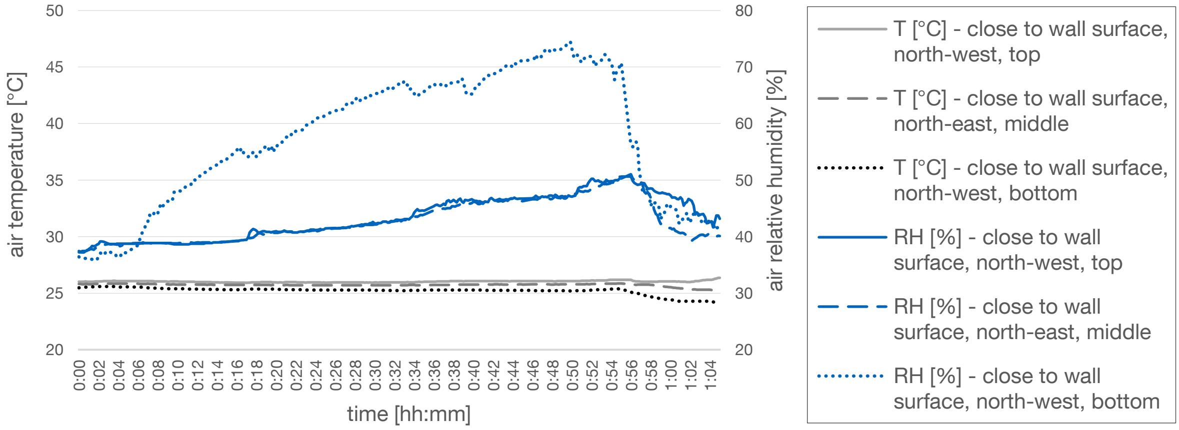

Figure 215: Relative humidity and temperature of air, measured close to the wooden surface in different locations of the test cube

It is noticeable that the curves for the temperature differences *dT* show a minor rise even before the start of the controlled mechanical humidification. This could be due to fluctuations during the day or the presence of people shortly before closing the door. Compared to laboratory experiments, the challenge of measurements in the cross-laminated timber cube is to isolate these individual hygrothermal effects.

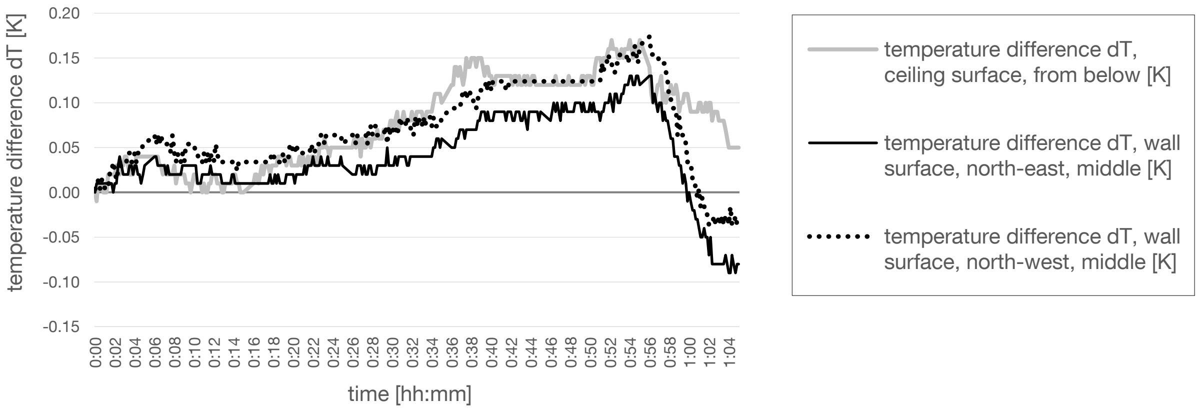

Figure 216: Resulting temperature differences on wooden surfaces, recorded in different locations within the test cube

9.10 Appendix J: Selection of in-situ monitoring results from modified CLT walls

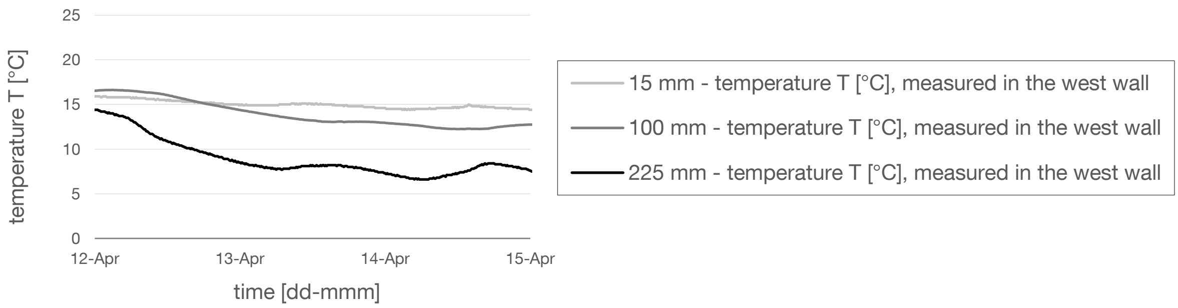

Figure 217: Temperatures measured in April of 2021 in the west-facing wall of the project Einfach Bauen

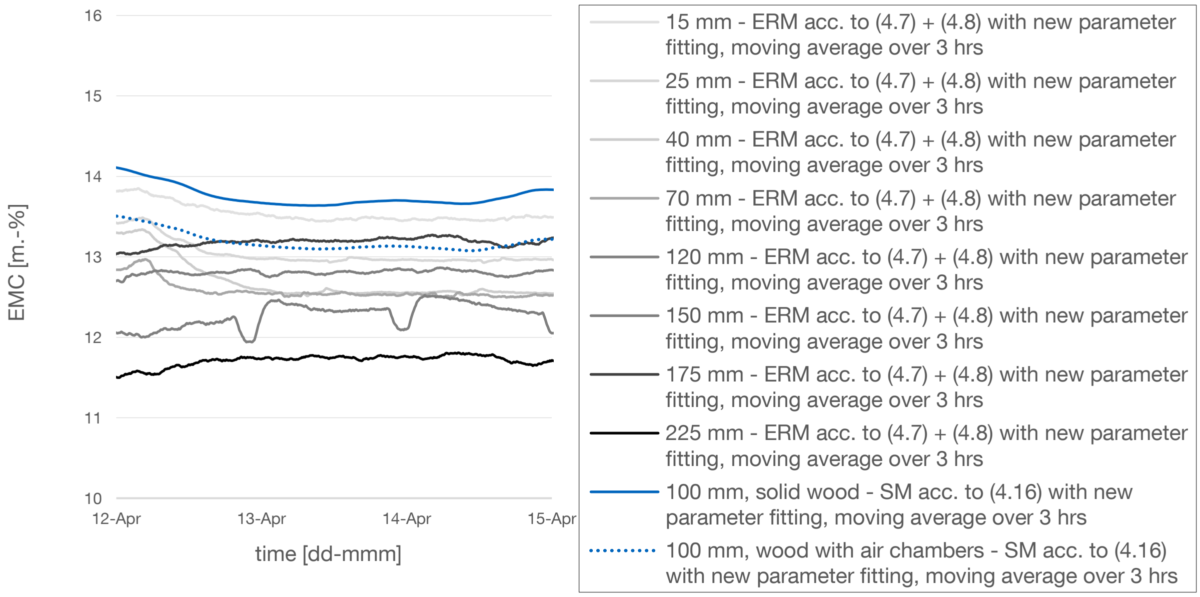

Figure 218: EMCs [m.-%] determined using two different methods (ERM and SM) in the west-facing wall

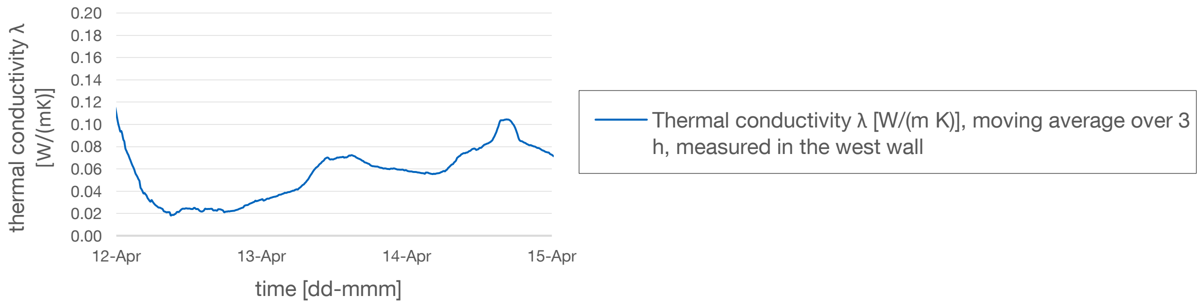

Figure 219: Thermal conductivity computed from the heat flux density measured inside the west-facing wall

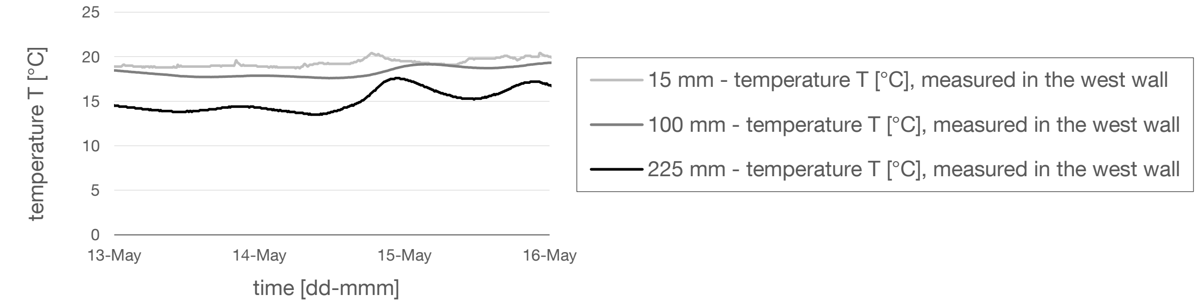

Figure 220: Temperatures measured in May of 2021 in the west-facing wall of the project Einfach Bauen

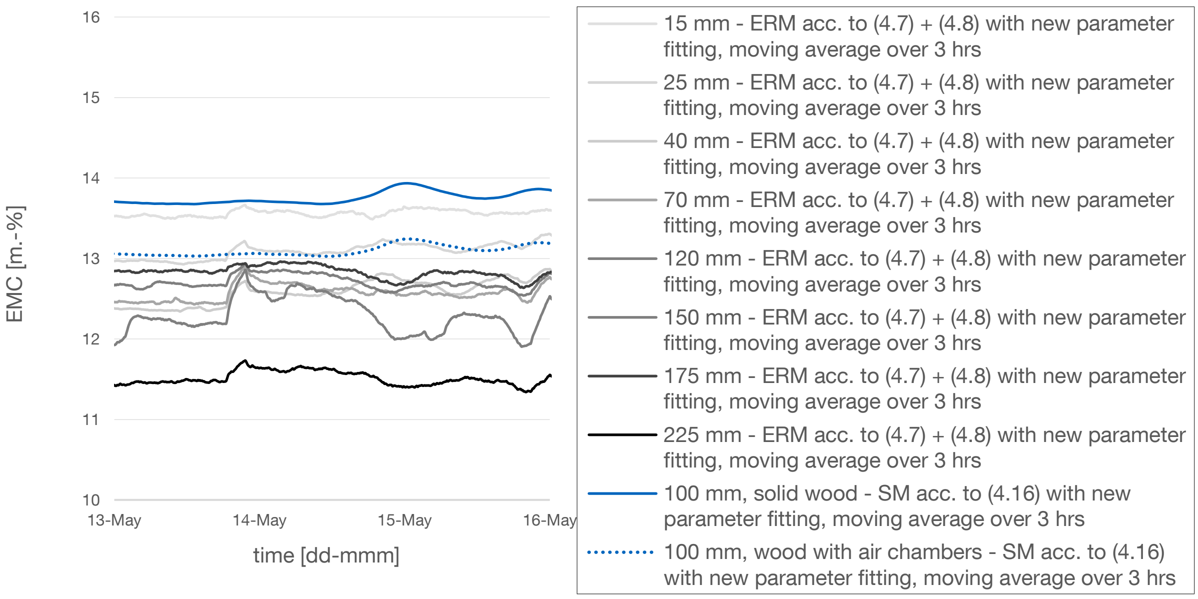

Figure 221: EMCs [m.-%] determined using two different methods (ERM and SM) in the west-facing wall

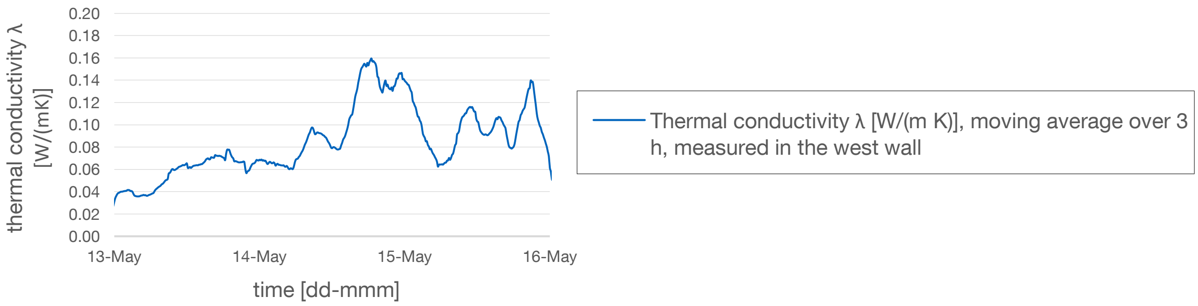

Figure 222: Thermal conductivity computed from the heat flux density measured inside the west-facing wall

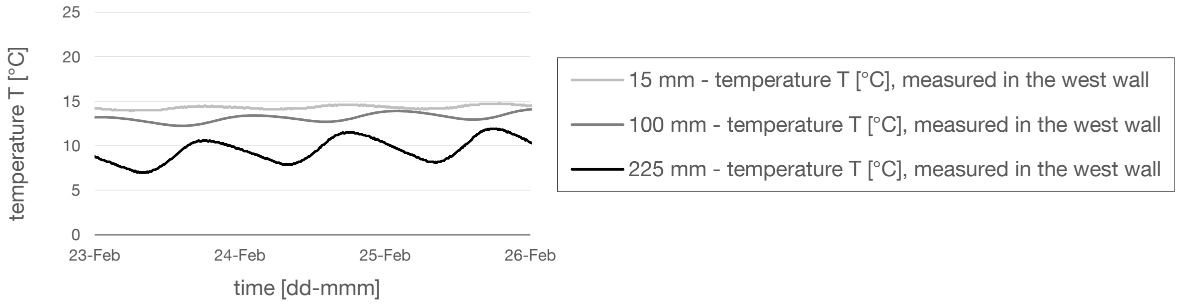

Figure 223: Temperatures measured in April of 2021 in the west-facing wall of the project Einfach Bauen

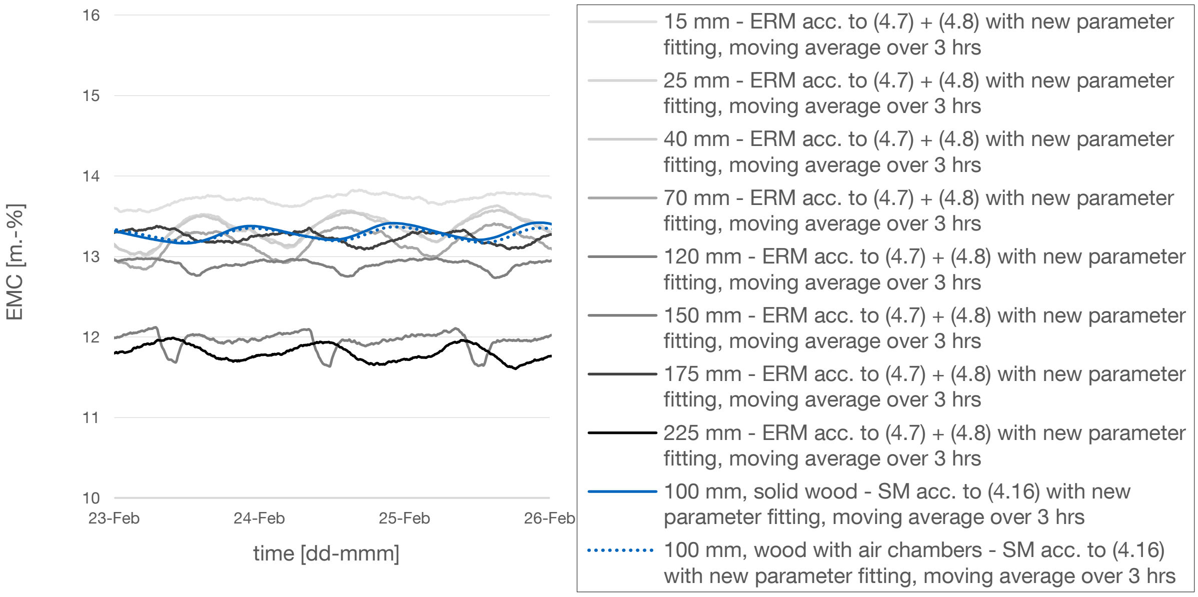

Figure 224: EMCs [m.-%] determined using two different methods (ERM and SM) in the west-facing wall

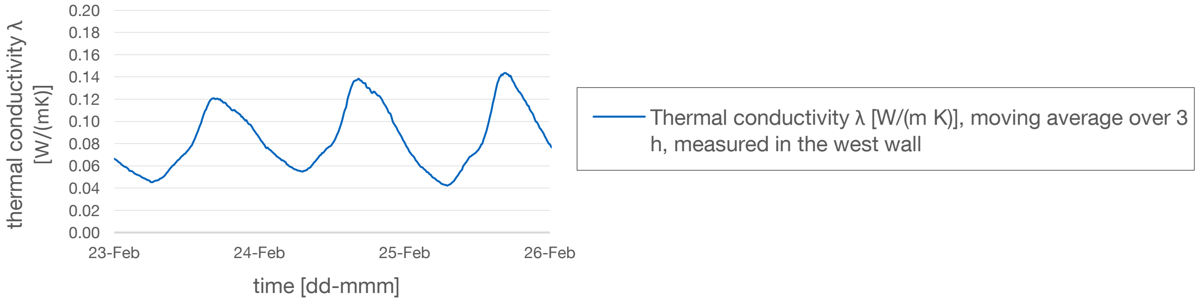

Figure 225: Thermal conductivity computed from the heat flux density measured inside the west-facing wall

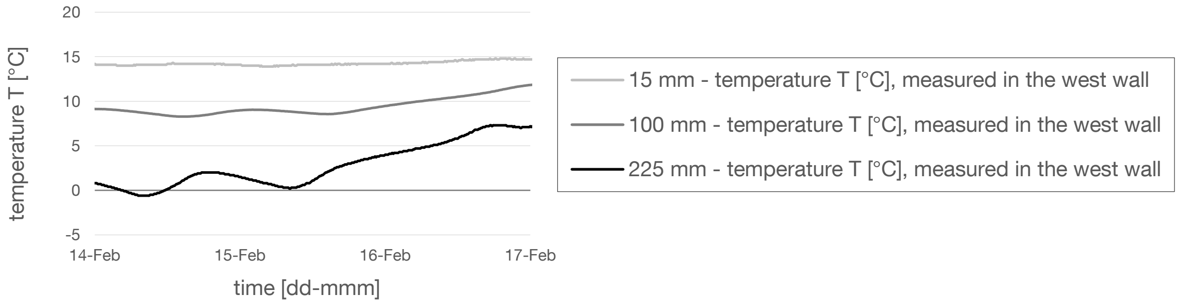

Figure 226: Temperatures measured in February of 2021 in the west-facing wall of the project Einfach Bauen

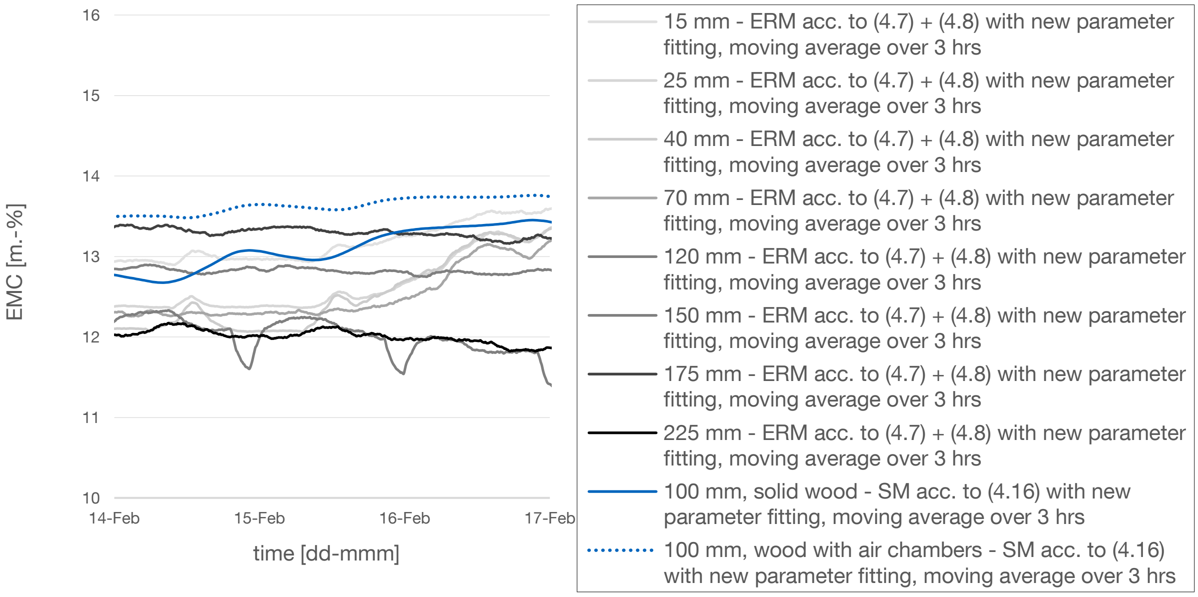

Figure 227: EMCs [m.-%] determined using two different methods (ERM and SM) in the west-facing wall

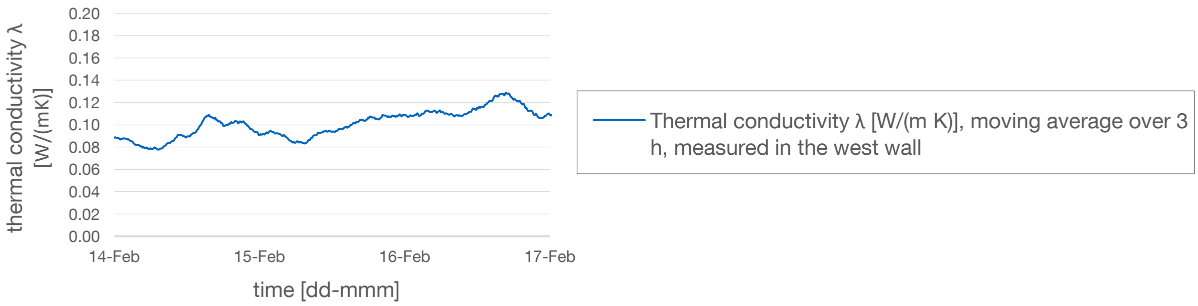

Figure 228: Thermal conductivity computed from the heat flux density measured inside the west-facing wall

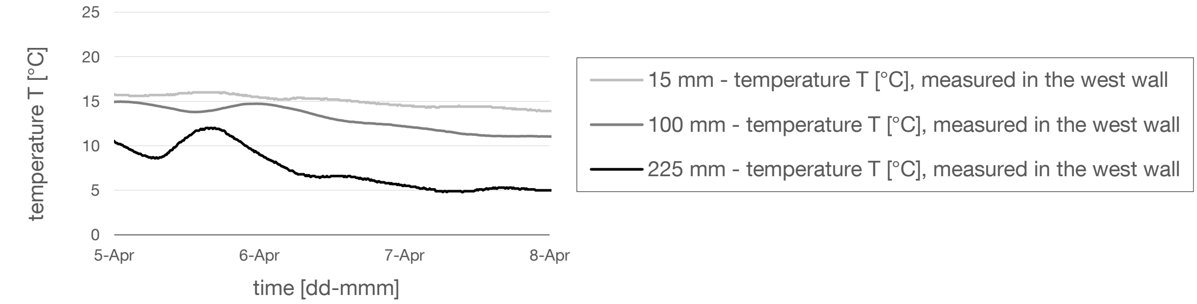

Figure 229: Temperatures measured in April of 2021 in the west-facing wall of the project Einfach Bauen

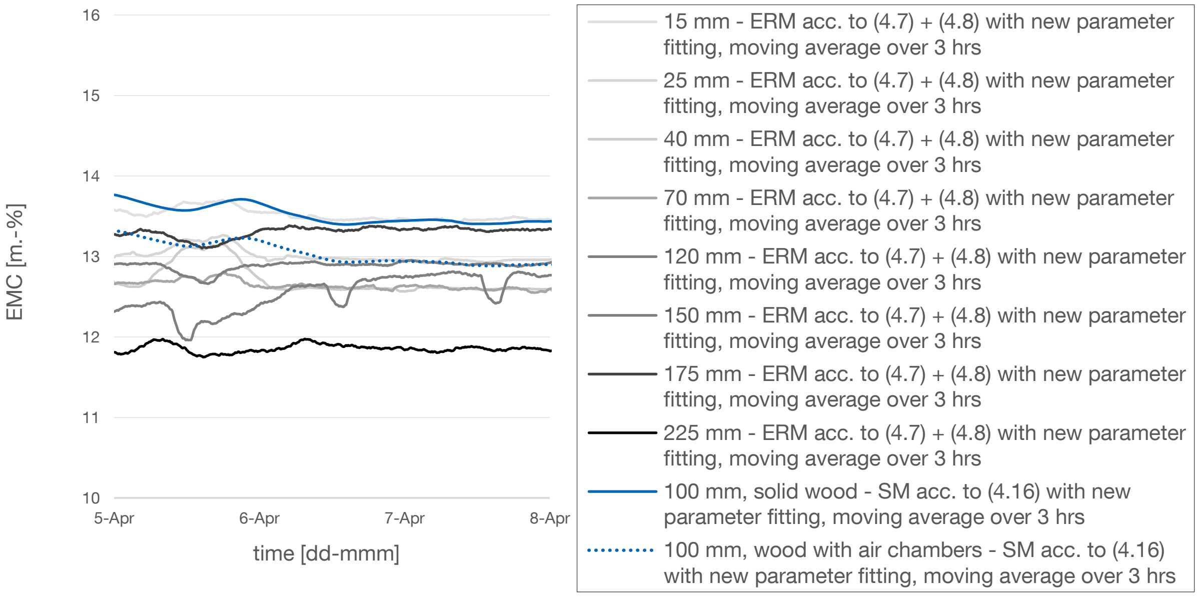

Figure 230: EMCs [m.-%] determined using two different methods (ERM and SM) in the west-facing wall

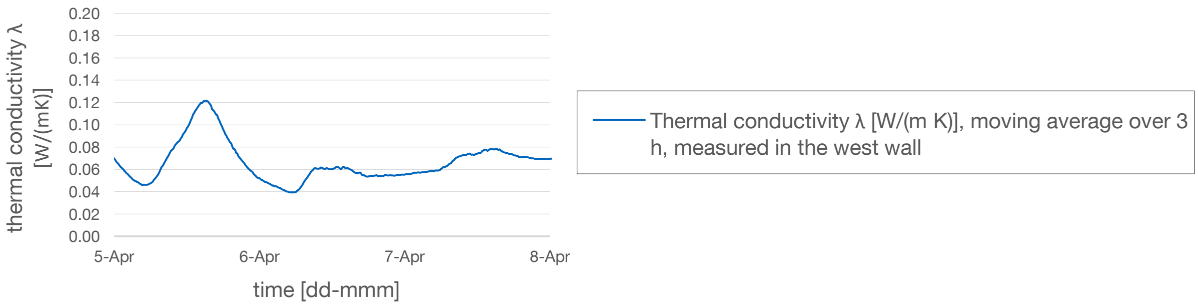

Figure 231: Thermal conductivity computed from the heat flux density measured inside the west-facing wall

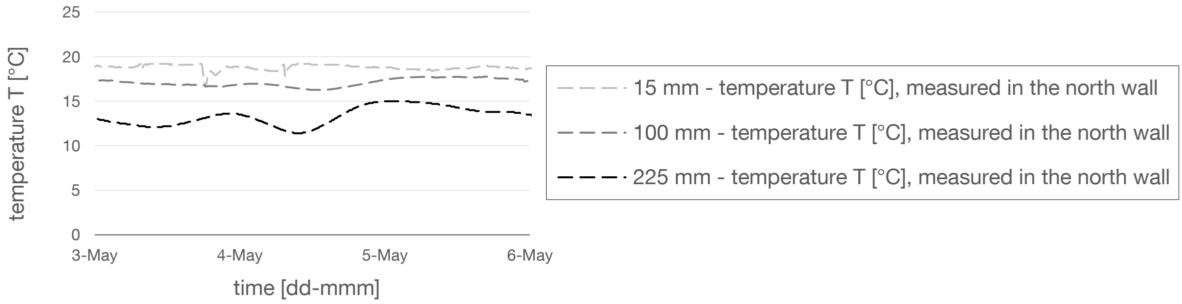

Figure 232: Temperatures measured in May of 2021 in the north-facing wall of the project Einfach Bauen

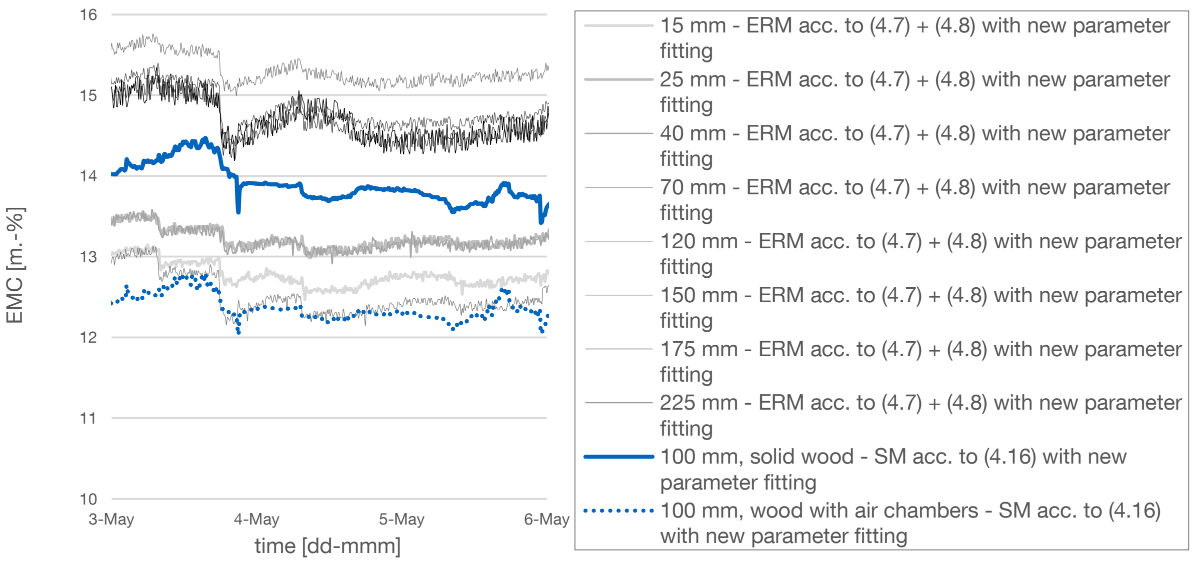

Figure 233: EMCs [m.-%] determined using two different methods (ERM and SM) in the north-facing wall

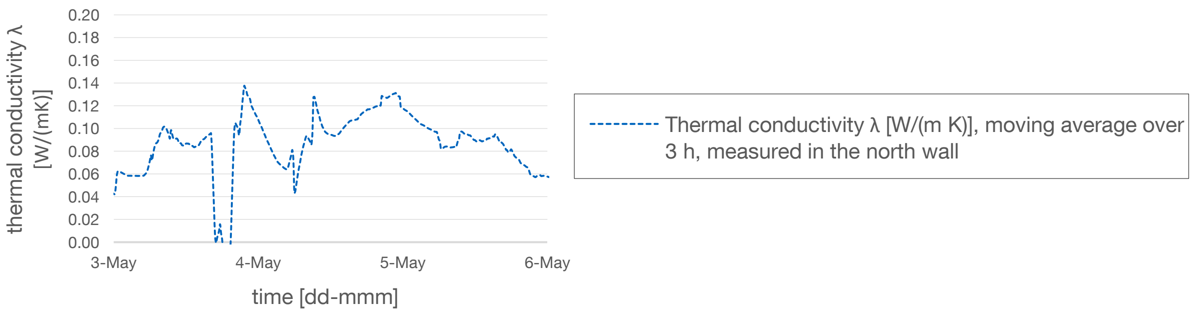

Figure 234: Thermal conductivity computed from the heat flux density measured inside the north-facing wall

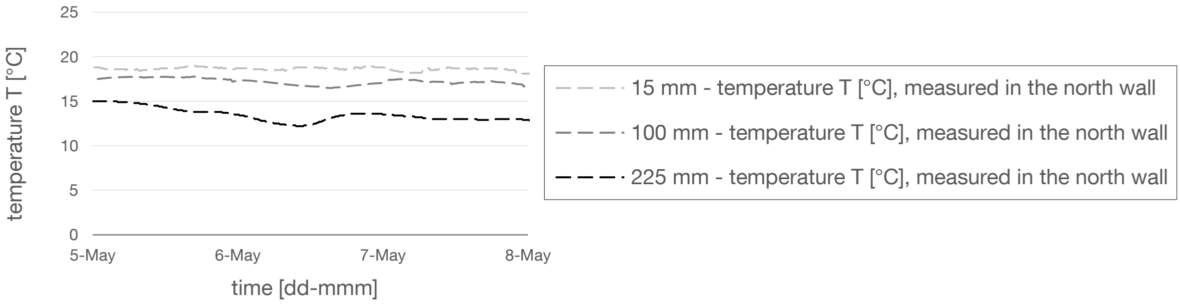

Figure 235: Temperatures measured in May of 2021 in the north-facing wall of the project Einfach Bauen

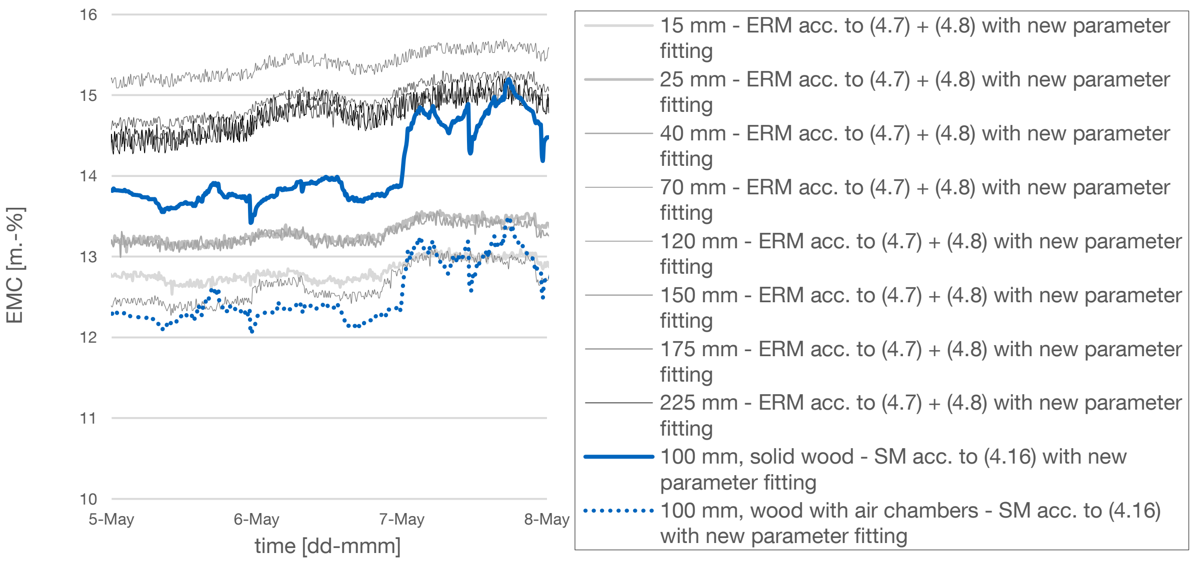

Figure 236: EMCs [m.-%] determined using two different methods (ERM and SM) in the north-facing wall

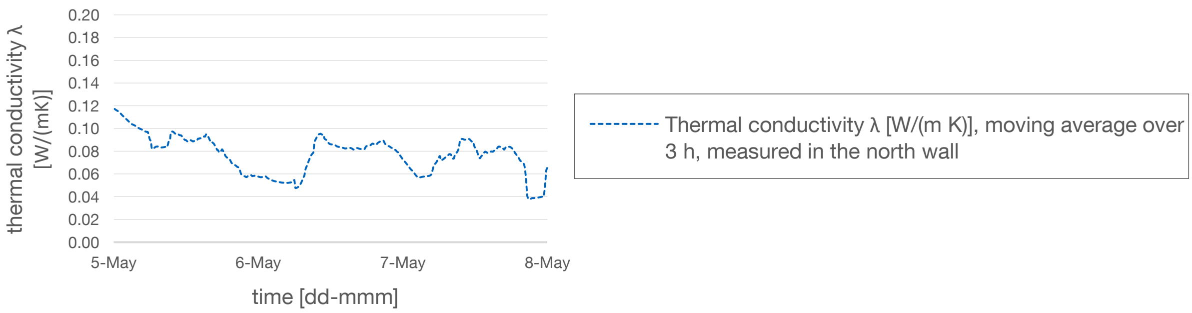

Figure 237: Thermal conductivity computed from the heat flux density measured inside the north-facing wall

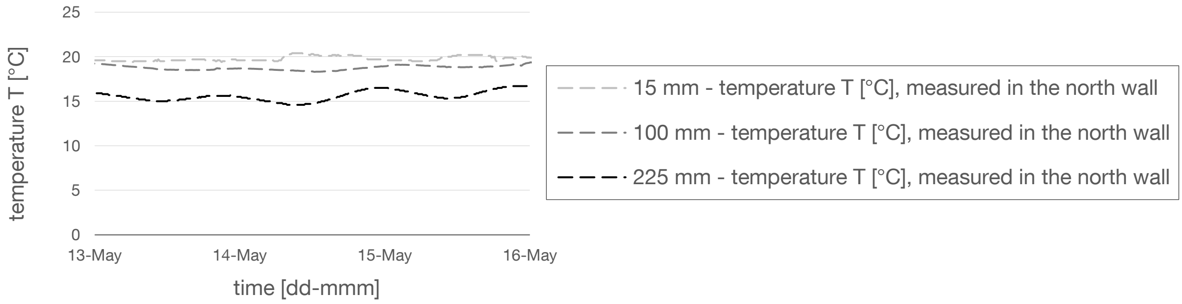

Figure 238: Temperatures measured in May of 2021 in the north-facing wall of the project Einfach Bauen

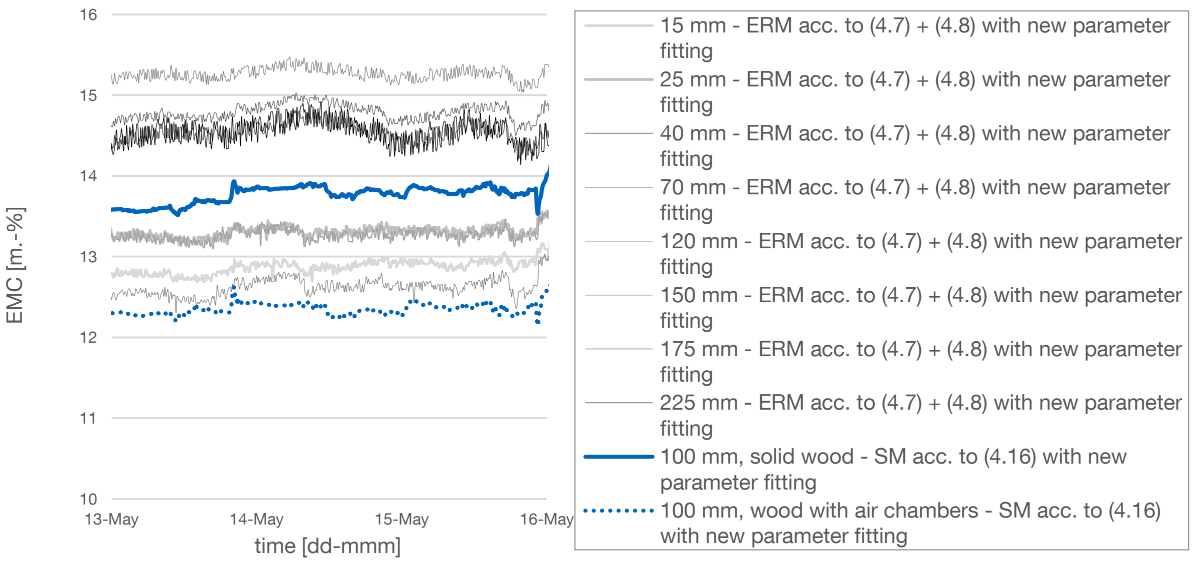

Figure 239: EMCs [m.-%] determined using two different methods (ERM and SM) in the north-facing wall

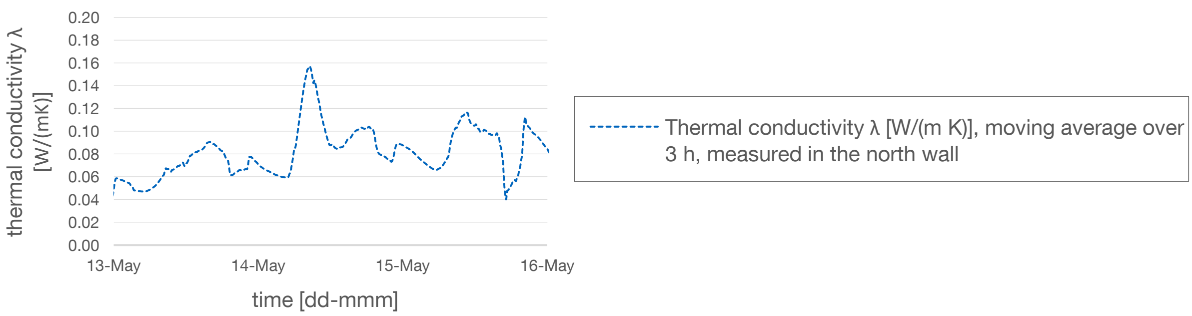

Figure 240: Thermal conductivity computed from the heat flux density measured inside the north-facing wall

9.11 Appendix K: Declaration of authorship

Selbstständigkeitserklärung

Hiermit versichere ich, dass ich die vorliegende Arbeit selbstständig verfasst und keine anderen als die angegebenen Quellen und Hilfsmittel benutzt sowie Zitate kenntlich gemacht habe.

Declaration of authorship

I hereby declare that I have written this thesis independently and that I have not used any sources or aids other than those specified and that I have indicated any quotations.

München, 2. September 2024

Munich September 2nd 2024

Nina Flexeder